Philipps Universität Marburg

From CoA ester supply to a yeast communication toolkit in *Saccharomyces cerevisiae*

Dissertation

zur
Erlangung des Doktorgrades
der Naturwissenschaften
(Dr. rer. nat.)

Dem Fachbereich Biologie
der Philipps-Universität Marburg
vorgelegt von

Nicolas Krink
geb. Koutsoubelis
aus Hagen

Marburg, September 2019

Die Untersuchungen zur vorliegenden Arbeit wurden von November 2014 bis September 2019 am Max-Planck-Institut für Terrestrische Mikrobiologie in Marburg unter der Leitung von Prof. Dr. Victor Sourjik durchgeführt.

Vom Fachbereich Biologie der Philipps-Universität Marburg

als Dissertation angenommen am: 01.11.2019

Erstgutachter: Prof. Dr. Victor Sourjik
Zweitgutachter: Prof. Dr. Tobias Erb

Weitere Mitglieder der Prüfungskommission:
Prof. Dr. Michael Bölker
Dr. Hannes Link

Tag der mündlichen Prüfung: 12.11.2019

Erklärung

Hiermit erkläre ich, dass ich die vorliegende Dissertation mit dem Titel:

„ From CoA ester supply to a yeast communication toolkit in *Saccharomyces cerevisiae* “

selbstständig verfasst, keine anderen als die im Text angegebenen Hilfsmittel verwendet und sämtliche Stellen, die im Wortlaut oder dem Sinn nach anderen Werken entnommen sind, mit Quellenangaben kenntlich gemacht habe.

Die Arbeit wurde in dieser oder ähnlicher Form noch keiner Prüfungskommission vorgelegt.

Marburg, den _____._____._____

_____
Nicolas Krink

Part of this work was published in the following articles:

Nicolas Krink-Koutsoubelis, Anne C. Loechner, Anna Lechner, Hannes Link, Charles M. Denby, Bastian Vögeli, Tobias J. Erb, Satoshi Yuzawa, Tadas Jakociunas, Leonard Katz, Michael K. Jensen, Victor Sourjik, and Jay D. Keasling: Engineered Production of Short-Chain Acyl-Coenzyme A Esters in *Saccharomyces cerevisiae*. *ACS Synthetic Biology* 2018, *7* (4), 1105-1115. DOI: 10.1021/acssynbio.7b00466

Nicolas Krink, Alexander Anders, Timo Glatter, Stefan Rensing, and Victor Sourjik: YCTK – A yeast communication toolkit for multicellular networks in *S. cerevisiae* (in preparation)

“Experience is what you get when you didn't get what you wanted. And experience is often the most valuable thing you have to offer.”

Randy Pausch

“Never lose the childlike wonder. Show gratitude... Don't complain; just work harder... Never give up.”

Randy Pausch

Meinen Wegbegleitern
Meiner Mama

Abbreviations

Abbreviation	Full form
2mb-CoA	2-methylbutyryl-CoA
3HP	3-hydroxypropionate pathway
3HP-CCR	3-hydroxypropionate CCR pathway
3'UTR	3' untranslated region
ACP	Acyl carrier protein
AHL	Acyl-homoserine-lactone
AIB	Alternative isovaleryl-CoA biosynthetic pathway
a.u.	Arbitrary units
BkD	branched-chain α-keto acid dehydrogenase (BCKDH) complex pathway
(k)bp	(Kilo) Base pair
BUT	Butyryl-CoA and hexanoyl pathway
but-CoA	Butyryl-CoA
Ca/C. a.	*Candida albicans*
CDK	Cyclin-dependent kinase
cMT	methyltransferase
CPEC	Circular polymerase extension cloning
CREBP	cAMP response element-binding protein
CRISPR	Clustered regularly interspaced short palindromic repeats
C-terminus/ terminal	Carboxyl-terminus/terminal
DBTL	Design, test, build, and learn cycle of SynBio
dCas9	Deactivated Cas9
ddH_2O	Sterile ultra-pure water
DH	Dehydrogenase
DMA-CoA	3,3-dimethylacrylyl-CoA
DMSO	Dimethyl sulfoxide
DNA	Deoxyribonucleic acid
DNT	2,4-Dinitrotoluene
dNTP	Deoxyribonucleotide triphosphate
dox	Doxycycline
Ec/E. c.	*Eremothecium cymbalariae*
EDTA	Ethylenediaminetetraacetic acid
EM	Extraction method
ER	Enoylreductase/endoplasmatic reticulum
FAD	flavin adenine dinucleotide
FCC	Frozen competent cell solution
Gal	Galactose
GPCR	G-protein-coupled receptor
hex-CoA	Hexanoyl-CoA
HMG-CoA	3-hydroxy-3-methylglutaryl-CoA
ib-CoA	Isobutyryl-CoA
IRES	Internal ribosome entry sites
IV-CoA	Isovaleryl-CoA
Ka/K. a.	*Kazachstania africana*
Kn/K. n.	*Kazachstania naganishii*
Kl/K. l.	*Kluyveromyces lactis*
KR	Ketoreductase

Abbreviations

LB	Luria broth medium
LCR	Ligase chain reaction
Lf/L. f.	*Lachancea fermentati*
Lm/L. m.	*Lachancea mirantina*
Lt/L. t.	*Lachancea thermotolerans*
*MAT*a	Mating type a
*MAT*α	Mating type α
MAPK pathway	mitogen-activated protein kinase pathway
MEK	Mitogen-activated protein kinase
MEKK	Mitogen-activated protein kinase kinase
MEKKK	Mitogen-activated protein kinase kinase kinase
MG-CoA	3-methylglutaconyl CoA
mm-CoA	Methylmalonyl-CoA
mNeonGreen	Green/yellow fluorescent protein
mRuby	Monomeric red fluorescent protein
N-terminus/terminal	Amino terminus/terminal
OD	Optical density at 600 nm
ORF	Open reading frame
PCR	Polymerase chain reaction
PEG	Polyethylene glycol
PHBA	p-hydroxybenzoic acid
PKS	Polyketide synthase
PNP	Plant natural products
P-pant	phosphopantetheinyl transferase
PrpE	PrpE pathway
P-CoA/Prop-CoA	Propionyl-CoA
QS	Quorum sensing
RNA	Ribonucleic acid
RPKM	Reads per kilobase per million
SC	Synthetic complete
Sc/S. c.	*Saccharomyces cerevisiae*
SCRaMbLE	Synthetic chromosome rearrangement and modification by loxP-mediated evolution
SD	Synthetic dropout
SGD	*Saccharomyces* Genome Database
SOB	Super optimal broth
SOC	Super optimal broth with catabolite repression
SSU rRNA	small subunit ribosomal ribonucleic acid
TAE	Tris-Acetate-EDTA
TE	Thioesterase
Tris	2-Amino-2-hydroxymethyl-propane-1,3-diol
Tp/T. p.	*Tetrapisispora phaffii*
T_m	Melting temerature
TULIP	Tunable and light-inducible light dimerization tag
Venus	Yellow fluorescent protein
Vp/V. p.	*Vanderwaltozyma polyspora*
YCTK	Yeast Golden Gate Communication Toolkit
YNB	Yeast nitrogen base
YPD	Yeast extract peptone dextrose
YTK	Yeast Golden Gate Toolkit

Zusammenfassung

Saccharomyces cerevisiae ist das am häufigsten verwendete eukaryotische Chassis in der Synthetischen Biologie, weil die Menschheit und diese Hefe eine lange und fruchtbare Geschichte miteinander verbindet. Bei Anwendungen in der Synthetischen Biologie wurde *S. cerevisiae* häufig für biotechnologische Biosynthesewege sowie den Aufbau künstlicher Netzwerke eingesetzt. Unser Beitrag zur biotechnologischen Nutzung der Hefe *S. cerevisiae* ist, dass wir deren metabolischen Kapazitäten erweiterten, indem wir nicht natürlich vorkommende kurzkettige Acyl-Coenzym-A-Ester als Stoffwechselvorläufer bereitgestellt haben. Um den Bau künstlicher Netzwerke zu mehrzelligen Systemen voranzutreiben, haben wir einen umfassenden Hefekommunikations-Baukasten (YCTK) bereitgestellt und gezeigt, dass es für den schnellen Aufbau synthetischer Zell-Zell-Kommunikationssysteme verwendet werden kann.

Designte Bereitstellung von kurzkettigen Acyl-Coenzym A-Estern in *Saccharomyces cerevisiae*

Weltweit ist *S. cerevisiae* einer der am häufigsten verwendeten Organismen in der modernen Biotechnologie und stellt einen hohen wirtschaftlichen Wert für die wachsende Bioökonomie dar. Mit dem Ziel, in *S. cerevisiae* neuartige Naturprodukte herzustellen, wurde ein Mangel des Organismus offensichtlich. Kurzkettige Acyl-Coenzym A-Ester dienen als Vorstufen für wertvolle Produkte, wie Fettsäuren, Polyketide, Biopolymere und anderen Chemikalien. Das begrenzte Repertoire von *S. cerevisiae* an kurzkettigen Acyl-CoAs verhindert jedoch, dass *S. cerevisiae* als Produktionswirt für eine Vielzahl an Naturstoffen eingesetzt werden kann. Um diese Einschränkung zu beseitigen, haben wir die Biosynthesewege zu fünf verschiedenen Acyl-CoA-Estern in *S. cerevisiae* etabliert. Wir entwickelten Hefen, welche die Biosynthesewege für Propionyl-CoA, Methylmalonyl-CoA, n-Butyryl-CoA, Isovaleryl-CoA und n-Hexanoyl-CoA von Plasmiden exprimierten. Für die Herstellung von Propionyl-CoA und Methylmalonyl-CoA haben wir einen veröffentlichten, fütterungsabhängigen Produktionsweg unter Verwendung von PrpE und Pcc Enzymen eingesetzt, der als Maßstab für unsere fütterungsunabhängigen Produktionswege diente, die in unserer Studie vergleichbare Produktkonzentrationen ergaben. Um eine effiziente Extraktion der produzierten Metaboliten sicherzustellen, haben wir ein hefespezifisches Metabolitenextraktionsprotokoll erstellt, um die intrazellulären Acyl-CoA-Konzentrationen in den gentechnisch hergestellten Stämmen zu bestimmen. Für die Herstellung von Isovaleryl-CoA haben wir zwei verschiedene Wege getestet, aber nur Produktbildung aus dem alternativen Isovaleryl-CoA-Biosyntheseweg (AIB) erhalten, der aus *Myxococcus xanthus* stammt und 5,5 ± 1,2 µM Isovaleryl-CoA produzierte. Unseres Wissens nach ist dies die erste funktionelle artfremde Expression dieses Stoffwechselweges in *S. cerevisiae*. Für die Herstellung von n-Butyryl-CoA und n-Hexanoyl-CoA haben wir den Butanol-Produktionsweg für unsere Zwecke angepasst und ca. 6 µM intrazelluläre Konzentration von Butyryl-CoA und Hexanoyl-CoA gemessen. Für den fütterungsabhängigen Weg zu Propionyl-CoA erhielten wir intrazelluläre Konzentrationen von 5,3 ± 2,4 µM, während der fütterungsunabhängige 3HP-Weg 8,5 ± 3,7 µM produzierte. Die Verlängerung beider Propionyl-CoA-Wege zur Produktion von Methylmalonyl-CoA führte nur zur Produktion von 0,5 ± 0,1 µM und 0,3

± 0,3 µM Methylmalonyl-CoA. Nicht nur, aber insbesondere für die Herstellung von Methylmalonyl-CoA, ist eine weitere Optimierung erforderlich. Wir haben einen kurzkettigen Acyl-CoA-Golden-Gate-Baukasten etabliert, um Prototypenentwicklung, Optimierung und das Testen von alternativen Enzymen zu vereinfachen. Diese Sammlung ermöglicht zusammen mit dem bekannten Hefe-Baukasten Dueber YTK sowohl die Untersuchung verschiedener Enzymvarianten als auch die optimierte Expression der entsprechenden Gene.
Wir kommen zur Schlussfolgerung, dass die hier produzierten Acyl-CoAs, welche häufige Vorstufen von Sekundärmetaboliten sind, den Grundstein für die künftige gentechnische Herstellung von Naturstoffen in *S. cerevisiae* legen. Diese Acyl-CoA-produzierenden Stämme bilden zusammen mit dem kurzkettigen Acyl-CoA-Baukasten die Grundlage für die weitere Erforschung von *S. cerevisiae* als heterologem Produktionsorganismus zur Herstellung hochwertiger sekundärer Stoffwechselprodukte.

Hefe Kommunikationsbaukasten
Die Konstruktion mehrzelliger Netzwerke wurde schon früh in der Synthetischen Biologie als Ziel definiert. Auch heute sind mit ihnen vielversprechende Vorteile, wie die Arbeitsteilung und die Lösung komplizierter Netzwerkfunktionen, verknüpft. Die meisten Systeme wurden bisher in bakteriellen Organismen etabliert und es existieren nur wenige Beispiele für eukaryotische Organismen wie *S. cerevisiae*. Speziell für gramnegative Bakterien bietet das Quorum-Sensing-System eine Vielfalt gebrauchsfertiger Kommunikationssysteme. Hefen entwickelten auch ein Kommunikationssystem unter Verwendung von Peptidpheromonen, um mit dem entgegengesetzten Paarungstyp zu interagieren. Wir haben die natürliche Diversität der Peptid-α-Faktor-Pheromone, der entsprechenden GPCR-Rezeptoren sowie der Proteasen, welche ähnlich wie Quorum-Quenching-Enzyme funktionieren, genutzt. Mit der Einrichtung unseres Golden Gate Hefekommunikations-Baukastens stellen wir eine standardisierte Sammlung von Teilen zur Verfügung, die den schnellen Aufbau von vielzelligen Netzwerken im Modellorganismus *S. cerevisiae* ermöglichen.
Die möglichen Netzwerkdesigns und die daraus resultierenden denkbaren Anwendungen sind sehr vielseitig. Die YCTK-Sammlung besteht aus Rückmelder- (Pheromon-induzierbaren Promotoren), Sender- (*mfa1*-Gene - α-Faktoren), Empfänger- (Ste2-Rezeptoren) und Barriere- (Bar1-Proteasen) -teilen. Wir haben die Dynamik der Pheromon-induzierbaren Promotoren in den verschiedenen Hintergründen der Paarungstypen charakterisiert und die Dosisreaktion auf den α-Faktor sowie deren zeitliche Reaktion bestimmt. Die verschiedenen Promotoren zeigten eine Reihe unterschiedlicher Dynamiken und Eigenschaften, die die Umsetzung unterschiedlicher Designs ermöglichen. Die Charakterisierungsergebnisse der Ste2-Rezeptoren zeigten, dass unsere Sammlung aus Rezeptoren mit hoher Promiskuität für den α-Faktor und aus Rezeptoren mit hoher Substratspezifität für ihren zugehörigen α-Faktor besteht. Ferner fanden wir, dass verschiedene Ste2-Rezeptoren unterschiedliche Empfindlichkeiten gegenüber dem verwandten sowie dem nicht verwandten α-Faktor aufweisen. Die Promiskuität der Ste2-Rezeptoren korrelierte nicht mit den α-Faktor-Sequenzen. Unsere Wahrscheinlichkeitsanalyse der Ste2-Rezeptoren ergab, dass diejenigen, die eng mit *S. cerevisiae* verwandt sind, tendenziell durch die α-Faktoren verwandter Spezies stimuliert werden. Unsere Stammbaumanalyse der Ste2-Rezeptoren stimmt mit den phylo-

genetischen Beziehungen der Spezies überein. Interessant ist auch die Feststellung, dass α-Faktoren von Spezies, für die der Rezeptor eine hohe Promiskuität gegenüber α-Faktoren aufweist, nur wenige Rezeptoren stimulieren. Obwohl nur fünf der ausgewählten Proteasen funktionell exprimiert wurden, war die Charakterisierung der Proteasepromiskuität unseres Wissens die bislang umfassendste Studie dieser Art. Ähnlich wie bei den Rezeptoren identifizierten wir promiskuitive und substratspezifische Proteasen. Das vorgeschlagene Modell der Koevolution zwischen Rezeptoren und Proteasen zur Erkennung ähnlicher Sequenzmotive des α-Faktors wurde teilweise durch unsere Ergebnisse bestätigt, das Modell ist jedoch nicht universell anwendbar. Das erweiterte Wissen über die Pheromon-induzierbaren Promotoren, den Crosstalk zwischen α-Faktoren, Rezeptoren und Proteasen und der Einstellbarkeitstest der Teile ermöglichten die Anwendung des modelhaften Aufbaus von mehrzelligen Systemen unter Verwendung der YTCK-Sammlung. Wir haben mehrzellige logische Gate-ähnliche Populationsnetzwerke entwickelt, die es den Empfängerzellen ermöglichten, auf die Populationszusammensetzung zu reagieren. Während das α-Faktor-Signalmotiv funktionsfähig ist und erfolgreich zur Etablierung von OR- und AND-Gate-ähnlichen Systemen verwendet wurde, muss die Signalstörung durch eine Barriereprotease eines selbststimulierenden oder eines Signalmotivs weiter optimiert werden. Insgesamt hat sich die Realisierung mehrzelliger Netzwerke mit dem YCTK als erfolgreich erwiesen.
Zusammenfassend haben wir mit den YCTK Baukasten Teilen sowie eine umfassende Charakterisierung von Sender-, Empfänger- und Barriereteilen bereitgestellt, um die Implementierung von Zell-Zell- und damit mehrzelligen Kommunikationsnetzwerke in *S. cerevisiae* zu erleichtern.

Summary

Saccharomyces cerevisiae is the most widely used eukaryotic chassis in synthetic biology, as humanity and yeast share a long and fruitful history. For synthetic biology applications, *S. cerevisiae* was extensively used for metabolic engineering as well as for the construction of artificial networks. To contribute to the metabolic engineering achievements conducted in *S. cerevisiae,* we extended its metabolic capacities by providing non-native short-chain acyl-coenzyme A esters as metabolic precursors. In order to advance the construction of artificial networks to multicellular systems we provided a comprehensive yeast communication toolkit (YCTK), and demonstrated its usability for the rapid assembly of synthetic cell-cell communication systems.

Engineered production of short-chain acyl-coenzyme A esters in *Saccharomyces cerevisiae*

Globally, *S. cerevisiae* is one of the most commonly used chassis organisms in modern biotechnology and constitutes a high economic value to the growing bioecomomy. With the objective to produce novel natural products in *S. cerevisiae* a bottleneck of the chassis was uncovered. Short-chain acyl-coenzyme A esters serve as intermediate compounds in fatty acid biosynthesis, and are building blocks for the production of polyketides, biopolymers, and other value-added chemicals. However, *S. cerevisiae*'s limited repertoire of short-chain acyl-CoAs effectively prevents its application as a production host for a plethora of natural products. To address and resolve this limitation, we introduced metabolic pathways to five different acyl-CoA esters into *S. cerevisiae*. We engineered plasmid-based yeast strains that provide propionyl-CoA, methylmalonyl-CoA, n-butyryl-CoA, isovaleryl-CoA, and n-hexanoyl-CoA. For the production of propionyl-CoA and methylmalonyl-CoA, we reestablished a published feeding-dependent production route using the PrpE and Pcc enzymes to serve as benchmark for our feeding-independent production pathways that provided in our study comparable product concentrations. To ensure efficient extraction of the produced metabolites we established a yeast-specific metabolite extraction protocol to determine the intracellular acyl-CoA concentrations in the engineered strains. For the production of isovaleryl-CoA, we tested two different pathways but only obtained product formation from the alternative isovaleryl-CoA biosynthetic (AIB) pathway originating from *Myxococcus xanthus* and obtained 5.5±1.2 µM isovaleryl-CoA. To our knowledge, this is the first reported functional heterologous expression of this pathway in *S. cerevisiae*. For the production of n-butyryl-CoA and n-hexanoyl-CoA, we adapted the butanol production pathway for our purposes and measured approximately 6 µM intracellular concentration of butyryl-CoA and hexanoyl-CoA. For the feeding-dependent pathway towards propionyl-CoA we obtained intracellular concentrations of 5.3 ± 2.4 µM while the feeding independent 3-hydroxypropionate (3HP) pathway produced 8.5 ± 3.7 µM. The extension of both propionyl-CoA pathways to produce methylmalonyl-CoA resulted only into production of 0.5 ± 0.1 µM and 0.3 ± 0.3 µM methylmalonyl-CoA. Not only but particularly for the production of methylmalonyl-CoA further optimization is required. To allow rapid pathway prototyping, optimization and testing of alternative enzymes, we established a short-chain acyl-CoA Golden Gate collection. This collection enables together with the well-known Dueber yeast toolkit YTK collection the examination of different enzymes variants and to investigate optimized expression of the corresponding genes.

We conclude that the acyl-CoAs produced here, that are common building blocks of secondary metabolites, prepared the ground for prospective engineered production of a variety of natural products in *S. cerevisiae*. These acyl-CoA producing strains together with the short-chain acyl-CoA collection lay the foundation to further explore *S. cerevisiae* as a heterologous production host for high-value secondary metabolite production.

Yeast communication toolkit

The construction of multicellular networks was a proposed aim already early on in synthetic biology. Today, they still hold many promises like the division of labor or the performance of more complex tasks. Most of the systems so far were implemented in bacterial chassis and only a few examples exist for the eukaryotic chassis *S. cerevisiae*. Especially for gram-negative bacterial chassis, the quorum sensing system provides a large diversity of ready to use communication systems. Also, yeast species evolved a communication system using peptide-based pheromones to interact with the opposite mating type. Here, we employed the natural diversity of the peptide α-factor pheromones, the corresponding GPCR receptors, as well as of barrier proteases, that function similarly to quorum quenching enzymes. With the establishment of the Golden Gate yeast communication toolkit (YCTK) we provide a standardized collection of parts that allow the rapid construction of multicellular networks in the model organism *S. cerevisiae*. The feasible designs are limitless as well as the number of envisioned applications. The YCTK collection consists of responder (pheromone-responsive promoters), sender (*mfα1* genes – α-factors), receiver (Ste2 receptors) and barrier (Bar1 proteases) parts. We characterized the dynamics of the pheromone-inducible promoters in the different mating-type strain backgrounds and determined the dose-response to the α-factor as well as their temporal response. The different promoters exhibited a range of different dynamics and properties that enable the implementation of different prospective network design motives. The characterization results of the Ste2 receptors indicated that our collection is comprised of receptors with high α-factor promiscuity and of receptors with high substrate specificity for their cognate α-factor. Further we found that different Ste2 receptors exhibit different sensitivities towards the cognate as well as to non-cognate α-factors. The promiscuity of the Ste2 receptors did not correlate with the α-factor sequences. Our likelihood analysis of the Ste2 receptors indicated that the ones closer related to *S. cerevisiae* tend to be stimulated by the α-factors of related species. Our likelihood analysis of the Ste2 receptors coincided with the phylogenetic relationships of the species. Interesting is also the finding that α-factors of species for which the receptor exhibited high α-factor promiscuity stimulated only a few receptors. Even though only five of the selected barrier proteases were functionally expressed the characterization of the protease promiscuity was to our knowledge the most comprehensive study of its kind so far. Similar to the receptors we identified promiscuous and substrate specific barrier proteases. The proposed model of a coevolution between the receptor and barrier proteases to recognize similar sequence motives of the α-factor was partly validated, however, the model is not universally applicable according to our results. The extended knowledge of the pheromone-inducible promoters, the crosstalk between α-factors, receptors and barrier proteases, and an initial tunability test enabled proof of principle construction of multicellular systems using the YTCK

collection. We engineered multicellular logic gate-like population networks that allow the receiver cells to conditionally respond to the population composition. While the α-factor signaling motif is functional and was used to successfully establish OR and AND gate-like systems, signal disruption by a barrier protease of a self-stimulating or a signaling motif requires further optimization. Overall, the realization of multicellular networks using the YCTK was proven to be successful.

To summarize, with the YCTK we provide a set of comprehensively characterized sender, receiver, and barrier parts to facilitate the implementation of cell-cell and thus multicellular communication networks in *S. cerevisiae*.

1 Introduction

1.1 The model organism *Saccharomyces cerevisiae* – a brief history of yeast

Microorganisms are part of our everyday life. Here, we define microorganisms a unicellular organism including all bacteria and archaea but also single-celled eukaryotic organisms. Microorganisms are the most important organisms on earth for mankind. Life on earth as we know it would not be possible without them, as for example most of the oxygen in our atmosphere was produced by single-celled phototrophic microorganism. A vast majority of biological processes found in nature are performed by microorganism and they are thus essential for a steady nutrition cycle. Even though only a relatively small fraction of microbes is harmful to humans, these microorganisms had a great impact on our evolution since our immune system constantly needed to adapt in order to be able to defend these pathogens. Symbiotic microorganisms had an even greater effect on human biology, resulting in the human gut microbiome that allows humans to digest complex nutrition and helps us fighting pathogenetic infectious microbes. Besides many biological examples of how microorganism had an impact on the biological evolution of humankind, it is thought that they also had a significant influence on our cultural evolution.

Among these culturally important microorganisms are yeasts, especially *Saccharomyces cerevisiae*, and they were discussed to be the driving factor for the Neolithic revolution [1–3]. With the Neolithic revolution the human lifestyle changed from hunting and gathering to agriculture and settlements. Going along with these changes was an adaptation to a grain-based diet. Evidence in Göbekli Tepe, an archeological site for the Neolithic age, suggest that the population used (unknowingly) yeast and grains for fermentation to produce alcohol (Figure 1) [4]. *S. cerevisiae* is today considered as the first unknowingly domesticated microorganism by humans [5]. Interestingly, this cultural revolution was found to not only have taken place in southern Turkey but also occurred for example in the Mekong river delta or the Andes region [6]. All mentioned areas were naturally rich in starch-containing plants that in the course of time were enriched by agricultural cultivation, and that were ideal for alcoholic fermentation. Besides the development of the social-cultural competence of fermenting alcohol, fermented beverages and foods also had health advantages, since they contained essential trace elements and nutrition as well as exhibited reduced harmful bacterial contamination. In the following centuries, the fermentation of food was found to be of great importance for many of the advanced civilizations. The best-known example is Babylon where a beer recipe was found. But also in ancient Egypt archeological evidence proved that beer was economically important for this state (Figure 1) [6]. Until today, different cultures ferment food for preservation, nutritional enrichment, and to make it easier to process.

In the 19th century, microorganisms gained scientific interest. On the one hand because of their utilization for food and beverage fermentation and on the other hand due to the diseases some of them caused. It took until 1858 that Louis Pasteur described the essential role of *S. cerevisiae* in alcoholic fermentation [7,8]. Pasteur's research made him the father of microbiology and he could also be considered as the father of biochemistry. The first visual description of yeast found in beer was made by Cagniard-Latour in 1837 [9]. In 1875, Emil Christian Hansen, a researcher at the Carls-

berg Laboratory, isolated the pure yeast strain responsible for beer production, laying the technological foundation of the usage of yeast as a model organism for basic and applied research [10]. This history of *S. cerevisiae* is closely connected with beer production and even the scientific name *Saccharomyces cerevisiae* is derived from the beer terminology. While *Saccharomyces* means sugar mold or fungus, *cerevisiae* was derived from the Gaelic word kerevigia and the French term cervoise, both translating to beer [11]. The research of Pasteur and his colleagues not only had an impact on biology but also on chemistry. Emil Fischer for example experimented with the fermentation of different sugars for beer in a brewery in Dortmund that his father had invested in [9]. His research may have led to the initial hypothesis of the molecular mechanism of enzyme specificity. Fischer and Thierfelder later on invented an apparatus that allowed the measurement of sugar fermentation by yeast as well as the produced CO_2 [12]. The re-evaluated findings of Pasteur that yeast could only ferment D- sugars and not L-sugars resulted in the famous lock and key enzymatic model by Fischer [13]. This finding initiated a series of concepts of enzyme-substrate specificity including the findings of Henri as well as Michaelis and Menten [14,15].

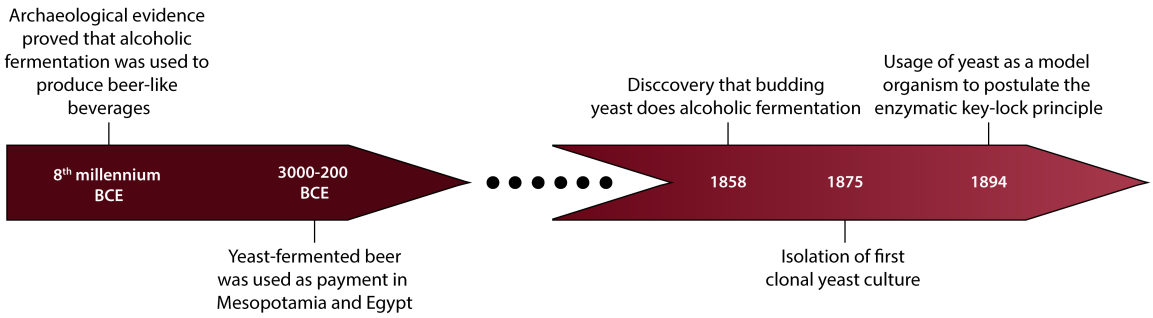

Figure 1: Timeline of the history of yeast from the 8th millennium BCE until 1894. The timeline ranges from the first archeological evidence of fermentation to the understanding of the enzymatic key-lock principle using yeast as model organism.

Besides an increasing research focus on the metabolism and biochemistry of *S. cerevisiae*, a lot of progress was observed in cell biological research using *S. cerevisiae* as a model organism. In the early 1900, innovations in the field of microscopy, both in optics and in sample preparation, like dyes that color specific cell structures, allowed the advancement of research studies using yeast as an easy and comparably large microorganism [16]. Several structures within yeast cells could be described, however often without the decipherment of their physiological function. Several researchers identified the nucleus, the vacuole and possibly organelles, which were described as granular structures. In 1946 Lindegren illustrated the previously observed mitotic cell division of *S. cerevisiae,* including the chromosomal structures within the nucleus that underlined the budding structure and the DNA location (Figure 2) [17]. The first reported observation of sexual reproduction of yeast was already found in 1891 by Hansen for which he reported the fusion between two spores, however he did not consider this as mating back then [16]. Mating was first observed in other yeast species but could not be identified in *S. cerevisiae*. Today we know that *S. cerevisiae* displays its mating behavior directly after sporulation and also it is likely that most *S. cerevisiae* strains investigated in early 1900 were diploid, therefore, no mating could be observed. Only in 1943 Lindgren and colleagues described the two mating types of *S. cerevisiae* and denoted them as **a** and α cells/mating types [18]. Already earlier on, Winge used mating of two mating types for

strain cross-breeding as an early genetic method to study *S. cerevisiae* [19]. The knowledge of the different mating types as well as the successful sexual reproduction resulted in the development of novel methods, like mass mating to study cellular function as well as metabolism on a genetic level in *S. cerevisiae* [20,21]. The mating pathway, with its G protein-coupled receptor (GPCR) that senses pheromones became quickly a model of signal transduction in eukaryotic organisms and can today be considered as one of the best understood signal pathways [22]. Modern research, which is based on heterologous gene expression in *S. cerevisiae*, started in 1978 with the demonstration of the Fink group that yeast can be transformed with foreign DNA (Figure 2) [23]. Shortly after this breakthrough for yeast research, an *Escherichia coli - S. cerevisiae* shuttle vector was developed [24]. Both advancements laid the foundation for the establishment of S. *cerevisiae* as a model organism for basic research and later for industrial applications. The rapid technological development allowed many breakthrough innovations in *S. cerevisiae*, for example, *S. cerevisiae* was the first organism with a systematic collection of bar-coded gene deletion mutants [25]. Despite the long history of *S. cerevisiae* as a model organism for modern life sciences, there are still many unanswered questions about its natural life cycle and its native ecological niche [26]. As unicellular eukaryotic model organism, *S. cerevisiae* was utilized by researchers and a plethora of genetic and molecular tools and methods were developed over the centuries. The *S. cerevisiae* strain S288C was the first eukaryotic organism for which the entire genome was sequenced in 1996 (Figure 2) [27]. The natural recombination efficiency of *S. cerevisiae*, its fast sexual and asexual propagation (cell division occurs every 90min under optimal conditions) and easy cultivation of cultures fostered innovation in yeast. Also, the establishment of the *Saccharomyces* Genome Database (SGD), in which most *S. cerevisiae*-based knowledge is collected improved research efforts tremendously (http://www.yeastgenome.org/) (Figure 4). The long and shared history of humans and *S. cerevisiae* resulted in many important findings that laid the foundation for lasting and continuous scientific discoveries using *S. cerevisiae* as a model organism. As several key processes, including autophagy, protein folding, modification, translocation, secretion, and degradation, and many more are conserved between yeast and higher eukaryotic cells, including human cell lines, *S. cerevisiae* was established as model organism for the discovery and description of cellular processes. The multitude of findings only marked the beginning of basic as well as applied research in *S. cerevisiae*. Until today, many researchers who made breakthrough findings using *S. cerevisiae* as a model organism were awarded the Nobel Prize [28]. In 2001, Prof. Hartwell received a Nobel prize for the discovery of a key regulator of the cell cycle, in 2013 Prof. Scheckman was awarded one for his ground-breaking work on cell membrane vesicle trafficking, and in 2016 Prof. Ohsumi obtained the Nobel Prize for his discovery of the mechanisms of autophagy (Figure 4) [29]. We can thus assume that the ongoing research in the eukaryotic model organism *S. cerevisiae* will continue to foster the development of novel technologies and new scientific concepts that will result in ground-breaking discoveries shaping our understanding of biology. Also, today *S. cerevisiae* has great economic importance and can be considered as a major production host for many of the established biotechnological products. The history of biotechnology is tightly linked to *S. cerevisiae* and for example Nova Nordisk started using yeast as a production chassis for the production of human insulin already in in 1987 (Figure 2). Today, about 20% of the biopharmaceuticals

are produced in *S. cerevisiae*, including insulin, insulin analogs, human serum albumin, hepatitis vaccines and virus-like particles for vaccines [30].

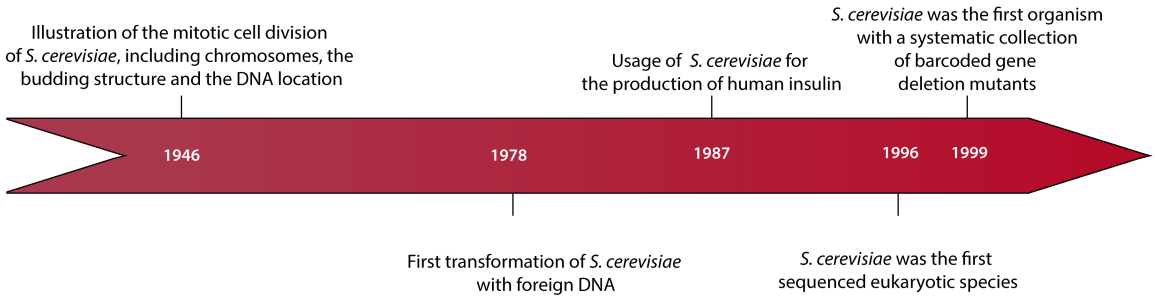

Figure 2: Timeline of the history of yeast from 1946 until 1999. Achievements ranged from the illustration of cellular structures and cell division to a systematic barcoded gene deletion mutant collection of *S. cerevisiae*.

Compared to bacterial chassis, *S. cerevisiae* as a eukaryotic host organism can perform post-translational modifications like glycosylation, subunit assembly, acylation and it can also secrete products to the media and therefore allows easier product purification [31]. Since *S. cerevisiae* has been investigated for applied as well as basic research for a very long time, it might be the best studied eukaryotic model organism. The great knowledge allowed high-throughput studies, generation of system models of cell signaling and metabolism, and many molecular methods have been developed and established [32–34]. Besides previously mentioned advantages over microbial chassis, *S. cerevisiae* is also preferred in comparison to mammalian chassis like HEK or HeLa cell lines that require more complex media and can be infected by viruses or bacterially contaminated. *S. cerevisiae's* life style mostly prevents bacterial contamination, as well as almost no infectious viruses are known. Taking all these advantages together, *S. cerevisiae* is designated generally recognized as safe (GRAS) (FDA 21 CFR §172.325).

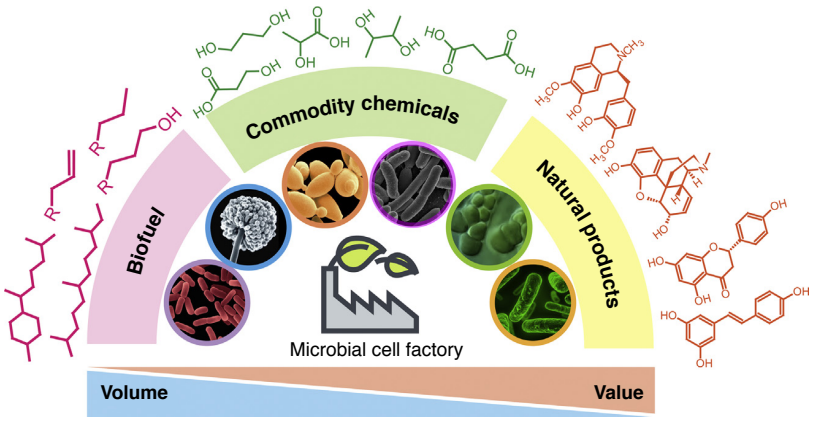

Figure 3: Biotechnological products separated by the most useful microbial cell factories. A wide range of chemical products can be fabricated in engineered microorganisms. These products range from biofuels, commodity chemicals to natural products and differ in the economically required volumes and values. Adapted from [35].

Besides the production of biopharmaceutical proteins, the alcohol fermenting ability of *S. cerevisiae* is still of great economic importance today for the production of bioethanol as fuel. In 2017, the USA produced 60 billion liters of bioethanol by fermentation mostly using *S. cerevisiae* (Figure

5) [10]. Separate from the production of high-volume low-value compounds like biofuels, *S. cerevisiae* was also engineered to produce higher value commodity chemicals as well as natural products that can be used for example as medication (Figure 3) [35]. Apart from ethanol production as biofuel, more sophisticated molecules need to enter the market that have a higher energy content, octane number, and freezing point [36]. Fatty acids, higher alcohols, and terpenoids are meeting these criteria and *S. cerevisiae* was engineered to produce these by targeting the fatty acid synthesis pathway, the 2-keto acid pathway, the isoprenoid pathway, the CoA-dependent reverse beta-oxidation pathway, and polyketide synthetic pathways (Figure 3) [35]. As previously mentioned, *S. cerevisiae* is a well-established model organism and the availability of many methods, tools and techniques, and computational models made this species also the preferred chassis for metabolic engineering approaches, including but not only, for biofuel production. A wide range of different approaches was implemented ranging from state of the art genome editing technology, to adaptive evolution, rewiring the metabolic fluxes or model-driven experimental optimization based on -omics data [37–40]. For the high-volume production of low-value compounds it is of high importance to obtain an efficient turnover of product formation. Therefore, besides the production of new compounds improving yields and product titers up to industrial-scale production is required. Since *S. cerevisiae* uses carbon sources like glucose it was often discussed whether the production of biofuels is in direct conflict with food production. To address and overcome this problem, *S. cerevisiae* was engineered to utilize alternative carbon sources like lignocellulose [41–43]. In addition to the production of biofuels, metabolic engineering in yeast addresses the need of sustainable bio-based commodity chemicals for the chemical industry that is consuming large percentages of the petroleum production every year. Several commodity chemicals were already produced in engineered *S. cerevisiae* like diols, and organic acids [44]. Apart from the production of commodity chemicals that are used already in industry, synthetic biology and metabolic engineering could provide alternative commodities that have advantages for the industry compared to currently used ones. High-value compounds do not need to be produced in highest yields and titers to be economical feasible and are established as proof of concepts. However, for an economic production, initial fermentation optimization is required. Many of these compounds have great pharmaceutical importance and therefore already entered the market [45]. These are mostly bioactive compounds and natural products derived from various organisms like bacteria, e.g. polyketides of *Streptomyces*, or are secondary metabolites of plants, e.g. opioids of poppy [46]. Heterologous production in for example *S. cerevisiae* is of interest, since a production in the native host is not always feasible. Plant natural product production for example requires high plant biomass and therefore agricultural land and also the concentration of the target compound might be very low and additionally vary with the season and year. Many recent innovations like the accessibility of enzymes and natural products in databases, rapid enzyme engineering, model-guided pathway design, rapid parallel pathway assembly, genome engineering, and many novel analytic methods accelerated compound production in *S. cerevisiae* and other chassis organisms [46,47]. The first and well-known example of metabolic engineering of a plant-derived secondary metabolite in *S. cerevisiae* was the semi-synthetic production of the antimalarial drug precursor artemisinic acid [48]. Since then, other implemented metabolic pathways increased in size and complexity. For the heterologous production of artemisinic acid four genes had to be expressed, while

25 gene were introduced for the production of noscapine and halogenated alkaloids in *S. cerevisiae* (Figure 5) [49]. Comparable progress had been made by the expression of bacterial or fungal secondary metabolic pathways. Previously, naturally found pathways were transferred into chassis organisms for heterologous production. More recently however, to achieve the most effective compound production, enzymes are obtained from various different species and selected for their ability and effectivity of catalyzing a required reaction and combined with other enzymes into the pathway of interest. In 2014 and 2015, the production of semisynthetic and natural opioids was accomplished in *S. cerevisiae*, which drew a lot of attention (Figure 5) [50,51].

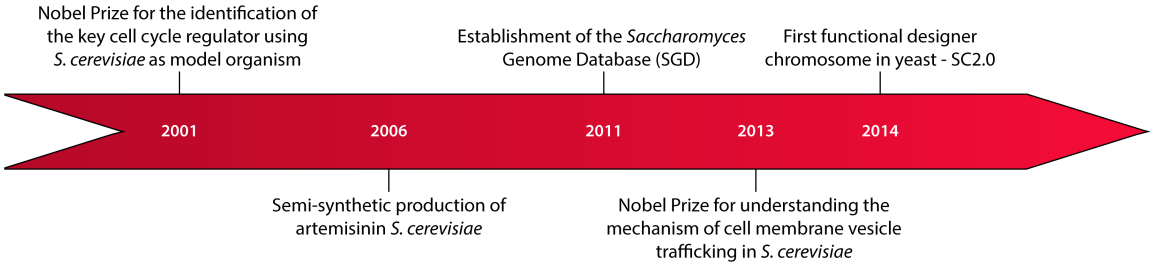

Figure 4 Timeline of the history of yeast from 2001 until 2014. Achievements ranged from the awarding of a Nobel prize for the identification of key regulators of the cell cycle in *S. cerevisiae* to the functional synthetically designed chromosome in yeast.

Also, the recent expression of the complete cannabinoid pathway in *S. cerevisiae* should be noted (Figure 5) [52]. Having said that *S. cerevisiae* is generally used as model organism for basic research and as production host for various compounds of interest, in synthetic biology *S. cerevisiae* was also established as chassis for various other applications. The examples range from employing GPCR yeast pheromone receptors as biosensor to serving as an assembly chassis for the first synthetic organism, since *S. cerevisiae* exhibits a high recombination efficiency [53,54]. An ongoing research effort in the field of synthetic biology of *S. cerevisiae* is also to synthesize its complete genome and to integrate it back into *S. cerevisiae*, and therefore transforming it into the so-called Sc2.0 organism (Figure 4) [55]. An international consortium of research groups collaborates to reassemble the different chromosomes of *S. cerevisiae*. Apart from the assembly of the different chromosomes from chemically synthesized DNA fragments, different design principles are applied. This includes for example the reduction the genome by 8% while maintaining the wild type phenotype. Additionally, several genetic adjustments constitute the Sc2.0 design principles. The first adjustment is the replacement of the TAG stop codon with TAA so that the TAG codon can be used for an amber amino acid integration into proteins. Second, is the addition of the loxPsym sites to all open reading frames, which allows inducing evolution by SCRaMbLE. Third, collecting all tRNAs genes on a neochromosome. Fourth, integration of PCRTags into open reading frames to allow the discrimination between wild type and synthetic yeast DNA. Fifth, the removal of enzyme recognition sites to facilitate assembly of the synthetic chromosomes [56]. Altogether, this is an indication that *S. cerevisiae* was not only the first fully sequenced eukaryotic organism but will also be the first eukaryote with a synthetic genome that was thoughtfully designed and assembled. Such endeavors prepare one of the most important model organisms for a glorious future. It is undeniable that it is very likely that once again *S. cerevisiae* will be at the forefront of the next level of scientific innovation in the near future.

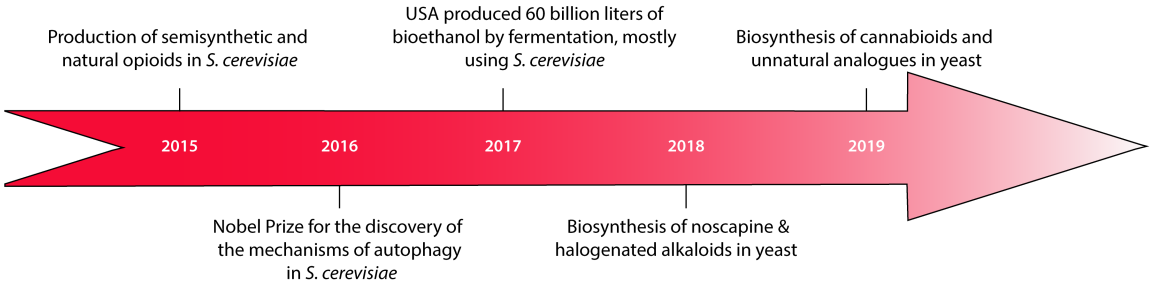

Figure 5: Timeline of the history of yeast from 2015 until today. Achievements ranging from the production of semisynthetic and natural opioids to the biosynthesis of natural and unnatural cannabinoids in *S. cerevisiae*.

1.2 Introduction to synthetic biology

As highlighted in the previous chapter on the example of *S. cerevisiae*, biology has come a long way and different groundbreaking scientific discoveries are shaping today our understanding of life itself. For many of the biological research projects the model organism *S. cerevisiae* has been primarily studied and also in synthetic biology, many proofs of principle studies ranging from genetic networks to metabolic engineering applications have been developed in yeast [57,58].

In the middle of the 19th century, the analytical and descriptive science of chemistry evolved and constituted the productive science of synthetic chemistry. This transition was initiated by Friedrich Wöhler, who first synthesized the small organic molecule urea [59]. This discovery was not only a technological innovation but also changed the mindset of chemists from a solely analytical to an engineering perspective, which considerably shaped the 19th and 20th century [60]. Besides the synthesis of several natural molecules, also molecules that did not exist in nature were synthesized [60]. This was resulting in an extended and in-depth understanding of the fundamental principles of chemical structures and reactions [60]. A similar technological transition could be observed at the end of the 20th and the beginning of the 21st century in biology with the dawn of the establishment of modern synthetic biology. The postulation of cellular regulation by molecular networks by Jacob and Monod in the 1960s laid the foundation of synthetic biology [61]. The establishment of DNA transfer, DNA cloning and sequencing until the 1990s were other key milestones required for the formation of the new engineering discipline synthetic biology [61]. A key feature of the engineering discipline is to apply the engineering cycle to biological systems, which is comprised of the design, build, test, and learn (DBTL) phases (Figure 6) [62].

Following these considerations allows the generation of artificial systems but it can also be employed to examine fundamental design principles in biology. Apart from applying the DBTL cycle for the construction of systems, all engineering sciences commonly rely on the usage and implementation of standardized parts [63]. In computer engineering, standardized parts are constituted by e.g. transistors; in synthetic chemistry by molecular precursors; and in synthetic biology by genetic parts [64]. Genetic parts can be combined and thus be arranged in different abstraction levels (Figure 7). Consisting of DNA, the second lowermost abstraction layer is comprised of genetic parts, encoding promoters, terminators, or open reading frames (ORF). A functional combination of genetic parts are genetic devices that can perform a specific task. Several or single devices can form a system that features a more complex behavior. In synthetic multicellular systems,

one system can be encoded in one organism that is interacting with other organisms carrying another system [65].

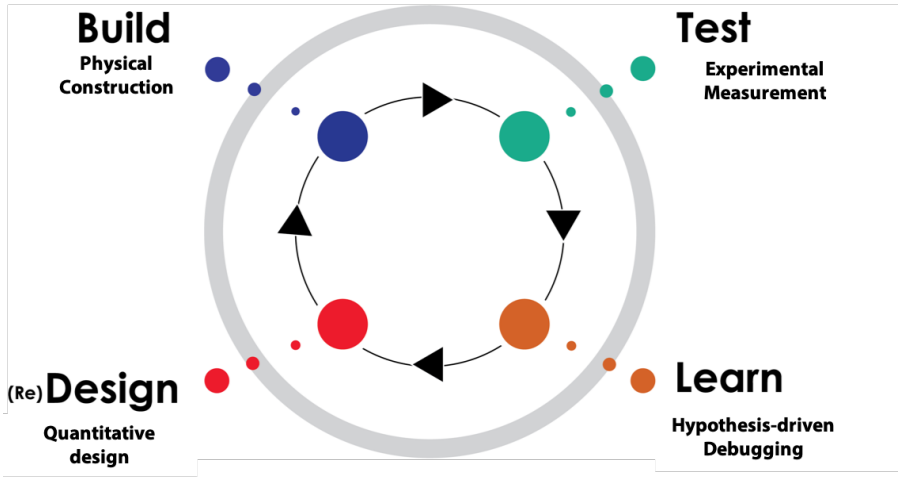

Figure 6: The engineering cycle in synthetic biology. As an engineering discipline, synthetic biology follows the design, build, test, learn (DTBL) cycle. Adapted from SynCTI.org.

Besides the standardization of biological parts, assembly standards were proposed for construction of synthetic biological devices, systems, and networks. This first widely accepted assembly standard was the BioBrick standard that was fostered and promoted by the international genetically engineered machine competition (iGEM) [67]. The part library that was generated over the different years of iGEM has to be considered the largest collection of biological parts.

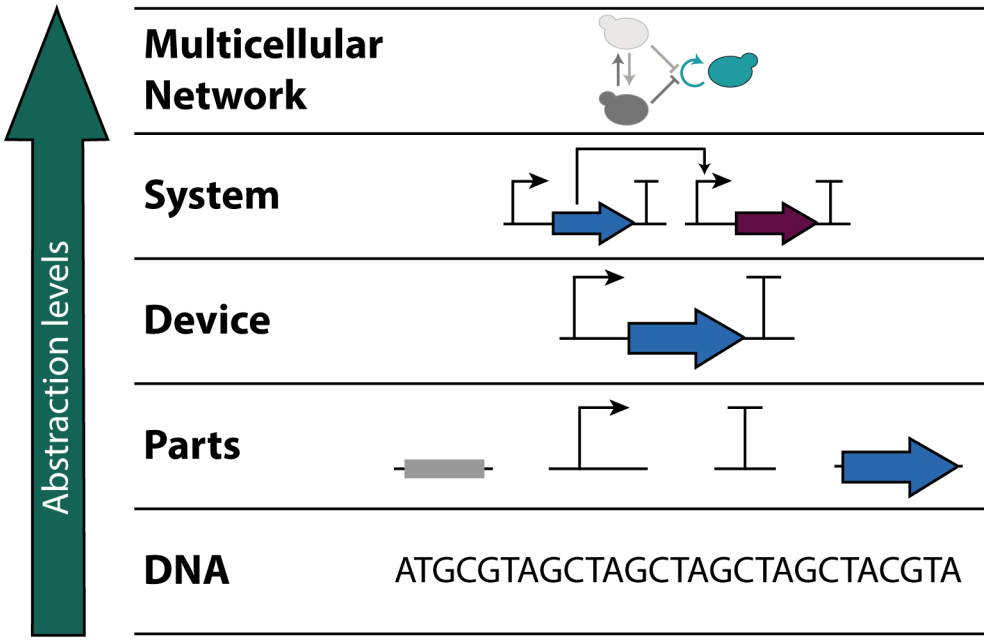

Figure 7: Abstraction levels in synthetic biology. The basis for parts, devices, systems, and networks is DNA. Different DNA sections form functional parts like promoters, genes of interest, terminators, or homology sequences for genomic integrations. Devices are functional genetic constructs that are built from parts in the order of promoter, gene, terminator. Devices can be further combined into genetic systems. Several systems in different cells can function as multicellular networks. Inspired by [63,66].

However, disadvantages of this collection is the absence of quality control or peer review processes in order to verify and characterize all collected parts. Since the introduction of the BioBrick standard, many more recent DNA assembly methods like circular polymerase extension cloning (CPEC), Gibson assembly, ligase chain reaction (LCR), or Golden Gate cloning have been established [68]. Some of these methods (e.g. CPEC, Gibson, and LCR) are restriction enzyme-independent methods and thus do not require specific enzyme recognitions sites or the domestication of the DNA from these. The disadvantage of these methods is though that they are PCR-based and therefore prone to mutations in comparison to non-PCR based DNA assembly methods. BioBrick as well as Golden Gate cloning require DNA sequence domestication of enzyme recognition sites. Golden Gate assembly is favored over BioBrick cloning since it allows the assembly of several parts at once as well as combinatorial assembly. Several Golden Gate toolkits, which include a collection of parts, have been developed for different chassis, including plants, *E. coli*, the bee microbiome and the yeast toolkit (YTK) [69–72]. These toolkits had a strong impact on the development of synthetic biology and improved the turnover of the DBTL cycle tremendously.
Using standardized biological parts and DNA assembly methods, synthetic biologists developed from the construction of simple intracellular genetic networks to the establishment of artificial complex cellular network or metabolic pathways [61,65].
Within the last 20 years, synthetic biology advanced and comparably complex systems can be engineered today, however, biology's full potential is by far not harnessed yet. One example highlighting these limitations are native enzymes. Many of them have already been implemented into metabolic pathways and genetic circuits or they have been adapted from native enzymes by protein engineering. However, a full *de novo* design of enzymes is currently impossible. One other limitation synthetic biologists still face is standardization [73,74]. Even though part libraries and DNA assembly methods have been established, genetic parts usually exhibit context specificity [74,75]. This means that the expression of one ORF from a promoter varies from the expression of another ORF from the same promoter. Also, if one genetic device is expressed in one strain background, the behavior in another strain background is mostly not alike. Thus, prediction of the behavior of genetic parts and systems remains challenging, since characterization of parts and device can only be limitedly deduced to other contexts. Also, our knowledge of natural living systems that are able to self-replicate, to age and that are highly dynamic is still limited in comparison to the fundamental knowledge in chemistry. This means that different to synthetic chemistry, synthetic biology is still at the beginning of the transition from the descriptive biological science to becoming an engineering discipline. Despite its current limitations, synthetic biology already contributed to our basic understanding of biology, accelerated the establishment of artificial cellular systems and gained economic importance [76]. Thus, synthetic biology can be considered as one of revolutionary technologies for the 21st century which is shaping prospective innovations in medicine or compound production and will provide solutions for various current challenges.

1.3 Metabolic engineering of *S. cerevisiae*

As previously highlighted, humans share a long and fruitful history with the yeast *S. cerevisiae*, both in research as well as in everyday life (chapter 1.1). Therefore, it is not surprising that until today, *S. cerevisiae* is one of the most commonly used model organisms as well as biotechnological production hosts. Yeast is also an important organism for the production of food, including

beer, wine, or bread and *S. cerevisiae* is therefore deployed at industrial scale [77]. This century-long operating experiences *with S. cerevisiae* for food production, the molecular comprehension, the genetic accessibility, and the fact that it is a higher eukaryotic organism paved the way for the establishment of *S. cerevisiae* as chassis for synthetic biology, and more specifically for metabolic engineering (Figure 8) [78].

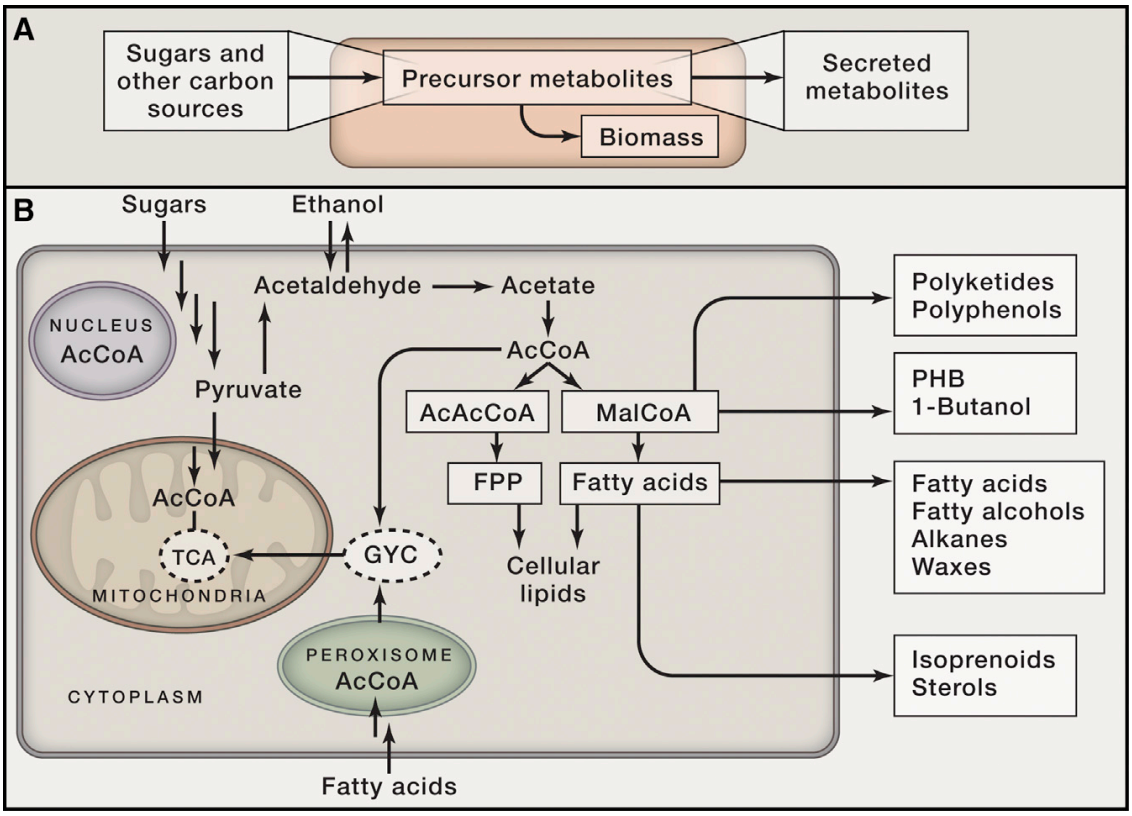

Figure 8: Production flow in metabolic engineering systems. A) Different carbon sources can be processed to precursor metabolites that serve as the basis for many secreted metabolites. **B)** Overview of the acetate metabolism of *S. cerevisiae* as a basis for the precursor formation that are required for the production of higher-value chemicals like polyketides, fatty acids, and isoprenoids. Adapted from [79].

The engineering of cellular factories has become a relevant approach for the transition from a petroleum-based industry to a bio-based economy [34]. However, not only *S. cerevisiae* is a suitable chassis for metabolic engineering applications, also *E. coli*, C*orynebacterium glutamicum* or *Aspergillus niger* hold potential, to name only a few organisms that are currently industrially employed [79]. Several parameters need to be fulfilled in order to be selected as chassis organism. The explicit advantages of *S. cerevisiae* include that it can be relatively easy engineered, plant enzymes (especially P450) can be comparatively well expressed, it exhibits a high pH tolerance, it is fairly robust, and that there is great knowledge of it (Figure 9)[10].

Already early on, *S. cerevisiae* was engineered to produce pharmaceutically relevant proteins like antibodies or insulin as previously highlighted [30]. Here, we will focus on the engineered production of chemical compounds in *S. cerevisiae*. Most of the examples that will be introduced are low-

scale proof of principle compound production that demonstrate what is generally feasible to produce in microorganisms and which lay the foundation for large-scale production for a future bio-based economy.

Traits	*E. coli*	*Corynebacterium glutamicum*	*S. cerevisiae*	*Aspergillus niger*
Rate	*****	****	***	**
Ease of engineering	*****	**	*****	*
Use of biomass as by-product	*	*	*****	*
Expression of plant enzymes[a)]	**	**	****	*****
pH tolerance	*	*	****	*****
Temperature tolerance	*****	****	***	***
Salt tolerance	***	***	****	****
Substrate spectrum	****	***	***	*****
Robustness[b)]	**	**	*****	*****
Knowledge base	*****	***	*****	**

[a)] P450 enzymes often used for the production of plant natural products.
[b)] Robustness is here defined as a general property associated with being robust at industrial conditions, e.g., resistance to phages and other contaminants.

Figure 9: Scoring different metabolic engineering chassis organisms according to important properties. Comparing the chassis organisms *E. coli*, *C. glutamicum*, *S. cerevisiae*, and *A. niger* with regard to rate, easiness of engineering, use of biomass as a by-product, expression of plant enzymes, pH tolerance, temperature tolerance, salt tolerance, substrate spectrum, robustness, and knowledge base. This scoring indicates the befits of *S. cerevisiae* as chassis organism for metabolic engineering applications. Adapted from [10].

Except for a few examples, like artemisinin, an anti-malaria drug produced by Amyris and Sanofi, adipoyl-7-aminodeacetoxycephalosporanic acid (adipoyl-7-ADCA) produced by DSM, or 1,3-propanediol produced by Dupont, the production of valuable compounds in cellular factories is currently not competitive with petrochemical-based production and thus not economically feasible [80]. For the transition from proof of principle production in the lab to industrial scale production, titers, rates and yields need to be evaluated. Improving these parameters requires multidimensional optimization, since not only the heterologous production pathway has to be adapted but rather the entire cellular metabolism of the chassis. Rewiring as well as heterologous expression of additional enzymes allowing the channeling of metabolic fluxes can be required [79]. Recent innovations in genome engineering, like the establishment of the CRISPR/Cas9 methodology, have improved and simplified the possibility of several genetic interferences, including knockdown, knockout, over- and controlled expression, and expression of alternative heterologous genes [81]. Apart from these genetic interferences also the optimization of culture conditions, like media composition, temperature, and perturbation can affect production efficiency [38]. Optimization attempts can be supported by mathematical models of *S. cerevisiae* that help predicting the most promising enhancement strategy. Kinetic models describe detailed kinetic reactions of, e.g., yeast glycolysis, while genome-scale flux balance models give an overall view on the metabolic fluxes

in a chassis [82]. Using previously gained knowledge and combining it with modeling mostly results in a directed optimization approach for enhanced production titers and yields, as it was previously achieved for example for the production of ethanol [83]. Historically, yeast is best known as a production host for alcohol. Compared to other industrially utilized microorganisms like *E. coli*, *S. cerevisiae* naturally exhibits a high tolerance to alcohols. Despite the production of ethanol with increased titers and yields, *S. cerevisiae* has also been engineered to produce higher alcohols like butanol, isobutanol, and 2,3-butanediol [84]. Both ethanol and higher alcohols produced from biomass serve as biofuels. With increasing production volumes of biofuels from engineered microorganisms, the public raised the concern that fuel production might be in conflict with food production. To clear this conflict, *S. cerevisiae* was engineered to utilize alternative carbon sources like lignocellulosic biomass [85,86]. Also, fatty acids are potential biofuels and commodity chemicals that are utilized in the nutrition, cosmetics and pharma industry [87]. To alter the fatty acid profile of *S. cerevisiae,* the TCA cycle was engineered [88]. To further extend the production to alternative fatty acids like dihomo-g-linolenic acid or stearodonic acid, the heterologous expression of desaturase and elongase enzymes in *S. cerevisiae* was required [89,90]. To allow biodiesel production in *S. cerevisiae*, the wax synthase of *Marinobacter hydrocarbonoclasticus* was heterologously expressed [91]. Overall, the production of the fatty acid-derived products holds great potential and undoubtedly, an increase in pathway variants and further optimization of these in *S. cerevisiae* will be observed in the future.

Other compounds of economic interest include for example terpenoids. Terpenoids are a large class of natural products and can be grouped according to the number of isoprene units that have been incorporated into their structure [92]. As previously highlighted, *S. cerevisiae* is a suitable chassis for the expression of plant-derived proteins as well as plant natural products (PNP) and also has sufficient precursor supply, for example, for terpene production (Figure 10).

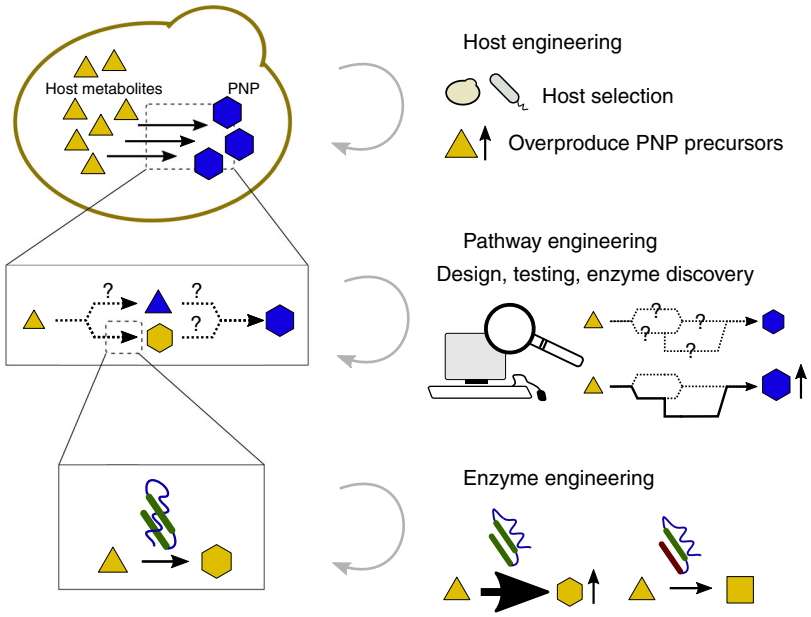

Figure 10: Synthetic biology strategies for microbial biosynthesis of plant natural products. The engineering approaches range from enzyme engineering, to pathway engineering, including the design, testing and if required enzyme discovery, as well as host engineering, including selecting the optimal organism as well as further optimization like precursor engineering. Adapted from [46].

The best-known example for terpene production in yeast is the production of amorpha-4,11-diene as precursor of the artemisinic acid pathway and downstream the production of artemisinic acid [93,94]. A diterpene of high interest is the cancer drug taxol. Different strategies have been developed to produce taxol in yeast, including the division of the pathway and the implementation into two host organisms, namely *E. coli* and *S. cerevisiae* [95]. Several studies achieved successful production of taxadiene, a pathway intermediate of taxol production, in *S. cerevisiae* as well as yield optimization efforts that resulted in a 40-fold increase in taxadiene production [96]. Rewiring the central metabolism was shown to increase required precursor levels for taxol production and can therefore be considered as a possible optimization strategy for the production of many other terpenoids [97]. Also, the engineering of a biosensor allowing high-throughput screening of suitable pathway designs was investigated [98]. Until today, the heterologous production of taxol in yeast could not be achieved since still several pathway enzymes remain uncharacterized. Currently, the taxol is produced from plant cell culture [99]. Furthermore, the production of the plant sesquiterpenes, valencene, cubebol, and patchoulol had been established in yeast [100]. To improve terpenoid production in yeast, the geranyl diphosphate and farnesyl diphosphate precursor supply was optimized [101]. The most recent example was the production of hoppy beer without the supplementation of hops, instead, heterologous production of the monoterpenes linalool and geraniol in *S. cerevisiae* imparting hoppy taste. Denby and colleagues thereby illustrated the potential of terpenoid production in yeast (Figure 11) [102].

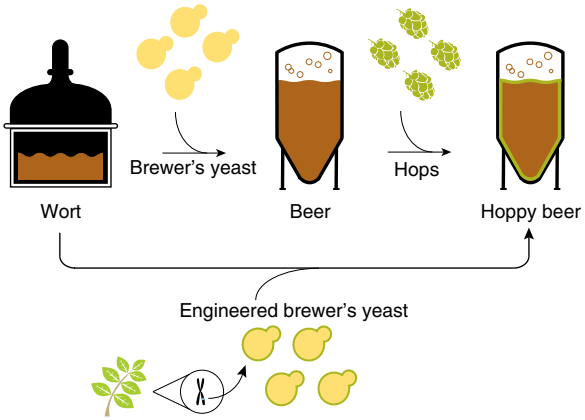

Figure 11: Overview of the classical beer brewing process as well as beer brewing with engineered yeast. The hoppy flavors of beer are usually a result from adding hops. Using engineered yeast strains, the hoppy flavor was imparted by monoterpenes produced by synthetic yeast. Adapted from [102].

An additional class of interesting components that are suitable for a bio-based production are aromatic compounds. They can be used as precursors for polymer production but also for nutritional and therapeutic purposes [103]. For the production of aromatic compounds, engineering of the shikimate pathway is required [104]. One benefit of producing aromatic compounds in yeast is the functional expression of plant proteins like cytochrome P450s. Resveratrol is an example for the successful production of an aromatic compound in *S. cerevisiae*, even on an industrial scale [105]. An additional example is the *de novo* biosynthesis of vanillin and its *in silico* guided production optimization approach [106,107].

Polyketides as a highly diverse class of natural products is gaining more attention, not only but also because of the possibility of tailored production of unnatural products. Polyketides are a

structurally diverse group of bioactive, mostly secondary, natural products [108]. The examination of the polyketide-synthesizing enzymes polyketide synthases (PKS) has to lead to the discovery of the possibility of engineering (un)natural products [109]. PKSs are using a variety of different acyl-coenzyme A building blocks and join theses for the formation of complex polyketides. Polyketides and their synthases are found in all kingdoms of life and can be classified into three groups. Type II and Type III PKSs differ from the type I PKSs. Type I PKSs, mostly found in bacteria, are highly modular megasynthases with several catalytic domains organized in modules and structured in an assembly line-like fashion (Figure 12). In type II PKSs the catalytic parts are freestanding monofunctional proteins. The type III PKSs on the other hand are freestanding iteratively-acting condensing enzymes that can also be non-ribosomal peptides (NRPS) [110]. Typically, type I PKSs possess an acyltransferase (AT) domain that builds, selects and loads the monomers to the acyl carrier protein (ACP) carrying with the 4'-phosphopantetheine arm the nascent polyketide chain. Then, the ketoynthase (KS) domain catalyzes decarboxylative Claisen-like condensations for chain elongation. The full-length polyketide chain is released by a thioesterase (TE) domain, and is subsequently often further modified by downstream tailoring enzymes [111]. Besides the mentioned domains, also, several optional catalytic domains including ketoreductase (KR), dehydratase (DH), enoylreductase (ER), and methyltransferase (cMT) can be found. A recently improved understanding of the structure of type I PKS made domain shuffling, swaps, and directed assembly possible, enlarging the range of potential applications of engineered PKS for the production of novel products [111]. These products could be used as pharmaceuticals but also hold potential as commodity chemicals or biofuels and are often difficult or even impossible to produce by chemical synthesis [112]. The large-scale production of heterologously produced polyketides has been limited to around 100 mg/L of for example for multi-methyl-branched esters and pentadecane in *E. coli* [113]. The expression of the megasynthases as well as the polyketide production is challenging since a high metabolic burden, folding and stability problems, redox balance, product toxicity, and building block CoA monomer supply could be limiting. Natural hosts like *Streptomycetes* are slow-growing and difficult to engineer but are nevertheless currently considered as production chassis, alongside *E .coli* and *S. cerevisiae* [111]. *S. cerevisiae* has already been explored as a chassis for the expression of fungal, plant as well as bacterial PKSs. It has been shown that *S. cerevisiae* can be used as a production host for 6-MSA, a polyketide naturally produced in *Penicillium patulum* [114]. The production of 6-MSA was improved by increasing the supply of the precursor malonyl-CoA [115]. Additional optimization was achieved by the expression of a mutated Acc1, which synthesizes malonyl-CoA. The mutated Acc1 could not be targeted by the Snf1 kinase anymore and therefore prevention of the deactivation of Acc1 resulted in increased 6-MSA production [116]. Another fungal polyketide that was successfully produced in *S. cerevisiae* is rubrofusarin, naturally found in *Fusarium graminearum* [117]. Apart from the production of fungal polyketides, *S. cerevisiae* has been established for the heterologous expression and subsequent discovery and *in vitro* characterization of fungal PKS and NRPS [118–120]. Very often, PKS build hybrid megasynthases with NRPS. Xu and colleagues have shown for the aspyridone synthase of *Aspergillus nidulans* that the expression of these and subsequently the production of preaspyridone could be achieved in *S. cerevisiae* [121]. However, PKS are not only found in fungi but also in plants. Plant-derived polyketides

often have a long history as pharmaceuticals including for example cannabinoids. With the identification of the olivetolic cyclase in *Cannabis sativa* that is required by the plant type III PKS tetraketide synthase, an improved understanding of the cannabinoid biosynthetic pathway was obtained [122]. These findings enabled researchers to engineer *S. cerevisiae* to produce natural as well as unnatural cannabinoids. Apart from the expression of the PKS and other synthases, the expression of the required hexanoyl-CoA precursor pathway had to be achieved [52,123].

As previously highlighted, type I PKS, which are often found in bacteria hold great promise for the production of (un)natural polyketides due to their modularity. *S. cerevisiae* was already successfully established as chassis for the expression of simple fungal polyketides [124]. However, it is lacking a phosphopantetheinyl (P-pant) transferase that is essential for the post-translational modification of the ACP domain of the 6-MSA synthesizing PKS. Thus, the expression of surfactin P-pant transferase (Sfp) of *Bacillus subtilis* was a prerequisite [114]. These experiments resulted in the investigations of Mutka and colleagues, whether *S. cerevisiae* is a suitable host for the expression of bacterial type I PKS [125]. Therefore, they engineered *S. cerevisiae* to produce the unavailable precursors propionyl-CoA and methylmalonyl-CoA via a propionate/methylmalonate-depending feeding pathway route. Furthermore, they expressed module 2 of the 6-Deoxyerythronolide B Synthase (DEBS) linked to a TE domain and showed that the production of triketide lactone (TKL) was achieved, when fed with N-acetyl-cysteamine thiol (SNAC) ester [125]. Overall, *S. cerevisiae* is a suitable chassis for the expression of type I, type II and type III PKS naturally found in fungi, plant, and bacteria, as well as associated NRPS.

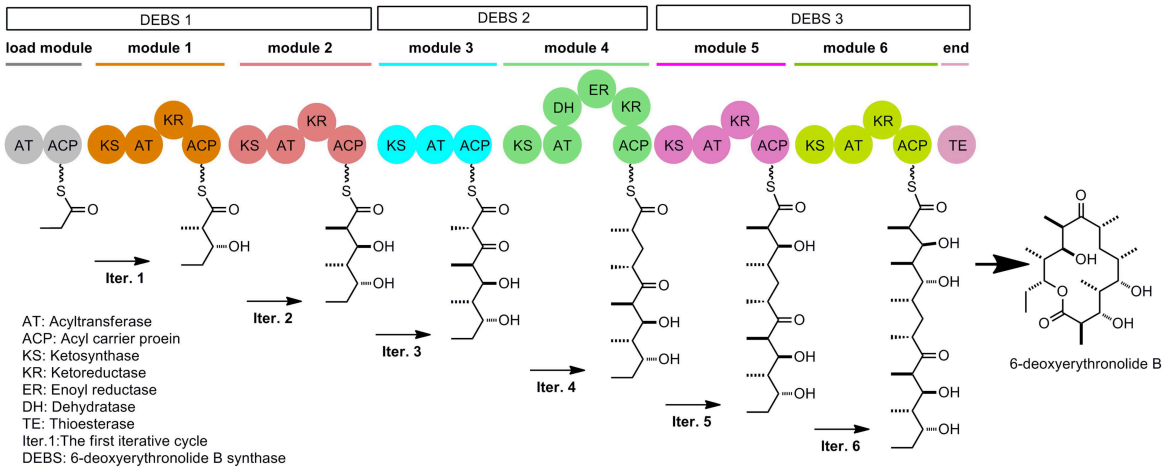

Figure 12: Exemplary model organization of a bacterial type I polyketide synthase (6-Deoxyerythronolide B Synthase (DEBS) PKS). The DEBS PKS consists of different modules that are comprised of different domains. Each domain catalyzes a specific reaction step of the polyketide synthesis. Adapted from [126].

However, the limiting factor of rapid production of polyketides in *S. cerevisiae* is often the lack of appropriate precursor supply, as for most published examples, natively available precursors were utilized. The naturally occurring precursors acetyl-CoA and malonyl-CoA have been engineered for increased pools to subsequently improve the production yields of polyketides however, several non-natural acyl-CoA ester precursors would be required to be supplied in *S. cerevisiae* to unleash its full potential for polyketide production [115,127].

Taken together, *S. cerevisiae* is an indispensable chassis in metabolic engineering for the production of various valuable compounds and will also in the future play a significant role for the bio-based production of chemicals after the renunciation of a petroleum-based economy.

1.4 Cell-cell communication in natural and synthetic systems

For every organism, receiving environmental signals is essential and thus it is not surprising that some of the key characteristics of life are directly or indirectly depending on it. Examples include the response to stimuli or homeostasis and adaptation [128]. Apart from the sensing of the abiotic environment, organisms evolved convergent ways of sensing cells from the same species as well as unrelated organisms [129]. It is likely that at first organisms secreted metabolic waste products that served as signaling molecules for cell-cell communication. The disadvantage was that these products were also just found in the environment and were therefore lacking specificity. Evolving more specific compounds solely dedicated for cell-cell communication thus evolved, compensating this disadvantage [130]. With increasing cellular complexity, cell-cell signaling molecules evolved to be more complex. In multicellular organisms, contact-dependent cell-cell signaling pathways like the delta notch system in animal embryos, plant hormone communication systems like auxin in plants, or highly complex hormones are utilized to orchestrate cell-cell communication to enable highly complex cell-cell interactions [131,132].

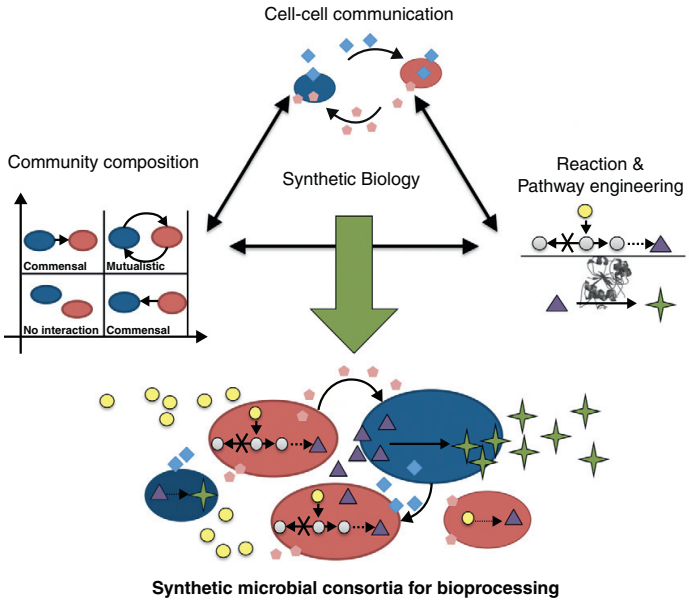

Figure 13: Schematic overview of required features for an engineered microbial consortium for bioprocessing. Important features include cell-cell communication, community composition, as well as suitable pathway and reaction engineering. Adapted from [139].

Cell-cell communication is essential for all types of cellular communities to coordinate organized interaction or specialization [133]. Without the evolution of an efficient cell-cell communication mechanism, the development of multicellular organisms would not have been possible [130]. But not only higher organisms feature cell-cell signaling mechanisms, also, in unicellular organisms like bacteria or yeasts, advanced cell-cell communication systems can be found [134,135]. Cell-cell

communication in microorganisms serves several purposes like coordination of collective behaviors, including violence, bioluminescence, biofilm formation, differentiation, and sporulation, or to find the opposite mating type for sexual reproduction, like the pheromone mating system of many yeast species [136–138]. Since cell-cell communication plays in many biological research areas an important role, for example, bacterial virulence (microbiology), compartmentalization of embryos (developmental biology) or immune response (immunology), it is not surprising that cell-cell communication is of high scientific interest. Thus, it should also not be surprising that also synthetic biologists employ cell-cell communication to develop tools for programming populations, communities, or even tissues, as well as to target these signaling processes for potential medical applications (Figure 13).

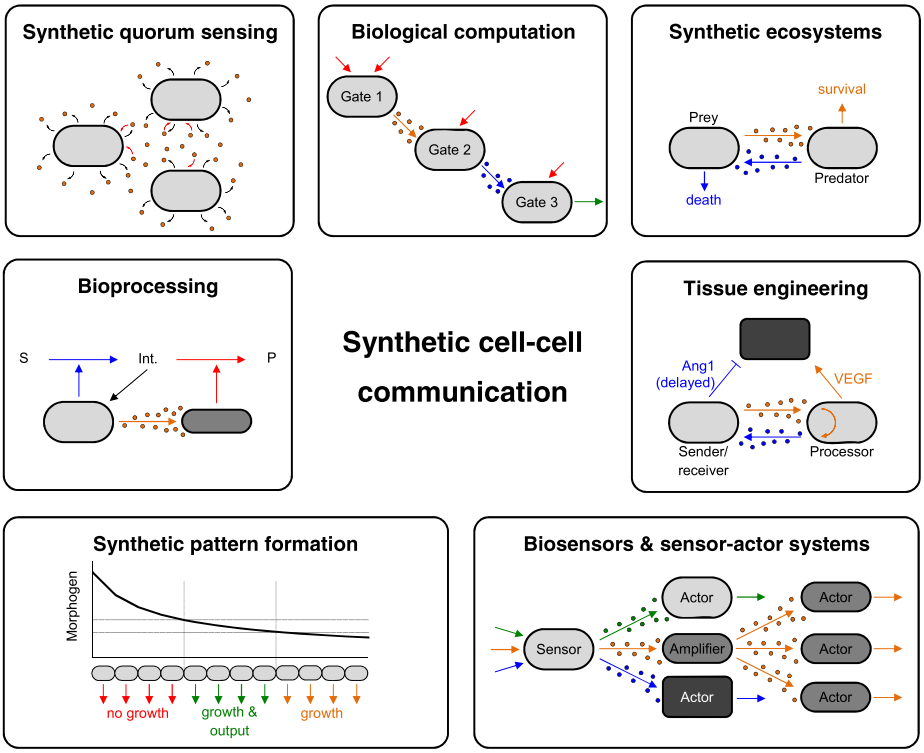

Figure 14: Scope of applications of cell-cell communication in synthetic biology. Using cell-cell communication systems it is possible to engineer a wide range of multicellular systems, including synthetic quorum sensing, multicellular biological computing, synthetic ecosystems, tissues, biosensors, pattern formation, or bioprocessing systems. Adapted from [140].

Apart from the employment of synthetic cell-cell communication for various applications, engineered multicellular systems that are comprised of known and characterized parts can also be utilized to study natural signaling system, following the Freeman credo: "What I cannot build I do not understand". In the following, we will highlight some but certainly not all the engineered systems that implemented signaling molecules to enable efficient cell-cell communication.

Cell-cell signaling is found in many different organisms and convergent systems have evolved over time. Most of the engineered cell-cell communication systems so far were implemented into bacterial chassis. Bacterial cell-cell communication is very diverse and the different signaling mol-

ecules range from metabolic side or end products like autoinducer 2, to a large diversity of different acyl homoserine lactones (AHL) in gram-negative bacteria, to peptide-based cell-cell communication in gram-positive bacteria [141–143]. Irrefutable, the bacterial AHL-based cell-cell communication is the most commonly used system in synthetic biological setups, however, there are also examples for the implementation of peptide-based communication systems for gram-positive bacteria. One of these examples was the engineering of the gram-positive bacterium *Bacillus megaterium* to express the peptide-based quorum sensing system originating from *Staphylococcus aureus* that enabled cell-cell communication between a sender and a receiver cell population of *B. megaterium* [144].

To employ natural cell-cell communication systems, they need to be made accessible for synthetic biology. Therefore, sender as well as the receiver systems need to be isolated and characterized, where necessary, in a heterologous chassis. The first bacterial communication system that was isolated was the Lux quorum sensing system from *Vibrio fischeri*. After identification of the responsible *lux* operon, the signaling molecule-producing enzyme, the responsive promoter and the associated transcription factor were characterized [145].

Since then, bacterial quorum sensing systems were intensively investigated, adapted and engineered for a variety of different applications (Figure 15).

Initially, it was possible to engineer a sender population that expressed under tetracycline-inducing conditions LuxI, which is responsible for the production of the communication molecule 3-oxohexanoyl-homoserine lactone (AHL-C6), that was subsequently transmitted as signal to the receiver population. The receiver cells expressed the LuxR transcription factor, which was activated upon AHL-C6 binding, resulting in the induction of the corresponding promoter and thereby initiated the expression of a reporter gene [146]. This implemented system was later used to engineer a self-regulating growth control circuit in *E. coli*. The production of the communication molecule AHL-C6 was applied to measure the density of the population. Upon reaching of an AHL threshold concentration, the expression of the CcdB cytotoxin was triggered leading to cell death and therefore stabilized the cell density of the population [147]. A similar system was intensively studied over a longer time period in a microchemostat, affirming the stability of the system [148]. Besides the characterization and employment of natural cell-cell communication systems, synthetic biologist also developed and engineered new to nature signaling communication systems [149–151].

Also, systems that are naturally not intended for cell-cell communication were already engineered to serve as such, for example, it was shown that the chemotaxis system of *E. coli* could be established as an artificial cell-cell communication system. In a two-population system, one population was expressing a heterologous enzyme that converted target molecules into ligands that served as attractants to the *E. coli* chemoreceptors in the second population. Since the ligand-producing population could induce chemotaxis in the receiver population, the hitchhiker effect was employed to obtain a complex multicellular system and an AND gate-like dynamic could be observed [152].

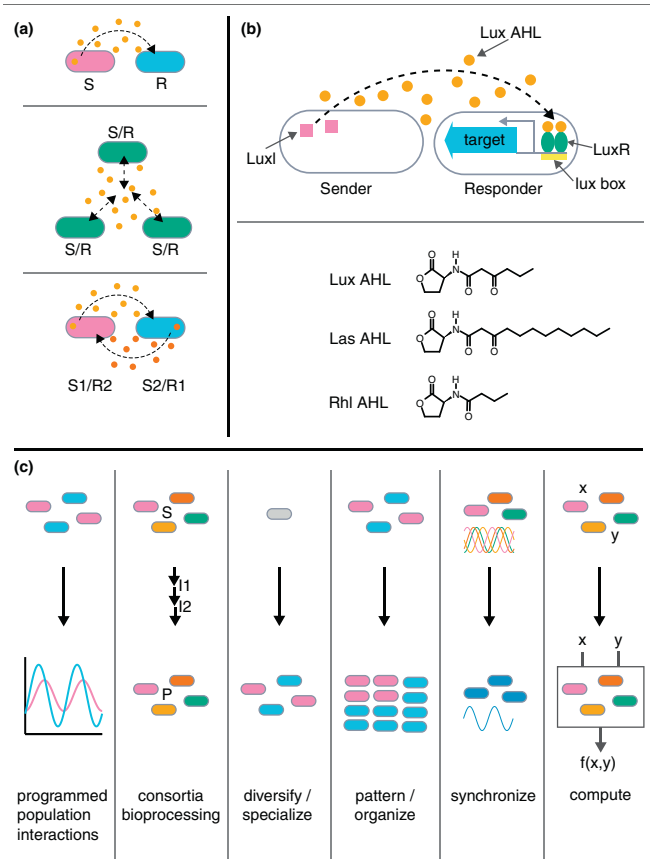

Figure 15: Network design motives, basic functions, and application systems of a bacterial cell-cell communication system in synthetic biology. A) Design motives of multicellular sender and receiver systems. **B)** Function AHL-based cell-cell communication system and AHL variants. **C)** Synthetic biological applications of bacterial cell-cell communication systems. Adapted from [153].

Another example for the development and implementation of a heterologous communication system was shown by the establishment of two cytokinin isopentenyladenine (IP)-dependent cell-cell communication system variants that were derived from the plant *Arabidopsis thaliana* and implemented into *S. cerevisiae* [151]. For the first system, the sender population synthesized and secreted IP. The receiver system expressed the AtCRE1 cytokinin receptor of *A. thaliana* as well as the native Ypd1 and Skn7 signaling proteins. Furthermore, they engineered the *SNK7*-binding promoter to reduce basal gene expression. In the presence of the IP signal it bound to the AtCRE1 receptor, resulting in AtCRE1-Ypd1-Skn7 phosphorylation and subsequently in induced GFP expression from the *SSRE* promoter. For the second signaling system variant, they adapted the system for IP production and sensing in one population. Taken together, they implemented an artificial cell-cell communication system that exhibited a two-population signal-response behavior as well as a network featuring a quorum sensing-like cell density-dependent behavior [151].
An example of a non-quorum sensing-based engineered cell-cell communication system was the implementation of metabolites as communication molecules [154,155]. *E. coli* was engineered to produce and secrete acetate at a constant rate. Acetate production was achieved via amino acid biosynthesis, while the natural acetate production pathway was disrupted. This alternative acetate production route resulted in acetate production proportional to the cell growth. Within the cells,

acetate was converted to acetyl phosphate (AcP), that phosphorylated NR_I in absence of the histidine kinase NR_{II} that subsequently indirectly activated the *glnAp2* promoter. With their approach of an engineered metabolism they showed that acetate could serve as communication molecule and thus established an alternative communication molecule and cell-cell signaling pathway [154,155].

Overall, it has been shown with various approaches and with increasing levels of complexity that cell-cell communication can be used as a versatile tool for synthetic biology applications to engineer diverse multicellular networks.

This was required since with increasing complexity of biological circuits, the metabolic burden of the chassis cells elevated as a result of their composition from many parts and the performance of more complex tasks. Different approaches were explored to reduce that burden, like automated circuit design improvement with minimal part usage or by establishing division of labor by distributing the circuits to several cells within a multicellular population [156–158]. This led to a physical separation of, for example, a gate function that generally reduced noise, crosstalk, or burden and increase at the same time the robustness of the computing elements [76,140,159–161]. One example for noise reduction by the implementation of cell-cell communication as a tool was obtained for the timed cell division of an entire population [162]. A similar trend was observed for the model-guided implementation of a minimal quorum sensing motif with a fast turnover rate of the transcription factor [159].

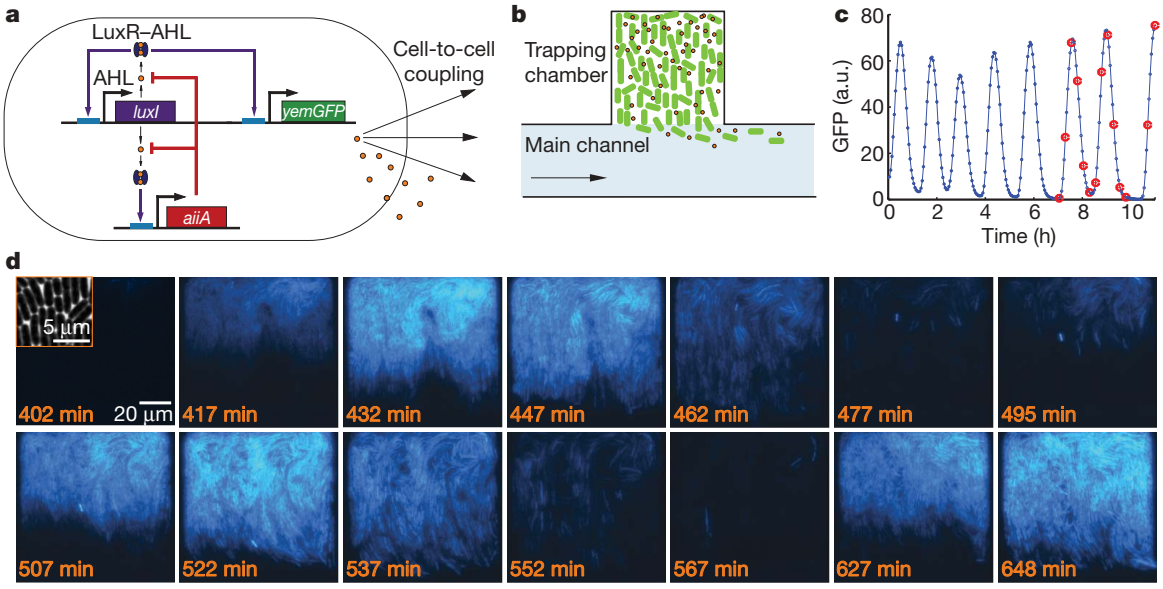

Figure 16: Design, experimental setup, and results of the synchronized quorum of a genetic clock. A) Genetic network design of the bacterial synchronized quorum of a genetic clock. **B)** Design of the microfluidic chamber for the experimental validation of the oscillator. **C)** Overall measured fluorescence intensity dynamics in the microfluidic trap over time. **D)** Microscopy images of the microfluidic trap over time for the synchronized quorum of a genetic clock. Adapted from [165].

Due to heterogeneity as well as expression noise, the first engineered population oscillators collapsed over longer time frames resulting in unsynchronized gene expression in the cells [163]. To synchronize the cells and cope with heterogeneity and noise, it was proposed and modeled to

implement a quorum sensing-based cell-cell communication system [164]. The proposed regulation to ensure synchronization of the population was achieved by the engineering of the synchronized genetic clock that used quorum sensing molecule as metronome for the expression of a reporter gene (Figure 16) [165].

One of the biggest achievements in circuit engineering in synthetic biology was the implementation of Boolean logic gates. Initially, simple AND gates were engineered in clonal chassis populations, later, also more complex multi-input and more complex gates were implemented as well as analog computing systems and networks that were able to count [166–178]. With increasing circuit complexity, amongst others metabolic burden and crosstalk, limited further circuit development in clonal populations. Thus, one approach to overcome this limitation was the separation of computing functions in order to reduce for example the metabolic burden of the single cells, and therefore, division of labor approaches were investigated. The separation of a genetic network into different populations can be beneficial but it requires efficient transport of information between the different subpopulations. A distribution of the computing power has additional advantages like the reduction of metabolic burden, lower noise, and overall increased stability. The conceptual idea of engineering multicellular circuits was discussed and reviewed to highlight the tasks that could be addressed, as well as the possibilities and potentials of division of labor [65,179,180].

The first implemented multicellular synthetic logic gates were engineered AND gates in different contexts that utilized various communication molecules for information transportation. One example was the engineered bidirectional communication system that mediated the consensus in a biofilm consortium [181]. In another example, benzoic acid, a new to nature wiring molecule, was implemented to obtain a logic AND gate which was shown to be functional in an engineered *Pseudomonas putida* strain [161].

Theoretical and model-based studies later on laid the fundament for the engineering of more complex multicellular networks and even synthetic multicellular computers and provided constraints for the implementation of the circuits by suggesting the implementation of Boolean units [182]. A more complex *in vivo* multicellular computing system was implemented into *E. coli*, for which the different logic operations of the subpopulations were wired using an AHL-based communication system [160]. Each single subpopulation was performing one Boolean gate function that could be induced as well as wired with other subpopulations performing another Boolean gate function. One subpopulation was represented by one colony and by spatially arranging the colonies, even difficult logics like OR or EQUALS could be engineered. Every single colony was acting as a module that performed a different function and by spatial distribution, like on a microchip, different and more complex computations were achieved [160].

Despite previously described systems, there are still remaining challenges to overcome that would allow a more rapid and improved design of multicellular logic networks. Attempts were made to formalize the engineering of multicellular logic networks by determining basic logic functions with biological as well as mathematical constraints: implementing rules for the ideal distribution; building and testing of the basic logic systems; model-guided tuning of the multicellular networks [183]. This system formalization was functional but also limited since only a small subset of currently available parts was included in the model. Further characterization and po-

tential machine-learning approaches would be required to be conducted to achieve full integration of model-guided designs and subsequent implementation of multicellular systems. The previously highlighted systems for multicellular computing were based on bacterial systems. Similar approaches were also investigated in *S. cerevisiae* as a chassis organism that will be highlighted in detail in a separate chapter (chapter 1.6).

Apart from the engineering of logic computing, also more dynamic systems were designed and engineered that were based on prior modeled population behavior. One example was a multicellular network using cell-cell communication to mimic ecological dynamics like the predator-prey system [184]. An ecological predator prey system is characterized by two populations that exhibit a time-shifted oscillatory relation of the population density. To mimic these oscillatory dynamics, a predator as well as a prey genetic circuit were implemented. The repeated increase and decrease in population densities was ensured by cell-cell communication-coupled expression of a toxin/antitoxin pair. Overall the system exhibited under specific conditions the model-predicted predator-prey oscillatory behavior [184].

In nature, cell-cell communication often orchestrates spatial arrangements of populations. For the spatial arrangement of biofilms, cell-cell communication is vital to obtain optimal spatial organization and information propagation [185]. Spatial arrangements can also have a significant impact on synthetic biology applications like the formation of biomaterials. For example, by the expression of different types of bioplastics, composite materials with improved characteristics could be formed. An early example of engineered multicellular pattern formation using cell-cell communication was a system that consisted of a sender strain expressing LuxI upon tetracycline induction for the production of AHL-C6, as well as a receiver strain [186]. The receiver strain carried the LuxR transcription factor that was expressed upon induction, the LacIM1 that could repress the expression of the reporter gene, as well as the CI that repressed the expression of an additional copy of LacI. However, in case the receiver cells were further distant to the sender cells, the AHL-C6 induction was not strong enough to express LacI, resulting in incomplete repression of the reporter gene and CI, required for the repression of an additional copy of LacI. In case the receiver cells were not stimulated by AHL-C6 due to the great distance to the sender cells, no LacIM1 or CI was expressed. CI was thus no longer able to repress the additional copy of LacI resulting in repression of the reporter gene expression. The multicellular cell-cell communication-based system allowed the engineering of multiple patterns, depending on the initial spatial distribution of sender and receiver cells on solid media [186]. More recently, a genetic multicellular system of clonal cells was published that displayed stochastic Turing pattern formation (Figure 17) [187]. The system was model-guided and comprised of two main modules. Abstracted, it was based on two signaling molecules, A3OC12HSL and IC4HSL. The first served as an activator catalyzing the biosynthesis of both signaling molecules, the second signaling molecule was an indirect inhibitor. IC4HSL was indirectly repressing the synthesis of both signaling molecules and additionally repressed A3OC12HSL by competitive binding. IPTG served as an external inducer that allowed the modulation of the dynamics of the system. The diffusion of the signaling molecules in a 1D space resulted subsequently in an alteration of the expression of the reporter gene and in pattern formation. By implementing this genetic system and varying the external modulating inducer, they

were able to generate various Turing patterns, as predicted in their model [187]. Prior to this publication, the implementation of a multicellular system exhibiting Turing pattern was already proposed and modeled [188].

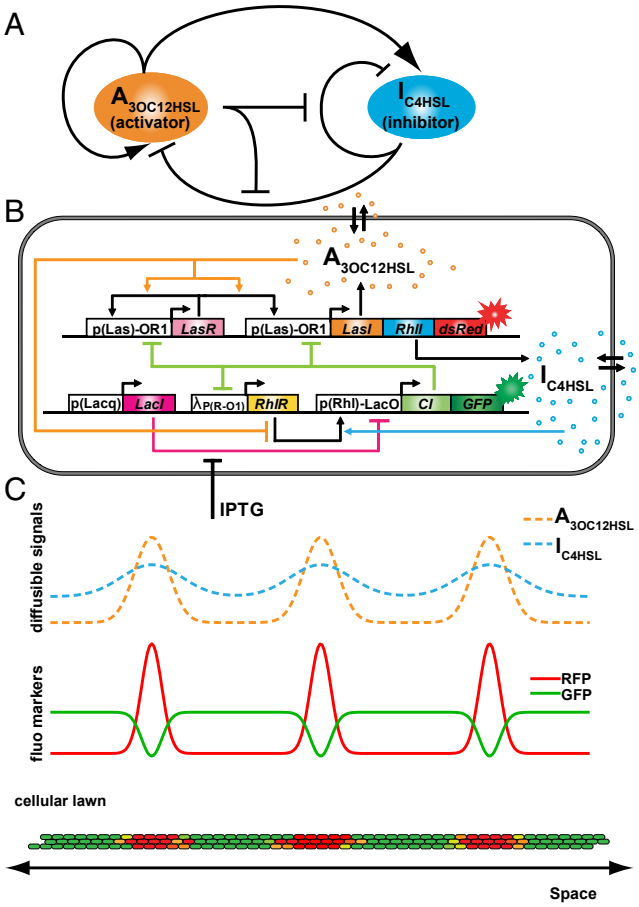

Figure 17: Multicellular network design, genetic circuit design, and expected results for the synthetic multicellular Turing pattern formation. A) Abstraction of the multicellular network design and interactions. **B)** Detailed genetic circuit design. **C (Top))** Desired communication molecule distribution in a 2D culture. **C (middle))** Expression of the reporter genes. **C (bottom))** Pattern formation on the cellular lawn. Adapted from [187].

Especially for the spatial organization of multicellular systems, the detection of edges was an unsolved problem. By designing an edge detection system that used AHL for cell-cell communication, the generation of a precisely structured multicellular system could be achieved [189].
One of the bottlenecks preventing further expansion of multicellular systems is the limitation of well-characterized wiring molecules for cell-cell communication. Even for the well-established and characterized group of AHLs, only in a few studies used more than two different signaling molecules in one multicellular system [190]. AHLs are very diverse and thus represent a source of further currently unknown wiring molecules, however, their usage in chassis and their orthogonality to other signaling molecules, including AHLs, need to be verified [190]. This potential limitation could be addressed by either using a different communication system, like the previously described utilization of metabolism-based wiring molecules, or by a comprehensive characteri-

zation of the plethora of AHL-based cell-cell communication systems. Scott and colleagues investigated and characterized four different quorum sensing system to unravel crosstalk and to identify orthogonal modules that can be combined in multicellular systems [191]. Two different types of crosstalk were identified: signal crosstalk that occurs when the transcription factor exhibits promiscuity towards other AHLs and then activates its cognate promoter; promoter crosstalk on the other hand appears when a transcription factor bound to cognate AHL can activate a non-cognate promoter. Also, a combination of signal and promoter crosstalk can take place. Thus, in order to obtain a comprehensive characterization, both parameters need to be examined before different QS system can be combined in the same cell or in multicellular systems, in order to avoid unintentional crosstalk and thereof resulting miswiring of a signaling circuit. By engineering of hybrid promoters as well as through protein engineering of one transcription factor, Scott *et al.* obtained four functional quorum sensing systems were generated that were further characterized by testing all combinations of AHLs, promoters and transcription factors [191]. This characterization allowed the identification of AHL-based wiring molecules that could be combined in one multicellular system without crosstalk and thus served as blueprint for future characterization [191]. Based on these results, the same authors were able to engineer a stabilized microbial ecosystem by implementing a quorum sensing-regulated lysis system in *Salmonella typhimurium*. In order to maintain a stable community composition within a community, self-limiting growth dynamics were modeled and implemented [192]. This stabilized microbial ecosystem constituted a first perspective of the prospects of systems based on non-interacting fully orthogonal wiring molecules. The different previously introduced cell-cell communication systems have different drawbacks but also many advantages and could also be combined with other systems and circuits in cells. For example, cell-cell communication could be coupled with any state-of-the-art downstream reaction or could be adapted to further engineer a cellular function [139]. An example of such an engineered system was the coupling of the sender molecule auxin with an engineered CRISPR transcription factor in *S. cerevisiae* [149]. This was achieved by implementing the biosynthetic auxin pathway of *Agrobacterium tumefaciens* into *S. cerevisiae,* to engineer a sender population that produced auxin from indole-3-acetamide (Figure 18). The main focus, however, laid on the engineering of auxin-degradable CRISPR transcription factors. The core of the artificial transcription factor was comprised of a deactivated Cas9 (dCas9) that still interacted with the desired DNA sequence upon gRNA binding. The dCas9 was fused to a nuclear localization sequence, an activation domain, a library of different auxin-sensitive degrons, and a transcriptional activator VP64. Upon auxin stimulation, the auxin-sensing F-box was recruited by the degron and formed the SCF complex, which ligated ubiquitin that induced the degradation of the engineering auxin-degradable CRISPR transcription factors, resulting in promoter deactivation [149] .

Several of the described proof of principle systems could be used for biosensors, bioprocessing like metabolic engineering, and even in very sophisticated medical applications. One example of a medical application using AHL molecules was developed by Din and colleagues [193]. They synchronized the lysis cycle of engineered bacteria to employ them as a drug delivery system to fight cancer. The engineered *Salmonella enterica* cells lysed at a threshold population density and released a therapeutic agent. Since a small number of engineered cells did not lyse, the population could regrow resulting in turn in a lysis cycle. The engineered system exhibited a continuous

pulsed drug delivery at threshold cell densities. The engineered population behavior was proven *in vitro* first, followed by testing in a microfluidics system together with human cancer cells and was eventually implemented into an *in vivo* mouse model. Finally, they explored whether a synergistic effect could be observed, when classical chemotherapy and treatment using engineered bacteria were combined [193].

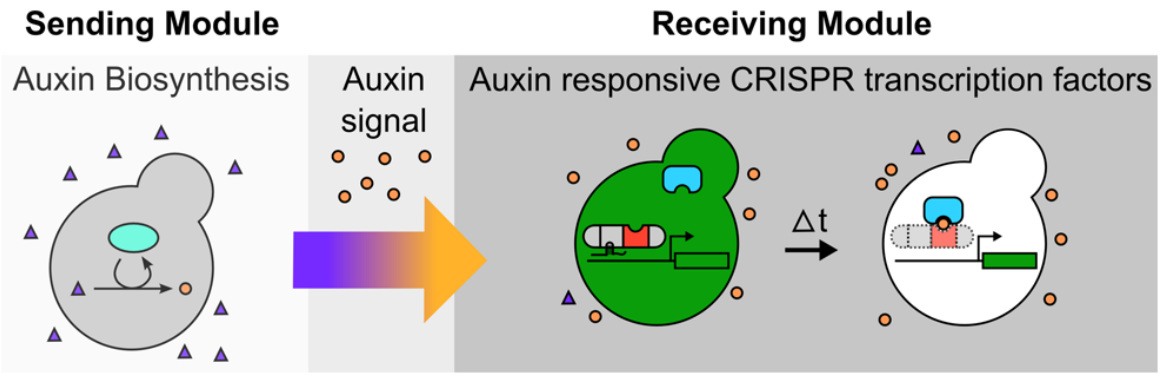

Figure 18: Schematic overview of the auxin-based cell-cell communication and responsive CRISPR transcription factor system in yeast. Using auxin biosynthesis to implement an artificial cell-cell commutation system to control expression by CRISPR-based transcription factors. Adapted from [149].

Another example of a medical application of engineered cell-cell communication was also shown by the complex network that was engineered in *E. coli* to target tumor cells. The cells were engineered to invade cancer cells by expressing invasin, which is required for tumor cell entry cell density-dependently, which was determined by cell-cell communication, hypoxia-responsive environmental conditions, and in addition upon arabinose induction [166].
Besides the employment of cell-cell communication molecules as a tool to synchronize engineered bacteria, it was also previously used as a target for medical applications. One example was the engineering of a complex genetic network in *E. coli* Nissel that could first sense and thereby detect the AHL signaling molecule produced by the human pathogen *Pseudomonas aeruginosa*, thereupon lysed to release anti-biofilm enzymes and anti-*P. aeruginosa* toxins to kill the pathogens. Several optimization cycles were passed through to obtain a proof of principle system that successfully worked in an animal model [194]. A similar approach with a different mode of action was recently published ,highlighting that such cell-cell communication-based medical treatment systems are still under development. Here, the engineered bacteria displayed biofilm degrading enzymes on the cell surface as well as expressed themselves quorum sensing molecules. Upon a threshold cell density, the cells secreted a biotherapeutic molecule to disrupt biofilms [195].
So far, we mostly highlighted engineered multicellular bacterial systems but also in other chassis organisms, multicellular networks have been engineered. By using nitric oxide signaling elements, an artificial cell-cell communication system could be implemented into mammalian cells. Therefore, they engineered the nitric oxide pathway and implemented it into a sender population that triggered the c-fos promoter in receiver cells [196].
Cell-cell communication in mammalian cells is vital for the implementation of tissue engineering setups. Different communication systems with this goal have been previously implemented, for example by using amino acids, second messengers, growth factors, or even volatile compounds

as communication molecules or by establishing contact-based interactions [196–200]. Examples in fungal chassis like *S. cerevisiae* will be highlighted in detail in the following chapter. Besides the engineered communication within one chassis genus, also communication systems can be engineered that bridge these boundaries. One example for an engineered cell-cell communication system that crossed the species boundaries was designed, implemented and tested by Weber *et al.* [201]. They used the volatile compound acetaldehyde to establish communication between bacterial *E. coli* cells, fungal *S. cerevisiae* cells, plant *Lepidium sativum* cells, and mammalian CHO or HEK cell line cells. They engineered communication-based networks mimicking predator prey, parasitic as well as mutualistic interactions and consisted of up to three community members [201]. To conclude, cell-cell communication is not only an important aspect of biology in general but was also already used as a tool in numerous synthetic biology research projects. Also, heterologous communication as well as entirely artificial communication systems have been developed and implemented. Overall, the majority of the systems were established in bacterial chassis, though also eukaryotic chassis like yeast and mammalian cells have been tested. However, *S. cerevisiae* as a workhorse organism of synthetic biology, especially for metabolic engineering applications, exhibits unused potential for the implementation of artificial cell-cell communication systems. Naturally, yeasts but mostly *S. cerevisiae* was also examined for cell-cell communication systems. Despite the discovery of quorum sensing-like signaling in some yeast species, they employ peptide-based pheromone signaling for sexual reproduction [202]. This mating pathway as well as its applications in synthetic biology will be discussed in the following.

1.5 The mating pathway in *S. cerevisiae*

In the previous chapter we highlighted the importance of cell-cell communication in biology in general and in synthetic biology in particular, mostly introducing bacterial signaling molecules. Briefly, we mentioned that yeast possesses quorum sensing-like systems. Additionally, their peptide-pheromone-dependent mating pathway plays an important role in cell-cell communication between the haploid mating types (Figure 19) [202]. It can be postulated that the *S. cerevisiae* mating pathway is one of the best-studied signaling pathways to date. Many general principles of signaling pathways on molecular, genetic, biochemical as well as cell biological level have been unraveled using the *S. cerevisiae* mating pathway [22]. The similarity to mammalian and other signaling pathways made the yeast mating pathway the optimal model for studying general concepts [203].

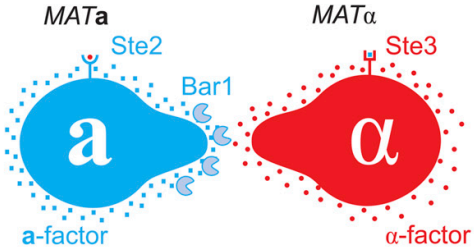

Figure 19: Schematic overview of *S. cerevisiae* mating types and expressed pheromones, corresponding receptors, and protease. The *MAT***a** cells express the α-factor-responsive Ste2 receptor, the α-factor degrading protease Bar1, and the **a**-factor. The *MAT*α cells express the **a**-factor-responsive Ste3 receptor and the α-factor. Adapted from [204].

As an overview, in *S. cerevisiae* two different haploid forms, the *MAT***a** and the *MAT*α mating type, exist that can sexually reproduce by mating. Before mating takes place, the two cell types need

to find each other and subsequently, the mating process is initiated. This process is based on a cell-cell communication system. *MAT***a** cells secrete the peptide pheromone **a**-factor and *MAT*α cells produce the peptide pheromone α-factor. The two mating types sense the peptide pheromone of the opposite mating type through a G protein-coupled receptor (GPCR). Upon pheromone binding, the receptor activates a signal transduction pathway resulting in the expression of around 200 genes, which are required for the mating phenotype, followed by cell cycle arrest in the G1 phase [205,206]. Historically important for yeast mating research was the identification of sterile strains, meaning haploids that did not enter cell cycle arrest upon pheromone stimulation, for example due to a mutation in the GPCR receptors [207]. The two peptide pheromones, the **a**- and the α-factor considerably vary in their composition and properties. The **a**-factor of *S. cerevisiae*, which is produced by *MAT***a** cells and sensed by *MAT*α cells, consists of 12 amino acids, YIIKGVFWDPAC and is post-translationally modified and covalently bound to a farnesyl group [208]. The farnesyl group constitutes the high hydrophobicity of the **a**-factor, resulting in reduced diffusion and therefore accumulates in close proximity to the producing cells. It was thus proposed that the **a**-factor serves for short distance communication and sensing [209]. The α-factor of *S. cerevisiae*, which is produced in the *MAT*α mating type and sensed by *MAT***a** cells, interestingly differs in its chemical properties from the **a**-factor. The α-factor peptide of *S. cerevisiae* consists of 13 amino acids, WHWLQLKPGQPM, and is less hydrophobic than the **a**-factor, which is reflected by increased diffusion of this pheromone. Therefore, the α-factor was considered to be important for long distance communication and sensing [209].

The pheromone-induced gene regulation engenders the mating phenotype which includes filamentous bipolar growth, increased cell volume, and directed growth towards the opposite mating type, which is together also referred to as protrusion formation or shmooing [210]. If the cells are in an early mating phenotype phase, the process is reversible, in case mating was unsuccessful. Generally, pheromone-induced gene expression leads to a significant fitness disadvantage when mating cannot be executed since the expression as well as pheromone stimulation are tightly regulated. The entire mating process can be abstracted into several phases, namely in pheromone production, G protein-coupled receptor pheromone detection, mitogen-activated protein (MAP) kinase signal transduction and downstream target gene expression regulation. A distinctiveness of the mating components that has not been highlighted yet is the barrier protease Bar1 that is exported by *MAT***a** cells and that degrades the α-factor [211]. In the following we will provide insights into cell-cell communication in *S. cerevisiae* using their peptide pheromones and how the natural mating procedure operates.

1.5.1 Pheromone processing

The α-factor of *S. cerevisiae* is encoded in the *mfα1* and in the *mfα2* gene [212–214]. Each gene encodes several mature α-factors. The pre-pro-α-factor consists of 165 and 120 amino acids for MFα1 and MFα2. The posttranslational modification is similar for MFα1 and MFα2. As MFα1 was at first and overall more intensively investigated, we will introduce α-factor processing on the example of MFα1. The pre-pro-α-factor consists of an N-terminal signal sequence also referred to as pre-region, and a pro-region, as well as four copies of the mature α-factor that are separated by spacer sequences, which contain protease cleavage sites (Figure 20, Table 3)[214]. In other yeast species, one to five mature α-factor copies are encoded in the MFα1. The pre-pro-α-factor undergoes a series of posttranslational modifications, also known as pheromone processing or maturation, before the mature α-factors are secreted into the extracellular environment [208]. After transcription and translation of the *mfα1* gene, the resulting MFα1 pre-pro-α-factor is translocated into the endoplasmic reticulum (ER) guided by the signaling sequence. In the ER lumen, the signaling sequence is cleaved and the N-linked glycosylation of the three asparagines in the pro-region takes place [215]. The α-factor precursor is then transported from the ER to the Golgi apparatus in a vesicle. In the lumen of the Golgi apparatus, the glycan chains undergo remodeling and the protease-mediated proteolytic cleavage steps occurs that remove the spacer regions (Figure 20) [216]. The first cleavage step is performed by Kexin2 (Kex2), that recognized a KR or RR amino acid sequence motif and separates the four copies of the α-factor [217]. The dipeptidyl aminopeptidase Ste13 cleaves on the carboxyl side of the N-terminal X-A sequence and removes it [218]. The final maturation step it performed by Kex1 by cleaving the remaining amino acid residues of the C-terminus off the α-factor (Figure 20) [219]. After this processing, the mature α-factor follows a secretory vesical transport from the Golgi apparatus to the plasma membrane and is subsequently released into the extracellular environment [217].

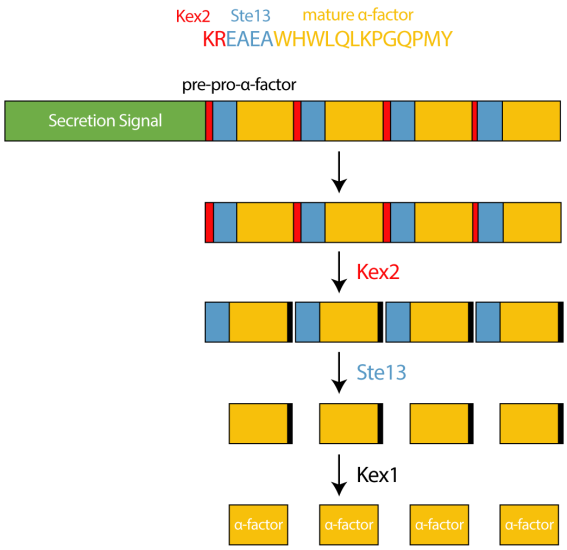

Figure 20: Visualization of the α-factor processing. The product of the expression of the *mfα1* gene is the pre-pro-α-factor which consists of a secretion signal sequence (green), processing protease recognition sites (red, black, blue) and the mature α-factors (yellow). The pre-pro-α-factor is processed by the Kex2 protease, that splits the pre-pro-α-factor. The Ste13 protease removes the spacer sequences form the α-factors. The final processing step is the removal of the remaining Kex2 recognition sequence by Kex1. Subsequently, the mature α-factor is secreted. Inspired by [220].

Even though the α-factor and the **a**-factor have similar roles in cell-cell communication and the subsequent mating process, the pheromones are considerably differing in their chemical properties and also in their pheromone processing procedure (Figure 21, Figure 22, Figure 23). While the α-factor secretion pathway can be considered as a classic secretion pathway, the **a**-factor secretion pathway is fairly unique to the **a**-factor [221]. Before its processing, the unprocessed **a**-factor is 36 amino acids long. The **a**-factor precursor contains an N-terminal extension, the final mature **a**-factor, as well as the CAAX box (Figure 21).

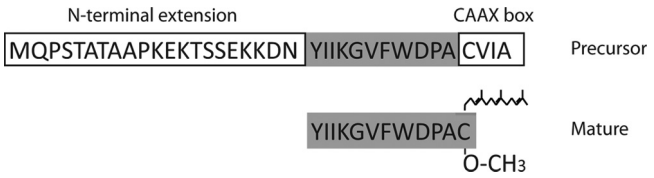

Figure 21: Scheme of the precursor and mature a-factor. Adapted from [208].

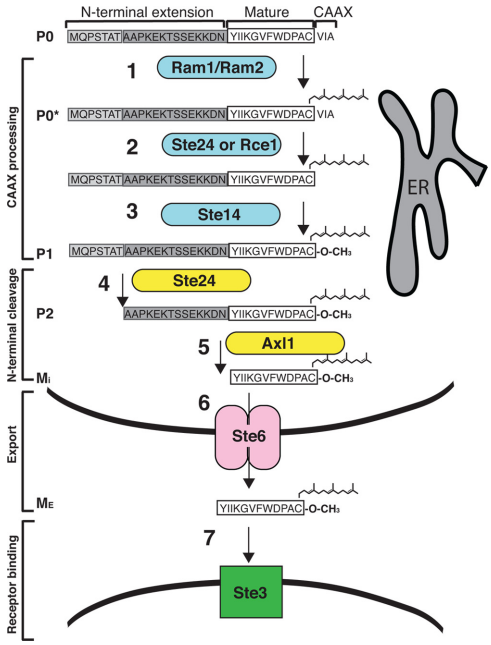

Figure 22: Detailed visualization of the a-factor processing. The precursor of the **a**-factor undergoes a series of chemical modifications a well as protease-mediated processing before its secretion. Adapted from [208].

The complete six-step biogenesis of the **a**-factor can be separated into three processing modules [208]. The first of the **a**-factor posttranslational processing modules is the CAAX processing. Different from the α-factor the **a**-factor is not translocated into the ER membrane but the enzymatic steps that are involved in the CAAX processing take place at the ER membrane. Ram1 and Ram2, two subunits of a cytosolic farnesyltransferase, recognize the CAAX motif and perform a farnesylation [222–224]. Next, Ste24, an ER-bound protease, initiates the proteolysis of VIA of the CAAX motif, resulting in the cleavage of these three C-terminal amino acids [225–228]. The final step of CAAX processing is performed by Ste14, an isoprenyl cysteine carboxyl methyltransferase that extends the

farnesylcysteine of the **a**-factor with a carboxymethyl group. Subsequently, this final CAAX processing step results in a fully C-terminally modified unmatured **a**-factor [229,230]. Afterwards, the N-terminus of the **a**-factor is processed. Two zinc metalloproteases are involved in this process. First, Ste24 cleaves off the N-terminal MQPSTAT sequence, followed by Axl1 that removes the remaining N-terminal part of the unmatured **a**-factor, providing the mature, fully processed and modified **a**-factor for the extracellular export [227,228,231,232]. Differently, from the α-factor, the **a**-factor has to be actively exported by the ABC transporter Ste6 [221,233,234]. After the ATP-dependent export, the mature **a**-factor can diffuse in the extracellular environment but due to its hydrophobic properties, only short distance diffusion takes place [208,209].

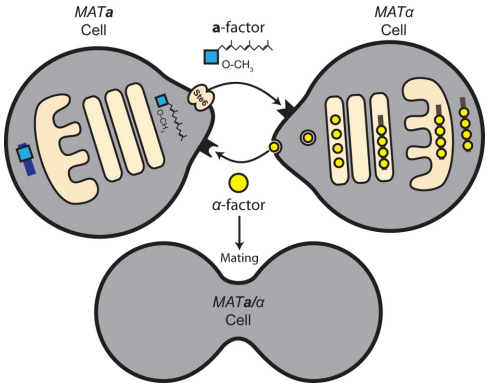

Figure 23: A brief overview of the production and processing of the a- and the α-factor and the resulting mating response. Adapted from [208].

1.5.2 GPCR pheromone receptors and effectors

The secreted pheromones stimulate their corresponding receptors that subsequently results in the activation of the mating pathway. In *MAT*α cells, the Ste3 receptor is stimulated by the **a**-factor, while in *MAT***a** cells, the Ste2 receptor is stimulated by the α-pheromone. Exemplary for all GPC receptors, Ste2 and Ste3 have seven transmembrane helices (Figure 24) [22]. Overall, the Ste2 receptor has been described more extensively and is better characterized due to the fact that the α-factor does not require chemical posttranslational modifications and can therefore be easier chemically synthetized, purified and utilized in experiments. The Ste2 receptor has been studied since 1970, and was first identified in sterile *S. cerevisiae* mutant strains and later cloned and further analyzed [207,235]. However, until today, no 3D structure of the Ste2 receptor has been obtained and published yet, most likely due to the difficulties in purification and crystallization of membrane proteins [236]. Besides the lack of a 3D structure, topological structures of Ste2 have been proposed and publicized, providing a general understanding of the receptor. Nevertheless, several studies based on mutagenesis approaches shed light on the function of the Ste2 and the Ste3 receptors (Figure 24) [237–239]. A general understanding of the structures of Ste2 as well as of the Ste3 receptor was obtained from mutant strains coining today's overall understanding of the receptor proteins [239]. Differently from Ste2, it has been proposed that the Ste3 receptor features larger extramembrane regions. Interestingly, mutagenesis studies of Ste2 and Ste3 revealed that several mutations in Ste2 led to non-stimulating phenotypes but not to hyperactive phenotypes, while hyperactive phenotypes were primarily found for Ste3. These findings conformed to the knowledge about the varying gene expression strategies of *ste2* and *ste3* [239]. The two pheromone

receptors represent also an example for convergent evolution of receptors. Since both receptors activate the same G protein, some regions are thought to have similar sequences and structures [239].

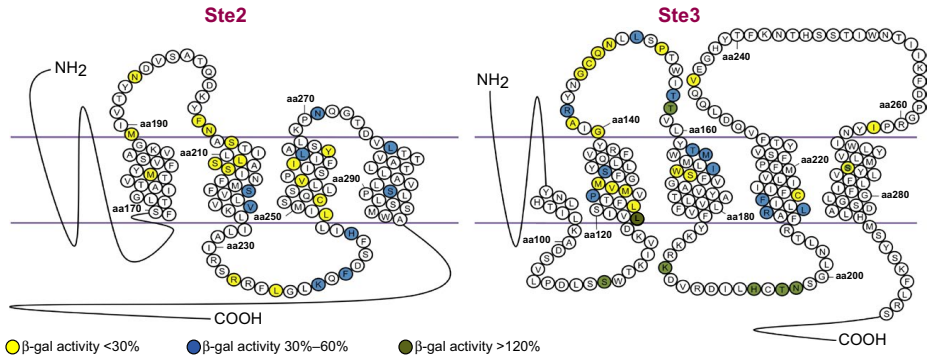

Figure 24: Prediction of the topological structure of the Ste2 and Ste3 receptors based on mutagenesis studies. Adapted from [239].

The currently most comprehensive model of a 3D structure of the Ste2 receptor bound to the α-factor obtained from mutagenesis studies and experimental validation showed that 26 residues of the Ste2 receptor are likely to interact with the α-factor and are therefore critical for receptor stimulation [236]. Further, the third cytoplasmic loop had been identified to interact with the G proteins, as it was shown that this region was very sensitive to mutations resulting in a loss of function of the receptor [240,241]. A follow up study identified the importance of the positive net charge of the region, which is conserved also in other species besides *S. cerevisiae* [242]. Apart from the third cytoplasmic loop, parts of the seventh transmembrane loop had been identified to be essential for the function of the Ste2 receptor. The region was thought to be responsible for the structural integrity and is crucial during the conformational change [243]. Termination of the receptor stimulation is achieved by ligand-induced endocytosis of the receptor [244]. When the α-factor is bound to Ste2, a conformational change of the receptor is induced leading to the exposure of 132 residues of the C-terminus that is also referred to as stimulated or active state [245]. This change allows, for example, the binding of Sst2 to the receptor [246]. Due to the phosphorylation of Ser and Thr within these 132 residues by Yck1 and Yck2, this conformational change becomes irreversible [247]. The stimulated receptor is associating with Rod1/Art4 and Rog3/Art7, members of the adaptor proteins of the arrestin family [248]. These are recruiting the plasma membrane-anchored Rsp5 ubiquitin ligase to the receptor [249]. Upon Rsp5 Ste2 binding, the clathrin-mediated endocytosis machinery is activated which results in the endocytosis of the Ste2 ligand complex [250]. Subsequently, the complex is degraded in the vacuole [251]. In *MAT*α cells the α-arrestins Aly1 and Aly2 are responsible for the endocytosis of the Ste3 receptor upon a-factor binding [252]. After the stimulation of the receptor Gpa1, the G protein α subunit is phosphorylated from GDP to GTP which leads to a subsequent release or lost binding of Ste4, which guides Ste18 to the G protein β and γ subunits [253–256]. The signal is further transmitted by the G protein β and γ complex by interacting with other effector proteins. The Gβ subunit binds Ste4 after being linked to the membrane by the Gγ subunit to the other effector proteins. By binding Ste20, a p21-activator protein kinase, and Ste11, a MEK kinase, the Gβγ complex is responsible for the establishment of a closer spatial organization of the two effector proteins [257,258]. This subsequently results in the transmission of

the signal by phosphorylation of Ste11 by Ste20 [259,260]. Next Ste5, a scaffold effector protein, binds to Gβ as well as Ste11 near the Ste20 binding site [261–265]. Hereupon, the Far1-Cdc24 complex is recruited by the Gβγ system. While Far1 binds to the Gβγ complex, the C-terminal part of Far1 binds Cdc24 [266]. Upon translocation of Far1-Cdc24 to the membrane, Cdc24 can act on Cdc42 by changing it from a GDP to a GTP state. The activated Cdc42 thus interacts with several effector proteins including Ste20 that was mentioned previously [267,268]. Subsequently, Cdc42 binds to other effector proteins that are required for the regulation of the cell polarity, triggering the mating specific shmooing phenotype [269]. Shmooing is defined as polarized growth or morphological change towards to highest abundance of the stimulating pheromone. The Gβ-Far1-Cdc24-Cdc42 is required for the expression of the phenotype as Cdc42 is regulating Bem1, Bni, Gic1, and Gic2 [266,270–278].

1.5.3 Mating mitogen-activated protein kinase signaling pathway

After introducing the first steps of the signaling cascade upon pheromone binding to the GPCRs, the downstream mitogen-activated protein kinase (MAPK) signaling pathway will be highlighted in more detail (Figure 25). The previously mentioned Ste11 is a MEK kinase (MEKK), the hierarchical first kinase of the Ste5 scaffold module that is regulating Ste7, another MEK. Two more MAPKs are involved in the mating pathway, Kss1 and Fus3. As previously highlighted, after the membrane-associated recruiting of Ste5, Ste11 and Ste50, the phosphorylation by the activated Ste20 is regulated. Subsequently, Ste11 activates Ste7 via phosphorylation, which leads to the downstream activation of Fus3 and Kss1 by Ste7. The scaffold protein Ste5 spatially arranges and organizes Ste11, Ste7, Fus3, and Kss1 and is thus crucial for the successful signal transduction through the MAP kinase pathway [264,279–284]. Subsequently, the Fus3 and Kss1 MAP kinases are interacting with the Ste12/Dig1/Dig2 transcription factor complex that is responsible for downstream gene regulation as well as with the Far1 protein, which is the main regulator for cell cycle arrest. These regulators are in charge of the regulation of around 200 genes in the haploid cells. Ste12 serves as transcriptional transactivator [206]. Dig1 and Dig2 are acting as antagonists to Ste12 by binding and subsequently repressing it [285,286]. Interestingly, several mating signaling pathway-involved genes are regulated by Ste12, some gene products promote the mating pathway, including Ste2, Fus3, and Far1, others have a demoting effects like Sst2, Msg5, and Gpa1 and even others are involved within the mating pathway like Fus1, Fus2, Fig1, Fig2, and Aga1 [287]. Ste12 also regulates its own expression. If the MAP kinase Kss1 is not phosphorylated it can bind the mating process transcription factor Ste12 and subsequently represses Ste12 activity which prevents downstream gene expression regulation [288]. Upon phosphorylation of Kss1 by Ste7, Ste12 repression gets released. Besides Ste12, Dig1, and Dig2, Far1 acts as a multifunctional regulator. Next to the promotion of polarized growth by binding to Gβ and Cdc24, it functions as regulator for cell cycle arrest as previously briefly highlighted. However, the exact mechanisms are so far not completely understood. One possibility could be that Far1 is interacting with Cdc28, the cycline-dependent kinase, which regulates the cell cycle in yeast [289]. It was observed that *far1*Δ strains and mutant strains in which Far1 cannot be phosphorylated by Fus3 do not exhibit cell cycle arrest [290]. Apart from induction of gene expression, around 100 genes are repressed by Far1 during the mating response [291]. Also mating pathway involved genes like *ste5*, *ste11*, and *ste7* as well as antagonistic genes including *sst2* and *msg5* are regulated [292]. Since the stimulation and subsequent

signal transduction of the mating pathway is highly complex and constitutes a high fitness disadvantage, the signal modulation plays an important role to regulate the signal intensity as well as to promote the decision making process [22]. Overall, the G protein effectors and the MAP kinase signaling pathway and most of the downstream regulated genes are similar in the *MAT*α and the *MAT***a** mating type. However, most of the introduced research results and finding were generated in the *MAT***a** strain background upon stimulation with the α-factor due to simpler experimental accessibility [22].

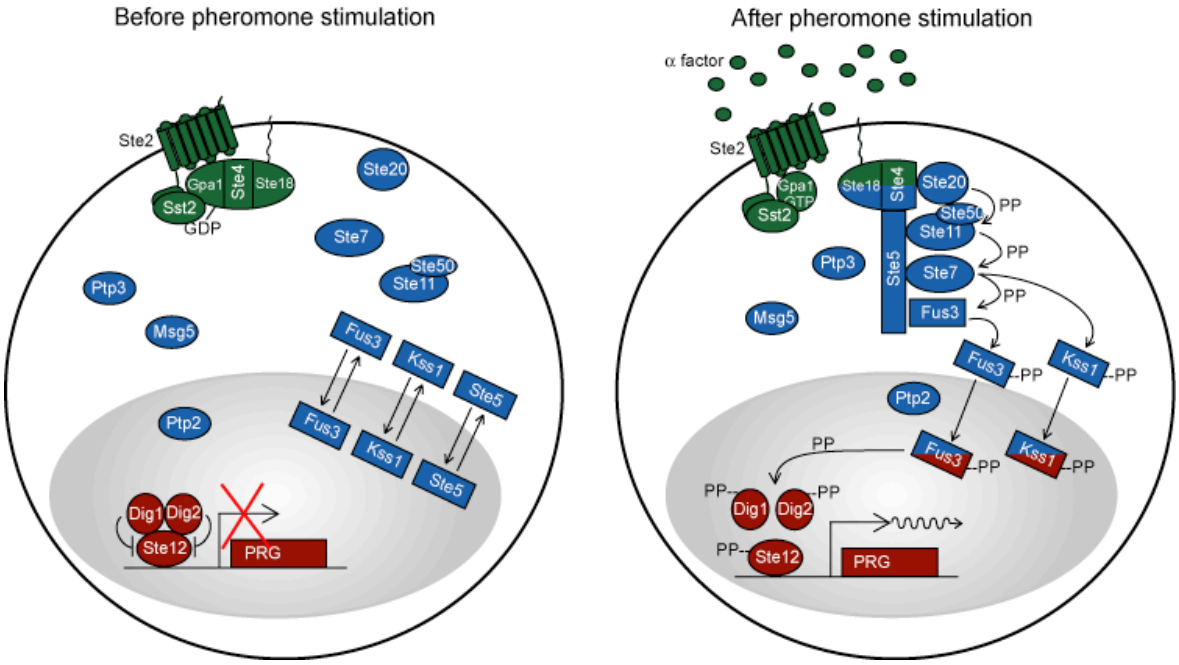

Figure 25: Overview of the MAPK signaling pathway in *MAT*a cells before (left) and after pheromone stimulation (right). The signaling pathway requires three main groups of factors: the extracellular α-factors as signaling molecules, the GPCR receptor Ste2 with the associated G proteins, as well as Sst2 (green), the signaling factors that are responsible for the MAPK singling pathway (blue) and the factors acting on the transcriptional level (red). Adapted from [293].

A unique attribute of the *MAT***a** mating type is the barrier proteases Bar1 that is secreted upon pheromone induction and degrades the α-factor [22,294,295]. The expression of Bar1 results in a steeper gradient of α-factor, which in turn positively influences the chemotropism and subsequently the mating efficiency [296,297]. Further studies in *Candida albicans* indicated that the expression of the barrier protease also reduces α-factors crosstalk of closely related species [298]. Taken together, we provided an overview of the mating pathway including the processing of the **a**- and α-factor, the GPCRs Ste2 and Ste3, the MAP kinase signaling pathway as well as the barrier protease Bar1.

1.6 The yeast mating pathway in synthetic biology

We already highlighted in the previous chapter the importance of cell-cell communication in synthetic biology (chapter 1.4). Several systems were engineered that used signaling molecules to build multicellular networks, logic gates, to reduce noise, to synchronize populations, to mimic synthetic ecosystems, or in medical applications as pharmaceutical targets, or to perform com-

plex tasks [150,162,165]. Most of the systems were implemented in bacterial chassis using AHLs as wiring molecules [65]. Previously, the implementation of cell-cell communication based on molecules derived from more distantly related organism, like the utilization of cytokinin isopentenyladenine as a signaling molecule in *S. cerevisiae*, had been achieved [151]. But also *S. cerevisiae* itself evolved an innate cell-cell communication system which is employed to find the opposite mating type and to subsequently sexually reproduce [299]. This cell-cell communication system, including the peptide-based pheromones **a**-factor and α-factor, the GPCRs Ste2 and Ste3, the successive MAP kinase signaling pathway as well as the downstream target genes have been intensely studied [22,138,253,300,301]. Continuous research is performed to further extend our knowledge of the *S. cerevisiae* mating pathway. One recent discovery includes the possibility of ratio sensing of the two mating types via signal input attenuation [209].

Generally, the MAP kinase pathway in *S. cerevisiae* is one of the best studied eukaryotic signaling pathways and served as a model, even for signaling pathways in mammalian cells, which were shown to be homologous [22]. Due to these homologies it was even possible to engineer yeast/mammalian G protein α-subunit chimera for drug screening [302]. Despite the pathway modularity of *S. cerevisiae* and mammalian cells, it has also been shown that different components can be interchanged with homologues variants from other fungal species [303]. This opportunity was utilized to identify mating factors and receptors of fungi that were prior reported to not sexually reproduce [304]. Thereupon, these discovered mating properties were employed for mating-derived strain development [305]. Taking the vast knowledge about the mating pathway and the plethora of tools available for *S. cerevisiae* into consideration it was not surprising that many synthetic biology projects targeted the mating pathway [306]. The yeast mating pathway is suitable to be implemented into various applications, for example into biosensor applications [140,307–309].

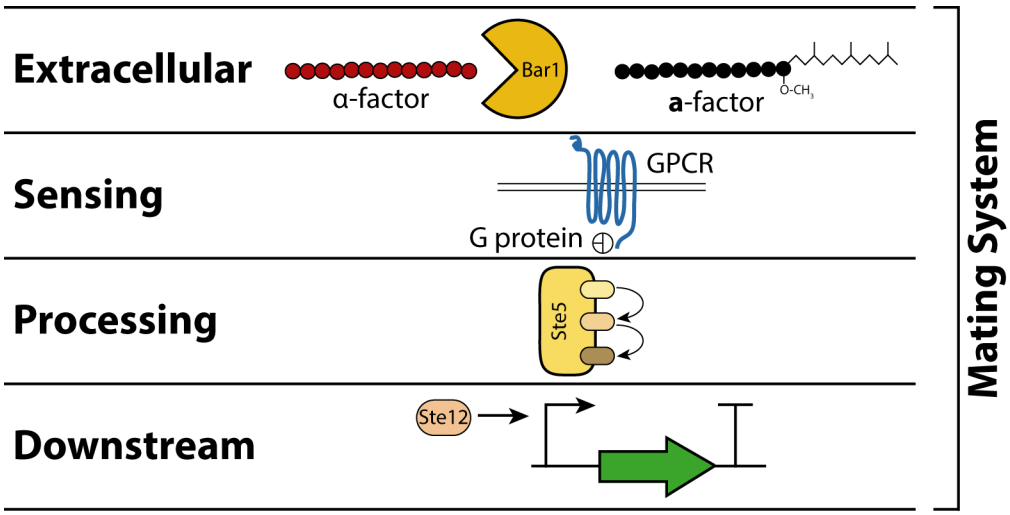

Figure 26: Abstraction levels of the yeast mating pathway for synthetic biology applications. The yeast mating pathway can be separated into four abstraction levels that can be the objectives of engineering approaches. Also, the entire system can be targeted for a synthetic biology application. The extracellular level is comprised of the wiring molecules **a**-factor, α-factor, and the α-factor-degrading protease Bar1. The sensing level consists of the GPCR receptors Ste2 and Ste3 as well as the associated G proteins. The scaffold and kinase proteins of the MAPK signaling pathway are part of the processing level and transcription factors like Ste12 as well as the pheromone-inducible promoters are part of the downstream level.

Overall, the yeast mating system can be abstracted into different units (Figure 26). The extracellular or communication unit is comprised of the peptide-based mating factors, the **a**-factor and the α-factor, as well as the barrier protease Bar1. The sensing unit includes the GPC receptors Ste2 and Ste3 and the associate G proteins. The processing unit consists of the MAP kinase signaling pathway and affects the activity of transcription factors and subsequently of promoters of the downstream unit. In each unit, components can be replaced with heterologous parts that interact with the native ones. Many research projects utilized the natural mating pathway system units and only altered one unit of the system or adapted the entire system to the meet the engineered parameters. Below, we will introduce synthetic biology *S. cerevisiae* mating pathway applications categorized according to the mentioned units and will eventually review systems that adapted the entire mating pathway.

1.6.1 Extracellular unit

The extracellular unit of the yeast mating pathway consists of the pheromones **a**-factor and α-factor as well as the barrier protease Bar1 that degrades the α-factor.

Interestingly, the barrier protease has rarely been implemented into synthetic biology yeast mating-based systems. Overall, the investigations focused on Bar1, including heterologous expression and detailed characterization, remain limited. However, the importance and benefits of the barrier protease for successful mating have been investigated [295,310]. Meanwhile, the secretion sequence of Bar1s have been identified and for some also the putative recognition and cleavage sites [298,311]. Apart from the native *S. cerevisiae* barrier protease $Bar1_{Sc}$, the *C. albicans* barrier protease was expressed and investigated in more detail. The specificity of this aspartyl protease revealed potential biotechnological applications [298]. To date, no protease similar to the α-factor-degrading protease Bar1 has been identified targeting the **a**-factor. Earlier reports of an **a**-factor protease could not be confirmed and remain therefore questionable [204].

Compared to the barrier protease, the pheromones have been intensely investigated and were frequently utilized in synthetic biology applications, though mostly the α-factor was utilized [220,312]. The usage of the **a**-factor was rare, due to experimental limitations and the requirement of post-transcriptional modifications [22]. Different heterologously expressed α-factors were previously employed as wiring molecules to engineer multicellular systems with *S. cerevisiae* and other yeast species, which will be highlighted below [312]. For the engineering of multicellular systems, the availability of the different heterologously expressed α-factors as sender molecules to wire the cells is crucial. Billerbeck and colleagues explored α-factors from 45 different species and found 32 to be functionally produced in *S. cerevisiae* [220]. Besides the expression and successful processing of α-factors, it is also of high importance that the corresponding sensing unit, mainly consisting of the GPCRs, can be functionally expressed. Additionally, Billerbeck *et. al.* examined if non-cognate α-factors could stimulate the GPCRs, resulting in crosstalk [220]. Due to the design of the α-factor genes to encode several mature pheromone copies and variants, it is possible to engineer chimeric α-factor genes. Chimeric genes could thus express two or more different α-factors, for example, the α-factor of *Schizosaccharomyces pombe* and *S. cerevisiae*. These chimeras enabled the engineering of an interspecies communication system [312]. Besides the heterologous expression of α-factors, it is also possible to engineer the α-factors directly. Artificial extracellular splicing

or N-terminal cleavage using a split intein-mediated reaction were implemented [313]. For the extracellular splicing, the α-factor was divided into two fragments and each of them was modified with N-intein or C-intein. After the protein trans-splicing, the mature α-factor was reconstituted and capable of Ste2 stimulation. An N-terminal extension of an α-factor reduces its binding to the Ste2 receptor. Thus, to implement N-terminal cleavage, an N-intein was added to the N-terminus. In the presence of a mutated C-intein, the N-terminus of the α-factor was cleaved off resulting in active α-factor that could stimulate the Ste2 receptor. These approaches highlight the potential of altering the pheromones to perform for instance logic gate functions [313]. A limitation was though that the α-factor was not produced by yeast cells but rather chemically synthesized or heterologously expressed and purified from *E. coli*. At present it is uncertain, whether the engineered α-factors could be processed and secreted by *S. cerevisiae* cells. In preceding studies, it was discovered that an amino-terminal truncated version of the α-factor (WLQLKPGQP(N1e)Y) competed with the natural α-factor by binding to the receptor. The truncated α-factor was however not able to activate the downstream signal transduction resulting in the MAP kinase pathway and therefore acted as an α-factor antagonist. The carboxyl-terminal truncated variant of the α-factor (WHWLQLKPGQP) on the other hand acts in presence of the natural α-factor synergistically. Both truncated α-factors versions have not been employed for synthetic biology approaches so far but bear a lot of potential for future engineering of multicellular systems [314].

1.6.2 Sensing unit

The sensing unit of the mating pathway consists of the pheromone-stimulated GPC receptors Ste2 and Ste3 and the associated G proteins (Figure 27). The G protein consists of the Gα, Gβ, and Gγ subunits, the latter two from a heterodimer that couples the receptor to the signaling pathway [22]. Upon pheromone stimulation, the receptor undergoes a structural conformation change, subsequently releasing the Gβ/γ dimer form the Gα subunit. The Gβ/γ dimer propagates at the membrane following the activation of downstream effector proteins resulting in the signal transduction of the MAPK pathway [22,315,316].

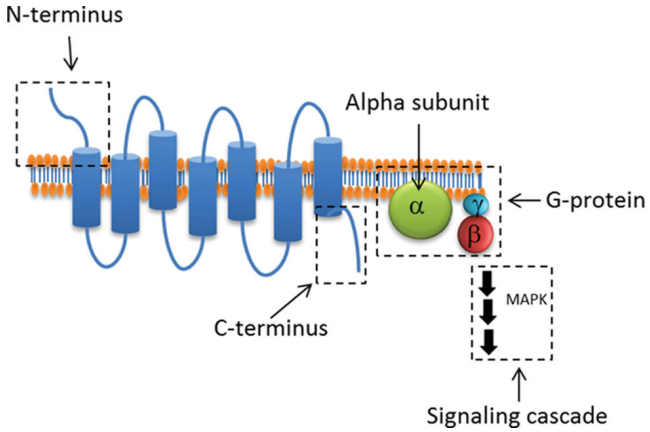

Figure 27: Scheme of targeted optimization of heterologously expressed GPCRs in yeast. For the functionality of heterologous GCPRs, optimization of the N-terminus, the C-terminus, as well as G proteins (especially the α-subunit), or the MAPK signaling pathway can be beneficial. Adapted from [307].

GPCRs exhibit in general structural similarities and are able to sense a wide range of different molecules, from small peptides and proteins, to photons, ions, and small molecules [317]. These properties make GPCRs vital parts for the construction of biosensors for various applications, especially based on the Ste2 receptor [307].

The potential of engineering the sensing unit by heterologous expression of alternative GPCRs, as well as engineering the receptors themselves was already extensively reviewed in literature [308,315]. It was shown that the $Ste2_{Sc}$ receptor could be replaced with heterologous Ste2 receptors from other yeast species, including infectious species, and that they could be used as biosensors. Based on the approach of heterologous expression of G protein-coupled receptors, major food fungal pathogen GPCRs could be expressed and the pathway activity was coupled to the production of colorful lycopene to obtain a functional ready to use and easy readout biosensor for peptides of other species (Figure 28) [318].

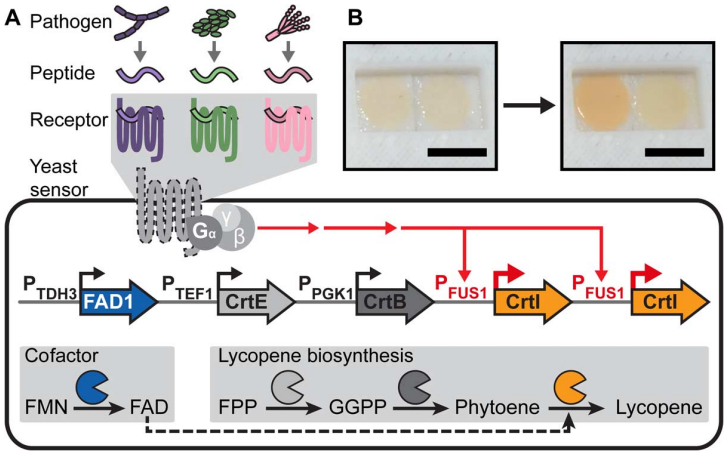

Figure 28: Function, genetic design, and results of the low-cost biosensor for pathogenetic fungi. A) Using the pheromone peptides of pathogenic fungi as a diagnostic indication. The genetic design shows that upon stimulation of the heterologously expressed GPCRs, lycopene is expressed for signal generation upon cognate peptide binding. **B)** Positive test result of the biosensor. Adapted from [318].

The heterologous expression of fungal pheromone-responsive GPCRs was also established as a basic research tool, for instance to study pheromone receptor induction in *Schizophyllum commune* that possesses more than two receptor-pheromone systems [319]. An important basis for future synthetic biology applications was also the investigation of crosstalk among different *Candida* species [320].

Further, the wiring of heterologous GPCRs originating from plants, insects, and mammalian cells to the yeast mating pathway can be achieved [321]. Generally, structural and functional similarities between the Gα subunit of *S. cerevisiae* and mammalian cells allow the expression of GPCRs from higher organisms in yeast [301]. In some cases, though, heterologous expression of unadjusted GPCR resulted in false localization or degradation [315]. It was found that the N-terminus of the GPCRs plays an important role in translocation as well as for receptor stability [322]. In order to successfully express heterologous GPCRs in *S. cerevisiae*, it had been shown that adjusting the N-terminus of the heterologous GPCRs was beneficial [323]. Also, the C-terminus of GPCRs is of high

importance for the interaction with downstream G proteins and thus of interest to enable functional heterologous expression of GPCRs [324]. Many mammalian GPCRs are linked to a specific Gα protein, acting as a threshold system which needs to be replaced or adjusted to be functional in a heterologous chassis like yeast [325]. Therefore, replacement of the Gα protein with the native homolog from *S. cerevisiae*, the implementation of other mammalian Gα proteins, or utilization of chimeric Gα proteins from yeast and mammals was examined [302,326–330]. Ten yeast-mammalian Gα protein chimeras were obtained by exchanging the five C-terminal amino acids of the yeast Gα protein with mammalian residues. Using this approach, the functional expression of a mammalian GPCR and downstream mating pathway-coupling was accomplished for the first time in *S. cerevisiae*. [302].

With the achievement of successful coupling of heterologous mammalian GPCRs in yeast with the mating pathway, the human neurotensin receptor could be expressed. It was shown that *S. cerevisiae* cells that were expressing this heterologous receptor were able to mate upon neurotensin stimulation. Interestingly, here no chimera development was required to enable interaction with the mating MAPK signaling pathway and this was therefore the first reported example of a mammalian receptor that replaced the Ste2 receptor though maintaining full signaling efficiency resulting in successful mating [331]. For other mammalian GPCRs, engineering the signal pathway was required, for example for the functional expression of the somatostatin receptor, or the lysophosphatidic acid receptor [327,330]. Successful heterologous expression of G protein receptors in yeast also allowed the development of biosensors to detect the GPCRs of major human, plant, and food pathogens [318]. Also, the expression of heterologous GPCRs in *S. cerevisiae* as a chassis allowed high throughput screening of pharmacological substances that affect these GPCRs in the yeast model organism [203,332,333]. GPCRs are of high interest as drug targets, since many modern therapeutics target as antagonists or artificial substrates the GPCRs and therefore represent potential treatment strategies [334].

It has also been shown that even olfactory receptors, that are also members of the GPCR family, can be functionally expressed in yeast and coupled to the mating signaling pathway [335]. To successfully express and couple olfactory receptors, the N- as well as the C-terminus of the GPCRs were replaced with regions from the rat I7 receptor. Additionally, the G protein was adjusted and taken together, these adaptions considerably improved the expression, functionality as well as localization of this GPCR. Apart from the heterologous expression of an olfactory receptor that sensed DNT, they also decoupled the GPCR from the yeast mating pathway by replacing the processing unit with the human cAMP response element-binding protein (CREBP) that activated their output signal [336]. This study highlighted that *S. cerevisiae* can also serve as chassis for GPCR expression that are not coupled to the native MAPK signaling pathway. However, the activity and sensitivity of the receptors was below prior expectations. By co-expressing the odorant-binding proteins from the silkworm, the sensitivity of heterologously expressed olfactory receptors was improved. These results indicated that accessory proteins can improve GPCR expression in yeast[337].

Besides the expression of heterologous GPCRs and their coupling to the native mating MAPK signaling pathway, they can also be engineered using directed evolution approaches to generate novel GPCRs [53,338,339]. The human glucose GPCR was heterologously expressed in *S. cerevisiae* and

evolved to specifically discriminate between multiple ligands. Using different resulting GPCRs in pairwise manner, it was possible to detect different compounds in a solution [340]. As previously highlighted, GPCRs are important drug targets, therefore it is not surprising that many of the directed evolution projects investigated pharmacogenomics [334]. Similar strategies could be used for the directed evolution of GPCRs for biosensing, addressing low stimulation of the natural compound as well as low basal stimulation. Therefore, it might be also important to not only target and evolve the GPCRs themselves but also the downstream G proteins, if applicable [307]. It is not only possible to evolve heterologously expressed GPCRs in *S. cerevisiae* but also the native Ste2 receptor, in order to sense a different target compound. The first example of directed evolution of a peptide-sensing GPCR was performed by Adeniran *et al.* [307]. Interestingly, they performed a primary screen of the mutated Ste2 receptor with chimeric ligands before screening with the diagnostically relevant Cystatin C. The results validated their model and indicated a general strategy for directed evolution of peptide-stimulated GPCRs (Figure 29) [341].

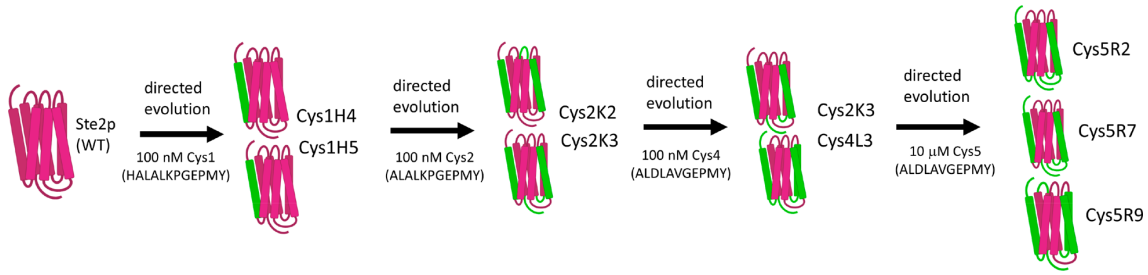

Figure 29: An abstraction of the substrate-walking directed evolution strategy of the Ste2 receptor. Adapted from [341].

A non-medical application of the GPC receptors in yeast is their employment as sensors in metabolic engineering. With the development of a sensor as well as a producer population, it was shown that the most efficient serotonin producer cells could be selected. In the sensor cells, upon serotonin stimulation of the GPCRs, the mating MAPK pathway was induced resulting in downstream reporter gene expression (Figure 30) [342].

A similar approach was taken to screen for medium-chain fatty acids by heterologous expression as well as mating pathway-coupling of a mammalian GPCR in *S. cerevisiae* [343]. Generally, directed evolution can also be utilized to gain a better understanding of GPC receptors. The $Ste2_{Sc}$ receptor is the optimal model for extended investigations, to get more insights into structure, functionality, and general principles of GPCRs. Mutating the $Ste2_{Sc}$ and screening for altered binding affinity as well as downstream mating pathway activity upon cognate or non-cognate α-factor stimulation disclosed two evolutionary paths. The first path reflected the binding affinity of the GPCR receptor towards the α-factor, while the second path was based on the signal transduction mediated by the stimulation of the receptor [344]. To reduce experimental workload for drug screenings and biosensor development, results from directed mutagenesis studies and the knowledge about structural and functional similarities of GPCRs were also implemented into the models [345]. Altogether, many approaches have been taken to study and utilize the Ste2 receptor and other GPCRs in *S. cerevisiae* for fundamental research but also for the development of various applications.

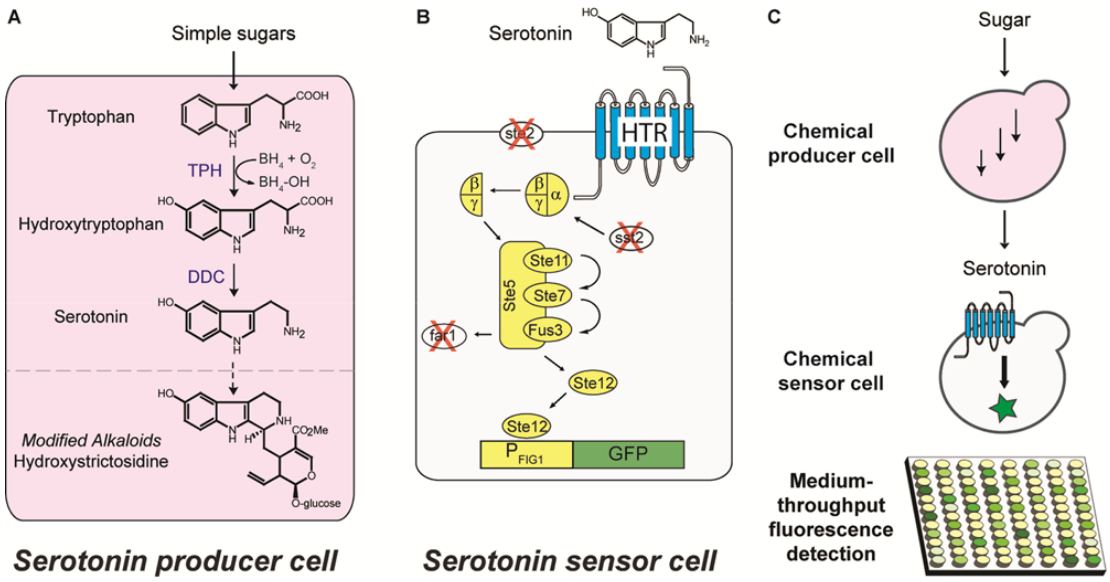

Figure 30: The workflow of a medium-throughput screen using yeast as compound producer as well as the sensor by expressing a GPCR. A) Production pathway for serotonin in yeast. **B)** Using the serotonin-sensitive GPCR receptors (HTR) and coupling to the mating MAPK signaling pathway in the sensor cells. **C)** Workflow of the medium-throughput screen. Adapted from [342].

1.6.3 Processing unit

By using traditional genetic approaches like the establishment of large knockout collections, most singling components of the yeast mating pathway have been identified and are well understood [346]. The MAPK signal transduction is based on cascading sequential activations of three kinases. MAPK activates via phosphorylation the MAPKK that subsequently phosphorylates and thereby activates the MAPKKK, that then initiates the cellular regulatory mechanisms [22]. In general, rational signaling pathway engineering is a promising approach and of interest and since the *S. cerevisiae* mating MAPK signaling pathway is very well understood, it is a suitable model system to explore these possibilities [347–349]. Many computational models supporting the understanding of MAPK singling pathways in yeast are available that can be adapted to guide engineering attempts [350,351]. Engineering signaling transduction pathways is advantageous in comparison to genetic networks, since they rapidly respond, allow applications within the pathway by the implementation of kinase feedback loops, they exhibit spatial and subcellular responses within the cell, and are overall highly modular [352].

One signal transduction engineering approach was taken by incorporating heterologous components and therefore replacing native parts within the signal transduction pathway in *S. cerevisiae* [353–355]. These studies emphasized the modularity of the yeast mating MAPK signaling pathway and laid the foundation for synthetic biology applications, like its employment for drug screenings [356]. Apart from the heterologous expression of pathway components, signaling proteins were directly targeted or engineered. One example was the usage of optogenetic tools in the mating pathway. Several studies have highlighted the advantages of light-inducible dimerization of the LOV2 domain tags from *Avena sativa*. Based on the LOV2 domain and an engineered PDZ domain, a tunable and light-inducible light dimerization tag (short TULIPs) was developed to be used in

the yeast mating pathway [357]. Examples include the attachment of the PDZ domain to Ste5, which was mutated to no longer bind the G protein, or addition of the PDZ domain to Ste11, or the heterologous expression of the membrane associated LOV2 domain. Upon light stimulation, the LOV2 domain recruited the engineering PDZ-Ste5 protein or the PDZ-Ste11, resulting in an activation of the mating pathway and expression of the mating phenotype. Attachment of the PDZ domain to Cdc24 led even to controlled directional shmooing of the cells upon localized light stimulation [357]. It is also possible to rewire the mating pathway resulting in a depletion of the evolved stimulus-response causality. For example, Ste11 is involved in two MAPK pathways, the osmoresponse as well as the mating signaling pathway. In case genes of the osmoresponse or mating MAPK signaling pathways were knocked out, increased signal crosstalk between both pathways was observed [358,359]. Normally, specific scaffolding proteins, inhibitors, or kinetic insulators prevent signal crosstalk [360]. Taking this into consideration, synthetic biologist wanted to rewire the MAPK signaling pathway in a predicted fashion by targeting and engineering the scaffolding protein Ste5. By using Ste5 mutant scaffold proteins that could not recruit Ste11 (MAPKKK) and Ste7 (MAPKK) kinases anymore, they reverse-engineered artificial kinase recruitment by using PDZ domain-mediated recruitment [282]. They also engineered an artificial kinase-kinase recruitment by attaching the PDZ domain to the kinase that could still be recruited by Ste5, thereby also recovering the mating efficiency (Figure 31) [282].

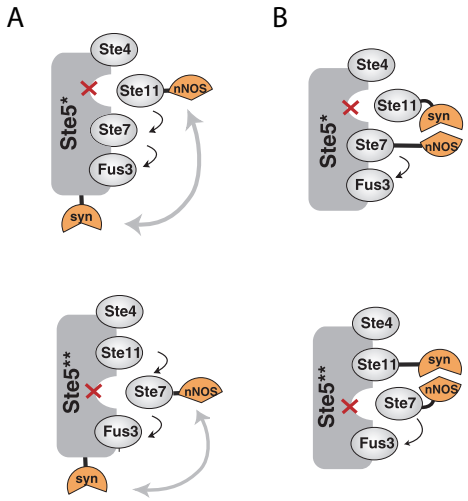

Figure 31: Schematics of the reconstitution of the Ste5 scaffold using a heterologous PDZ domain. A) Reconstitution of Ste5 using the scaffold-kinase recruitment design. **B)** Reconstitution of Ste5 using the kinase-kinase recruitment design. Adapted from [282].

Taking this approach even further, they accomplished the engineering of a non-natural signaling pathway, meaning, they rewired the signaling cascade to obtain an osmolarity response upon pheromone stimulation. To do so, they fused the mating scaffold protein Ste5 to the osmoregulator scaffold protein Pbs2. This fused scaffold was further modified to not interact with Sho1, the upstream osmoregulator, and with Ste7, thereby triggering the mating phenotype. The engineered MAPK signaling pathway was shown to be functional since the harboring cells were only able to survive an osmoshock when they were previously stimulated with α-factor (Figure 32) [282].

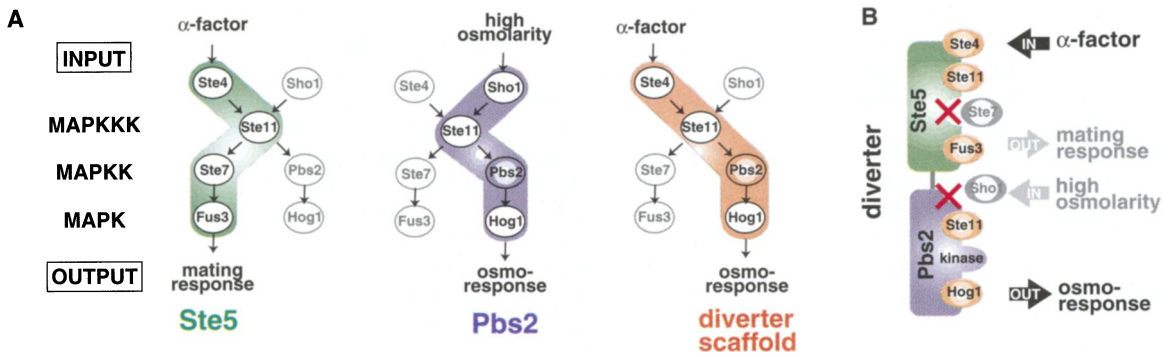

Figure 32: Abstraction of the mating and osmolarity shock MAPK signaling pathways as well as the engineered diverter scaffold pathway and system in detail. A) Visualization of the mating and high osmolarity signaling pathway with the MAPKKK Ste11 as important node, and the signaling pathway with the engineered diverter scaffold protein. **B)** Detailed visualization of the diverter protein. Adapted from [282].

Further pursuing the MAPK pathway engineering, they implemented a synthetic recruitment site by attaching a zipper to the scaffold protein Ste5 as well as Msg5 and Ste50, enabling an additional regulation of the MAPK signal transduction (Figure 33) [361]. The synthetic recruitment site blocked the propagation of the signaling cascade upon Msg5 (negative modulator) binding, resulting in no or strongly reduced mating phenotype upon α-factor stimulation. It was also possible to recruit the engineered Ste50 (positive modulator), which promoted the MAPK signaling pathway, resulting in an enhanced pathway output upon α-factor stimulation [361]. The negative feedback was additionally engineered by transcriptional up-/downregulation or affinity altering of the leucine zipper of Msg5. Following, a decoy module was expressed acting as competitors to Ste5 allowing the implementation of further response behaviors. Taken together, they compiled a set of recruitment approaches, enabling the establishment of versatile response behaviors, including a pulse generator, an accelerator, delay response, or an ultrasensitive switch [361].

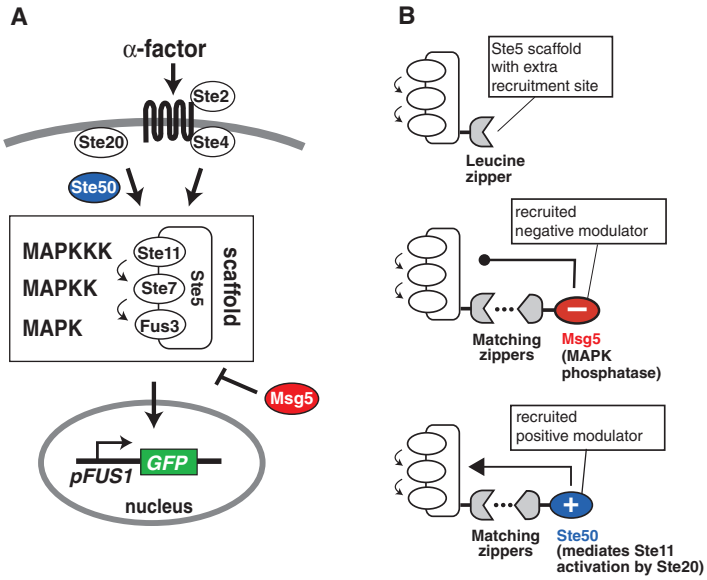

Figure 33: Output tuning of the yeast MAPK signaling pathway using artificial modulator recruiting. A) Signaling cascade upon Ste2 stimulation by α-factor resulting in downstream gene expression regulation. **B)** Synthetic pathway modulator recruitment to Ste5 through leucine zipper interaction. A positive and a negative modulator were engineered. Adapted from [361].

Altering and engineering the mating MAPK singling pathway was also utilized to address basic research questions, which were important for subsequent applications. By *in vitro* reconstitution of the signaling pathway, the role of the scaffold protein Ste5 was further examined. A minimal scaffold version of Ste5 that binds Ste7 well and has only weak binding affinity for Fus3 was constructed. Experiments revealed that Fus3 has to be catalytically unlocked by Ste5, resulting in a significant (about 5000-fold) increase of the phosphorylation of Fus3 by Ste7 [362]. Research on functional characteristics as well as insulation mechanisms were continued and data were obtained supporting the model that Ste5 supports conformational switching to streamline the information flow. This means, Ste5 insulates the mating signal from other signaling pathways like the starvation signal, that could highlight a strategy to block information crosstalk in signaling pathways that share components [363].

As previously highlighted, scaffolding proteins exhibit great potential for signaling pathway engineering but to unleash their full potential, a comprehensive understanding, especially of their modularity, is required. By deploying a directed evolution approach, Lai and colleagues generated a library of randomly shuffled protein interaction domains [364]. Interestingly, they identified different engineered protein interaction domain variants that were capable of processing the mating signal in Ste5 deletion strains [364]. These finding laid the foundation for the engineering of signaling scaffold proteins that could be highly beneficial in engineered signaling pathways, including the mating pathway. Also, the engineering of artificial signaling pathways with new and different dynamic properties and competences was facilitated by their directed evolution approach. Apart from synthetic biology approaches, their attempts and other signaling pathway rewiring approaches can also be adapted to address basic research questions [364]. Examples of signaling pathway rewiring that shed light on the native essential and non-essential roles of a protein, was the rewiring of the osmoregulation signaling MAPK pathway unraveling the role of Hog1 [365]. Beside the signal processing in a MAPK pathway, complex spatial arrangements within the cell take place [366]. These arrangements can be also employed for synthetic biological application to spatially arrange specific proteins within the cell upon signal stimulation.

Within the processing unit, also the decision-making process of the cell fate takes place, which is controlled by several regulators [367]. When these regulators are engineered, the cell fate can be rationally controlled. In the native system, the cell fate, meaning to mate or not to mate, is based on receptor stimulation as a function of pheromone concentration in relation to the abundance and distance of the opposite mating type. Experiments revealed that Ste4 is as MAPK promoting and Msg5 is MAPK repressing regulator protein [367]. By controlling the expression and transcript stability of Ste4 and Msg5, the cell fate decision under different α-factor concentrations could be controlled. By further optimizing the system, a tradeoff between tunability and system's robustness was achieved, resulting in the control of three distinct cells fates, the MAPK on, the MAPK off and the MAPK wt fate [367].

Overall, much is known about the signaling processes within MAPK pathways in *S. cerevisiae* and more specifically on the mating signaling pathway. Many different engineering approaches have been taken, providing a broad base of knowledge for further artificial interferences.

1.6.4 Downstream unit

Subsequent to the MAPK signaling pathway, the Fus3 MAP kinase interacts with different transcription factors, namely Ste12, Dig1, and Dig2 [368]. Reduced expression of Dig1 and Dig2 resulted in stabilization of Ste12 and thus subsequently promoted the transcription of downstream genes [368]. The best studied Ste12 is a transcription factor that interacts with different other transcription factors and subsequently regulates gene-specific expression [369]. Ste12 served repeatedly as starting point for transcription factor engineering by combining this pheromone-induced transcription with innovative approaches in transcription factor engineering [369]. Also, a small domain of the Ste12 protein that depends on the activation of the MAP kinase pathway had been identified [369]. To identify this minimal pheromone response element of Ste12, Pi and colleagues constructed several hybrids proteins of Ste12 and the DNA binding domain of Gal4. Doing so, they obtained a pheromone-responsive transcription factor that could bind the operator sequence of the *GAL4* promoter instead of the Ste12 induced promoter sequence [369]. They also engineered a hybrid transcription factor by combining the Ste12 phosphorylation domain, the synthetic B42 activation domain and the bacterial LexA DNA binding protein [343,370]. Upon pheromone-induced phosphorylation of the Ste12 domain of the artificial transcription factor, it bound to an engineered promoter consisting of a synthetic minimal promoter and four LexA binding sites [343]. The kinetics of the promoter that bound Ste12-Gal4 and Ste12-B42-LexA could be altered by varying the number of DNA binding sites, resulting in different dose-response dynamics. The engineering and characterization of artificial minimal promoters in yeast that do not exhibit homologies to natural yeast promoters contributed also to the provision of inducible promoter systems [371]. Apart from the implementation of DNA binding domains from other transcription factors, it is also possible to utilize artificial DNA binding domains. It has been shown that zinc fingers combined with a transcriptional activation domain and a protein interaction domain can act as artificial transcription factors with an engineered DNA binding motif [372]. Employment of this system revealed that the Ste12 DNA binding domain could be replaced with a zinc-finger motif to obtain an artificial transcription factor acting like Ste12 [220]. These engineered pheromone-induced transcription factor bound a synthetic promoter containing the corresponding zinc finger-responsive element [220]. These two examples highlighted that tools that were not directly engineered to be used in the yeast mating pathway can be adapted to it. The downstream unity engineering approaches and available tools in *S. cerevisiae* are numerous and could be further expanded to be used with its mating pathway.

1.6.5 Systems level

In most previous cases, the components within one unit were altered to obtain new to nature functions. By rewiring the natural mating MAPK signaling pathway it was possible to obtain a cell density-dependent gene expression as it is naturally observed for quorum sensing [373]. In their initial genetic design, the α-factor was expressed from a pheromone-induced promoter and therefore, a positive feedback loop was obtained when a threshold cell density was reached. In a secondary design, the *mfα1* or the *mfα2* gene were expressed from a promoter that could be induced by aromatic amino acids, resulting in a density-sensing behavior. In case the barrier protease was not expressed, the system exhibited a rather linear response compared to digital dynam-

ics, when the protease was expressed [374]. The cell density-dependent expression of genetic constructs has a great potential for biotechnological applications. It was for example shown that the system could be linked to the autonomous expression of RNA interference that required the metabolic flux in a production cell, here, towards the shikimate pathway to produce PHBA [373].
The mating system from yeast was also already utilized and adapted for other synthetic biology approaches. To engineer a multicellular memory device, a pheromone-induced NOT logic system was implemented [375]. The α-factors as well as the corresponding GCPRs from *C. albicans* and *S. cerevisiae* were split into two population (Figure 34). In case the cognate α-factor bound the GPCR, the stimulation resulted in the expression of LacI that subsequently repressed the production of the respective other α-factor. When these two populations were cocultured and induced with either α_{Ca}-factor or α_{Sc}-factor, the system's output was set to an "On" or "Off" state. After α-factor removal, the multicellular system was turned off and then autonomously returned to the state prior α-factor removal, exhibiting the memory capacities of the system. To switch from the α_{Ca}-factor-induced memory "On" state to the "Off" state, induction with the α_{Sc}-factor was required or by addition of the barrier protease $Bar1_{Ca}$ that removed the α_{Ca}-factor [375].

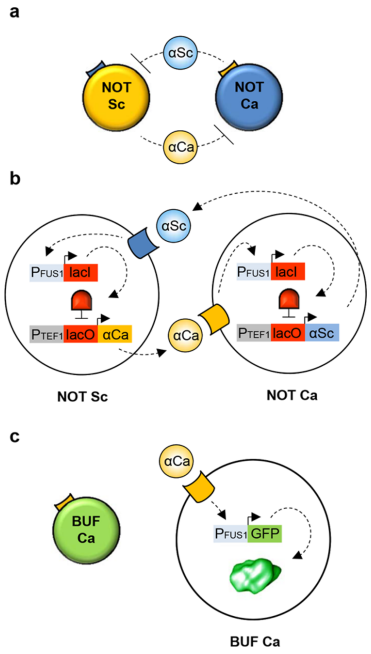

Figure 34: Abstraction of the genetic design of the multicellular memory system. A) Abstraction of the multicellular memory system representing the NOT Sc and NOT Ca system. **B)** Genetic design and cellular interactions of the multicellular memory system. **C)** Abstraction of the genetic design and molecular activity of the reporter cells of the system. Adapted from [375].

By utilizing characterized α-factors and Ste2 receptors, in another study, Billerbeck and colleagues implemented different multicellular networks including a scalable ring, a bus and a tree-like multicellular network topology [220].
These examples highlighted how different heterologous mating pathway components can be combined to obtain new systems. The implementation of pheromones and barrier proteases into multicellular systems bears a lot of the potential for instance for medical applications. The yeast mating pathway could serve as model to explore the correlation between the network architecture and the resulting output. A glucose-induced promoter was for example utilized to induce

α_{Sc}-factor production that in return induced the expression of a reporter gene, or the production of pharmaceutical substance like insulin or glucagon [376]. The network dynamics confirmed a preceding model. They also added a repressive network node that served as modulator. It consisted of a Bar1 that degraded the α_{Sc}-factor that was in turn induced by a second signaling molecule, the α_{Ca}-factor [376]. Using this network architecture, the dynamics could be altered. Depending on the population composition, the output signal could be fully repressed or reduced. The results indicated the importance of the composition of and the ratios within multicellular networks [376]. Implementing α-factors of yeast as wiring molecules in eukaryotic multicellular systems is a promising approach to obtain for example a division of labor-like systems or to distribute biological computations. Regot *et al.* showed that the computation of complex logic gates could be distributed among several cells [158]. The input signals of these multicellular logic networks were transcriptional inducers or repressors. Depending on the network architecture, addition of the input signal led to the expression/repression of α-factor production or inhibited/promoted the signal processing in the α-factor responding cells. Here, the yeast mating pathway served as signal communication system with all its components of all units. When the system was extended by other α-factors it was also possible to wire the gates together and to perform more complex computations [158].

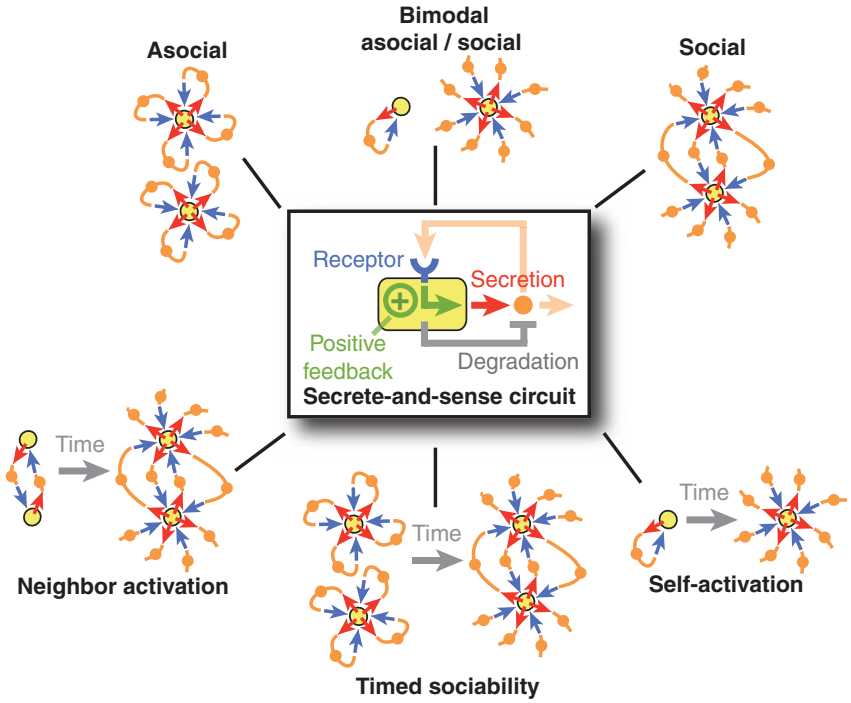

Figure 35: Overview of the different population behaviors that can be generated with the secrete-and-sense circuit. Adapted from [378].

This study further served as basis for a theoretical quantitative study, resulting in a kinetic model of several gates. Using deterministic as well as stochastic frameworks for the model, the most sensitive parameters were identified allowing the design of multicellular networks that can respond to three discrete inputs [377]. Using the yeast mating pathway as a model, a deeper understanding of the relationship between the communication circuit motif and the population behavior was obtained [378]. To mimic different naturally occurring circuit motives, the extracellular and

sensing unit were modified. For one motif including a positive feedback regulation, self- and neighbor-communication were examined both for low and high cell density conditions. The results revealed that Ste2 and α-factor expression with a strong positive feedback at low cell densities led to self-communication. For high cell densities, Ste2 and α-factor expression with a weak positive feedback resulted in neighbor-communication while for a strong positive feedback, self- and neighbor-communication could be observed. When this network motif was extended by the tunable expression of a Bar1 protease that degraded the α-factor, the population behavior was modulated. At low cell densities with a strong positive feedback, instead of self-activation a bimodal activation was observed. The same result was also obtained for high cell densities and weak positive feedback, while for low cell densities, low neighbor activation occurred. Feeding the results into a mathematical model revealed that with their circuit motif population behaviors including asocial, social, bimodal, neighbor activation, timed sociability and self-activation behavior can be obtained (Figure 35) [378].

Another example demonstrating the use of the mating pathway was the engineering of a multicellular network of sensor-actor systems. A multicellular sensor-actor system was split between two populations, thus sensing, and response were distributed [379]. Besides the implementation of multicellular systems using the mating pathway for signal transition, the temporal and spatial properties of the mating pathway can also be employed to build biosensor systems. The control of distance and ratios of sensor and reporter cells allows the exploration of additional network dynamics. Detailed analysis and data collection thus enabled the implementation of mathematic models that fostered the engineering of multicellular systems, taking the spatial and temporal dimension into consideration [380]. Generally, validated mathematical models represent a valuable approach of facilitating the establishment of functional multicellular networks, also ones based on the yeast mating pathway. Hoffmann and colleagues utilized a rather simple multicellular yeast network, consisting of a sender population secreting the α-factor and a receiver strain that responded to the stimulus by expression a reporter gene. Based on the experimental data, their mathematical model was parameterized allowing subsequent predictions of the growth dynamics and the overall system's behavior [381].

In order to use or even combine the different presented engineering approaches within the units, an understanding of the interplay on a systems level is essential. A recent retrosynthesis approach of the GPCR signaling pathway generated a model strain to study the core singling elements and it demonstrated the possibility of tuning the GPCR singling pathway [382]. By varying the expression of key components, Shaw *et al.* were able to tune the sensitivity, basal activity and signal amplitude of the response network, which was also reflected in their model (Figure 36) [382].

Using their different tunable parameters, they demonstrated the implementation and rapid improvement of a heterologously expressed GPCR from *S. pombe* in *S. cerevisiae*. Their optimization improved tightness, sensitivity, operational range, maximal output, and dynamic range. Having biosensor applications in mind, Shaw *et al.* addressed the need for a linear and digital response of the GPCR pathway [382]. By expressing different levels of an adenosine-responsive GPCR and through promoter output tuning, they established a heterogeneous population to obtain an average linear output response and thus a suitable biosensor for the medically relevant metabolite adenosine [382]. For the sensing of melatonin, a digital response was required, which was realized

by an amplifier-like two strain population network. The sender cells produced α-factor upon melatonin stimulation of the corresponding GPCR. The receiver cells responded to the α-factor and additionally constitutively expressed the barrier protease Bar1 to obtain an activation threshold [382].

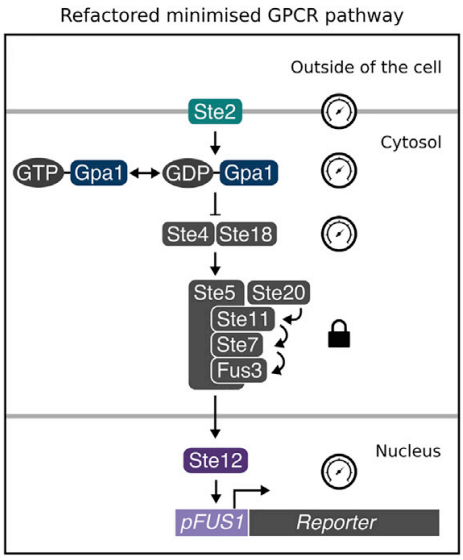

Figure 36: Schematic overview of the refactored and minimized GPCR signaling pathway, including titration possibilities of the pathway components. Adapted from [382].

Altogether, the well characterized yeast mating pathway was already used for several synthetic biology studies [383]. Engineering approaches within the different units have highlighted its great potential, modularity, and range of possible applications based on the yeast mating pathway. Altering the extracellular unit by expressing heterologous α-factors and in some case barrier protease opened up the opportunity to utilize them as wiring molecules and quenching enzymes for cell-cell communication. These systems were further used to engineer multicellular networks as well as to gain a deeper understanding of how circuit motives influenced population behavior [378]. The heterologous expression of GPCRs (extracellular unit) in yeast facilitated tool development for GPCR-based drug screenings with great pharmacological importance [342]. By engineering components of the processing unit, design features of the MAPK signaling pathway were obtained that can be further used to engineer cellular responses on a protein level [348]. Linking the yeast mating pathway to downstream networks further extended its implementation into potential applications. Apart from the plethora of success stories previously highlighted, the potential of the yeast mating pathway has not been fully unleashed yet. Most of the prior approaches altered components of maximally two units, most likely due to a lack of easy incorporation and standardization of the different available engineered units. After they have been overcome, the potential applications of the yeast mating pathway in synthetic biology are innumerable.

1.7 Aim of this dissertation

Saccharomyces cerevisiae is one of the oldest but still one of the most used model organisms in basic as well as in applied research [21,26]. For synthetic biology, *S. cerevisiae* became the eukaryotic workhorse for metabolic engineering, rewiring of cellular signaling, protein scaffold and translocation engineering as well as for biosensor applications [45,318,382].

Thus, the overall aim of this thesis was to extend and contribute to the existing synthetic biology research tools for *S. cerevisiae* and to provide the research community of synthetic biologists working with yeast novel capabilities for basic and applied research projects. Therefore, we developed two projects, one targeting the establishment of *S. cerevisiae* for non-native secondary metabolite production, while the aim of the second project was to introduce a yeast communication toolkit.

1.7.1 Engineered production of short-chain acyl-coenzyme A esters in *S. cerevisiae*

As previously highlighted, *S. cerevisiae* has already been engineered to be a versatile host for the production of several natural and engineered small molecules that belong to wide biochemical classes such as flavonoids, isoprenoids, alkaloids, and polyketides [51,384–386]. However, a limiting factor for the plug and play production of various high-value chemicals is a limitation of biosynthetic precursors, like the lack of a number of short-chain acyl-CoA metabolites that are required in the biosynthesis of many pharmacological and economically important compounds. To secure the potential usage of *S. cerevisiae* as chassis for the production of many valuable compounds, we engineered yeast to produce five platform short-chain acyl-CoA esters [123]. We determined to produce isovaleryl-CoA, which is incorporated into some polyketides; butanol-CoA and hexanoyl-CoA, which are for example required for the production of cannabinoids; propionyl-CoA that is important for odd-chain fatty acids production and serves as polyketide starter unit; and methylmalonyl-CoA, an essential extender unit for example utilized by the DEBS PKS [52,387–390]. To meet our objectives, we implemented the production of isovaleryl-CoA via the branched-chain α-keto acid dehydrogenase complex pathway (BkD) originating from *B. subtilis* and the alternative isovaleryl-CoA biosynthetic pathway (AIB) of *Myxococcus xanthus* [391]. For the establishment of the production of butyryl-CoA and hexanoyl-CoA we adjusted the previously engineered butyraldehyde and butanol production pathway [389,392]. To ensure of propionyl-CoA and methylmalonyl-CoA production we engineered the established propionate feeding-dependent biosynthesis route as a benchmark pathway as well as the feeding-independent 3HP and 3HP-CCR pathway branching off malonyl-CoA [125,393–395]. For future pathway optimization approaches we established a CoA ester engineering toolkit by domesticating a selection of suitable genes to be cloned into the pathways using the commonly used Golden Gate cloning standard of the yeast toolkit of Lee *et al.* [71]. Taken together, with this study we aimed to lay the foundation for the successful engineering and establishment of *S. cerevisiae* as production host for the next wave of bio-based molecules [123].

1.7.2 Yeast communication toolkit - YCTK

After the implementation of metabolic pathways and artificial genetic circuits into living cells, researchers quickly aimed to build multicellular circuits to control population behavior and implement for example division of labor between different organisms in one culture [95,376]. Thus, a key function is the efficient information propagation between the different organisms, for example between sender and receiver cells. The majority of such systems has been installed in bacterial chassis and the examples in eukaryotic host organisms, including *S. cerevisiae,* remain limited. Compared to bacterial systems, for *S. cerevisiae* only a limited number of communication devices is available and so far, no standardized communication part collection has been established.

Therefore, it was our aim to contribute a set of different communication parts to the most commonly used Golden Gate toolkit in *S. cerevisiae,* which was previously provided by Lee *et al.* [71]. By extending the toolkit with eleven sender and receiver parts based on yeast α-factors and GPCRs as well as with seven barrier parts constituted by Bar1-like proteases that act like quorum quenching enzymes in bacteria, it was our objective to foster the rapid generation of multicellular systems in *S. cerevisiae*. In addition, we wanted to add a set of seven pheromone-responsive promoters, exhibiting different response dynamics for downstream gene expression regulation. To ensure and to facilitate versatile applications using this toolkit, one of our aims was to thoroughly characterize all parts with regard to crosstalk, modularity, and expression dynamics. Apart from the primary goal of establishing a communication toolkit for *S. cerevisiae*, we wanted to gain insights into coevolution and specificity of α-factor-mediated communication. Finally, our objective was to utilize the toolkit for proof of principle design and implementation of multicellular networks in *S. cerevisiae*. Taken together, here, we aimed to facilitate the engineering of multicellular networks in *S. cerevisiae* by, providing a characterized and established α-factor-based yeast communication toolkit.

2 Results:

2.1 Engineered production of short-chain CoA esters in *S. cerevisiae*

2.1.1 Pathway design

The construction of large genetic systems still requires a great amount of time. However, standardization and the allocation of tool boxes consisting of characterized parts or even customizable devices improved the turnover time tremendously. For the construction of the acyl-CoA expression systems we generated a small cloning library of pre-fabricated expression devices. This allowed fast and convenient cloning in a standardized fashion. The device collection was generated based on the yeast 2µ plasmids pRS425 and pRS424. This library contains pairs of glycolytic promoters and terminators to be combined with any gene of interest and to be further assembled into pathway cassettes of up to five expression units. The promoters were selected based on a reanalysis of a large promoter screen of Keren *et al.* [396]. The selected promoters are known to exhibit high expression levels of the controlled genes and are commonly used in metabolic engineering setups for the heterologous expression of pathway components. We selected the *TEF1*, *TEF2*, *PGK1*, *ADH1*, *FAB1*, and *TDH3* promoters. For the controlled expression of metabolic pathways, we additionally used different galactose-inducible promoters, namely the *GAL1*, *GAL10*, and *GAL7* promoters. To reduce the likelihood of homologous recombination within the pathway cassettes, we mostly collocated associated promoters and terminators in close proximity, meaning within the cassette, the promoter was directly downstream of its associated terminator. Overall, we ensured that the terminators were not placed downstream of their corresponding promoters. Generally, to avoid homologous recombination, heterologous DNA fragments containing similar sequences are integrated into different loci of the *S. cerevisiae* genome.

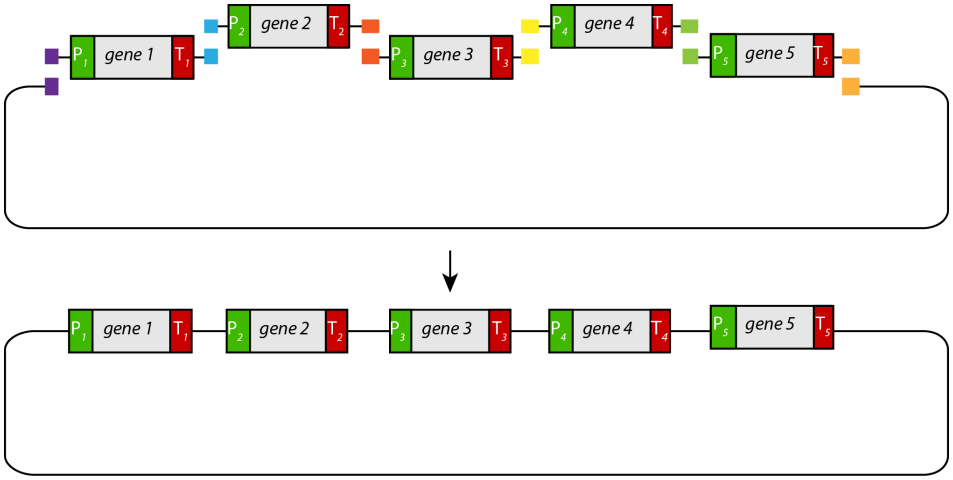

Figure 37: Pathway expression cassette design. Pathway plasmids were assembled as modular cassettes using CPEC, Gibson assembly or yeast homologous recombination and expressed from 2µ plasmids. Each fragment contains a promoter (P_1-P_5), gene, and terminator (T_1-T_5) as well as overlapping regions to flanking parts [123].

However, in this study, we assembled the different biosynthetic pathway genes into cassettes. This cassette design provides greater engineering flexibility and allows ultimately rapid integration into multiple loci if required. Here, we utilized the 2µ high-copy number plasmid system. The current plasmid library can be used to build pathways consisting of up to five genes (Figure 37). By using standardized primers that add standard homology arms to the different devices of the collection, final cassettes can be assembled using different cloning methods: yeast homologous recombination, Gibson assembly, or circular polymerase extension cloning (CPEC).

2.1.2 Optimization of acyl-CoA metabolite extraction

Acyl-CoAs are difficult to quantify in cell extracts because they are prone to hydrolysis and degradation. Thus, for unstable metabolites like acyl-CoAs, the development of a suitable and most importantly gentle extraction method is necessary. Since different methods available are not specific to acyl-CoA quantification in *S. cerevisiae*, we adapted and optimized a previously established metabolite extraction protocol [393].

We used the yeast strain expressing the AIB pathway genes as a test case for our method optimization efforts. We altered different steps in the extraction method, starting with testing different total optical densities of the harvested cells. The total optical density of cells can influence the cell lysing and thus metabolite extraction efficiency. We tested a total OD of 10 and 50 to compare the relative recovery. Next, we examined two cell lysis approaches: mechanical lysis using a homogenizer and solely chemical lysis combined with filtration. The filtration method allows a more rapid sample preparation and would be ideal for example for time course experiments. Last, we tested whether lyophilization for concentrating the acyl-CoAs in the metabolite extracts resulted in improved compound detection. To identify the best acyl-CoA extraction conditions, we tested all three protocol steps in all combinations. Figure 38 summarizes the different extraction methods (EM) tested and their relative extraction efficiencies. Our results showed that using mechanical force (i.e., homogenization) to disrupt the cell wall was necessary to achieve efficient extraction. Furthermore, we observed that concentration steps by lyophilization strongly reduced measurable titers up to 90% in our hands, probably due to acyl-CoA instability under tested conditions. From these results, we chose the extraction method EM3 as the standard extraction protocol for our study. EM3 is based on a total cell amount of OD 10, includes a bead beating step and recovers acyl-CoAs in almost 6-fold higher concentrations compared to the original extraction method EM1. Method EM3 was applied for all metabolite extractions. We quantified the concentration of each acyl-CoA ester based on a calibration curve of synthesized standards using LC–MS/MS and calculated intracellular metabolite pools taking cell concentration and extraction volume into account.

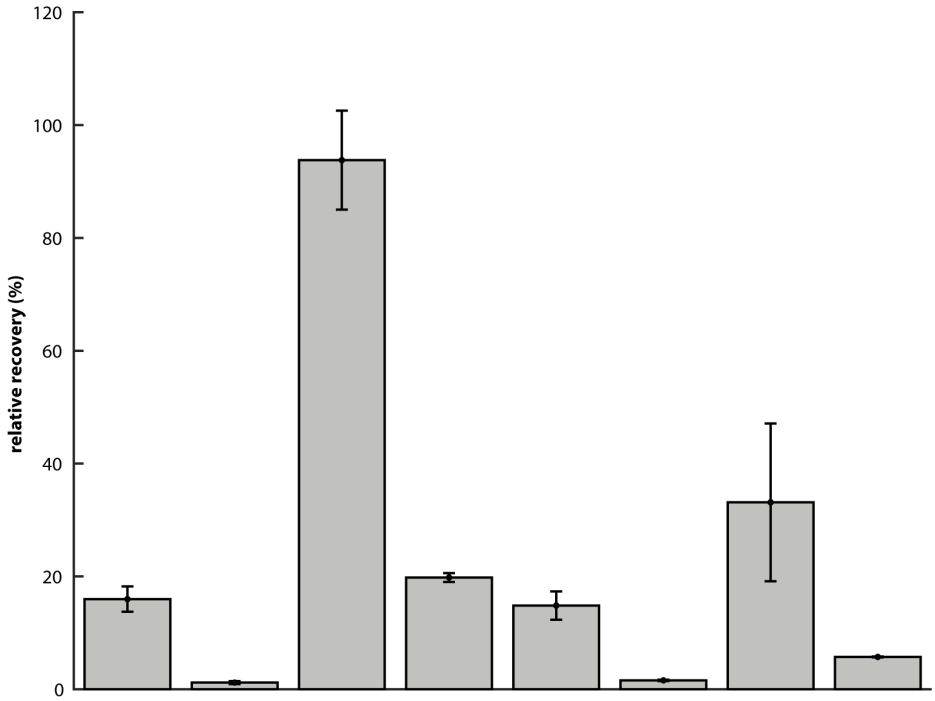

Extraction method	1	2	3	4	5	6	7	8
OD of cells	10	10	10	10	50	50	50	50
Filtration	x	x			x	x		
Centrifugation and homogenization			x	x			x	x
Lyophilization		x		x		x		x

Figure 38: Evaluation of several acyl-CoA extraction methods. Relative extraction efficiencies achieved for isovaleryl-CoA using different extraction methods (EM). For EM 1-4, a culture volume corresponding to a total OD of 10 was used; for EM 5-8, a total OD of 50 was used. For EM 1, 2, 5, and 6, cells were lysed using filtration and quenching. For EM 3, 4, 7 and 8, cells were lysed by homogenization in quenching solution. The extracted metabolite solution was additionally lyophilized in EM 2, 4, 6 and 8 and resuspended in 150 µl quenching solution. Bars show mean values of two biological replicates ± standard deviation with highest measured intracellular concentration set as 100% [123].

2.1.3 Isovaleryl-CoA production

Isovaleryl-CoA, a branched-chain acyl-CoA, is a commonly used precursor for the production of various secondary metabolites and can also serve as a branched-chain starter unit of some polyketides [387]. Certain bacteria, e.g., *B. subtilis*, *P. putida*, and *M. xanthus*, and plants, e.g., *Humulus lupulus,* produce branched-chain acyl-CoAs using various pathways [397,398]. These branched-chain acyl-CoAs are used for the production of branched-chain fatty acids, are incorporated into diverse bioactive compounds or used for the synthesis of long-chain hydrocarbons.

2.1.3.1 Branched-chain acyl-CoA pathway

The most common pathway in bacteria for the production of branched-chain acyl-CoAs, including isovaleryl-CoA, is via the branched-chain α-keto acid dehydrogenase complex (BCKDH-complex) that is used in the branched-chain α-keto acid dehydrogenase (BkD) pathway [399–401]. Besides the production of isovaleryl-CoA, we also wanted to produce isobutyryl-CoA and 2-methylbutyryl-CoA with the BkD pathway. The BCKDH-complex can be found in different bacteria, including *B. subtilis* [399]. The BCKDH complex originating from *B. subtilis* was previously isolated and biochemically analyzed [399]. Since the complex was previously used for the production of

branched-chain acyl-CoAs in *E. coli*, we also wanted to utilize the complex in *S. cerevisiae* for the production of branched-chain acyl-CoAs. To produce these, the amino acids valine, isoleucine, and leucine are required that are naturally produced by S. *cerevisiae* but could also be supplemented by feeding. These amino acids are made accessible for the BCKDH-complex by the Bat2 branched-chain amino acid transaminase of *S. cerevisiae*. This enzyme catalyzes the transamination of valine, isoleucine, and leucine to the corresponding 2-keto acids (Figure 39). The BCKDH-complex originating from *B. subtilis* consists of three major components: the decarboxylase (E1), the dihydrolipoyl acyltransferase (E2), and the flavoenzyme (E3) [399]. The decarboxylase consists of two homodimers that form a heterotetramer, and multiple of these heterotetramers are functional in the complex. It can be hypothesized that similar to the BCKDH-complex of *Azozobacter vinelandii*, for which the protein structure is available, the acyltransferase E2 consists of multiple trimers that form together the core of the multienzyme complex [402]. Several of the flavoenzyme E3 homodimers are associated with the core of the multienzyme complex [403].

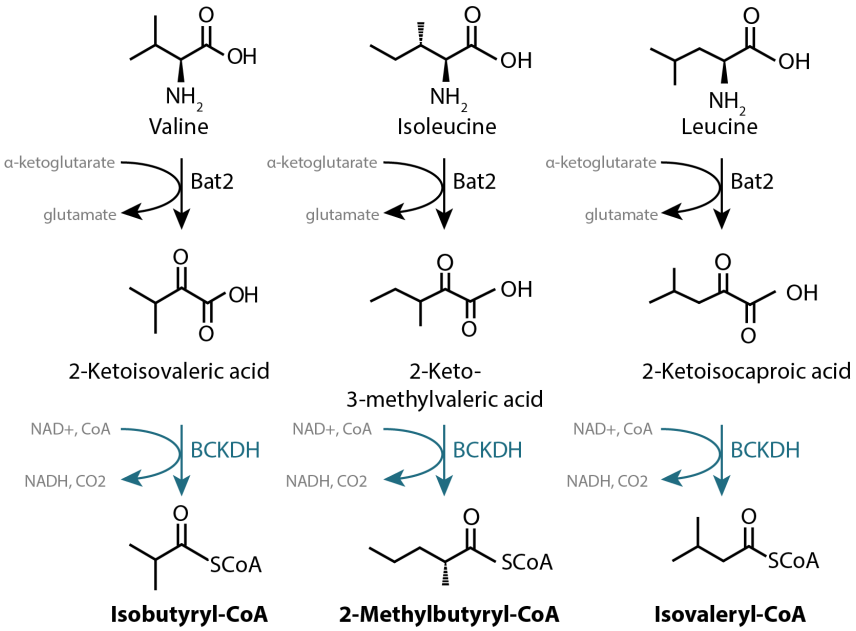

Figure 39: BkD pathway scheme. Biosynthetic pathway towards isobutyryl-CoA (ib-CoA), 2-methylbutyryl-CoA (2mb-CoA), and isovaleryl-CoA (iv-CoA) production: the protein Bat2 catalyzing the conversion of valine/isoleucine/leucine to 2-ketoisovaleric acid/3-keto-mehylvaleric acid/2-ketoisocaproic acid is native to yeast (black), whereas the BCKDH-complex originates from *B. subtilis* (turquoise).

The BCKDH-complex is a multienzyme complex that is catalyzing several reactions and therefore requires the cofactors vitamin B1, FAD and lipoamide. First, the branched-chain 2-keto acids are decarboxylated to branched-chain 2-oxo acids and an intermediate between the 2-oxo acids and the coenzyme thiamine diphosphate (vitamin B1) is formed. Subsequently, the substrate is transferred to the lipoamide. The substrate-lipoamide complex propagates to the next active site, where the branched-chain acyl-CoA is formed and the lipoamide is reduced. To recycle the lipoamide, it is oxidized in the presence of FAD and NAD^+ is reduced to NADH [404,405]. This showcases very well the high complexity of the reactions that are performed by the multienzyme complex. The different cofactors play a crucial role in the activity of this enzyme complex, especially lipoamide that is covalently bound to a lysine residue in the lipoyl domain of the second subunit

of the BCKDH complex. As in yeast, the lipoylation enzymes are localized in the mitochondrial lumen where they post-translationally modify the pyruvate and 2-oxoglutarate dehydrogenase complexes, we co-expressed the lipoyl ligase LplJ from *B. subtilis* to ensure cytosolic lipoic acid scavenging [406].

To express the BCKDH-complex and the supporting lipoyl ligase, we built a four-gene expression system (Figure 40). All genes were cloned into a pathway cassette, as previously described, on a high-copy 2µ plasmid. The lipoyl ligase *lplJ* gene was expressed by the *TEF1* promoter and terminated by T_{PGK1}. The gene for the E2 subunit of the BCKDH-complex, *bkdB*, was controlled by the *PGK1* promoter. The termination of the gene was ensured by the *ADH1* terminator. The first gene of the homodimer subunit of E1, *bkdAα* , was expressed by P_{ADH1} and terminated by T_{HXT7}. The gene of the other E1 subunit, *bkdAβ*, was expressed by the *FAB1* promoter and terminated by T_{TDH3}. As previously described, both subunits form homodimers first, and then build the heterotetramer of the E1 of the BCKDH complex. The gene of the last BCKDH-complex subunit E3, *lpdV*, was expressed by the *THD3* promoter and terminated by the terminator of *ACT1*. All genes together formed the BkD pathway expression cassette on a plasmid that was transformed into the BJ5465 strain background.

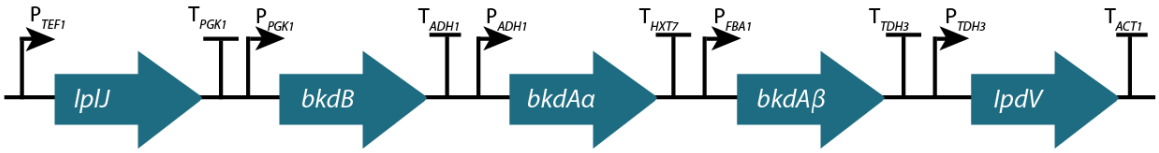

Figure 40: Scheme of the gene cassette encoding the BkD pathway enzymes. The engineered pathway contains five biosynthetic genes originating from *B. subtilis* and each gene was assembled with unique promoter and terminator pairs.

To ensure lipoic acid supply, we added 5 ng/mL lipoic acid to the production culture media. First, we tested the growth of three BkD pathway transformants. We observed that the maximal growth rate was reduced compared to the empty plasmid control strain and reached a maximal growth rate of about 0.2 1/h (Table 1). The reduced growth could be interpreted as an indication of the expression of the BCKDH-complex and the lipoyl ligase. Also, we hypothesized that this might be due to the fact of a metabolic burden of the pathway and the use of NAD^+. However, these hypotheses were falsified since no production of the branched-chain acyl-CoAs could be detected using LC/MS-MS [123]. The proteins were detected using shotgun proteomics (data not shown) in the soluble fraction of yeast cell lysate, which indicates successful expression of the BCKDH-complex proteins. However, the proteomics data did not indicate if the subunits were correctly assembled into a functional BCKDH-complex. We hypothesized that it is likely that no functional enzyme complexes were formed under the conditions tested.

Potential bottlenecks could be an unfavorable ratio of BCKDH-complex subunits and/or improper folding of its polypeptide chains as well as different expression dynamics preventing assembly of a functional BCKDH-complex. A labor-intensive optimization of the expression conditions could be performed to identify optimal expression ratios.

Table 1: Growth rates of acyl-CoA pathway-harboring strains. Growth was compared between the different *S. cerevisiae* BJ5465 strains carrying the acyl-CoA pathways. Propionate was supplemented for the strains harboring the PrpE or PrpE-PCC1 pathway. The strain harboring the BUT pathway was cultured in media with galactose as carbon source. A MATLAB script was used to determine the growth rate. The maximal growth rate in h^{-1} as well as the time point at which the maximal growth rate was reached are listed below. Normal growth was observed when carrying the empty vector pRS424.

Plasmid	Construct	Propionate feed in mM	Maximal growth rate in h^{-1}	Time of maximal growth in h
pRS424	Empty plasmid	0	0.35±0.004	11.3±1.0
pNK45	BKD	0	0.22±0.011	17.7±1.8
pNK23	AIB	0	0.22±0.008	15.7±1.5
pNK44	BUT	0	0.05±0.008	52.4±12.8
pNK30	3HP	0	0.16±0.065	25.2±10.3
pNK42	3HP-CCR	0	0.26±0.010	27.8±13.4
pNK36	PrpE	50	0.10±0.022	24.7±38.5
pNK37	PrpE-PCC1	50	0.17±0.043	17.2±8.8

2.1.3.2 Alternative isovaleryl-CoA biosynthetic pathway

Since no production of isovaleryl-CoA (iv-CoA) was obtained using the BkD pathway, we utilized another biosynthetic pathway that branches off the mevalonate pathway. This pathway was identified in *M. xanthus* by BCKDH knockout mutants that were still capable of incorporating iv-CoA into secondary metabolites [407]. This alternative isovaleryl-CoA biosynthesis (AIB) pathway may have evolved for the production of iv-CoA during sporulation since leucine is limited under these conditions [408]. Feeding experiments revealed that 3-hydroxy-3-methylglutaryl-CoA (HMG-CoA) was a compound in the biosynthetic pathway. The laboratory of Prof. R. Müller identified the non-active operon and renamed it alternative isovaleryl-CoA biosynthesis pathway [391]. This pathway is comprised of the HMG-CoA synthase, a transcriptional regulator, two subunits of a glutaconate-CoA transferase (AibA/B) as well as a dehydrogenase (AibC). In addition, they described the activity of the 3-methylglutaconyl CoA (MG-CoA) hydratase LiuC in the pathway [391]. The proposed and *in vitro* verified pathway starts with the dehydration of HMG-CoA by LiuC resulting in MG-CoA. The heterodimer of AibA and AibB then decarboxylates MG-CoA to 3,3-dimethylacrylyl-CoA (DMA-CoA) [391]. In the final catalytic step, AibC reduces DMA-CoA to iv-CoA by dehydration of NADPH to $NADP^+$ (Figure 41) [409].

When the AIB pathway is heterologously expressed in *S. cerevisiae*, it utilizes the central metabolite acetyl-CoA, which is naturally converted to acetoacetyl-CoA by the acetyl-CoA-C-acetyltransferase Erg10 by transferring an acetyl group from one acetyl-CoA to another. Similar to the HMG-CoA synthase in *M. xanthus*, native Erg13 in *S. cerevisiae* catalyzes the formation of HMG-CoA from acetyl-CoA and acetoacetyl-CoA. We then heterologously expressed LiuC, AibA, AibB, and AibC in *S. cerevisiae* for the production of iv-CoA. The AIB pathway has the advantage in comparison to the BkD pathway that no large multisubunit-containing complex needs to be expressed as well as no cofactors are required to be supplemented with the media.

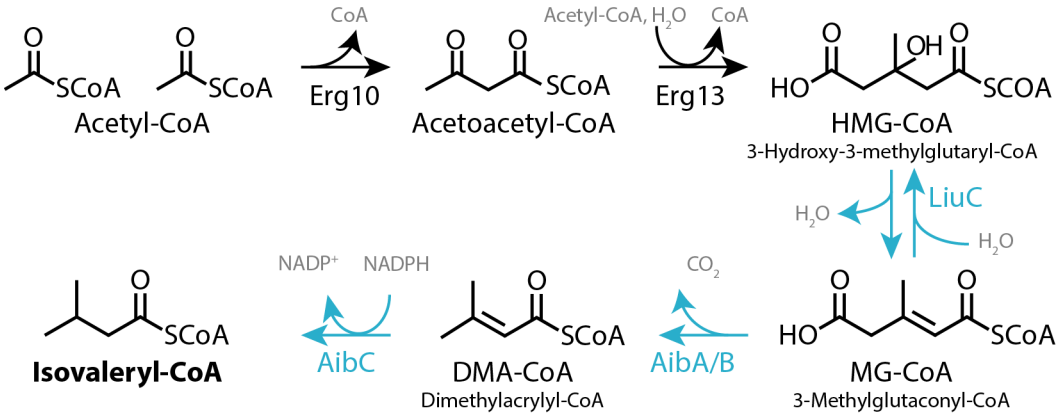

Figure 41: AIB pathway scheme. Biosynthetic pathway towards isovaleryl-CoA (iv-CoA) production: Proteins catalyzing the conversion of acetyl-CoA to HMG-CoA are native to yeast (black), whereas the 3-methylglutaconyl CoA hydratase LiuC, the glutaconate CoA transferase AibA/B and the dehydrogenase AibC originate from *M. xanthus* (light blue).

The AIB pathway expression system consists of a four-gene cassette (Figure 42). The *liuC* dehydrogenase gene was expressed by the *FAB1* promoter and terminated by T_{TDH3}. The first subunit gene of the glutaconate-CoA transferase *aibA* was expressed by the *TEF1* promoter and terminated by the terminator of *PGK1*. The second subunit gene *aibB* of the heterodimer was under the control of the *ADH1* promoter and terminated by the T_{HXT7}. The *aibC* gene was expressed by the *PGK1* promoter and terminated by T_{ADH1}. All pathway genes were combined into an expression cassette that was cloned into the high-copy 2µ plasmid.

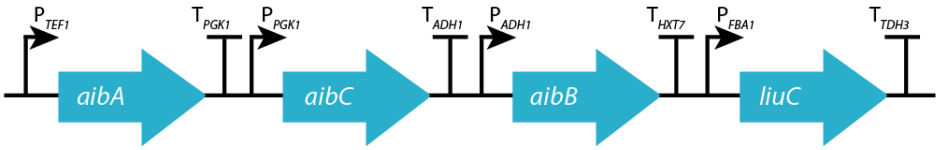

Figure 42: Scheme of the gene cassette encoding the AIB pathway enzymes. The engineered pathway contains four biosynthetic genes originating from *M. xanthus* and each gene was assembled with unique promoter and terminator pairs.

The three transformants of the AIB pathway-expressing strains had similar growth rates as the BkD pathway-expressing strain and exhibited reduced maximal growth rates in comparison to the empty plasmid control strain (Table 1). This reduced growth is most likely the result of the burden of the expression of this heterologous pathway as well as the metabolic burden due to the CoA limitation resulting from the expression of the AIB pathway.
Followed by monitoring the growth of the AIB pathway-expressing strain, we verified the production of iv-CoA in three transformants. Therefore, we cultured the strains for 48 h, subsequently extracted the metabolites and measured iv-CoA concentrations using LC/MS-MS. The LC/MS-MS chromatogram exhibited a clear detection of iv-CoA in the cell lysate compared to no iv-CoA for the empty vector control strain (Figure 43A). Based on the measurement we computed the intracellular concentrations of iv-CoA, taking the harvested total OD of cells, the cell volume and cell number into account. We calculated 5.5 ± 1.2 µM iv-CoA intracellular concentration in the AIB pathway-expressing strains (Figure 43B) [123].

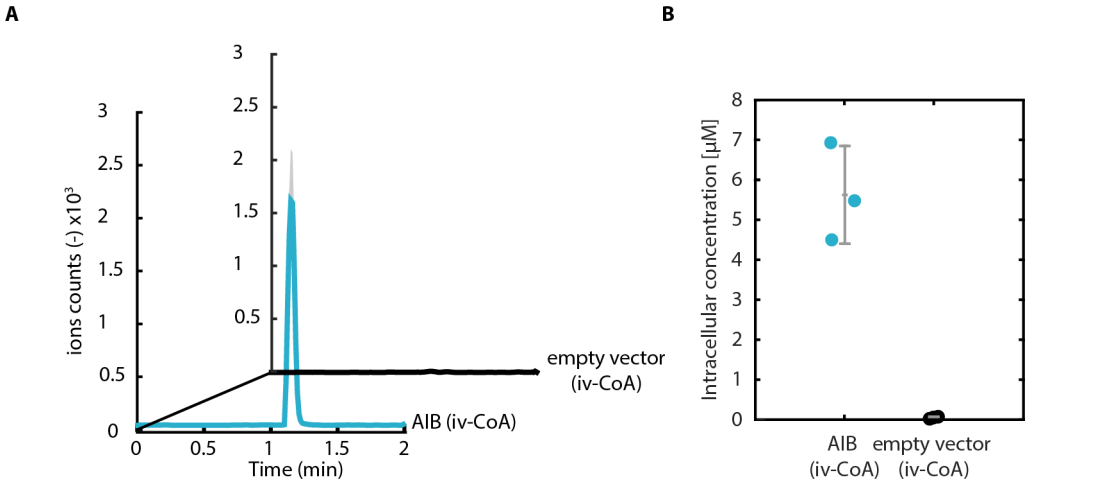

Figure 43: Engineered production of isovaleryl-CoA via the alternative isovaleryl-CoA pathway (AIB). A) LC-MS/MS chromatograms for strains transformed with the AIB pathway (light blue) or the empty vector control (black). Shown are the means of three biological replicates and respective standard deviations (grey). **B)** Intracellular concentrations of isovaleryl-CoA with respective standard deviations for three biological replicates of *S. cerevisiae* BJ5465 harboring pNK23 (light blue) or the empty vector control pRS424 (black).

For polyketides, isovaleryl- CoA and other branched-chain acyl-CoAs serve as starter units and the levels of acyl-CoAs produced within this study are consistent with the reported binding constants for various characterized PKSs [410,411]. The intracellular concentrations of isovaleryl-CoA we measured using our AIB strain, are comparable to acyl-CoAs pool sizes of natural producer strains, suggesting that the engineered pathways can support polyketide biosynthesis in yeast [411,412]. As such, this engineered yeast strain can serve as a platform to convert isovaleryl-CoA into various high-value chemicals like polyketides or novel fatty acids. However, the intracellular iv-CoA pools could be optimized by the adjusting *erg10* and *erg13* gene expression and by preventing side-fluxes. To summarize, isovaleryl-CoA was produced via the alternative isovaleryl biosynthetic (AIB) pathway from *M. xanthus*, which is the first heterologous expression example of the AIB pathway, to our knowledge, in *S. cerevisiae*.

2.1.4 Butyryl-CoA and hexanoyl-CoA production

Next, we aimed to produce sufficient intracellular concentrations of butyryl-CoA (but-CoA) and hexanoyl-CoA (hex-CoA). But-CoA and hex-CoA are intermediates of the production of butyraldehyde and butanol. The production of butanol via but-CoA has been accomplished in *E. coli* and *S. cerevisiae* [389,392,413–416]. Also, it has been shown that several type I, II and III PKSs are capable of incorporating hexanoyl-CoA into (un)-natural polyketides [417–419]. By providing a *S. cerevisiae* platform strain which produces hexanoyl-CoA and additional other short- and medium-chain acyl-CoAs, the establishment of yeast as polyketide production host would be accelerated. To reach this goal, we adapted the n-butanol (BUT) pathway previously described in *E. coli* for the expression in *S. cerevisiae* [389,392].

The tetrameric beta-ketothiolase (BktB) catalyzes the condensation of two acetyl-CoAs into acetoacetyl-CoA (Figure 44) [420]. It has been shown that the BktB of *Ralstonia eutropha* can accept besides acetyl-CoA also butyryl-CoA as substrate, which is required for downstream hexanoyl-CoA production [389]. The dimeric 3-hydroxybutyryl-CoA dehydrogenase/reductase (PaaH1) is catalyzing the dehydration reaction to 3-hydroxybutyryl-CoA [421]. The PaaH1 we utilized originated

from *Clostridium acetobutylicum* since it was shown to be promiscuous towards 3-ketohexanoyl-CoA and thus converts it to 3-hydroxyhexanol-CoA [389]. The crotonase (Crt) from *Clostridium acetobutylicum* forms a complex structure, a hexamer is formed by the dimerization of two trimers and subsequently catalyzes a dehydration of 3-hydroxybutyryl-CoA resulting in crotonyl-CoA [422]. The final reaction step required for the production of butyryl-CoA is catalyzed by the trans-enoyl-CoA reductase (Ter) from *Treponema denticola,* which hydrogenates crotonyl-CoA to form but-CoA. As previously mentioned, $BktB_{Re}$ is also promiscuous towards but-CoA and thus catalyzes an additional condensation with acetyl-CoA to form 3-ketohexanoyl-CoA [389]. The 3-hydroxybutyryl-CoA dehydrogenase/reductase ($PaaH1_{Ca}$) also accepts 3-ketohexanoyl-CoA and catalyzes the reaction to form 3-hydroxyhexanol-CoA. The Crt_{Ca} accepts besides 3-hydroxybutyryl-CoA also 3-hydroxyhexanoyl-CoA which is dehydrated to trans-2-hexanoyl-CoA. The last reaction step to hexanoyl-CoA is catalyzed by Ter_{Td}.

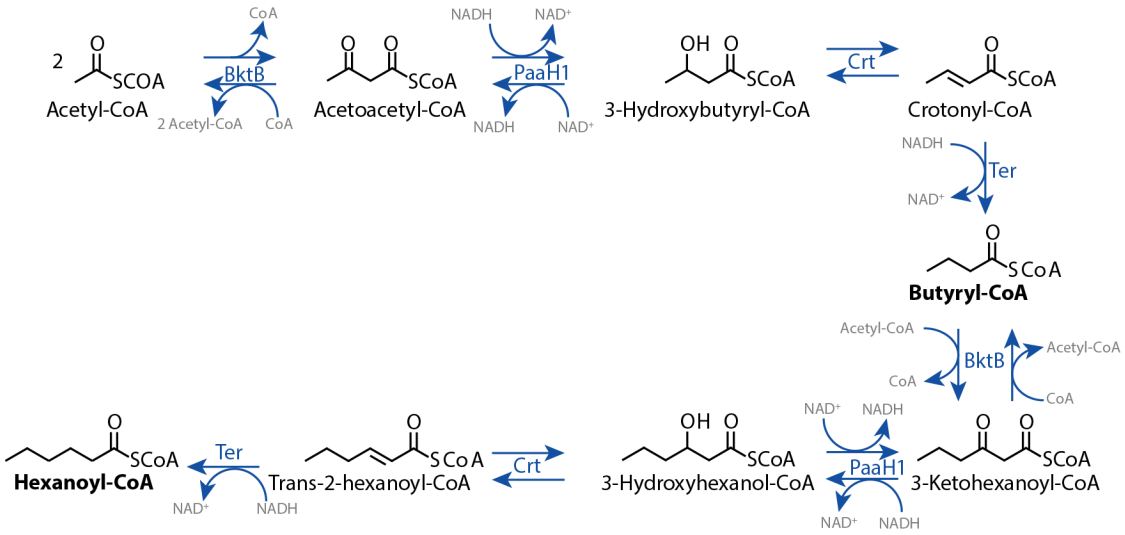

Figure 44: BUT pathway scheme. Biosynthetic pathway towards butyryl-CoA and hexanoyl-CoA production: Production from acetyl-CoA via the beta-ketothiolase BktB from *R. eutropha*, the 3-hydroxyacyl-CoA dehydrogenase PaaH1 from *C. acetobutylicum*, the crotonase Crt from *C. acetobutylicum* and the trans-enoyl-CoA reductase Ter from *T. denticola*.

Overall, the biosynthetic pathway for the production of both but-CoA and hex-CoA requires heterologous gene expression of only four genes and branches off the central metabolism using acetyl-CoA (Figure 45). For the expression of this pathway, we used galactose-inducible promoters in order to be able to control the expression of the pathway, if necessary. The cassette design that was previously used for the BkD and AIB pathways was maintained. The *bktB* gene was expressed under the *GAL10* promoter and terminated by T_{SSA1}. The gene for the 3-hydroxybutyryl-CoA dehydrogenase/reductase, *paaH1*, was expressed by the *GAL1* promoter and terminated by the *ENO1* terminator. The *crt* gene was constitutively expressed by the *TEF2* promoter and terminated by the terminator of *PGK1*. The *ter* gene was expressed by the *GAL7* promoter and terminated by T_{ADH1}. All expression devices were cloned into the pathway expression cassette on a 2µ plasmid and transformed into the BJ5465 strain background.

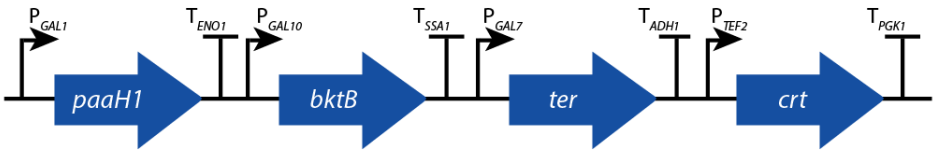

Figure 45: Scheme of the gene cassette encoding the BUT pathway enzymes. The engineered pathway contains four biosynthetic genes originating from *R. eutropha, C. acetobutylicum,* and *T. denticola* and each gene was assembled with unique promoter and terminator pairs.

For the strain carrying the BUT-pathway plasmid, we observed considerably reduced maximal growth rates and also visibly shifted timepoint of maximal growth rate compared to the empty plasmid control (Table 1). It has to be noted that the growth reduction is not only a result of the metabolic and expression burden of the pathway but also due different growth conditions. As glucose is a natural repressor of galactose-inducible promoters, the acyl-CoA production and thus also the growth examination were conducted in media containing galactose as carbon source. Since *S. cerevisiae* generally exhibits reduced growth in galactose media, the observed reduced growth of the strain carrying the BUT plasmid is both a result of growth in galactose media and of the protein and metabolic burden.

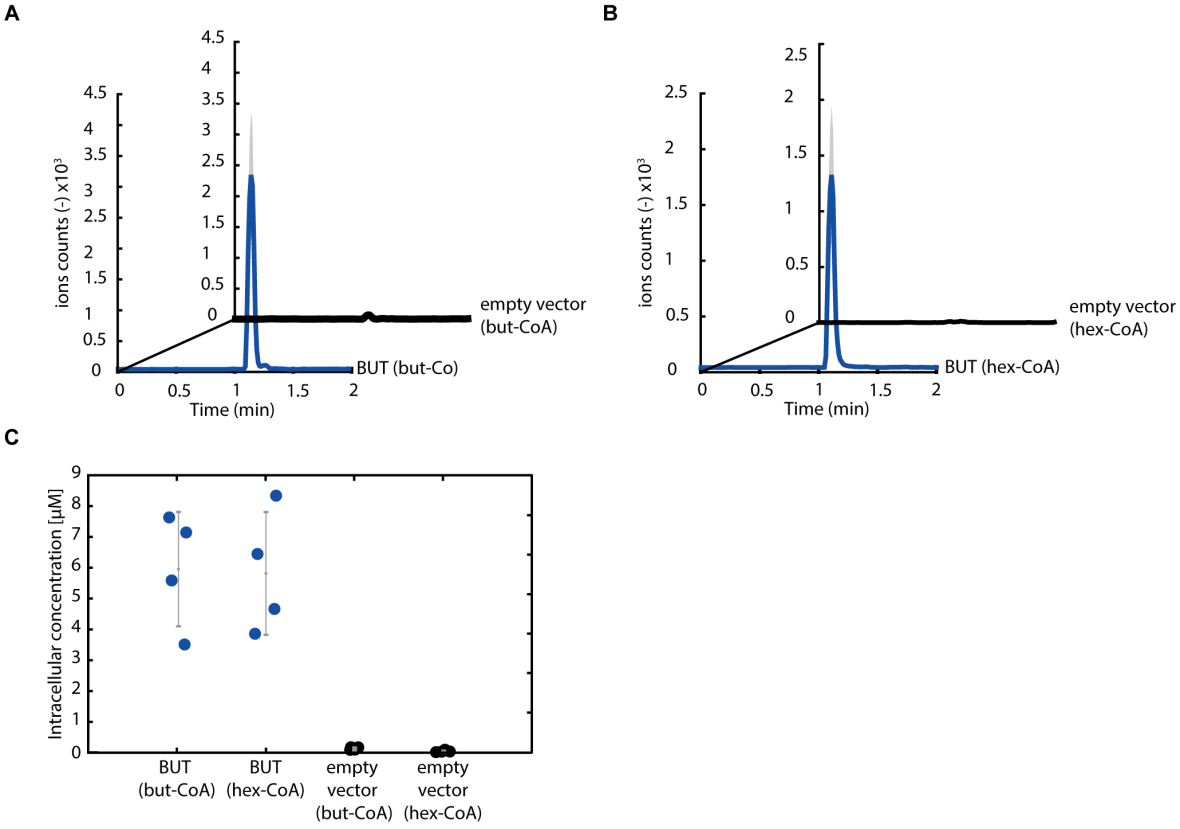

Figure 46: Engineered production of butyryl-CoA (but-CoA) and hexanoyl-CoA (hex-CoA) via the BUT pathway. **A)** LC-MS/MS chromatograms for strains transformed with the BUT pathway (blue, butyryl-CoA) or the empty vector control (black). Shown are the means of four biological replicates and the standard deviations (grey). **B)** LC-MS/MS chromatograms for strains transformed with the BUT pathway (blue, hexanoyl-CoA) or the empty vector control (black). Shown are the means of four biological replicates and the standard deviations (grey). **C)** Intracellular concentrations of but-CoA and hex-CoA with respective standard deviations for four biological replicates of the production strain BJ5465 harboring pNK44 (blue) or the empty vector control pRS424 (black).

The acyl-CoA production was performed using four transformants. BUT pathway expression in *S. cerevisiae* resulted in detectable amounts of butyryl-CoA and hexanoyl-CoA in the engineered strain BJ5464 harboring pNK44 (Figure 46A, B). The LC/MS-MS chromatograms exhibited clear peaks for butyryl-CoA and hexanoyl-CoA. No visible peak was detected for the empty vector control strain that was used as negative control. Using the peak intensities, we calculated the intracellular concentrations of both butyryl-CoA and hexanoyl-CoA (Figure 46C). We determined intracellular concentrations of 6 ± 1.9 µM for butyryl-CoA and 5.8 ± 2 µM for hexanoyl-CoA [123]. The relatively high variability could have been due to plasmid copy number variation or to differences during metabolic sample preparation. The intracellular concentration is reflecting the required concentrations for the incorporation into secondary metabolites including polyketides [411]. By providing a *S. cerevisiae* platform strain producing hexanoyl-CoA and additional other short- and medium-chain acyl-CoAs, the establishment of yeast as polyketide production host has been accelerated.

2.1.5 Propionyl-CoA production

Propionyl-CoA (p-CoA) is a building block for polyketides, fatty acids and bioplastics. Multiple propionyl-CoA biosynthesis routes exist in nature and were already used for the propionyl-CoA supply in different host organism [388].

2.1.5.1 Propionyl-CoA ligase pathway

One of the natural pathways for the production of propionyl-CoA is via the propionyl-CoA ligase (PrpE) pathway. This pathway is the most commonly used pathway for heterologous expression and it is based on exogenous propionate supply and the expression of the propionyl-CoA synthetase PrpE from *S. typhimurium* [394]. This pathway was already previously implemented into yeast and serves here as a reference production pathway [125]. The propionate CoA ligase catalyzes the ATP-dependent ligation of free CoA to propionate resulting in propionyl-CoA (Figure 47).

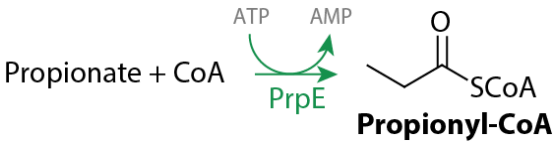

Figure 47: PrpE pathway scheme. Biosynthetic pathway towards propionyl-CoA production: Production from propionate via the propionyl-CoA ligase PrpE from *S. typhimurium*.

The *prpE* gene was expressed by the *TDH3* promoter and terminated by T_{ACT1}. The *prpE* gene expression device was inserted into a high-copy 2µ plasmid (Figure 48).

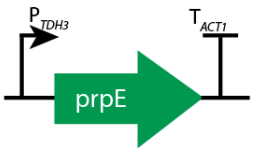

Figure 48: Scheme of the gene cassette encoding the PrpE pathway enzyme. The engineered pathway contains one biosynthetic gene originating from *S. typhimurium* which was assembled with a unique promoter and terminator pair.

Previously it was described that high propionate concentrations in the media are toxic for *S. cerevisiae* [406,423–425]. Therefore, we tested a propionate feeding concentration of 50 mM (Table 2). We observed a slight reduction of the maximal growth rate for the strain carrying the empty vector with propionate in the media. We therefore concluded that the propionate toxicity could be neglected for the concentrations used in this study. However, for the strain carrying the *prpE*-expressing plasmid, we observed a considerable reduction of the maximal growth rate and a shifted timepoint of the maximal rate, also, when no propionate was fed. This observation could be explained by the fact that the PrpE is also promiscuous towards other substrates resulting in a CoA as well as an ATP sink in the cell. Upon addition of propionate to the media this sink might be even more rapid, since PrpE has a faster turnover rate for propionate. In addition to this induced metabolic burden it was reported that propionyl-CoA can be toxic to the yeast cells. The peroxisomally located citrate synthase Cit2p shows promiscuity towards propionyl-CoA and catalyzes the reaction to the toxic 2-methylcitrate [406]. This indirect toxicity of propionyl-CoA could account for an additional reduction of growth.

Table 2: Growth rates with propionate supplementation.

Plasmid	Construct	Propionate feed in mM	Maximal growth rate in h^{-1}	Time of maximal growth in h
pRS424	Empty plasmid	0	0.35±0.004	11.3±1.0
pRS424	Empty plasmid	50	0.32±0.019	12.0±0.4
pNK36	PrpE	0	0.21±0.013	16.3±3.5
pNK36	PrpE	50	0.10±0.022	24.7±38.5
pNK37	PrpE-PCC1	0	0.16±0.019	25.4±0.6
pNK37	PrpE-PCC1	50	0.17±0.043	17.2±8.8

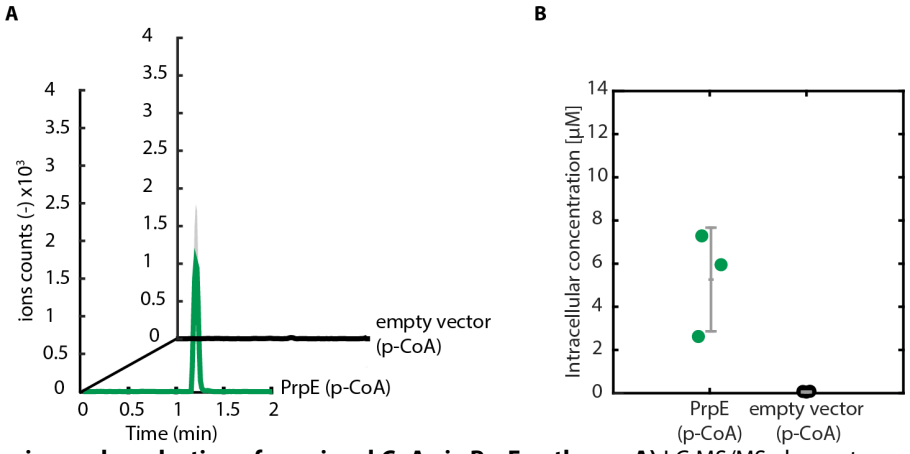

Figure 49: Engineered production of propionyl-CoA via PrpE pathway. A) LC-MS/MS chromatograms for strains transformed with the PrpE pathway (green) or the empty vector control (black). Shown are the means of three biological replicates and respective standard deviations (grey). **B)** Intracellular concentrations of propionyl-CoA with respective standard deviations for three biological replicates of *S. cerevisiae* BJ5465 harboring pNK36 (green) or the empty vector control pRS424 (black).

When the PrpE-expressing strain was cultured in media with 50 mM propionate, we detected propionyl-CoA in the metabolite extract using LC/MS-MS (Figure 49A). Based on this measurement we computed the intracellular concentrations of propionyl-CoA, which were around 5.3 ±

2.4 µM (Figure 49B) [123]. The large heterogeneity of the intracellular concentration might have resulted from differences in plasmid copy number but could also have been due to the fact that the induced burden of the pathway increased the likelihood of mutations that may have reduced the pathway activity.
Overall, when this pathway is utilized, a trade-off between increased propionyl-CoA production by additional propionate feeding and a reduction of cell growth and toxicity needs to be found.

2.1.5.2 3-hydroxypropionate pathway

To avoid economically unfeasible propionate feeding, we implemented a direct propionyl-CoA production route from malonyl-CoA. Therefore, propionyl-CoA can be directly produced from feedstock and precursor feeding is not required. Malonyl-CoA is a commonly used branching point for synthetic and heterologous metabolic pathways and different approaches have been taken to increase the malonyl-CoA supply in yeast [426–429]. The 3-hydroxypropionate (3HP) pathway to produce propionyl-CoA has been previously established in *E. coli* [393]. The enzymes for the production of 3-hydroxypropionate are found in the carbon assimilation cycle in some auxotrophic archaea and bacteria [393,430–432]. Here, we utilized the pathway that was previously implemented into *E. coli* as a blueprint for the design of the 3-hydroxypropionate pathway to produce propionyl-CoA in *S. cerevisiae*. Differently, we utilized the bifunctional malonyl-CoA reductase Mcr_{Ca} from *Chloroflexus aurantiacus*. The C-terminal domain of the Mcr_{Ca} reduces malonyl-CoA using NADPH to the free intermediate malonate semialdehyde (Figure 50). The N-terminal domain further reduces the malonate semialdehyde to 3-hydroxypropionate [431].The Mcr_{Ca} catalyzes both reaction steps, differently from the pathway implemented in *E. coli,* for which the Mcr from *Sulfolobus tokodaii* catalyzes the reaction from malonyl-CoA to malonic semialdehyde and the malonic semialdehyde reductase (Msr) catalyzes the substrate further to 3-hydroxypropionyl-CoA [393]. This alternative pathway route requires a precise expression of both enzymes to prevent the formation of a bottleneck. With the Mcr_{Ca} we overcame this potential drawback. As Mcr_{St}, Mcr_{Ca} originates from a thermophilic archaeon. It has been shown that Mcr_{Ca} exhibits its maximal relative activity at 57 °C, while its activity is reduced to 40 % at 33 °C [433]. However, a recent study has shown that Mcr_{Ca} exhibits increased activity in comparison to Mcr_{St}, resulting in the advantage of both having one gene less and improved activity [393,434,435]. The ATP-dependent esterification to ligate CoA to 3-hydroxypropionate and therefore the formation of 3-hydroxypropionyl-CoA is catalyzed by the 3-hydroxypropionyl-CoA synthase (3Hpcs) of *Metallosphaera sedula*. Also, *M. sedula* is a thermophilic archaeon which was originally found in a volcanic field and therefore it is not surprising that the maximal enzyme activity was reported to be ≥ 65 °C [436]. A similar optimal temperature was reported for the hexameric hydroxypropionyl-CoA dehydratase (3Hpcd) of *S. tokodaii*, which catalyzes the dehydration of 3-hydroxypropionyl-CoA to acryloyl-CoA [437]. The final catalytic step in the 3HP pathway is performed by the zinc-containing acryloyl-CoA reductase Acr, also originating from *M. sedula*. The Acr reduces acryloyl-CoA with NADPH to propionyl-CoA.

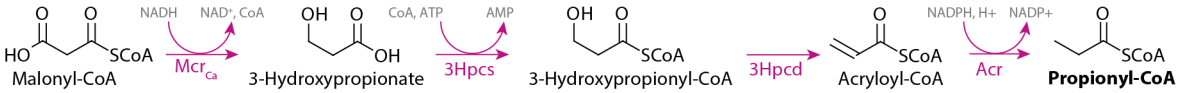

Figure 50: 3HP pathway scheme. Biosynthetic pathway towards propionyl-CoA production: Production from malonyl-CoA using the malonyl-CoA reductase Mcr_{Ca} from *C. aurantiacus,* the 3-hydroxypropionyl-CoA synthase 3Hpcs from *M. sedula*, the 3-hydroxypropionyl-CoA dehydratase 3Hpcd from *S. tokodaii*, and the acryloyl-CoA reductase Acr from *M. sedula*.

To implement the pathway in *S. cerevisiae* we placed the four genes under strong glycolytic promoters and constructed a pathway expression cassette (Figure 51). The bifunctional mcr_{Ca} gene was expressed by the *TEF1* promoter and terminate by T_{CYC1}. The $3hpcs_{Ms}$ gene was cloned under the control of the *TDH3* promoter and is terminated by the *ACT1* terminator, while $3hpcd_{St}$ was expressed by the *FAB1* promoter and terminated by the *TDH3* terminator. The acr_{St} gene was placed under the control of the *ADH1* promoter and was terminated by T_{HXT7}. As previously mentioned, all pathway devices were combined into the pathway cassette on a high-copy 2µ plasmid.

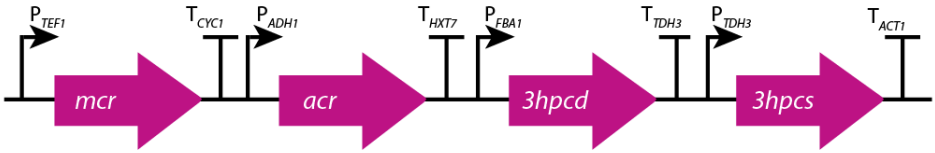

Figure 51: Scheme of the gene cassette encoding the 3HP pathway enzymes. The engineered pathway contains four biosynthetic genes originating from *C. aurantiacus, M. sedula,* and *S. tokodaii* and each gene was assembled with unique promoter and terminator pairs.

The maximal growth rates of the strains carrying the 3HP pathway plasmid differed visibly between the three transformants (Table 1). Overall, we observed a considerably reduced maximal growth in comparison to the empty vector control strain. We hypothesized that the heterogeneity of the maximal growth rate of the three biological replicates was a result of differences in plasmid copy number. Since we did not further investigate whether different mutations accumulated in the faster growing strains, it might be also possible that the replicates with the highest growth rate produced lower amounts of propionyl-CoA. The overall reduction of the maximal growth rated could be explained with the high burden by the enzyme expression. Similar to the propionyl-CoA production pathway via the propionate CoA ligase route (PrpE), we could assume that propionyl-CoA was toxic for the cells. However, it was surprising to see that the maximal growth rates of the strains with the 3HP pathway was higher in comparison to the strains carrying the PrpE pathway in media containing 50 mM propionate. We interpreted these findings as an indication that the 3HP pathway might produce lower amounts of propionyl-CoA. However, when we tested the production of propionyl-CoA using LC/MS-MS, we detected visible amounts of propionyl-CoA (Figure 52A). In the empty plasmid negative control, we did not detect visible amounts of propionyl-CoA. Based on the measurements we calculated the intracellular concentration of propionyl-CoA to be around 8.5 ± 3.7 µM (Figure 52B) [123]. Similar to the results of the growth rates, we have to report a high variation between our biological replicates. The variation might be, as previously discussed, due to plasmid copy number variability or instability. Differently to our previous hypothesis, we detected overall higher intracellular propionyl-CoA concentrations via the 3HP biosynthetic route than with the PrpE pathway. We could thus conclude that

the 3HP pathway was more efficient for the production of propionyl-CoA and has the additional advantage that propionate supplementation is not required.

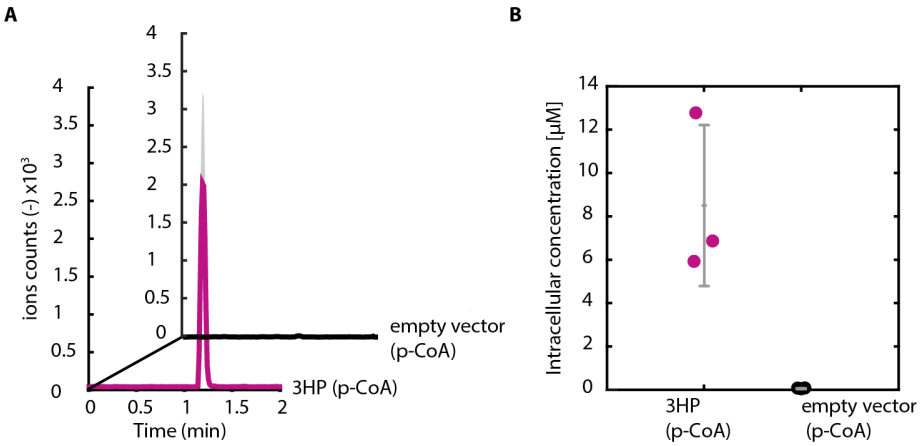

Figure 52: Engineered production of propionyl-CoA via the 3HP pathway. A) LC-MS/MS chromatograms for strains transformed with the 3HP pathway (purple) or the empty vector control (black). Shown are the means of three biological replicates and respective standard deviations (grey). **B)** Intracellular concentrations of propionyl-CoA with respective standard deviations for three biological replicates of *S. cerevisiae* BJ5465 harboring pNK30 (purple) or the empty vector control pRS424 (black).

2.1.6 Methylmalonyl-CoA production

To establish *S. cerevisiae* as a prospective production host for diverse polyketides with great biological and economic value, not only the starter unit supply needed to be engineered but also the allocation of commonly used extender units like methylmalonyl-CoA (mm-CoA). It was shown that triketide lactone (TKL) can be successfully produced in *S. cerevisiae* by expression of the module 2 of the deoxyerythronolide B synthase (DEBS) fused to its cognate thioesterase (TE) [125]. One prerequisite for the TKL production in *S. cerevisiae* was the allocation of methylmalonyl-CoA, which is not naturally produced in yeast, and which was established by the implementation of a production pathway from propionate. However, the exogenous supply of propionate is economically unfeasible. Also, as previously shown here, the expression of the propionyl-CoA ligase PrpE as well as the feeding of propionate resulted in a visible reduction of the maximal growth rates. Therefore, we provided an alternative biosynthetic pathway for the production of mm-CoA from feedstock.

2.1.6.1 Propionyl-CoA ligase and propionyl-CoA carboxylase pathway

We established the propionyl-CoA ligase, propionyl-CoA carboxylase pathway (PrpE-PCC1) based on the previously described feeding-dependent propionyl-CoA production pathway, mainly to use it for the comparison with the feeding-independent biosynthetic route (Figure 53) [125]. Towards this goal, we implemented in addition to PrpE the ATP-dependent carboxylation of propionyl-CoA, catalyzed by the biotin-dependent propionyl-CoA carboxylase complex (Pcc).

The Pcc complex is composed of six homodimers of each subunit that form together a dodecamer [438]. The Pcc complex from *Streptomyces coelicolor* that we utilized is comprised of three subunits and requires a post-translational modification. The α-subunit AccA1 harbors two domains, the biotin carboxylase, and biotin-carboxyl carrier protein domain [439]. Interestingly, it was reported

that the α-subunit is alternatively encoded in the *accA2* gene, that serves as α-subunit when stationary/transition phase is not reached [440]. The Pccβ-subunit PccB1 is a carboxyl transferase carboxylating propionyl-CoA to methylmalonyl-CoA. The ε-subunit is not necessarily required for the enzymatic activity of the Pcc complex [439,441,442].

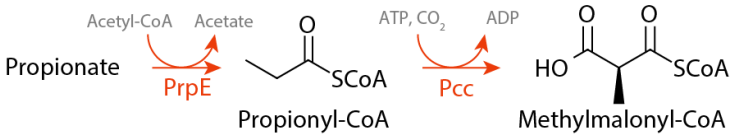

Figure 53: PrpE-PCC1 pathway scheme. Biosynthetic pathway towards methylmalonyl-CoA production: Production from propionate using the propionyl-CoA ligase PrpE from *S. typhimurium* and the biotin-dependent propionyl-CoA carboxylase complex Pcc from *S. coelicolor*.

This mm-CoA biosynthetic pathway has been successfully implemented in the past using a multiplasmid approach using the *accA1* and *pccB1* genes to form the Pcc complex [125]. Here, we combined gene expression units for *prpE*, *accA1* and *pccB1* into a pathway cassette constituting the PrpE-PCC1 pathway (Figure 54). As for the PrpE pathway, we expressed the *prpE* gene from the *TDH3* promoter and terminated it by T_{ACT1}. The *accA1* gene encoding the α-subunit was expressed by the *TEF1* promoter and terminated by T_{TDH3}. The *pccB1* gene that encodes the β-subunit of the Pcc complex was expressed by the *PGK1* promoter and terminated by T_{HXT7}. The cassette was integrated into a 2μ high-copy plasmid.

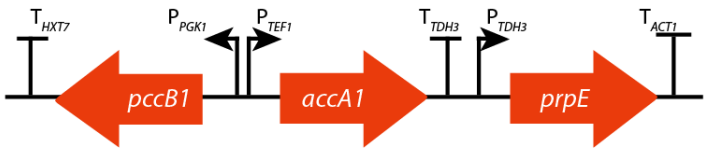

Figure 54: Scheme of the gene cassette encoding the PrpE-PCC1 pathway enzymes. The engineered pathway contains three biosynthetic genes originating from *S. typhimurium,* and *S. coelicolor* and each gene was assembled with unique promoter and terminator pairs.

As previously reported for the propionyl-CoA production via the PrpE route, we saw a reduction of the maximal growth rate in propionate-containing media. Thus, we also tested the growth rate for methylmalonyl-CoA production via the PrpE-PCC1 pathway with and without propionate in the media (Table 2). Also, for 0 mM propionate in the media, we monitored a reduced growth of the three transformants, when compared to the empty plasmid control strain as well as compared to the PrpE strain. The reduced maximal growth rate could be explained with increased metabolic burden of additional Pcc complex expression. Interestingly, we could report slightly increased maximal growth rate in media with 50 mM propionate in comparison to the PrpE strain. This was an indication that the growth reduction of the PrpE strain was most likely due to the toxicity of a downstream product of propionyl-CoA, 2-methylcitrate [406]. When the Pcc was co-expressed, the propionyl-CoA was carboxylated to methylmalonyl-CoA, which cannot be recognized by Cit3p and therefore no toxic side-product formation could occur.
In the chromatogram of the metabolite extract exhibited that the strain containing the PrpE-PCC1 pathway produced both propionyl-CoA and methylmalonyl-CoA (Figure 55A, B). No acyl-CoA was detected in the empty plasmid control metabolite extract. Based on these data we calculated the

intracellular concentrations of propionyl-CoA to be 4.6 ± 2.2 µM and methylmalonyl-CoA to be 0.5 ± 0.1 µM (Figure 55C) [123]. The propionyl-CoA concentrations were slightly lower compared to the PrpE pathway. The variation between the biological replicates was most likely due to plasmid copy number variability. The intracellular concentration of methylmalonyl-CoA was rather low and would have to be increased by different optimization steps for successful production of polyketides in yeast.

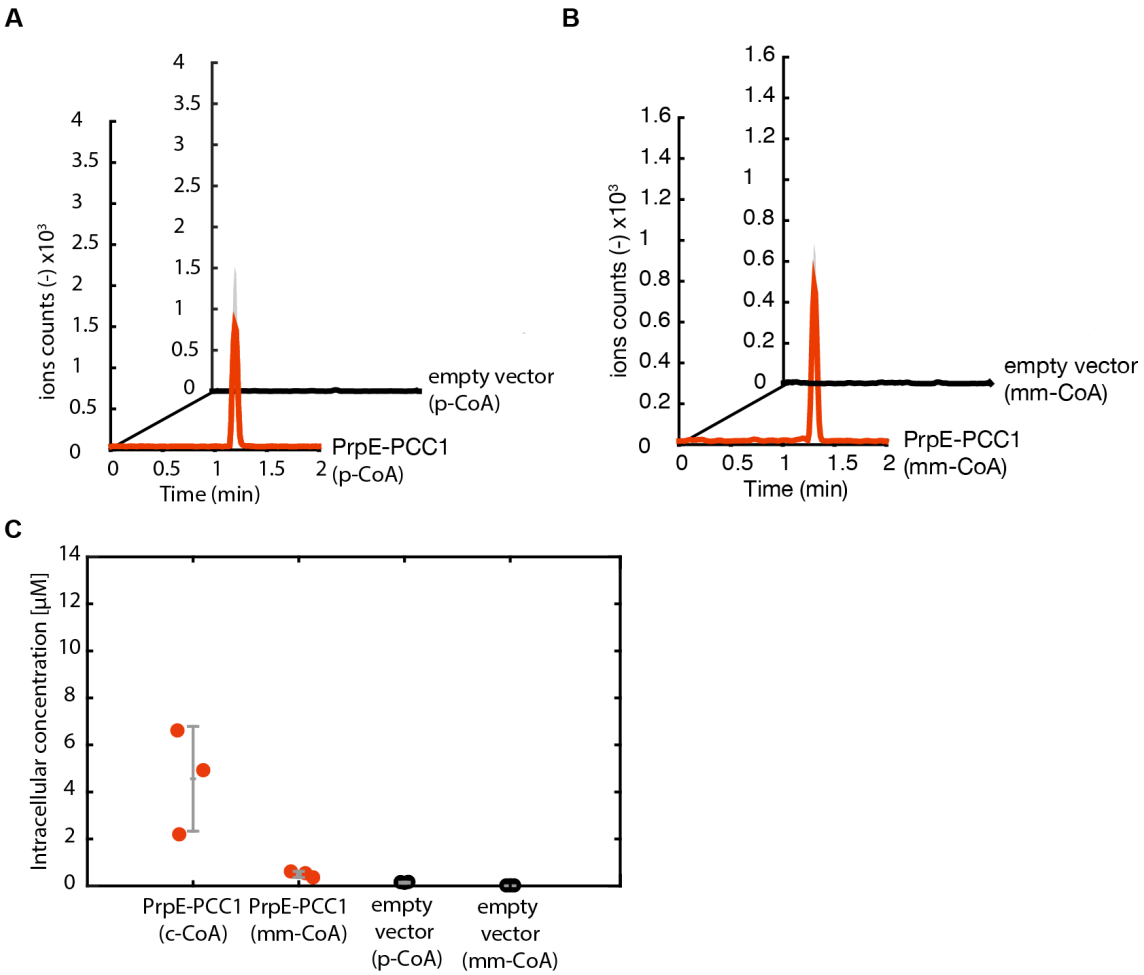

Figure 55: Engineered production of propionyl-CoA (p-CoA) and methylmalonyl-CoA (mm-CoA) via the PrpE-PCC1 pathway. A) LC-MS/MS chromatograms for strains transformed with the PrpE-PCC1 pathway (red, p-CoA) or the empty vector control (black). Shown are the means of three biological replicates and the standard deviations (grey). **B)** LC-MS/MS chromatograms for strains transformed with the PrpE-PCC1 pathway (red, mm-CoA) or the empty vector control (black). Shown are the means of four biological replicates and the standard deviations (grey). **C)** Intracellular concentrations of p-CoA and mm-CoA with respective standard deviations for three biological replicates of the production strain BJ5465 harboring pNK37 (red) or the empty vector control pRS424 (black).

Since the intracellular concentrations of methylmalonyl-CoA were lower than expected, we wanted to improve the pathway. It was previously reported that the Pcc complex exhibits higher enzymatic activity and stability when it also contains the ε-subunit [439,441,442]. The ε subunit is thought to stabilize and improve the complex formation of the α-(6)- β (6)-dodecamer [439,441,442]. To improve the reaction efficiency of the Pcc complex, we additionally aimed to improve its biotinyl-

ation by expressing the biotin ligase BirA of *E. coli* heterologously that was shown to be functionally expressed in yeast [443]. The improved pathway was cloned into a cassette expression system (Figure 56). The *accA1* and *pccB1* genes were expressed from the same promoters as previously. The gene encoding the ε-subunit was cloned under the control of the *TDH3* promoter and was terminated by T_{ACT1}. The *prpE* gene was expressed from the *FAB1* promoter and was terminated by T_{TDH3}. The biotin ligase *birA* gene was expressed by the *ADH1* promoter and terminated by T_{HXT7}. All expression devices were again cloned into the expression cassette system on a high-copy 2µ plasmid.

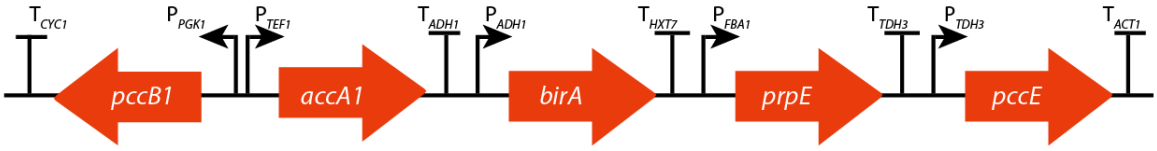

Figure 56: Scheme of the gene cassette encoding the PrpE-PCC2 pathway enzymes. The engineered pathway contains five biosynthetic genes originating from *S. typhimurium, S. coelicolor,* and *E. coli* and each gene was assembled with unique promoter and terminator pairs.

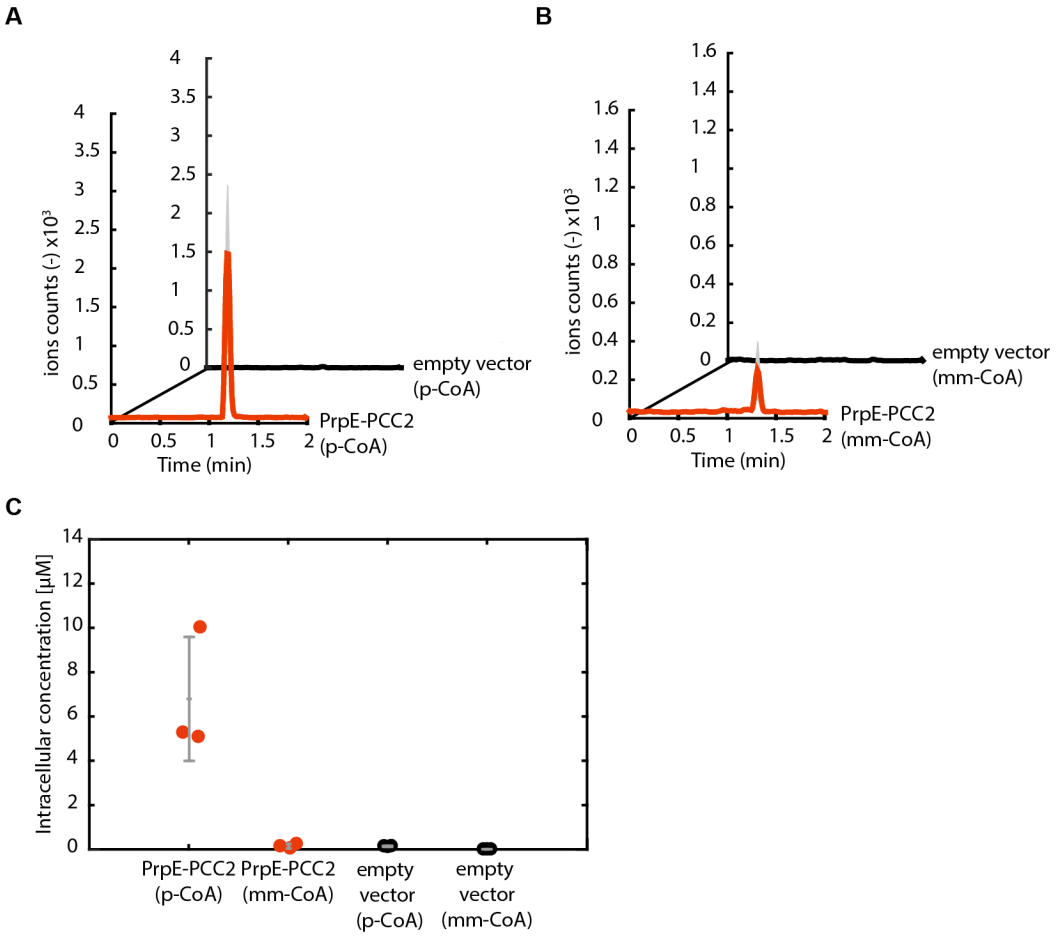

Figure 57: Engineered production of propionyl-CoA (p-CoA) and methylmalonyl-CoA (mm-CoA) via the PrpE-PCC2 pathway. A) LC-MS/MS chromatograms for strains transformed with the PrpE-PCC2 pathway (red, p-CoA) or the empty vector control (black). Shown are the means of three biological replicates and the standard deviations (grey). **B)** LC-MS/MS chromatograms for strains transformed with the PrpE-PCC2 pathway (red, mm-CoA) or the empty vector control (black). Shown are the means of four biological replicates and the standard deviations (grey).**C)** Intracellular concentrations of p-CoA and mm-CoA with respective standard deviations for three biological replicates of the production strain BJ5465 harboring pNK54 (red) or the empty vector control pRS424 (black).

When we tested the acyl-CoA production levels from the improved PrpE-PCC2 pathway in three transformants, we did not detect considerably increased amounts of methylmalonyl-CoA in the metabolite extract (Figure 57). Differently from the initial PrpE-PCC1 pathway though, we detected higher intracellular concentrations of propionyl-CoA as a result of PrpE expression from a stronger promoter. Overall, the attempted improvements of the PrpE-PCC pathway resulted in lower intracellular methylmalonyl-CoA concentrations. It is likely that complex formation of AccA1, PccB1, and PccE was suboptimal for our expression conditions, resulting in more non-functional protein. Also, it is questionable if the biotin ligase was efficiently biotinylating the Pcc complex. Overall it should be noted that for further optimization of the PrpE-PCC pathway, the focus should be on improved expression and activity of the Pcc. Additionally, a knockout of the *cit2p* gene could reduce the toxicity of propionyl-CoA.

2.1.6.2 3-hydroxypropionate and crotonyl-CoA carboxylase/reductase pathway

Similar to the production of propionyl-CoA directly from feedstock, we aimed to engineer a feeding-independent production pathway for methylmalonyl-CoA to ensure the supply of this important extender unit. A feeding-independent production of methylmalonyl-CoA would have economic benefits as well as the previously reported side effects of intermediate production of propionyl-CoA would be reduced.

Therefore, we modified the previously described 3HP pathway for propionyl-CoA production in order to generate methylmalonyl-CoA. The first three pathway steps, resulting in the formation of acryloyl-CoA, were identical to the 3HP pathway. However, the acryloyl-CoA reductase Acr was replaced by the crotonyl-CoA carboxylase/reductase (Ccr) of *Caulobacter crescentus*, thus forming the 3HP-CCR pathway (Figure 58). It was previously shown for the Ccr of *Rhodobacter sphaeroides* that besides crotonyl-CoA ,also acryloyl-CoA was efficiently carboxylated and reduced [444]. Since the Ccr_{CC} exhibited the overall most robust expression as well as faster carboxylation of crotonyl-CoA, it was assumed that it would also efficiently carboxylate acryloyl-CoA. The NADPH-dependent Ccr_{CC} thus catalyzes the reduction of acryloyl-CoA to propionyl-CoA that is then further carboxylated to methylmalonyl-CoA, during which one CO_2 is fixated [395].

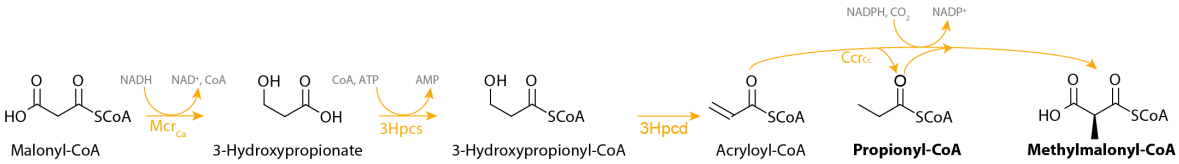

Figure 58: 3HP-CCR pathway scheme. Biosynthetic pathway towards methylmalonyl-CoA production: Production from malonyl-CoA using the malonyl-CoA reductase Mcr_{Ca} from *C. aurantiacus,* the 3-hydroxypropionyl-CoA synthase 3Hpcs from *M. sedula*, the 3-hydroxypropionyl-CoA dehydratase 3Hpcd from *S. tokodaii*, and the crotonyl-CoA carboxylase/reductase Ccr from *C. crescentus*.

The 3HP-CCR gene expression cassette was adapted from the 3HP cassette. We replaced the *acr* gene by the ccr_{CC} gene, which was now expressed by the *ADH1* promoter and terminated be the T_{HXT7} (Figure 59). The maximal growth rate of three biological replicates carrying the 3HP-CCR expression system exhibited the weakest reduction of growth compared to all production strains (Table 1). However, the growth rate was still lower in comparison to the empty vector control strain, most likely due to the burden resulting from protein expression. Compared to the 3HP

production pathway we could report an improved maximal growth rate. This indicated that in the 3HP production strain, the toxicity of propionyl-CoA and not the burden of the protein expression was the main factor for growth reduction.

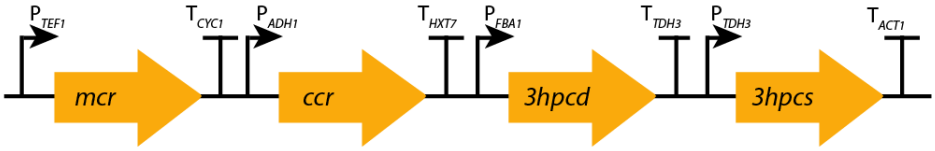

Figure 59: Scheme of the gene cassette encoding the 3HP-CCR pathway enzymes. The engineered pathway contains four biosynthetic genes originating from *C. aurantiacus, M. sedula, S. tokodaii,* and *C. crescentus* and each gene was assembled with unique promoter and terminator pairs.

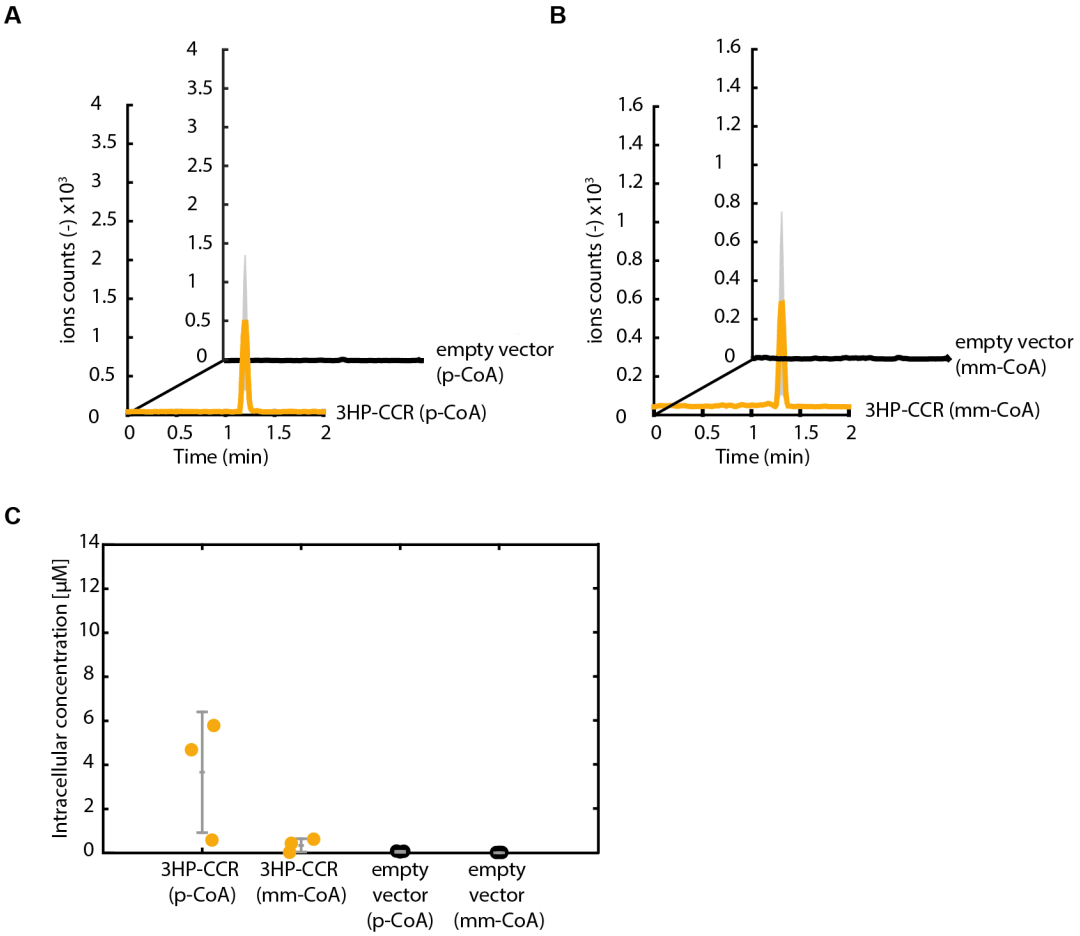

Figure 60: Engineered production of propionyl-CoA (p-CoA) and methylmalonyl-CoA (mm-CoA) via the 3HP-CCR pathway. A) LC-MS/MS chromatograms for strains transformed with the 3HP-CCR pathway (yellow, p-CoA) or the empty vector control (black). Shown are the means of three biological replicates and the standard deviations (grey). **B)** LC-MS/MS chromatograms for strains transformed with the 3HP-CCR pathway (yellow, mm-CoA) or the empty vector control (black). Shown are the means of four biological replicates and the standard deviations (grey). **C)** Intracellular concentrations of p-CoA and mm-CoA with respective standard deviations for three biological replicates of the production strain BJ5465 harboring pNK42 (yellow) or the empty vector control pRS424 (black).

When we tested the production of methylmalonyl-CoA in 3HP-CCR productions strains, we detected visible amounts of methylmalonyl-CoA using LC/MS-MS in comparison to the empty plasmid control. Unexpectedly, we also detected production of propionyl-CoA (Figure 60A, B). Based

on the LC/MS-MS results we computed propionyl-CoA concentrations of 3.7 ± 2.7 µM [123]. We observed high variation in the production amounts of propionyl-CoA and methylmalonyl-CoA, indicating that one replicate was not expressing the 3HP-CCR pathway efficiently. When this outlier was neglected we measured mean intracellular concentrations of 0.5 µM methylmalonyl-CoA and 5.2 µM propionyl-CoA (Figure 60C). Recent investigations on Ccrs revealed that they are able to catalyze a single reduction step in addition to a combined reduction/carboxylation, which explains the detection of propionyl-CoA besides methylmalonyl-CoA [445,446]. The ratio of the two products indicated that the reduction reaction of Ccr_{CC} was more efficient compared to the carboxylation under the tested conditions *in vivo*. Overall, the methylmalonyl-CoA concentrations were comparable to the concentrations found for the PrpE-PCC pathways. To our knowledge, this is the first time that a Ccr was expressed in yeast and that production of methylmalonyl-CoA from feedstock was achieved. However, the measured methylmalonyl-CoA concentrations were not sufficient for efficient production of polyketides and further pathway optimization is required. Nevertheless, it should be highlighted that during the reactions catalyzed by the Ccr_{Cc}, CO_2 was fixated in methylmalonyl-CoA, featuring the possibility of carbon fixation using a Ccr in yeast.

2.1.7 Golden Gate collection of short-chain acyl-coenzyme A ester pathway genes

As previously highlighted, the biosynthetic pathways of the short-chain acyl-CoAs partially require further optimization. The production amounts of isovaleryl-CoA, butyryl-CoA, hexanoyl-CoA and propionyl-CoA were reaching intracellular concentrations similar to the reported concentrations in the natural host organism and should thus be sufficient for secondary metabolite production like polyketides [52,112,410,447]. However, the optimization of the production of methylmalonyl-CoA remains to be achieved. Also, all pathways were expressed from high-copy plasmids that resulted in high gene expression heterogeneity and thus in variation of protein amounts. For future commercial production of natural products, chromosomally integrated precursor pathways would be a prerequisite. However, also with recent advances of the in CRISPR/Cas9 technology, only a few chromosomal integrations of the pathways would be feasible. It has to be presumed that the gene copy number of the integrated pathways would be lower than on the high-copy 2µ plasmid. This would result in overall lower expression of the genes and therefore into a lower production amount of the acyl-CoAs.

To optimize the pathways, different approaches can be taken requiring genetic adaption of the expression cassettes. Due to recent innovations in high throughput cloning, fast and efficient construction of multiple pathways is feasible. The YTK provided by Dueber and colleagues constitutes the most comprehensive cloning system for *S. cerevisiae* and is comprised of many useful parts [71]. However, in order to use this cloning standard for our purposes, domestication, meaning the removal of Golden Gate enzyme restriction sites in the genes, promoters and terminators was required. To this end, we provide all pathway genes required for the production of isovaleryl-CoA, butyryl-CoA, hexanoyl-CoA, propionyl-CoA, and methylmalonyl-CoA in a domestic form (Figure 61). The YTK provides a large number of promoters and terminators that could be utilized for the expression of the different pathway genes [71]. Also, different integration systems and plasmid-based (2µ and CEN) systems are provided in the toolkit. With the domesticated pathway genes, a targeted optimization is possible. One approach could be the determination of flux bottlenecks using metabolomics. Another one to shuffle promoter and terminators for each gene and to

measure whether increased production yields could be obtained. As already highlighted for the optimization of the PrpE-PCC pathway, the expression of a Pcc from a different organism could be beneficial. To explore this possibility, we added the Pcc of *Methylobacterium extorquens* to the collection. Since also the structure of the biotin ligase BirA from *E. coli* exhibits visible differences compared to the biotin ligase of *S. coelicolor*, we added the $birA_{Sc}$ and the $birA_{Me}$ to the collection and that could thus be tested. These part extensions together with the Dueber Golden Gate toolkit allow the exploration of multiple approaches.

For an optimization of methylmalonyl-CoA production, it should be additionally examined whether methylmalonyl-CoA can be further metabolized intracellularly. As methylmalonyl-CoA has structural similarities to succinyl-CoA, it could be hypothesized that succinyl-CoA-accepting enzymes are promiscuous towards methylmalonyl-CoA. Thus, methylmalonyl-CoA production using for example labeled methylmalonate could give revealing insights. To produce methylmalonyl-CoA from methylmalonate, we added the methylmalonate CoA ligase gene *matB* to the collection.

The acyl-CoA toolkit provides different gene variants that will allow the rapid improvement of the production of short-chain acyl-CoAs in *S. cerervisiae* based on our previously obtained results.

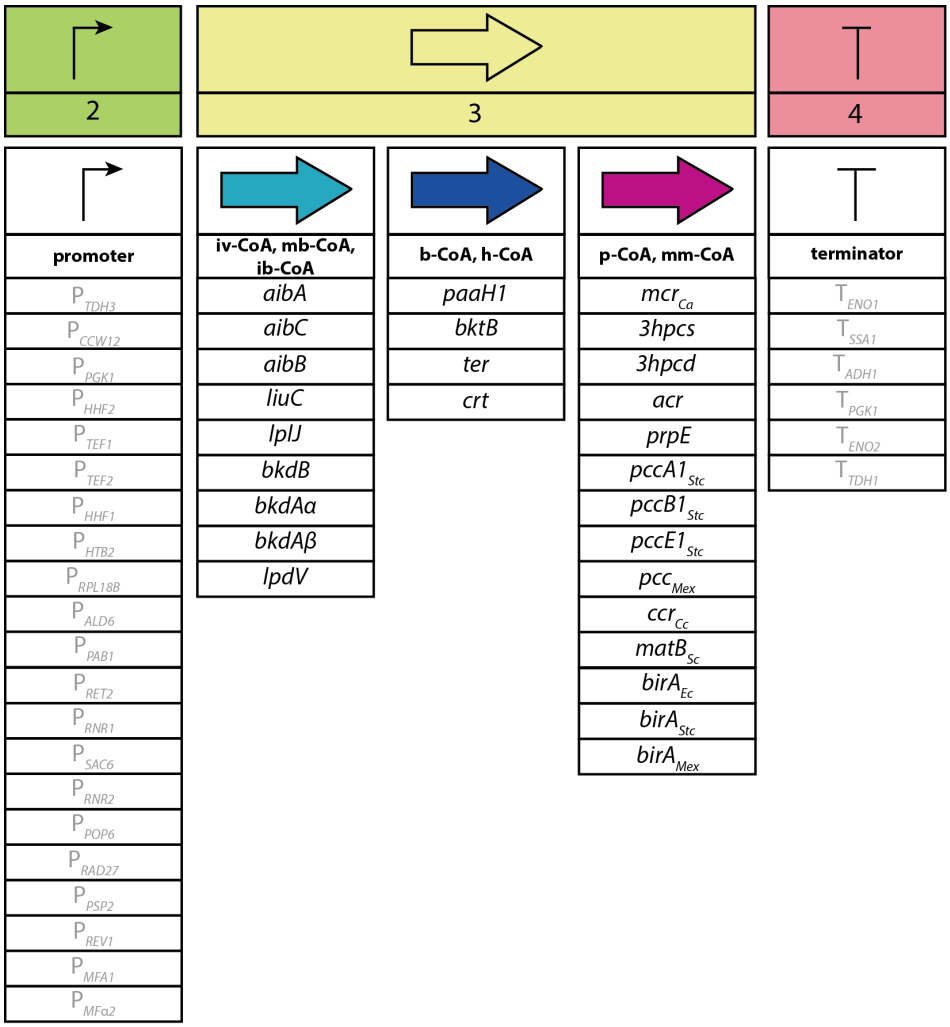

Figure 61: Schematic overview of the promoter and terminator parts of the yeast Golden Gate toolkit and genes encoding acyl-CoA pathway enzymes. Parts originating from the YTK are represented in grey. Figure inspired by Lee *et. al.* [71].

2.2 YCTK – a yeast communication toolkit

A bottleneck for the engineering of higher-order multicellular networks in *S. cerevisiae* is the lack of a highly characterized toolkit for inter- and intracellular communication. The yeast communication toolkit (YCTK) is thus providing sender (α-factors), receiver (Ste2 receptors), and barrier (Bar1 proteases) parts as well as pheromone-responsive promoters as responder parts. Following the Yeast Golden Gate Toolkit (YTK) Standard, the YCTK can be used in combination with this existing toolkit [71]. The YCTK provides essential parts for the construction of multicellular networks in *S. cerevisiae* as an extension to the YTK.

2.2.1 Selection of parts for the YCTK

The selection of the parts to be included into the YCTK is of high importance for the usability of the toolkit. Selecting components that will be utilized by many researchers, as well as parts covering a wide range of characteristics is essential. Apart from providing a reasonable set of parts, we were also aiming to get a better understanding of the interaction between the different parts, how they can be shuffled and combined into multicellular communication networks.

With their mating pathway and their intercellular pheromone sensing system, yeasts provide a natural, sophisticated communication system. The parts in our YCTK will employ this natural communication system and allow their engineering to serve our purposes. As the sender modules of the YCTK, we selected α-factors since they do not require further chemical modification (Figure 62) [22]. The α-factors are small peptides and thus more easily diffuse than the **a**-factor. Not all selected α-factors are natively named that way, however, they exhibit the same properties and will thus be named α-factors in the following. The cognate Ste2-like receptors serve as receivers. The α-factors can be degraded by Bar1-like proteases, which we implemented as barrier parts. A selection of pheromone-inducible promoters will function as responders to generate output signals by controlling the expression of downstream genes.

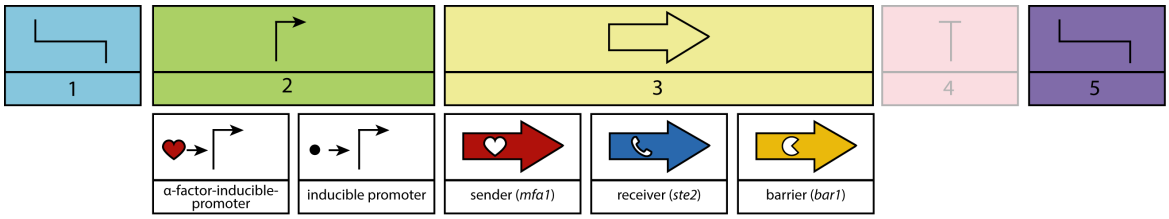

Figure 62: Schematic overview of the parts included in the YCTK. We extended the YTK by providing additional 1) L-connectors, 2) pheromone-inducible and inducible promoters, 3) sender, receiver and barrier parts, and 5) R-connectors. Figure inspired by Lee *et. al.* [71].

2.2.1.1 Promoter part selection

Besides the sender, receiver, and barrier parts we included seven pheromone-inducible promoters (part level 2) into our YCTK to be used to drive downstream gene expression. Pheromone-inducible promoters are promoters, which are active in the mating pathway and that are therefore responsive to pheromone induction. This means their activity is downstream upregulated upon binding of α-factor to the Ste2 receptor. Since these promoters natively drive the expression

of different genes in the cell, they are expected to exhibit different expression profiles. The promoters are only indirectly induced by α-factor, yet we will refer to them as pheromone-inducible promoters below.

Besides the pheromone-inducible promoters, we also added the P_{TETO7} promoter to the toolkit that can be induced or repressed with doxycycline as function of the corresponding transcription factor system [448]. Our seven pheromone-inducible promoters are an addition to the 19 constitutive promoters, two pheromone-induced and two inducible promoters available in the YTK. For our promoter characterization, P_{THD3}, P_{REV1}, and P_{RPL18B} served as benchmark promoters.

The pheromone-responsive promoters were selected based on RNA sequencing data previously obtained by A. Anders in the Sourjik Lab. The RNA-Seq results served solely as a basis to identify suitable promoters, and our later findings cannot be directly compared with this data set since strains, pheromone concentrations, and culturing methods differed.

Figure 63 displays the RNA levels in reads per kilobase per million (RPKM) of our selected genes that were upregulated in *S. cerevisiae MAT***a** cells upon α-factor stimulation by different α-factor concentrations. The RPMK values on the y-axis were normalized by the reads per genome of the represented gene and further normalized by the total numbers of reads in the experiment. The RNA levels were correlating with the transcription of the gene. Therefore, the promoter strength can be deduced. We chose promoters exhibiting different maximal induction levels in dependency of increasing α-factor concentrations. We also included the *REV1* RNA levels as a lower expression reference. *DIG2* and *MSG5* featured low maximal induction levels and these two were the weakest promoters we selected for our set and exhibited RNA levels below 250 RPKM. The RNA levels of *FUS1* and *FUS3* showed similar dynamics upon pheromone induction. The maximal induction of *FUS1* was higher with RNA levels of approximately 750 RPMK in comparison to *FUS3* RNA levels with around 500 RPKM. *SST2* RNA levels followed a similar trend as *FUS1* and *FUS3,* however, responded already to low α-factor concentrations but saturated at similar pheromone levels.

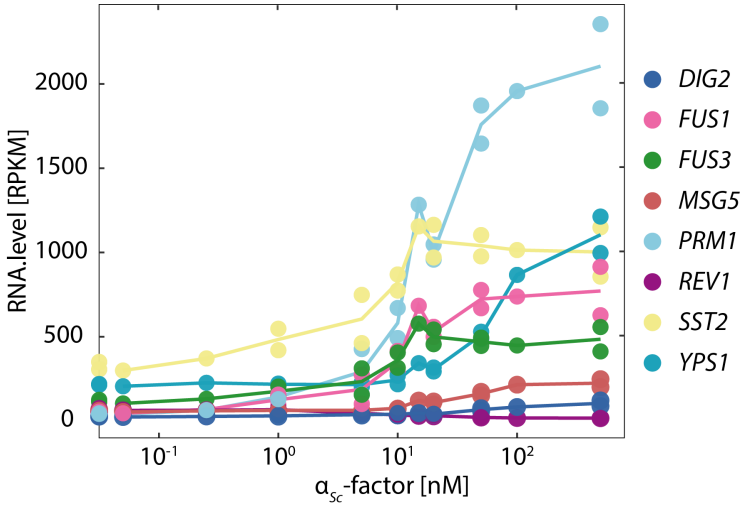

Figure 63: RNA levels of pheromone-induced genes. Displayed are RNA levels of selected pheromone-induced genes of two biological replicates. These data exhibit the α-factor-responsive promoters we selected for our toolkit. Data and plot provided by A. Anders.

Also notable were the high basal RNA levels of more than 250 RPMK for *SST2* in absence of any α-factor. The basal RNA levels of *YPS* were visibly lower. An increase in the RNA levels of *YPS* was observed at 10 nM and steadily increased up to the maximal pheromone concentrations added to the cells. The maximal transcription levels of *YPS* were higher than for *SST2*. Differently from *SST2* we could not observe a saturation of RNA levels for *YPS1* for maximal pheromone concentrations. The RNA level of *PRM1* were with 2000 RPMK the highest. The RNA levels of *PRM1* also exhibited the highest dynamic range as well as comparably low (< 200 RPMK) basal levels.
Based on this RNA data set, we selected and thus aimed to cover a wide dynamic range of α-factor-responsive promoters with different maximal expression levels and varying expression profiles.

2.2.1.2 Sender part selection – α-factor *in silico* identification

To select suitable α-factor-like pheromones, a literature and database search was conducted. This search resulted in a set of *mfa1*-like genes from 49 different yeast species. Our general approach was to utilize the natural pheromone sequences for our toolkit, which require to be enzymatically processed in order to obtain the mature α-factor. Thus, we verified that the conservation of the maturation process and the compatibility with the natural one of *S. cerevisiae* was given. We scanned *in silico* for the lysine-arginine (KR) or arginine-arginine (RR) motif within the 49 pre-pro-α-factor-like sequences (gene products before the maturation process). These motives are recognized by Kexin2 (Kex2), the serine protease that cleaves the pre-pro-α-factor. The recognition sequences are highlighted in Table 3 in red for the example of *S. cerevisiae*.

Table 3: Result of the *in silico* identification of α-factors for the example *S. cerevisiae*. Green: secretion signaling sequence, red: Kex2 motif, blue: Ste13 motif, yellow: mature α-factor. Appendix Table 1 lists the results for our initial set of 49 sequences.

Name of organism	Pre-pro-α-factor sequence	α-factor
Saccharomyces cerevisiae	MRFPSIFTAVLFAASSALAAPVNTTTEDETAQIPAEAVIGYLDLEGDFD VAVLPFSNSTNNGLLFINTTIASIAAKEEGVSLDKREAEAWHWLQLKP GQPMYKREAEAEAWHWLQLKPGQPMYKREADAEAWHWLQLKPG QPMYKREADAEAWHWLQLKPGQPMY	α_{sc}-factor: WHWLQLKPGQPMY

A complete table of all 49 pre-pro-α-factor sequences and identified mature α- factors can be found in Appendix Table 1. The Kex2 recognition motif was identified in 47 of the selected sequences. No Kex2 recognition motif was found in *Ashbya aceri*, *Ashbya gossypii*, and *Naumovozyma dairenensis*, which indicates that the maturation process is not conserved in these organisms. For *Aspergillus fumigatus*, *Naumovozyma dairenensis*, and *Penicillium chrysogenum* the Kex2 motif was found but no mature α-factor could be identified. During the MFα1 sequence scanning, we also determined the repetitive x-alanine and x-proline sequences that are cleaved by the dipeptidyl aminopeptidase Ste13, which is required for the full maturation of the α-factors. For some species, the XA, and XP sequences are incomplete or exhibit alternative motives, e.g., for S. pombe the sequence contains the EFE motif. Our findings allow the hypothesis that homologous aminopeptidases in these organisms may have different promiscuities. The Ste13 motives are highlighted in blue in Table 3 and Appendix Table 1. We further identified the N-terminal secretion signaling sequence that is responsible for the translocation, secretion and processing

of the pre-pro-α-factor. The N-terminal secretion signaling sequence is shown in green in Table 3 as well for all remaining pre-pro-α-factors in Appendix Table 1. Subsequently, we identified potential α-factors in 44 of the set of 49 sequences, highlighted in Table 4 and Appendix Table 1 in yellow.

In 22 of these selected pre-pro α-factors, we identified up to five alternative mature pheromones. These findings are in accordance with previously described analyses [214]. We determined the mature α-factors based on the identified Kex2, Kex1, and Ste13 recognition sites and predicted downstream processing. Our identified mature α-factors thus do not necessarily correspond to natively resulting sequences.

Table 4: List of all predicted mature α-factors of the 50 species. Not for all species a mature α-factor could be identified, for others up to 5 variants of mature α-factors were identified.

Name of Organism	α-factor
Ashbya aceri	no mature pheromone identified
Ashbya gossypii	no mature pheromone identified
Aspergillus fumigatus	no mature pheromone identified
Babjeviella inositovora	α_{Bi}-factor 1: KWGWLTLRFNQPLF
Candida albicans	α_{Ca}-factor 1: KSKGGFRLTNFGYFEPG α_{Ca}-factor 2: GFRLTNFGYFEPG
Candida auris	α_{Cau}-factor 1: KWGWLRFFPGEPFV
Candida glabrata	α_{Cg}-factor 1: WHWWKIRKGQGLF α_{Cg}-factor 2: WHWVRLRKGQGLF
Candida intermedia	α_{Ci}-factor 1: WGWIKFFPGQPIG
Candida orthopsilosis	α_{Co}-factor 1: HWTTYGYYEPQ
Candida tenuis	α_{Ct}-factor 1: FSWNYRLKWQPIS
Clavispora lusitaniae	α_{Cl}-factor 1: WGWIHFLNTDVIG α_{Cl}-factor 2: KWKWIHFRNTDVIG α_{Cl}-factor 3: KWKWIKFRNTDVIG α_{Cl}-factor 4: KWRWINFRNTDVIG
Eremothecium cymbalariae	α_{Ec}-factor 1: WHWLRFDRGQPIH
Eremothecium sinecaudum	α_{Es}-factor 1: WKWMKFGRGGSYW α_{Es}-factor 2: WKWVKFGRGGSYW
Fusarium langsethiae	α_{Fl}-factor 1: WCTWKGQPCWKEKMA α_{Fl}-factor 2: WCWWKGQPCWKT α_{Fl}-factor 3: ANEPRWCWWKGQPCWKSKS α_{Fl}-factor 4: WCWWKGQPCWKA
Hanseniaspora guilliermondii	α_{Hg}-factor 1: WIRMXNVARWCYVHQ
Hanseniaspora opuntiae	α_{Ho}-factor 1: WIRMWPGGVMFT
Hanseniaspora osmophila	α_{Hos}-factor 1: WHWLKFDVGEPLYA α_{Hos}-factor 2: SLWHWLKFDVGEPLYA
Hanseniaspora uvarum	α_{Hu}-factor 1: WIRMWPGGVMFT
Kazachstania africana	α_{Ka}-factor 1: WHWLSISPGQPMYI α_{Ka}-factor 2: WHWLSIAPGQPMYI

Name of Organism	α-factor
Kazachstania naganishii	α_{Kn}-factor 1: WHWLRLSYGQPIY
Kluyveromyces dobzhanskii	α_{Kd}-factor 1: WSWISLRPGQPIF
Kluyveromyces lactis	α_{Kl}-factor 1: WSWITLRPGQPIF
Kluyveromyces marxianus	α_{Km}-factor 1: WKWLSLRVGQPIY α_{Km}-factor 2: WEWLSLRVGQPLY
Kluyveromyces thermotolerans	α_{Kt}-factor 1: WRWLSLSRGQPMY α_{Kt}-factor 2: WRWLSLARGQPMY
Lachancea dasiensis	α_{Ld}-factor 1: WQWLRLGRGQPMY α_{Ld}-factor 2: WSWLRLGRGQPMY α_{Ld}-factor 3: WKWLRLGRGQPMY α_{Ld}-factor 4: WRWLRLGRGQPMY α_{Ld}-factor 5: WRWLRLDRGQPMY
Lachancea fermentati	α_{Lf}-factor 1: WHWLRLKGPMY
Lachancea kluyveri	α_{Lk}-factor 1: WHWLSFSKGEPMY
Lachancea lanzarotensis	α_{Ll}-factor 1: WRWLSLARGQPMY
Lachancea meyersii	α_{Lme}-factor 1: WHWLKLDRGQPMY α_{Lme}-factor 2: WHWLRLDRGQPMY
Lachancea mirantina	α_{Lm}-factor 1: WRWLSLRAGEALH α_{Lm}-factor 2: WQWLSLRAGEALH α_{Lm}-factor 3: WSWLSLRAGEALH
Lachancea nothofagi	α_{Ln}-factor 1: WSWLRLDRGQPMY α_{Ln}-factor 2: WRWLRLDRGQPMY α_{Ln}-factor 3: WTWLKLDRGQPMY
Lachancea quebecensis	α_{Lq}-factor 1: WRWLSLSRGQPMY
Lachancea thermotolerans	α_{Lt}-factor 1: WRWLSLSRGQPMY α_{Lt}-factor 2: WRWLSLARGQPMY
Metschnikowia bicuspidata	α_{Mb}-factor 1: WHWVRLKIGQPFF α_{Mb}-factor 2: WRWLSLSRGQPMY α_{Mb}-factor 3: WHWVALKIGQPFF

Name of Organism	α-factor
Millerozyma farinosa	α_{Mf}-factor 1: KFHWFTYSNFDPIT α_{Mf}-factor 2: KFHWFKYNNFDPIT α_{Mf}-factor 3: KFHWFTYNNFDPIT α_{Mf}-factor 4: KFHWFKYNKYDPIT
Naumovozyma castellii	α_{Nc}-factor 1: GWHWLRLDPGQPLY α_{Nc}-factor 2: NWHWLRLDPGQPLY
Naumovozyma dairenensis	no mature pheromone identified
Penicillium chrysogenum	no mature pheromone identified
Sordaria macrospora	α_{Sm}-factor 1: QWCRIHGQSCWKKA α_{Sm}-factor 2: QWCRIHGQSCWK α_{Sm}-factor 3: QWCRIHGQSCWKA α_{Sm}-factor 4: QWCRIHGQSCW
Saccharomyces cerevisiae	α_{Sc}-factor 1: WHWLQLKPGQPMY
Saccharomyces kudriavzevii	α_{Sk}-factor 1: WHWLQLKPGQPMY
Saccharomyces naganishii	α_{Sn}-factor 1: WHWLRLSYGQPIY
Saccharomyces paradoxus	α_{Spa}-factor 1: WHWLQLKPGQPMY
Scheffersomyces stipitis	α_{Ss}-factor 1: WHWTSYGVFEPG α_{Ss}-factor 2: WHWTSYGVFEPGK
Schizosaccharomyces pombe	α_{Sp}-factor 1: YADFLRAYQSWNTFVNPDRPNLK α_{Sp}-factor 2: YADFLRAYHSWNTFVNPDRPNLK
Tetrapisispora blattae	α_{Tb}-factor 1: HWLRLGRGEPLY
Tetrapisispora phaffii	α_{Tp}-factor 1: WHWLRLDPGQPLY
Torulaspora delbrueckii	α_{Td}-factor 1: GWMRLRLGQPLK α_{Td}-factor 2: GWMRLSPGKPMK α_{Td}-factor 3: GWMRLRIGQPL
Vanderwaltozyma polyspora	α_{Vp}-factor 1:WHWLRLRYGEPIY
Yarrowia lipolytica	α_{Yl}-factor 1:WRWFWLPGYGEPNW
Zygosaccharomyces rouxii	α_{Zr}-factor 1: HFIELDPGQPMF α_{Zr}-factor 2: HFVELDPGQPMF

The amino acid alignment of all predicted α-factors exhibited high heterogeneity of the central amino acids (Figure 64). These positions were previously described to be recognized by the Ste2 receptors. In case we obtained several different mature α-factor variants for one organism, these central sequences were conserved. The C-terminal sequences of the peptides were quite similar and the motif GQOMY was identified, with some variation, in the majority of α-factors. Also, the N-terminal motif WXWLXL was relatively conserved.

Interestingly we identified organisms for which the mature pheromone sequences were identical, but the pre-pro-α-factors varied. The similarity of mature α-factors is expected to result in signaling crosstalk between the species. This similarity of α-factor sequences was observed for the ones originating from *Hanseniaspora opuntiae* and *Hanseniaspora osmophila*; *Lachancea lanzarotensis*, *Lachancea thermotolerans*, *Lachancea quebecensis* and *Metschnikowia bicuspidata*; L*achancea nothofagi* and *Lachancea dasiensis*; *Saccharomyces cerevisiae*, *Saccharomyces kudriavzevii* and *Saccharomyces paradoxus*. This finding indicated the relatedness of these species.

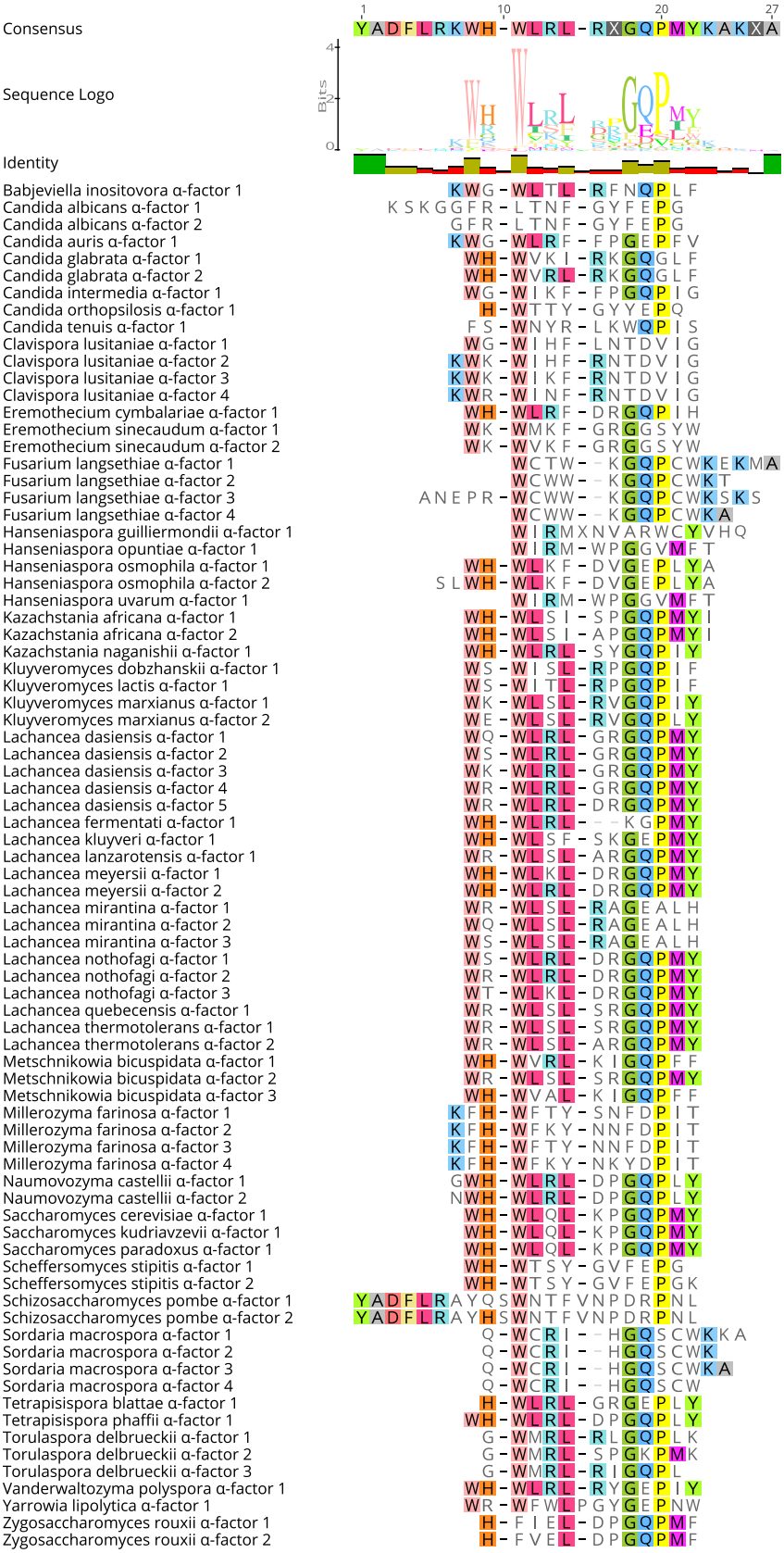

Figure 64: Alignment of the mature α-factor sequences from different *ascomycetes*. Amino acid sequence alignment of α-factor sequences that were identified by *in silico* identification of the *MFa1*s.

Based on the *in silico* identification and mature pheromone amino acid sequence alignment we selected α-factors from 11 different organisms to obtain a sequence diversity for our toolkit (Figure 65). Additionally, we took previously published studies on the mating of these organisms and heterologous expression of in *S. cerevisiae* into account [158,220,449]. We thus codon-optimized and synthesized these *mfα1*-like genes and incorporated them into our communication toolkit as sender parts. The toolkit can be extended by, e.g. α-pheromones, which are highlighted in the selection above (Figure 64) or by newly identified sequences containing the Kex2 motif.
To our set of α-factors we added the pheromone from *C. albicans* which exhibits no sequence similarity. For our evolutionary studies *C. albicans* served as outgroup species. The α-pheromone of *L. fermentati* is three amino acids shorter than the average α-factor.
To learn more about possible crosstalk, we selected α-factors with conserved C- and N-terminal motives. Except for *C. albicans,* all α-factors contain tryptophan (W) at position one and three. Furthermore, the fourth position is also highly conserved in our selection, all pheromones besides *C. albicans* and *Klyveromyces lactis* contain a leucine (L). The N-terminal motif GQP is also conserved in the majority of selected pheromones.

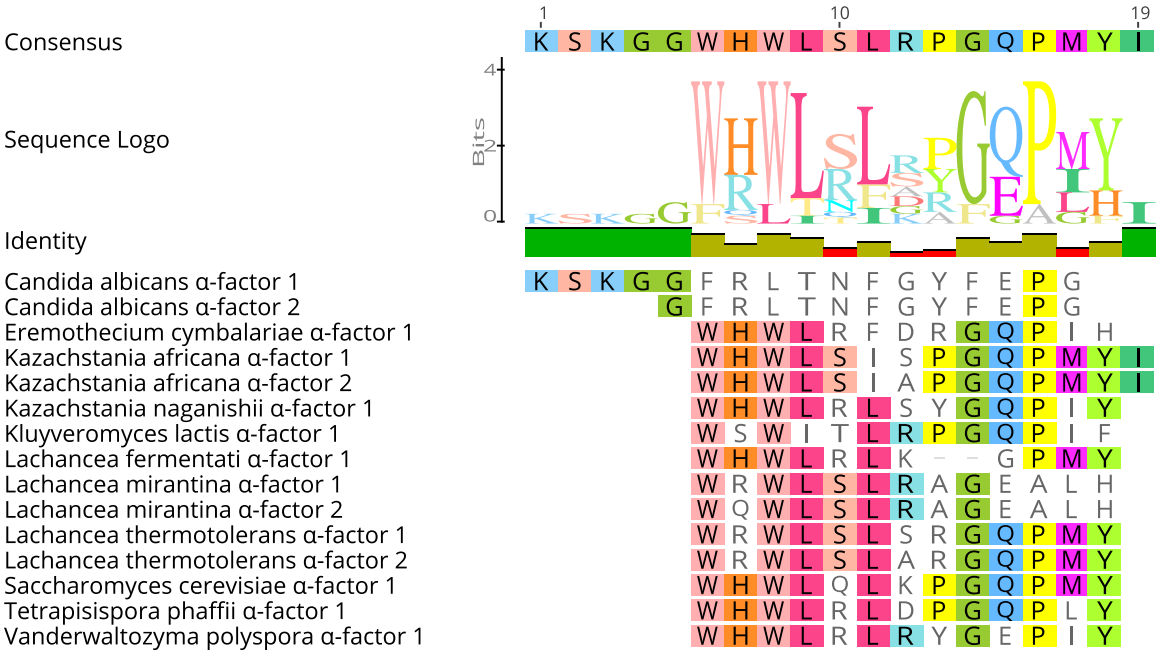

Figure 65: Alignment of the selected α-factor sequences for the toolkit. We selected MFα1 pheromones from 11 different species, covering a large diversity of different sequence motives.

2.2.1.3 Receiver part selection- Ste2 receptors

Based on our set of 11 α-factors, we identified the cognate Ste2-like receptors from the corresponding yeast species. For downstream signal propagation upon on α-factor binding, the third cytoplasmic loop and part of the seventh interacting transmembrane domain of Ste2 are crucial [242]. To ensure that our selected Ste2-like receptors will be functionally expressed in *S. cerevisiae*, we extracted the sequences of both domains. The alignment of the third cytoplasmic loops in Figure 66 revealed that these sequences are highly conserved. This loop was proposed to be responsible for the interaction with the G protein α subunit. Interestingly, also the Ste2 sequence

of *C. albicans* exhibits high homology, even though the α-factor sequence and the entire Ste2 receptor sequence vary visibly, suggesting signal transduction will be feasible.

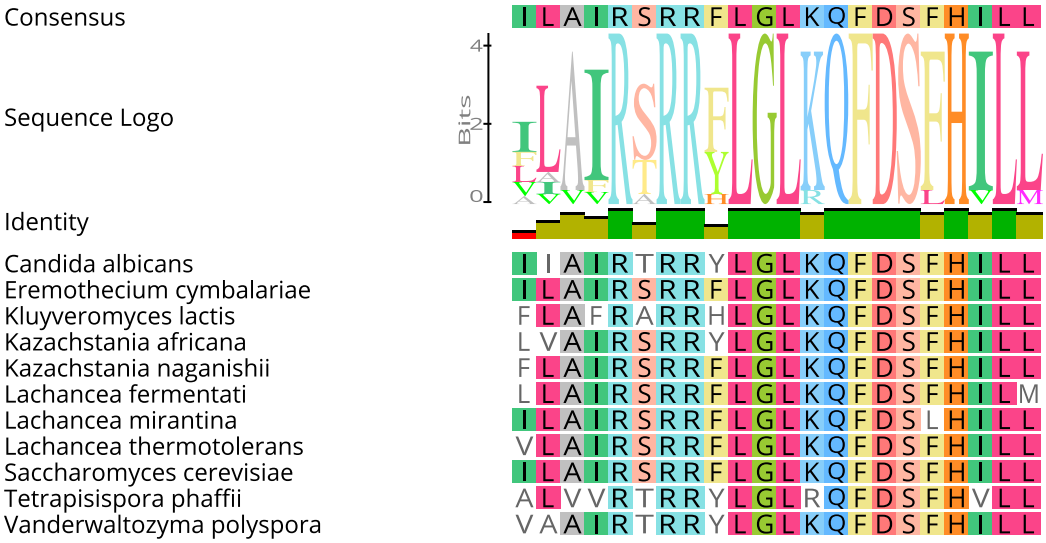

Figure 66: Third cytoplasmic loop sequence alignment of the selected Ste2 receptors. The third cytoplasmic loop is essential for signal transduction upon pheromone stimulation by interacting with the Gα subunit. High sequence conservation suggests functional coupling to the downstream *S. cerevisiae* signaling cascade.

Likewise, part of the seventh transmembrane motif is highly conserved among the different species. The alignment indicates (Figure 67) that all selected receptors should be suitable to be incorporated into the membrane and to transduce the signal to the native signaling pathway in *S. cerevisiae*. A sequence alignment of the entire receptor sequences can be found in Appendix Figure 1.

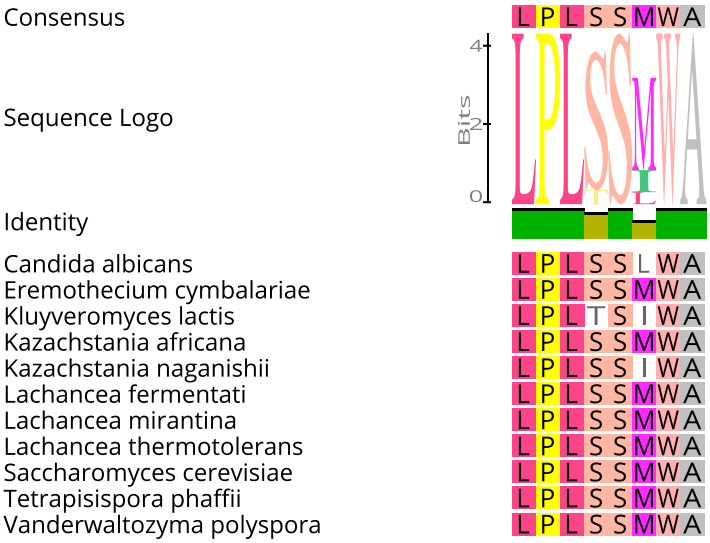

Figure 67: Seventh transmembrane region sequence alignment of the selected Ste2 receptors. The seventh transmembrane region was proposed to be crucial for the structural integrity of the receptor. High sequence conservation suggests that the heterologous receptors are functional in *S. cerevisiae*.

2.2.1.4 Barrier part selection – Bar1 proteases

To complete the yeast communication toolkit, we included barrier parts that exhibit part level 3 characteristics, as it is required for the cloning standard using the YTK. To allow quenching (degradation) of α-factors that serve in our toolkit as signaling parts, we selected seven Bar1-like proteases (barrier parts). Our selection of barrier parts is based on our previously compiled collection of α-factors from eleven different yeast species (Figure 65). So far, not for all of these species Bar1 proteases have been described. To date, it remains challenging to identify the Bar1 proteases through homology studies within the *ascomycetes*. The proteases are only distantly related and share only little sequence identity, indicating that the evolution of the Bar1-like proteases was convergent. We examined literature and protein alignments and identified seven potential Bar1 proteases. The selection of some of the proteases was only based on sequence homology or chromosomal positioning. For the majority of the identified proteases, the annotation score of UniProt was low, or they were hypothetical proteases according to sequencing data. The predicted $Bar1_{Vp}$ protease is visibly shorter than the other proteases, while the well-studied $Bar1_{Sc}$ is with 587 amino acids the longest. All Bar1-like protease contain a signaling peptide sequence, which is required for extracellular export. These signaling peptides exhibit high leucine content but no highly conserved motives. Based on structural predictions and alignments, our barrier proteases are annotated to a peptidase A1 family domain on Uniport. Also based on these predictions, active sites are annotated for some of the proteases. When we aligned the peptidase A1 domains, the annotated actives sites were conserved in all our Bar1-like proteases (Figure 68). Starting with amino acid residue 20 on the N-terminal end of the protease, a conserved DXGSXD sequence can be found. The N-terminal sequence constitutes the aspartic protease family and is annotated as one of the catalytic sites of the proteases. Starting at amino acid 180, the GXLGXG sequence is conserved in all of our selected Bar1 proteases, as well as the YXNXP sequence around amino acid residue 200. Similar to the first predicted active site, the amino acids sequence of the second active site is with its DSG sequence highly conserved among our selection of proteases. Solely $Bar1_{Ec}$ exhibits a slight deviation with a DTG motif. Overall, we could identify different conserved regions and further biochemical and structural studies of these proteases could be of importance to unravel their biotechnological potential.

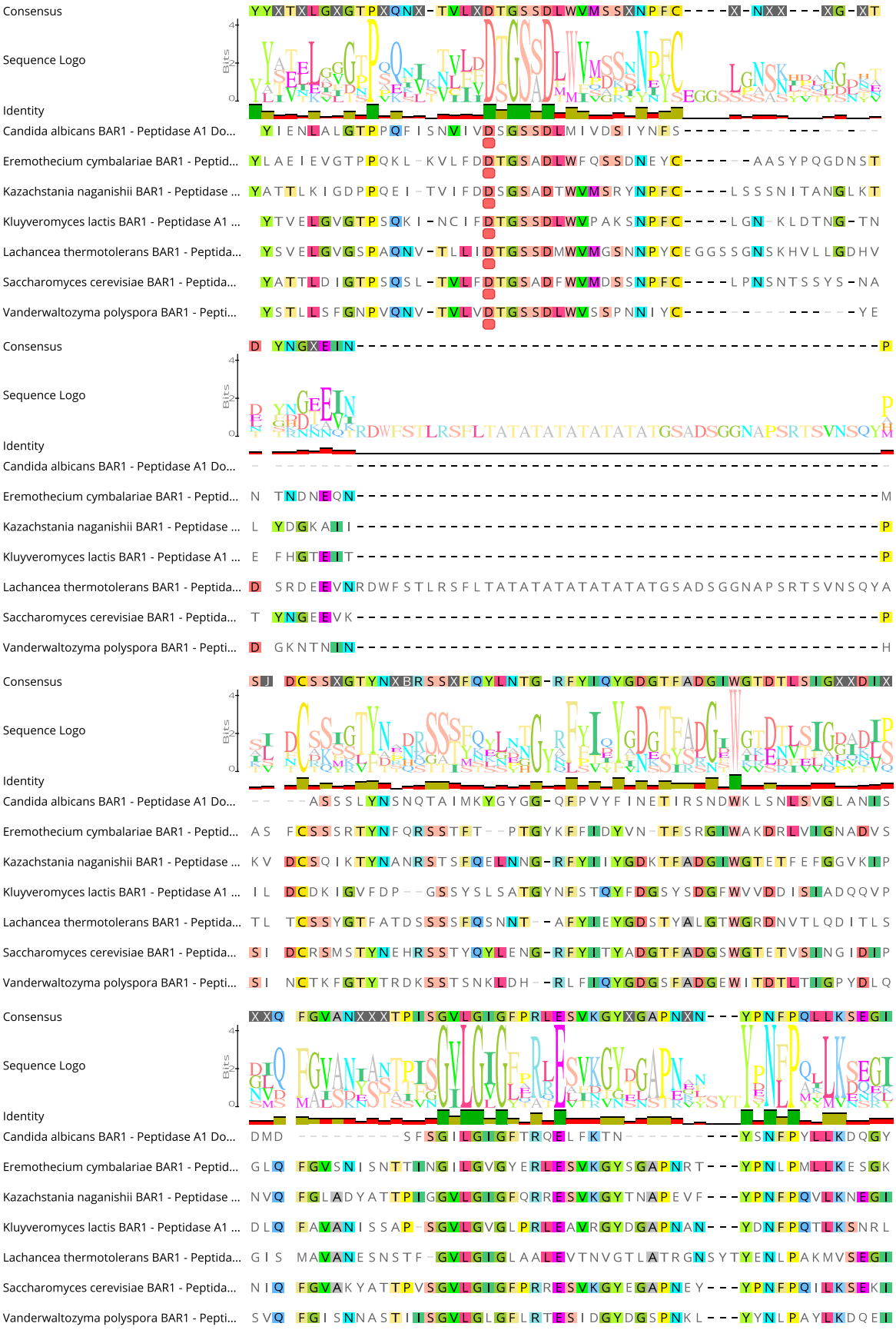
Consensus
Sequence Logo
Bits
Identity
Candida albicans BAR1 - Peptidase A1 Do...
Eremothecium cymbalariae BAR1 - Peptid...
Kazachstania naganishii BAR1 - Peptidase ...
Kluyveromyces lactis BAR1 - Peptidase A1 ...
Lachancea thermotolerans BAR1 - Peptida...
Saccharomyces cerevisiae BAR1 - Peptida...
Vanderwaltozyma polyspora BAR1 - Pepti...

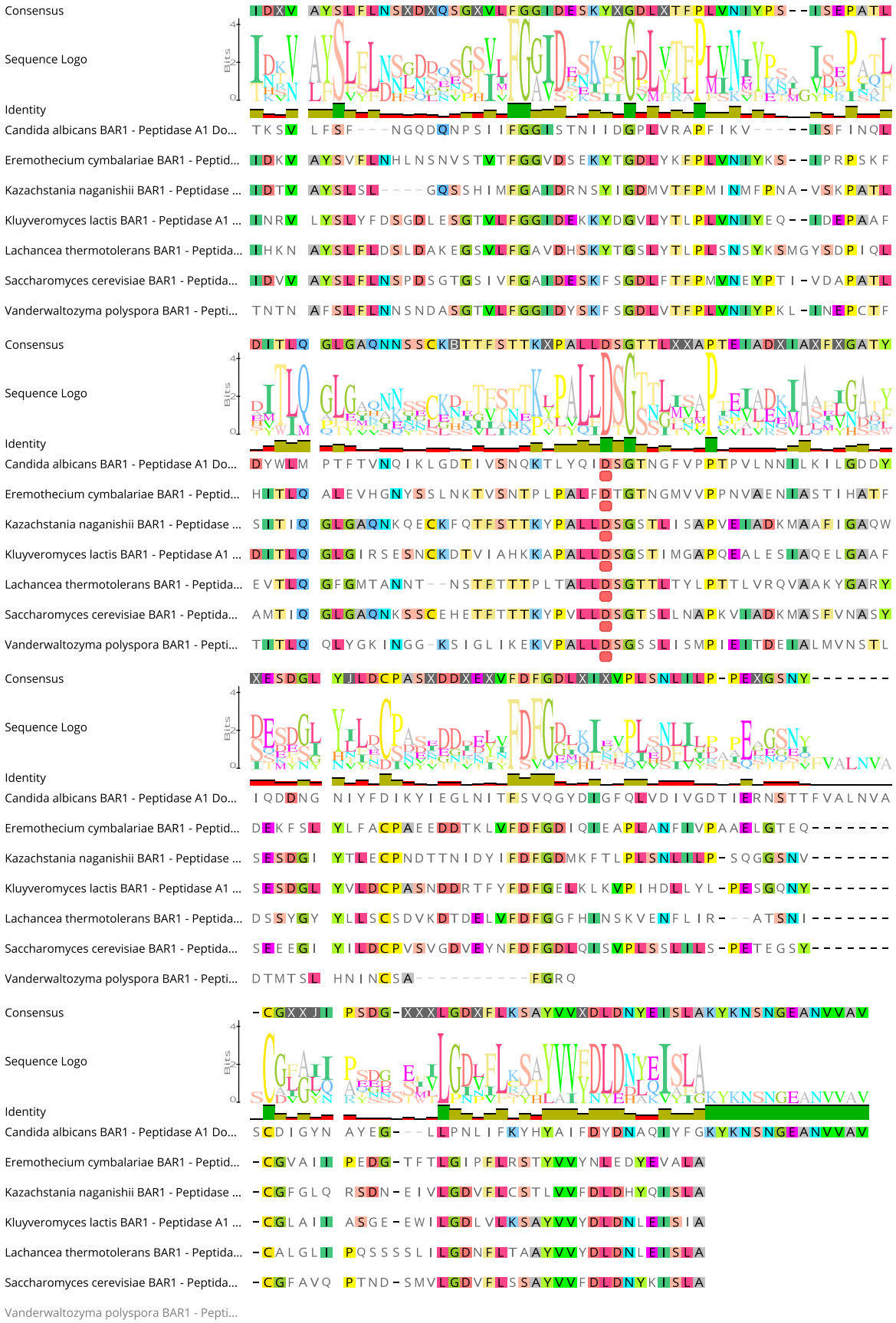
Consensus
Sequence Logo
Bits
Identity
Candida albicans BAR1 - Peptidase A1 Do...
Eremothecium cymbalariae BAR1 - Peptid...
Kazachstania naganishii BAR1 - Peptidase ...
Kluyveromyces lactis BAR1 - Peptidase A1 ...
Lachancea thermotolerans BAR1 - Peptida...
Saccharomyces cerevisiae BAR1 - Peptida...
Vanderwaltozyma polyspora BAR1 - Pepti...

Figure 68: Alignment of the peptidase A1 domains of Bar1s identified in our set of selected species. The annotated peptidase A1 domains were determined by structural homology studies and obtained from Uniprot. Annotated in red are amino acid sequence positions 21 and 300 of the proposed active centers. These two sequences are conserved for all depicted species.

2.2.2 Evolutionary relationships of the selected species

All selected sender parts (α-factors) belong to different classes of the *Ascomycota* phylum of the kingdom fungi and are part of the subdivision of *Saccharomycotina*. Of the analyzed yeast species, the most distantly related one is *C. albicans* and constitutes the only representative of the *Debaryomycetaceae/Metschnikowiaceae*, a sub-family within the order of *Saccharomycotina*. Recent and more extended studies of this phylum led to updated phylogenetic trees as well as the renaming of some species. At present, the most comprehensive phylogenetic trees are based on genome-scale data. Using these data, Xing-Xing Shen and colleagues reconstructed and updated the phylogeny of *Saccharomycotina* [450]. Except for *Lachancea fermentati* and *Lachancea mirantina*, all species we chose were integrated in their study and, those two remaining species were part of another phylogenetic study, exhibiting the relationship between several *Lachancea* species [451].To obtain a comprehensive phylogenetic tree that includes all selected species we obtained parts from, we generated one based on the small subunit ribosomal ribonucleic acid (SSU rRNA) sequences of these species. The SSU rRNA is commonly used for phylogenetic studies, constituting an overview of the evolutionary relationships between different species. For the majority of known species, the SSU rRNA sequence has been identified and the information were deposited and curated in large public databases and are therefore accessible for phylogenetic studies. However, differences between a phylogenetic tree based on SSU rRNA and whole-genome-scale trees are expected. Figure 69 depicts the phylogenetic tree of the selection of eleven species based on the alignment of their SSU rRNAs. The overall structure of the SSU rRNA tree reflects the structure of the whole-genome tree. *C. albicans* was the only member of the separate clade of the subfamily *Debaryomycetaceae*. All the other species built the clade of *Saccharomycetaceae*. Within this clade, two subgroups could be distinguished that included all species except for *Lachancea thermotolerans*, *Tetrapisispora phaffii*, and *Lachancea fermentati*. The whole-genome tree could not be compared with the SSU rRNA tree for *L. fermentati* and *L. mirantina*, since these species were not included in the study. *L. thermotolerans* and *T. phaffii* however were part of the Shen *et al.* study [450]. Differently from the SSU rRNA tree, in the whole-genome tree *L. thermotolerans* was part of the clade of *K. lactis* and *Eremothecium cymbalariae*. In the SSU rRNA-based tree, *K. lactis*, *E. cymbalariae*, and *L. mirantina* built one clade. The clade of *K. lactis* and *E. cymbalariae* was in line with our results. In our tree, the second clade consists of *K. africana*, *K. naganishii*, *Vanderwaltozyma polyspora*, and *S. cerevisiae*. This evolutionary relation was consistent with the one found in the publication of the Shen *et al.* study, in which also the common ancestor of *K. africana* and *K. naganishii* was shown. The branch of *V. polyspora* and *S. cerevisiae* was not entirely in line with the whole-genome tree what we would have expected. Also, we did not expect that *T. phaffii* did not cluster with this clade, since according to the tree of Shen *et al.*, this species is closely related to *V. polyspora* [450]. Overall, the SSU rRNA-based tree reflected the phylogenetic relationship between the species, the observed differences were expected when taking into consideration the differ-

ences in analysis, e.g. the SSU rRNA analysis does not account for genome duplications. Nevertheless, both phylogenetic trees served as reference to compare phylogenetic analyses of the α-factors, α-factor receptors (Ste2), and the barrier proteases (Bar1).
In higher organisms, the natural occurrence of non-sterile reproduction is an indicator for species discrimination. By determining the evolutionary relation of the mating components (α-factors, Ste2 receptors, Bar1s), we sought to study if species separation was also noticeable in the mating communication in yeast. We additionally examined the correlation between species separation, protein evolution and if signaling crosstalk could be found. Furthermore, we explored the predicted co-evolution of the Ste2 receptor, α-factor, and the Bar1 proteases.

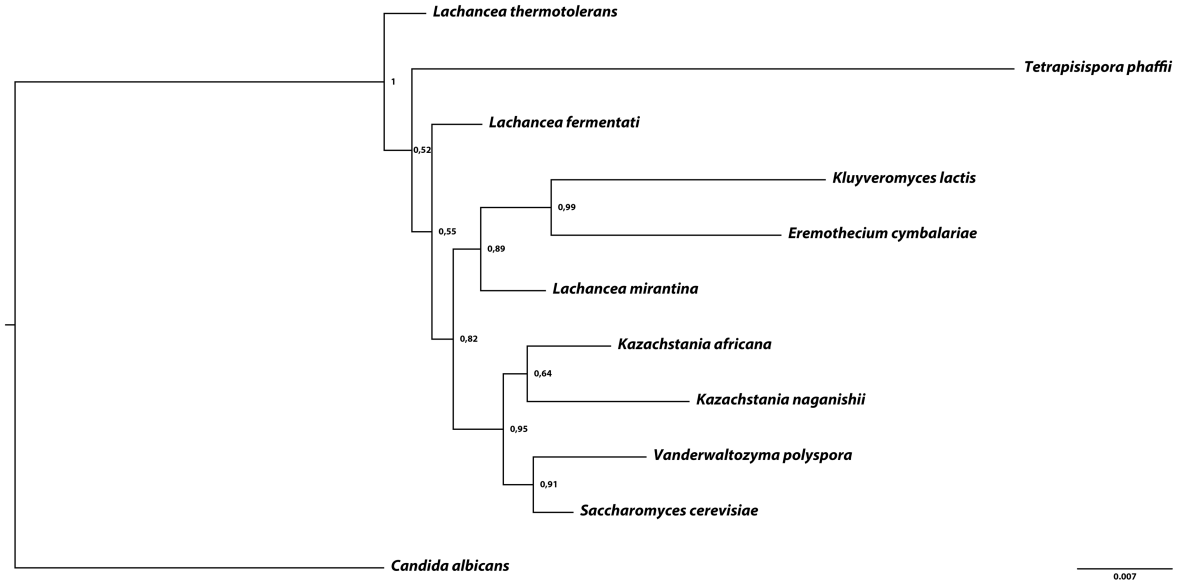

Figure 69: Phylogenetic tree based on the SSU rRNA sequences of the selected species. The phylogenetic tree represents the likelihood analysis of the SSU rRNA sequences obtained from the ribosomal RNA database SILVA (Table 29).

In Figure 70 the phylogenetic tree of the amino acid sequences of the mature α-factor is shown. The resulting clades varied from the SSU rRNA and whole-genome tree, most likely due to the shortness of the amino acid sequences, which increases the difficulty to differentiate between sequence homologies. However, also for the mature α-factors we identified two clades and six unrelated α-factors. As previously, *C. albicans* represented an outgroup species. The α-factors of *K. africana*, *K. lactis, L. fermentati*, *L. mirantina*, *L. thermotolerans*, and *S. cerevisiae* each exhibited a separate branch point, which indicates that no closer relationship was found for these mature α-factors. The pheromones of *E. cymablariae*, *K. naganishii*, *V. polyspora*, and *T. phaffii* form a clade, having a common branching point. Within this branch, the pheromones of *E. cymablariae*, *K. naganishii*, *and V. polyspora* were the closest related. However, the closer evolutionary relation between *E. cymablariae* and *V. polyspora* pheromones stands in contrast to both the whole-genome and the SSU rRNA trees. Due to the short mature α-factor sequences, this tree could only provide limiting insights into the actual relationship between the species but it could nonetheless be helpful and of importance in terms of signaling crosstalk.

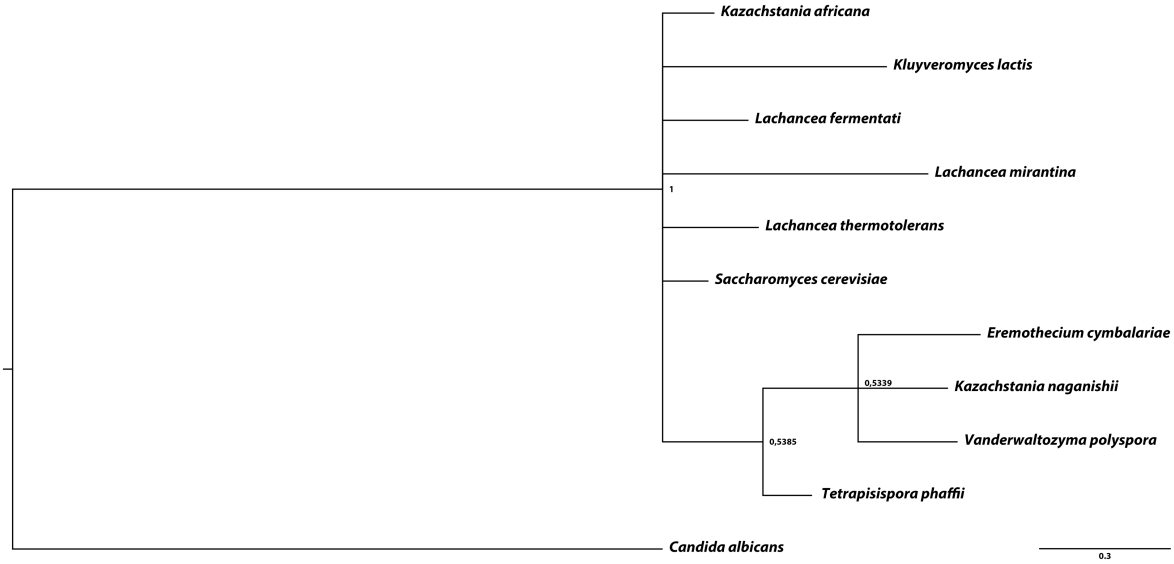

Figure 70: Phylogenetic tree of the amino acid sequences of the mature α-factors. The tree represents the likelihood analysis of the amino acid sequences of the mature α-factors of the selected species. We used the most abundant or first pheromone that was identified by the *in silico* identification of the MFfα1-like sequences from 11 different species.

Next, we generated a tree of the amino acid sequences of the pre-pro-α-factors to investigate, whether its structure was more resembling the reference trees. The likelihood analysis of the pre-pro-pheromones was depicted as a phylogenetic tree in Figure 71. The clade of *C. albicans* remained an outgroup as for the analysis of the amino acid sequences of the mature pheromones. However, for the remaining pre-pro-α-factors ,we obtained a more defined tree structure. The pre-pro-α-factoris of *K. africana*, *K. lactis*, *L. fermentati*, *L. mirantina*, *L. thermotolerans*, *S. cerevisiae*, and *T. phaffii* were now structured in one clade. Except for the α-factors of *S. cerevisiae* and *T.phaffi*, all others were closely related and formed a subclade. The relatedness of the pre-pro-α-factors of *K. lactis* and the *Lachancea spec.* reflected the one found in the whole-genome phylogenetic analysis [450]. However, we had also expected *E. cymablariae* to be part of this clade.
When comparing the relationships between the amino acid sequences of the mature and the pre-pro-pheromones, visible differences could be found. For the analysis of the mature pheromones, we identified a clade consisting of *E. cymablariae*, *K. naganishii*, and *V. polyspora* (Figure 70). In opposition, the pre-pro-α-factor alignment revealed though that each of them had their own branching point (Figure 71). The mature α-factor of *T. phaffii,* which exhibited higher similarities, was similar to the pre-pro-pheromone sequence closer related to *S. cerevisiae*.
Overall, the phylogenetic analysis based on the likelihood analysis of the mature as well as on the pre-pro-α-factors remained inconclusive. It can be hypothesized that the selection pressure was focused on the mature pheromone. Large parts of the pre-pro-α-factor are cleaved off during the maturation process and therefore, have no phenotypic effect. Repetitive sequences within the pre-pro-α-factors indicate that duplication of entire pheromone units might have occurred.

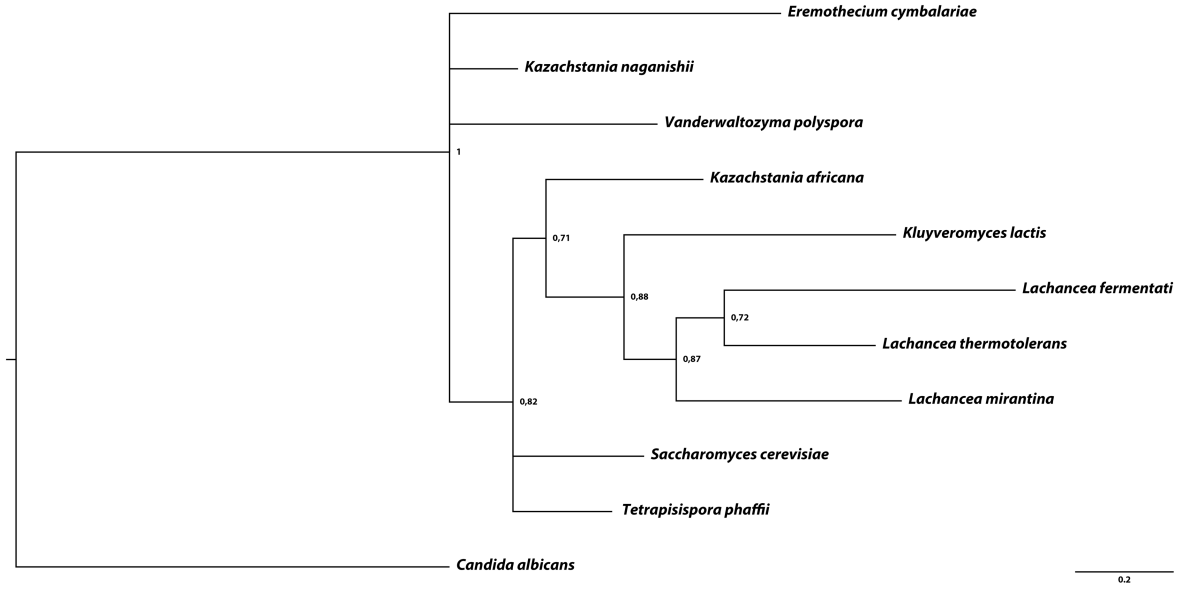

Figure 71: Phylogenetic tree of the amino acid sequences of the pre-pro-α-factors. The tree represents the likelihood analysis of the amino acid sequence of the pre-pro-α-factors of the selected species.

Figure 72 shows a phylogenetic tree based on the likelihood analysis of the protein sequences of the Ste2 -like α-factor binding GPCRs. The tree contained three clades, while one only consisted of *C. albicans*, the outgroup of this tree. The receptors of *E. cymbalariae*, *L. fermentati*, *L. thermotolerans*, *L. mirantina*, and *K. lactis* exhibited a common ancestor. With this clade, all *Lachancea spec.* receptors were part of one subclade. This was in accordance with the genome-based tree, with the exception of *L. fermentati* and *L. thermotolerans* which were not considered in this tree [450]. In comparison to the SSU rRNA tree we only saw a common ancestor for the Ste2 receptors of *K. lactis*, *E. cymablariae*, and *L. mirantina*. The GPCRs of *L. thermotolerans* and *L. fermentati* were not part of this clade in the SSU rRNA tree. Also, the more detailed branching was in line with the genome-based phylogenic tree that depicted a closer relatedness between *E. cymablariae and L. thermotolerans* than with *K. lactis*. We registered that the $Ste2_{Kl}$ receptor exhibited a separate branching point and possessed therefore less homology with the other species in this group. The other clade of the phylogenetic tree was formed by a common ancestor of the *K. africana*, *K. naganishii*, *S. cerevisiae*, *T. phaffii*, and *V. polyspora* receptor. This tree branch was fully in line with the whole-genome tree [450]. With the exception of *T. phaffii*, all members of this clade were also found to be grouped in one clade in the SSU rRNA tree (Figure 69). The $Ste2_{Sc}$, $Ste2_{Ka}$, and $Ste2_{Kn}$ are closer related than $Ste2_{Tp}$ and $Ste2_{Vp}$. The latter two were separating from the others and built their own subclade. Besides the closer relation of the Ste2 receptors of *T. phaffii* and *V. polyspora*, as well as *K. africana* and *K. naganishii*, also their whole genomes indicated a closer relationship of the species. Overall, the $Ste2_{Sc}$ had less homology with the other receptors in this group, which was again in line with the tree generated by Shen *et al.* [450]. Taken together, the tree of the Ste2-like receptors was similar to the genome-based phylogenetic tree, which indicated more conclusive results. A similar trend was observed for the comparison of the receptor tree with the SSU rRNA tree, with some exceptions.

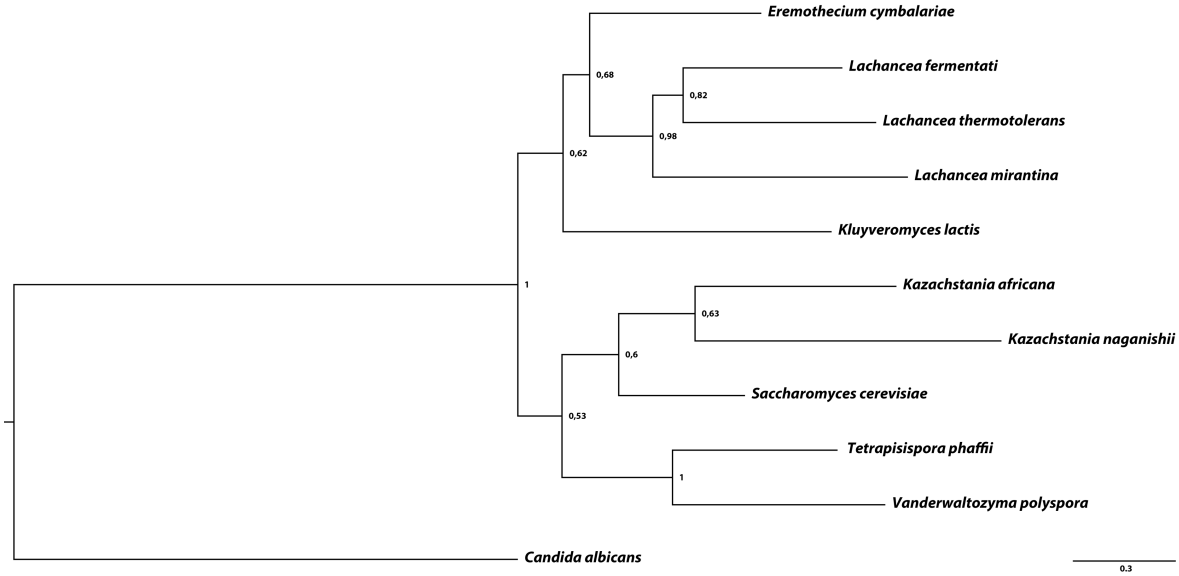

Figure 72: Phylogenetic tree of the amino acid sequences of the Ste2 receptors. The tree represents the likelihood analysis of the amino acid sequences of Ste2 receptors of the selected species.

Besides the α-factors and the Ste2 receptors, the barrier proteases Bar1 are part of the mating process [211]. Furthermore, it was proposed that the Bar1 proteases closely co-evolved with the Ste2 receptors and recognize similar amino acid sequences as the Ste2 receptors [298]. In Figure 73 we plotted the phylogenetic tree-based likelihood analysis of the amino acid sequences of the Bar1 proteases. Similar to the Ste2 receptors, we identified four general clades. As for the α-factors and the receptors, *C. albicans* was in a separate clade and served as the outgroup during tree generation. The Bar1 proteases of *E. cymablariae*, *L. thermotolerans* and *K. lactis* were grouped in one clade. Also, the whole-genome phylogenetic tree indicated a closer relationship between these three species. A clade consisting of $Bar1_{Ec}$, $Bar1_{Lt}$, and $Bar1_{Kl}$ was similarly found for the Ste2 receptors. A crosstalk experiment studying the binding of pheromones to the Ste2-like receptors and Bar1 pheromone degradation, which takes these evolutionary findings into account, is of interest to answer the question, whether receptors and proteases recognize the same amino acid sequences of the α-factors. When we compared the Bar1-based tree with the SSU rRNA tree, K. *naganishii* and *S. cerevisiae* were grouped into one clade. Also *K. lactis* and *E. cymbalariae* showed a common ancestor in the SSU rRNA tree. The similarity of the clades underlined the hypothesis of a co-evolution of the receptors and the proteases. The other clade was formed by $Bar1_{Sc}$ and $Bar1_{Kn}$. Also, in this case the receptors of *S. cerevisiae* and K. *naganishii* were grouped in the same clade as $Bar1_{Sc}$ and $Bar1_{Kn}$. Differently from the receptors, in the Bar1 amino acid phylogenetic tree the Bar1 originating from *V. polyspora* was not grouped together with $Bar1_{Sc}$ and $Bar1_{Kn}$. All our selected Bar1-like proteases belonged to the peptidase A1 subgroup but for the protease of *V. polyspora*, the α-factor protease activity was only derived from sequence homology studies [452]. However, it was hypothesized that the Bar1-like proteases evolved from different ancestors, since for example for *S. pombe,* the Bar1 protease does not belong to the peptidase A1 subgroup. The functionality of the $Bar1_{Vp}$ as an α-factor protease thus remained to be proven.

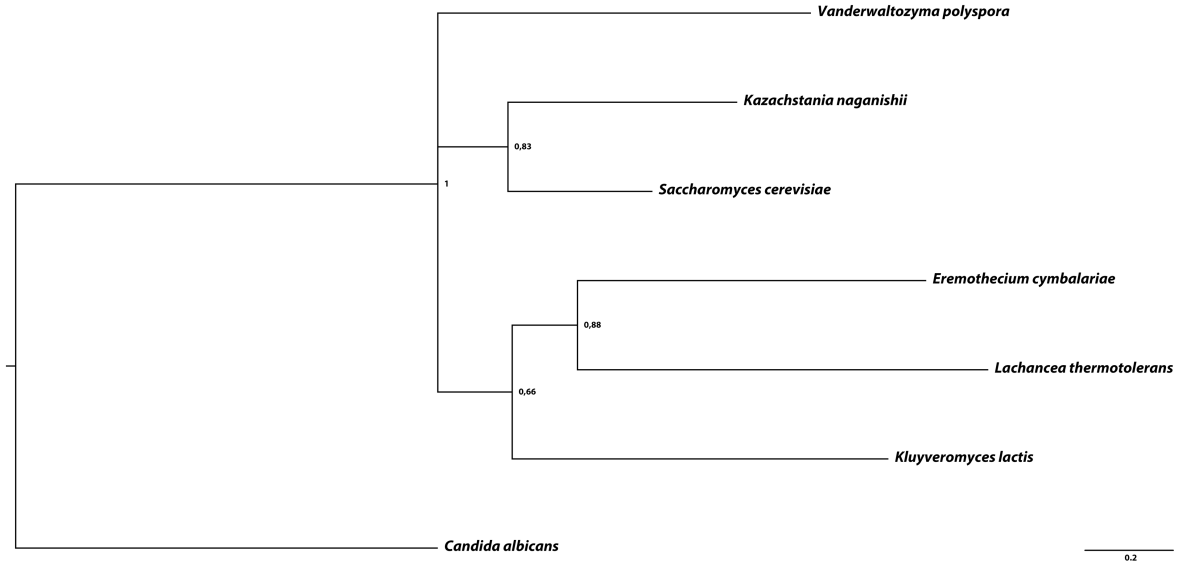

Figure 73: Phylogenetic tree of the amino acid sequences of the Bar1 proteases. The tree represents the likelihood analysis of the amino acid sequences of Bar1-like proteases identified in our set of the selected species.

To summarize, the SSU rRNA-based phylogenetic trees exhibited partial agreement with the whole-genome-based phylogenetic tree and can thus further be used as a reference to compare with the characterization results below. The phylogenetic analyses of the pheromones remained challenging and inconclusive and further investigation is required. We assume that the results of the pre-pro-α-factor analysis could be more suitable for phylogenetic analyses. We were thus aiming to correlate the upcoming results of our pheromone-receptor experiments and pheromone-protease experiments with the phylogenetic trees to identify if crosstalk patterns could be explained by the relationship of the species.

2.2.3 Growth of *MAT***a** and *MAT*α chassis cells under α-factor stimulation

First, we wanted to test, whether addition of α-factor to the media had an effect on growth. Throughout our studies, we utilized different strains, both *MAT*α (*ste3Δ::klTRP1 mfa1Δ::natNT2 mfa2Δ::hphNT1)* and *MAT***a** (*MAT***a** *lys2::rttAS2 mfa2Δ::hphNT1 mfa1Δ::klTRP1 bar1Δ::kanMX ste2Δ::natNT*) background strains. The mating genes were knocked-out in these strain backgrounds. In order to stimulate the strains with α-factor, the $Ste2_{Sc}$ receptor was reconstituted and expressed and under the control of a constitutive promoter. Additionally, we knocked-out *far1*, which is responsible for cell cycle arrest upon mating pathway induction by inhibiting the CDK [453]. Cells with a deletion of the *far1* gene were expected to not exhibit any cell cycle arrest, other pheromone-responsive cell physiological phenotypes however may still be observed. We measured the optical density of three biological replicates of the four different strains over time using a plate reader. Each line represents the mean optical density and the grey shadow indicates the standard deviation. Figure 74 displays the growth over time of the strains in absence and presence of α_{Sc}-factor. First, we monitored the growth of the *MAT*α strain background both with and without α-factor (Figure 74A). The growth of the *MAT*α strain in media with α_{Sc}-factor was slightly reduced in comparison to the growth in absence of α-factor. This was expected since the cells should exhibit an arrested cell cycle. Though, the cell cycle was arrested only for a short period since the cells quickly resumed growth. In contrast, for the growth of the *MAT*α strain with the

deletion of the *far1* gene we could not observe a reduction in growth upon pheromone induction (Figure 74B).

For the *MAT***a** strain background, we saw a noticeable reduction of the growth upon α-factor induction in comparison to the absence of α-factor (Figure 74C). The observed increase of the optical density at later timepoints was most likely a result of the increase in cell volume due to shmooing and increased cell size. The Far1 knockout *MAT***a** strain didn't exhibit any cell cycle arrest upon α-factor stimulation, as it was previously indicated in literature (Figure 74D) [453].

Overall the experimental results were as predicted and in line with previous findings [453,454]. Since the *MAT***a** *far1* gene deletion strain background exhibited no or only minor reduction of the growth in presence of α-factor, this strain was used for our multicellular networks.

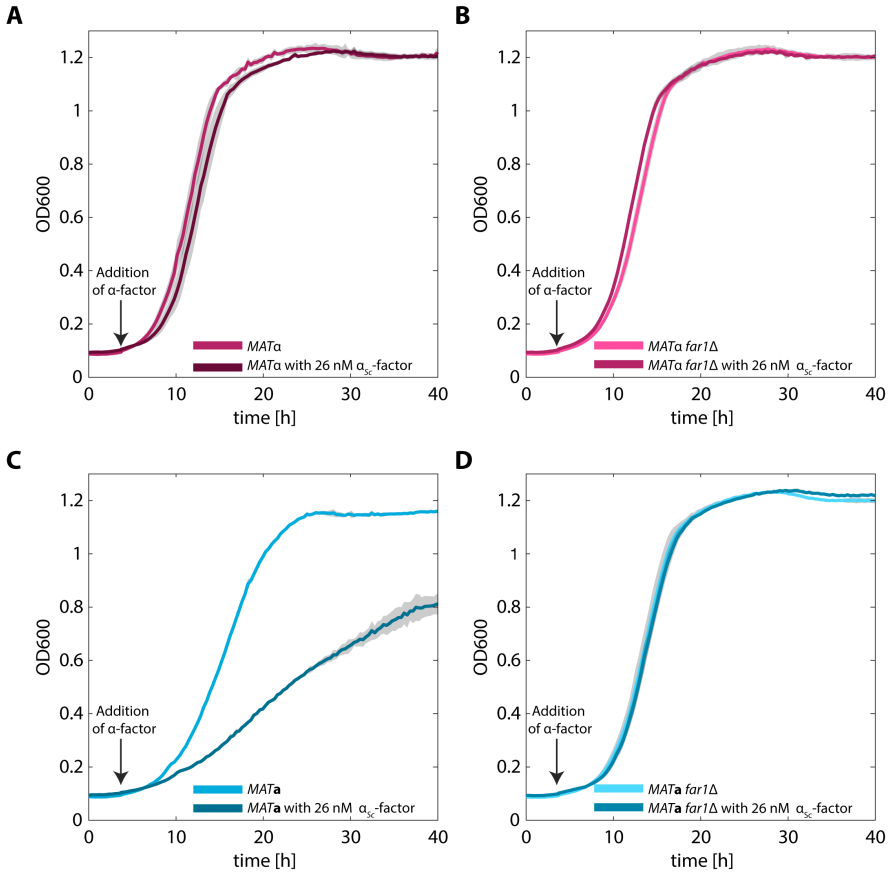

Figure 74: Growth curves of strains utilized in this study with 0 and 26 nM α-factor (added at t= 4 h). A) *MAT*α *ura3 Δ*::[P_{PAB1}-*ste2*$_{Sc}$-T_{ENO1}-*leu2*]. **B)** *MAT*α *Δfar1*::*ura3 ura3 Δ*::[P_{PAB1}-*ste2*$_{Sc}$-T_{ENO1}-*leu2*]. **C)** *MAT***a** *ura3 Δ*::[P_{PAB1}-*ste2*$_{Sc}$-T_{ENO1}-*leu2*]. **D)** *MAT***a** *Δfar1*::*ura3 ura3 Δ*::[P_{PAB1}-*ste2*$_{Sc}$-T_{ENO1}-*leu2*].

2.2.4 Design of the yeast communication toolkit

The YCTK consists of eleven sender (α-factors), eleven receiver (Ste2 receptors) and five functional barrier (Bar1 proteases) parts (Figure 75). Besides, the toolkit contains seven promoters that are induced by the stimulation of the mating pathway upon α-factor induction. In addition, we also included the P_{TetO7} promoter into the collection. This promoter can either be repressed or activated in response to the availability of the TetR transcription factor. In our studies, we used the Tet-ON system, which is induced upon addition of doxycycline. All parts are fully compatible with

the Yeast Golden Gate Toolkit (YTK) published by Lee *et al.* [71]. This toolkit is among the most commonly used cloning kits for the assembly of circuits and pathways in yeast and served as the starting point for the communication toolkit extension. Although our parts are compatible with their toolkit parameters, we did not follow all their design rules. For all parts, the NotI, BsaI, and BsmBI enzyme recognition sites were removed, further referred to as domesticated. Also, they include the linker sequences required to be compatible as part 2 (promoter parts) and part 3 (ORF). Differently, the YCTK sender and receiver parts include a stop codon within their part sequences. Thus, C-terminal tagging as intended for the YTK parts was omitted. This design feature was not included since the processing during the pheromone maturation process cleaves and digests all C-terminal extensions of the pre-pro-α-factors. In addition, it is unknown how sequence additions to the C-terminus might influence the processing during α-factor maturation. As the impact of C-/N-terminal tagging of these Ste2-like receptors remains under investigation to date, no alteration from the natural sequences was desired to ensure and maintain functionality. For the barrier parts, all design features for part 3 of the YTK were included. Therefore C-terminal tagging of the Bar1 like proteins is possible, allowing the purification of the proteases for further analysis. All of our parts can be easily adapted to the entire YTK standard by point directed mutagenesis, if required. To extend the flexibility of the assembly of devices to more complex networks, we designed and built five pairs of assembly connectors (part level 1 and 5). These parts exhibit the design features of ConL' and ConR' parts and are based on the design of ConL1-ConL5 and ConR1-ConR5. The ConL' and ConR' parts were utilized in entry vectors. The parts of the YCTK in combination with the YTK allow the rapid assembly of various communication devices.

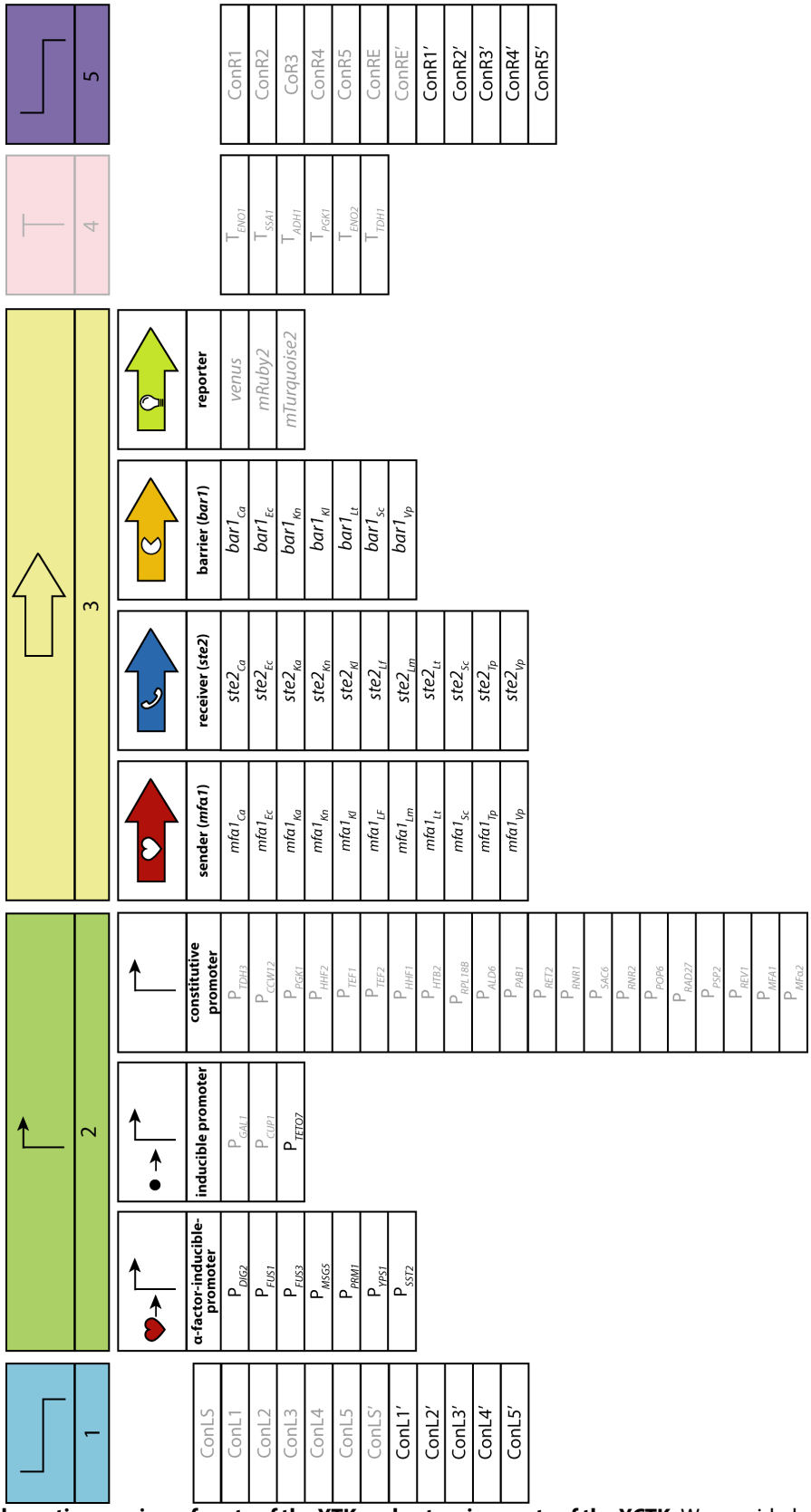

Figure 75: Schematic overview of parts of the YTK and extension parts of the YCTK. We provided additional connectors, pheromone-inducible and inducible promoters, sender, receiver and barrier parts. Parts originating from the YTK are represented in grey. Figure inspired by Lee *et. al.* [71].

2.2.5 Characterization of YCTK parts

For the design of biological systems that will behave in a predicted manner, standards are of high importance. Since for present biological standards prediction of their behavior is limited, characterization of all parts to be used in the design of circuits and networks is required to ensure the functionality of a system. For the YCTK, we characterized all sender, receiver and barrier parts, as well as the promoters that we added to the existing YTK collection. To assure that the characterization results were comparable to the YTK collection, we selected for the promoter characterization benchmark promoters that were previously characterized for the YTK. For the communication toolkit parts (sender, receiver, and barrier) we also investigated crosstalk between the different components and the influence of the expression strength onto the communication system.

2.2.5.1 Responder part characterization - promoter

2.2.5.1.1 Inducible promoter parts

To engineer complex networks like, e.g., an amplifier, inducible promoters are a prerequisite. The YTK comprises the P_{GAL1} and the P_{CUP1} promoter. The P_{GAL1} promoter is galactose-inducible, and the P_{CUP1} promoter can be stimulated by copper ($CuSO_4$) in the media. We extended this selection by introducing the P_{TETO7} promoter into our YCTK. The P_{TETO7} promoter can either be induced or repressed by doxycycline, depending on the associated transcription factor system in the chassis strain background. In our study, the chassis strain expresses the reverse tetracycline trans-activator (rtTA) from the *LYS2* locus on the chromosome. Thus, the P_{TETO7} promoter is induced upon addition of doxycycline.

For the engineering and circuit design process, it is essential to obtain the main characteristics of each part. For promoters, the dose-response, leakiness, and maximal induction are most crucial. We hence determined these properties for different constructs containing the P_{CUP1} and the P_{TETO7} promoter.

2.2.5.1.1.1 P_{CUP1} dose-response characterization

First, we characterized P_{CUP1} in our *MAT***a** *far1*Δ, *mfa2*Δ, *mfa1*Δ, *ste2*Δ LYS::*rtTA* strain background. Since we were planning to utilize the P_{CUP1} promoter to investigate the behavior of sender, receiver, and barrier parts under different expression strength conditions, we built several P_{CUP1} characterization constructs. P_{CUP1} was compared on the one hand with P_{PGK1}, the promoter that was implemented to express the sender parts, with P_{PAB1}, which was used in the receiver devices, and with P_{HHF1} expressing the barrier protease genes. Each part device also contained a dedicated terminator and integration site sequence, which we also applied to our P_{CUP1} characterization constructs. As the readout for our characterization modules, we utilized the fluorescent protein Venus as it exhibits the shortest maturation time of the reporter genes available in the toolkit. Each expression characterization device consists of an integration site (*HO* or *URA3*), the P_{CUP1} or benchmark promoter (P_{PGK1}, P_{PAB1}, or P_{HH1}), the *venus* gene as reporter, a unique terminator (T_{TDH1}, T_{ENO}, or T_{ENO2}), and a selection marker (*LEU2* or *HIS2*) (Figure 76). Especially the promoters were selected to be similar to the estimated native expression strengths of the promoters of sender, receiver and barrier parts. Each device was chromosomally integrated and colony PCR-verified. To characterized each strain, we induced the cells with different $CuSO_4$ concentrations measured for each

condition and replicate 50,000 cells using flow cytometry. More information on the approaches of gating and data processing can be found in material and methods (chapter 4.6.5).

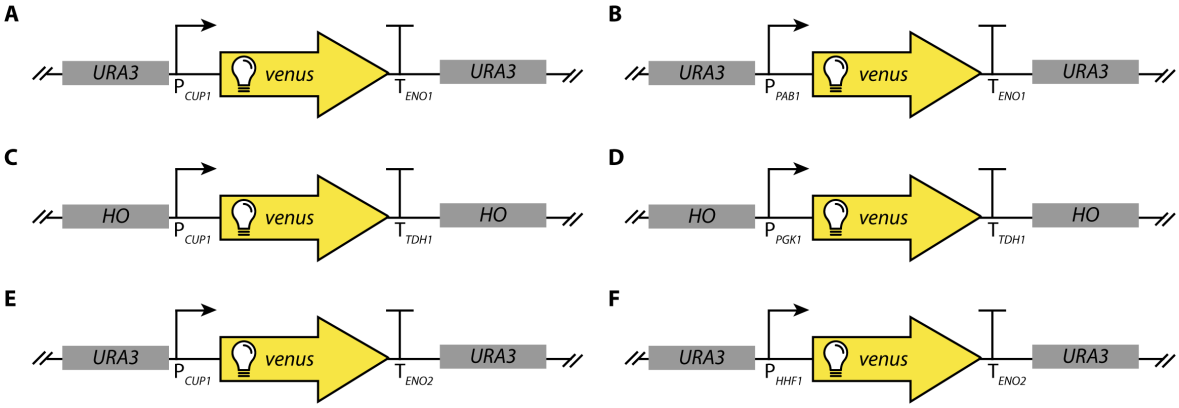

Figure 76: Genetic constructs for the P_{CUP1} promoter characterization. A) P_{CUP1}-*venus*-T_{ENO1} construct with *URA3* homology sequences. **B)** P_{PAB1}-*venus*-T_{ENO1} construct with *URA3* homology sequences. **C)** P_{CUP1}-*venus*-T_{TDH1} construct with *HO* homology sequences. **D)** P_{PGK1}-*venus*-T_{TDH1} construct with *HO* homology sequences. **E)** P_{CUP1}-*venus*-T_{ENO2} construct with *URA3* homology sequences. **F)** P_{HHF1}-*venus*-T_{ENO2} construct with *URA3* homology sequences. The constructs were designed to be compared in pairs, A-B, C-D, and E-F.

For each replicate, we utilized the mean fluorescence intensity of 50,000 cells and calculated a mean and standard deviation from three replicates. Figure 77 displays the dose-response curves of the P_{CUP1} promoter constructs with the curves of their corresponding benchmark characterization devices. For all three P_{CUP1} constructs, we observed promoter leakiness as it had previously been reported [71]. The effect of the terminator sequence on the fluorescence output can be deduced from the P_{CUP1}-*venus*-T_{ENO1} and P_{CUP1}-*venus*-T_{ENO2} constructs, which only vary in their terminators. The dynamic range of P_{CUP1} was monitored to be between 0.75 µM and 25 µM $CuSO_4$. Most essential for us was the comparison of the expression strength to the ones of our selection of constitutive promoters (P_{PGK1}, P_{PAB1}, P_{HHF1}), utilized for the expression of the sender, receiver and barrier genes. While the expression profile of P_{CUP1} was in a similar range as P_{PAB1} and P_{HHF1}, P_{CUP1} could not reach to the expression strength of P_{PGK1}. For the P_{PGK1} promoter, an approximately three-fold higher Venus signal was measured in comparison to the P_{CUP1} promoter (Figure 77). With fluorescence intensities of about 1,900 a.u., the P_{HHF1} promoter resulted in expression strength similar to the maximally induced expression of the P_{CUP1} promoter (Figure 77). When the P_{CUP1} expression was compared to the P_{PAB1} promoter, a three-fold higher maximally induced expression was detected than for the constitutive one (Figure 77). The expression strength of the P_{PAB1} promoter was similar to the expression of the P_{CUP1} promoter induced with 3.13 µM $CuSO_4$. These results indicated that the titration of the expression of the sender and the barrier parts in the same expression strength range as from the constitutive promoters is feasible, when being expressed from the P_{CUP1} promoter. For the sender genes, expression levels similar to the constitutive gene expression would not be reached when using the P_{CUP1} promoter. Overall, the P_{CUP1} promoter is suitable to study the effect of expression strength for receptor and barrier parts by also covering the levels of the constitutive expression range. For the sender parts, only significantly reduced expression levels could be studied. Drawbacks, when utilizing this promoter are

the limited dynamic range, the relatively low maximal expression strength, a visible leakiness of the expression as well as slight toxicity of $CuSO_4$ for the cells [71].

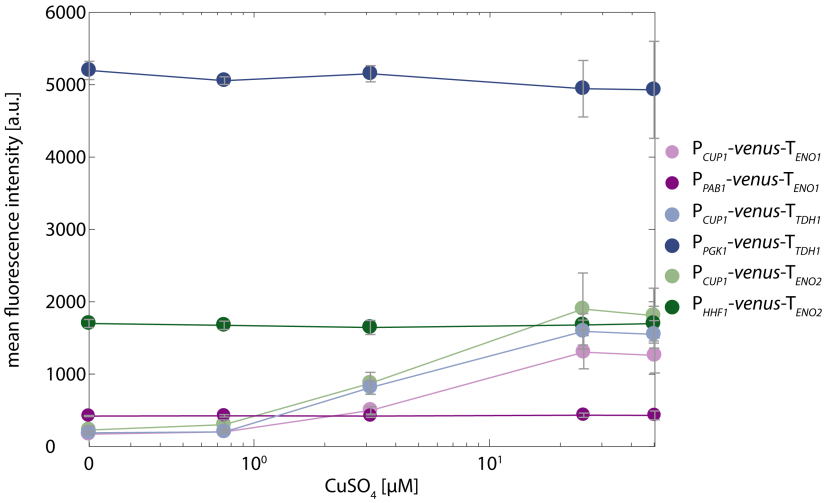

Figure 77: Dose-response curve of the P_{CUP1} promoter characterization in comparison to constitutive promoters. Dose-response curve of three biological replicates of the strains harboring P_{CUP1}-venus-T_{ENO1} or P_{PAB}-venus-T_{ENO1}, dose-response curve of three biological replicates of the strains harboring P_{CUP1}-venus-T_{TDH1} strain or P_{PGK1}-venus-T_{TDH1}, and dose-response curve of three biological replicates of the strains harboring P_{CUP1}-venus-T_{ENO2} strain or P_{HHF1}-venus-T_{ENO2}. Plotted are the mean fluorescence intensity of Venus in response to five $CuSO_4$ concentrations.

2.2.5.1.1.2 P_{TETO7} dose-response characterization

In comparison to the copper-inducible promoter, the P_{TETO7} promoter exhibited a greater dynamic range as well as reduced basal expression in absence of the inducer. The characterization device for the P_{TETO7} promoter was integrated into the *URA3* locus and consists of the P_{TETO7}, the reporter gene *venus* as well as the T_{ENO1} terminator (Figure 78).

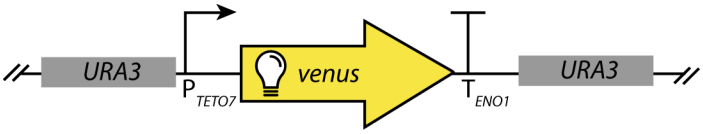

Figure 78: Genetic construct for the P_{TETO7} promoter characterization. P_{TETO7}-*venus*-T_{ENO1} construct with *URA3* homology sequences. The construct was integrated into the *MAT***a** *far1Δ* strain background.

The data acquisition, gating, and data processing were similar to the characterization of the P_{CUP1} promoter. We tested twelve different doxycycline concentrations ranging from 0 µM to a maximal concentration of 20 µM. Promoter induction with the maximal concentration of doxycycline did not result in a saturation of the promoter activity in our chassis background (Figure 79). This indicated that the dynamic range of this promoter might be suitable for higher induction requirements. Overall, the fluorescence intensities resulting from the induction with 20 µM doxycycline were comparable to the maximal induction of the P_{CUP1} promoter, while the latter one already reached its saturation. An almost linear dynamic range was measured for the P_{TETO7} promoter between 0.45 µM and 20 µM doxycycline. With a 14-fold induction between 0 and 20 µM doxycycline, the P_{TETO7} is an adequate promoter to be employed in engineered inducible systems.

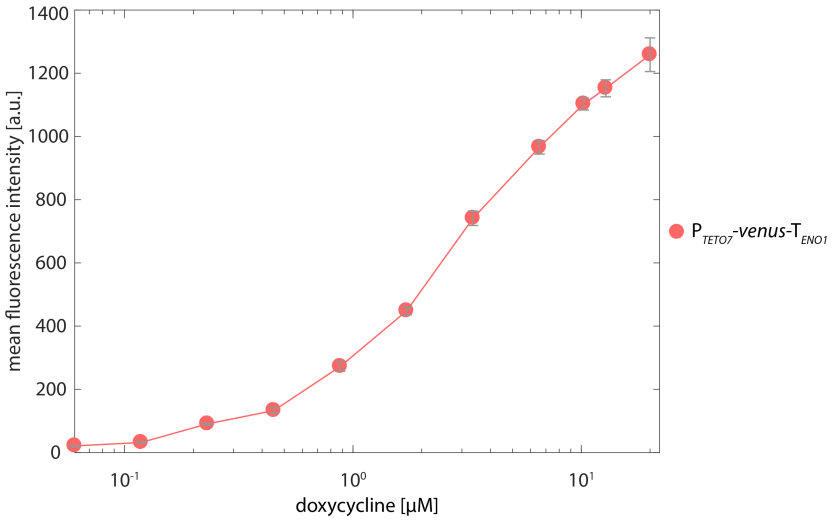

Figure 79: Dose-response curve of the P_{TETO7} promoter. Dose-response curve of three biological replicates of the *MAT***a** *far1Δ* strain carrying P_{TETO7}-*venus*-T_{ENO1} as mean fluorescence intensity of Venus for 12 different doxycycline concentrations.

2.2.5.1.2 Pheromone-inducible promoter parts characterization

Determining the characteristics of promoters is of high importance in order to allow the construction of complex networks and to be able to predict their behavior in these contexts. Since the genetic background of a chassis strain might influence the performances of the promoters, we tested all promoters in different strains. We tested promoter expression both in *MAT*α and in *MAT***a** cells, in which the $Ste2_{Sc}$ receptor was deleted. To enable the characterization of the pheromone-responsive promoters, we reconstituted the $Ste2_{Sc}$ by expressing it from the constitutive P_{PAB1} promoter, which was integrated into the *URA3* locus, if not noted differently. The reporter gene, terminator, integration site, and selection marker are identical for all promoter constructs, if not noted differently, to facilitate direct comparison and to be able to identify the effects of the strain background on the promoter dynamics. All constructs were chromosomally integrated into the *HO* locus of the respective strain (Figure 80). To classify the behavior of our selected promoters into the profiles of the promoters of the YTK collection, we included three constitutive benchmark promoters, namely P_{TDH3}, P_{RPL18B}, and P_{REV1} into the set of promoters being characterized. These promoters were selected as they represented the strongest (P_{TDH3}), the medium (P_{RPL18B},), and the lowest (P_{REV1}) constitutive promoters of the YTK collection. Since all of the α-factor-responsive promoters exhibited significantly lower expression levels than P_{TDH3}, we did not include the dynamics of P_{TDH3} in our graphs.

The reporter Venus reporter was expressed from the different α-factor-inducible mating-pathway response promoters. Thus, the measured fluorescence intensities reflected mating pathway activity but will only be referred to a fluorescence intensity upon α-factor stimulation throughout this study.

For all data points, we utilized the mean fluorescence intensities of approximately 50,000 single cells, which were recorded using flow cytometry. The experimental setup, gating, and data processing can be retraced in the material and methods section (chapter 4.6.5).

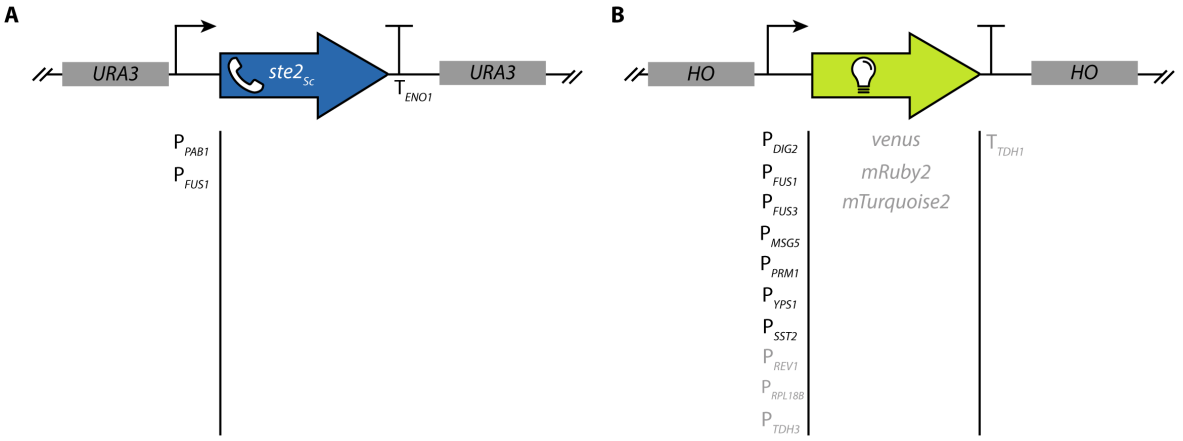

Figure 80: Constructs used for the characterization of the α-factor-inducible promoters. A) P_{PAB1}-ste2$_{Sc}$-T_{ENO1} construct with URA homology sequences or P_{FUS1}- ste2$_{Sc}$ -T_{ENO1} construct with URA3 homology sequences that were integrated into the different strains utilized for the pheromone-inducible promoter characterization. **B)** The design scheme for the α-factor-inducible promoter characterization construct including promoters, reporter genes, terminators, and *HO* homology sequences. Construction overview of all pheromone-inducible promoters (black) and benchmark promoters (grey) that were combined with the three reporter genes (*venus*, *mRuby2*, *mTurquoise2*) and terminated by the T_{TDH1} terminator. Grey parts were obtained from the YTK collection [71]. Each promoter was combined with each reporter gene and subsequently characterized.

First, we investigated the influence of the reporter gene itself on the expression profile of the promoters. Therefore, we designed three different versions of the characterization device differing in their reporter genes (Figure 80). We introduced *mTurquoise2*, *mRuby2*, or the *venus* gene into the constructs as three different fluorescent markers to investigate expression variation. These constructs were chromosomally integrated into the *HO* locus of the *MAT*α strain background for initial testing.

For all three resulting strains, we studied the dose-response to twelve different concentrations of α-factor. As expected, according to literature, as well as the analysis of the RNA sequencing data, all selected α-factor-inducible promoters exhibited an increase in fluorescence intensity upon addition of pheromone. We observed slight differences in the dynamics of the dose-response curves depending on the reporter gene being expressed. While the profiles of the different promoters expressing mTurqoise2 or Venus were comparably similar, the ones of cells expressing mRuby2 deviated. One self-evident explanation for the differences are the different maturation times and half-lives of the fluorescent proteins, being reflected in the monitored intensities.

To further highlight the differences in promoter behavior in relation to the gene being expressed, we correlated the fluorescence intensities of two colors. The responses at the maximal dosage of 26 nM α-factor were selected for plotting. For the expression of mTurquoise2 and Venus, the intensities resulted in an almost linear correlation (Figure 81). The only visible divergence was observed for the P_{FUS1} promoter. In case P_{FUS1} was driving the expression of mTurquoise2, the resulting fluorescence intensities were relatively higher in comparison to the values of Venus, thus deviating from the otherwise linear correlation between the two colors.

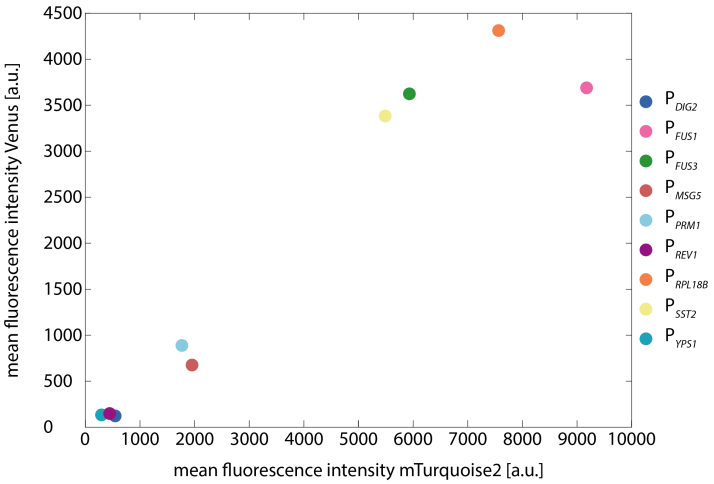

Figure 81: Fluorescence intensity correlation between Venus and mTurquoise2 of pheromone-inducible and benchmark promoters. Correlation between the mean fluorescence intensity of Venus- and mTurquoise2-expressing cells of pheromone-inducible and benchmark promoters induced with 26 nM α_{Sc}-factor in the *MAT*α strain background with constitutively expressed $Ste2_{Sc}$.

For both correlations including mRuby2, namely the correlation of mTurquoise2 (Figure 82) or Venus (Figure 83) with mRuby2, the correlation was less apparent and exhibited more outliers deviating from a linear correlation. Most striking were the differences for the two constitutive promoters P_{RPL18B} and P_{REV1}. Since mRuby2 exhibits a comparably long maturation time of about three hours and a long half-life, the signal for the two constitutive promoters was relatively stronger than for mTurquoise2 and Venus [455]. The fluorescence intensities for the α-factor-inducible promoters, on the other hand, were weaker since they were recorded three hours after the induction with the α-factor, which is similar to the maturation time of mRuby2. The comparably reduced fluorescence intensities resulted most likely from mRuby2 proteins not being fully matured yet at our measuring point. Besides the constitutive promoters, the pheromone-responsive promoters also correlated almost linearly, with mRuby2 fluorescence intensities being relatively lower than mTurquoise2 or Venus intensities.

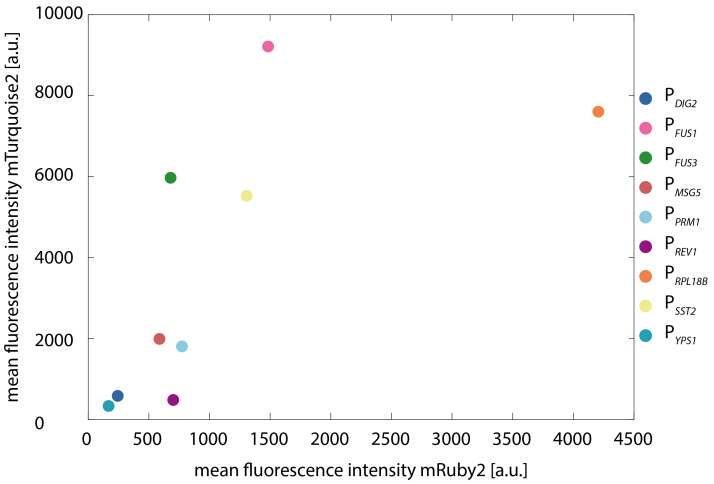

Figure 82: Fluorescence intensity correlation between mTurquoise2 and mRuby2 of α-factor-inducible and benchmark promoters. Correlation between the mean fluorescence intensity of mRuby2- and mTurquoise2-expressing cells of pheromone-inducible and benchmark promoters induced with 26 nM α_{Sc}-factor in the *MAT*α strain background with constitutively expressed $Ste2_{Sc}$.

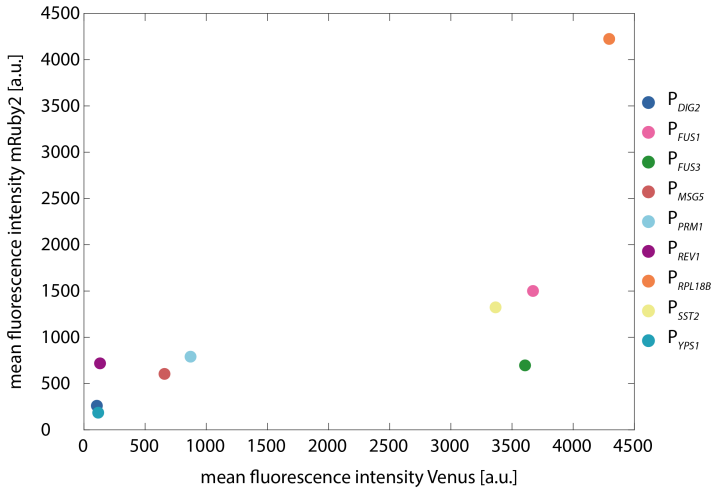

Figure 83: Fluorescence intensity correlation between mRuby2 and Venus of α-factor-inducible and benchmark promoters. Correlation between the mean fluorescence intensity of mRuby2- and Venus-expressing cells of pheromone-inducible and benchmark promoters induced with 26 nM α_{Sc}-factor in the *MAT*α strain background with constitutively expressed $Ste2_{Sc}$.

Our experimental results led to the decision to omit mRuby2 as a reporter for subsequent promoter characterization. Since mTurquoise2 exhibits also slightly increased maturation times in comparison to Venus, we proceeded with Venus as our standard reporter for further characterization of our toolkit parts. It should be noted though that a drawback of Venus is a lower brightness and reduced photostability in comparison to e.g., mTurquoise2. However, the maturation time was more important to us than the latter characteristics and could thus be neglected.

2.2.5.1.2.1 Pheromone-inducible promoter dose-response characterization

We characterized our selection of seven α-factor-inducible promoters and the two constitutive ones in different *MAT***a** and *MAT*α strain backgrounds to be utilized for the different aspects of this study. Figure 84 displays the dose-response curve of the promoters in the *MAT*α stain background with reconstituted $Ste2_{Sc}$ receptor expressed from the constitutive promoter P_{PAB1}. Each data point is the mean fluorescence intensity of approximately 50,000 single cells. The grey curve is a regression curve determined from the dose-responses using MATLAB (chapter 4.6.5). P_{DIG2} and P_{YPS} exhibited a weak response during mating pathway activity. The basal, as well as the maximal induction levels were slightly lower than the ones of the low-expression reference promoter P_{REV1}. For P_{YPS1} the response upon maximal induction of 26 nM α-factor was not saturated. In comparison to the RNA sequencing data, the P_{YPS1} promoter strength was visibly weaker than predicted and expected. Since the response was not saturated, one explanation could be that a maximal response was not reached yet for 26 nM α-factor and increased output signals could be observable at higher pheromone concentrations. For the P_{MSG5} promoter, an approximately five-fold stronger induction in comparison to P_{DIG2} was observed. The promoter of the *PRM1* gene showed responses for lower pheromone concentrations similar to P_{MSG5}, at higher levels though, the fluorescence intensities were 1.5-fold increased compared to P_{MSG5}. This was surprising since these findings were not in accordance with the results of the RNA levels (see Figure 63). The dose-response profiles of P_{FUS1} and P_{FUS3} were similar but different maximal induction levels were detected. The reporter gene expression intensities saturated at 2,600 a.u. when expressed from the

P_{FUS3} promoter. In comparison, Venus being expressed by the P_{FUS1} promoter reached fluorescence intensities up to 3,600 a.u.. The P_{FUS1} promoter featured with a 70-fold response increase the highest fold change between its uninduced and induced state. The P_{SST2} promoter reached similar maximal fluorescence intensities in comparison to the P_{FUS3} promoter. Remarkably, the P_{SST2} promoter exhibited dose-response dynamics differing from all other α-factor-inducible promoters in our set, which was characterized by high promoter leakiness with basal expression levels of approximately 273 a.u.. Additionally, we observed for this promoter a maximal response at a pheromone concentration of 11 nM, for 17 and 26 nM the fluorescence signal already resulted in reduced output intensities.

It has to be noted that both benchmark promoters from the YTK, namely P_{REV1} and P_{RPL18B}, also showed a response to increasing α-factor concentrations. We hypothesized that these increasing fluorescence intensities were an artifact resulting from an increase in cell size and volume in response to pheromone sensing. This effect could be smoothened by normalization to cell size and volume.

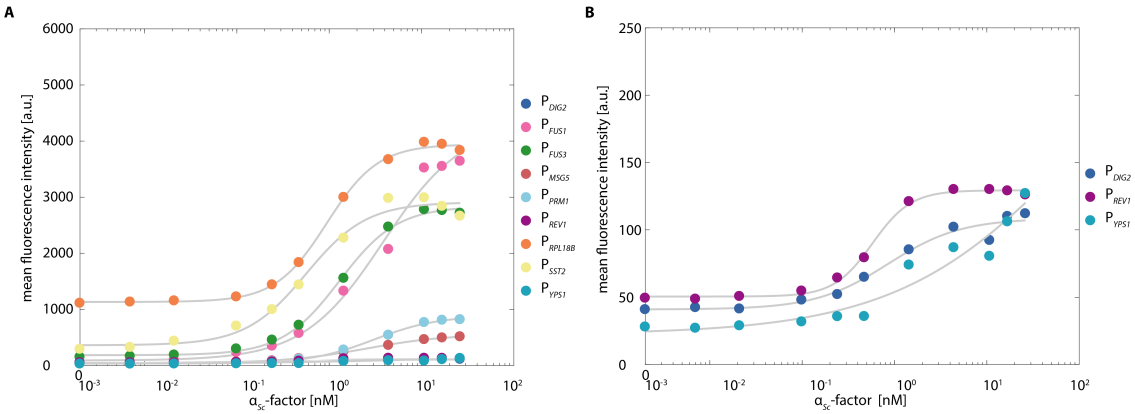

Figure 84: α_{Sc}-factor dose-response curves of the pheromone-inducible and benchmark promoters in the *MAT*α strain background with constitutively expressed Ste2$_{Sc}$. A) Mean fluorescence intensity of Venus of 50,000 single cell events for each pheromone-inducible and benchmark promoter strain for different α_{Sc}-factor concentrations. **B)** Plot of the dose-response of the three weakest promoters with a response-adjusted y-axis scale.

In Table 5, we listed the basal expression levels, the fluorescence intensities upon maximal induction, the fold change between minimal and maximal fluorescence intensities as well as the computed EC_{50} of our set of pheromone-responsive promoters. In the *MAT*α strain, the EC_{50} of P_{FUS1} as well as of P_{YPS1} can only be considered conditionally since the dose-response curves were not saturated. The EC_{50}s of the promoters ranged from 0.56 nM α-factor for P_{SST2} up to 5 nM for P_{YPS1}. With our selection of promoters, we covered a variety of different dynamics and characteristics, including a wide dynamic range and different sensitivities, laying the foundation for the design of complex communication networks.

Table 5: Summary of the key characteristics of the pheromone-inducible promoters in the different strain backgrounds. The hashtag (#)-labeled EC_{50} values indicate that these values could only be considered conditionally since the corresponding dose-response curves were not saturated. N.A. indicates that no dataset was obtained. Double hashtag (##) indicates inconclusive correlation curve.

Promoter	**Mean fluorescence intensity [a.u.] - Unindcued**				**Mean fluorescence intensity [a.u.] - Induced 26 nM α-factor**				**Fold change**				**EC_{50}**			
Strain background	*MATα*, const. $Ste2_{Sc}$	*MATα*, phero. $Ste2_{Sc}$	*MATα* Δ far1, const. $Ste2_{Sc}$	*MAT***a**Δ far1, const. $Ste2_{Sc}$	*MATα*, const. $Ste2_{Sc}$	*MATα*, phero. $Ste2_{Sc}$	*MATα* Δ far1, const. $Ste2_{Sc}$	*MAT***a**Δ far1, const. $Ste2_{Sc}$	*MATα*, const. $Ste2_{Sc}$	*MATα*, phero. $Ste2_{Sc}$	*MATα* Δ far1, const. $Ste2_{Sc}$	*MAT***a**Δ far1, const. $Ste2_{Sc}$	*MATα*, const. $Ste2_{Sc}$	*MATα*, phero. $Ste2_{Sc}$	*MATα* Δ far1, const. $Ste2_{Sc}$	*MAT***a**Δ far1, const. $Ste2_{Sc}$
P_{DIG2}	39.0	N.A.	28.1	24.1	112	N.A.	105	83.5	3	N.A.	4	4	0.85	N.A.	39##	0.97
P_{FUS1}	52.0	114	47.5	46.8	3641	5408	3019	4495	71	48	64	97	3.90#	0.94	7.80#	2.00
P_{FUS3}	154.0	238	147	139	2715	3354	2118	2622	18	15	15	19	1.30	0.81	2.10	1.50
P_{MSG5}	50.2	61.1	42.8	39.3	513	889	332	490	11	15	8	13	2.50	1.70	8.50	2.30
P_{PRM1}	30.8	34.2	19.6	16	818	1100	499	699	27	33	26	44	3.10	2.00	8.40#	4.60#
P_{SST2}	273.0	227	220	189	2663	2622	1961	2250	10	12	9	12	0.56	0.83	0.81	0.82
P_{YPS1}	28.1	32.2	19.2	20.9	127	189	110	72.4	5	6	6	4	5.00#	1.90#	0.23#	1.70#

Next, we characterized the pheromone-responsive promoters in the *MAT*α strain background in which the $Ste2_{Sc}$ was reconstituted under the control of the α-factor-inducible promoter P_{FUS1}. It has to be noted that P_{FUS1} exhibited under maximal pheromone induction a slightly higher expression level than the previously implemented P_{PAB1} promoter. The fluorescence intensities of the dose-response curves for this strain exhibited overall higher expression levels of the reporter, also for the constitutive promoters, in comparison to the strain constitutively expressing $Ste2_{Sc}$ (Figure 85).

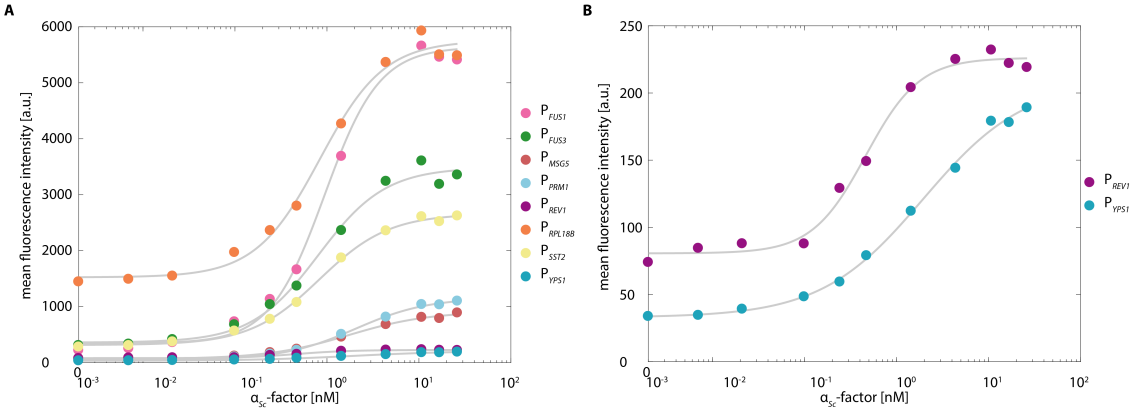

Figure 85: α_{Sc}-factor dose-response curves of the α-factor-inducible and benchmark promoters in the *MAT*α strain background with pheromone-induced expression of $Ste2_{Sc}$. A) Mean fluorescence intensity of Venus of 50,000 single cell events for each pheromone-inducible and benchmark promoter strain for different α_{Sc}-factor concentrations. **B)** Plot of the dose-response of the two weakest promoters with a response-adjusted y-axis scale. For P_{DIG2} no dose-response curve was obtained.

Increased fluorescence levels most likely resulted from higher receptor density due to the stronger expression of the Ste2 receptor. Another explanation could also be that the cell volume and size increased comparably more, and an overall stronger mating response could be the cause, thus higher fluorescent protein accumulation would be a consequence. The P_{DIG2} promoter was missing in this set due to experimental difficulties. P_{FUS1} reached visibly highest promoter activities of the α-factor-inducible promoters, and a rather step-like response was observed. An interesting finding was that P_{FUS1} exhibited two-fold basal expression levels in this strain background in comparison to the previous one (Table 5). The fold change between its uninduced and full induced state was 48-fold, with maximal fluorescence intensities of 5408 a.u.. The EC_{50} of P_{FUS1} was with 0.94 considerably lower, and the fluorescence intensities were fully saturated. Especially the comparison of P_{FUS1} in the strain with constitutively expressed receptor with the strain expressing the receptor from an α-factor-responsive promoter highlighted the alteration of its dynamics. Similar trends were also observed for most of the other promoters. Such observations are frequent and expected for positive feedback regulation as we implemented in our circuit design. We did however, not see a strong increase in the leakiness of the promoters, only exceptions were P_{FUS1} and P_{FUS3}. Overall, all promoters except for P_{SST2} exhibited higher fluorescence intensities when expressed in this strain background compared to the previous one. Based on these data sets, we concluded that the implementation of a positive feedback loop for the expression of the receptor led to different expression profiles and dynamics of the promoters. The fold change between uninduced and α-factor-induced fluorescence intensities in the two strains was increased

in the strain with pheromone-induced receptor expression except for P_{FUS1} and P_{FUS3}. The EC_{50} of the *SST2* promoter increased from 0.56 in the strain with constitutively expressed $Ste2_{Sc}$ to 0.83 in the strain with pheromone-induced expression of the $Ste2_{Sc}$, while for all other promoters, a lower EC_{50} was determined. The implementation of a positive feedback loop for the expression of the receptor could prospectively be utilized for increased signals and a higher sensitivity of the mating pathway. However, this would come with the cost of reduced fold changes and for some promoters with increased basal expression levels.

In wild-type cells, cell response to pheromone results amongst others in cell cycle arrest [453]. Since these cellular changes are undesirable for network performances, we knocked out the *far1* gene, which is regulating the cell cycle arrest during mating response upon phosphorylation by Fus3 [290]. We introduced the *far1* knockout into the *MAT*α strain that constitutively expressed $Ste2_{Sc}$. In Figure 86 A and B we display the dose-response curves for our set of promoters in this strain Far1 knockout strain background. The overall dynamics of the promoters were similar to the strain expressing Far1.

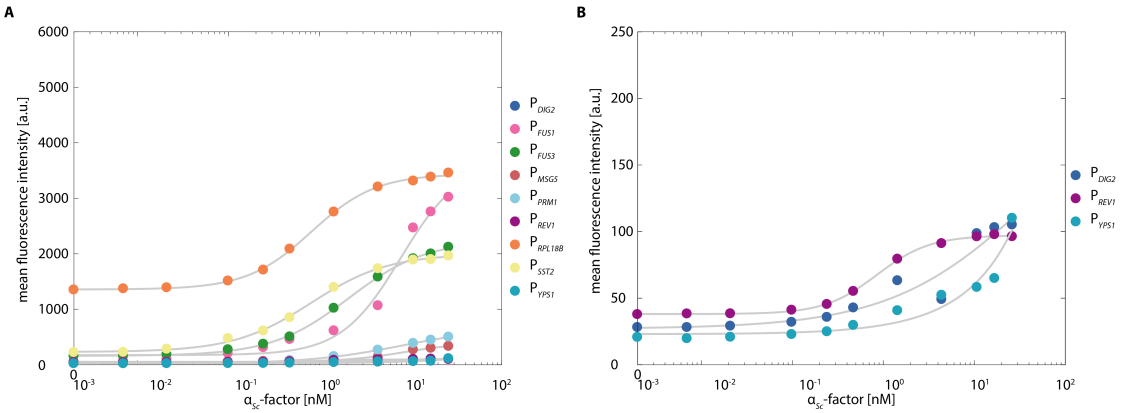

Figure 86: α_{Sc}-factor dose-response curves of the pheromone-inducible and benchmark promoters in the *MAT*α *far1Δ* strain background with constitutively expressed $Ste2_{Sc}$. A) Mean fluorescence intensity of Venus of 50,000 single cell events for each pheromone-inducible and benchmark promoter strain for different α_{Sc}-factor concentrations. **B)** Plot of the dose-response of the three weakest promoters with a response-adjusted y-axis scale.

P_{FUS1} remained the promoter with the strongest gene expression and the highest fold change of 64 upon induction with α-factor. As previously observed, P_{SST2} exhibited with fluorescence intensities of 220 a.u. the highest basal expression levels. Overall, we saw reduced pathway activity resulting in reduced leakiness of the uninduced promoters and lower maximal expression levels. The fold changes between uninduced and fully induced states of the promoters were comparable to in the parental strain (Table 5). One consequence of the weaker response in this strain background was that many of the promoters were not saturated at maximal pheromone concentrations we added to the media. Therefore, the EC_{50}s of the promoters were only estimations and need to be validated by additional experiments with higher pheromone concentrations.

So far, we characterized the set of promoters in different *MAT*α strains. For the implementation of future networks and to ensure a flexible use of the YCTK in every strain background, we additionally characterized the promoters in a *MAT***a** strain background. All relevant mating genes were knocked out in this strain background (chapter 4.5.1). In addition, we knocked out the *far1* gene to repress the cell cycle arrest. When we compared the promoter dynamics in the *MAT***a** strain

background with the ones in the *MAT*α *far1*Δ strain background, we could monitor differences in the expression profiles of the promoters. A visible difference was found for example in the dynamics of the P_{YPS1} promoter. In the *MAT***a** strain background, the YPS1 promoter featured an overall weaker response. Also, P_{FUS1} exhibited a different expression profile than in the other strains. In all *MAT*α background strains, the *FUS1* promoter showed similar or slightly lower fluorescence intensities than the benchmark promoter *RPL18B*. In the *MAT***a** chassis, we observed a higher expression for P_{FUS1} under maximal pheromone concentrations (Figure 87). Taken all characterizations together, we achieved the strongest fold change of 97-fold between its uninduced and maximally induced state of P_{FUS1} in this background (Table 5). Besides P_{PRM1} and P_{FUS1}, all other promoters had similar fold changes as in the *MAT*α strain background. In the *MAT***a** background, we saw an increased fold change of 44 for the P_{PRM1} promoter, which was higher than for all other *MAT*α strains tested. Overall, we observed a slight difference in leakiness, maximal induction, and dynamics of the dose-response curve as well as for the EC_{50} of the promoters in the *MAT***a** strain background versus in the *MAT*α background.

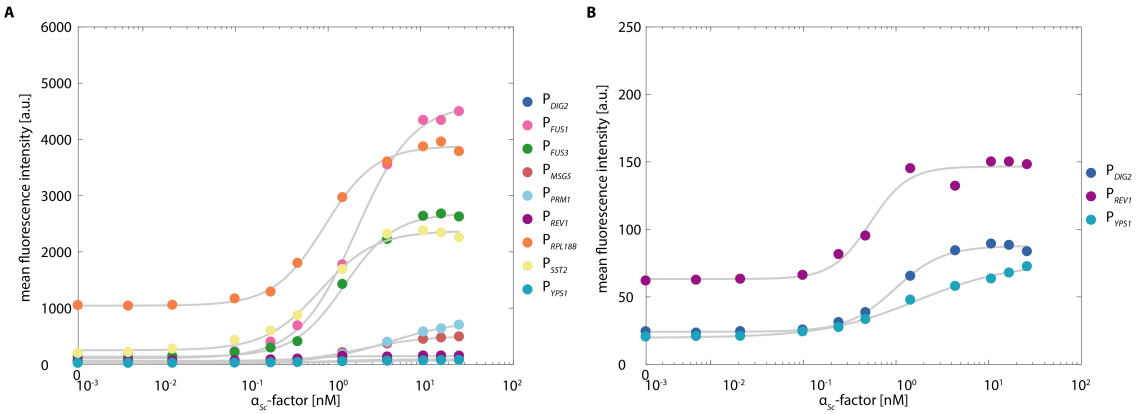

Figure 87: α_{Sc}-factor dose-response curve of the pheromone-inducible and benchmark promoters in the *MAT*a *far1Δ* strain background with constitutively expressed $Ste2_{Sc}$. A) Mean fluorescence intensity of Venus of 50,000 single cell events for each pheromone-inducible and benchmark promoter for different α_{Sc}-factor concentrations. **B)** Plot of the dose-response of the three weakest promoters with a response-adjusted y-axis scale.

To summarize the results of the characterization of the α-factor-inducible promoters, the selected promoters display when induced with 26 nM α-factor, a promoter strength that was slightly weaker than P_{REV1}, the weakest promoter of the YTK, and about a similar strength to P_{RPL18B}, the medium-strength promoter of the YTK. The different pheromone-responsive promoters also exhibited a range of different dynamics upon pheromone induction. They differed in their basal and maximal activity, and also in the fold change, depending on the different background strains. The calculated EC_{50}s however, were comparable for the different strain backgrounds but further validation is required.

To give an overall overview of the differences in expression under maximal induction, we plotted a selection of the fluorescence intensities against each other. Figure 88 shows the maximally α-factor-induced expression of all pheromone-responsive and benchmark promoters in the *MAT*α chassis with the constitutively and the feedback-induced expressed $Ste2_{Sc}$ receptors. Interestingly, the differences were most notably for P_{FUS1}. We clearly distinguished a stronger induction of the *FUS1* promoter in the $Ste2_{Sc}$ feedback loop strain (Figure 85) compared to the constitutively

expressed Ste2$_{Sc}$ strain (Figure 84). P$_{SST2}$, on the other hand, exhibited higher fluorescence intensities in the strain with constitutive expression of the Ste2$_{Sc}$ receptor (Table 5).

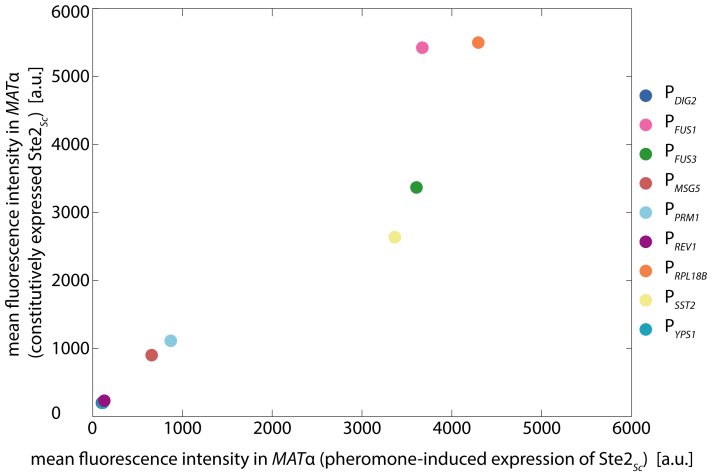

Figure 88: Fluorescence intensity correlation of induced α-factor-inducible and benchmark promoters expressed in two *MAT*α background strains with either constitutive or pheromone-induced expression of Ste2$_{Sc}$. Plot shows the correlation between the mean fluorescence intensity of 50,000 single cell event for Venus-expressing cells of the pheromone-inducible and benchmark promoters induced with 26 nM α$_{Sc}$-factor in the *MAT*α strain background with either constitutive or α-factor-induced expression of Ste2$_{Sc}$.

As all genes of the selected promoters are part of the mating pathway and we thus expected to see similar trends for all of them. Overall the promoters followed a similar linear trend, even though for the promoters with higher fluorescence intensities, increased deviations of the linear correlation were found.

In Figure 89 we compared the maximally induced fluorescence levels of the promoters in the *MAT*α and the *MAT*α chassis with the deletion of the *far1* gene, both having the Ste2$_{Sc}$ receptor reconstituted under the P$_{PAB1}$ constitutive promoter.

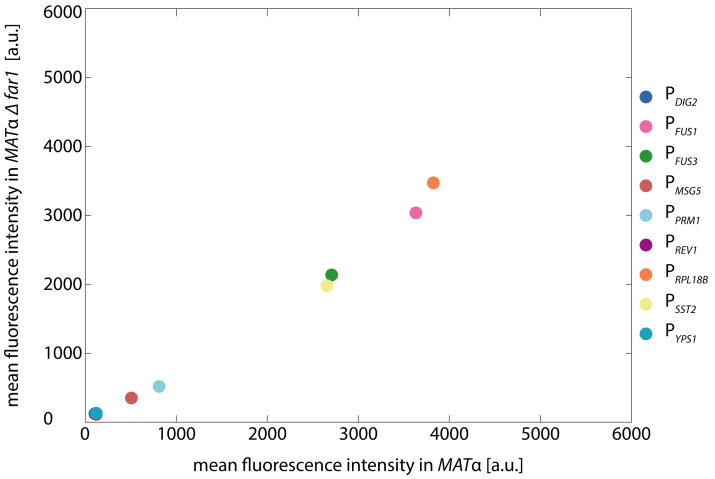

Figure 89: Fluorescence intensity correlation of induced α-factor-inducible and benchmark promoters expressed in *MAT*α and *MAT*α *far1Δ* background strains with constitutively expressed Ste2$_{Sc}$. Plot shows the correlation between the mean fluorescence intensity of 50,000 single cell event for Venus-expressing cells of the pheromone-inducible and benchmark promoters induced with 26 nM α$_{Sc}$-factor in the *MAT*α and *MAT*α *far1Δ* strain background with constitutively expressed Ste2$_{Sc}$.

In this case, the overall correlation between both strains was stronger than for the previous comparison. The general trend was that the *MAT*α strain with active Far1 exhibited a slightly higher pathway activity, resulting in overall increased promoter activity compared to the *MAT*α *far1*Δ strain. On the x-axis, we plotted the maximal expression of the α-factor-inducible promoters in the parental strain and on the y-axis the fluorescence intensities of the *MAT*α *far1*Δ strain. One reason for the increased fluorescence intensity could be the dilution of the reporter protein Venus in the *MAT*α *far1*Δ strain due to ongoing cell division, while the parental strain with an active Far1 discontinued cell division upon cell cycle arrest resulting in an accumulation of Venus. Since also the constitutive benchmark promoters *RPL18B* and *REV1* exhibited higher fluorescence values, these findings supported this hypothesis. By additional cell size normalization, it would be possible to compensate for these differences.

Figure 90 depicts the correlation between both *MAT*α *far1*Δ and the *MAT***a** *far1*Δ strains. Overall, we observed a higher mating pathway activity of all our selected promoters in the *MAT***a** strain background. Most distinct was the increase for the P_{FUS1} promoter but also all other promoters exhibited higher fluorescence intensities in the *MAT***a** strain versus the *MAT*α strain. Overall, it was unexpected to find differences in the expression profiles of the promoters between the different strain backgrounds. Especially, we could not identify a common trend for all promoters, even though all promoters are found in or downstream of the mating response pathway. All previous findings need to be repeated with more biological replicates as well as with a wider range of α-pheromone concentrations to reach saturating fluorescence intensities required for exact EC_{50} determination.

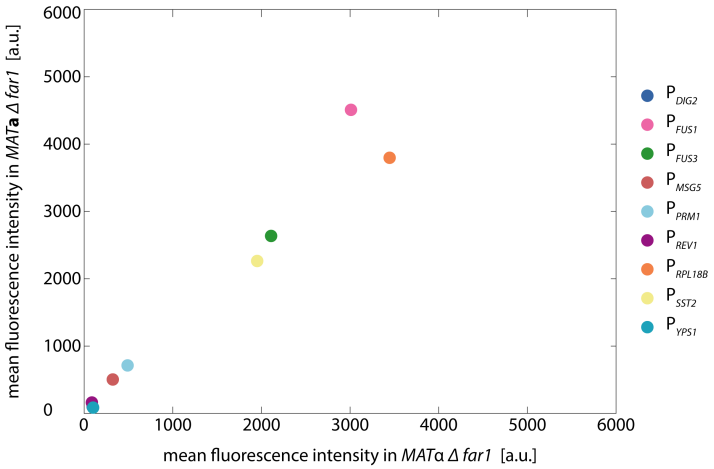

Figure 90: Fluorescence intensity correlation of induced α-factor-inducible and benchmark promoters expressed in *MAT*a *far1Δ* and *MAT*α *far1Δ* background strains with constitutively expressed $Ste2_{Sc}$. Plot shows the correlation between the mean fluorescence intensity of 50,000 single cell event for Venus-expressing cells of the pheromone-inducible and benchmark promoters induced with 26 nM α_{Sc}-factor in the *MAT***a** *far1Δ* and *MAT*α *far1Δ* strain background with constitutively expressed $Ste2_{Sc}$.

To conclude, the correlations of the promoter characterization in the different strain backgrounds provided interesting insights. The predicted increased fold change between uninduced and induced state in the *MAT*α strain background when the Ste2 receptor was expressed by a pheromone-induced promoter, could not be observed. The implementation of the positive feedback

loop should have theoretically led to a more stepwise promoter response that might be observable though, when monitored over a longer time period. The correlation between the promoter characteristics in the *MAT*α *far1*Δ and the *MAT*α did not reveal any considerable differences. The experimental results indicated though that the promoters exhibited a decreased basal and increased maximal activity, in the *MAT***a** strain background in comparison to the *MAT*α strain background.

2.2.5.1.2.2 Time course of pheromone-inducible promoter parts

Besides the dose-response characterization of the promoters, we investigated the promoter dynamics over time. We compared three strain backgrounds: the *MAT*α strain with constitutively expressed the $Ste2_{Sc}$ receptor, the *MAT*α stain with the knockout of the *far1* gene as well as the *MAT***a** strain with the same knockout. We chose 26 nM α-factor to induce the mating pathway and determined fluorescence levels every hour for 5 hours, by measuring 50,000 single cells using flow cytometry. Each data point represents the mean of these cells. The gating, as well as the experimental setup, can be recalled from material and methods (chapter 4.6.5).

Figure 91 depicts our set of pheromone-inducible promoters of and the benchmark promoters in the *MAT*α strain background induced with 26.2 nM α-factor over a time course of five hours after α-factor addition. Besides $P_{DIG2,}$ all other promoters exhibited maximal induction levels after four hours of pheromone induction. Differently, the *DIG2* promoter showed a constant increase of expression levels over the entire experimental time course. Unexpectedly, all other promoters featured a noticeable reduction of fluorescence intensities after 4 hours. We hypothesized that the *MAT*α cells were no longer responding to the pheromone stimulus and, therefore, the mating pathway was no longer active, resulting in a reduction of the expression of the reporter and other in the mating pathway involved genes. The reduction was most evident for the *SST2* promoter but was also observed for the constitutive benchmark promoters. Overall P_{FUS1} exhibited the highest expression levels and reached fluorescence values of 7,000 a.u. after four hours.

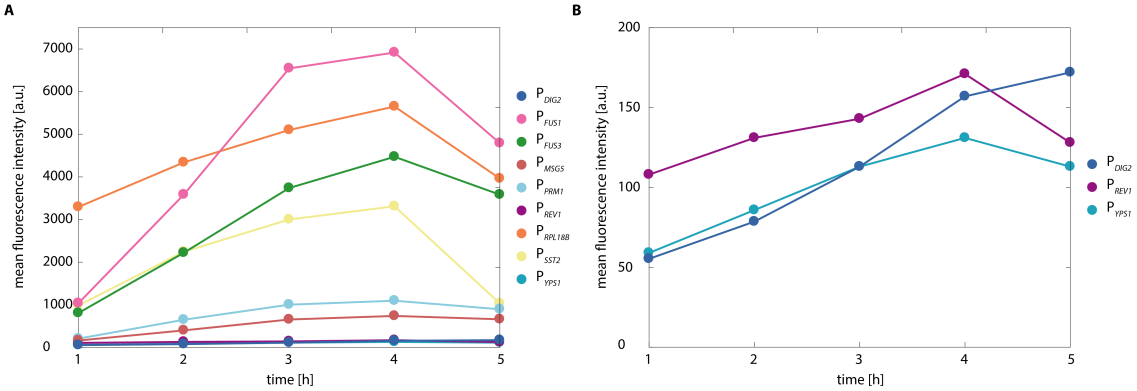

Figure 91: Fluorescence intensity time course of pheromone-inducible and benchmark promoters upon α_{Sc}-factor induction in the *MAT*α strain background. A) Mean fluorescence intensity of Venus for 50,000 single cell events for each pheromone-inducible and benchmark promoter for 26 nM α_{Sc}-factor over a time period of 5 h post-induction. **B)** Plot of the time course of the three weakest promoters with a response-adjusted y-axis scale.

The time course dynamics of the promoters in the *MAT*α *far1*Δ strain background varied visibly from the ones in the background strain with Far1 since the overall outputs were lower (Figure 92).

In general, we could see also slight changes in time dependency, which were observed best for the time courses of the *YPS1* and *DIG2* promoters. The timely response for *DIG2* in this *MAT*α *far1*Δ background exhibited a steeper increase than in the parental strain. Similarly, to the parental strain, we saw after four hours of induction a reduction of the fluorescence for all our promoters. However, the effects were less strong in comparison to the parental strain. Also, in this strain background only, the expression from the *DIG2* promoter resulted in a decrease in fluorescence intensities after 4 hours.

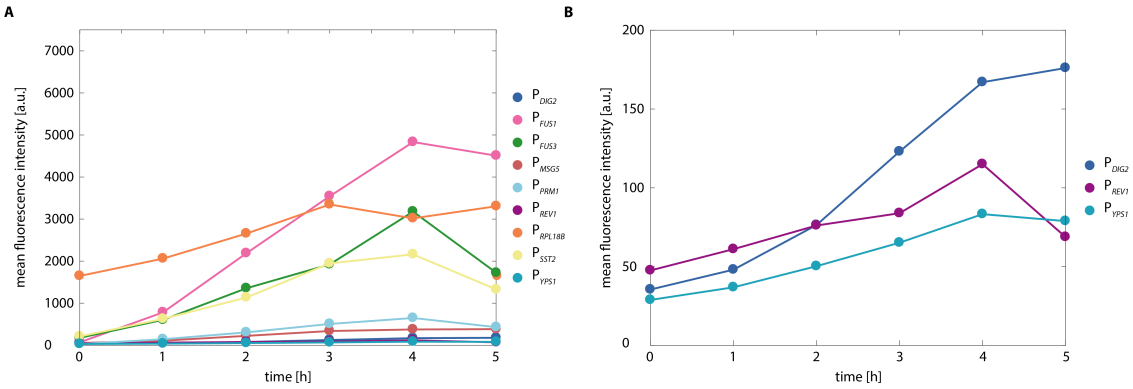

Figure 92: Fluorescence intensity time course of pheromone-inducible and benchmark promoters upon α_{Sc}-factor induction in the *MAT*α *far1Δ* strain background. A) Mean fluorescence intensity of Venus for 50,000 single cell events for each pheromone-inducible and benchmark promoter for 26 nM α_{Sc}-factor over a time period of 5 h post-induction. **B)** Plot of the time course of the three weakest promoters with a response-adjusted y-axis scale.

In Figure 93 the results of the *MAT***a** *far1*Δ are plotted. The overall fluorescence of the reporter Venus expressed by the pheromone-inducible promoters was slightly higher as in the *MAT*α *far1*Δ strain (Table 5). Interestingly, we observed saturation of fluorescence intensities after 4 hours of α-factor induction for most of the promoters. Besides the constitutive benchmark promoters, we only observed for the *YPS1* and the *FUS3* promoters a minor reduction of the output over time. However, a strong reduction in fluorescence intensities as it was monitored for both *MAT*α strains could not be observed for the *MAT***a** strain. This led to the hypothesis that the *MAT*α strains lose the sensitivity to the α-factor over time, an interesting feature that could be utilized for the engineering of dynamic networks if the responsible regulator would be identified.

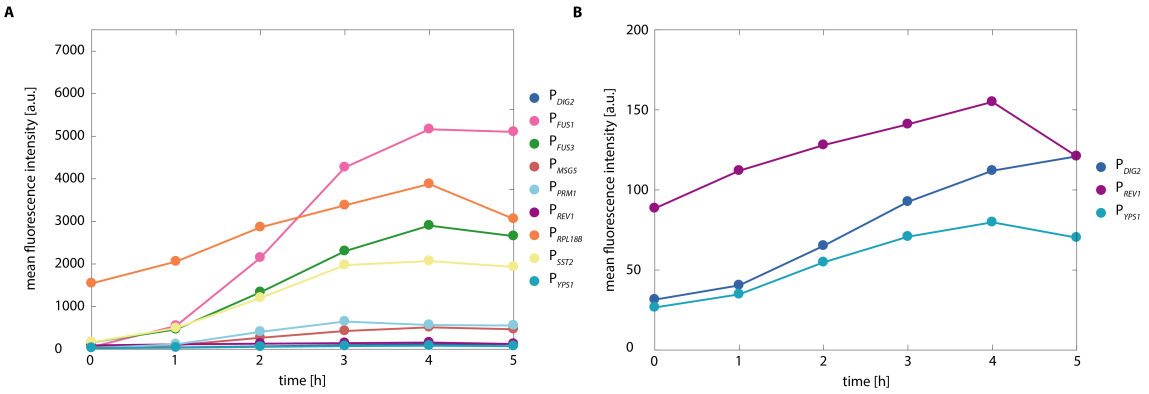

Figure 93: Fluorescence intensity time course of α-factor-inducible and benchmark promoters upon α_{Sc}-factor induction in the *MAT*a *far1Δ* strain background. A) Mean fluorescence intensity of Venus for 50,000 single cell events for each pheromone-inducible and benchmark promoter for 26 nM α_{Sc}-factor over a time period of 5 h post-induction. **B)** Plot of the time course of the three weakest promoters with a response-adjusted y-axis scale.

To conclude, results of the time course experiment displayed that all promoters started responding to the α-factor stimulus at the same time but we observed varying time-dependent response dynamics of the different promoters. The maximal fluorescence intensities were reached after 4 h in all strain backgrounds. Notably, the promoter activity in the *MAT*α background strains was drastically reduced after 5 h, indicating that the cells no longer responded to the α-factor. The time course gave insights into the induction dynamics of the selected promoters. These parameters are valuable for the engineering of complex dynamic or timed networks.

2.2.5.2 Sender part characterization – α-factor

The sender parts of the YCTK were the α-factor genes *mfa1,* originating from our selection of eleven yeast species. The goal was to cover a large diversity of different α-factors to gain a deeper insight into the relevant sequence motives and to obtain orthogonal sender and receiver part combinations that could be utilized for the design of multicellular communication systems. The *mfa1* gene encodes the pre-pro-α-factor that is further processed, resulting in the formation of several partially variable mature α-factors that are subsequently secreted into the environment. Using *in silico* identification, we wanted to predict successful processing and secretion of the heterologously expressed α-factors. If functionally expressed, the α-factors could be used as sender parts, which are required for the stimulation of the Ste2 receptors that are serving as the receiver parts in the YCTK.

Since the majority of our selected α-factors have never been expressed in *S. cerevisiae*, successful expression, processing, and secretion of the eleven selected α-factors had to be proven. The selected *mfa1* genes were codon-optimized as well as domesticated to follow the here utilized Golden Gate cloning standard. The *mfa1* genes were expressed by the P_{PGK1} promoter and terminated by T_{TDH1} and then chromosomally integrated into the *HO* locus and selected with the *HIS3* marker (Figure 94).

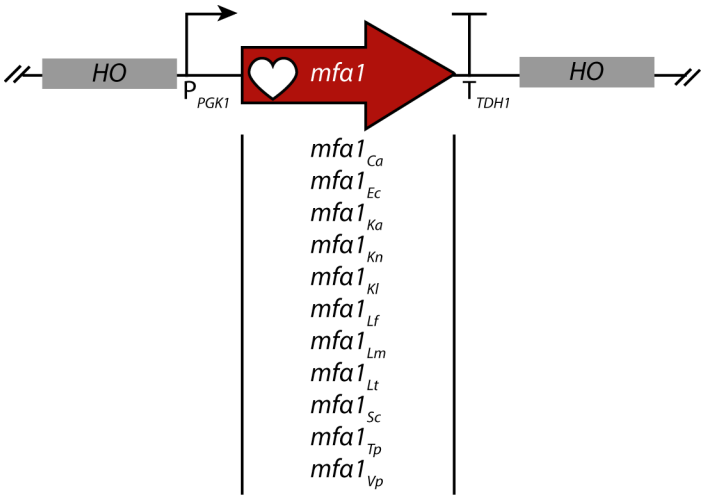

Figure 94: Constructs of the experiment to verify functional α-factor expression, processing and secretion. Genetic construct of the sender cells consisting of P_{PGK1}- *mfa1*-T_{TDH1} and *HO* homology sequences. This construct was built for all eleven *mfa1* genes originating from the selected species. The construct was integrated into the *MAT*α strain background.

We utilized a *MAT*α strain background, defective in the Ste2 receptors and mating factors for the characterization of the sender parts. To verify if the heterologous α-factors were expressed,

properly processed and secreted, we used a proteomics-based approach and directly verified the α-factors in the supernatant of cultures. We detected the computed mass for ten of the eleven heterologously expressed α-factors and plotted the extracted chromatograms in comparison to the negative control (Figure 95). The α_{Ka}-factor could not be detected since the strain exhibited a functional genetic problem when proteomics results were compiled and had to be reconstructed subsequently. The proteomics-based verification has thus to be repeated for the detection of the α_{Ka}-factor. For the negative controls of α_{Ca}-factor, α_{Kn}-factor, and α_{Lt}-factor we detected a clear peak in the chromatogram. However, when the mass of the peak was further analyzed we could not detect ionization or a mass of an α-factor and could therefore conclude that this peak could be considered as background or artifact and was only displayed due to the similar elution time point of the α-factors. Overall, we proved with this experiment the functional expression, processing, and secretion of all sender parts, except the α_{Ka}-factor.

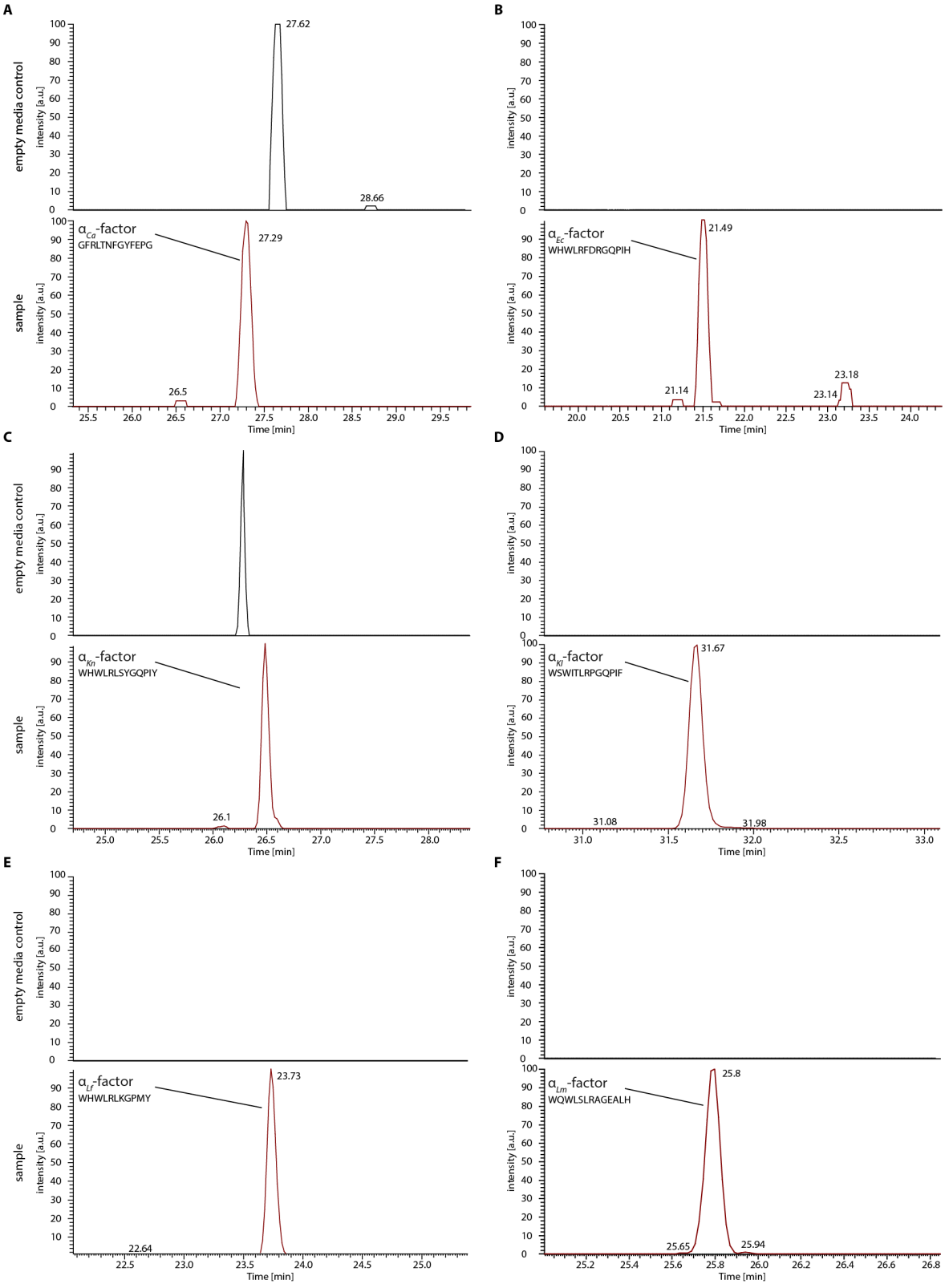
A
empty media control
intensity [a.u.]
27.62
28.66
sample
αCa-factor
GFRLTNFGYFEPG
27.29
26.5
Time [min]
B
αEc-factor
WHWLRFDRGQPIH
21.49
21.14
23.14
23.18
C
αKn-factor
WHWLRLSYGQPIY
26.1
D
αKl-factor
WSWITLRPGQPIF
31.67
31.08
31.98
E
αLf-factor
WHWLRLKGPMY
23.73
22.64
F
αLm-factor
WQWLSLRAGEALH
25.8
25.65
25.94

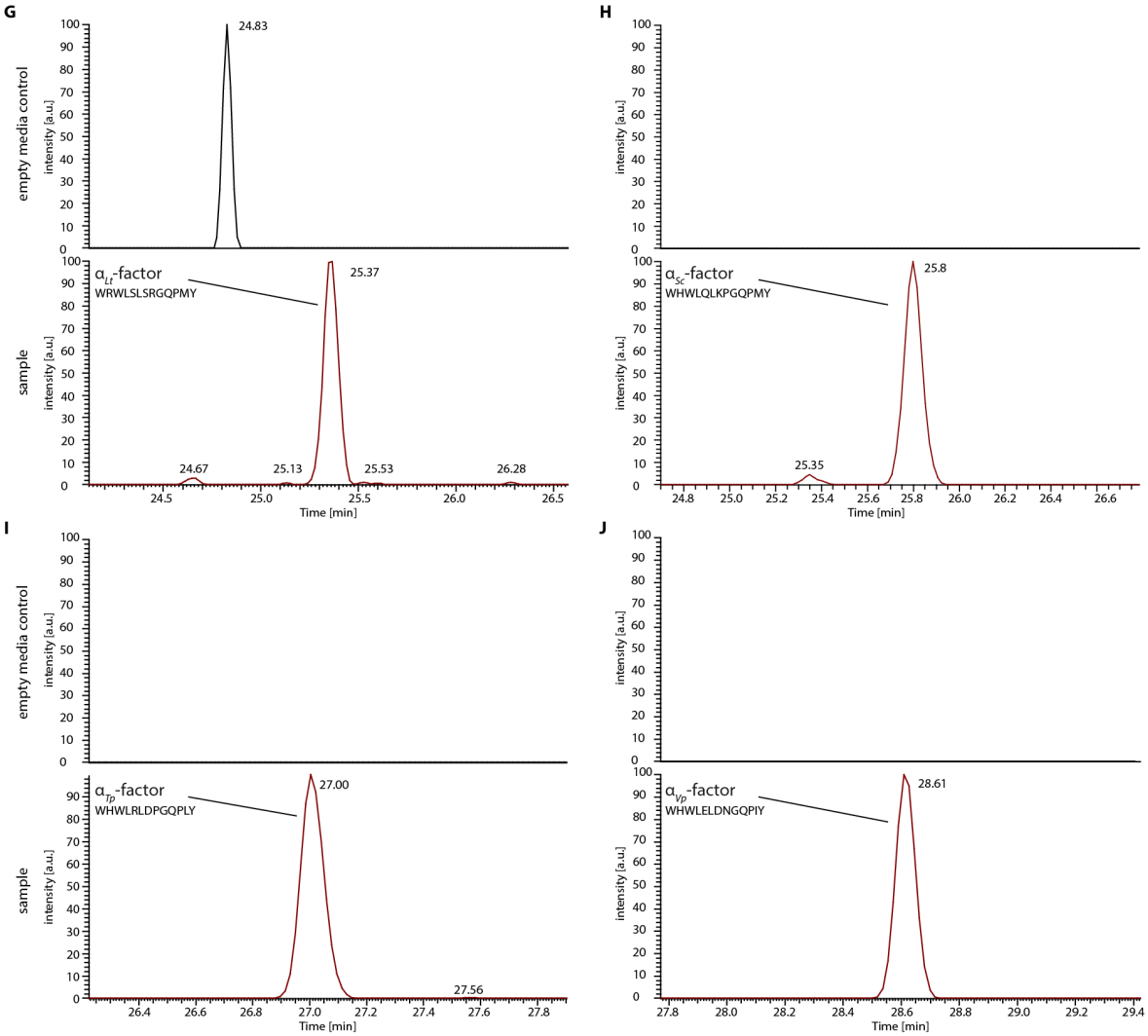

Figure 95: Extracted chromatograms of the supernatant of α-factor producing strains and negative controls. A) The extracted chromatogram for the empty media control (black) and the α_{Ca}-factor (red). **B)** The extracted chromatogram for the empty media control (black) and the α_{Ec}-factor (red). **C)** The extracted chromatogram for the empty media control (black) and the α_{Kn}-factor (red). **D)** The extracted chromatogram for the empty media control (black) and the α_{Kl}-factor (red). **E)** The extracted chromatogram for the empty media control (black) and the α_{Lf}-factor (red). **F)** The extracted chromatogram for the empty media control (black) and the α_{Lm}-factor (red). **G)** The extracted chromatogram for the empty media control (black) and the α_{Lt}-factor (red). **H)** The extracted chromatogram for the empty media control (black) and the α_{Sc}-factor (red). **I)** The extracted chromatogram for the empty media control (black) and the α_{Tp}-factor (red). **J)** The extracted chromatogram for the empty media control (black) and the α_{Vp}-factor (red).

To gain a better understanding of the α-factor amounts produced, we wanted to quantify the pheromone concentrations in the media by correlating the sample peak intensity with a dose-response curve of synthetic α-factors. The results have to be considered conditionally since further optimization of the purification and detection method is required, most likely due to the high chemical properties of the α-factors. We were able though to quantify the produced α-factor amounts for nine of the eleven strains. Again, the α_{Ka}-factor-producing strain was not part of the experiment. The α_{Vp}-factor was difficult to quantify due to difficulties in the ionization and in the detection of low concentrations. This resulted in a non-linear standard curve that could not be utilized for quantification. Overall, we were surprised by the large differences in produced

amounts for the different α-factors, ranging from about 3 µM for the α_{Ca}-factor and α_{Lm}-factor up to 48 µM for α_{Tp}-factor (Table 6). To include the variation in optical densities at the time point of α-factor quantification (the same volume was taken from each culture), we normalized to the OD of the cell cultures. However, still variation in the concentrations between the different strains was the result. We could not identify a correlation between the concentrations and the copy number or variants of the mature α factor encoded in the *mfα1* gene. Further investigations would be required, for example, using targeted proteomics or correlating between the quantified α-factor concentrations and the receptor activity, to confirm these preliminary results.

Table 6: Quantification of produced α-factor. Proteomics-based quantification of the heterologously produced α-factors in the *MAT*α stain background. Concentrations computed from synthetic standard dose-response and subsequently normalized to the optical density.

α-factor	Mean concentration [µM]	Normalized concentration [µM/OD]
α_{Ca}-factor	3±0.3	9±1.2
α_{Ec}-factor	13±0.4	33±2.2
α_{Ka}-factor	N.A.	N.A.
α_{Kn}-factor	27±1.3	116±11.8
α_{Kl}-factor	32±1.5	94±7.9
α_{Lf}-factor	37±4.5	101±11.4
α_{Lm}-factor	3±1.5	8±3.0
α_{Lt}-factor	25±3.8	66±10.2
α_{Sc}-factor	10±1.3	27±3.5
α_{Tp}-factor	49±8.0	119±10.1
α_{Vp}-factor	N.A.	N.A.

To conclude, all α-factors of our set of selected species, excepted for α_{Ka}-factor and α_{Vp}-factor were successfully heterologously expressed, processed and secreted in the *MAT*α strain background and could be detected and quantified using mass spectrometry.

2.2.5.3 Receiver part characterization – Ste2

The receiver parts of the YCTK are Ste2-like GPC receptor proteins originating from the eleven selected *ascomycete* species. Ste2 receptors are naturally expressed in *MAT***a** cells and are stimulated by the corresponding α-factors, which are synthesized by *MAT*α cells [205,206]. The Ste2 receptors are membrane-bound proteins and thus not only the expression itself but also the transmembrane localization is crucial for successful heterologous expression. Furthermore, the Ste2 receptors require interaction with downstream proteins that are part of a MAP kinase signaling cascade in order to respond to α-factor in the environment.

2.2.5.3.1 Verification of functional Ste2 expression by stimulation of cognate α-factor

To examine, whether the receptors were functionally heterologously expressed, we cocultured the *MAT*α receiver strain with a strain that was expressing the cognate pheromone. The same pheromone-producing strain was previously used to verify the expression and secretion of the α-factors. All receiver parts were constitutively expressed by the *PAB1* promoter and terminated by T_{ENO1} (Figure 96). The devices were chromosomally integrated into the *URA3* locus and selected with the *LEU2* marker. We used a *MAT*α strain with deletions of the mating genes, similar to the

background strain that was used for the promoter characterization. The strain contained a mating response output device that consisted of the *FUS1* promoter driving the expression of the mNeonGreen reporter gene.

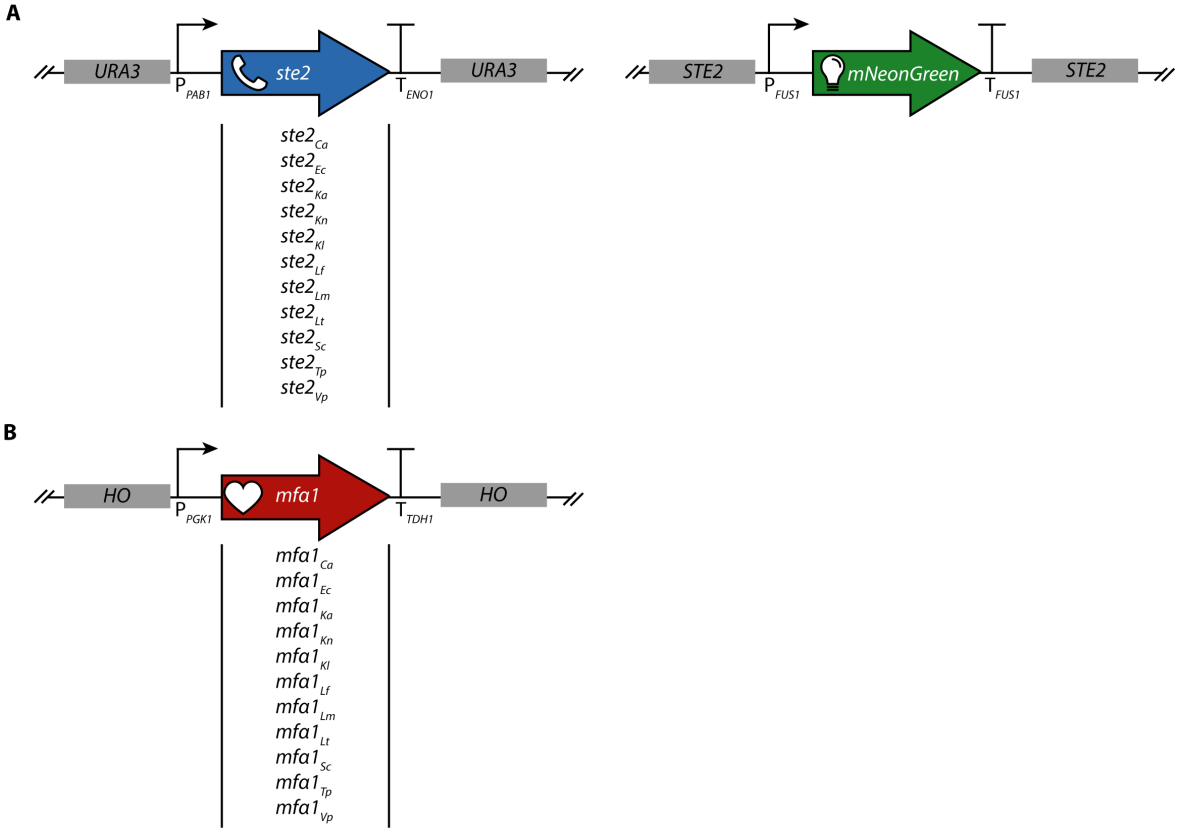

Figure 96: Constructs for receptor crosstalk experiment to verify functional α-factor and Ste2 receptor expression. A) Genetic constructs of the receiver cells consisting of P_{PAB1}-*ste2*-T_{ENO1} and *URA3* homology sequences. This construct was built for all eleven *ste2* genes originating from the selected species. The reporter construct consists of P_{FUS1}-*mNeonGreen*-T_{FUS1}, and Ste2 homology sequences. Both constructs were integrated into the *MAT*α strain background. **B)** Genetic construct of the sender cells consisting of P_{PGK1}- *mfa1*-T_{TDH1} and *HO* homology sequences. This construct was built for all eleven *mfa1* genes originating from the selected species. The construct was integrated into the *MAT*α strain background.

Figure 97 shows the results of the cognate cocultivation experiments: the histograms of the receiver cells include the cell density as well as the mNeonGreen fluorescence intensity of approximately 50,000 single cells for three biological replicates. The cell count is shown on the y-axis and the mNeonGreen intensity is plotted on the x-axis. The color code indicates the log of the mean fluorescence intensity. These settings also apply to the following Ste2 promiscouity results towards non-cognate α-factor. First, we co-cultivated the empty receptor strain (Ø Ste2, *MAT*α P_{FUS1}-*mNeonGreen*) with the strains expressing the pheromones (α_x-factor, *MAT*α) (Figure 97 upper row). The results indicated that only basal fluorescence levels could be detected due to a lack of a receptor and thus no activation of the mating pathway, even in presence of α-factor. As a second control, we inoculated the receptor strains (Ste2$_x$, *MAT*α P_{PAB1}-*ste2*$_x$-T_{ENO1}, P_{FUS1}-*mNeonGreen*) with an empty pheromone strain (Ø α-factor, *MAT*α) (Figure 97 middle row). A first indication of successful receptor expression and transmembrane localization was the slightly reduced basal

mating pathway activity, constituted by slightly lower fluorescence intensities, compared to the strain lacking the Ste2 receptor. It has previously been reported that the mating pathway exhibits higher basal activity, when no receptor is expressed, which could be confirmed by our results. Last, we cocultured each receptor strain with its cognate α-factor-producing strain (Figure 97 bottom row). For all receiver strains, an explicit activation of the mating pathway, measured by the expression of mNeonGreen from the *FUS1* promoter was observed. However, for the different receptor-α-factor pairs, distinctions in the mating pathway activity were recorded. The strain expressing the Ste2 receptor of *V. polyspora* exhibited a comparably weak mating pathway activity. A stronger mating response compared to *V. polyspora* but reduced compared to all others, was detected for the $Ste2_{Ca}$ and $Ste2_{Ka}$ strains. All other receiver strains showed similarly strongly induced mating pathway activity. Since for the coculture of the receiver strains with an empty α-factor-producing strain no mating pathway activity was observed, we could conclude that all receptors were successfully expressed in the *MAT*α strain background. The previously reported lower mating pathway activity of the $Ste2_{Ca}$ and the $Ste2_{Vp}$ expression strains might be due to an inefficiency in transmembrane localization, expression of each of the receptors or insufficient amounts of pheromone in the media. Nevertheless, we found functional heterologous Ste2 receptor expression and mating pathway stimulation by cognate α-factor. We also indirectly verified the production of α_{Ka}-factor and α_{Vp}-factor, which was previously not achieved using the proteomics-based approach.

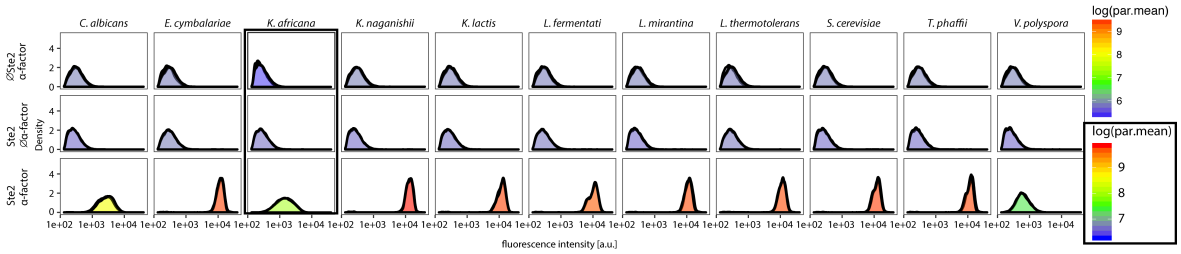

Figure 97: Verification experiment of functional Ste2 and α-factor expression. The x-axis shows the Venus fluorescence intensity indicating the mating pathway activity of the measured single cells events and the y-axis the density, depicting the cell number. The color code depicts the mean fluorescence intensity as log scale. The black-framed $Ste2_{Ka}$ and α_{Ka}-factor crosstalk experiment was performed with a new flow cell in the flow cytometer and can therefore not be quantitatively compared to the other data. The black-framed legend belongs to these results. Each α-factor producing strain was cocultured with a receiver strain lacking a Ste2 receptor (**upper row**), indicating no fluorescence output in the receiver strains. Also, each Ste2-expressing strain was cocultured with a strain lacking the *mfα1* gene (**middle row**), resulting in no fluorescence output. Only, when Ste2-expressing and corresponding α-factor strains were cocultured, the mating response in the receiver cells was activated resulting in a fluorescence output (**bottom row**). This indicated that both the receptors and α-factors were functionally expressed.

To conclude, all Ste2 receptors of our set of selected species were functionally expressed in the *MAT*α strain background. The experimental results proved that all α-factors were functionally produced and secreted and that the receptors could be stimulated by these. The Ste2 receptor stimulation resulted in activation of the MAPK signaling pathway and downstream reporter gene expression.

2.2.5.3.2 Investigation of Ste2 promiscuity towards α-factors

For the implementation of many synthetic biological systems, orthogonality is essential and we thus aimed to obtain an orthogonal communication system to be used for the engineering of multicellular communities. After having proven that the heterologous Ste2 receptors were functionally expressed in *S. cerevisiae*, we investigated their promiscuity as well as the ability of α-factors to stimulate the different receptors, to identify possible crosstalk between non-cognate sender and receiver parts. We utilized a similar experimental setup and the same strains as for the previous cognate α-factor and Ste2 receptor functional expression experiment (Figure 96). To ensure reproducibility, we utilized in one experiment three biological replicates of the receiver strains with one sender strain and in another one, three biological replicates of the sender strains with one receiver strain (data not shown). No visible differences were observed between the two experiments.

The histograms in Figure 98 consist of single cells events of the receiver strains (50,000 cells), measured using flow cytometry. Most of the receptors exhibited promiscuity towards several different α-factors. It has to be noted that in case the mating pathway was not maximally induced, a higher heterogeneity of the pathway activity in the cells was observed. Among the selected Ste2 receptors only the variants originating from *C. albicans* and *K. africana* exhibited solely mating pathway activity upon stimulation with their cognate α-factor, meaning these receptors are highly orthogonal. For *C. albicans* this was expected since the receptor as well as the α-factors have little sequence homology with the other sender and receiver parts. Therefore, it was also not surprising that also the α_{Ca}-factor was not recognized by any of the Ste2 receptors. That the $Ste2_{Ka}$ exhibited high substrate specificity however, was unexpected, since *K. africana* itself as well as its receptor and α-factor sequences are fairly closely related to the other species of our set of organisms (Figure 69, Figure 71, Figure 72). Thus, it would be interesting to biochemically investigate the $Ste2_{Ka}$ structure and its binding properties to unravel, why it exhibited such a high substrate specificity. In contrast to the α_{Ca}-factor though, the α_{Ka}-factor could stimulate other receptors besides its cognate, for instance $Ste2_{Ec}$, $Ste2_{Lf}$, and $Ste2_{Lt}$. In comparison to the high pheromone specificity of the $Ste2_{Ca}$ and $Ste2_{Ka}$, the $Ste2_{Ec}$ receptor was very promiscuous since it was stimulated by all α-factors except the α_{Ca}-factor. Weaker stimulation of $Ste2_{Ec}$ was observed upon stimulation with α_{Kl}-factor and α_{Lm}-factor. In contrast to $Ste2_{Ec}$, the α_{Ec}-factor was only stimulating one non-cognate receptor, $Ste2_{Lm}$, as well as its cognate receptor. For the $Ste2_{Kn}$ we reported a strong mating pathway activity when it was stimulated by its cognate α_{Kn}-factor as well as the α_{Tp}-factor and α_{Vp}-factor. Also, addition of the α_{Kl}-factor and α_{Sc}-factor resulted in a weak mating response. Interestingly, α_{Kn}-factor was recognized by the majority of the Ste2 receptors, except for $Ste2_{Ca}$ and $Ste2_{Ka}$. Also, the α_{Kl}-factor originating from *K. lactis* was stimulating several Ste2 receptors, namely $Ste2_{Ec}$, $Ste2_{Kn}$, $Ste2_{Kl}$, $Ste2_{Lf}$, $Ste2_{Lm}$, and $Ste2_{Sc}$. The strongest activation of the mating pathway though was observed upon induction of the cognate receptor. The $Ste2_{Kl}$ receptor was also promiscuous towards α_{Kn}-factor, α_{Tp}-factor, and α_{Vp}-factor. However, none of these α-factors resulted in a strong mating response.

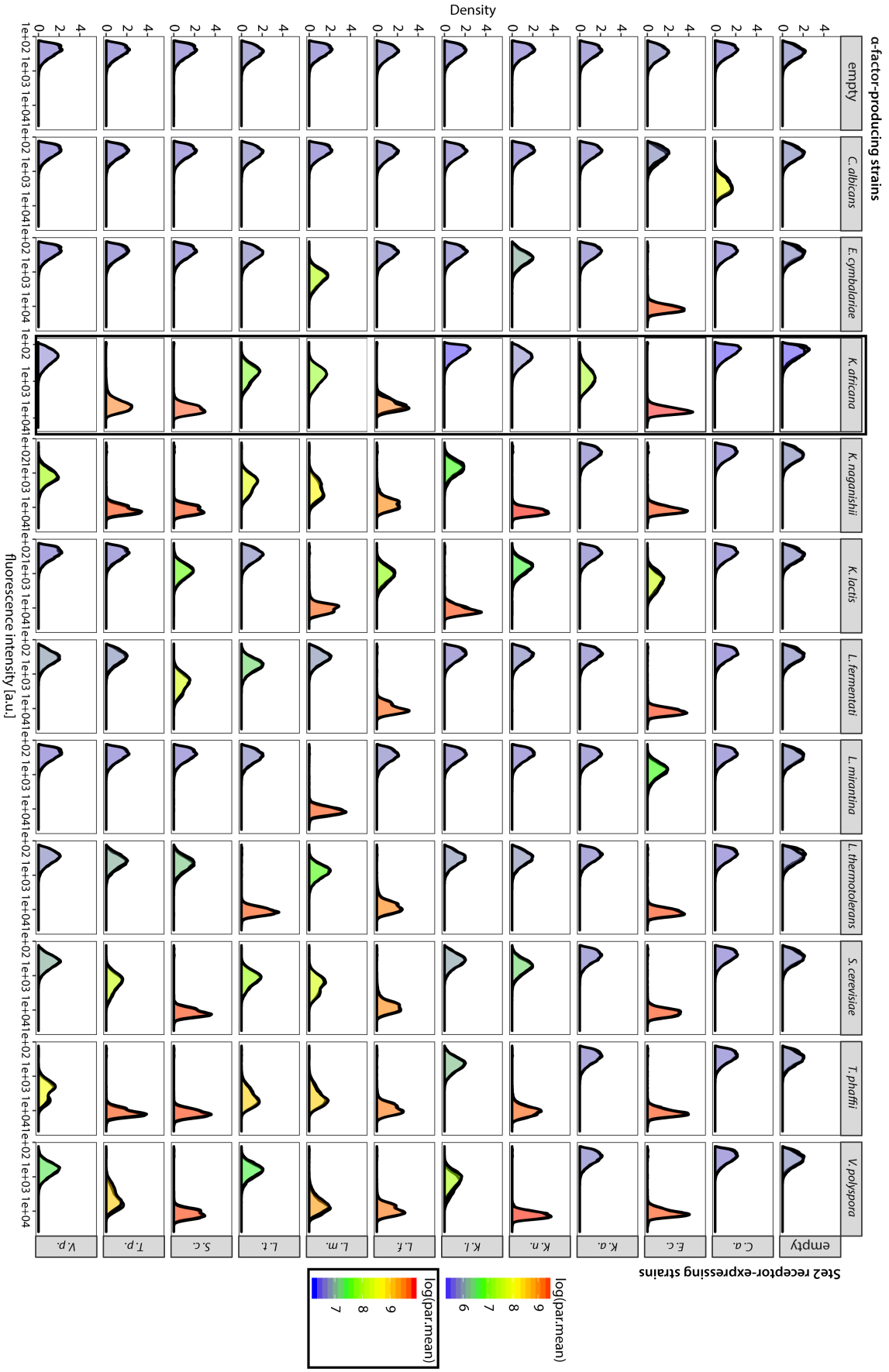

Figure 98: Results of the Ste2 and α-factor crosstalk experiment. The x-axis shows the Venus fluorescence intensity

indicating the mating pathway activity of the measured single cells events and the y-axis the density, depicting the cell number. The color code depicts the mean fluorescence intensity as log scale. The black-framed $Ste2_{Ka}$ and α_{Ka}-factor crosstalk experiment was performed with a new flow cell in the flow cytometer and can therefore not be quantitatively compared to the other data. The black-framed legend belongs to these results. Each α-factor producing strain was cocultured with every Ste2-expressing receiver strain. For those receptor-α-factor combinations for which a fluorescence output could be measured, indicate that these α-factors could stimulate non-cognate receptors, which exhibits crosstalk between the different sender and receiver parts of the YCTK.

The Ste2 receptor of *L. fermentati* was strongly stimulated by the α-factors α_{Kn}-factor, α_{Lt}-factor, α_{Sc}-factor, α_{Tp}-factor, α_{Vp}-factor, and its cognate α_{Lf}-factor. A weaker stimulation could be reported for the α_{Kl}-factor. The α_{Lf}-factor induced besides its cognate receptor also $Ste2_{Ec}$, as well as with a weaker stimulation $Ste2_{Lt}$ and $Ste2_{Sc}$. The α-factor of *L. mirantina* was only strongly stimulating its cognate receptor. However, also the $Ste2_{Ec}$ receptor was induced, as previously noted. In contrast to the α_{Lm}-factor, $Ste2_{Lm}$ exhibited mating pathway activity upon addition of nine out of the eleven pheromones, only for the α_{Ca}-factor and α_{Lf}-factor, no stimulation was detected. Overall, the stimulation of the $Ste2_{Lm}$ receptor was lower than for most others and exhibited only for its cognate as well as for α_{Kl}-factor higher mating pathway activity. For the $Ste2_{Lt}$ receptor of *L. thermotolerans*, the highest mating activity was reported with its cognate α_{Lt}-factor but the receptor was also activated by α_{Kn}-factor, α_{Lf}-factor, α_{Sc}-factor, α_{Tp}-factor, and α_{Vp}-factor. The α_{Lt}-factor induced the receptors $Ste2_{Ec}$, $Ste2_{Lf}$, and $Ste2_{Lm}$ whereas the pathway activity levels were similar for $Ste2_{Ec}$ and the $Ste2_{Lt}$ strain. For the $Ste2_{Sc}$ expression strain, we observed high mating pathway activity when the strain was cocultivated with the strains that were expressing the α-factors α_{Sc}-factor, α_{Kn}-factor, α_{Tp}-factor, and α_{Vp}-factor. The $Ste2_{Sc}$ was also stimulated by the α_{Kl}-factor and α_{Lf}-factor, however, the α-factor-receptor interaction resulted in a weaker mating pathway response. The α_{Sc}-factor of *S. cerevisiae* was stimulating the receptors $Ste2_{Ec}$, $Ste2_{Kn}$, $Ste2_{Lf}$, $Ste2_{Lm}$, $Ste2_{Lt}$, and $Ste2_{Tp}$. Except for $Ste2_{Ec}$, the mating pathway activity was not maximally induced by α_{Sc}-factor. The $Ste2_{Tp}$ receptor of *T. phaffii* was stimulated besides its cognate α-factor also by the α_{Kn}-factor, α_{Sc}-factor, and α_{Vp}-factor. However, maximal mating pathway activity was only found for the $Ste2_{Tp}$ stimulation with its cognate α-factor as well as the α_{Kn}-factor. The *T. phaffii* α_{Tp}-factor was recognized by the receptors $Ste2_{Ec}$, $Ste2_{Kn}$, $Ste2_{Lf}$, $Ste2_{Lm}$, $Ste2_{Lt}$, $Ste2_{Sc}$, and $Ste2_{Vp}$. The $Ste2_{Vp}$ receptor of *V. polyspora* exhibited overall the lowest mating pathway activity compared to the other receptors. Differently from the other receptors, we could report higher mating pathway activity upon stimulation of $Ste2_{Vp}$ with non-cognate α_{Kn}-factor and α_{Tp}-factor than with its cognate α_{Vp}-factor. Compared to most other receptors, $Ste2_{Vp}$ exhibited lower promiscuity towards other α-factors. The α_{Vp}-factor on the other hand was recognized by all other receptors, with the exception of $Ste2_{Ca}$ and $Ste2_{Ka}$, resulting in lower up to maximal induction of the mating pathway upon binding of these receptors.

Overall, this experiment gave us a qualitative overview of the α-factor production as well as the receptor promiscuity. From this experimental setup, we could however not draw any conclusions about the kinetics of the receptors, for which utilization of defined α-factor concentrations would be required. Interestingly, we noted that in our selection of mating systems originating from different *Saccharomycetaceaes,* α factors of species with high Ste2 receptors promiscuity tend to stimulate less Ste2 receptors than of species with more specific Ste2 receptors. Figure 99 outlines the correlation between the number of Ste2 receptors that can be stimulated by an α-factor and

the Ste2 promiscuity, resulting in an R^2 value of 0.53. For a solid validation of this observation and seubsequent conclusion, a more comprehensive analysis of other Ste2 receptors and α-factors should be conducted.

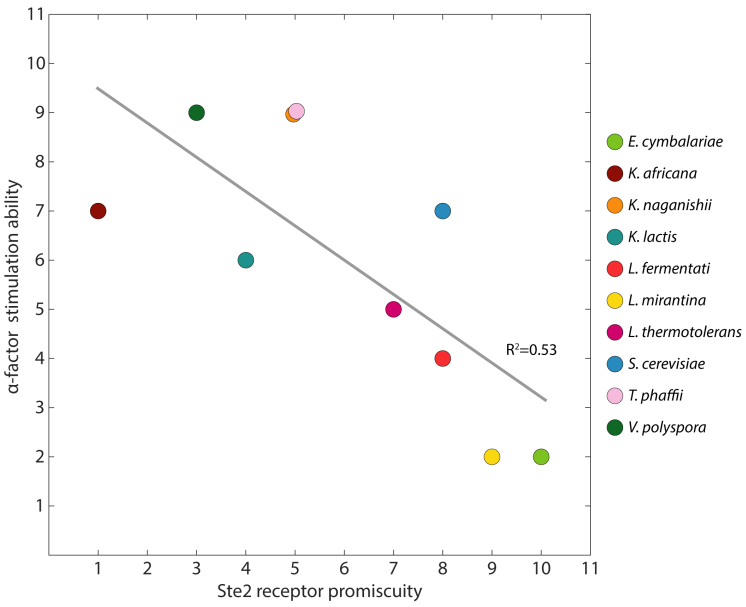

Figure 99: Correlation of α-factors stimulation ability with Ste2 receptor promiscuity. Plotted on the the x-axis is the Ste2 receptor promiscuity by number of α-factors that stimulate one Ste2 receptor. The y-axis represents the α-factor stimulation ability by the number of Ste2 receptors that one α-factor can stimulate. The color code indicates the species. The grey line depicts the linear correlation with an calculated R^2 value of 0.53.

Korrelation der Anzahl der alphafactokr stimulierenden Rezeptoren
Anzahl der durch einen α-factor stikumlierten Rezetoren. Anzahl der alpha-factoren die ein Rzepetro erkennt

To conclude, the Ste2 promiscuity experiments illustrated that all receptors, except for $Ste2_{Ca}$ and $Ste2_{Ka}$, exhibited crosstalk with at least one other α-factor apart from the cognate one. No strong general correlation between receptor α-factor crosstalk and phylogenetic relationship of the species or the likelihood analysis of the Ste2 receptors could be identified. Interestingly, a coherence between pheromone and receptor crosstalk could be reported, the α-factors of species for which the receptor exhibited high promiscuity tended to stimulate only a low number of receptors.

2.2.5.3.3 Ste2 sensitivity for cognate and non-cognate α-factors in *MAT***a** strain background

In this experiment, we investigated the dose-response of the eleven selected receiver parts, the Ste2 receptors, to all eleven α-factors. We utilized synthetic α-factor for this experiment which was synthesized according to the most common α-factor sequence variant found in the pre-pro-α-factor sequence (
Appendix Table 2). All receiver parts were constitutively expressed from the *PAB1* promoter and terminated by T_{ENO1} in the *MAT***a** *far1*Δ strain background (Figure 100). To measure mating pathway activity, we genomically integrated a fluorescence output module which consisted of the mating-responsive promoter *FUS1* expressing *venus* as a reporter gene. We utilized this fluorescence output to determine the mating response of the receptors to the different pheromones.

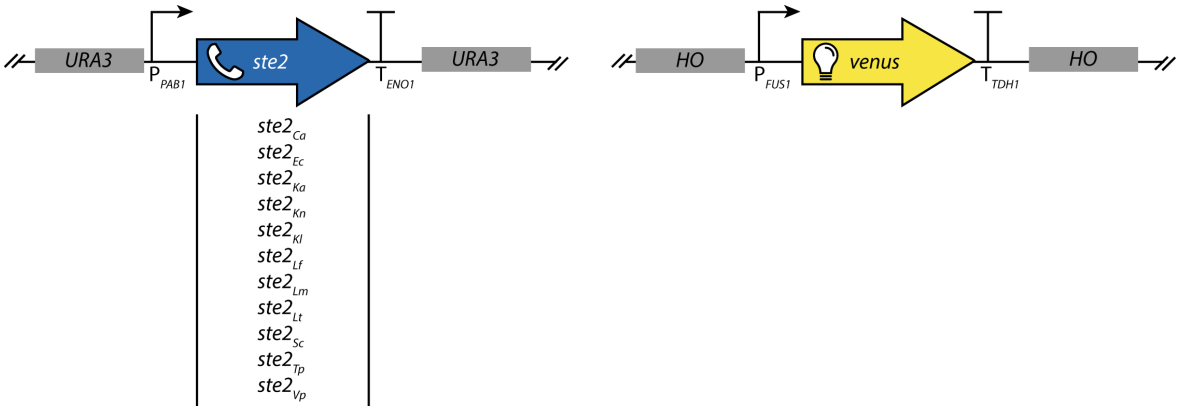

Figure 100: Constructs for the Ste2 receptor sensitivity experiment. Genetic constructs of the cells consisting of P_{PAB1}-*ste2*-T_{ENO1} and *URA3* homology sequences. This construct was built for all eleven *ste2* genes originating from the selected species. The reporter construct consists of P_{FUS1}-*venus*-T_{TDH1}, and *HO* homology sequences. Both constructs were integrated into the *MAT***a** *far1*Δ strain background.

The results of the α-factor dose-response analysis are plotted in Figure 101 and were split into three columns. The first column displays the histograms of the acquired 50,000 single cells for all eleven receptor strains, stimulated with their cognate α-factor. We tested eight different concentrations of α-factor, ranging from 0 nM to 26.2 nM. The second column represents the dose-response curve of the Ste2 receptor strains stimulated with cognate pheromone. Each measuring point depicts the mean fluorescence intensity of the 50,000 recorded events. The light grey line is a regression curve of the measuring points which was utilized for the determination of the EC_{50}. Some computed EC_{50} values were preliminary, since saturation was not reached by the α-factor concentrations. The EC_{50} values are summarized in Table 7. The third column displays heatmaps of the mating pathway activity for each receptor under the stimulus of all α-factors for different concentrations.

For $Ste2_{Ca}$ (Figure 101A) we observed that for an α_{Ca}-factor concentration of 0.2 nM the histogram was more heterogeneously distributed, meaning that the cells exhibited a more divergent activity of the mating pathway. 0.2 nM α_{Ca}-factor was also the lowest concentration for which pathway activation was detected. The computed EC_{50} for the dose-response was 0.91 nM and a linear dose-response was identified between 0.2 nM and 4.4 nM α_{Ca}-factor. Since *C. albicans* is part of the subfamily of *Debaryomycetaceae* and thus only distantly related to the other species of this study, which belong to the *Saccharomycotina* subfamily, no $Ste2_{Ca}$ stimulation by the other species α-factors was expected, which was confirmed in this experiment. Overall, the maximal mating pathway activity resulting from an induction with 26.2 nM α_{Ca}-factor was lower in comparison to the other receptors.

For $Ste2_{Ec}$ (Figure 101B) we also observed high cell to cell variability of the receptor strain for the output reporter upon mating pathway induction with low α_{Ec}-factor concentrations. For the dose-response with cognate α_{Ec}-factor, the overall lowest EC_{50} of 0.02 nM was computed. The linear dynamic range of the $Ste2_{Ec}$ ranged from 0.002 nM to 4.4 nM of α_{Ec}-factor. The $Ste2_{Ec}$ was in comparison to $Ste2_{Ca}$ very sensitive and could be induced with lower concentrations of cognate α-factor, suggesting further dose-response characterization with concentrations < 0.002 nM α_{Ec}-factor, in order to obtain a full range of the dose-response. As it was already observed in the crosstalk experiment, the $Ste2_{Ec}$ exhibited very broad α-factor promiscuity. A mating response upon on

pheromone binding to $Ste2_{Ec}$ was detected for all α-factors, even low response at maximal concentrations to the α_{Ca}-factor. Also, for α_{Ka}-factor and α_{Lm}-factor, only a weak stimulation of the mating pathway for maximal pheromone concentrations was observed.

The stimulation of $Ste2_{Ka}$ (Figure 101C) in response to α_{Ka}-factor was similar to the one observed for $Ste2_{Ca}$. The histograms revealed that the first indication of mating pathway response in presence of cognate pheromone was detected for 0.2 nM. The dose-response curve correlation exhibited a linear range of pathway induction for concentrations ranging from 0.2 nM to 10.7 nM α_{Ka}-factor. At an α_{Ka}-factor concentration of 26.2 nM, the response was almost saturated, however full saturation of the mating pathway response could not be reached at maximal concentrations utilized during this study. Thus, the computed EC_{50} of 2.1 nM was not accurate and the response to even higher α_{Ka}-factor concentrations needs to be determined in order to compute the EC_{50}. Interestingly, the $Ste2_{Ka}$ receptor was only stimulated by cognate pheromone as it was already suspected during the crosstalk experiment and confirmed here. This was surprising since *K. africana* is closely related to all other species. Especially the mature α_{Ka}-factor exhibited strong homologies to the other pheromones, in contrast to α_{ca}-factor that has no similarities to any of the other pheromones.

For the $Ste2_{Kn}$ (Figure 101D) a mating pathway response was already observed for the lowest concentration of α_{Kn}-factor of 0.002 nM, which was similar to $Ste2_{Ec}$. The $Ste2_{Kn}$ linear induction range of the mating pathway was between 0.002 nM and 1.4 nM cognate α-factor and the computed EC_{50} of 0.31 nM was comparably low. For the $Ste2_{Kn}$ the strongest mating pathway activity was detected in response to its cognate pheromone. The receptor was also stimulated by α_{Tp}-factor but exhibited lower reporter fluorescence intensities in comparison to α_{Kn}-factor. A rather weak stimulation of $Ste2_{Kn}$ was also reported for α_{Ec}-factor, α_{Kl}-factor, α_{Sc}-factor, and α_{Vp}-factor.

We noticed that there was no crosstalk between the pheromones and the receptors of the members of the *Kazachstania* genus. Taking the results of the likelihood analysis-based phylogenetic tree of the amino acid sequences of $Ste2_{Ka}$ and $Ste2_{Kn}$ into account, we saw a close relation between the two species (Figure 72). A similar finding was also identified in the SSU rRNA tree (Figure 69). In contrast to the Ste2 and the SSU rRNA tree though, α_{Ka}-factor and α_{Kn}-factor did not exhibit high sequence homologies (Figure 71). This was likely the reason that no crosstalk between these two closely related species was observed.

For $Ste2_{Kl}$ (Figure 101E) the lowest α_{Kl}-factor concentration for which a mating response was observed was 0.241 nM, as for $Ste2_{Ca}$ and $Ste2_{Ka}$. Since with the tested range of concentration the dose-response was not yet fully saturated, the EC_{50} of 2.0 nM was only an estimation and the response to higher α_{Kl}-factor concentrations needs to be tested to validate this result. A linear induction range of the mating pathway activity was exhibited for α_{Kl}-factor concentrations of 0.2 nM up to 10.7 nM as it was already observed for the previous Ste2 receptors except $Ste2_{Ec}$. Stimulation with cognate α-factor resulted in the highest activation of the mating pathway. In contrast to literature, we detected only a weak induction of $Ste2_{Kl}$ with α_{Sc}-factor [450]. One reason for this contradicting result could by the utilization of a different strain background, or stronger expression of the receptor itself. Besides a weak stimulation of $Ste2_{Kl}$ by α_{Sc}-factor, we also monitored a slightly stronger stimulation with α_{Kn}-factor.

Table 7: EC_{50} computed from the Venus mating response reporter under the P_{FUS1} promoter of the dose-response of α-factor with cognate Ste2 receptor: The hashtag (#)-labeled EC_{50} values indicate that these values could only be considered conditionally since the corresponding dose-response curves were not saturated.

Ste2 receptor	α-factor	EC_{50} [nM]
$Ste2_{Ca}$	α_{Ca}-factor	0.91
$Ste2_{Ec}$	α_{Ec}-factor	0.022
$Ste2_{Ka}$	α_{Ka}-factor	2.1#
$Ste2_{Kn}$	α_{Kn}-factor	0.31
$Ste2_{Kl}$	α_{Kl}-factor	2.0#
$Ste2_{Lf}$	α_{Lf}-factor	0.94
$Ste2_{Lm}$	α_{Lm}-factor	2.9#
$Ste2_{Lt}$	α_{Lt}-factor	1.2
$Ste2_{Sc}$	α_{Sc}-factor	0.79
$Ste2_{Tp}$	α_{Tp}-factor	1.2#
$Ste2_{Vp}$	α_{Vp}-factor	2.5#

The next receiver part that we investigated was $Ste2_{Lf}$ (Figure 101F). Upon induction with its cognate α_{Lf}-factor, a first visible mating response was found for 0.2 nM. In comparison to the other Ste2 receptors, the linear induction range was rather small, ranging from α_{Lf}-factor concentrations of 0.2 nM to 4.4 nM. The dose-response regression curve-based computation of the EC_{50} resulted in a concentration of 0.91 nM. The heatmap crosstalk results for the $Ste2_{Lf}$ revealed that this receptor was rather promiscuous towards non-cognate α-factors. Additionally, to the $Ste2_{Lf}$ induction with α_{Lf}-factor, a reporter output was observed in case the cells were induced with α_{Kn}-factor, and the fluorescence intensities were comparably high to cognate α-factor stimulation. Despite the strong response to α_{Kn}-factor, a medium stimulation of $Ste2_{Lf}$ could be reported upon addition α_{Lt}-factor, α_{Sc}-factor and α_{Tp}-factor, while a weak stimulation was observed for α_{Ka}-factor, α_{Kl}-factor, and α_{Vp}-factor. No stimulus of the $Ste2_{Lf}$ receptor was measured in presence of α_{Ca}-factor, α_{Ec}-factor, and α_{Lm}-factor.

As it was reported for the majority of previously described receptor strains in this study, a mating response upon stimulation of $Ste2_{Lm}$ receptor with cognate α-factor was observed at a concentration of 0.2 nM (Figure 101G). For the dose-response of $Ste2_{Lm}$, a response saturation could not be reached for maximal inducer concentration of 26.2 nM α_{Lm}-factor. The computed EC_{50} of 2.9 nM could thus only be considered conditionally. The linear stimulation range of $Ste2_{Lm}$ was observed for concentrations from 0.2 nM up to 26.2 nM and saturating conditions were not conceivable within the range of tested α_{Lm}-factor concentrations. Similar maximal induction levels of $Ste2_{Lm}$ were reached by stimulation with α_{Kl}-factor. Like $Ste2_{Lf}$, also $Ste2_{Lm}$ exhibited a broad α-factor promiscuity. Notably, no stimulation of $Ste2_{Lm}$ was detected upon addition of α_{Lf}-factor as well as for α_{Ca}-factor, and α_{Vp}-factor. Furthermore, we only reported low stimulation of $Ste2_{Lm}$ by α_{Ec}-factor, α_{Sc}-factor, and α_{Tp}-factor. A medium mating response was measured upon addition of α_{Kn}-factor, while for α_{Kl}-factor and α_{Lm}-factor, a strong mating response was observed

Also, for the $Ste2_{Lt}$ receptor (Figure 101H), mating pathway activity could be detected from α_{Lt}-factor concentrations higher than 0.2 nM, as previously reported for most of the other receptors. Similar to the dose-response of $Ste2_{Lf}$, stimulation of $Ste2_{Lt}$ with 26.2 nM cognate α_{Lt}-factor did not result in a saturated response, however the dose-response curve started falling suggesting a

trend towards saturation. Therefore, the computed EC_{50} of 1.2 nM has to be verified by further testing of a wider range of α_{Lt}-factor concentrations. The crosstalk results visualized in the heatmap suggested that $Ste2_{Lt}$ was most sensitive for its cognate α_{Lt}-factor for which we also determined the strongest stimulation. Besides its cognate pheromone, $Ste2_{Lt}$ could also be induced by α_{Kn}-factor, α_{Sc}-factor, and α_{Tp}-factor. A weaker stimulation of $Ste2_{Lt}$ was observed upon addition of α_{Ka}-factor and α_{Lf}-factor. Interestingly, $Ste2_{Lt}$ exhibited no mating pathway activity in response to α_{Lm}-factor. Since our set of parts contained three species of the *Lachancea* genus, we further wanted to analyze and compare the results of the crosstalk within this genus. We identified that $Ste2_{Lf}$ and $Ste2_{Lt}$ were stimulated by the respective other α-factors. $Ste2_{Lm}$ however, did not react to α_{Lf}-factor, and could only be weakly stimulated by α_{Lt}-factor. The observed minimal crosstalk was surprising since all three receptors were overall very promiscuous towards many of the other α-factors of this set. It was interesting to compare the promiscuity of $Ste2_{Lm}$ but also the fact that $Ste2_{Lt}$ could be stimulated by α_{Lf}-factor. The α_{Lf}-factor is two amino acids shorter than the average of our selected pheromones (Figure 65). This raised the question of a minimal size of a functional α-factor. By comparing the crosstalk results with the phylogenic trees that we previously explained, we might get a better understanding of the observed interactions. However, the SSU rRNA phylogenetic tree of the *Lachancea* genus remained inconclusive, thus we could not draw a clear conclusion based on this tree (Figure 69). Unfortunately, *L. mirantina* was not part of the whole-genome based phylogenetic tree by Shen *et al.* [450]. However, Pereira and colleagues proved, that *L. mirantina*, which was first isolated in 2011, is related to *L. fermentati* but is part of a separate taxonomic group within the *Lachancea* clade [451]. Further, their analysis showed that *L. fermentati* and *L. thermotolerans* are closer related than *L. mirantina*. We obtained similar results supporting the finding of Pereira *et al*. for the likelihood analysis of the amino acid sequences of the pre-pro-α-factors as well as for the receptors. Overall, the crosstalk results we gathered for the *Lachancea* genus were in line with findings in literature and our previous phylogenetic studies[450,451].

Next, we investigated the sensitivity of $Ste2_{Sc}$ (Figure 101I) and the first outstanding observation was that $Ste2_{Sc}$ exhibited a very high sensitivity as well as we measured overall maximal pathway activity constituted by the highest output fluorescence intensities. The histograms revealed that $Ste2_{Sc}$ was already stimulated by 0.002 nM α_{Sc}-factor. Only for $Ste2_{Ec}$ and $Ste2_{Kn}$, a comparably low cognate α-factor concentration resulted in a mating response, suggesting the three Ste2 receptors were very sensitive. For the dose-response, a response saturation was almost reached for 26.2 nM α_{Sc}-factor. In order to obtain a full dose-response, both lower as well as higher concentrations should be tested, nevertheless, the computed EC_{50} of 0.79 nM was a good preliminary estimation. The $Ste2_{Sc}$ receptor could not only be stimulated by α_{Sc}-factor. Interestingly, also induction of $Ste2_{Sc}$ with α_{Kn}-factor resulted in a very similar dose-response as with α_{Sc}-factor and also the maximal mating response was comparable. A slightly weaker but still strong response was measured for the $Ste2_{Sc}$ stimulation with α_{Tp}-factor. An overall weaker but still measurable output was obtained upon addition of α_{Vp}-factor, α_{Lt}-factor, and α_{Ka}-factor to the $Ste2_{Sc}$-expressing strain.

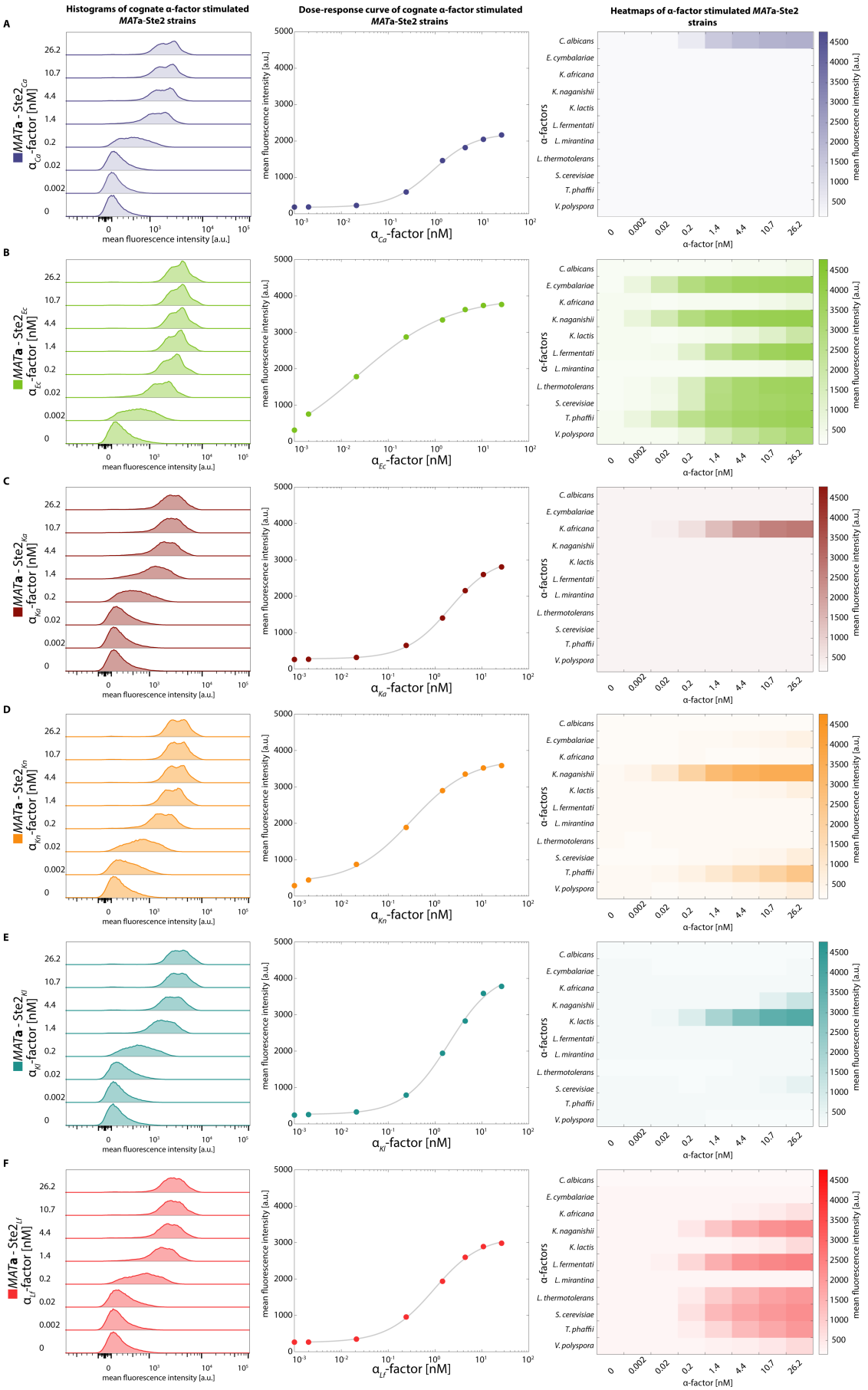
Histograms of cognate α-factor stimulated MATa-Ste2 strains
Dose-response curve of cognate α-factor stimulated MATa-Ste2 strains
Heatmaps of α-factor stimulated MATa-Ste2 strains
A
B
C
D
E
F
MATa - Ste2Ca α-factor [nM]
MATa - Ste2Ec α-factor [nM]
MATa - Ste2Ka α-factor [nM]
MATa - Ste2Kn α-factor [nM]
MATa - Ste2Kl α-factor [nM]
MATa - Ste2Lf α-factor [nM]
26.2
10.7
4.4
1.4
0.2
0.02
0.002
0
mean fluorescence intensity [a.u.]
αCa-factor [nM]
αEc-factor [nM]
αKa-factor [nM]
αKn-factor [nM]
αKl-factor [nM]
αLf-factor [nM]
C. albicans
E. cymbalariae
K. africana
K. naganishii
K. lactis
L. fermentati
L. mirantina
L. thermotolerans
S. cerevisiae
T. phaffii
V. polyspora
α-factors
α-factor [nM]

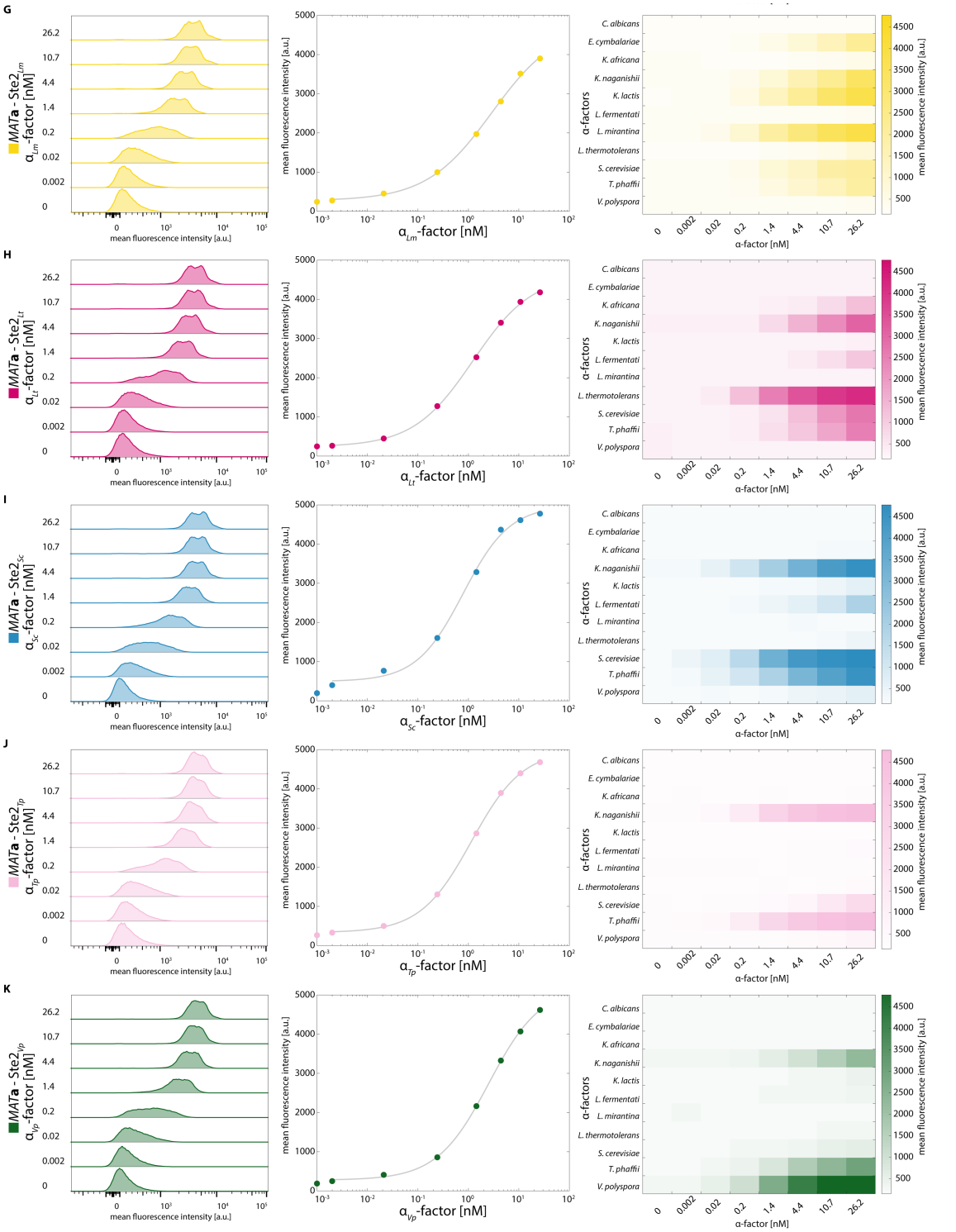

Figure 101: Results of the Ste2 receptor sensitivity towards cognate and non-cognate α-factors in the *MAT*a *far1*Δ strain background. The colors reflect the different Ste2 receptor expressing strains (MAT**a** *far1*Δ strain background). The first column displays the fluorescence histograms of 50,000 measured single cell events of the receptor strains for stimulation with different concentrations of cognate α-factor. The second column depicts the dose-response of the receptor strain to different concentrations of cognate α-factor. The grey line is the computed dose-response regression curve, from which EC_{50}s were computed (Table 7). The third column lists the heatmaps of the fluorescence intensities of the receptor strains stimulated with all α-factors of this study. Within the heatmaps, each row represents the response to one α-factor and the columns depict a different α-factor concentration. The color code indicates the resulting mating pathway activity by measuring the mean Venus fluorescence intensity for 50,000 single cell events.

A) Results of Ste2$_{Ca}$ sensitivity experiment. **B)** Results of Ste2$_{Ec}$ sensitivity experiment. **C)** Results of Ste2$_{Ka}$ sensitivity experiment. **D)** Results of Ste2$_{Kn}$ sensitivity experiment. **E)** Results of Ste2$_{Kl}$ sensitivity experiment. **F)** Results of Ste2$_{Lf}$ sensitivity experiment. **G)** Results of Ste2$_{Lm}$ sensitivity experiment. **H)** Results of Ste2$_{Lt}$ sensitivity experiment. **I)** Results of Ste2$_{Sc}$ sensitivity experiment. **J)** Results of Ste2$_{Tp}$ sensitivity experiment. **K)** Results of Ste2$_{Vp}$ sensitivity experiment.

The histograms of the Ste2$_{Tp}$ response to α$_{Tp}$-factor (Figure 101J) exhibited that this receptor was less sensitive than Ste2$_{Ec}$ and Ste2$_{Sc}$ since it only featured a mating response for α$_{Tp}$-factor concentrations higher than 0.2 nM. The dose-response revealed that the range of concentrations were almost sufficient to reach saturation, however testing more higher concentrations would result in a more refined characterization. Thus, the computed EC_{50} 1.2 nM was a good estimation but subsequent to further characterization, the computation should be repeated. Overall, the maximally measured output fluorescence intensities upon addition of 26.2 nM α$_{Tp}$-factor were comparably high as for Ste2$_{Ec}$. Interestingly, the dose-response for α$_{Tp}$-factor was very similar to the stimulation of Ste2$_{Tp}$ with α$_{Kn}$-factor. The α-factors of *S. cerevisiae* and *V. polyspora* though, resulted only in weak mating response. In comparison to most of the other Ste2 receptors of our selected species, of Ste2$_{Tp}$ exhibited reduced promiscuity since it could only be stimulated by four α-factors.

Similar to the majority of Ste2 receptors of this study, the histograms highlighted that higher α$_{Vp}$-factor concentrations were required to induce the mating pathway upon Ste2$_{Vp}$ stimulation (Figure 101K). Also, for Ste2$_{Vp}$ the dose-response curve was not saturated for the maximal α$_{Vp}$-factor concentration of 26. 2 nM, the resulting fluorescence intensities were comparably high to the ones observed for cognate α-factor stimulation of Ste2$_{Sc}$. Thus, the computed EC_{50} of 1.2 nM could only be considered conditionally. The linear induction range of the mating pathway of Ste2$_{Vp}$ was between 0.2 nM and 26.2nM cognate α-factor. Besides the stimulation with cognate α-factor, Ste2$_{Vp}$ also reacted to α$_{Tp}$-factor and α$_{Kn}$-factor with a medium strong mating response, while only a very weak stimulation of Ste2$_{Vp}$ could be observed upon addition of the α$_{Sc}$-factor.

This was an interesting finding, since in the likelihood analysis of the protein sequences, the Ste2 receptors of *T. phaffii* and *V. polyspora* exhibited visible homologies placing them close in the phylogenetic tree (Figure 72). However, Ste2$_{Tp}$ could not be stimulated by α$_{Vp}$-factor, but Ste2$_{Tp}$ responded to α$_{Tp}$-factor, and both receptors were stimulated by the α$_{Kn}$-factor. Both receptors exhibited lower promiscuity towards the other α-factors.

To compare the overall activation of the mating pathway as well as to gain a summarizing overview of the crosstalk, we generated a heatmap for all Ste2 receptor responses to all α-factor concentration of 26.2 nM (Figure 102). The mating pathway activity was represented by the expression of the reporter Venus, which was expressed from the mating-responsive promoter P$_{FUS1}$. Overall, we observed that the strongest mating pathway activities for all Ste2 receptors was measured for the stimulation with cognate α-factor. Also, we could report that mating response fluorescence intensity was varying between the different Ste2 receptor-expression strains. For Ste2$_{Ca}$, the maximal pathway activity was only half of what was observed for Ste2$_{Sc}$, each time for a receptor induction with 26.21 nM cognate α-factor. Also, the maximal output of Ste2$_{Ka}$ was comparably low, but higher as for Ste2$_{Ca}$. One cause for these observations might be variation in Ste2 receptor expression. Even though we utilized the same expression components, gene expression and thus transcription and translation are context-dependent and may have led to different protein amounts of the different Ste2 receptors [74,456]. As the receptors are membrane-bound proteins,

also the process of transmembrane localization of the heterologous receptors might account for differences in receptor abundancy in the membrane. Another possible explanation was that the signal transfer from the receptor to the downstream MAP kinase pathway was less sufficient for heterologous Ste2 receptors.

Most of the Ste2 receptors exhibited promiscuity towards non-cognate α-factor. The highest promiscuity was found for $Ste2_{Ec}$ for which a mating response was measured for all α-factor, partially only a weak response but nevertheless the $Ste2_{Ec}$ interacted with all pheromones. Most Ste2 receptors were stimulated by six to eight α-factors, including their cognate α-factor. Rather limited promiscuity was found for $Ste2_{Tp}$, $Ste2_{Vp}$, and $Ste2_{Kl}$ that only exhibited mating pathway activity for three or four α-factors. A high α-factor selectivity on the other hand was identified for $Ste2_{Ca}$ and $Ste2_{Ka}$. Both receptors only exhibited a mating response by addition of their cognate α-factors. Since we selected *C. albicans* as outgroup species, which was only distantly related to the other species, and the α_{Ca}-factor as well as the $Ste2_{Ca}$ had low sequence homology, it was not surprising to obtain these results. For the α_{Ka}-factor, however, this pheromone selectivity was unexpected since both the α_{Ka}-factor as well as $Ste2_{Ka}$ receptor were sequence homolog to the other α-factors and Ste2 receptors. Yet, the α_{Ka}-factor was stimulating other Ste2 receptors, including $Ste2_{Ec}$, $Ste2_{Lf}$, and $Ste2_{Lt}$. Another interesting finding was that α_{Kn}-factor stimulated most of the Ste2 receptors in our study, while the $Ste2_{Kn}$ responded only to a subset of non-cognate α-factors.

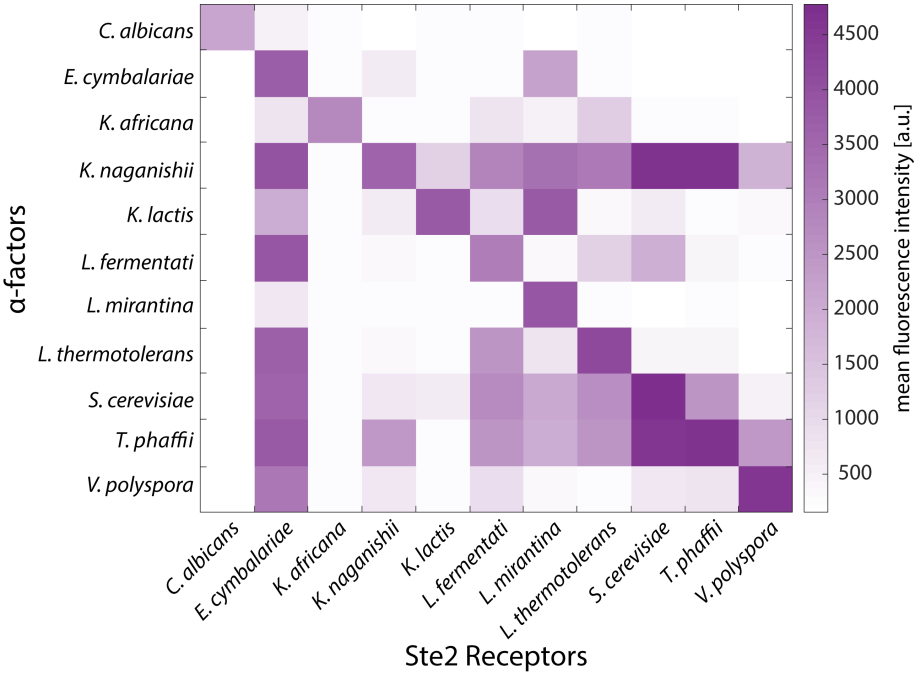

Figure 102: Heatmap of fluorescence intensities of the different Ste2-expressing strains induced with 26 nM α-factors in the *MAT*a *far1*Δ strain background. Each column displays the responses of one Ste2 receptor-expressing *MAT***a** strain and each row exhibits the synthetic α-factor used for Ste2 induction. The color intensity indicates the Ste2 stimulation as mating pathway activity by measuring the Venus fluorescence intensity for 50,000 single cell events, expressed from the P_{FUS1} promoter.

Overall, the results were in line with the data of the crosstalk study, in which α-factor-producing strains were cocultured with receptor-expressing strains (Figure 98). For example, some qualitative results for the $Ste2_{Kl}$, $Ste2_{Lm}$, and $Ste2_{Vp}$ strains exhibited some differences, including weaker

mating pathway activity. However, it needs to be noted that a different strain background (*MATα*) was used for the crosstalk experiment as well as a different reporter gene (*mNeonGreen* versus *venus*), limiting direct comparison. The data of the receptor sensitivity experiments were generated using a *MAT***a** strain with a deletion of the *far1* gene and Venus as a reporter. The data of the receptor sensitivity experiment need to be validated by repetition of the study with biological replicates. Also, it should be pointed out that the receptor sensitivity, and subsequently maximal mating pathway activity, can be modulated by the expression strength of the receptor.

Concluding from the experimental results of the Ste2 sensitivity experiment, the different Ste2 receptors exhibited a range of dynamics when stimulated with their cognate α-factor. Further, the promiscuity towards non-cognate α-factors did not result in similar mating pathway activation, indicating different binding affinities of the receptors to the various α-factors. Qualitatively, the reported crosstalk of the Ste2 receptors expressed in the *MAT***a** strain background were in line with the results for the receptor crosstalk study in the *MAT*α stain background.

2.2.5.4 Barrier part characterization – Bar1

The barrier parts in the YCTK play an essential role to suppress the signal of the sender parts in a multicellular network. Characterization of the barrier parts is required, to gain information that is essential for the implementation of these parts into multicellular networks in a predicted manner. As described in the barrier part selection chapter, we identified seven potential Bar1-like protease parts.

2.2.5.4.1 Verification of functional Bar1 expression and activity by degradation of cognate α-factor

Similar to the characterization of the sender and receiver parts, we verified if the barrier parts were functionally expressed and secreted. All *bar1* genes were constitutively expressed from the *HHF1* promoter and terminated by the *ENO2* terminator. The barrier devices were chromosomally integrated into the *URA3* locus and selected with the *LEU2* maker (Figure 103).

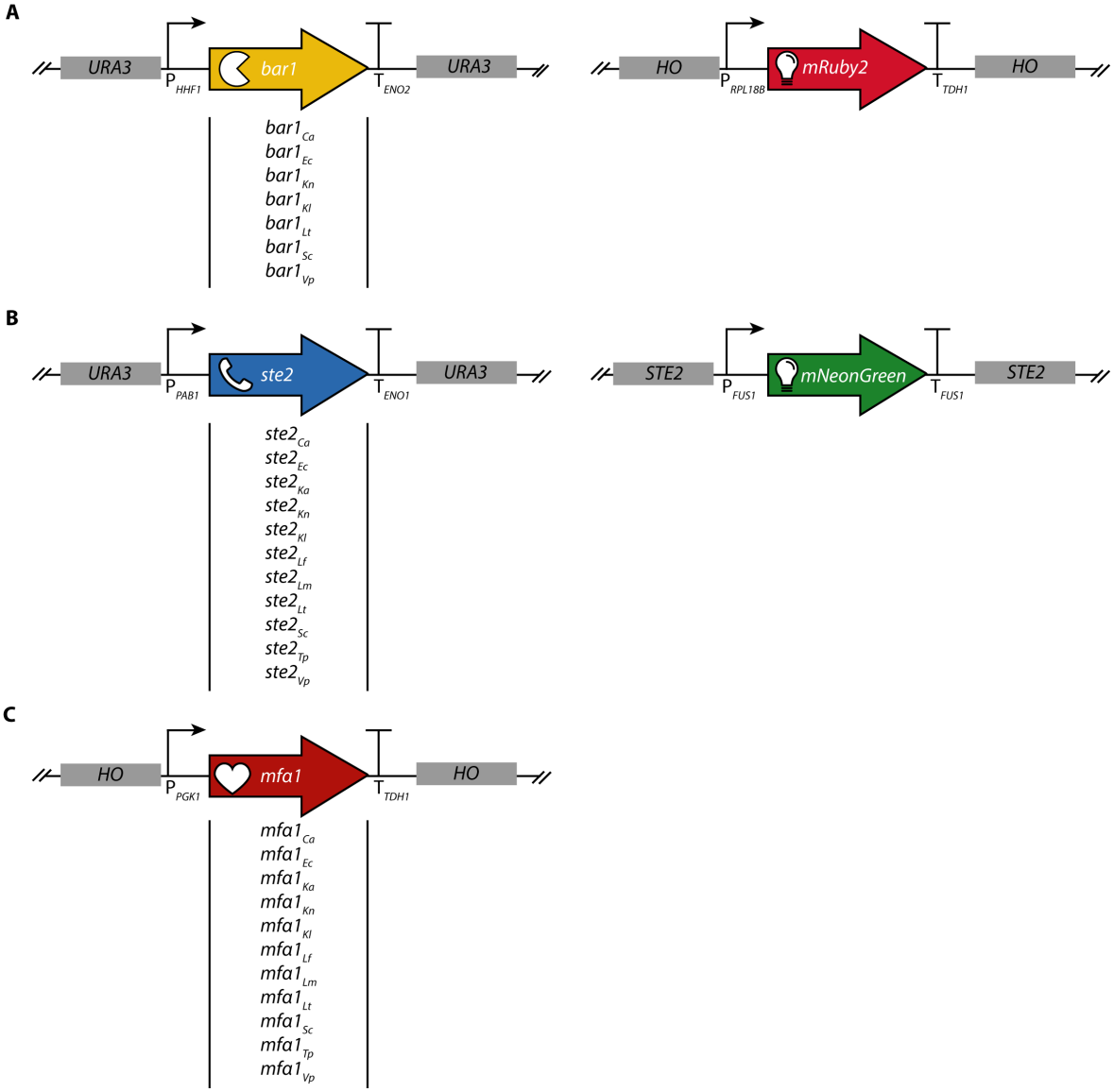

Figure 103: Constructs for the Bar1 protease crosstalk experiment. A) Genetic constructs of the Bar1 expression strain consisting of P_{HHF1}-*bar1*-T_{ENO2} and *URA3* homology sequences and P_{RPL18B}-*mRuby2*-T_{TDH1} and *HO* homology se-

quences. The *bar1* construct was built for all seven *bar1* genes originating from the selected species. For the discrimination of different strains in the coculture, the Bar1 strain harbored a reporter construct expressing mRuby2. Each *bar1* construct and the reporter construct were integrated into the *MAT*α strain background. **B)** Genetic constructs of the Ste2 expression strain consisting of P_{PAB1}-*ste2*-T_{ENO1} and *URA3* homology sequences (Ste2 device) and P_{FUS1}-*mNeonGreen*-T_{FUS1} and Ste2 homology sequences (mating reporter device). The *ste2* construct was built for all eleven *ste2* genes originating from the selected species. Each *ste2* construct and the mating pathway reporter construct were integrated into the *MAT*α strain background. **C)** Genetic construct of the α-factor expression strain consisting of P_{PGK1}- *mfα1* -T_{TDH1} and *HO* homology sequences. The *mfα1* construct was built for all eleven *mfα1* genes originating from the selected species. Each *mfα1* construct was integrated into the *MAT*α strain background.

Since direct characterization of the barrier proteases was challenging, an indirect functionality assay was implemented. By cocultivating the Bar1-expressing strain together with the cognate α-factor-producing and receptor-expressing strains (Figure 96, Figure 98), we could measure the mating pathway activity of the receiver strain by the recording the fluorescence intensity of the mating reporter Venus using flow cytometry. In case the barrier part would be functionally expressed, we expected a reduction in the mating pathway activity, since the α-factor should be degraded by the protease and thus reduce the mating response. The mating pathway activity of the receiver strains cocultivated with the strain that expressed the barrier parts was compared with the mating pathway activity of the receiver strains cocultivated with a strain lacking the barrier protease.

Figure 104 displays the histograms of the recorded single cell events of the Ste2-expressing strains for three biological replicates of the cognate protease expressing strains (upper line) and for three biological replicates of strains lacking the *bar1* gene as a control. For the *C. albicans* components observed a weaker mating pathway activity in the receiver strain when cocultivated with the $Bar1_{Ca}$-expressing strain. Therefore, we concluded that the $Bar1_{Ca}$ protease was functionally expressed and able to degrade the α_{Ca}-factor. Similar results were obtained for the parts originating from *E. cymbalariae*. Also, here the $Ste2_{Ec}$-expressing strain exhibited reduced mating pathway activity in coculture with the $Bar1_{Ec}$ strain and the α_{Ec}-factor strain. The reduction of the fluorescence intensity in comparison to the control was higher for $Bar1_{Ca}$ than for $Bar1_{Ec}$. The coculture of the three strains harboring the parts of K. *naganishii* also revealed functional protease activity since reduced mating pathway activity for the $Ste2_{Kn}$-expressing receiver strain was measured. Also, for the coculture of the three strains expressing $Bar1_{Kl}$, $Ste2_{Kl}$ and α_{Kl}-factor, a lower mating pathway activity was detected, suggesting functional $Bar1_{Kl}$ and therefore degradation of α_{Kl}-factor, which resulted in reduced fluorescence intensities of the receiver strain. Unfortunately, no reduction of the mating pathway activity was found for the cocultivation of the $Bar1_{Lt}$-expressing strain with the corresponding receiver and pheromone-producing strains. Since the identified *bar1* gene was only predicted to exhibit α-factor protease activity, it could be that in fact this was not a Bar1-like protease. Other reasons could have been inefficient degradation of the α_{Lt}-factor, expression, or secretion difficulties. Further investigations are required to verify the activity and functionality of this barrier protease. A reduction of the mating pathway activity of the *S. cerevisiae* receiver strain in comparison to the control was also observed, when cocultivated with the $Bar1_{Sc}$ strain and the α_{Sc}-factor strain. As for $Bar1_{Vp}$ we could not detect functionally expressed and secreted $Bar1_{Vp}$, as the mating pathway was not reduced in the $Ste2_{Kl}$ -expressing strain, when

cocultivated with the strains expressing the $Bar1_{Vp}$ and the α_{Vp}-factor. Causes for no detection of Bar1 activity were similar to previously mentioned ones for $Bar1_{Lt}$.
Overall, the Bar1 expression did not result in full inactivation of the mating pathway for all tested. cocultures. One reason explaining this observation was the weaker promoter used to express *bar1* genes in comparison to the strong promoter expressing the α-factors. In a follow-up experiment, we would aim to investigate whether stronger barrier part expression would result in a more efficient reduction of the mating pathway activity in the receiver strains.
To conclude, we observed protease activity for five of the seven identified Bar1-like proteases. The initial Bar1 functionality screening revealed that not activity of $Bar1_{Lt}$ and $Bar1_{Vp}$, could be detected. However, we continued characterizing them, since there was still the chance for an activity of other α-factors of our set of sender parts.

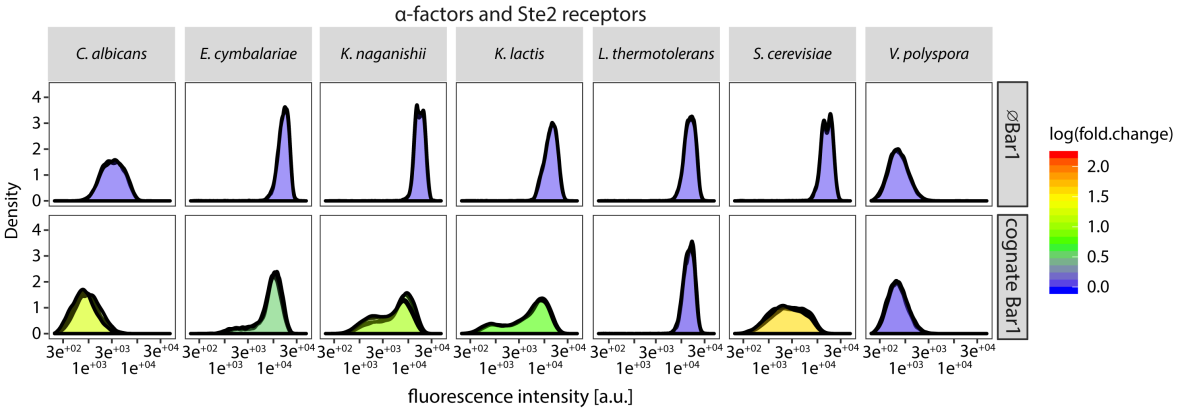

Figure 104: Verification experiment of functional Bar1 expression. The x-axis shows the Venus fluorescence intensity indicating the mating pathway activity of the measured single Ste2-expressing cell events and the y-axis the density, depicting the cell number. The color code indicates the mean fluorescence intensity of Venus as fold change reduction in log scale, constituting the reduction of the mating pathway activity. The higher the log (fold change), the higher is the activity of a Bar1 on an α-factor, reducing the mating pathway activity in the receiver strain due to reduced α-factor concentrations. Each column represents a different cognate α-factor and Ste2 strain combination. Bar1 activity was measured indirectly by cocultivation of cognate α-factor-, Ste2-, and Bar1-expressing strains and the mating pathway activity was measured in the Ste2 receiver strain, additionally harboring a α-factor-responsive mNeonGreen reporter construct. The **upper row** displays the mating pathway activity in the receiver strain when an empty Bar1 strain was part of the coculture. The **bottom row** indicates the mating pathway activity in the receiver strain for a coculture with the cognate Bar1-expressing strain. The results suggested that $Bar1_{Ca}$, $Bar1_{Ec}$, $Bar1_{Kn}$, $Bar1_{Kl}$, and $Bar1_{Sc}$ were functionally expressed and secreted since the cognate α-factor was degraded resulting in a reduced mating pathway activity in the receiver strain. No difference in the mating pathway activity was observed for the expression of $Bar1_{Lt}$ and $Bar1_{Vp}$.

2.2.5.4.2 Investigation of Bar1 promiscuity towards α-factors

After testing the functionality of the Bar1 proteases, we wanted to examine the barrier part promiscuity. Therefore, we tested the seven barrier parts against the eleven α-factors. To measure the barrier part activity, we utilized the same experimental setup as for the previous functionality assay by indirectly determining the barrier part activity by measuring the mating pathway activity of the receiver strain expressing the corresponding Ste2 receptor of an α-factor (Figure 105).
The $Bar1_{Ca}$ was very selective since we only observed a reduction of the mating pathway activity in the coculture with the cognate receiver- and sender-expressing strains. We could therefore conclude that the $Bar1_{Ca}$ exhibited a substrate specificity towards the cognate pheromone. This

result was expected, as Bar1$_{Ca}$ had the lowest sequence homology with the other identified Bar1 proteases. This little sequence homology was also identified for the α$_{Ca}$-factor and the Ste2 receptor. Overall, *C. albicans* was phylogenetically more distantly related to the other species. Also, we could report that the α$_{Ca}$-factor was not recognized by any other Bar1 in our study. Overall, for all parts (Ste2 receptor, α-factor and Bar1 protease) originating from *C. albicans,* we perceived a similar pattern: the α $_{Ca}$-factor was not stimulating any other Ste2 receptor or was degraded by any Bar1, the Ste2$_{Ca}$ receptor could not be activated by any other α-factor as well as the Bar1$_{Ca}$ protease was not degrading other α-factors. We could thus conclude that the *C.a albicans* sender, receiver and barrier parts were fully orthogonal parts in our YCTK.

Surprisingly, for Bar1$_{Ec}$ we obtained similar results as for Bar1$_{Ca}$. Bar1$_{Ec}$ reduced the mating pathway activity in its cognate receiver strain when cocultured with an α$_{Ec}$-factor-producing strain. However, we did not observe any Bar1$_{Ec}$ activity on any of the other α-factors. And also, here, none of the other Bar1s in our experiment was able to degrade the α$_{Ec}$-factor. Differently from the results of the parts originating from *C. albicans*, we did not expect these results for Bar1$_{Ec}$. *E. cymbalariae* is closely related to the other species, as we determined in our SSU phylogenetic tree (Figure 69). Similar to the Bar1$_{Ec}$, α$_{Ec}$-factor could only interact with its cognate Ste2 receptor, while Ste2$_{Ec}$ recognized almost all α-factors in this study. Since it was previously proposed that the Ste2 receptors and Bar1 proteases recognize similar amino acid sequences of the α-factor, we expected to observe Bar1 protease activity on most of the α-factors as well [298]. We could therefore conclude that also Bar1$_{Ec}$ was orthogonal and exhibited a high substrate specificity.

Differently from the previously described barrier proteases, Bar1$_{Kn}$ showed a large α-factor promiscuity, which was determined by the reduction of the mating pathway activity in cocultures of the Bar1$_{Kn}$ expression strain with non-cognate sender- and receiver-expressing strains. We observed a reduced mating pathway activity in Ste2$_{Kn}$-, Ste2$_{Kl}$-, Ste2$_{Lm}$-, Ste2$_{Tp}$-, Ste2$_{Sc}$ and Ste2$_{Vp}$-expressing strains, when cocultured with their corresponding strains producing the cognate pheromones. This indicated that the Bar1$_{Kn}$ was degrading the α$_{Kn}$-, α$_{Kl}$-, α$_{Lm}$-, α$_{Tp}$-, α$_{Sc}$-, and α$_{Vp}$-factor. These results should be critically reviewed though, since the results indicated a weaker reduction of the α$_{Tp}$-, α$_{Sc}$-, and α$_{Vp}$-factor, constituted by lower reduction of the mating pathway activity in the corresponding receiver strains. When we compared the Bar1$_{Kn}$ activity results with the Ste2$_{Kn}$ results (Figure 98), we observed a correlation between the α-factors that stimulated the Ste2$_{Kn}$ receptor and that were degraded by Bar1$_{Kn}$. Both components were interacting with the same α-factors except for α$_{Lm}$-factor, which was not recognized by Ste2$_{Kn}$ but degraded by Bar1$_{Kn}$.

Besides Bar1$_{Ca}$ and Bar1$_{Ec}$, also the barrier part originating from *K. lactis,* Bar1$_{Kl}$, exhibited a high substrate specificity. A reduction of the mating pathway activity could only be observed for the coculture of the Bar1$_{Kl}$ strain with the cognate α-factor-producing and receiver-expressing strains. A minor reduction of the mating response was also determined in the Ste2$_{Lt}$ strain, however, in order to confirm this result, further experiments are required. The Bar1$_{Kl}$ protease was part of one clade with Bar1$_{Ec}$ and Bar1$_{Lt}$ in the Bar1 phylogenetic tree that was based on the likelihood analysis of Bar1 protein sequences (Figure 73). That finding indicated a closer relationship between these proteases constituted by higher sequence homology. Overall, *E. cymbalariae* and *K. lactis* were also closer related according to our SSU rRNA phylogenetic tree (Figure 69).

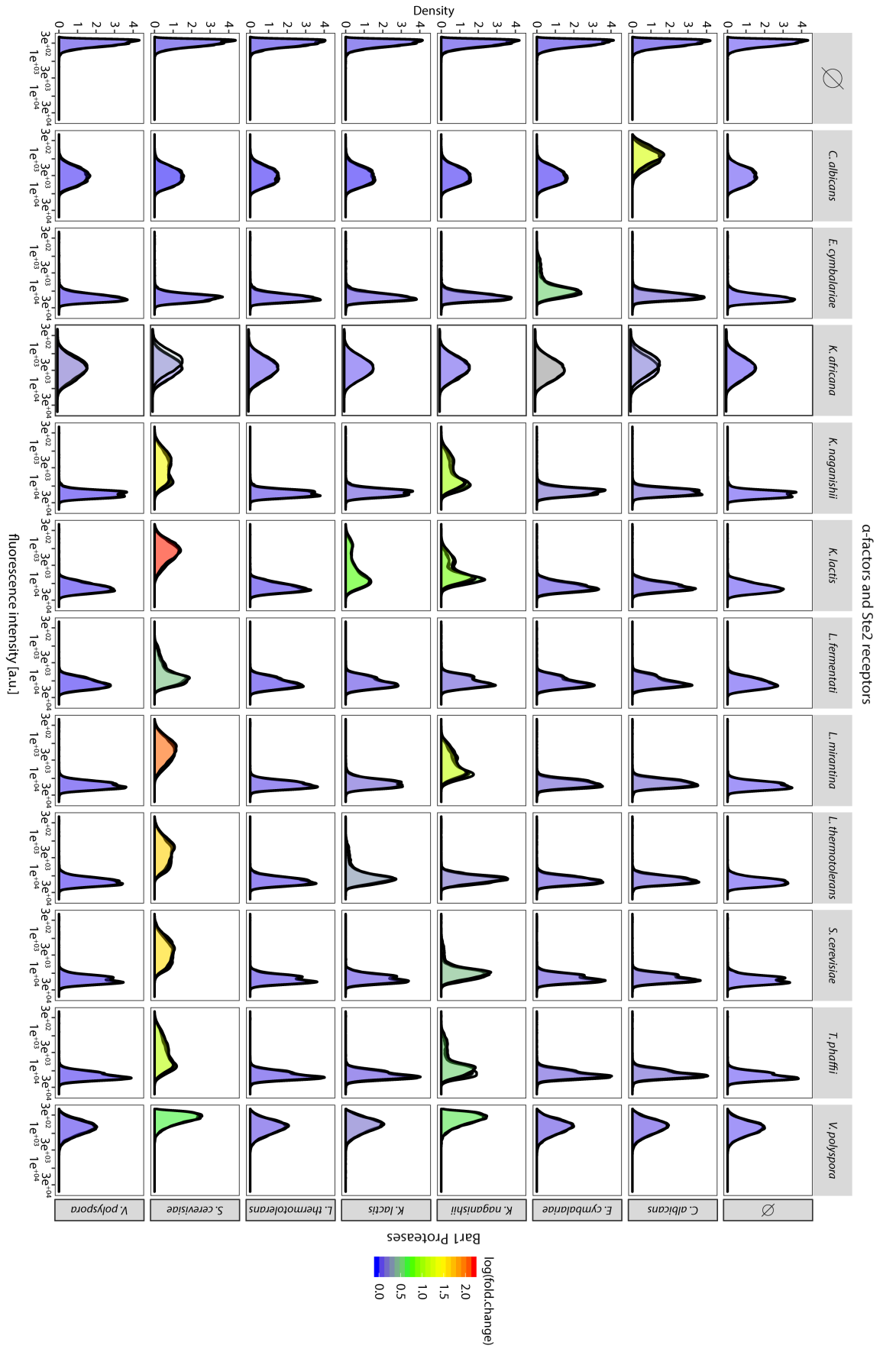

Figure 105: Results of the Bar1 and α-factor crosstalk experiment. The x-axis shows the Venus fluorescence inten-

sity indicating the mating pathway activity of the measured Ste2-expressing single cell events and the y-axis the density, depicting the cell number. The color code indicates the mean fluorescence intensity of Venus as fold change reduction in log scale, constituting the reduction in mating pathway activity. The higher the log (fold change), the higher is the activity of a Bar1 on an α-factor, reducing the mating pathway activity due to reduced α-factor concentrations. Each column represents a different cognate α-factor and Ste2 strain combination, while each row represents a different Bar1-expressing strain. Bar1 activity was measured indirectly by cocultivation of α-factor-, Ste2-, and Bar1-expressing strains and the mating pathway activity was measured in the Ste2 receiver strain additionally harboring a α-factor-responsive mNeonGreen reporter construct. The higher the fold change of fluorescence intensities was in comparison to the empty Bar1 control, the more efficiently the corresponding Bar1 was able to degrade the α-factor, resulting in reduced mating pathway activity and thus lower fluorescence reporter values. The Bar1 and α_{Ka}-factor/Ste2$_{Ka}$ crosstalk experiment was performed with a new flow cell in the flow cytometer and can therefore not be quantitatively compared to the other others.

The highest promiscuity towards non-cognate α-factors was found for the Bar1$_{Sc}$ protease. Bar1$_{Sc}$ and Bar1$_{Kn}$ share high sequence identity and were thus close related and part of the same clade in the Bar1 phylogenetic tree (Figure 73). Both species are closely related, as it had been indicated by the whole-genome phylogenetic tree [450]. Bar1$_{Sc}$ activity resulted in a reduction of the mating pathway activity in all the receptor-expressing strains in our study, except for Ste2$_{Ca}$ and Ste2$_{Ec}$, when the Bar1$_{Sc}$ strain was cocultured with cognate Ste2- and α-factor-expressing strains. Interestingly, the Bar1$_{Sc}$ protease degraded more α-factors than were recognized by the Ste2$_{Sc}$, which itself already exhibited high promiscuity towards many α-factors. When we considered the quantitative reduction efficiency of the mating pathway activity, we could report that Bar1$_{Sc}$ exhibited higher degradation activity on α_{Kl}-factor than on the cognate α_{Sc}-factor. However, further experiments are required to confirm this finding. For the Bar1 proteases originating from *L. thermotolerans* and *V. polyspora* we did not detect any reduction of mating pathway activity in any of the Ste2-expressing strains cocultured with the corresponding pheromone-producing strains and either the Bar1$_{Lt}$ or Bar1$_{Vp}$ expression strain. Therefore, we had to conclude that these proteases, as already indicated during the functionality assay, did not exhibit any degradation activities that could be monitored with our indirect measurement method and that they were most likely not functionally expressed or secreted.

This was to our knowledge the most comprehensive study of barrier proteases and their promiscuity towards α-factors that was conducted up to now. These Bar1 proteases are a highly interesting class of proteins, since they are not only secreted but are also highly stable in different conditions [298]. A more detailed biochemical analysis of these proteases to understand their α-factor recognition sites and cleavage pattern could be beneficial for future biotechnological applications.

The conclude, studying the Bar1 promiscuity, we could identify for each α-factor, except for α_{Ka}-factor, a degrading barrier protease. When we compared the promiscuity results to the likelihood analysis of the barrier protease, we saw that the closely related barrier proteases originating of *K. naganishii* and *S. cerevisiae* had the greatest promiscuity towards non-cognate α-factors. The Bar1 promiscuity did not always correlate with the receptor promiscuity. However, the α-factors originating from the same species as the most promiscuous Bar1s were able to stimulate the most Ste2 receptors.

2.2.5.4.3 Determination of Bar1 cleavage sequences in α-factors

To better understand the Bar1 activity and to determine potential recognition as well as cleavage sites of the α-factors, we conducted a proteomics-based experiment. Therefore, we cultivated the Bar1-expressing strains with defined concentrations of synthetic α-factors and determined the resulting peptide fragments (Figure 106). As the α-factors themselves are already relatively small (11-14 amino acids), the resulting peptide fragments might be below the detection limit of the mass spectrometry. After method optimization, we were able to detect the larger fragments for most α-factors after Bar1 degradation. Overall, the α_{Kn}-factor remained difficult to detect prior to protease activity and could not be detected after Bar1 cleavage. Also, the results of the smallest α-factor, which originated from *L. fermentati*, were inconclusive and will thus not be considered here. We tested all α-factors against all Bar1 proteases, as it was previously conducted for the Bar1 characterization (Figure 105). In Figure 106, each tile represents the results of the degradation of one Bar1 of one α-factor. The length of one bar in a tile represents the sequence of one detected α-factor fragment, the full sequence is depicted above. The y-axis of the tile, as well as the color code represent the log2 values normalized to the control, in which no Bar1 protease was expressed (full length α-factor). The color intensity of the bars reflects the log intensity of the peptide fragment. We expected to find a lower log2ratio of the complete α-factor and a higher ratio of a fragment, when an α-factor was cleaved by a Bar1. In case either of these two findings did not occur, the results were considered as inconclusive.

For all α-factors, we detected also smaller, non-classifiable fragments, in some case with an increased log2ratio. Up to this point, we could not determine the origin of these fragments or if they were artifacts resulting from sample treatment.

Similar to the results of the initial Bar1 characterization, we only observed a clear activity of $Bar1_{Ca}$ on its cognate α-factor. The results indicated that the α_{Ca}-factor was cleaved by $Bar1_{Ca}$ at the TN site. We also obtained an increase of the log2ratio of a peptide fragment for α_{Ka}-factor and α_{Lt}-factor, but no considerable reduction in the log2ratios of the full-length α-factors. Therefore, these findings were not considered as α-factor fragments resulting from $Bar1_{Ca}$ cleavage. The proteomics-based experiment also confirmed our previous findin that the α_{Ca}-factor was not degraded by any of the other tested Bar1 proteases.

For the $Bar1_{Ec}$ we could report a reduction of the complete α_{Ec}-factor, when the protease was expressed, together with the detection of an α_{Ec}-factor peptide fragment. This result indicated that the $Bar1_{Ec}$ barrier protease was cleaving the α_{Ec}-factor at the FD site. This result was correlating with the findings that we obtained in the Bar1 characterization experiment. Expression of $Bar1_{Ec}$ in media with any of the other α-factors resulted in peptide fragments but no reduction of the full-length α-factor, suggesting that only α_{Ec}-factor was cleaved by $Bar1_{Ec}$.

For $Bar1_{Kl}$ we detected protease activity on the α_{Kl}-factor as well as on the α_{Lt}-factor. Interestingly, we obtained similar results as for the initial Bar1 protease characterization, however, since the mating pathway activity in the $Ste2_{Lt}$-expressing strain was not considerably reduced, we considered the result as inconclusive (Figure 105). Because the results of the proteomics-based Bar1 experiment confirmed our previous finding, we could conclude that $Bar1_{Kl}$ could cleave α_{Lt}-factor. α_{Kl}-factor and α_{Lt}- factor share only the GQP motif, which however is also found in other pheromones that are not cleaved by $Bar1_{Kl}$. The α_{Kl}-factor was also cleaved at the LR amino acids and

α_{Lt}-factor at the LS motif. Both pheromones have a leucine residue two amino acids downstream of the GQP motif. However, similar motives are also found in α_{Sc}-factor, α_{Tp}-factor, and α_{Vp}-factor, which are not degraded by $Bar1_{Kl}$.

As we previously described, $Bar1_{Kn}$ exhibited great substrate promiscuity. Unfortunately, we were not able to detect the α_{Kn}-factor. The $Bar1_{Kn}$ cleaved most of the detected α-factors, excepted for α_{Ca}-factor and α_{Ec}-factor. For the α_{Ec}-factor we found an increase in the log2ration of an α_{Ec}-factor fragment but no reduction of the log2ratio of entire pheromone. These fragments were also found in the sample of $Bar1_{Ec}$ with α_{Ec}-factor. Overall, weaker activity was found for the degradation of α_{Ka}-factor and α_{Lm}-factor by $Bar1_{Kn}$. The α_{Ka}-factor was cleaved at the TS motif. Interestingly, we could also report a small peptide fragment of α_{Lt}-factor. During the initial protease characterization, we could not detect $Bar1_{Kn}$ activity on α_{Lt}-factor. The α_{Lt}-factor factor was cleaved at LS, similar to the cleavage observed for the $Bar1_{Kl}$ protease. Also, the α_{Lt}-factor factor was cleaved at the same sequence as previously described. The α_{Sc}-, α_{Tp}-, and α_{Vp}-factors were cleaved at the second N-terminal leucine residue. The α_{Lm}-factor, which had less homology to the other α-factors, was cleaved at the SL amino acid sequence. The proteomics-based experimental results suggested that α_{Lm}-factor was degraded less efficiently by $Bar1_{Kn}$, however, the previous flow cytometry-based experiment revealed a visible reduction of mating pathway activity in the $Ste2_{Lm}$-expression strain upon expression of $Bar1_{Kn}$. Except for the α_{Lm}-factor, all other pheromones that were cleaved by $Bar1_{Kn}$ have a GQP motif two amino acids upstream of the cleavage sequence. This sequence could also be found in the α_{Ec}-factor but the obtained results were inconclusive, as previously mentioned. Also, for this experiment, we could not report any protease activity for $Bar1_{Lt}$, which was in accordance with the previous Bar1 characterization experiment using flow cytometry. Similar high promiscuity as for $Bar1_{Kn}$ was found for the $Bar1_{Sc}$ protease, with protease activity for all α-factors, except for α_{Ca}-factor. During initial characterization, we did not detect degradation of α_{Ec}-factor, though. All of the pheromones that were cleaved had the previously mentioned GQP motif, except for α_{Lm}-factor. The $Bar1_{Sc}$ protease was also the only Bar1 protease that exhibited cleavage of α_{Ka}-factor. Interestingly, we detected higher log2 ratios of the peptide fragment of α_{Ec}-factor, when treated with the $Bar1_{Sc}$ than with $Bar1_{Ec}$. This observation suggested that $Bar1_{Sc}$ was degrading the α_{Ec}-factor more efficiently than the $Bar1_{Ec}$. Also, the proteomics-based experiment did not reveal any protease activity for the barrier protease $Bar1_{Vp}$, which was already excepted based on our previous findings.

Overall, the results correlated with the initial indirect Bar1 characterization findings. The few differences were most likely due to the experimental setup, as for example the Bar1 proteases were longer incubated with the α-factors and most importantly, a defined amount of α-factor was supplied and thus degraded over time. For the indirect Bar1 characterization experiment, continuous production of α-factor was warranted, resulting in overall higher concentrations of α-factor. As described for the *in silico* identification, some *mfα1* genes contain several different α-factors resulting a mixture of different mature pheromones, which not all might be not recognized by the proteases. This would result in mating pathway stimulation that could be detected in the initial Bar1 characterization experiment.

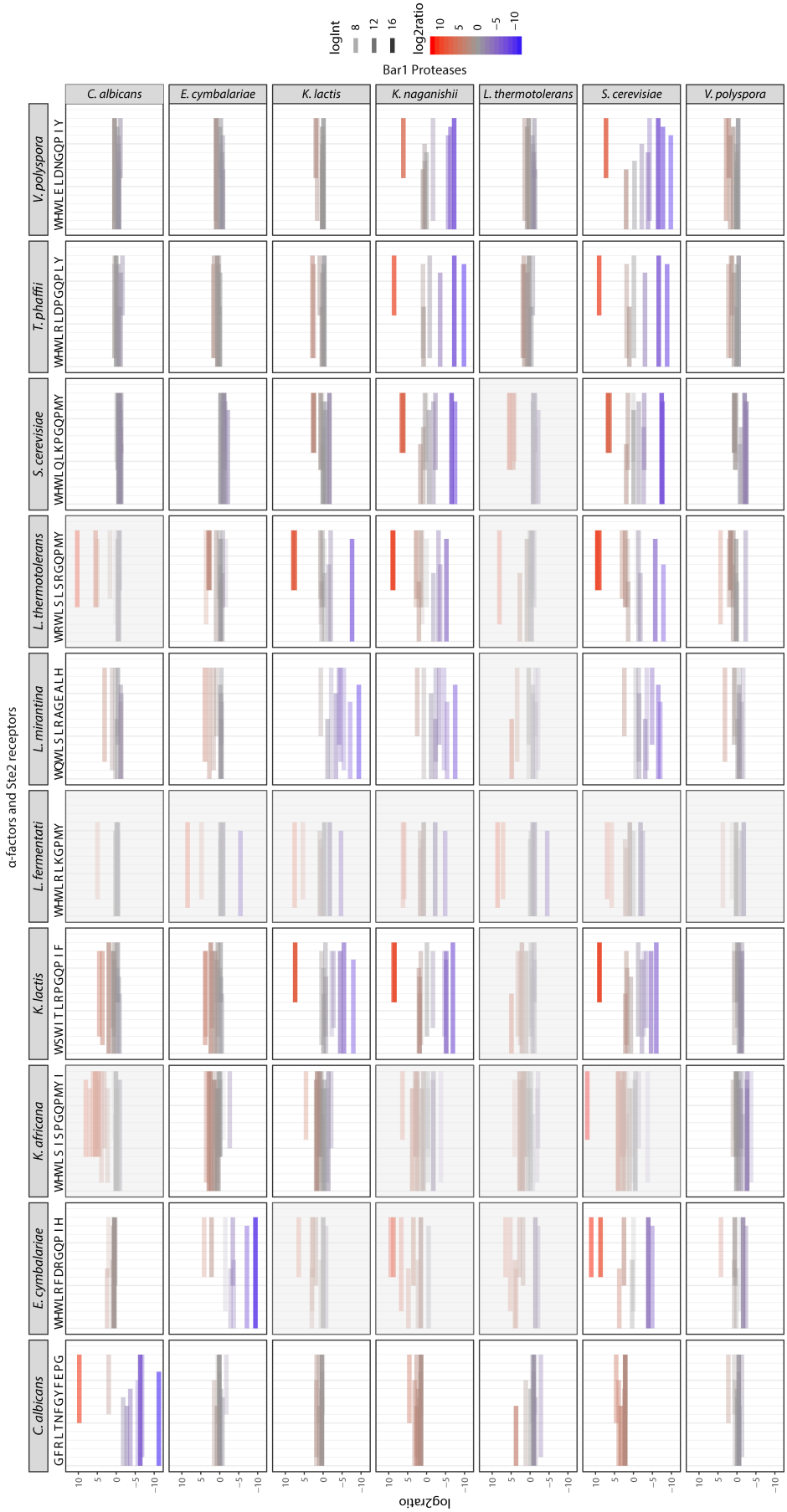
logInt
8
12
16
log2ratio
10
5
0
−5
−10
Bar1 Proteases
C. albicans
E. cymbalariae
K. lactis
K. naganishii
L. thermotolerans
S. cerevisiae
V. polyspora
α-factors and Ste2 receptors
C. albicans GFRLTNFGYFEPG
E. cymbalariae WHWLRFDRGQPIH
K. africana WHWLSISPGQPMYI
K. lactis WSWITLRPGQPIF
L. fermentati WHWLRLKGPMY
L. mirantina WQWLSLRAGEALH
L. thermotolerans WRWLSILSRGQPMY
S. cerevisiae WHWLQLKPGQPMY
T. phaffii WHWLRLDPGQPLY
V. polyspora WHWLELDNGQPIY
log2ratio

Figure 106: Proteomics-based investigation of Bar1 cleavage sites of α-factors. Each column depicts a different synthesized α-factor and each row represents a different Bar1-expressing strain. At the top of each column, the amino acid sequence of each full-lengthα-factor that is listed, with each letter forming one sub-column. The size of the bars within each panel indicates the sequence of the detected α-factor peptide fragments of two technical replicates normalized by the negative control as a result of the corresponding Bar1 activity. The y-axis and color code illustrate the log2ratio of each detected fragment to the negative control. The intensity of the color code reflects the log intensity of the detected fragments. Positive results, meaning one Bar1 was effectively cleaving an α-factor, should exhibit a log2ratio increase for fragments, constituted by red bars, and a reduction of the log2ratio of the full-length α-factor, depicted by blue bars. Inconclusive experimental results are masked in grey. Plot provided by A. Anders.

For the proteomics-based experiment, we utilized synthetic α-factor, which was synthesized according to one of the sequences.
Appendix Table 2 lists the α-factors of the different species and highlights the synthetic α-factor that was utilized. Interestingly, when the Bar1 proteases were degrading α-factors, the resulting peptide fragments were the same, independently from the Bar1. For most of the pheromones we detected cleaving at the second N-terminal leucine residue.

In summary, this is to our knowledge the most comprehensive analysis of the promiscuity of different Bar1 proteases towards different α-factors that was performed so far. To confirm these results, repetition with more biological replicates as well as further optimization of the proteomics method, in order to be able to also detect smaller peptide fragments after protease treatment, would be required.
To conclude, the results were overall qualitatively mostly coinciding with the data obtained from the Bar1 promiscuity investigation. In some cases, the results did not fully reflect these results which will be further investigated. Independent from the barrier proteases, the peptide fragments of the Bar1-degraded α-factors remained consistent, possibly indicating similar recognition and cleavage sites of the barrier proteases.

2.2.5.5 Investigating the effects by expression tuning of the YCTK parts

In our previous experiments, the Ste2 receptors, the α-factors and Bar1 proteases were mostly expressed from constitutive promoters. Now, we wanted to investigate if by modulating the expression strength of these receiver, sender and barrier parts, the output could be altered by expressing the corresponding genes from an inducible promoter. This is an important parameter required for the design, potential improvement, and implementation of multicellular networks in which many different parts have to interact with each other. With the large collection of parts provided with the YTK and YCTK, exchanging e.g. promoters to modulate the expression of the desired part could be easily achieved. To cover a range of expression strengths, we utilized the previously characterized P_{CUP1} promoter, which can be induced by $CuSO_4$. Exemplarily, we used the sender, receiver, and barrier parts originating from *S. cerevisiae*.
As it was shown earlier for the characterization of the *CUP1* promoter (Figure 77), maximal induction of P_{CUP1} resulted in lower expression as from the *PGK1* promoter that was used for the expression of *mfα1* genes (Figure 95, Figure 98, Figure 104). The expression levels of the *PAB1* promoter, which was implemented for the expression of *ste2* genes (Figure 98, Figure 101 Figure 104), were similar to the maximally induced P_{CUP1} promoter. For the rather weak *HHF1* promoter, that was utilized for the expression of *bar1* genes (Figure 105, Figure 106), the expression strength was in

the dynamic range of the P_{CUP1} promoter (Figure 77). To summarize, we investigated how lower expression of the sender parts, lower or a similar expression strength of the receiver parts, and lower and higher expression of the barrier parts altered the mating pathway activity.

2.2.5.5.1 Tuning of sender parts- α-factor

To measure the differences in expression strength of the *mfα1* gene, which encoded the α_{Sc}-factor, we measured the induction levels of the mating pathway in a receiver strain, in which the $Ste2_{Sc}$ receptor was constitutively expressed. With the receiver strain, we could indirectly measure the production levels of the α_{Sc}-factor, since the dose-response characterization of the promoter revealed that higher α-factor concentrations result in stronger activation of the mating pathway, indicated by increased fluorescence reporter output. The receiver strain contained thus two devices: the $ste2_{Sc}$ gene was constitutive expressed by the *PAB1* promoter and terminated by T_{ENO1}. To monitor the mating pathway activity, we utilized the P_{FUS1} promoter that expressed the Venus reporter upon mating pathway activation. This receiver and mating reporter strain was cocultured with the sender strain. This strain carried the sender system, which consisted of the $mfα1_{Sc}$ gene expressed from the copper-inducible promoter P_{CUP1} and the T_{TDH1} terminator. As a positive control we used the previously constructed strain, which constitutively expressed the $mfα1_{Sc}$ gene. For the negative control, we utilized a strain that was not producing any pheromone (Figure 107).

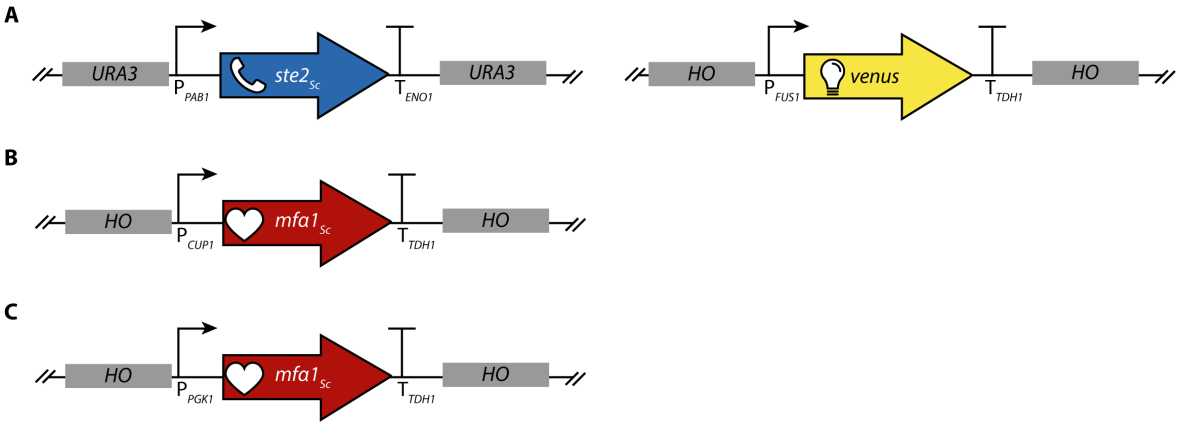

Figure 107: Constructs for the $mfα_{Sc}$ gene expression titration experiment. A) Genetic constructs of the $Ste2_{Sc}$ receiver and reporter strain consisting of P_{PAB1}-$ste2_{Sc}$-T_{ENO1} with *URA3* homology sequences and P_{FUS1}-*venus*-T_{TDH1} with *HO* homology sequences. Both constructs were integrated into the *MAT***a** *far1Δ* strain background. **B)** Genetic constructs of the *mfα1* gene expression titration strain consisting of P_{CUP1}- $mfα1_{Sc}$ -T_{TDH1} and *HO* homology sequences. The construct was integrated into the *MAT***a** *far1Δ* strain background. **C)** Genetic constructs of the *mfα1* gene expression control strain consisting of P_{PGK1}- $mfα1_{Sc}$ -T_{TDH1} and *HO* homology sequences. The construct was integrated into the *MAT***a** *far1Δ* strain background.

The data were obtained using flow cytometry and each dataset consisted of 50,000 recorded single cell events of the receiver strain. The error bars represented the standard deviation of three biological replicates.

Figure 108 displays the mean fluorescence intensity of the dose-response of the receiver strain output, representing mating pathway activity. We tested six different concentrations of $CuSO_4$, namely 0, 0.2, 0.75, 3.13, 25, and 50 µM. For the coculture of the receiver strain with the P_{CUP1}-$α_{Sc}$-

factor strain, we observed with increasing $CuSO_4$ concentrations, higher fluorescence intensities in the receiver strain, suggesting higher mating pathway activity and thus higher amounts of α-factor in the media. We could therefore report that stronger expression of the *mfa1*$_{Sc}$ gene resulted in stronger activation of the mating pathway in the receptor strain. The strong mating pathway response in media without copper was resulting from the leakiness of the *CUP1* promoter. For the coculture of the receiver strain with the strain constitutively producing the α-factor, we monitored that in absence of $CuSO_4$ and for low concentrations, high fluorescence intensities could be measured. However, at higher $CuSO_4$ concentrations, a reduction of the mating pathway activity was detected. This could be explained by the cytotoxic effect of copper resulting in a reduction of protein expression. The negative control, for which we cocultured the receiver strain with a strain lacking an expression module for the *mfa1*$_{Sc}$ gene, we only measured basal fluorescence intensities.

Based on this experiment we could conclude that by modulating the expression of the sender part, we could tune the response in the receiver strain, thus providing the possibility for adjustment of part expression, which is of importance for multicellular network designs. Since we only investigated the effects for the expression of the *mfa1*$_{Sc}$ gene, comprehensive analysis of the modulation of the other sender parts would be required to obtain all characteristics of all parts. For now, we assumed that the results for the other sender parts would be comparable.

To conclude, the experimental results determined that by upregulating the expression and thus production of α_{Sc}-factor, the mating pathway activity in the receiver cells could be increased.

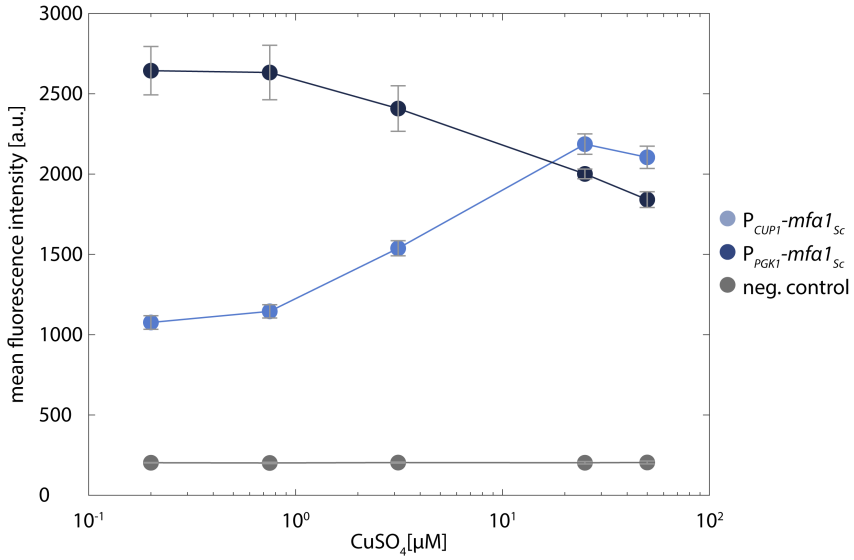

Figure 108: Result of the *mfa1*$_{Sc}$ gene expression titration experiment. The dose-response of *mfa1*$_{Sc}$ gene expression and subsequently the production of the α_{Sc}-factor was indirectly measured by Venus expression from the P_{FUS1} α-factor-responsive promoter as a function of the mating pathway activity in the reporter strain. Displayed are the mean Venus fluorescence intensities of the reporter strain, cultivated with three biological replicates of the α-factor producing strain for increasing $CuSO_4$ concentrations, to induce *mfa1*$_{Sc}$ gene expression. The constitutive promoter *PGK1* that was previously used for *mfa1*$_{Sc}$ gene expression was utilized as a control.

2.2.5.5.2 Tuning of receiver parts- Ste2

To investigate the effect of Ste2 receptor expression tuning on the mating pathway activity, we constructed a receiver system consisting of two devices, the receiver and output device. The receiver device consisted of the $Ste2_{Sc}$ that was expressed by the *CUP1* promoter and terminated byT_{ENO1}. The output device was, a before, and P_{FUS1} was driving the expression of the *venus* reporter gene to monitor the mating pathway activity. As positive control we utilized a strain constitutively expressing the $ste2_{Sc}$ gene from the *PAB1* promoter and which also contained the output device. As a negative control, we used a strain harboring the reporter device but lacking the receiver device, meaning this strain was not expressing any Ste2 receptor (Figure 109).

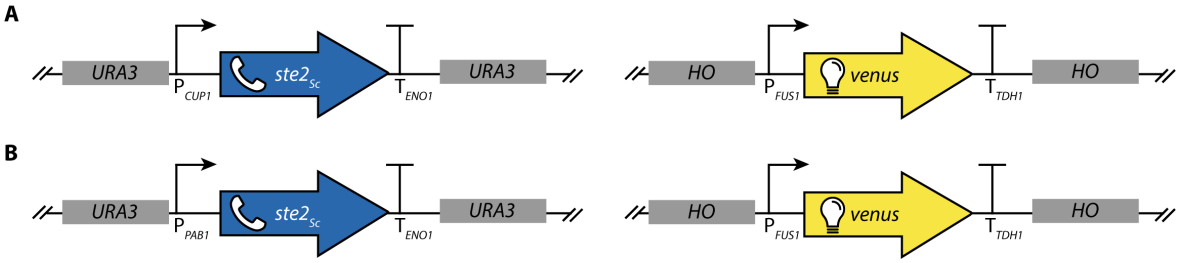

Figure 109: Constructs for the $ste2_{Sc}$ gene expression tuning experiment. A) Genetic constructs of the $Ste2_{Sc}$ tuning receiver and reporter strain consisting of P_{CUP1}-$ste2_{Sc}$-T_{ENO1} with *URA3* homology sequences and P_{FUS1}-*venus*-T_{TDH1} with *HO* homology sequences. Both constructs were integrated into the *MAT***a** *far1Δ* strain background. **B)** Genetic constructs of the $ste2_{Sc}$ gene expression control strain consisting of P_{PAB1}- $ste2_{Sc}$ -T_{ENO1} with *URA3* homology sequences and P_{FUS1}-*venus*-T_{TDH1} with *HO* homology sequences. Both constructs were integrated into the *MAT***a** *far1Δ* strain background.

Using this $Ste2_{Sc}$-expressing strain, we tested different Ste2 induction levels for different α-factor concentrations. As before, we tested 6 concentrations of $CuSO_4$ to induce Ste2 expression and additionally 8 concentration of synthetic α_{Sc}-factor. We measured 5,0000 single cell events by flow cytometry and plotted the mean fluorescence intensity. As before, we utilized the P_{FUS1}-*venus* output device to measure mating pathway activity and measured three biological replicates. Figure 110 A displays the heatmap of the fluorescence intensities for the copper-titratable Ste2 expression strain. The overall trend indicated that increased receptor expression resulted in a stronger activation of the mating pathway. Activation of the mating pathway in the absence of $CuSO_4$, meaning no Ste2 receptor should be expressed, could also here be explained with the leakiness of the P_{CUP1} promoter. We detected that with minimal expression of $Ste2_{Sc}$, earlier saturation of the mating pathway activity was observed. For $CuSO_4$ concentrations up to 3.13 µM, the fluorescence intensities saturated for 4.4 nM α_{Sc}-factor. For higher $CuSO_4$ concentrations though, the mating pathway activity was not reaching saturating levels for maximal α_{Sc}-factor amounts. We could therefore conclude that that the number of Ste2 receptors in the membrane were correlating with the mating pathway response activity. When all available receptors were stimulated, the mating pathway response saturated, as our data indicated. This suggested that by changing the expression of the Ste2 receptor, the mating pathway response could be de- or increased. Figure 110 B displays the heatmap-plotted mating pathway response for the strain constitutively expressing Ste2. As predicted, we did not observe any differences in the output response for increasing $CuSO_4$ concentrations. However, it was unexpected that in total higher mating pathway

activities were measured for this strain than for the P_{CUP1}-ste2 strain. Our P_{CUP1} promoter characterization had indicated that the *CUP1* promoter could be stronger induced than the P_{PAB1} promoter, which was the constitutive promoter utilized here for Ste2 expression (Figure 77). The only explanation we have so far for this finding is that the expression of a reporter gene does not necessarily represent the expression of a membrane protein and that each part exhibits context-dependent expression variation [74,75]. Appendix Figure 2 depicts the heatmap of mean fluorescence intensities resulting from the mating pathway activity of the negative control strain. As predicted, we did not measure any visible stimulation of the mating pathway and could only measure basal mating pathway activity.

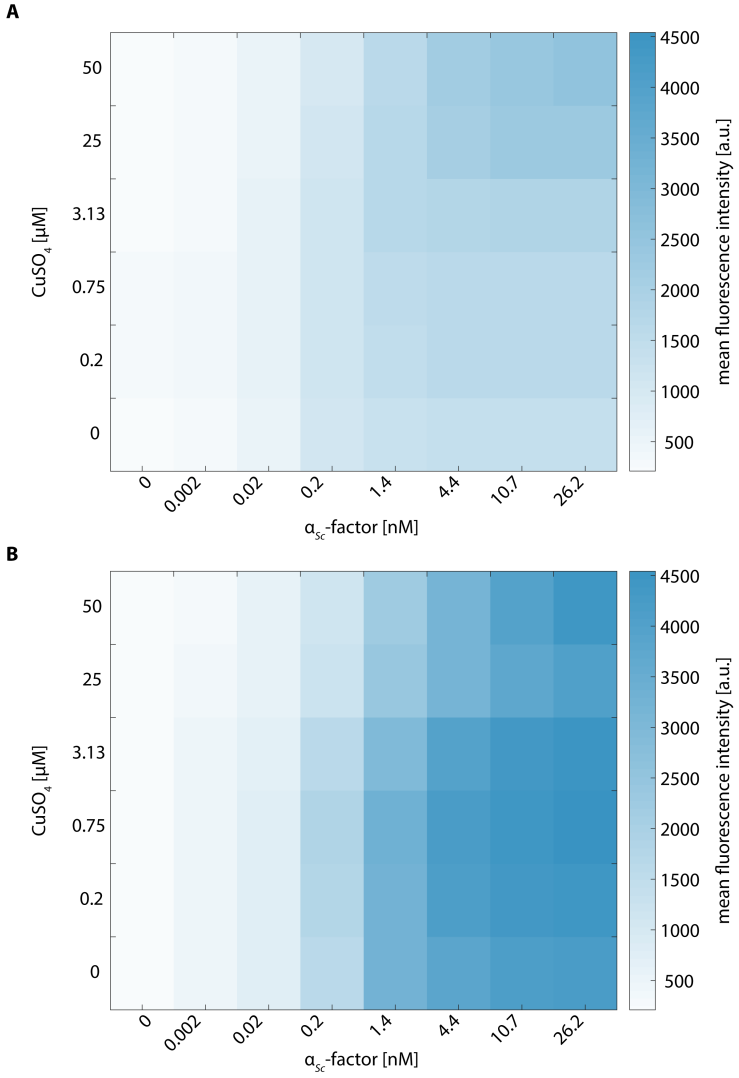

Figure 110: Results of the *ste2* gene expression tuning experiment. The expression of the Ste2 receptor was regulated by amounts of $CuSO_4$ in the media. To investigate the interplay between receptor expression levels and amounts of α-factor, synthetic pheromone was added in different amounts to the Ste2- expressing receptor strains. The columns of the heatmap display different α_{Sc}-factor concentrations and the rows the increasing $CuSO_4$ concentrations. The color code indicates the mating pathway activity as levels of Venus expressed from the P_{FUS1} α-factor-responsive promoter. Plotted is the mean fluorescence intensity of three biological replicates of 50,000 single-cell events of the receiver strain each. The constitutive promoter *PAB1* that was previously used for $ste2_{Sc}$ gene expression was utilized as a control. **A)** Heatmap for the P_{CUP1}-*ste2 MAT***a** *far1Δ* stain in increasing $CuSO_4$ and α_{Sc}-factor concentrations. **B)** Heatmap for the P_{PAB1}-Ste2 *MAT***a** *far1Δ* stain in increasing $CuSO_4$ and α_{Sc}-factor concentrations. See also Appendix Figure 2.

Overall, the results of the tuning of the receiver part revealed that by modulating the Ste2 expression we could change the response of the mating pathway. These results suggest that the modulation of receiver part expression is another control level that can be implemented into the design of multicellular systems.
To conclude, by modulating the Ste2 receptor expression, we altered the response of the mating pathway, especially the maximal pathway activity. This titration of the receiver part provided an additional opportunity to control the pathway response.

2.2.5.5.3 Tuning of barrier parts- Bar1

To investigate whether a stronger expression of the Bar1 proteases would result in higher quenching activity on the α-factors, we designed a device, in which $Bar1_{Sc}$ was expressed from the P_{CUP1} promoter. As controls, we utilized a strain constitutively expressing $Bar1_{Sc}$ as well as a strain that didn't express any barrier part. The constitutive *HHF1* promoter that was utilized for $Bar1_{Sc}$ expression was rather weak and exhibited similar expression strength as the P_{CUP1} promoter upon induction with 3.13 µM $CuSO_4$ (Figure 77). Since we could not measure the barrier part expression directly, we cocultured the $Bar1_{Sc}$-expressing strain with a strain harboring the previously utilized receiver system consisting of a constitutive $Ste2_{Sc}$ expression device as well as the mating response output device consisting of the *FUS1* promoter driving the expression of the reporter gene venus (Figure 111).

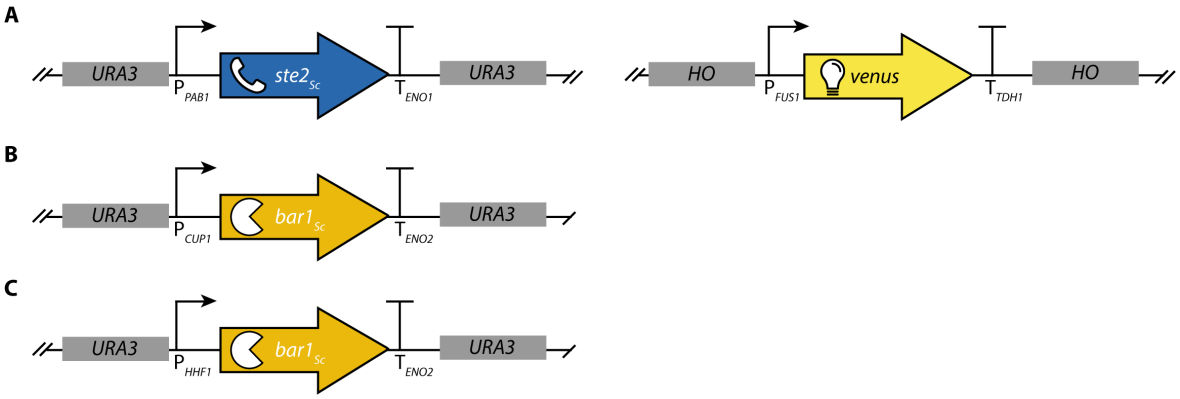

Figure 111: Constructs for the *bar1*$_{Sc}$ gene expression tuning experiment. A) Genetic constructs of the $Ste2_{Sc}$ receiver and reporter strain consisting of P_{PAB1}-*ste2*$_{Sc}$-T_{ENO1} with *URA3* homology sequences and P_{FUS1}-*venus*-T_{TDH1} with *HO* homology sequences. Both constructs were integrated into the *MAT***a** *far1Δ* strain background. **B)** Genetic constructs of the *bar1* gene expression titration strain consisting of P_{CUP1}- *bar1*$_{Sc}$ -T_{ENO2} and *URA3* homology sequences. The construct was integrated into the *MAT***a** *far1Δ* strain background. **C)** Genetic constructs of the *bar1* gene expression control strain consisting of P_{HHF1}- *bar*$_{Sc}$ -T_{TDH1} and *URA3* homology sequences. The construct was integrated into the *MAT***a** *far1Δ* strain background.

The mating pathway is activated upon α-factor stimulation, resulting in the expression of the reporter gene. In case the Bar1 protease is expressed, the α-factor is degraded, resulting in reduction of the activity of the mating pathway, which we recorded by measuring the Venus fluorescence intensity in the receiver strain. Here, we tested six different $CuSO_4$ concentrations to induce the expression of $Bar1_{Sc}$ in combination with 8 concentrations of synthetic α_{Sc}-factor. The heatmap in Figure 112 depicts the mean fluorescence intensity of three biological replicates. Figure 112A represents the results for the $CuSO_4$-inducible expression of $Bar1_{Sc}$. It should be noted

that higher Bar1$_{Sc}$ expression should result in weaker mating pathway activity, indicated by lighter color in the heatmap. When Bar1$_{Sc}$ expression was uninduced and 0 nM α_{Sc}-factor was added to the media, we detected only basal mating pathway activity. As previously mentioned, the *CUP1* promoter exhibits leaky gene expression, resulting in basal expression in uninduced culture conditions. For increasing α_{Sc}-factor concentrations and uninduced Bar1$_{Sc}$, we observed an increase in the mating pathway activity. With increasing $CuSO_4$ concentrations though, leading to stronger expression of Bar1$_{Sc}$, a reduction of the mating pathway activity was observed. For 0 µM $CuSO_4$ and 26.2 nM α_{Sc}-factor, we reported Venus fluorescence intensities of around 4000 a.u., while for 50 µM $CuSO_4$ and 26.2 nM α_{Sc}-factor, we only measured 900 a.u., which indicated that the mating pathway was less active.

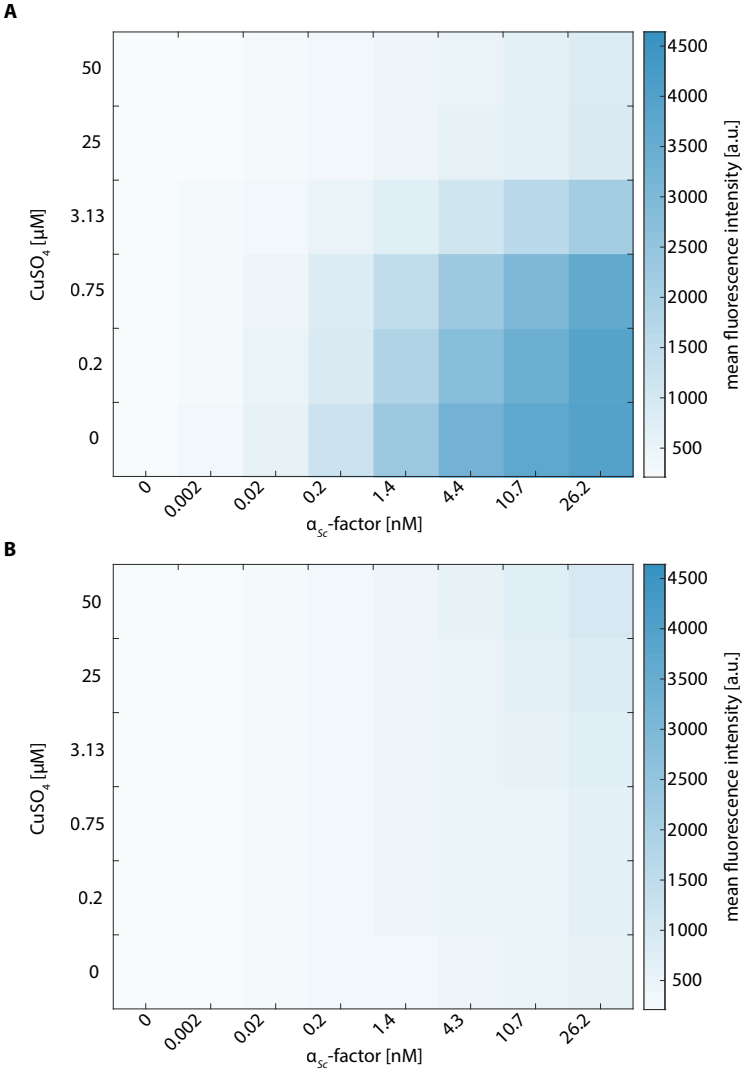

Figure 112: Results of the *bar1* gene expression titration experiment. The expression of the Bar1 protease was regulated by amounts of $CuSO_4$ in the media. To investigate the interplay between protease expression levels, amounts of α-factor and resulting mating pathway activation, synthetic pheromone was added in different amounts to the co-culture of the Bar1 and Ste2 strain. Higher expression levels of Bar1 should result in reduced mating pathway activity in the Ste2 receiver strain due to α-factor degradation. The columns of the heatmap display different α_{Sc}-factor concentrations and the rows the increasing $CuSO_4$ concentrations. The color code indicates the mating pathway activity as levels of Venus expressed from the P_{FUS1} α-factor-responsive promoter in the Ste2 strain. Plotted is the mean fluorescence intensity of three biological replicates of 50,000 single-cell events of the Ste2 strain each. The constitutive promoter *HHF1* that was previously used for *bar1*$_{Sc}$ gene expression was utilized as a control. **A)** Heatmap for the P_{CUP1}-*bar1*

*MAT***a** *far1Δ* stain in increasing $CuSO_4$ and α_{Sc}-factor concentrations. **B)** Heatmap for the P_{PAB1}-*bar1 MAT***a** *far1Δ* stain in increasing $CuSO_4$ and α_{Sc}-factor concentrations. See also Appendix Figure 3.

Overall, we could conclude that a stronger expression of the barrier part resulted in increased degradation of the α_{Sc}-factor and thus reduced mating response. However, it has to be noted that even for maximal $Bar1_{Sc}$ expression, the mating response could not be entirely prohibited. This result indicated that α_{Sc}-factor was not entirely degraded. This finding should be considered for the engineering of multicellular systems, in which an α-factor would not be added in a defined amount but rather constantly produced by an α-factor-expressing strain. We also monitored the coculture, in which $Bar1_{Sc}$ was constitutively expressed by the *HHF1* promoter (Figure 112B). Based on the previous promoter characterization, we expected lower $Bar1_{Sc}$ expression levels (Figure 77). Increasing $CuSO_4$ concentrations slightly influenced the $Bar1_{Sc}$ expression and but we observed a reduction of the mating pathway activity under all conditions. For the negative control, in which the barrier part was expressed, we obtained a full activation of the mating pathway with increased α-factor concentrations (Appendix Figure 3).
Overall, the experiment showed that by increasing the expression of the $Bar1_{Sc}$, we could reduce the mating pathway activity in the receiver strain by enhancing the degradation of the α-factor. Unfortunately, we could not report a full degradation of the α-factor and therefore were only able to reduce the mating pathway activity. To apply the barrier parts for a full reduction, further investigations are required to identify the optimal balance between sender, receiver and barrier part expression levels. Nevertheless, the results showed that the Bar1 proteases can degrade α-factors and are therefore a valuable component to be used for the engineering of multicellular systems.
To conclude, the barrier protease Bar1 can act as a buffer and change the α-factor concentration depending on its expression strength and thus the dose-response of the mating pathway in receiver strains.

2.2.6 Utilization of YCTK parts for the construction of multicellular networks

With our selection and characterization of responder, sender, receiver and barrier parts, we aimed to provide a toolkit for the rapid assembly of multicellular communication networks. We provided all parts in level 0 Golden Gate vectors, which can be assembled into genetic device (Level 1). One genetic device consists of one expression unit, which in turn is composed of a promoter (part 2), open reading frame (part 3) and terminator (part 4), as well as connectors, homology sequences for genomic integration, and selection markers. Genetic devices can function as genetic devices but also as systems, if they perform a more complex task. Several genetic devices can also be combined into systems in Golden Gate level 2 vectors. Each device/system is integrated into one cell, and several devices/systems in different cells can be combined to multicellular networks that perform the desired function.
For all upcoming networks, we utilized the *MAT***a** *lys2::rttAS2 mfα2Δ::hphNT1 mfα1Δ::klTRP1 bar1Δ::kanMX ste2Δ::natNT far1Δ::ura3* strain as chassis and built a variety of different multicellular systems using the sender, receiver and barrier parts of our YCTK. We thus constructed α-factor- and mating response-based communication network. Besides the genetic systems, each sender strain carried a reporter gene that was chromosomally integrated and constitutively expressed

and essential for strain discrimination during flow cytometry acquisition. Each multicellular system consisted of one to three sender strains and one receiver strain expressing the output reporter. We designed and built two different types of multicellular networks: for one type we utilized the population composition itself as the input (logic population networks) while in a second approach, external signals in form of inducers served as input (multicellular response networks). For each multicellular system, we conducted three experiments using biological replicates of each strain. We acquired 50,000 single cell events using flow cytometry. The results display the fluorescence intensities of the receiver strains and to visualize the results further, we calculated the fold change of the expression based on the mean intensity of the receiver strain in the absence of the sender system.

2.2.6.1 Logic population networks

The aim of this project was to use the parts of the YCTK for the construction of multicellular networks that function as self-organized logic population networks. Different from other Boolean Logic Gates, here, the output is not depending on input signals in form of inducers, rather on the community composition itself, which allows the receiver cells to conditionally respond and thus exhibiting the logics of various Boolean Gates.

2.2.6.1.1 Buffer-like population network

The goal of this multicellular network was to engineer populations that were acting as a buffer, meaning their population behavior for different conditions was following the Boolean logic of a buffer (Figure 114A). In order to exhibit a buffer-like output, the receiver cells should exhibit an output signal (💡)in case the sender population is present (1), in our case, the expression of the mTurquoise2 reporter. If the sender population is not present (0), meaning it was replaced with an empty strain, the receiver cells should not exhibit an output (-).

The sender cells (S) harbored the *mfa1*$_{Sc}$ gene, which was expressed by P_{TDH3} and terminated by T_{TDH1}. The device, here acting as a system, was chromosomally integrated into the *URA3* locus and selected with the *LEU2* auxotrophic marker. The receiver strain (R) carried two devices: the first was the *HHF2* promoter driving the expression Ste2$_{Sc}$ receptor, terminated by T_{ENO1}, the second device was the pathway response output module consisting of P_{FUS1} driving the expression of the mTurquoise2 reporter, terminated by T_{ADH1}. This receiver system, was also chromosomally integrated into the *HO* locus and selected by *LEU2* (Figure 113). The general design motif of the buffer is alike the experimental setup of the Ste2-α-factor crosstalk studies (Figure 98, chapter 2.2.5.3.2). To verify, if the populations acted as a buffer, we tested a coculture consisting of the sender and receiver strain or an empty and the receiver strain. We expected that if the sender cell was present, the constitutively expressed α_{Sc}-factor was produced and secreted into the medium. This α_{Sc}-factor then stimulated the Ste2$_{Sc}$ in the receiver strain, which resulted in an activation of the mating pathway, subsequently inducing the P_{FUS1} promoter and thus mTurquoise2 expression. In case no sender strain was in the coculture, we anticipated no fluorescence output in the receiver strain, since α-factor could stimulate the mating receptor Ste2.

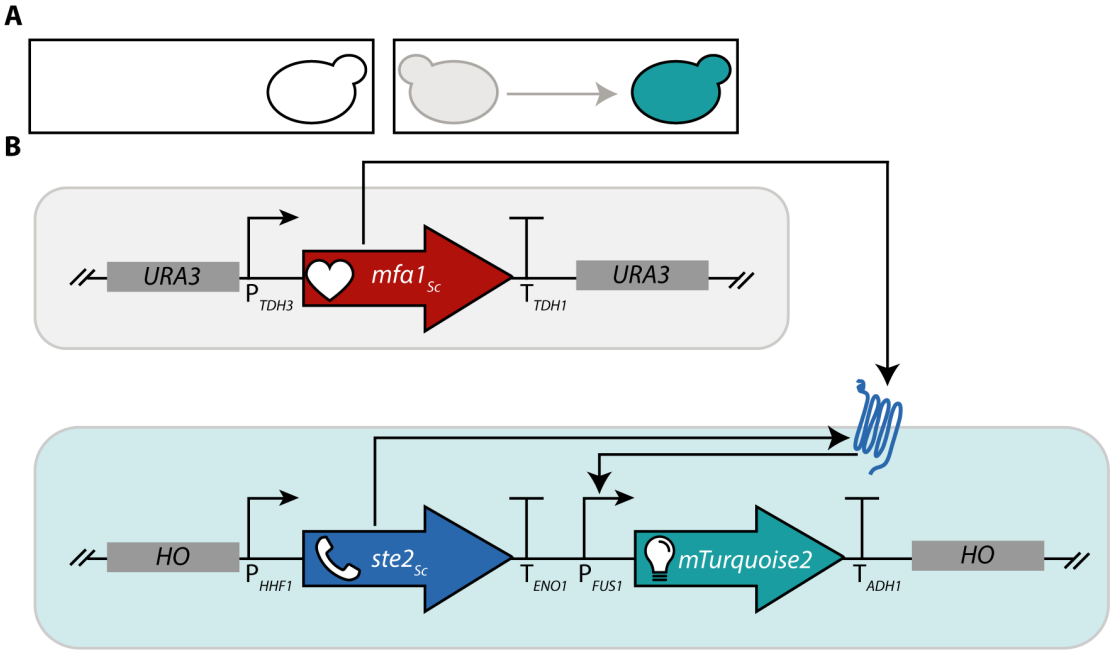

Figure 113: Network architecture and genetic constructs of the buffer-like population network. A) Network design for the Buffer-like population network. The sender population (grey) induces the receiver population (turquoise). If no sender cells are part of the community, the receiver cells do not express the output signal. **B)** Genetic constructs of the sender and receiver cells as well a circuit design. The construct of the sender strain (grey) consists of P_{TDH3}-*mfa1*$_{Sc}$-T_{TDH1} with *URA3* homology sequences. The construct was integrated into the *MAT***a** *far1Δ* stain background strain. The construct of the receiver strain (turquoise) consists of P_{HHF1}-*ste2*$_{Sc}$-T_{ENO1} (receiver device) and P_{FUS1}-*mTurquoise2*-T_{ADH1} (reporter device). Both devices were combined to the receiver system having *HO* homology sequences. The receiver system was integrated into the *MAT***a** *far1Δ* strain background.

We measured 50,000 single cell events of three biological replicates. By gating and data processing we selected the cells carrying the receiver system, for which the fluorescence intensities were plotted in Figure 114. In absence of the sender strain, we measured only basal mating pathway activity. One of the biological replicates exhibited slightly lower output intensities in comparison to the other two. This obervations was unexpected as we did not detect this phenomenon for the Ste2-α-factor crosstalk experiments that utilized similar design motives (Figure 98, chapter 2.2.5.3.2). When the sender cells were part of the coculture, all three biological sender replicates exhibited increased mating pathway activity, depicted by increased fluorescence intensities (Figure 114B). We computed a more than six-fold increase in fluorescence intensity (Figure 114C). Thus, we could conclude that the buffer like population network was exhibiting the behavior as intended. In case stronger/weaker outputs are required, the buffer-like population network could be improved by other parts from the YCTK, either different pheromone-inducible promoters for the output device or other sender and receiver parts originating from other species.

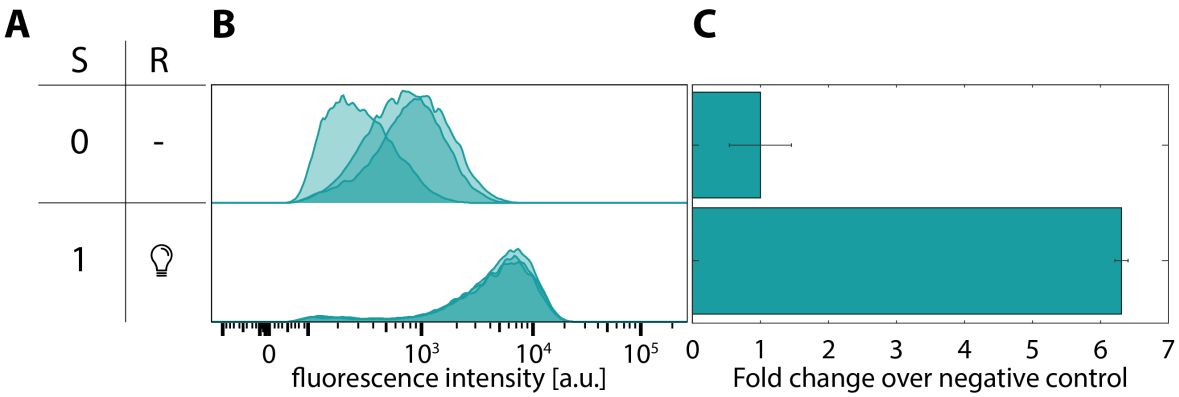

Figure 114: Results of the buffer-like population network. A) Truth table of the Boolean buffer gate. Zero (0) indicates in the left column that the sender population is not part of the coculture, resulting in the right column in no output in the receiver cells (-). One (1) in the left column indicates that the sender population is part of the coculture resulting in an output in the receiver cells (♡). **B)** Fluorescence histograms of the measured receiver cells for three biological replicates. The fluorescence output (♡) in the receiver cells indicates mating pathway activity. **C)** Fold change of the mean fluorescence intensity of mTurquoise2 of the receiver cells over the fluorescence intensity of the receiver cells when the sender population was not part of the coculture (negative control).

2.2.6.1.2 Inverter-like population network

Next, we tested an inverter-like population network. An inverter should reverse the buffer-like population behavior. This means, in case the sender cells are present, the signal should be repressed (Figure 115, Figure 116A).

For the inverter, sender cells contained a construct, consisting of the $Bar1_{Sc}$ protease under the control of the P_{TDH3} promoter and T_{ENO2} terminator, which was chromosomally integrated into the *URA3* locus and selected by *LEU2*. The receiver strain harbored three devices: 1. P_{REV1}-*mfα1*$_{Sc}$-T_{TDH1} 2. P_{RAD27}-*ste2*$_{Sc}$-T_{ENO1} and 3. P_{FUS1}-*mTurquoise2*-T_{ADH1}. All three devices were chromosomally integrated into the *HO* locus and selected with the *LEU2* marker (Figure 115B).

In this multicellular network, the receiver strain should express both $Ste2_{Sc}$ and α_{Sc}-factor, resulting in a positive feedback loop of the mating pathway activity, which should be monitored by the expression of mTurquoise2, the mating response output reporter. If the sender cells would be present, the $Bar1_{Sc}$ protease should act as a barrier by degrading α_{Sc} -factor, which would result in the deactivation of the mating pathway and thus in lower P_{FUS1} expression levels. For the coculture of the receiver with an empty control strain, we predicted to obtain self-induced mating pathway activity in the receiver strain.

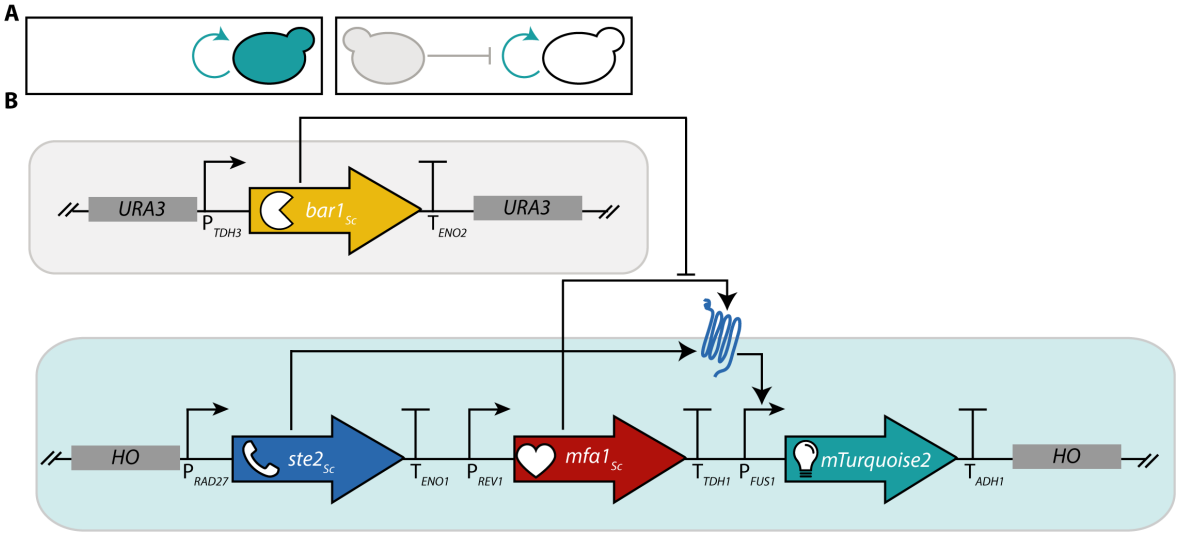

Figure 115: Network architecture and genetic constructs of the inverter-like population network. A) Network design for the inverter-like population network. The sender population (grey) represses the self-induced receiver population (turquoise). If no sender cells are part of the community, the receiver cells express the output signal dur to self-stimulation. **B)** Genetic constructs of the sender and receiver cells as well a circuit design. The construct of the sender strain (grey) consists of P_{TDH3}-*bar1*$_{Sc}$-T_{ENO2} with *URA3* homology sequences. The construct was integrated into the *MAT***a** *far1Δ* stain background strain. The construct of the receiver strain (turquoise) consists of P_{RAD27}-*ste2*$_{Sc}$-T_{ENO1} (receiver device), P_{REV1}- *mfa1*$_{Sc}$-T_{TDH1} (sender device) and P_{FUS1}-*mTurquoise2*-T_{ADH1} (reporter device). All three devices were combined to the receiver system having *HO* homology sequences. The receiver system was integrated into the *MAT***a** *far1Δ* strain background.

When we measured the network behavior, we cocultured the receiver strain either with or without the sender strain. The histograms of the receiver strain exhibited fluorescence cells in absence of the sender strain (Figure 116B). However, we could not report any difference in mating pathway activity of the receiver strain in the presence of the sender cells. For both coculture conditions, the results were alike. All biological replicates exhibited the same behavior, which in turn means that no visible fold change between the two conditions could be reported (Figure 116C). Our results indicated that the design of the multicellular system did not result in a functional system, since the predicted behavior could not be observed. It remained difficult to determine if the auto-stimulation was functional or not, since we measured low fluorescence intensities. Another possibility could have been that the barrier device of the sender system was not behaving as predicted. We previously proved the activity of the Bar1 protease in a coculture (Figure 104). The fundamental design difference between the coculture experiment and the inverter-like population network was that the α-factor was produced by a third strain. For the inverter-like population network, the α-factor was produced by the receiver strain itself. Thus, it is more likely that the auto-stimulation motif was the limiting factor. Further investigations and design optimizations are required to obtain the desired network dynamics.

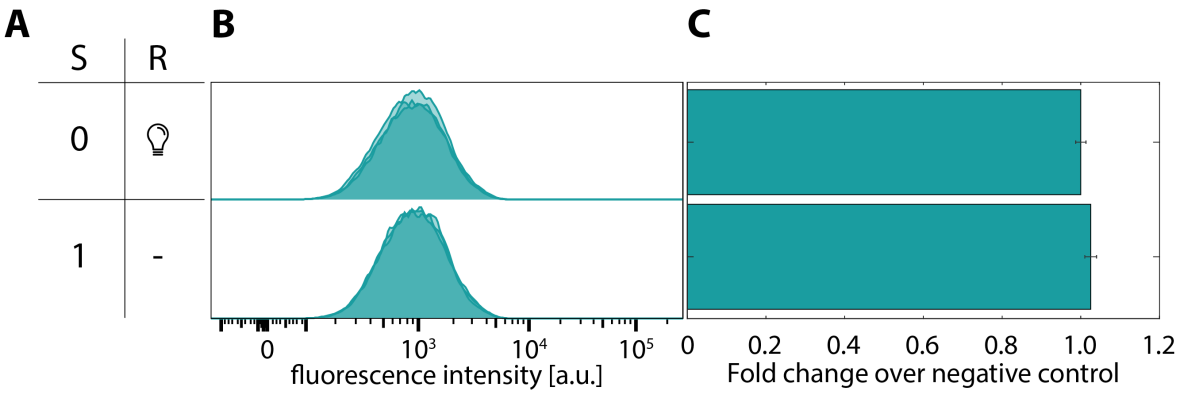

Figure 116: Results of the inverter-like population network. A) Truth table of the Boolean Buffer gate. Zero (0) indicates in the left column that the sender population is not part of the coculture, resulting in the right column in an output in the receiver cells (♀). One (1) in the left column indicates that the sender population is part of the coculture resulting in no output in the receiver cells (-). **B)** Fluorescence histograms of the measured receiver cells for three biological replicates. The fluorescence output (♀) in the receiver cells indicates mating pathway activity. **C)** Fold change of the mean fluorescence intensity of mTurquoise2 of the receiver cells over the fluorescence intensity of the receiver cells when the sender population was not part of the coculture (negative control).

2.2.6.1.3 OR-like population network

Here, we wanted to engineer a population network, that was acting as a Boolean logic OR gate (Figure 118A). To achieve this goal, we cocultured three strains together, two of them serving as sender strains and one as receiver strain. For a logic OR gate, in case either of the two or both sender strains were in coculture with the receiver population, we should obtain a fluorescence output in the receiver cells. Only in absence of both sender strains, the receiver cells should not express any reporter.

Each sender strain harbored a single device. The device of S1 contained P_{PGK1}- *mfα1*$_{Tp}$-T_{TDH1}. The second sender strain harbored a device consisting of P_{PGK1}- *mfα1*$_{Kn}$-T_{TDH1}. Both devices acted as systems and were integrated into the *URA3* locus and selected with *LEU2* (Figure 117B).

The receiver strain of the OR-like population network was comprised of two devices: 1. P_{RPL18B}-*ste2*$_{Sc}$-T_{ENO1} (receiver device) and 2. P_{FUS1}-*mTurquoise2*-T_{ADH1} (output device). Together, both devices formed the receiver system that was integrated into the *HO* locus and selected for by the *LEU2* marker (Figure 117B).

When no sender strain would be part of the coculture, no α-factor should be present and thus the Ste2$_{Sc}$ in the receiver strain should not be stimulated and therefore no mating pathway activity would be observable, indicated by no fluorescence intensities of the reporter mTurquoise2. In case the S1 population would be part of the coculture, α$_{Tp}$-factor would be produced, resulting in the stimulation of Ste2$_{Sc}$ in the receiver strain, subsequently inducing the expression of mTurquoise2. The same dynamics should be observable when only the population S2 is in the coculture, which produces the α$_{Kn}$-factor. Due to the α-factor promiscuity of the Ste2$_{Sc}$ receptor, the receiver cells could recognize both α-factors. This means, presence of either of the sender strains in the coculture should be sufficient to obtain a receiver output but also a coculture consisting of all three strains should result in a fluorescence output in the receiver cells (Figure 117).

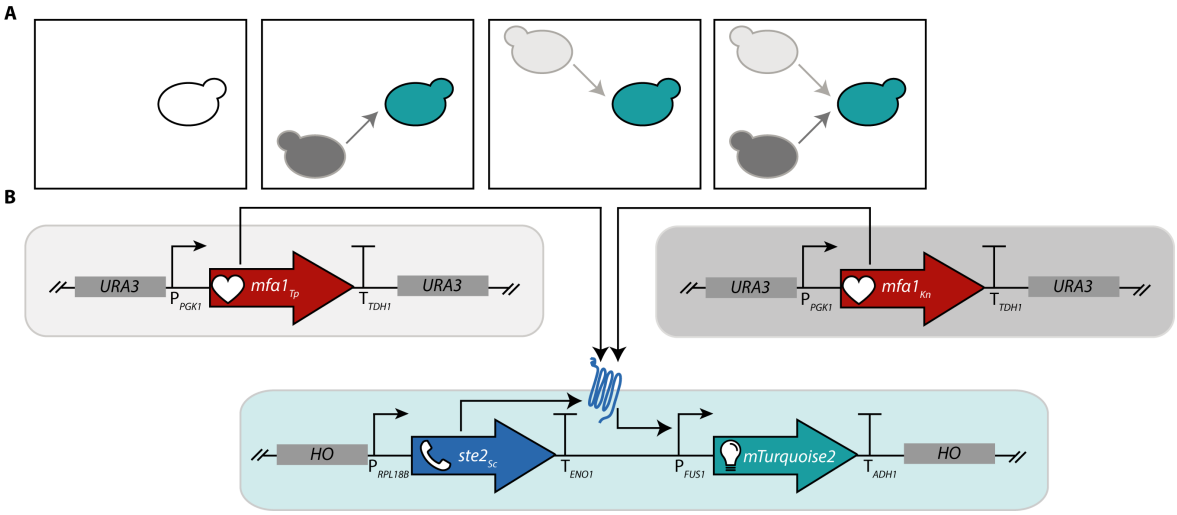

Figure 117: Network architecture and genetic constructs of the OR-like population network. A) Network design for the OR gate-like population network. Either the sender population 1 (light grey) or the sender population 2 (dark grey) or both together induce the receiver population (turquoise). If none of the sender populations are part of the community, the receiver cells do not express the output signal. **B)** Genetic constructs of the sender 1, sender 2 and receiver cells, as well a circuit design. The construct of the sender 1 strain (light grey) consists of P_{PGK1}- *mfa1*$_{Tp}$-T_{TDH1} with *URA3* homology sequences. The construct was integrated into the *MAT***a** *far1Δ* stain background strain. The construct of the sender 2 strain (dark grey) consists of P_{PGK1}- *mfa1*$_{Kn}$-T_{TDH1} with *URA3* homology sequences. The construct was integrated into the *MAT***a** *Δ far1* stain background strain. The construct of the receiver strain (turquoise) consists of P_{RPL18B}-*ste2*$_{Sc}$-T_{ENO1} (receiver device) and P_{FUS1}-*mTurquoise2*-T_{ADH1} (reporter device). Both devices were combined to the receiver system having *HO* homology sequences. The receiver system was integrated into the *MAT***a** *far1Δ* strain background.

The fluorescence histograms of the receiver strain for the different coculture conditions confirmed that in absence of both sender strains, the mating pathway only exhibited basal activity, indicated by low fluorescence intensities (Figure 118B). If either the S1 or the S2 population were present, we measured mating pathway activity as reporter gene expression. Also, when both sender strains were cocultured with the receiver population, an output in the receiver cells could be observed, which was very similar to the other two conditions, for which either of the sender strains was present. However, when we calculate the fold change over the negative control, we computed a stronger fold change, up to 14-fold, for the receiver strain that was cocultured with both sender strains (Figure 118C). This indicated that in presence of only one sensor population, the mating pathway in the receiver strain was not fully stimulated. Based on our titration experiments, a network improvement could be achieved by utilization of a weaker promoter for the expression of Ste2$_{Sc}$, thus lower α-factor concentrations would be sufficient to obtain a fully saturate mating response. Overall, the OR-like population network is functional and exhibited that crosstalk between the different sender and receiver parts can be also used as a design feature.

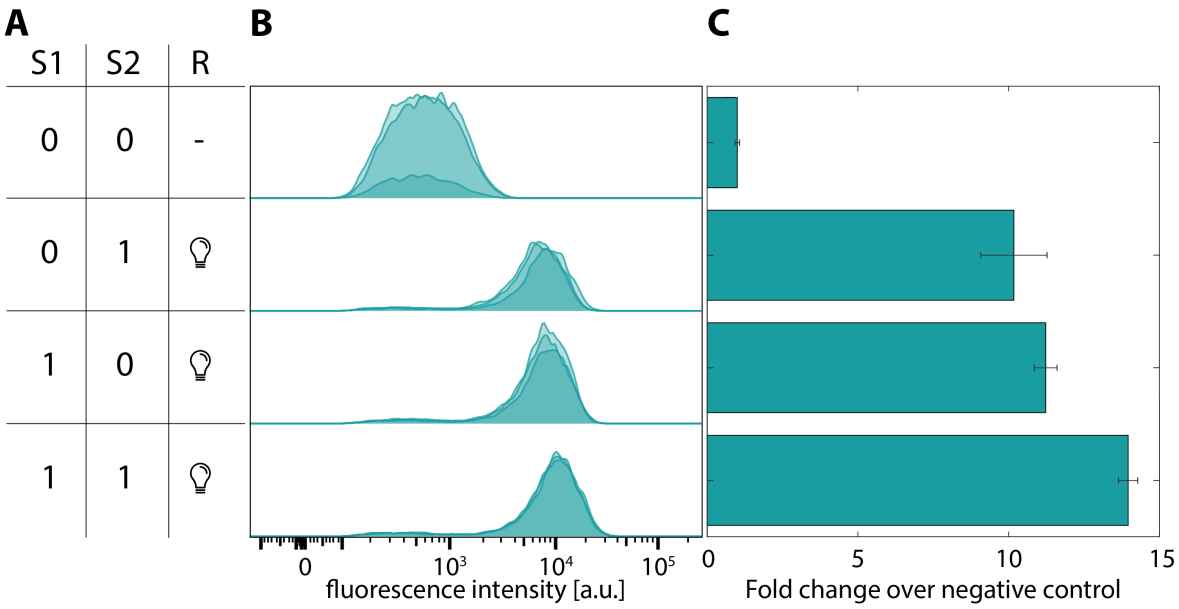

Figure 118: Results of the OR-like population network. A) Truth table of the Boolean OR gate. Zero (0) indicates in the S1 and S2 column that the sender population 1 or 2 is not part of the coculture, resulting, depending on the coculture composition, in the right column in an/no output in the receiver cells (♡/-). One (1) in the S1 and S2 column indicates that the sender population 1 or 2 is part of the coculture, resulting in an output in the receiver cells (♡). **B)** Fluorescence histograms of the measured receiver cells for three biological replicates. The fluorescence output (♡) in the receiver cells indicates mating pathway activity. **C)** Fold change of the mean fluorescence intensity of mTurquoise2 of the receiver cells over the fluorescence intensity of the receiver cells when the sender populations were not part of the coculture (negative control).

2.2.6.1.4 NOR-like population network

With this multicellular system, we wanted to establish a network exhibiting Boolean NOR gate-like behavior on a population level using the population composition as input. Therefore, we engineered two sender and one receiver strain to be cocultured under different conditions. Only in absence of both sender strains, we expected to observe an output signal in the receiver strain (Figure 119, Figure 120).

The S1 sender population carried one device, which consisted of P_{TDH3}-*bar*$_{Sc}$-T_{ENO2}, and the S2 sender harbored the P_{TDH3}-*bar*$_{Kl}$-T_{ENO2} device. Each of these two devices was integrated into the *URA3* locus and selected with the *LEU2* marker. The receiver strain comprised three devices: 1. P_{RPL18B}- *mfa1*$_{Kl}$-T_{TDH1} (sender device) 2. P_{POP6}-*ste2*$_{Kl}$-T_{ENO1} (receptor device) 3. P_{FUS1}-*mTurquoise2*-T_{ADH1} (output device). All three devices were combined into the receiver system and chromosomally integrated into the *HO* locus and selected using the *LEU2* marker (Figure 119B).

In case the receiver population was grown without any of the sender populations, the receiver strain should exhibit a positive feedback loop by producing the α_{Kl}-factor and therefore stimulating the Ste2$_{Kl}$ receptor. This stimulus in turn would induce the mating pathway, which should result in the expression of the reporter gene (Figure 119). If one or both of the sender populations would be part of the coculture with the receiver population, the expressed Bar1 proteases would be blocking the signaling feedback loop by α-factor degradation and thereby preventing the receiver output signal (Figure 119).

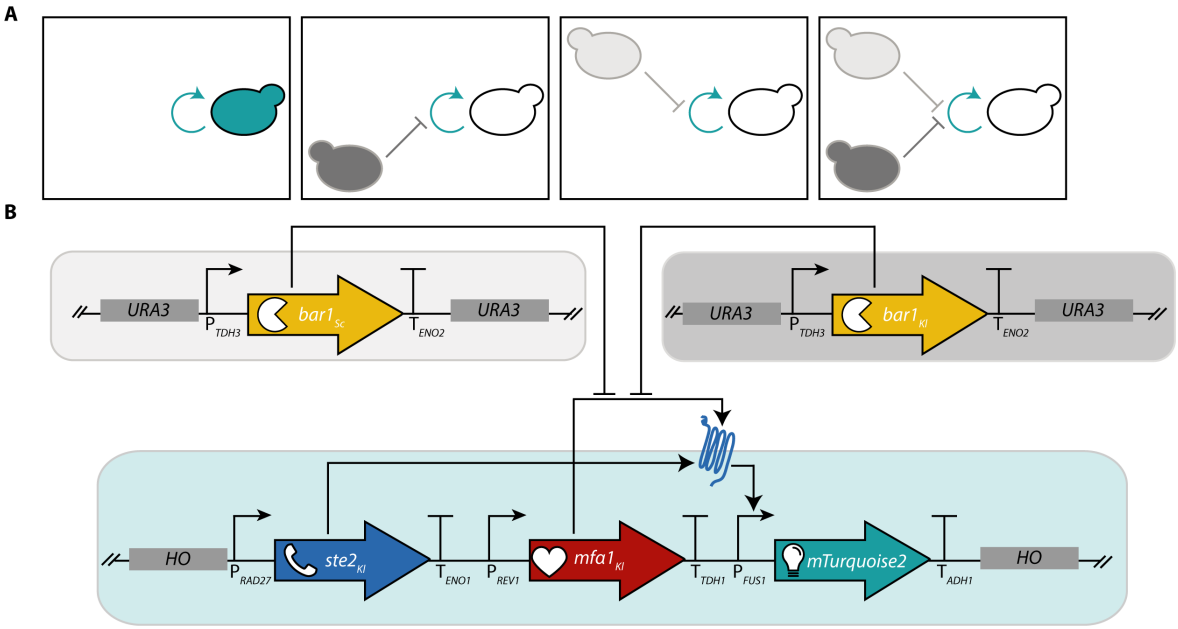

Figure 119: Network architecture and genetic constructs of the NOR-like population network. A) Network design for the NOR gate-like population network. Both the sender population 1 (light grey) and the sender population 2 (dark grey) repress the self-induced receiver population (turquoise). If none of the sender populations is part of the community, the receiver cells express the output signal. **B)** Genetic constructs of the sender1, sender 2 and receiver cells as well a circuit design. The construct of the sender 1 strain (light grey) consists of P_{TDH3}-*bar1*$_{Sc}$-T_{ENO2} with *URA3* homology sequences. The construct was integrated into the *MAT***a** *far1Δ* stain background strain. The construct of the sender 2 strain (dark grey) consists of P_{TDH3}-*bar1*$_{KI}$-T_{ENO2} with *URA3* homology sequences. The construct was integrated into the *MAT***a** *Δ far1* stain background strain. The construct of the receiver strain (turquoise) consists of P_{RAD27}-*ste2*$_{KI}$-T_{ENO1} (receiver device), P_{REV1}- *mfa1*$_{KI}$-T_{TDH1} (sender device) and P_{FUS1}-*mTurquoise2*-T_{ADH1} (reporter device). All three devices were combined to the receiver system having *HO* homology sequences. The receiver system was integrated into the *MAT***a** *far1Δ* strain background.

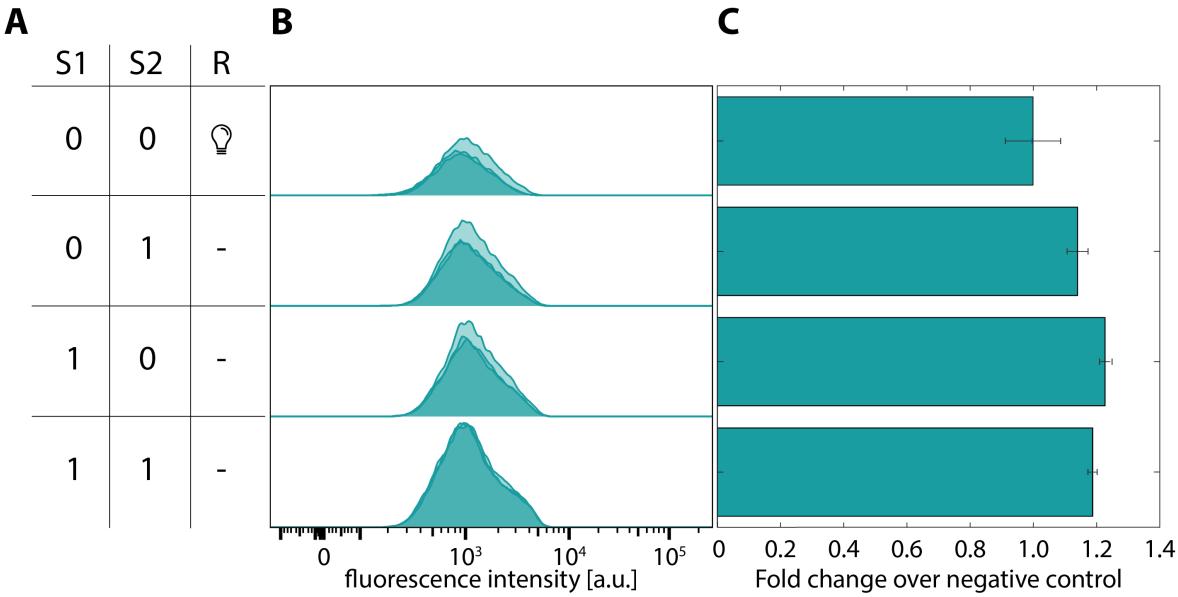

Figure 120: Results of the NOR-like population network. A) Truth table of the Boolean NOR gate. Zero (0) indicates in the S1 and S2 column that the sender population 1 or 2 is not part of the coculture, resulting, depending on the coculture composition, in the right column in an/no output in the receiver cells (💡/-). One (1) in the S1 and S2 column indicates that the sender population 1 or 2 is part of the coculture resulting in no output in the receiver cells (-). **B)**

Fluorescence histograms of the measured receiver cells for three biological replicates. The fluorescence output (♡) in the receiver cells indicates mating pathway activity. **C)** Fold change of the mean fluorescence intensity of mTurquoise2 of the receiver cells over the fluorescence intensity of the receiver cells when the sender populations were not part of the coculture (negative control).

However, when we cocultured the strains in different combinations together, the fluorescence histograms of the receiver cells revealed that there was no considerable difference for the different conditions (Figure 120). Similar to the inverter-like population network, we could not differentiate if the auto-stimulation of the receiver system was not functional or if the Bar1 proteases were not able to degrade the α-factors efficiently. Control experiments would be required to conclude which device should be improved.

2.2.6.1.5 AND-like population network

For the establishment of an AND-like population network, we had the premise that only in case two sender populations were part of the coculture, the receiver strain would exhibit an output signal (Figure 121A, Figure 122A). The coculture exhibiting AND-like logic gate behavior was comprised of three strains, two sender and one receiver population. The first sender strain (S1) was comprise of three devices: 1. P_{PGK1}- *mfa1*$_{Lf}$-T_{TDH1} (transmitter device) 2. P_{PAB1}-*ste2*$_{Ca}$-T_{ENO1} (receiver device) 3. P_{FUS1}- *mfa1*$_{Lm}$-T_{ENO2} (sender device) (Figure 121B). All three devices were combined to a system that was integrated into the *HO* locus and selected by *LEU2* marker. The second sender population network (S2) also contained three devices: 1. P_{PGK1}- *mfa1*$_{Ca}$-T_{TDH1} (transmitter device) 2. P_{PAB1}-*ste2*$_{Lf}$-T_{ENO1} (receiver device) 3. P_{FUS1}- *mfa1*$_{Lm}$-T_{ENO2} (sender device). The resulting system was also chromosomally integrated into the *HO* locus and selected with the *LEU2* marker. The receiver system (R) had only two devices: 1. P_{PAB1}-*ste2*$_{Lm}$-T_{ENO1} (receiver device) and 2. P_{FUS1}- *venus*-T_{ADH1} (output device). Also, these two devices were combined to the receiver system that was integrated into the *HO* locus and selected with the *LEU2* marker.

As shown in the network diagram in Figure 121, population S1 should be producing and transmitting the α_{Lf}-factor signal that could be recognized by the Ste2$_{Lf}$-expressing population S2. Upon on binding of α_{Lf}-factor to Ste2$_{Lf}$ in S2 cells, the expression of α_{Lm}-factor would be induced. S2 should be additionally producing α_{Ca}-factor, which in turn would stimulate the Ste2$_{Ca}$ receptor in population S1, upon which also in this population α_{Lm}-factor is produced. This cross-signaling using α_{Ca}-factor was not an essential design feature but thought to enhance the signal amplification. The α_{Lm}-factor, which would eventually be produced by both sender populations subsequently would induce the expression of the output reporter Venus in the receiver strain. Since both sender populations are required to induce the expression of α_{Lm}-factor, this network architecture acts as a AND-like logic gate (Figure 121). Additionally, in order to obtain a functional AND gate-like population network, it would haven been sufficient that only one sender strain produces the α_{Lm}-factor. However, for increased output signal, both sender populations produced the α_{Lm}-factor.

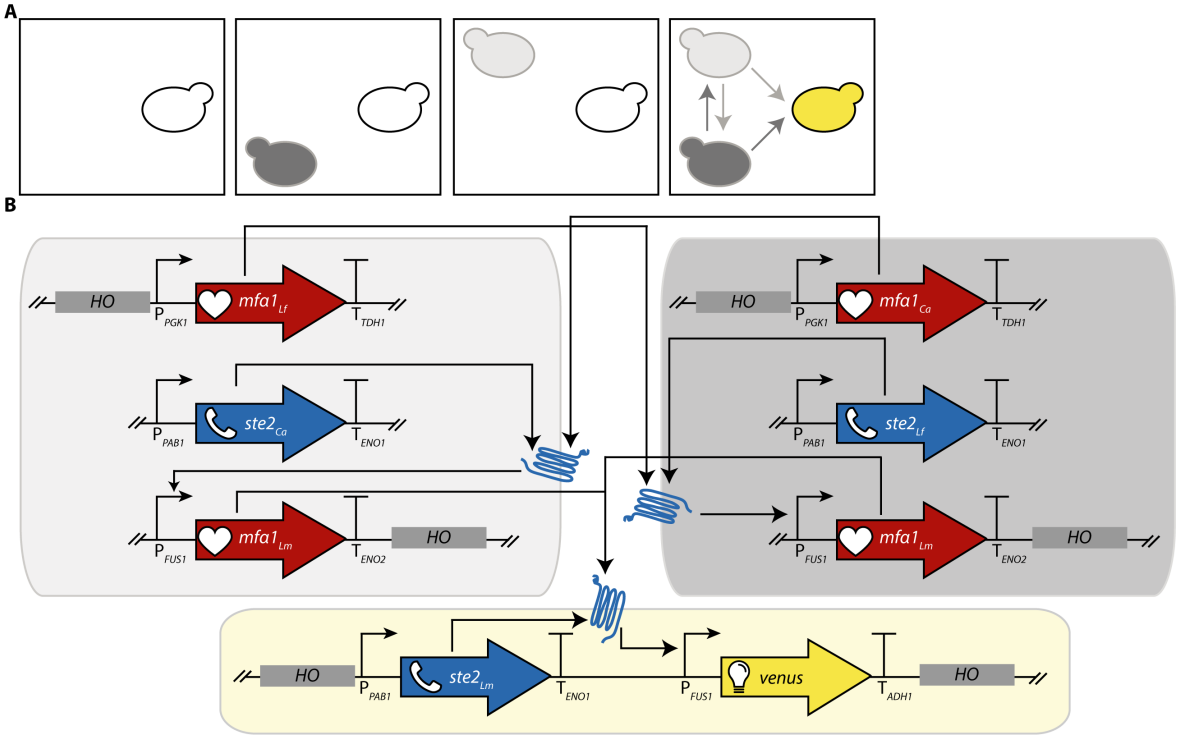

Figure 121: Network architecture and genetic constructs of the AND-like population network. A) Network design for the AND gate-like population network. Sender population 1 (light grey) and sender population 2 (dark grey) induce each other which is required in order to induce the receiver population (yellow), so if none or either of the sender populations is part of the community, the receiver population does not express an output signal. **B)** Genetic constructs of the sender1, sender 2 and receiver cells as well a circuit design. The constructs of the sender 1 strain (light grey) consists of P_{PGK1}-*mfa1*$_{Lf}$-T_{TDH1} (sender device), P_{PAB1}-*ste2*$_{Ca}$-T_{ENO1} (receiver device) and P_{FUS1}-*mfa1*$_{Lm}$-T_{ENO2} (2. sender device), which were combined into a system with *HO* homology sequences. The system was integrated into the *MAT***a** *far1Δ* stain background strain. The constructs of the sender 2 strain (dark grey) consists of P_{PGK1}-*mfa1*$_{Ca}$-T_{TDH1} (sender device), P_{PAB1}-*ste2*$_{Lf}$-T_{ENO1} (receiver device) and P_{FUS1}-*mfa1*$_{Lm}$-T_{ENO2} (2. sender device), which were combined into a system with *HO* homology sequences. The system was integrated into the *MAT***a** *far1Δ* stain background strain. The construct of the receiver strain (yellow) consists of P_{PAB1}-*ste2*$_{Lm}$-T_{ENO1} (receiver device) and P_{FUS1}-*venus*-T_{ADH1} (reporter device). Both devices were combined to the receiver system having *HO* homology sequences. The receiver system was integrated into the *MAT***a** *far1Δ* strain background.

The fluorescence histograms of three biological replicates indicated that the mating pathway was not activated in the absence of both sender strains in a coculture with the receiver population (Figure 122B). However, when one of the sender systems was part of the coculture, we measured a more than three-fold increase in fluorescence intensity, which indicated an activation of the mating pathway (Figure 122C). In a coculture with both sender populations, we observed a nearly eight-fold change of the reporter output fluorescence. Overall, we could report that the AND-like gate population network was exhibiting the features we intended. In order to obtain a more digital behavior, lower mating pathway activity, when only one sender strain was present, further optimization is required. Improvements could for example be achieved by reducing the production strength of the α-factors in the sender strains or by expressing the Ste2 receptor in the receiver strain from an mating-responsive promoter. This complex network architecture exhibited proof of principle for the generation of multicellular signaling networks that can be constructed using the YCTK.

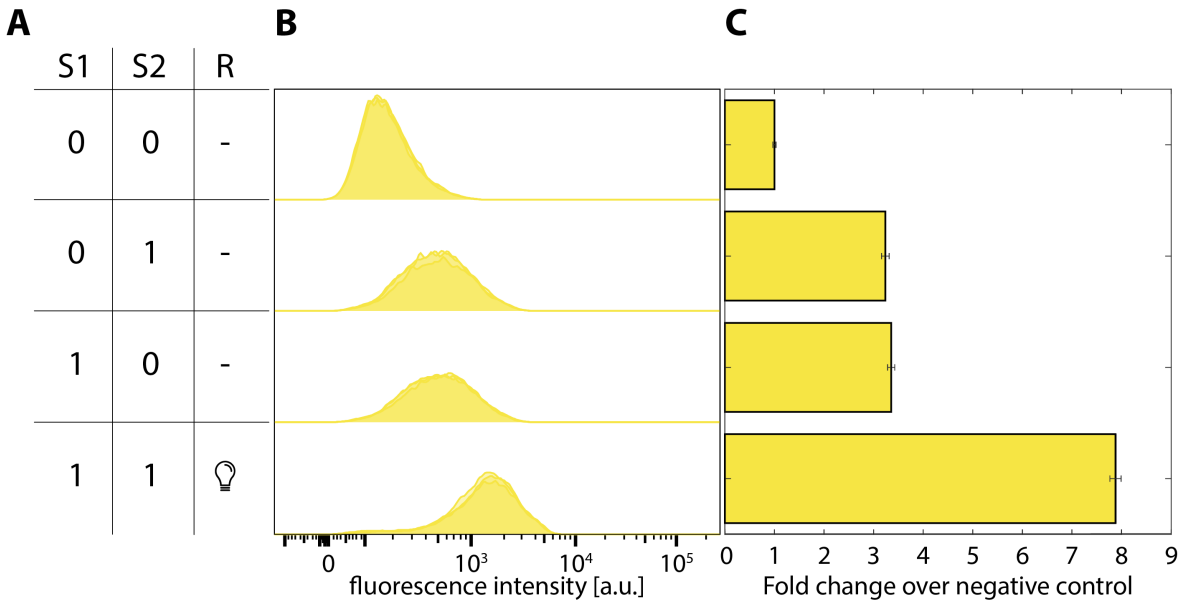

Figure 122: Results of the AND-like population network. A) Truth table of the Boolean AND gate. Zero (0) indicates in the S1 and S2 column that the sender population 1 or 2 is not part of the coculture, resulting, depending on the coculture composition, in the right column in no output in the receiver cells (-). One (1) in the S1 and S2 column indicates that the sender population 1 or 2 is part of the coculture resulting in an/no output in the receiver cells (♀/-). **B)** Fluorescence histograms of the measured receiver cells for three biological replicates. The fluorescence output (♀) in the receiver cells indicates mating pathway activity. **C)** Fold change of the mean fluorescence intensity of Venus of the receiver cells over the fluorescence intensity of the receiver cells when the sender populations were not part of the coculture (negative control).

2.2.6.1.6 NAND-like population network

With this multicellular network, we aimed to engineer a population network exhibiting the features of a NAND Boolean logic gate. Therefore, we engineered two sender and one receiver strain to be cocultured and perform NAND-like population dynamics. The receiver cells should always transmit an output signal for the different coculture strain combinations, only when both sender strains would be present, not output should be observable (Figure 124A, Figure 123).

The S1 population genetic system consisted of three devices: 1. P_{PGK1}-*mfa1*$_{Lt}$-T_{TDH1} (sender device) and 2. P_{PAB1}-*ste2*$_{Ca}$-T_{ENO1} (receptor device) and 3. P_{FUS1}-*bar*$_{Kl}$-T_{ENO2} (barrier device). All three devices were combined and formed the first sender system that was integrated into the *HO* locus and selected with the *LEU2* marker. The S2 population genetic system was similar to the S1 design and was also composed of three devices: 1. P_{PGK1}-*mfa1*$_{Ca}$-T_{TDH1} (sender device) and 2. P_{PAB1}-*ste2*$_{Lt}$-T_{ENO1} (receptor device) and 3. P_{FUS1}-*bar*$_{Kl}$-T_{ENO2} (barrier device). As for S1, the three devices were jointly integrated into the chromosome into the *HO* locus and selected by *LEU2*. Also, the receiver system consisted of three devices. Like for the inverter and the NOR network, the NAND-like receiver system harbored a self-induction feedback loop: 1. P_{PSP2}-*mfa1*$_{Kl}$-T_{ENO2} (sender device) and 2. P_{PAD1}-*ste2*$_{Kl}$-T_{ENO1} (receptor device) and 3. P_{FUS1}-*mTurquoise2*-T_{ADH1} (output device). The three devices were combined and then integrated into the *HO* locus and selected using the *LEU2* marker (Figure 123).

By expressing the α_{Kl}-factor, as well as the $Ste2_{Kl}$, the receiver strain should generate a positive auto-stimulation and thus activate the yeast mating pathway, which would result in the expression of the output reporter gene. When either the S1 or the S2 population would be cocultivated with the receiver population, solely α-factor would be produced, which should not affect the receiver population. Only when both sender strains would be in coculture with the receiver cells, the S1 population would induce the expression of the Bar1 protease in population S2 and vice versa. This barrier part expression would subsequently lead to the degradation of the α_{Kl}-factor produced by the receiver cells and thereby disrupting the feedback loop resulting in the deactivation of the mating pathway and thus no fluorescence output.

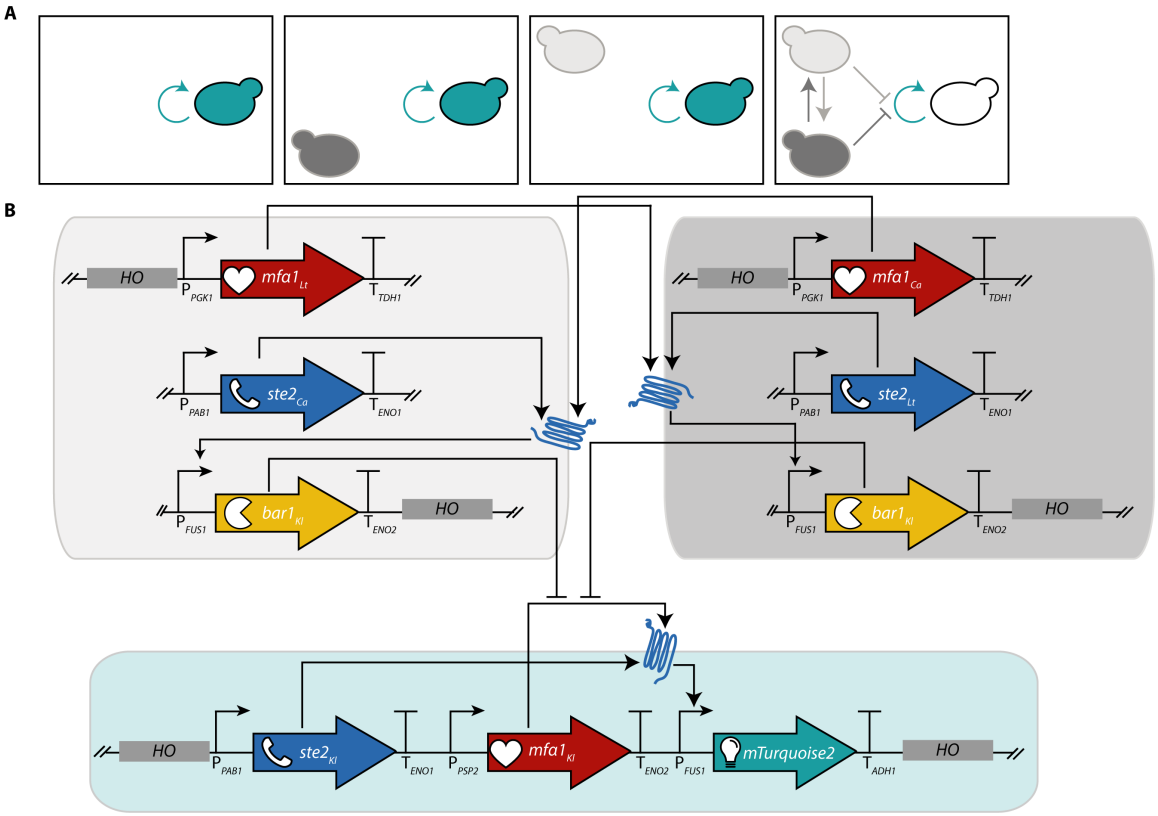

Figure 123: Network architecture and genetic constructs of the NAND-like population network. A) Network design for the NAND gate-like population network. Sender population 1 (light grey) and sender population 2 (dark grey) induce each other which is required in order to repress the self-induced receiver population (turquoise). Thus, the receiver always expresses an output signal, only when both sender populations are part of the coculture, no output signal is expressed. **B)** Genetic constructs of the sender1, sender 2 and receiver cells as well a circuit design. The constructs of the sender 1 strain (light grey) consists of P_{PGK1}-*mfa1*$_{Lt}$-T_{TDH1} (sender device), P_{PAB1}-*ste2*$_{Ca}$-T_{ENO1} (receiver device) and P_{FUS1}-*bar1*$_{Kl}$-T_{ENO2} (barrier device), which were combined into a system with *HO* homology sequences. The system was integrated into the *MAT***a** *far1Δ* stain background strain. The constructs of the sender 2 strain (dark grey) consists of P_{PGK1}-*mfa1*$_{Ca}$-T_{TDH1} (sender device), P_{PAB1}-*ste2*$_{Lt}$-T_{ENO1} (receiver device) and P_{FUS1}-*bar1*$_{Kl}$-T_{ENO2} (barrier device), which were combined into a system with *HO* homology sequences. The system was integrated into the *MAT***a** *far1Δ* stain background strain. The construct of the receiver strain (turquoise) consists of P_{PAB1}-*ste2*$_{Kl}$-T_{ENO1} (receiver device), P_{PSP2}-*mfa1*$_{Kl}$-T_{TDH1} (sender device) and P_{FUS1}-*mTurquoise2*-T_{ADH1} (reporter device). All three devices were combined to the receiver system having *HO* homology sequences. The receiver system was integrated into the *MAT***a** *far1Δ* strain background.

When we cocultured the three strains in different combinations though, the receiver cell fluorescence histograms revealed that we were not able to establish a population network exhibiting

NAND-like gate outputs (Figure 124B). For all different conditions, we measured mating pathway activity. No considerable fold change over the empty control could be reported (Figure 124C). We thus had to conclude that the NAND multicellular network was not functional and that most likely the positive feedback loop of the receiver strain was not sufficiently disrupted by the degradation of α_{KI}-factor by $Bar1_{KI}$. Additional experiments would be required to identify targets to improve the network architecture. One aspect that has to be further investigated is, if the local concentration maximum of the secreted α-factor might already have resulted in direct maximal stimulation of the $Ste2_{KI}$ receptor. Due to this local concentration maximum, the proteases most likely could not reduce the α-factor concentration sufficiently and therefore no reduction of the $Ste2_{KI}$ receptor stimulation and mating pathway response output.

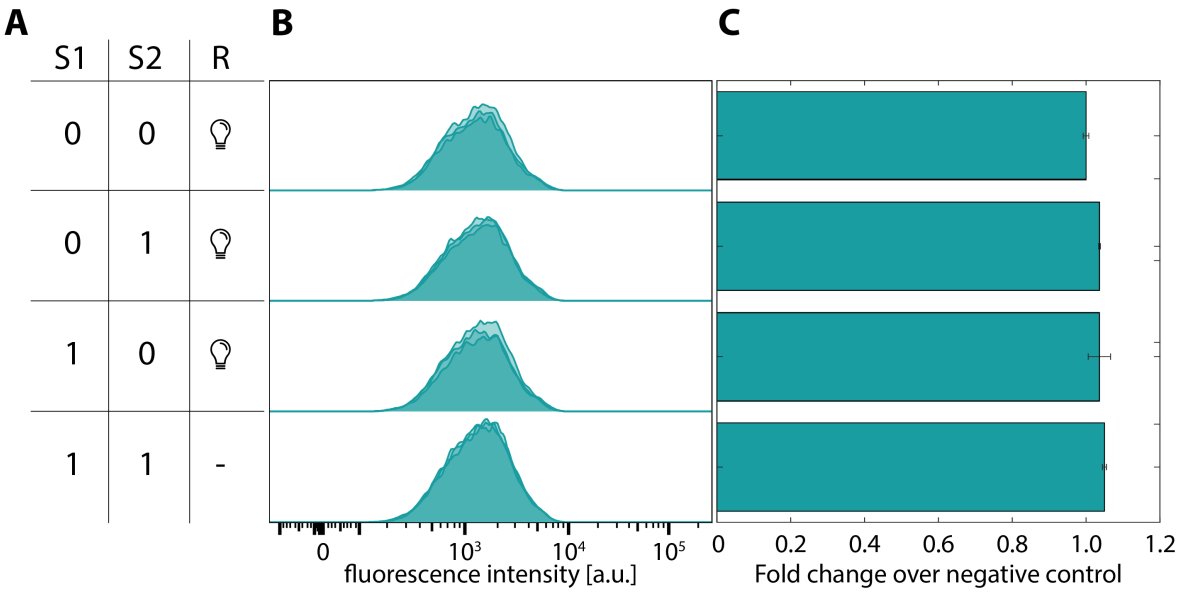

Figure 124: Results of the NAND-like population network. A) Truth table of the Boolean NADN gate. Zero (0) indicates in the S1 and S2 column that the sender population 1 or 2 is not part of the coculture, resulting depending on the coculture composition in the right column in an/no output in the receiver cells (♡/-). One (1) in the S1 and S2 column indicates that the sender population 1 or 2 is part of the coculture resulting in an/no output in the receiver cells (♡/-). **B)** Fluorescence histograms of the measured receiver cells for three biological replicates. The fluorescence output (♡) in the receiver cells indicates mating pathway activity. **C)** Fold change of the mean fluorescence intensity of mTurquoise2 of the receiver cells over the fluorescence intensity of the receiver cells when the sender populations were not part of the coculture (negative control).

2.2.6.1.7 XOR-like population network

A commonly utilized Boolean logic gate is the XOR gate. Thus, we also aimed to engineer a multicellular population network exhibiting XOR-like population dynamics. According to the specifications of a XOR gate, the receiver population should only exhibit an output when either of the sender populations is present. If none or both sender strains are part of the coculture, no output signal should be observable (Figure 125, Figure 126A). Based on these requirements, we designed two sender and one receiver system.

The sender system of the S1 sender population consisted of two devices: 1. P_{RAD27}- $mfa1_{Ec}$-T_{TDH1} (sender device) and 2. P_{TDH1}-bar_{Sc}-T_{ENO1} (barrier device) (Figure 125). Both deceives were combined and integrated into the *HO* locus. *LEU2* was used as the selection marker.

The second sender system was similar to the first one, only the sender device was harboring the *mfa1*$_{Sc}$ gene and the barrier gene *bar*$_{Ec}$. Also, the receiver system was composed of two devices: 1. P$_{RPL18B}$-*ste2*$_{Ec}$-T$_{ENO1}$ (receptor device) and 2. P$_{FUS1}$-*mTurquoise2*-T$_{ADH1}$ (output device). Combined to the receiver system, they were integrated into the *HO* locus and selected with the *LEU2* marker (Figure 125B).

If only one of the sender strains would be cocultured with the receiver population, either α$_{Ec}$-factor or α$_{Sc}$-factor should be expressed and the Ste2$_{Ec}$ in the receiver strain would get stimulated, due to its promiscuity it can recognize both α$_{Ec}$-factor and α$_{Sc}$-factor, which would result in the expression of the reporter, as an indicator of mating pathway activity. Each sender strain would also produce a Bar1 protease, but since Bar1$_{Sc}$ does not recognize α$_{Ec}$-factor and Bar1$_{Ec}$ does not recognize α$_{Sc}$-factor, in case where only one sender strain would be part of the coculture, no α-factor degradation should be observable. If both sender systems would be cocultured with the receiver strain, the expressed proteases should cleave the cognate α-factors, produced in the respective other sender population, which would result in the degradation of the sender pheromones. The receiver cell would thus not be stimulated and therefore, the reporter gene should not be expressed. In case neither of the sender populations would be part of the coculture, no α-factor should be present in the media and no signal in the receiver cells could be generated (Figure 125).

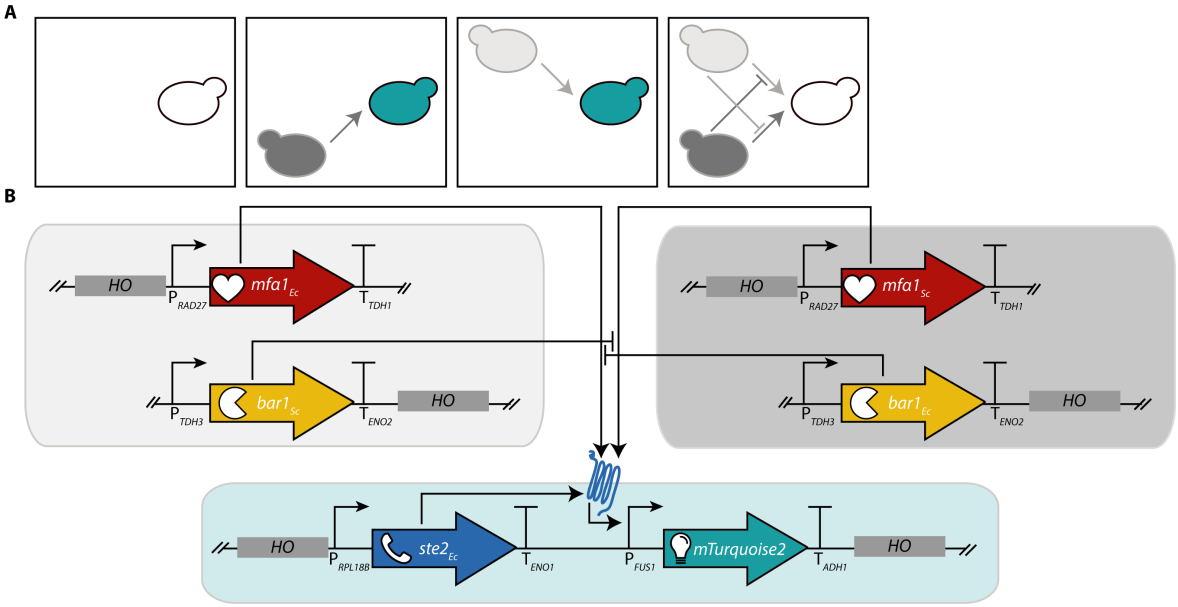

Figure 125: Network architecture and genetic constructs of the XOR-like population network. A) Network design for the XOR gate-like population network. Sender population 1 (light grey) and sender population 2 (dark grey) repress the inducer of the respective other population. Therefore, the receiver population only expresses an output signal (turquoise), when either of the two sender populations is part of the coculture. **B)** Genetic constructs of the sender1, sender 2 and receiver cells as well a circuit design. The constructs of the sender 1 strain (light grey) consists of P$_{RAD27}$- *mfa1*$_{Ec}$-T$_{TDH1}$ (sender device) and P$_{TDH3}$-*bar1*$_{Sc}$-T$_{ENO2}$ (barrier device) which were combined into a system with *HO* homology sequences. The system was integrated into the *MAT***a** *far1Δ* stain background strain. The constructs of the sender 2 strain (dark grey) consists of P$_{RAD27}$- *mfa1*$_{TDH1}$ (sender device) and P$_{TDH3}$-*bar1*$_{Ec}$-T$_{ENO2}$ (barrier device) which were combined into a system with *HO* homology sequences. The system was integrated into the *MAT***a** *far1Δ* stain background strain. The construct of the receiver strain (turquoise) consists of P$_{RPL18B}$-*ste2*$_{Ec}$-T$_{ENO1}$ (receiver device) and P$_{FUS1}$-*mTurquoise2*-T$_{ADH1}$

(reporter device). Both devices were combined to the receiver system having *HO* homology sequences. The receiver system was integrated into the *MAT***a** *far1Δ* strain background.

To verify the predicted population network behavior, we cocultured the strains in different combinations with each other. When none of the sender systems was in the coculture, we did not measure mating pathway activity (Figure 126B). When the second sender strain was present, we saw a weak activation of the mating pathway, as we predicted, resulting in a two-fold induction in comparison to the empty control (Figure 126C). This low output signal intensity might be due to the weak promoter that was used to express the α_{Sc}-factor. When however only the S1 population and the receiver strain we cocultured, we did not observe any mating pathway activity, indicating that the design of the S1 system needs to be improved. For a coculture of all three strains, S1, S2 and R, we could not detect any mating pathway activity, as predicted. When the barrier device of the S1 strain would function as predicted, we would expect a stimulation of the receiver system resulting in mating pathway activity, therefore it was most likely, that the sender device required optimization. First, increased production of the α-facotrs would be tested, to enhance the output signal in the receiver strain. Overall, we obtained a partially functional multicellular system exhibiting XOR gate-like dynamics, that required further optimization, for example, a stronger expression of the sender parts. Nevertheless, the results were promising and highlighted the successful utilization of Bar1 proteases in multicellular networks.

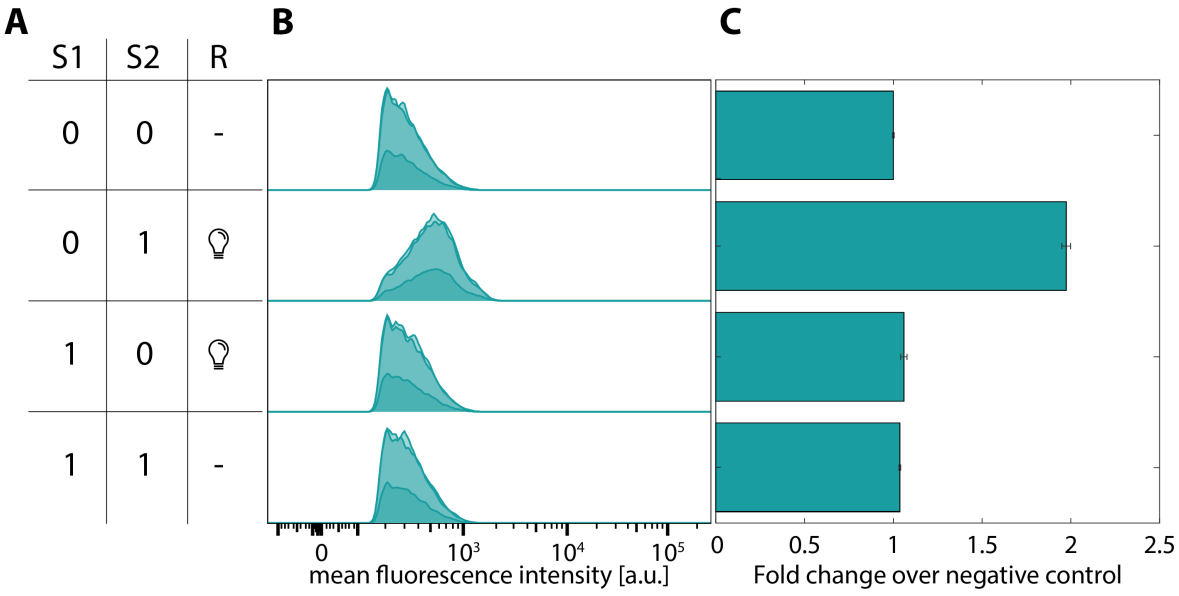

Figure 126: Results of the XOR-like population network. A) Truth table of the Boolean XOR gate. Zero (0) indicates in the S1 and S2 column that the sender population 1 or 2 is not part of the coculture, resulting, depending on the coculture composition, in the right column in an/no output in the receiver cells (♡/-). One (1) in the S1 and S2 column indicates that the sender population 1 or 2 is part of the coculture resulting in an/no output in the receiver cells (♡/-). **B)** Fluorescence histograms of the measured receiver cells for three biological replicates. The fluorescence output (♡) in the receiver cells indicates mating pathway activity. **C)** Fold change of the mean fluorescence intensity of mTurquoise2 of the receiver cells over the fluorescence intensity of the receiver cells when the sender populations were not part of the coculture (negative control).

2.2.6.1.8 XNOR-like population network

The design of the multicellular system below aimed to exhibit dynamics like the XNOR Boolean logic gate on a population level. According to the XNOR logics, an output should be observed when either none or both sender strains are cocultured with a receiver strain. If either of the two sender populations is cocultured with the receiver, no output should be observable (Figure 128A, Figure 127).

The first sender strain S1 consisted of four devices: 1. P_{PSP2}- *mfa1*$_{Lm}$-T_{ENO1} (sender device) and 2. P_{CCW12}-*ste2*$_{Lm}$-T_{SSA1} (receptor device) 3. P_{FUS1}-*bar*$_{Ca}$-T_{ENO2} (barrier device) 4. P_{TDH3}-*bar*$_{Ec}$-T_{TDH1} (barrier device). All four genetic devices were combined and chromosomally integrated into the *HO* locus and selected using the *LEU2* marker. The design of the second sender system S2 was similar to the first one: 1. P_{PSP2}- *mfa1*$_{Ec}$-T_{ENO1} (sender device) and 2. P_{CCW12}-*ste2*$_{Ec}$-T_{SSA1} (receptor device) 3. P_{FUS1}-*bar*$_{Ca}$-T_{ENO2} (barrier device) 4. P_{TDH3}-*bar*$_{Sc}$-T_{TDH1} (barrier device). Also, these four genetic devices were combined and integrated into the *HO* locus in the genome and selected using the *LEU2* marker. The receiver system consisted only of three deceives: 1. P_{PSP2}- *mfa1*$_{Ca}$-T_{ENO1} (sender device), 2. P_{CCW12}-*ste2*$_{Ca}$-T_{SSA1} (receptor device) and 3. P_{FUS1}-*mTurquoise2*-T_{ADH1} (output device). As previously, the devices were combined to the receiver system which was subsequently chromosomally integrated into the *HO* locus and selected by the *LEU2* marker.

The XNOR population dynamics should be based on the interactions between the strains in coculture, with different combinations of the strains: if none of the sender populations would be present, the receiver population should auto-induce itself by a positive feedback loop by the expression of the α_{Ca}-factor and the Ste2$_{Ca}$ receptor, which would result in the activation of the mating pathway, leading to the activation of the *FUS1* promoter and the expression of the reporter gene. In case only one of the sender strains would be cocultured with the receiver strain, the autoinduction signal α_{Ca}-factor would be degraded by the Bar1 $_{Ca}$ protease, which would result in a suppression of the reporter gene expression. The Bar1 $_{Ca}$ proteases themselves would be expressed by an auto-induced feedback loop in each of the sender populations. Within a coculture of both sender and the receiver strain, the Bar1$_{Ec}$ protease and the Bar1$_{Sc}$ protease would be expressed which would lead to the suppression of the expression of the Bar1$_{Ca}$ protease. Without the expression of the Bar1$_{Ca}$, the autoinduction of the receiver system is no longer prevented and the receiver could express the reporter gene (Figure 127).

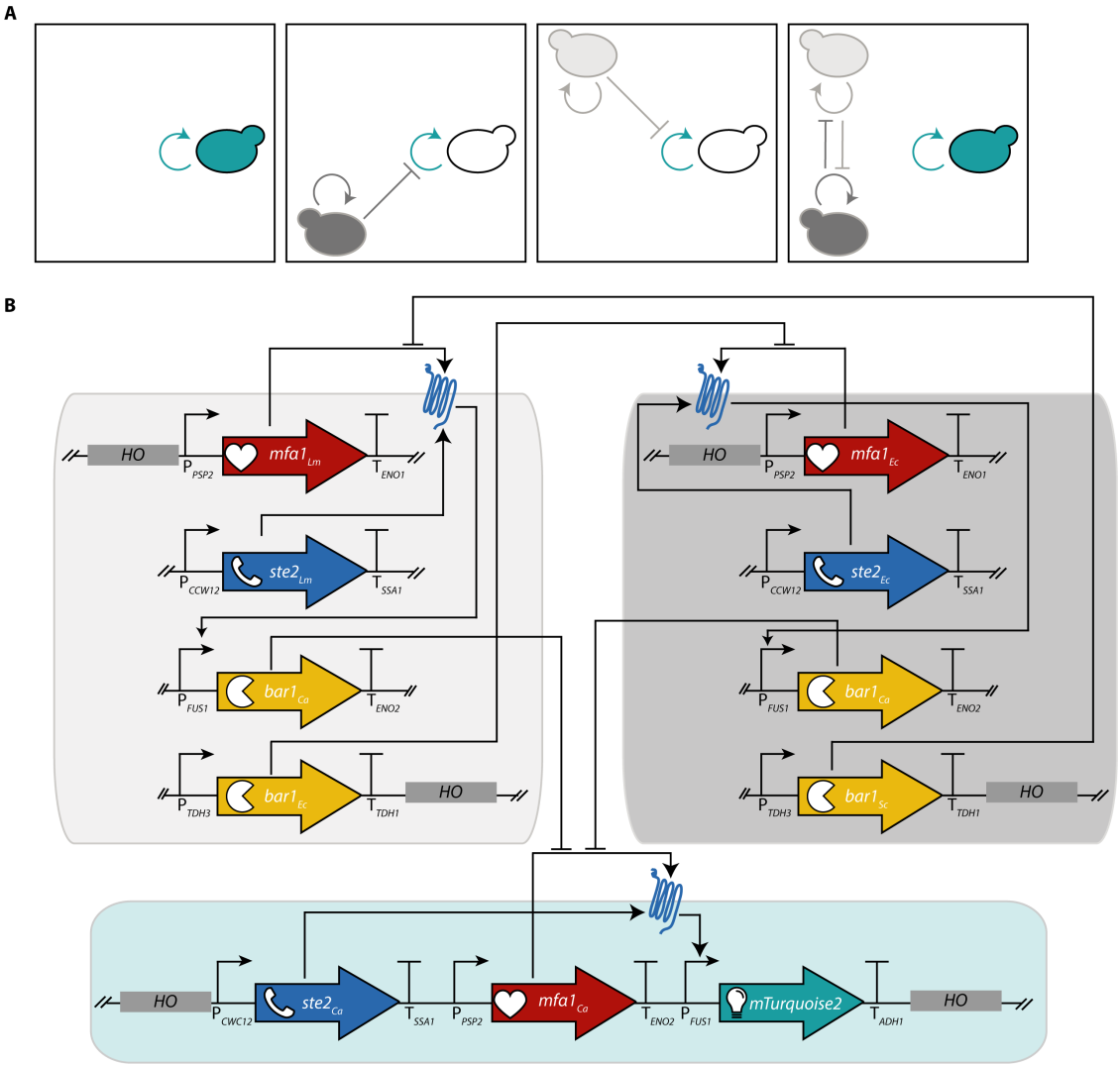

Figure 127: Network architecture and genetic constructs of the XNOR-like population network. A) Network design for the XNOR gate-like population network. Sender population 1 (light grey) and sender population 2 (dark grey) repress the induction feedback of the respective other sender population which is required in order to repress the self-induced receiver population (turquoise). So only when none or both sender populations are part of the community, the output signal is expressed. **B)** Genetic constructs of the sender1, sender 2 and receiver cells as well a circuit design. The constructs of the sender 1 strain (light grey) consists of P_{PSP2}- *mfa1*$_{Lm}$-T_{ENO1} (sender device), P_{CCW12}-*ste2*$_{Lm}$-T_{SSA1} (receiver device), P_{FUS1}-*bar1*$_{Ca}$-T_{ENO2} (1. barrier device), and P_{TDH3}-*bar1*$_{Ec}$-T_{TDH1} (2. barrier device) which were combined into a system with *HO* homology sequences. The system was integrated into the *MAT***a** *far1Δ* stain background strain. The constructs of the sender 2 strain (dark grey) consists of P_{PSP2}- *mfa1*$_{Ec}$-T_{ENO1} (sender device), P_{CCW12}-*ste2*$_{Ec}$-T_{SSA1} (receiver device), P_{FUS1}-*bar1*$_{Ca}$-T_{ENO2} (1. barrier device), and P_{TDH3}-*bar1*$_{Sc}$-T_{TDH1} (2. barrier device) which were combined into a system with *HO* homology sequences. The system was integrated into the *MAT***a** *far1Δ* stain background strain. The construct of the receiver strain (turquoise) consists of P_{CCW12}-*ste2*$_{Ca}$-T_{SSA1} (receiver device), P_{PSP2}- *mfa1*$_{Ca}$-T_{ENO1} (sender device) and P_{FUS1}-*mTurquoise2*-T_{ADH1} (reporter device). All three devices were combined to the receiver system having *HO* homology sequences. The receiver system was integrated into the *MAT***a** *far1Δ* strain background.

We then cocultured the three strains in different combinations, as depicted in the truth table (Figure 128A). The fluorescence histograms of the receiver population exhibited that for none of the conditions tested, the receiver population exhibited mating pathway activity (Figure 128). We could therefore conclude that this multicellular network was not acting as predicted and additional experiments are required to investigate which devices need to modified and improved.

Similar observations were found for all systems having auto-feedback, suggesting that auto-induction circuits cannot be utilized so far. Fundamental redesign or an intensive optimization of these networks is thus required to obtain population networks meeting our logic gate specifications.

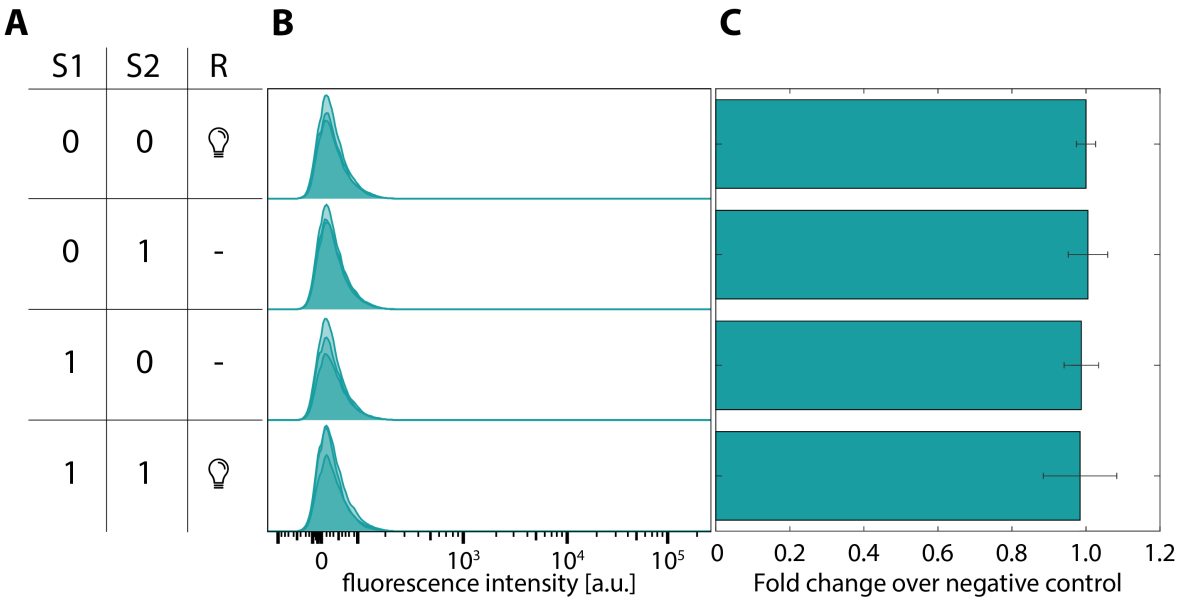

Figure 128: Results of the XNOR-like population network. A) Truth table of the Boolean XNOR gate. Zero (0) indicates in the S1 and S2 column that the sender population 1 or 2 is not part of the coculture, resulting, depending on the coculture composition, in the right column in an/no output in the receiver cells (♀/-). One (1) in the S1 and S2 column indicates that the sender population 1 or 2 is part of the coculture resulting in an/no output in the receiver cells (♀/-). **B)** Fluorescence histograms of the measured receiver cells for three biological replicates. The fluorescence output (♀) in the receiver cells indicates mating pathway activity, which was very low here. **C)** Fold change of the mean fluorescence intensity of mTurquoise2 of the receiver cells over the fluorescence intensity of the receiver cells when the sender populations were not part of the coculture (negative control).

To conclude, we demonstrated the successful implementation of α-factors as sender parts and Ste2 receptors as receiver parts into logic population networks. The effective establishment of α-factor-induced auto-stimulation, and in some cases the repression of it using barrier parts, remained to be proven. Overall, a complete repression of α-factor with the barrier part was not feasible. Addressing these, the successful implementation of previous and other logic population networks could be achieved.

2.2.6.2 Multicellular response networks

In contrast to the logic gate-like population networks, we aimed with the multicellular response networks to design, build and test multicellular systems that are stimulated by external inducer molecules. Distributed cellular computing can be achieved using the cascade design. A multicellular amplification system on the other hand should amplify the induction of the a sensor population.

2.2.6.2.1 Multicellular amplifier response network

The goal for the multicellular amplifier network was to separate sensing, the signal amplification and downstream signaling output. Therefore, we built one sensor strain and three signal amplification strains, which additionally exhibited the signal output (Figure 129A).

The sensor system consisted of three devices, each sensing a different input: 1. P_{CUP1}- *mfα1*$_{Ca}$-T_{TDH1} ($CuSO_4$ sensor device), 2. P_{TETO7}- *mfα1*$_{Lm}$ -T_{PGK1} (dox sensor device) and 3. P_{GAL1}- *mfα1*$_{Lf}$ -T_{ENO2} (galactose sensor device) (Figure 129B). These three devices were combined to the sensor system, which was integrated into the *HO* locus and selected by the *LEU2* marker.

The copper signal amplification system (Receiver 1) should respond to the transmitted signal of the sensor cell in the presence of $CuSO_4$. This system in turn was composed of three devices: 1. P_{FUS1}- *mfα1*$_{Ca}$-T_{TDH1} ($CuSO_4$ signal amplification device), 2. P_{RPL18B}- *ste2*$_{Ca}$ -T_{TENO1} (receptor device) and 3. P_{FUS3}- *venus* -T_{PGK1} (output device). The initial $CuSO_4$ input was converted into an α_{Ca}-factor, to which cells carrying the amplification system can respond to by expression of the Ste2$_{Ca}$ receptor (receptor device). Upon α_{Ca}-factor stimulation of the Ste2$_{Ca}$ receptor, the signal amplification device expresses then again α_{Ca}-factor, to further amplify the initial $CuSO_4$ signal. In order to be able to detect, whether the signal amplification from the sensor system to the signal amplification system was successful, the Venus reporter is expressed in response to α_{Ca}-factor (output device). The three devices were combined into a system and integrated into the *HO* locus and selected by the *LEU2* marker. The other two signal amplification systems were adapted from the one above described for $CuSO_4$.The dox amplification system (Receiver 2) consisted of: 1. P_{FUS1}- *mfα1*$_{Lm}$-T_{TDH1} (dox signal amplification device), 2. P_{RPL18B}- *ste2*$_{Lm}$ -T_{TENO1} (receptor device) and 3. P_{FUS3}- *mRuby2* -T_{PGK1} (output device) and the galactose amplification system (Receiver 3) of: 1. P_{FUS1}- *mfα1*$_{Lf}$-T_{TDH1} (galactose signal amplification device), 2. P_{RPL18B}- *ste2*$_{Lf}$ -T_{TENO1} (receptor device) and 3. P_{FUS3}- *mTurquoise2* -T_{PGK1} (output device) (Figure 129).

Together, this multicellular network should exhibit input amplification dynamics and responses. All four strains should be cocultured together. In case one of the inducers, either $CuSO_4$, doxycycline, or galactose would be added to the media, the sensor cell system would express the corresponding sender device ($CuSO_4$/dox/galactose sensor device). As an example, upon addition of $CuSO_4$, the α_{Ca}-factor would be produced. Subsequently, the corresponding amplifier cells would be stimulated by the α_{Ca}-factor, resulting in the expression of more α_{Ca}-factor and therefore in an amplification of the signal, and in the expression of the Venus reporter. Similar progression would be observable for the addition of the other inducers, with the corresponding devices and strains responding to the signal (Figure 129). Of course, also different combinations of inducers could be added to the coculture, which could be determined by the different fluorescence reporter colors.

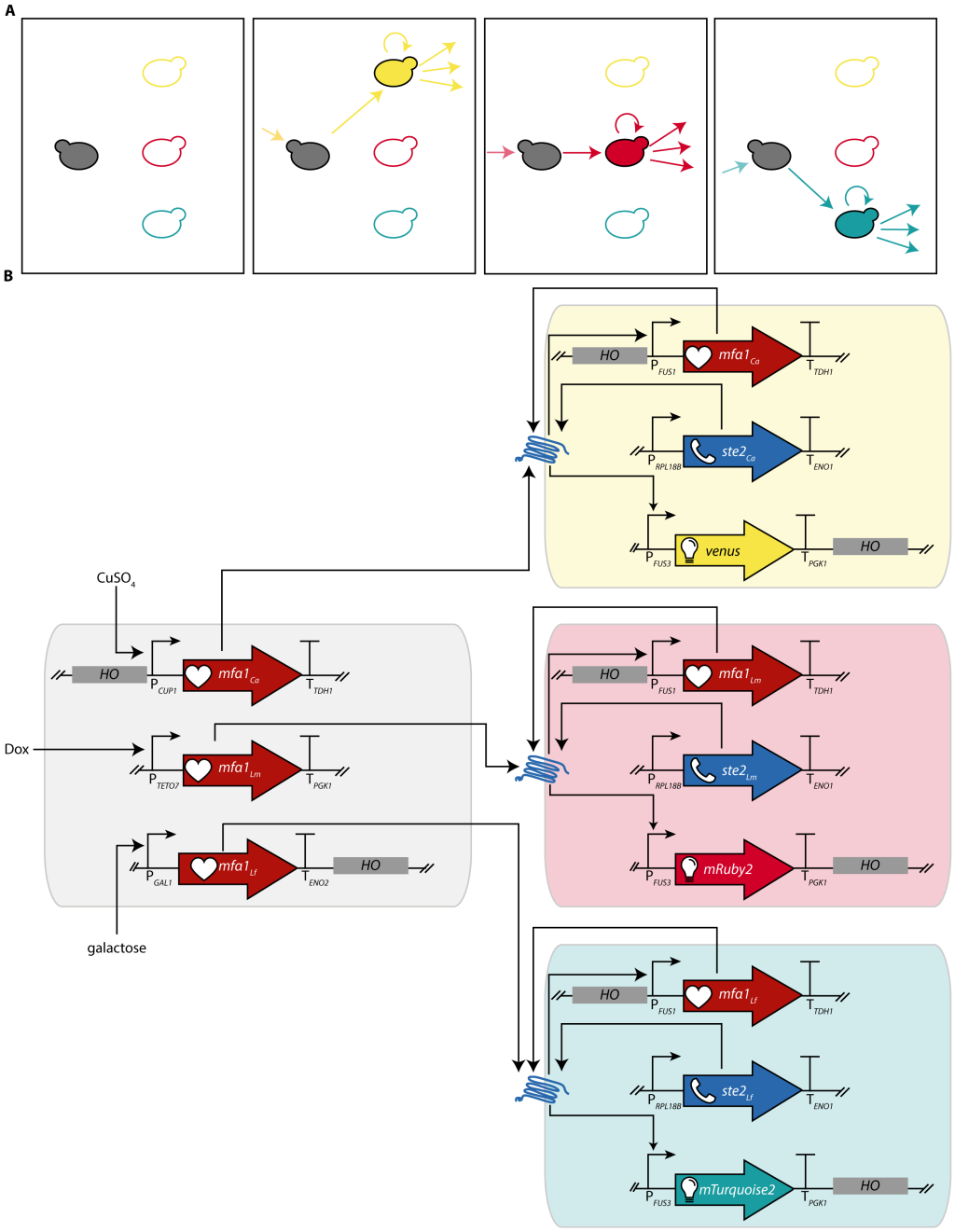

Figure 129: Network architecture and genetic constructs of the amplifier multicellular network. A) Network design for the amplifier multicellular network. The sender population (grey) can respond to different inducer inputs. Upon addition of inducer 1 (yellow) the sender population transmits the signal to receiver 1 cells (yellow), that amplify the signal and transmit the signal to other receiver 1 cells (yellow). Signal transmission of the sender population is similar for the addition of inducer 2 (red) and inducer 3 (turquoise), which in turn results in the signal amplification by receiver population 2 (red) or population 3 (turquoise). **B)** Genetic constructs of the sender1, receiver 1, receiver 2 and receiver 3 cells as well a circuit design. The construct of the sender strain (grey) consists of P_{CUP1}- *mfa1*$_{Ca}$ -T_{TDH1} (1. sender device), P_{TETO7}- *mfa1*$_{Lm}$ -T_{PGK1} (2. sender device), and P_{GAL1}- *mfa1*$_{Lf}$ -T_{ENO2} (3. sender device), which were combined into a system with *HO* homology sequences. The construct was integrated into the *MAT***a** *far1Δ* stain background strain. The construct of the receiver strain 1 (yellow) consists of P_{RPL18B}-*ste2*$_{Ca}$-T_{ENO1} (receiver device), P_{FUS1}- *mfa1*$_{Ca}$-T_{TDH1} (sender device) and P_{FUS3}-*venus*-T_{PGK1} (reporter device). All three devices were combined to the receiver 1 system having *HO* homology sequences. The receiver 1 system was integrated into the *MAT***a** *far1Δ* strain background. The construct of the receiver strain 2 (red) consists of P_{RPL18B}-*ste2*$_{Lm}$-T_{ENO1} (receiver device), P_{FUS1}- *mfa1*$_{Lm}$-T_{TDH1} (sender device) and P_{FUS3}-*mRuby2*-T_{PGK1}

(reporter device). All three devices were combined to the receiver 2 system having *HO* homology sequences. The receiver 2 system was integrated into the *MAT***a** *far1Δ* strain background. The construct of the receiver strain 3 (turquoise) consists of P_{RPL18B}-*ste2*$_{Lf}$-T_{ENO1} (receiver device), P_{FUS1}- *mfa1*$_{Lf}$-T_{TDH1} (sender device) and P_{FUS3}-*mTurquoise2*-T_{PGK1} (reporter device). All three devices were combined to the receiver 1 system having *HO* homology sequences. The receiver 3 system was integrated into the *MAT***a** *far1Δ* strain background.

To verify the amplifier population network, we cocultivated the four strains together under different inducer conditions. Since the chassis background strain had a *suc2* gene deletion resulting in a growth deficiency in raffinose-based media, which is usually utilized for induction experiments with galactose, we had to take a different cultivation approach. Thus, we set up all experiments with galactose as an inducer in media that contained solely galactose as carbon source. As the strains grew insufficiently in galactose, the resulting fluorescence output exhibited different intensities compared to the strains grown in glucose media. Nevertheless, with the acquired data, we got an overall impression of the dynamics of this multicellular amplifier system. The fluorescence histograms of the signal amplification strains carrying the output and amplifier system and the corresponding reporter genes depict the results of three biological replicates (Figure 130). The first row of histograms exhibited the initial conditions in absence of any inducer for which we expected that none of the reporter genes should be activated. However, we observed that all strains exhibited expression levels of the corresponding reporter genes. This indicated a high basal activity of the *FUS1* promoter. Unfortunately, we could not detect considerable changes of fluorescence intensities upon addition of any of the combinations of inducers. The overall lower expression levels of the Venus-expressing strain grown in galactose media was a result of the growth conditions and not a result of our system. Overall, we have to conclude that the system did not meet our initial specifications and the predicted dynamics could not be observed. Similar to the logic gates inverter, NOR, NAND and XNOR, also here, the positive feedback loop design feature was limiting. We additionally presumed that the expression of the sender devices of the signal amplifier system were leaky, which resulted in an activation of the system and thus a fluorescence output, even though gene expression was not induced. Another limitation of the entire system could be the leakiness of the inducible promoters of the sensor system. To improve this multicellular system and to obtain a functional system, also other network architectures could be explored.

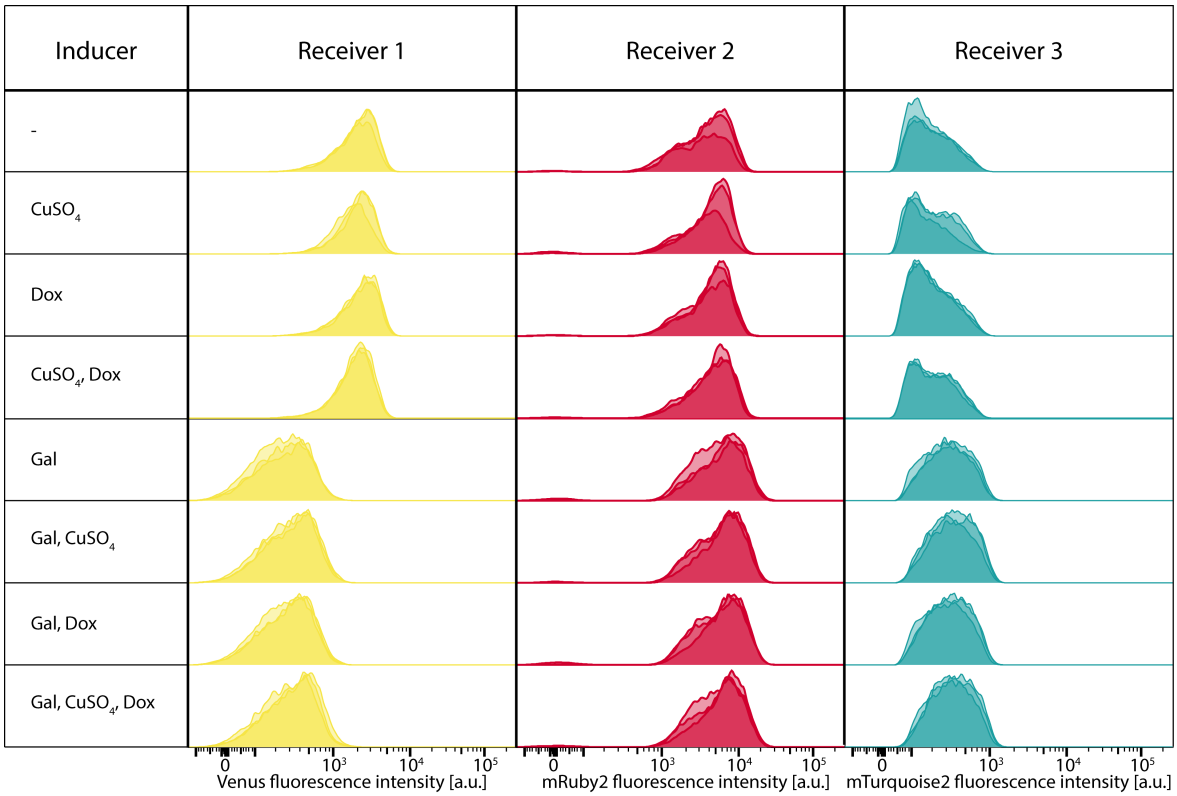

Figure 130: Results of the amplifier multicellular network. The fluorescence histograms represent the fluorescence intensities of the measured single-cell events of three biological replicates of the different receiver strains in different media and inducer conditions, together with the sender population. Each column displays one of the receiver strains and each row an inducer combination. Note, all cocultures containing Gal as an inducer were cultured in galactose media, while cocultures lacking Gal were cultured in glucose media.

2.2.6.2.2 Multicellular cascade response network

To develop distributed computing in a multicellular network on a population level, we designed a multicellular cascade that included two AND gates. Only when all inducers are added, the signal can be transmitted through the cascade and be converted into an output signal by the receiver strain (Figure 131A).

The S1 sender system consisted of one device, P_{CUP1}-*mfα1*$_{Ca}$-T_{TDH1}. The S2 sender and receiver system was composed of two devices, P_{TETO7}-*ste2*$_{Ca}$-T_{TDH1} and P_{FUS1}-*mfα1*$_{Lm}$-T_{ENO2}, the S3 system contained P_{GAL1}-*ste2*$_{Lm}$-T_{TDH1} and P_{FUS1}-*mfα1*$_{Lf}$-T_{ENO2} and the receiver system harbored P_{PAB1}-*ste2*$_{Lf}$-T_{TDH1} as well as the output device P_{FUS1}-*venus*-T_{ENO2} (Figure 131B). Each system for this cascade was chromosomally integrated in the *URA3* (S1) or the *HO* locus (S2, S3, R) and selected by the *LEU2* marker. The cascade should be functional, when all four strains are cocultured. When $CuSO_4$ would be added to the media, the S1 system in the cascade should be activated and produce the sender α_{Ca}-factor. Only when doxycycline would be in the media, the S2 system of the cascade could express Ste2$_{Ca}$ and thus be stimulated by α_{Ca}-factor from S1, which would lead to an activation of the production of α_{Lm}-factor. The S3 system of the cascade in turn could only react to the α_{Lm}-factor stimulus when galactose would be present to express Ste2$_{Lm}$. This stimulation would result in the production of α_{Lf}-factor. The receiver system should constitutively express Ste2$_{Lf}$ and would be stimulated by α_{Lf}-factor produced by the S3 population and thus induce the expression of the output Venus as a result of the induction of the mating pathway. If one of the inducers would not

be added, the cascade would be interrupted at this node and the receiver cell would not exhibit an output signal (Figure 131).

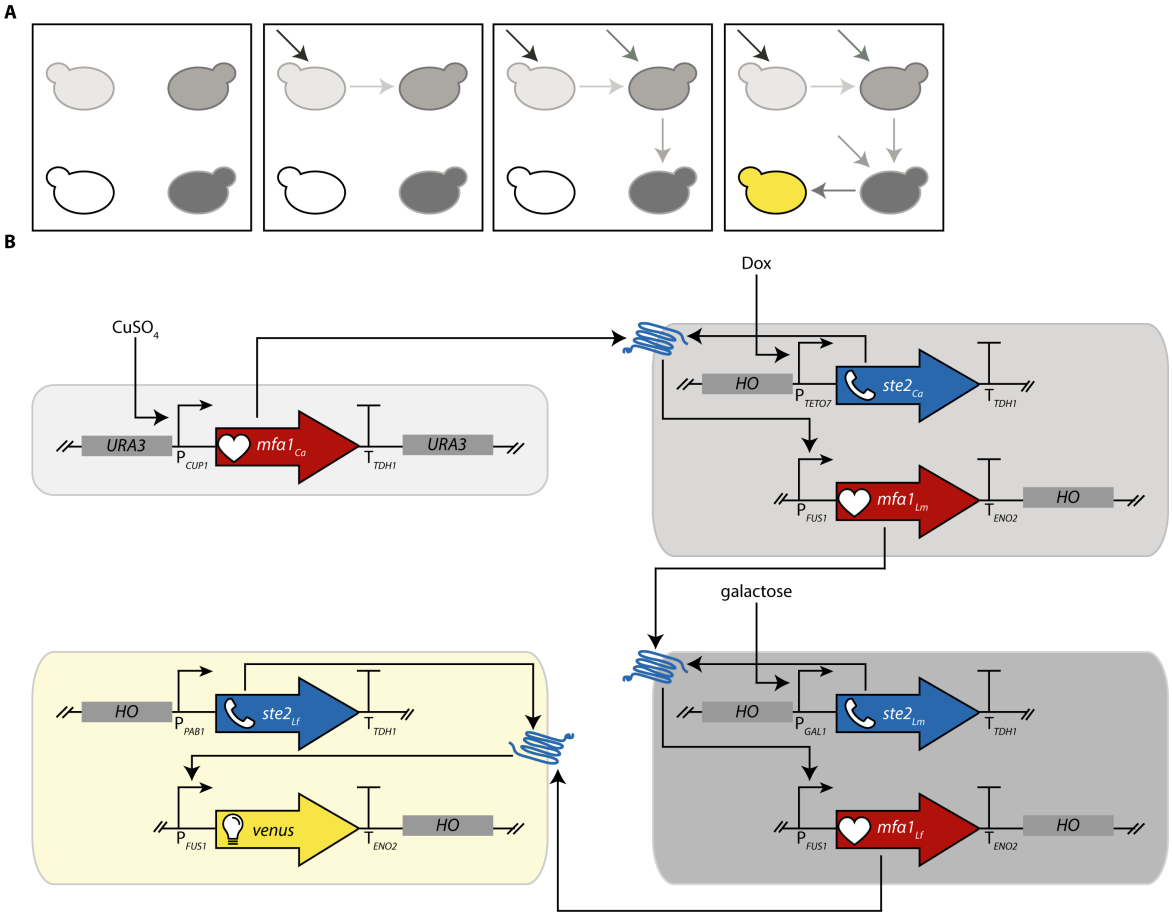

Figure 131: Network architecture and genetic constructs of the cascade multicellular network. A) Network design for the cascade multicellular network. The sender 1 population (light grey) responds to an inducer 1 and in response transmits a signal to the sender 2 population (grey) that can only respond to the signal, when stimulated with inducer 2. If this is the case sender 2 population transmits a signal to the sender 3 population (dark grey) that can only respond to the signal, when stimulated with inducer 3. If this is the case sender 3 population transmits a signal to the receiver population (yellow). **B)** Genetic constructs of the sender 1, sender 2, sender 3 and receiver cells as well a circuit design. The construct of the sender 1 strain (light grey) consists of P_{CUP1}- *mfa1*$_{Ca}$-T_{TDH1} with *URA3* homology sequences. The construct was integrated into the *MAT***a** *far1Δ* stain background strain. The system of the sender 2 strain (grey) consists of P_{TETO7}-*ste2*$_{Ca}$-T_{TDH1} (receiver device) and P_{FUS1}- *mfa1*$_{Lm}$-T_{ENO2} (sender device). The two devices were combined into a system with *HO* homology sequences. The system was integrated into the *MAT***a** *far1Δ* stain background strain. The system of the sender 3 strain (dark grey) consists of P_{GAL1}-*ste2*$_{Lm}$-T_{TDH1} (receiver device) and P_{FUS1}- *mfa1*$_{Lf}$-T_{ENO2} (sender device). The two devices were combined into a system with *HO* homology sequences. The system was integrated into the *MAT***a** *far1Δ* stain background strain. The system of the receiver strain (yellow) consists of P_{PAB1}-*ste2*$_{Lf}$-T_{TDH1} (receiver device) and P_{FUS1}-*mTurquoise2*-T_{ENO2} (reporter device). Both devices were combined to the receiver system having *HO* homology sequences. The receiver system was integrated into the *MAT***a** *far1Δ* strain background.

To test, whether the cascade population network was functional, we tested a coculture of all four strains under different media conditions with different inducer combinations. Since we utilized the same chassis strain as for the amplifier system, the we faced the same challenges of the deletion of the *suc2* gene, meaning that we grew the strains lacking galactose as inducer in glucose

media, while strains that were in induced with galactose grew in media containing solely galactose as carbon source. To verify the functionality of the cascade, we measured the fluorescence output of the receiver strain (Figure 132). The fluorescence histograms in Figure 132 of the receiver strain displays three biological replicates. In the first row, the histogram displays the receiver strain output in absence of any inducer. The cascade should not have been activated and no fluorescence of the reporter gene was expected. However, even in uninduced culture conditions, we detected the expression of the reporter Venus by increased fluorescence intensities. Comparing the histograms for the different culture conditions, it was evident that no differences of fluorescence intensities could be detected. We thus had to conclude that the cascade was not exhibiting the predicted dynamics. Differently, from the amplifier system no feedback loop had been implemented, which previously caused difficulties. Further experiments are required in order to debug the system. First, the receiver device should to be examined by testing if addition of synthetic α_{Lf}-factor would result in a visible induction of the output device. Also, here, one problem might be the leakiness of the utilized promoters, resulting in an activation of downstream gene expression, also in absence of the inducers. Taking these considerations into account, a modification and improvement of the design could be achieved and thus obtain a system meeting the initial design and dynamics specifications.

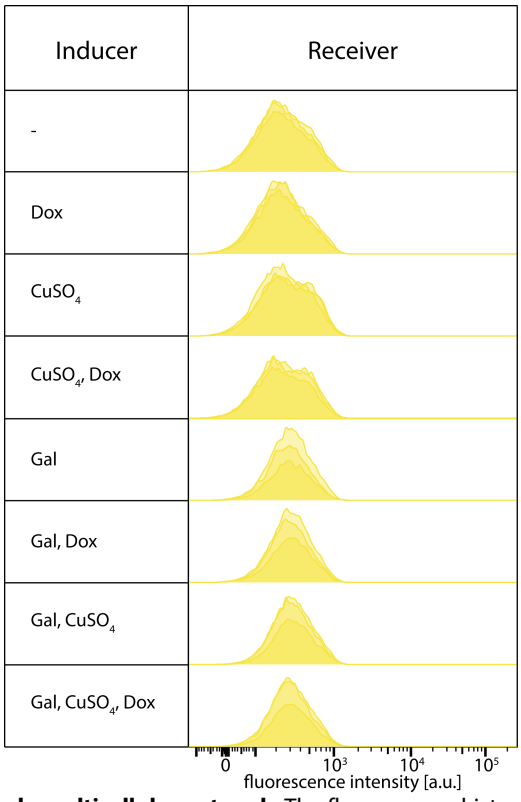

Figure 132: Results of the cascade multicellular network. The fluorescence histograms represent the fluorescence intensities of the measured single-cell events of three biological replicates of the receiver strain in different media and inducer conditions, together with the sender 1, sender 2, and sender 3 populations. Each row displays an inducer combination. Note, all cocultures containing Gal as an inducer were cultured in galactose media, while cocultures lacking Gal were cultured in glucose media.

In conclusion, for the successful implementation of multicellular response networks, each response element has to be optimized and tested individually to ensure their functionality. We further conclude that in our cases, the basal expression levels of the selected promoters was most likely responsible for the insufficient network performance.

3 Discussion

3.1 Engineered short-chain acyl-CoA ester supply in yeast

The aim of this research project was to lay the foundation for the usage of *S. cerevisiae* as a prospective polyketide production host by extending the availability of different acyl-CoA esters. We therefore engineered *S. cerevisiae* to produce unnatural propionyl-CoA, butyryl-CoA, isovaleryl-CoA, hexanoyl-CoA, and methylmalonyl-CoA [123].

3.1.1 Branched-chain acyl-CoA production

For the production of isovaleryl-CoA, we heterologously expressed the branched-chain α-keto acid dehydrogenase (BCKDH) complex pathway (BkD), originating from *B. subtilis* as well as the alternative isovaleryl-CoA biosynthetic pathway (AIB) of *M. xanthus* [391,399].

3.1.1.1 Branched-chain acyl-CoA pathway

The BkD pathway was designed to branch off the branched-chain amino acids valine, isoleucine, and leucine. The BkD pathway was previously implemented in *E. coli* and it was shown that by changing the amino acid concentration in the media, the amounts of produced branched-chain acyl-CoAs could be altered [458]. To heterologously express the BkD pathway in *S. cerevisiae*, we codon-optimized the pathway enzyme genes and assembled them in a cassette on a 2µ plasmid. To this end though, we were not able to detect production of any of the branched-chain acyl-CoA esters isobutyryl-CoA, 2-methylbutyryl-CoA or isovaleryl-CoA. As previously described, the BkD complex consists of the decarboxylase (E1), the dihydrolipoyl acyltransferase (E2), and the flavoenzyme (E3) [399]. Tow homodimers that form a heterotetramer are the base of the decarboxylase. The complex consists of multiple of these heterotetramers [402]. Based on the crystal structure of the homolog dehydrogenase complex of *Azozobacter vinelandii,* it can be hypothesized that the acyltransferase E2 consists of multiple trimers that form together the core of the multienzyme complex. The flavoenzyme consists of homodimers that are associated with the multienzyme complex [404]. Since we could not detect any branched-chain acyl-CoAs, we assumed that the pathway expression in our chassis organism led to unfavorable ratios of the complex subunits, resulting in an improper folding and formation of the multi-domain enzyme complex. In the Haushalter *et al.* study, as well as in the natural host *B. subtilis*, the BCKDH complex genes were and are organized in an operon structure, resulting in defined balanced ratios of the different subunits [399,458]. Also, the expression occurs simultaneously, since the genes are translated from the same mRNA. We therefore hypothesized that the operon arrangement of the pathway genes is optimal for the expression and timing, resulting in the formation of functional BCKDH complex. As a eukaryotic host, *S. cerevisiae* cannot express operons. Our approach was thus the usage of glycolytic promoters that exhibit similar transcriptional activity during similar growth stages, however, the expression dynamics are not alike to expression from an operon. An alternative strategy to mimic operon gene expression in *S. cerevisiae* could be the implementation of internal ribosome entry sites (IRES) or 2A self-cleaving peptides. IRES sequences allow cap-independent translation initiation and are found in viruses, e.g., polio, in plants, and have also been reported in yeast [459,460]. Since

multicistronic gene expression is naturally rarely found in eukaryotic organisms, IRES implementation was very promising. In *S. cerevisiae* it was proven that using viral IRES, a bicistronic gene expression can be achieved [461,462]. Only a limited number of viral IRES have been identified so far. The high recombination efficiency in yeast limits multicistronic gene expression since repeated insertion of IRES would results in homologous recombination and subsequently loss of function. 2A self-cleaving peptides are found in viral genomes and consists of 18-22 amino acid long sequences. After the translation of the 2A peptides, the cleaving is triggered by breaking the proline-glycine peptide bond on the C-terminus of the 2A peptide. More than 20 2A peptides have been characterized in *S. cerevisiae* and it has been shown that they could be implemented into metabolic engineering applications for multicistronic gene expression [463]. A drawback of the 2A systems is that the translation efficiency is reduced for very long mRNA sequences, which might result in lower protein abundancy of proteins encoded in the 3' region of the mRNA. Nevertheless, both systems, IRES as well as 2A, have been shown to be applicable for multicistronic gene expression in *S. cerevisiae* [459–462]. The use of either of the two systems could, in our case, improve the ratios of the different BCKDH complex subunits, which might result in an improved formation of the functional complex. However, this implementation would only have an effect in case the major bottleneck of the heterologous expression of the BkD pathway is the complex formation of BCKDH. Other limitations of the gene expression of the BCKDH in *S. cerevisiae* could be the lack of sufficient supply of the vitamin B1 cofactor or the lipoylation efficiency [399,404–406]. To ensure sufficient lipoylation, we expressed the lipoyl-ligase LplJ, however we did not verify the lipoylation state of the E2 subunit of the BCKDH [399]. Generally, also adequate amounts of insoluble protein of one of the subunits could be a limiting factor of BCKDH complex formation. To date, we did not have solid evidence that identified one of the hypothesized causes to be the limitation that the BkD pathway expression remained unfunctional, therefore optimization of the pathway expression would be very labor-intensive.

3.1.1.2 Alternative isovaleryl-CoA biosynthetic pathway

Since the production pathway using the BCKDH-complex did not produce branched-chain acyl-CoAs, we decided to investigate the alternative isovaleryl-CoA biosynthesis (AIB) pathway of *M. xanthus* [391]. The AIB pathway was not our first choice, since different from the BkD pathway, it only produces one branched-chain acyl-CoA, isovaleryl-CoA, and also simple product increase by exogeneous feeding of amino acids is impossible. However, the advantage of the AIB pathway is that no multienzyme complex consisting of several subunits is required to be expressed and therefore, the expression of the AIB pathway was thought to be achievable. With the expression of the AIB pathway enzyme genes we successfully produced intracellularly 5.5 ± 1.2 µM isovaleryl-CoA [123]. Isovaleryl-CoA and other branched-chain acyl-CoAs serve as starter units of polyketide synthesis [410,411]. The concentrations produced in our strains would be sufficient for the production of polyketides, since the levels of isovaleryl-CoA produced are consistent with the reported binding constants for various characterized PKSs [393,410,411]. To our knowledge, this was the first reported heterologous expression of the entire AIB pathway in *S. cerevisiae* and thus laid the foundation for the production of polyketides or other valuable compounds in *S. cerevisiae* that require the incorporation of isovaleryl-CoA. However, so far, the pathway was expressed from a 2µ plasmid, resulting in a visible heterogeneity of acyl-CoA ester production yields, which was also previously

reported [71]. Also, to ensure plasmid maintenance, the pathway plasmid-carrying strain had to be cultured in selective media, which would be unfavorable culture conditions for industrial production. To overcome this shortage, genomic integration of the pathway genes would be feasible, however, it can be expected that as a result the overall intracellular concentrations of isovaleryl-CoA would be reduced due to lower gene copy number within each cell. Generally, it would also be beneficial to eliminate competing pathways within the *S. cerevisiae* cells, e.g., the formation of mevalonic acid, which is also produced from HMG-CoA [464]. To test, whether elimination of this pathway would result in higher production of isovaleryl-CoA, the media could be supplemented with statins that are blocking the HMG-CoA reductase activity [464]. If utilization of statins resulted in successful increased isovaleryl-CoA production, interference of the HMG-CoA reductase could be genetically determined resulting in an overall increased metabolic flux from HMG-CoA towards propionyl-CoA. Also, adapting the expression of Erg10 and Erg13 should improve the metabolic flux towards isovaleryl-CoA. To identify other metabolic adjustments that would be beneficial to improve the productivity of the AIB pathway, a flux balance analysis (FBA) should be considered. Especially increasing the availability of acetyl-CoA would be a good starting point.

3.1.2 Butyryl-CoA and hexanoyl-CoA production

Besides the engineered precursor supply of branched-chain acyl-CoAs, we also wanted to provide butyryl-CoA and hexanoyl-CoA pools in *S. cerevisiae* as precursors for the production of alcohols, carboxylic acids, and polyketides [417–419]. Therefore, we modulated the previously in *E. coli* and *S. cerevisiae* expressed and described butyraldehyde and butanol production pathway [389,392]. By expressing the modified n-butanol (BUT) pathway from the 2µ plasmid in *S. cerevisiae*, we were able to produce 6 ± 1.9 µM butyryl-CoA and 5.8 ± 2 µM hexanoyl-CoA intracellularly [123]. Similar to the isovaleryl-CoA pathway, it would be expected that the intracellular concentrations of butyryl-CoA and hexanoyl-CoA would be lowered upon chromosomal pathway integration. The integration of several copies of the pathway into different chromosomal locations might be a possibility to increase gene copy number. One disadvantage of the BUT pathway utilized here is that both butyryl-CoA and hexanoyl-CoA are produced from one pathway, resulting in a mixture of both acyl-CoAs in the cell. The nature of the BUT pathway prohibits the formation of solely either of the two acyl-CoAs since all four pathway enzymes are promiscuous towards an intermediate of the production of butyryl-CoA as well as of hexanoyl-CoA [389,392]. Since several homologs of the pathway enzymes have been identified featuring different affinities to the intermediates, the pathway towards butyryl-CoA or hexanoyl-CoA could be adapted and subsequently improved to produce increased acyl-CoA amounts. Also, a directed evolution approach could be envisioned to alter the substrate specificity of the different pathway enzymes [389]. Rapid construction of alternative BUT pathways that include enzyme homologs is possible due to the allocation of our short-chain acyl-CoA toolkit in combination with the Dueber yeast toolkit [71]. This optimization strategy of testing and incorporating homolog enzyme variants originating from different species into the pathways could also be tested for the other acetyl-CoA production pathways. Since the BUT pathway is NADH-dependent, it would be possible to engineer a growth-coupled BUT pathway expression strain not only to improve the overall acyl-CoA production but also to allow effective screening of different pathway designs that exhibit enhanced acyl-CoA production and thus increased growth. The coupling of growth and production of butanol as a NADH consumption pathway has

been proven to be effective in engineered *E. coli* strains and could thus also be implemented in *S. cerevisiae* [465]. Also, for this pathway, engineered enhanced acetyl-CoA supply, as native key metabolite, would be beneficial for increased acyl-CoA production [429]. To conclude, the here produced butyryl-CoA and hexanoyl-CoA intracellular concentrations are sufficient to allow proof of principle production of polyketides in yeast. For prospective commercial biotechnological production, further optimizations like chromosomal integration and thus increased production efficiency would be required.

3.1.3 Propionyl-CoA production

Propionyl-CoA is a platform molecule required for the biotechnological production of bioplastics, polyketides, or fatty acids [388]. Since it is such an important compound, we aimed here to engineer *S. cerevisiae* to produce propionyl-CoA and therefore establish the producing strains as a platform for upcoming metabolic engineering projects. Different routes are known for the production of propionyl-CoA and thus we established two different pathways here. The pathway using the propionyl-CoA ligase (PrpE) was previously established and requires continuous feeding of propionate [125]. We implemented this pathway to compare the production of propionyl-CoA from feedstock via the 3HP pathway that branches off from malonyl-CoA.

3.1.3.1 Propionyl-CoA ligase pathway

After codon optimization of the *prpE* gene, we selected a glycolytic promoter for its expression, based on a re-analyzed promoter characterization data set obtained from Keren *et al*. [396]. With this enzymatic step, we were able to produce intracellular concentrations of 5.3 ± 2.4 µM propionyl-CoA, when 50 mM propionate were supplemented in the media [123]. A direct comparison to the propionyl-CoA amounts produced by Mutka and colleagues remained difficult because they only reported relative propionyl-CoA abundancy in comparison to the overall acyl-CoA pool [125]. In their study they reported that after a cultivation period of 103 hours, propionyl-CoA accounted for 90 % of the acyl-CoA pool [125]. They also measured a propionyl-CoA accumulation in absence of the *prpE* gene in propionate-containing media due to the native *S. cerevisiae* Acs1 propionyl-CoA ligase, however, the reported amounts were visibly lower compared to the PrpE-expressing strain [125]. Though, we did not detect any production of propionyl-CoA in our negative control. A reason could be that with our extraction and measuring method the detection of very low concentrations of propionyl-CoA could not be achieved.

Overall, we observed a strong reduction of the maximal growth rate of this strain, also, when no propionate was added to the media. Reduced growth was also thought to result in overall lower production of propionyl-CoA. This growth reduction was unlikely to be a result of protein expression burden of the *prpE* gene but rather to be a metabolic burden that was caused by catalyzing the CoA ligation. The most considerable growth reduction of the PrpE pathway-expressing strain was found when the cells were grown in media supplemented with 50 mM propionate. Also, for the control strain, we reported a reduction of the maximal growth rate when propionate was supplemented to the media. This was most likely due to the accumulation of propionyl-CoA produced by the native Acs1. The toxicity of propionate feeding could be further explained by a side reaction of the peroxisomally located Cit2p. It was shown that Cit2p is promiscuous towards pro-

pionyl-CoA and catalyzes a reaction resulting in the production of toxic 2-methylcitrate [406]. Naturally, Cit2p is involved in the peroxisomal production of succinate from acetyl-CoA [406]. Taking these considerations into account we could deduce a possible optimization strategy, namely knocking out the *cit2p* gene. It was already shown that knocking-out *cit2p* allowed growth on propionate without exhibiting visible growth reduction [406].
The observed reduced growth of the PrpE strain in the absence of propionate indicated that the CoA ligase could also be promiscuous towards other cellular substrates and thus resulting in CoA product accumulation in the cell. To overcome this, homologous PrpE enzymes of other organisms could be tested to identify, whether they exhibit higher substrate specificity for propionate. One optimization approach that would be suitable for all our engineered pathways but that would be especially important for the PrpE pathway, is to address the size of the free CoA pool. Since the ligation of free CoA to propionate might result in a strong CoA sink in the cell, increasing the size of the free CoA pool by feeding pantothenate, a precursor of CoA, should prevent CoA being depleted. It has previously been shown that by feeding pantothenate, the free CoA pools in the cell can be increased [466]. Since propionyl-CoA accumulation is toxic to *S. cerevisiae* and since it only serves as an intermediate for more complex products, it would be beneficial to implement just-in-time production of propionyl-CoA to prevent intracellular accumulation of propionyl-CoA. Overall, establishing the PrpE pathway for propionyl-CoA production is feasible though expensive. Thus, the implementation of a feeding-independent metabolic pathway towards propionyl-CoA would be favored over this propionate feeding route.

3.1.3.2 3-hydroxypropionate pathway

One major aim of this study was to implement a feeding-independent propionyl-CoA production pathway in *S. cerevisiae*. Therefore, we expressed genes derived from the 3-hydroxypropionate (§HP) carbon assimilation cycle found in many auxotrophic archaea and bacteria [393,430–432]. This pathway was previously successfully expressed in *E. coli* and we further improved it by replacing the first two pathway genes with the mcr_{Ca}, gene, encoding an enzyme capable of catalyzing both required reaction steps [393]. With the successful expression of the 3HP pathway we were able to produce intracellular concentrations of propionyl-CoA of 8.5 ± 3.7 µM [123]. Side-by-side comparison between both propionyl-CoA production routes revealed that the propionate-dependent production via the PrpE pathway resulted in a smaller propionyl-CoA pool compared to the 3HP pathway. Also, it should be noted that compared to the PrpE strain, the 3HP-carrying pathway exhibited increased growth and thus a higher maximal growth rate. One reason explaining this observation could be that the 3HP pathway does not require free CoA, since it branches off malonyl-CoA and thus doesn't create a free CoA sink, as previously discussed for the PrpE pathway. Furthermore, malonyl-CoA is differently regulated than free CoA in the cell. Many metabolic engineering projects used malonyl-CoA as the branching point from the central metabolism, as the cell can balance a reduction of internal malonyl-CoA pools [426–429]. Also, it should be noted that the measured propionyl-CoA concentrations, produced from the two pathways, do not necessarily reflect the metabolic fluxes in a cell. This means that the similar intracellular propionyl-CoA concentrations of both pathways do not necessarily represent alike fluxes towards propionyl-CoA and thus pathway production efficiency. Overall, these are only hypothetical explanations for the

obtained results and further detailed investigations would be required to draw a more comprehensive conclusion. Besides the PrpE and 3HP propionyl-CoA production routes, several alternative pathways towards propionyl-CoA have been described [467,468]. Recently, Bernhardsgrütter and colleagues described the homodimeric propionyl-CoA synthase (PCS) that consists of three-domain fusions. The PCS catalyzes the reaction from 3-hydroxypropionate to propionyl-CoA [469]. An expression of this enzyme in our chassis *S. cerevisiae* would provide a shortened alternative production pathway towards propionyl-CoA, which could additionally result in increased production levels. The enzymes utilized in our 3HP pathway for now mostly originate from thermophilic organisms. Biochemical investigations of the enzymes evidenced that their highest relative activity was found at 57 °C [393,430–432]. We cultured our strains at 25 °C, thus the enzyme activity was considerably reduced, since it was previously discussed that only 40 % of the relative activity would be reached under culture conditions at 33 °C [393,430–432]. The use of homolog enzymes from other organisms might be a possible solution to address this bottleneck however, generally, the 3-hydroxypropionate carbon assimilation cycle is mostly found in extremophiles. A rapid shuffling of different enzymes of the pathway could be performed using the acyl-CoA toolkit. The setup of the toolkit, which is following the Golden Gate cloning standard, also allows a directed evolution approach, like the Darwin Assembly by the Pinheiro lab, to evolve the current enzymes towards higher relative activity at lower temperatures [470]. A direct screening of higher propionyl-CoA production yields would be beneficial, ideally by using a biosensor with an easy readout. A propionate-induced promoter system was developed based on the PrpB promoter and the PrpR regulator in *E. coli* [471]. To detoxify, *E. coli* was expressing PrpE resulting in the production of propionyl-CoA from propionate. Propionyl-CoA was subsequently further metabolized to 2-methylcitrate which was the activator of the PrpR-PrpB regulator-promoter system [471]. This promoter system was then further adapted to be used as an indirect biosensor of propionyl-CoA in *E. coli* [472]. Theoretically, the promoter system could be adapted to also be functional in *S. cerevisiae*. Alternatively, a screen of propionate-induced gene expression in *S. cerevisiae* could identify a suitable promoter to be employed in a biosensor.

Overall, it would be of importance to identify pathway bottlenecks by identifying accumulating intermediates using LC/MS-MS. In case an intermediate accumulates, adapting the gene expression strength of the pathway genes could be performed using the acyl-CoA toolkit by increasing the expression of downstream enzymes. Beside this directed approach, it would also be possible to randomly shuffle pathway genes and promoter-terminator pairs to create a library of different pathway variants. Since currently no propionyl-CoA biosensor is available in yeast, high-throughput mass spectrometry would be required to identify the best producing pathway variant. Recently, a novel method was published for the high-throughput mapping of CoA metabolism using SAMDI-MS for cell-free biosynthesis [473]. This method could be adapted to also be functional using yeast cell lysate and would thus allow a better understanding and the identification of bottlenecks of the pathway. Also, it would be important to investigate the key metabolites in the central metabolism of *S. cerevisiae* to ensure sufficient precursor supply for our acyl-CoA production pathway. For the 3HP pathway, acetyl-CoA as well as malonyl-CoA are the precursors required for propionyl-CoA production. Since malonyl-CoA is a common branching point from the

central metabolism for the production of a variety of different valuable compounds, several studies aimed to improve its availability by different attempts [427]. One approach was to reduce non-essential site reaction that pull the metabolic flux away from acetyl- and malonyl-CoA. Reducing or knocking out the expression of the *cit2* as well as *mls1* genes would result in an increase of acetyl-CoA concentration since the channeling of acetyl-CoA towards the glyoxylate cycle would be limited [428,429]. The precursor of acetyl-CoA is acetaldehyde that is also required for the production of ethanol [474]. Reducing the flux towards ethanol formation would thus in turn increase the intracellular acetaldehyde concentrations and could be achieved by reducing or knocking out the expression of *adh1,3,4,5,6,* and *7*. This approach would generally be possible, however, it was shown that blocking the production of ethanol is fatal to *S. cerevisiae* [474]. Since malonyl-CoA is used for fatty acid biosynthesis, also here, a reduction might increase the intracellular malonyl-CoA pools but would also lead to a reduction of growth. Besides reducing or preventing flux to competing pathways, it would also be possible to increase the flux towards acetyl-CoA. The overexpression of Adh2 (encoding an alcohol dehydrogenase) and Ald6 (encoding a NADP-dependent aldehyde dehydrogenase) would increase the acetaldehyde concentrations [474]. Heterologous expression of the Acs (encoding an acetyl-CoA synthetase) of *Salmonella enterica* would improve the malonyl-CoA concentrations. The Acs_{Se} is differently from the natively expressed Acs_{Sc} acetylation-insensitive and therefore not regulated [435]. A key role in the formation of malonyl-CoA formation also plays the Acc1. Studies have shown that changing its native promoter to enhance the expression of Acc1 led to an increase in malonyl-CoA pools [124]. Since Acc1 is deactivated by Snf1, an AMP-activated serine/threonine-protein kinase under glucose limiting conditions, simple overexpression may prevent an increase of the malonyl-CoA concentrations. Wook Choi and colleagues identified the critical amino acid of Acc1 for the deactivation to be Ser-1157. When this serine residue was mutated to an alanine residue, Snf1 could no longer deactivate Acc1 [116,426]. Model-driven pathway improvements have predicted additional genetic interferences resulting in an increase of the intracellular malonyl-CoA pools [475]. Also, to optimize the precursor supply, dynamic flux control using for example a promotor-based biosensor for malonyl-CoA could be implemented [476,477]. Overall, it remains difficult to compare the different optimization strategies to increase the acetyl-CoA and malonyl-CoA pools in the cell since for the different proposed approaches different strains, media compositions, and analytical methods were employed. However, the availability of so many approaches highlights the great potential to optimize the 3HP pathway for the production of propionyl-CoA. Acetyl-CoA and malonyl-CoA are not only required for the production of propionyl-CoA, also the production efficiency of the AIB and BUT pathway would benefit from these adjustments.

To conclude, for both implemented propionyl-CoA production pathways, we could report sufficient intracellular concentrations of propionyl-CoA. The 3HP pathway route even exhibited slightly higher propionyl-CoA concentrations compared to the PrpE pathway and has the additional advantage of producing propionyl-CoA independently from feeding, as well as the strain was growing faster. Nevertheless, we discussed and highlighted different optimization strategies for both pathways, as well as other acyl-CoA ester production pathways that could improve the intracellular concentrations.

3.1.4 Methylmalonyl-CoA production

Apart from the production of isovaleryl-CoA, butyryl-CoA, hexanoyl-CoA, and propionyl-CoA, we wanted to establish methylmalonyl-CoA supply as a precursor for various valuable compounds in *S. cerevisiae*. Therefore, we improved the previously implemented pathway route via PrpE-PCC, by expressing the *prpE*, *accA1*, and *pccB1* genes from one plasmid [125]. This pathway was used as a reference to compare this route with the feeding-independent production pathway via a modified 3HP pathway.

3.1.4.1 Propionyl-CoA ligase and propionyl-CoA carboxylase pathway

With the implementation of the PrpE-PCC1 in *S. cerevisiae* we were able to produce intracellular concentrations of 4.6 ± 2.2 µM propionyl-CoA and 0.5 ± 0.1 µM methylmalonyl-CoA [123]. A direct comparison with the produced acyl-CoA ester amounts that were reported in the Mutka *et al.* study was not possible since they did not quantify the production [125]. However, recently, the PrpE-PCC pathway was re-established for the production of angelyl-CoA and they reported a production of methylmalonyl-CoA of 1.7 mg/L [478]. When we converted our measured methylmalonyl-CoA concentration to their computation, we produced about 0.4 mg/L, indicating that their pathway produced approximately 4-times more methylmalonyl-CoA than we did. Direct comparison between their and our pathway design and production procedures revealed that the pathway enzyme genes were expressed from different promoters as well as the metabolite extraction method was different [478]. Overall, we could assume that the different harvest and media conditions explained the discrepancy in methylmalonyl-CoA production yields. Since the Pcc is a biotin-dependent carboxylase, they increased the biotin supplementation in the media to 20 µg/L compared to our 10 µg/L [478]. This increase might have positively affected the biotinylation efficiency and thus the activity of the Pcc complex. One last apparent difference between the Callari *et al.* study and our study was that their production media was buffered to a pH of 4.5 compared to our media that was buffered to pH 6.5. It was previously discussed that a decreased pH allows improved passive diffusion of propionic acid into the cell [478]. Callari and colleagues reported that under lower pH conditions the cells exhibited an increased growth as well as an enhanced production of angelyl-CoA, which requires methylmalonyl-CoA as precursor. Changes of the media conditions could be easily implemented and tested with our PrpE-PCC pathway and thus result in an increase of the intracellular methylmalonyl-CoA concentrations, as it was reported [478].

Our attempt to improve the PrpE-PCC pathway by expressing the third Pcc subunit, ε, as well as the addition of the biotin ligase of BirA originating from *E. coli*, did not result in increased intracellular methylmalonyl-CoA concentrations (PrpE-PCC2 pathway). Expression of the ε subunit PccE has been reported to improve the Pcc complex formation and to increase Pcc activity significantly [439,441,442]. However, this could not be confirmed here. Reasons could have been the genetic construct design as the *prpE* gene was expressed from a different promoter. It is also likely that Pcc complex formation of the subunits AccA1, PccB1 and PccE was not optimal under the here tested conditions, resulting in the formation of unfunctional protein complex. This could be addressed by using the established CoA-ester toolkit and the YTK collection for rapid prototyping of an improved Pcc complex expression cassette. Since the expression of the Pcc and the production of methylmalonyl-CoA led to a slight growth rate recovery, this phenomenon could potentially be employed as a selection mechanism. Alternative approaches to improve the production

yields of methylmalonyl-CoA could be the implementation of the Pcc originating from *M. extorquens* that was shown to have a higher substrate specificity towards propionyl-CoA and therefore might be more suitable for our purposes [479]. Overall, the propionyl-CoA supply was found to be sufficient. However, we detected propionyl-CoA accumulation, even though the Pcc was expressed, suggesting the carboxylation activity remained the bottleneck of the PrpE-PCC pathway. Besides previously mentioned optimization approaches, insufficient biotinylation could be the limitation of methylmalonyl-CoA production efficiency. We already addressed an improvement of the biotinylation of the Pcc by expressing a biotin ligase of *E. coli*. However, we could not report increased methylmalonyl-CoA production. *S. cerevisiae* is natively expressing the biotin ligase Bpl1 that could potentially biotinylate the Pcc complex of our pathway [480]. Overexpression of Bpl1 could result in improved methylmalonyl-CoA yields. However, when we structurally compared the different biotin ligases originating from *E .coli*, *S. cerevisiae*, *S. coelicolor*, and *M. extorquens*, we could report visible differences accounting for insufficient binding to the Pcc complex and therefore inadequate biotinylation. To investigate Pcc biotinylation by the different biotin ligase variants, we included codon-optimized genes of the biotin ligase of *E. coli*, *S. coelicolor*, and *M. extorquens* to the CoA-ester toolkit. Using this Golden Gate toolkit, we could rapidly test different combinations of Pcc complex and biotin ligases for their efficiency of improving the production of methylmalonyl-CoA. Also, the availability of intracellular biotin could be increased by overexpression of the natural biotin symporter Vht1 [481].

Taking all the different optimization approaches into account, we are confident that we would improve the untracellular methylmalonyl-CoA production amounts and would reach similar concentrations as reported by Callari [478]. Overall, the re-establishment of the PrpE-PCC pathway, initially introduced by Mutka *et al.*, served as an optimal reference and test pathway to optimize Pcc activity [125]. After improving the expression of the Pcc complex as well as the biotin ligase, the Pcc pathway could also be combined with the 3HP propionyl-CoA production pathway, obtaining a feeding-independent methylmalonyl-CoA production route.

3.1.4.2 3-hydroxypropionate and crotonyl-CoA carboxylase/reductase pathway

To implement a feeding-independent production route towards methylmalonyl-CoA, we modified the 3HP propionyl-CoA production pathway. We replaced the Acr catalyzing the reaction towards propionyl-CoA with the Ccr_{CC}, catalyzing the reduction and carboxylation of acryloyl-CoA to methylmalonyl-CoA [445,446]. With this 3HP-CCR pathway we were able to detect intracellular concentrations of 3.7 ± 2.7 µM propionyl-CoA and 0.3 ± 0.3 µM methylmalonyl-CoA [123]. The unexpected formation of propionyl-CoA as well as the ratio of the two acyl-CoA esters indicated that the reduction performed by the Ccr_{CC} was more efficient compared to the carboxylation. The notable variation between the intracellular methylmalonyl-CoA concentrations of the different replicates was due to one replicate for which overall lower acyl-CoA ester production was observed. When that outlier would be neglected, the obtained intracellular concentrations of methylmalonyl-CoA of the 3HP-CCR pathway would be similar to the detected concentrations produced by the PrpE-PCC pathway. Similar to the PrpE-PCC pathway, further optimization would be required to ensure sufficient supply of methylmalonyl-CoA for downstream valuable compound production. Overall, the majority of potential improvement approaches discussed for the 3HP pathway, would also apply to the 3HP-CCR pathway. One approach specifically applying to the 3HP-CCR

pathway would be to alter the media and cultivation conditions to increase the production of methylmalonyl-CoA. As the carboxylation reaction seemed to be the limiting step, the first optimization approach could be to improve the CO_2 supply utilized in this reaction step, for example by supplementing the media with sodium bicarbonate or by growing the production strain under higher atmospheric CO_2 conditions. Addition of sodium bicarbonate to the media was shown to improve the formation of methylmalonyl-CoA in *Rhodopseudomonas spheroides* [482].
Besides previously mentioned media and cultivation adjustments, also the pathway design itself could be altered to obtain higher methylmalonyl-CoA yields. Since all utilized genes of the 3HP-CCR pathway were domesticated for the CoA-ester toolkit, rapid shuffling of promoters could be performed to identify optimal expression strengths and ratios of the pathway genes. The main focus though should be on the expression of the Ccr. Since the discovery of the first Ccr, many research projects were conducted to investigate the biochemical activities in the natural pathway, the evolutionary constraints as well as its biotechnological potential [483,484]. Peter and colleagues identified and heterologously expressed a library of Ecrs, including Ccrs, to characterize their substrate promiscuity [395]. Unfortunately, acryloyl-CoA was not part of their investigation but predictions suggested the acceptance of acryloyl-CoA as a substrate, which we successfully proved with the formation of propionyl-CoA and methylmalonyl-CoA from acryloyl-CoA using the Ccr_{CC}. To identify a Ccr being more promiscuous towards acryloyl-CoA and with an enhanced carboxylation reaction, we could revert to the previously published library of Ecrs and Ccrs to identify a more suitable variant producing more efficiently methylmalonyl-CoA from acryloyl-CoA [395]. In vitro studies could already be performed to identify a subset of potential suitable Ccrs, but if the performance would be similar *in vivo* remains to be investigated. Besides the implementation of the 3HP-CCR pathway with homologous Ccrs, the recent advances in the Golden Gate coupled directed evolution system of the Pinheiro group could be utilized to engineer an improved Ccr_{CC} [470]. Several studies have addressed and investigated the function and structure of the Ccr and therefore protein engineering approaches would be feasible [445,446,485,486]. In case the side product formation of propionyl-CoA remains, it would also be possible to convert more propionyl-CoA to methylmalonyl-CoA by additional expression of a Pcc. To summarize, many different approaches exist that could be tested to improve the production of methylmalonyl-CoA in *S. cerevisiae*, an important precursor for the production of valuable products.

3.1.5 Concluding remarks and outlook

With the here presented and discussed study we laid the foundation for establishing *S. cerevisiae* as a chassis host for the production of secondary metabolites, for which the different acyl-CoA esters serve as important platform precursor molecules (Figure 133) [123]. This plug-and-play approach further provides opportunities to discover and engineer novel bioactive compounds and valuable chemicals in the future. The engineered platform strains provide a metabolic engineering tool to produce diverse compounds of interest, such as fatty acids and polyketides from renewable carbon sources in *S. cerevisiae*. A recent publication of our collaborators from the Keasling Lab reported the successful production of cannabinoids, THC and CBD, in *S. cerevisiae* [52]. For the production of both cannabinoids, hexanoyl-CoA is an important precursor. By optimizing the BUT pathway they obtained sufficient precursor supply in yeast for the production of cannabinoids. They also showed that different fatty acid precursors could be incorporated into

olivetolic acid, a direct precursor of cannabinoids. Thereby they detected the production on unnatural cannabinoids that might exhibit different pharmacological properties. It could also for example be tested, if isovaleryl-CoA would be incorporated to form isovaleric-olivetolic acid. Generally, testing if plant, fungal or bacterial PKS would be promiscuous towards the produced acyl-CoA esters could be interesting and to identify synthesized novel compounds. It was already shown that the LipPks1, which utilizes isobutyryl-CoA as starter unit in its native host, is promiscuous towards other branched-chain acyl-CoA esters like isovaleryl-CoA. The LipPks1uses methylmalonyl-CoA as extender unit to synthesize the antibiotic α-lipomycin [447]. Here, we showed the successful production of both precursors in *S. cerevisiae* and therefore established yeast as a prospective chassis for the production of novel lipomycin-derived antibiotics. With the demonstrated production of propionyl-CoA as well as methylmalonyl-CoA in our engineered strains, we provided the opportunity of establishing a feeding-independent production of 6-deoxyerythronolide B by the polyketide synthase 6-deoxyerythronolide B (DEBS) in yeast. The DEBS PKS uses propionyl-CoA and methylmalonyl-CoA for the production of 6-deoxyerythronolide B, an erythromycin precursor [487]. Besides the utilization of our engineered acyl-CoA ester production strains for the manufacturing of polyketides, the precursors could be also incorporated into other higher value products. In *E. coli* it was shown that the fatty acid synthase (FAS) could also incorporate branched-chain-acyl-CoAs [458]. In contrast, the fungal FAS1 is more selective to the excepted substrates. However, the yeast FAS1 is at present under investigation and innovations in protein engineering will lead to a better understanding as well as to the possibility of engineering the FAS1 to exhibit higher substrate promiscuity [488]. Subsequently, the production of alternative fatty acids, to be used as biofuels could be envisioned, potentially also based on our set of acyl-CoA esters.

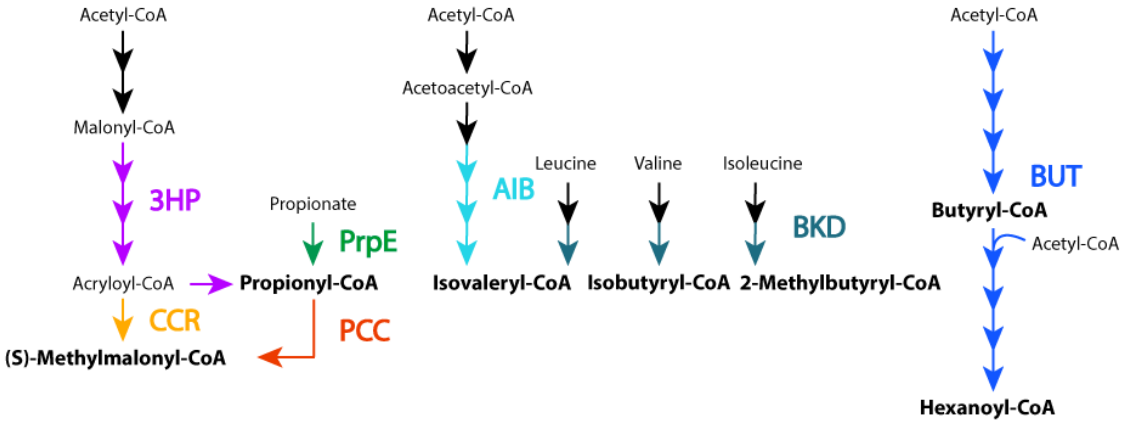

Figure 133: Graphical overview of established acyl-CoA ester-producing pathways in *S. cerevisiae* [123].

The 3HP pathway that was implemented for the production of propionyl-CoA and especially methylmalonyl-CoA exhibited also an additional potential for the fixation of carbon. The natively found 3HP pathway was implemented in *E. coli* for this purpose and exhibited sufficient activity [489]. Therefore, an implementation with further improvement into yeast would be conceivable. Solely the implementation of vitamin B12-dependent enzymes, which would be required, needs to be investigated independently, since to date it was not proven whether *S. cerevisiae* could take up and utilize vitamin B12.

As part of this study, we also expressed the alternative isovaleryl-CoA pathway originating from *M. xanthus* in *S. cerevisiae* and found a sufficient production of isovaleryl-CoA [391]. We also engineered *S. cerevisiae* for butyryl-CoA and hexanoyl-CoA production via the well-established n-butanol pathway [389,392].

Finally, we evaluated multiple routes towards propionyl-CoA and methylmalonyl-CoA biosynthesis and established a feeding-independent approach for the production of these acyl-CoA esters *in vivo*. Beside these achievements, further optimization to obtain higher production titers or an improved growth of the production strains would be beneficial and were previously discussed in detail. We highlighted different optimization strategies, including media and culture optimization, engineered regulation of the gene expression, metabolic flux optimizations, or the suppression of competing pathways. The establishment of the acyl-CoA ester Golden Gate toolkit allows future rapid testing of alternative pathway designs and the screening of homologous alternative enzymes that could result in improved pathway performance.

3.2 Yeast communication toolkit - YCTK

The aim of the YCTK project was to generate a toolkit that allows rapid engineering of multicellular networks in *S. cerevisiae*. To enable the implementation into an existing toolkit, we designed the YCTK to be fully compatible with the Golden Gate YTK of Lee *et al.* [71]. Initial comprehensive testing and characterization of the parts to be incorporated into the kit was vital for future successful utilization of the toolkit. By investigating the crosstalk between the sender (α-factors), receiver (Ste2 receptors), and barrier parts (Bar1 proteases), we gained new insights into Ste2 and Bar1 promiscuity towards α-factors. Together with the responder parts (α-factor-responsive promoters), the toolkit offers a coherent part selection for the engineering of multicellular communication systems in *S. cerevisiae*. First attempts of engineering multicellular networks showed limitations and possible bottlenecks that need to be addressed in the future.

3.2.1 *In silico* identification of α-factors

The *in silico* identification of the pre-pro-α-factor sequences from an initial set of 49 different species showed that the Kex2 motif was highly conserved in the different organisms. Even the pre-pro-α-factor seuqnce of *C. albicans*, the only species of our final set of species that does not belong to the family of *Saccharomycetaceae* but to the family of *Debaryomycetaceae/Metschnikowiaceae,* contained this motif [450]. Also, the Ste13 motif was conserved in most of the processed sequences. Notably, for *S. pombe* we identified the Kex2 motif but not the Ste13 motif, indicating that for the α-factor processing an alternative aminopeptidase might be required [218]. For the closely related species *A. aceri* and *A. gossypii* we could not identify the Kex2 or the Ste13 motif, suggesting that they evolved an alternative α-factor processing pathway. Interestingly, a conservation was not found for the secretion signaling sequence that is responsible for the translocation of the pre-pro-α-factors. Since the results of this project demonstrated the successful α-factor processing and subsequent secretion, we could assume that the translocation mechanism that recognizes the signaling sequence in *S. cerevisiae* can also recognize heterologous signaling sequences. When we compared the results for the *in silico* identification on a random basis with literature, we could validate our results [220,449]. Thus, we conclude that the α-factor processing is conserved within all our selected species and that the different *mfα1* genes can be heterologously expressed in *S. cerevisiae*. Also, we could report that the predicted processing was successfully performed in *S. cerevisiae* (chapter 2.2.5.2).

3.2.2 Growth of *MAT***a** and *MAT*α chassis strains for α-factor stimulation

The deletion of Far1 in the *MAT*α and *MAT***a** strain backgrounds led to strains that did not exhibit cell cycle arrest upon pheromone stimulation, as it was reported in literature [453]. However, pheromone-induced promoters could still be stimulated. Far1 is the main regulator of cell cycle arrest by inhibiting CDK [453]. With the deletion of Far1, we wanted to abolish the cell cycle arrest to overcome growth reduction but to still be able to use the mating MAPK signaling pathway and downstream regulated promoters for our toolkit. An alternative could have been to decouple the mating MAPK signaling pathway from downstream gene expression by deleting the global mating transcription factor Ste12. Different studies demonstrated the Ste12 deletion and its subsequent replacement with a different engineered transcription factor variant that bound synthetic promoters [220,382]. Since these systems remained limited to the different designs of the transcription

factors, they were not considered here. Interestingly, the *MAT*α stain with constitutive heterologously expressed Ste2 receptor, only exhibited short cell cycle arrest and quickly resumed growth. This phenomenon was previously described but has to our knowledge not been investigated in detail yet [204]. Therefore, we decided to utilize the *MAT***a** *far1Δ* strain background as chassis for the implementation of multicellular networks. However, to explore potential differences in the expression of pheromone-induced promoters, the expression of Ste2 receptor and α-factors, the *MAT*α as well as the *MAT***a** strain background was examined.

3.2.3 Sequence alignments

The sequence alignment of the α-factors, the Ste2 receptors, and the Bar1 protease gave use an indication of the functional expression in *S. cerevisiae* and served as correlation foundation to investigate the relationships of crosstalk and stimulation in more detail.

The alignment of the identified α-factors revealed that the N-terminus is fairly conserved with a WXW motif. Deletion of any of these amino acids has been reported to drastically reduce the bioactivity of the α-factors but only a minor reduction in receptor binding affinity to the receptor [490]. It was proposed that the N-terminus of the α-factor is responsible for the initiation of the signaling [491]. Also, the C-terminus of the majority of the α-factors exhibited a relative motif conservation. Because of a drastic reduction in the binding affinity of C-terminally mutated α-factors to the receptor, it was proposed that the C-terminus is responsible for binding to Ste2 [314]. We postulated based on this conservation and the reported proposed functionalities that the structure-function relationship is conserved in many of the identified α-factors.

The highest heterogeneity was found in the central residues of the α-factors. We could thus conclude that these residues are crucial for the specificity of the α-factors that can be validated by correlating crosstalk interactions with the α-factor sequences. It was proposed that these central residues are responsible for specific structural conformations and for the agonist efficacy [491]. For the α_{Ca}-factor, that does not obtain the previously described conserved N- and C-terminal sequence motives, it was shown that substitution of the central sevens residues resulted in a loss of function. These results indicated that also here, the central residues are essential [220].

To cover a variety of different sequence variants to hopefully obtain different characteristics and different crosstalk stimulation dynamics, we selected a set of 11 α-factors. These ranged from the α-factor originating from *C. albicans* that exhibits no common sequence homology to the remaining α-factors, to the α_{Lm}-factor lacking the otherwise conserved C-terminal sequence and the α_{Ec}-factor that has an extended unique central sequence, to the α-factor of *L. fermentati* that only consists of eleven amino acids and is thus the shortest identified α-factor (chapter 2.2.1.2).

Apart from the successful production of the pheromones in *S. cerevisiae*, also the Ste2 receptors have to be functionally expressed and to be incorporated into the membrane. The third cytoplasmic loop of the receptors was proposed to be essential to interact with the α subunit of the G protein and therefore to be important for the integration of the heterologously expressed receptors into the mating signaling pathway [242]. The alignment of the cognate receptors revealed high sequence conservation of the third cytoplasmic loop, suggesting functional coupling to the native Gα-protein. To conclude, we could validate the indication of the alignments by demonstrating the functional expression of the heterologous receptors and the downstream activation of the mating MAPK signaling pathway upon pheromone stimulation (chapter 2.2.5.3). The reduced

mating pathway activity of the $Ste2_{Ca}$- and $Ste2_{Ka\,a}$-expressing cells was unlikely due to inefficient signal transduction to the Gα subunit since similar sequence discrepancies were also found in other receptors with full activation of the mating signaling pathway. The seventh transmembrane domain was proposed to be vital for structural integrity as well as for conformational changes after pheromone stimulation. The corresponding alignment results indicated that the observed high conservation should result in functional heterologous receptor expression.

Besides the investigation of the potential crosstalk of the pheromones and receptors, we wanted to examine the pheromone recognition by the barrier proteases. The barrier protease Bar1 plays an important role in fungal mating as it was reported to increase the mating efficiency as well as it is partly responsible for the mating partner ratio sensing [209,310]. Only seven Bar1-like proteases were found in the databases for the selected species. All of them were annotated as aspartyl proteases (peptidase A1) with an identified N-terminal signaling peptide for the extracellular export. The sequence alignment indicated a conservation of two catalytic domains of the proposed barrier proteases, indicating functional activity. However, the test for functionality with the cognate pheromones showed that the proposed barrier protease of *L. thermotolerans* and *V. polyspora* did not exhibit considerable protease activities. Both Bar1 proteases exhibited in the sequence alignments uniqueness that might be responsible for their non-functional expression. The $Bar1_{Lt}$ contains a 56 amino acid long unique sequence that does not have any homology to any of the other proteases. The $Bar1_{Vp}$ is substantially shorter than the other proteases.

Assuming from the results of the alignment and the functionality assay, the proposed $Bar1_{Lt}$ and the $Bar1_{Vp}$ are unlikely barrier proteases and might have been inaccurately annotated. To validate this assumption, a proof of expression and secretion would be required. Nevertheless, the results of the remaining proteases indicated that the sequence alignment gave an indication of functional barrier protease activity and could thus be used in the future to screen for other barrier proteases within the *Saccharomycotina*. However, it is known that other families of *Archiascomycete* evolved alternative proteases acting as barrier proteases, for example, *S. pombe* uses the carboxypeptidase Sxa2 to degrade the α-factor homolog P-factor [492,493]. This convergent evolution of different proteases to function as barriers for the more hydrophilic pheromones indicates the evolutionary benefit of these proteases [298].

3.2.4 Evolutionary relationships of the selected species

To gain an overall understanding of the evolutionary relationships between the selected species in general, as well as more specifically between the α-factors, receptors, and barrier proteases, we generated different trees indicating the relationship of the species. We aimed to use the gained understanding of the evolutionary studies to assess correlations between observed crosstalk of the different pheromones, receptors, and barrier proteases with the evolutionary relation. The generated phylogenetic tree based on the likelihood analysis of the SSU rRNA of the selected yeast species is only partially conform with the evolutionary relationships of the species in a whole-genome alignment-based phylogenetic tree that included most of the selected species [450]. The relationship between *K. lactis* and *E. cymbalariae*, and *K. africana* and *K. naganishii*, coincides in both trees. However, for example the close relationship of *T. phaffii* and *V. polyspora* is not reflected in the SSU rRNA-based tree. We therefore conclude that the SSU rRNA tree can only serve as a first indication of the phylogenetic relationships between the species. *L. mirantina*, which was

first described in 2011, is thus mostly not part of phylogenetic studies [451]. The evolutionary relationships of *L. mirantina* to other *Lachancea,* including *L. fermentati* and *L. thermotolerans* has been investigated and revealed that *L. mirantina* belongs to a separate taxonomic group within the genus *Lachancea* [451]. These results were also reflected in our phylogenetic study since the *Lachanceas* are not forming a combined clade. In our analysis, *L. mirantina* was closer related to *K. lactis* than to the other *Lachancea* species. We can thus conclude, that overall it would be beneficial to use the whole-genome sequence of *L. mirantina* and incorporate it into a whole-genome phylogenetic tree for a more detailed understanding [450].
The phylogenetic tree based on the likelihood analysis of the mature α-factors remained inconclusive due to the short amino acid sequences. Therefore, we have to conclude that the tree could not be utilized to investigate the pheromone relationships in correlation to the crosstalk. The tree of the likelihood analysis of the pre-pro-α-factor sequence on the contrary reflected the relationships better. The *Lachancea* species formed one clade, which we did not find in our SSU rRNA-based tree but that coincides with the results of taxonomic investigations of *L. mirantina* [451]. Concluding, the pre-pro-α-factor based tree captured some of the phylogenetic relationships better than the SSU rRNA tree, at least for a clade of *Lachancea* in comparison to the whole-genome tree. However, the proposed closer a relationship between *T. phaffii* and *V. polyspora* was not reflected in the pre-pro-α-factor tree. The phylogenetic tree based on the likelihood analysis of the Ste2 receptors matched well the relationships in the whole-genome phylogenetic tree [450]. The Ste2 likelihood analysis enabled the investigation of the relationships of the receptors in correlation to the α-factor crosstalk. Also, the tree based on the barrier protease likelihood analysis reflects the basic structure of the whole-genome-based phylogenetic tree [450]. Interestingly, $Bar1_{Vp}$ and $Bar1_{Lt}$ that did not exhibit any protease activity in the functionality test, differed in their sequences from the others in the alignment. However, they fit the phylogenetic tree structure of the whole-genome tree. The previous conclusion that these annotated proteases might not be barrier protease should be further examined and validated as discussed.

3.2.5 Promoter characterization

To complete the toolkit, we added promoters as responder parts to the toolkit. It has been shown in several promoter characterization studies that the promoters behaved differently depending on the background strain as well as on the expressing gene, referred to as context-dependency [74,75]. Therefore, we wanted to thoroughly characterize especially the pheromone-inducible promoters under different conditions.

3.2.5.1 Inducible promoters

For our experiments, we also utilized the $CuSO_4$ inducible P_{CUP1} promoter that was already part of the YTK, and extended the kit by adding the doxycycline-inducible promoter P_{TETO7} to our toolkit [71,494]. However, the core of the promoter collection of the YCTK consists of pheromone-inducible promoters. Prior the implementation of the different inducible promoters into systems, we characterized them thoroughly. Since we utilized the P_{CUP1} promoter to drive the expression of the communication parts, we compared the P_{CUP1} expression profile with the one from the constitutive promoters utilized for the expression of these parts. The results of the experimental characterization of the inducible promoter P_{CUP1} exhibited that the basal expression of P_{CUP1} was lower

than the expression of the weakest reference promoter P_{PAB1}, and the maximal induction reached similar promoter strengths to P_{HHF1}. We could also see that the utilized terminator had a greater impact on the characteristics than the integration site, as it was reported in literature [495]. The dynamic range and the leakiness of the P_{CUP1} promoter was comparable to P_{TETO7}, however, saturation was not reached for the P_{TETO7} promoter. It could thus be possible that the dynamic range of P_{TETO7} is extended. The conclusion of these results is that both the P_{CUP1} and the P_{TET07} promoter can be utilized and implemented as functional and titratable promoters [71,494].

3.2.5.2 Pheromone-inducible promoters

The results of the characterization of the pheromone-inducible promoters exhibited that the promoter dynamics varied between the different strain backgrounds. Also, the selected promoters obtain different characteristics with regard to basal expression levels, maximal promoter strength, EC_{50}, and fold change. Thus, our characterization laid the foundation of the further use of these promoters in engineered systems.

We selected pheromone-inducible promoters based on RNA-Seq data that were available in our laboratory to get a first indication of the promoter activity. These data also allow the comparison of the results of our promoter characterization with the RNA-Seq data. However, it should be noted that the RNA-Seq data were generated using another strain background and also different pheromone concentrations and media conditions were utilized.

To determine the most suitable reporter gene for the pheromone-inducible promoter characterization, we first tested mRuby2, mTurquoise2, and Venus, that are available in the YTK collection [71]. We observed reduced fluorescence intensities due to incomplete maturation of the mRuby2 reporter protein, which were also previously reported in literature [71]. Concluding from the experiments of testing the promoter characteristics with different reporter genes, namely mRuby2, mTurquoise2, and Venus, Venus is the most suitable reporter for the promoter characterization using flow cytometry, hence we decided to continue using Venus. The only disadvantage of using Venus is the reduced brightness compared to mTurquoise2, which was not significant for us. The decisive parameter of Venus for us was the reduced maturation time in comparison to the other available reporter proteins [496]. Alternatively, mTurquoise2 would also be a suitable reporter.

Generally, the expression of a reporter gene is not only depending on the promoter strength and dynamics but also for instance on the utilized terminator (also called 3' untranslated region or 3' UTR) that influences the 3'-end processing, as well as the stability, and translational efficiency of the resulting mRNA. Therefore, the terminator region affects the expression of a gene of interest [495,497]. Thus, extending the available terminators in the Golden Gate toolkit could lead to an additional control layer for the expression of genes of interest. Also, it was reported that the untranslated 3' UTR region can be used to modulate the mRNA stability resulting in different noise levels of the expression [494]. To ensure comparability between the characterized constitutive and inducible promoters of the YTK, we utilized for our selected pheromone-inducible promoters the same T_{TDH1} terminator as well as the same chromosomal integration site [71]. Since the strain background and also the experimental setup slightly differed, a direct comparison with the characterizations of the promoters in the YTK is only limitedly possible. To facilitate the comparison of the pheromone-responsive promoters with the constitutive promoters of the YTK collection, we utilized three of them as benchmark promoters during our characterization experiments, namely, the

weak P_{REV1}, the medium-strength P_{RPL18B}, and the strongest promoter P_{THD3}. Since the expression strength of the *TDH3* promoter was substantially higher than of the α-factor-inducible promoters, we omitted P_{THD3}during the plotting of the results. The overall expression strengths of the constitutive benchmark promoters remained similar [71]. However, we noted that independent from the strain background, upon α-factor stimulation, an increase in fluorescence intensities of Venus was observed, creating the impression of pheromone induction of the constitutive promoters. It is unlikely though that for example the induction of the mating pathway led to increased DNA damage, which would be required to induce the expression of P_{REV1}. Also, an upregulation of the *RPL18B* promoter, which is driving the expression of the 60S ribosomal subunit, is unlikely upon pheromone stimulation and we thus conclude that the observed increase in fluorescence intensities of the constitutive promoters is an artifact [498,499]. The reason for the observed increase is most likely a result of an increase in cell volume and size due to pheromone stimulation, which was also indicated by the RNA levels of *REV1*, that did not show any increase upon α-factor induction (Figure 63). By normalizing to the cell volume or to the fluorescence intensities of an additional reporter, the artifact might be resolved and thus could result in an overall improved characterization.

The characterization of the pheromone-inducible promoters revealed that upon maximal α-factor induction, fluorescence intensities in the range of slightly above the medium reference promoter, P_{RPL18B} and slightly below the weakest reference promoter P_{REV1} were obtained. Interestingly, for most of the pheromone-responsive promoters, the results do not coincide with the RNA levels that we initially utilized for the selection of the promoters (Figure 63). We could not observe in any of the strain backgrounds higher fluorescence intensities from P_{PRM1} or P_{SST2} than P_{FUS1} like the RNA levels had indicated. Despite the usage of a different background strain and different α-factor induction concentrations, we did not expect such considerable differences. It is known that the RNA levels depend both on the promoter activity and on the transcript stability [500]. Thus, we conclude that our results indicated that the RNA levels did not reflect the promoter strength of the selected genes. However, it needs to be considered that we did not characterize the promoters in their native context, since the Ste2 receptor was reconstituted which might have altered the mating pathway response. Our characterization results showed that P_{FUS1} exhibited the highest maximal output levels as well as the greatest fold change. The lowest fold change for P_{FUS1} was measured in the *MAT*α strain background, in which the Ste2 receptor was expressed by P_{FUS1}, and thus already exhibited high basal expression levels. It was previously described that in case the Ste2 receptor is not expressed, the basal mating pathway activity is increased, explaining these results. For the remaining promoters, we also observed increased basal expression, with P_{SST2} constituting an exception. These results underlined the proposed explanation of increased basal pheromone-responsive promoter activity in the absence of the Ste2 receptor. Further, it might be possible that the mating pathway with this expression design took longer to reach full activity, which should be further investigated in more detail. To conclude, the positive feedback expression of the receptor did not lead to an improved fold change of the promoter dose-response. To give a final statement about the obtained EC_{50} values, additional biological replicates need to be tested as well as the range of α-factor concentrations should be increased, since the dose-response curve was not fully saturated for all promoters.

The weakest fold change and the weakest maximal output levels were measured for P_{DIG2} and P_{YPS1}. The *DIG2* promoter exhibited high basal expression levels in comparison to the maximal induction. Dig2 functions as a MAP kinase-responsive inhibitor with Kss1 to the central mating transcription factor Ste12 [501]. The low fold change and general low expression of the *DIG2* promoter might point out the supporting function of Dig2 to Dig1 in Ste12 inhibition. It was shown that deleting Dig1 led to an increase in the mating pathway activity compared to the wild type, while deletion of Dig2 seemed not have any effect [502]. The promoter of Yps1 displayed lower basal activity and exhibited a very long dynamic range, however full saturation was not obtained. The native function of Yps1 is not fully understood and different roles of the protease have been proposed, including the processing of the α-factor [503]. The protease was also thought to interact with Msb2 and activates it by cleaving an inhibitory domain, thus generating a filamentous growth phenotype [504]. It was hypothesized that Yps1 is also involved in the filamentous growth and it is assumed to also be involved in the shmooing phenotype upon pheromone stimulation. The P_{YPS1} showed a similar behavior as found for the RNA levels. We can conclude that P_{YPS1} has a long dynamic range and might be beneficial to control expression upon pheromone induction.
The promoter of Sst2 exhibited independent from the strain background the highest basal expression levels of all pheromone-induced promoters and had an about 10-fold increase upon maximal pheromone stimulation. The high basal expression of the *SST2* promoter could be indirectly explained by the fact that the GTPase-activating protein Sst2 serves as a principal regulator of the pheromone signaling pathway [505]. Basal expression of Sst2 is thus required to control the sensitivity of the mating pathway by regulating the desensitization and internalization of the Ste2 receptor [246]. The results of the promoter characterization of P_{SST2} that expresses Sst2, which initiates a negative feedback loop upon pheromone stimulation, are matching with the RNA levels. P_{MSG5} also exhibited increased leaky expression, however less prominent in comparison to P_{SST2}. Also, Msg5 acts as an antagonist to the MPAK singling pathway by dephosphorylating Fus3 and therefore repressing the activation of the transcription factor Ste12 that regulates the downstream expression of pheromone-induced genes [506,507]. To conclude, the high basal expression levels of P_{SST2} and partly of P_{MSG5} might serve as thresholds prior initiation of the mating MAPK signaling pathway.
Comparing the pheromone-inducible promoter activities in the *MAT*α *far1Δ* and the *MAT***a** *far1Δ* strain backgrounds, in which the Ste2 receptor was constitutively expressed, the promoters exhibited a wider dynamic range in the *MAT***a** strain background. We reported lower basal expression levels in the *MAT***a** strain background as well as increased maximal induction levels for all our selected pheromone-inducible promoters, with P_{YPS1} constituting an exception to this observation. Also, the fold change of the promoters was overall increased in the *MAT***a** compared to the *MAT*α strain background. We assumed that this might indicate additional effects that promote the Ste2 receptor stability in the *MAT***a** cells or the downstream signal transduction. It was reported that the expression of the receptor and the proteins that are involved in the MAPK signaling pathway can affect the expression profiles of pheromone-responsive promoters [382].
Apart from the α-factor dose-response of the promoters, the temporal response upon pheromone induction also indicates an important parameter for subsequent artificial network implementations. Independent from the strain background, all α-factor-inducible promoters started

responding to pheromone stimulus at the same time point. However, since we plotted the mean fluorescence intensities, we potentially lost a more detailed temporal resolution as some cells of the population might respond prematurely or delayed. It would be possible to examine the temporal resolution of a single cell using microscopy in combination with an adapted microfluidic device like a mother machine [508]. Despite, all promoters started responding at the same time after the pheromone stimulus, however, we observed varying time-dependent response dynamics. We can assume that all of the pheromone-induced promoters are directly or indirectly controlled by the transcription factor Ste12 and that the different temporal dynamics are affected by the promoter expression strength and the binding of the transcription factor.

We noted that for the timely response to α-factor in the *MAT*α cell background, a decrease in the fluorescence output could be observed after four hours. As it was already indicated by the growth results of the different strain backgrounds upon pheromone induction, the *MAT*α cells resumed growth after a short cell cycle arrest due to response to α-factor in the media. We can conclude based on the time response results of the *MAT*α cells that not only the cell cycle arrest was released but that also the MAPK singling pathway was no longer active after 4 hours of pheromone induction, resulting in a decrease in fluorescence intensities of the output reporter driven by pheromone-responsive promoters. This phenomenon should be further investigated. Overall, the maximal promoter activity was obtained four hours post pheromone induction.

Altogether, the presented results were only a first indication and further validation of the obtained results is required. Additional biological replicates, as well as improved normalization, as previously discussed, should be tested to draw final conclusions.

To conclude, the characterization of the pheromone-inducible promoters gave important insights into the expression dynamics of the promoters in the different strain backgrounds. Correlating the observed promoter dynamics to the native functions of the corresponding proteins gave helpful indications to predict the behavior of the promoters in engineered systems. The time courses revealed that the maximal promoter activity of the selected pheromone-inducible promoters was reached 4 hours after initial stimulation with the α-factor. Further, we can conclude that in *MAT*α cells the MAPK signaling pathway activity was reduced after 4 hours, indicating that the cells were no longer stimulated by the α-factor.

3.2.6 Sender part characterization – α-factor

Based on the *in silico* identification, we postulated that the selected α-factors should be expressed and that the processing of the pre-pro-α-factors should be successful. To validate the *in silico* identification, we tested the expression, processing, and secretion of the α-factors in the *MAT*α strain background and examined the pheromone accumulation in the media supernatant. All of the selected α-factors, except for the α_{Ka}-factor and α_{Vp}-factor, were identified in the supernatant using LC-MS/MS. We can, therefore, conclude that most of the heterologously expressed α-factors can be expressed, processed, and successfully secreted. Another approach based on the generation of chimeric pre-pro-α-factors has also shown the successful heterologous expression of α-factors in *S. cerevisiae* [220]. The two α-factors we could not identify using LC-MS/MS might have been difficult to detect due, for example, insufficient ionization required for detection. However, the functional expression of the α_{Ka}-factor and α_{Vp}-factor was verified in coculture by the stimulation of the cognate Ste2 receptor and the subsequent activation of the mating MAPK signaling

pathway. In order to quantify the expression of the α-factors, we generated a standard curve for the different α-factors using synthetic peptides. The computed concentrations of the α-factors that were further normalized to the cell density were unexpected. We anticipated similar concentrations for the different α-factors, as they were expressed from the same promoter. However, the concentrations varied widely between 8 µM/OD and 118 µM/OD for the different α-factor producing strains. No correlation could be identified between the number of encoded mature α-factors per *mfα1* gene or the different α-factor variants.
To conclude, the obtained concentrations of produced α-factors should be considered conditionally and need the be further validated. One other approach of obtaining the produced α-factor concentrations could be to use the supernatant with produced α-factor and adding Ste2-expressing cells to it. The resulting mating response could then be correlated to the dose-response curve of the mating response obtained with synthetic α-factor. Further, the utilized LC-MS/MS-based quantification method could be optimized and validated.

3.2.7 Receiver part characterization - Ste2 receptor expression

The validation of functional expression and the investigation of the promiscuity of the Ste2 receptors provide the basis for the future use of the receiver parts in engineered systems. We gained novel insights into the promiscuity and the binding affinities towards non-cognate α-factors that can be compared to the proposed α-factor-Ste2 receptor interaction model [509,510]. Overall, our selection of parts contains Ste2 receptors that are very specific and only recognize cognate α-factor, as well as very promiscuous ones, recognizing almost all α-factors. Taken together, we obtained a diverse set of Ste2 receptors and α-factors allowing the establishment of numerous different artificial networks. As already briefly mentioned in the previous chapter, apart from the validation of the production of the heterologous pheromones, we tested their successful production by stimulating their cognate Ste2 receptors. Therefore, we cocultured α-factor-producing and Ste2 receptor-expressing strains. From the obtained experimental results, we can conclude that the heterologous receptors could be functionally expressed in the *MAT*α strain background and were functionally connected to the natural mating MAPK signaling pathway. This was already indicated by our alignment studies since the third cytoplasmic loop as well as the seventh transmembrane region were conserved. Some of the selected Ste2 receptors had been previously heterologously expressed in *S. cerevisiae* and were shown to be functional [158,220,449]. Our results are, therefore, in line with previously reported findings. However, the results also exhibited that the stimulation of the receptors did not always result in maximal stimulation of the mating pathway, indicated by the expression levels of the α-factor inducible P_{FUS1} promoter. Only for the α_{Ca}-factor, we obtained quantitative results of the pheromone production, that revealed lower α-factor production levels and therefore subsequently lower receptor stimulation. The dose-responses of the receptors was separately investigated by stimulation with standardized synthesized α-factors (Figure 101).
To study the promiscuity of the Ste2 receptors and the resulting crosstalk, we tested the stimulation of all receptors by all our selected pheromones. The results showed that the $Ste2_{Ca}$ as well as $Ste2_{Ka}$ could not be stimulated by non-cognate α-factors. The $Ste2_{Ca}$ and the α_{Ca}-factor showed no visible homologies to any of the other selected species, which was also reflected by the evolutionary distance of *C. albicans* to the other species.

Interestingly, the likelihood analysis of $Ste2_{Ka}$ indicated a closer relationship to the other sequences and especially to *K. naganishii* that was also reflected in the overall closer relationship of *K. africana* to the other selected species. Also, the α_{Ka}-factor sequence contains several of the key motives that are also found in the other α-factors like the N-terminal WHWL and the C-terminal GQP motif. However, none of the other α-factors could stimulate $Ste2_{Ka}$. We can, therefore, conclude that based on these results, the $Ste2_{Ka}$ receptor evolved a high substrate specificity. All other remaining Ste2 receptors exhibited crosstalk to other α-factors apart from the cognate pheromone. $Ste2_{Ca}$, $Ste2_{Kl}$, $Ste2_{Sc}$, and $Ste2_{Vp}$, which were previously examined, exhibited crosstalk with the respective α-factors similar to our experimental results [220]. Overall, no striking correlation between the amino acid sequences of the α-factors and receptor crosstalk could be determined. Thus, we conclude that Ste2 promiscuity towards α-factors could not be derived from the amino acid sequences of the α-factors. In order to determine characteristics of the α-factors and Ste2 receptors that are enabling crosstalk, further analyses would be required. It was previously postulated that the C-terminal region of the α-factor could be responsible for binding to the receptor, while the N-terminal region promotes the conformational change, and therefore, signal propagation [314,490,491]. Peptide polarity or secondary structures of the α-factors could also play a role in non-cognate pheromone binding to the Ste2 receptors. However, due to the fact that the interaction between the α-factor and the Ste2 receptor is not fully understood yet, mostly because no crystal structure of the Ste2 receptor was obtained so far, drawing a conclusion remains difficult. Even though a working model of the interaction of the α-factor with the Ste2 receptor for *S. cerevisiae* had been postulated this does not explain the observed receptor promiscuity, as the interacting α-factor residues 1, 3, 10 and 13 are also conserved in other α-factors that did not stimulate a receptor [509,510].

One other interesting finding from the crosstalk experiment was for instance that the shortest α-factor, α_{Lm}-factor, only strongly stimulated its cognate receptor while a rather weak stimulation was observed for only one other receptor, $Ste2_{Ec}$. Contrary, $Ste2_{Lm}$ recognized a wide range of different α-factors. A similar trend was also observed for the α_{Ec}-factor and the $Ste2_{Ec}$. Notably, a coherence between pheromone and receptor crosstalk could be reported, species for which the receptor exhibited high promiscuity towards non-cognate α-factors, the α-factors tended to stimulate only a low number of non-cognate receptors.

Using the likelihood analysis of the Ste2 receptors, we were able to examine the correlations between the Ste2 homologies and the observed crosstalk. Apart from $Ste2_{Ca}$, all other receptors are overall grouped in two clades. Within the first clade, consisting of *K. lactis*, *E. cymbalariae*, and the members of the *Lachancea* family, we could not identify any correlation between the receptor relationships and crosstalk. Interestingly, within the *Lachancea* family, the closely related Ste2 receptors of *L. fermentati* and *L. thermotolerans* exhibited promiscuity towards the other α-factors. The receptor of *L. mirantina* could not be stimulated by α_{Lm}-factor or α_{Lt}-factor. Also, α_{Lm}-factor did not stimulate the $Ste2_{Lf}$ and $Ste2_{Lt}$. However, towards other α-factors, the receptors were similarly promiscuous, like other Ste2 receptors. It could be assumed that the insulation of the $Ste2_{Lm}$ receptor from other α-factors of the *Lachancea* family promoted the clade separation of *L. mirantina* within the *Lachancea* family that was described in literature [451]. For, the second clade of the Ste2

likelihood tree, consisting of *T. phaffii*, *V.polyspora*, *S. cerevisiae*, and the members of the *Kazachstania* family, we identified a crosstalk pattern. The trend was that their receptors tended to be better stimulated by the α-factors of the same clade members and thus were overall stimulated by similar α-factors. To conclude, at least for the members of the second Ste2 receptor clade, a correlation between receptor relationship and observed crosstalk could be drawn. Overall, the likelihood analysis of the Ste2 receptors reflected the phylogenetic relationships found in the SSU rRNA as well as the whole-genome-based phylogenetic tree well [450]. Therefore, the discussed correlations of the Ste2 relationships also constitute the phylogenetic relationships of the species.
After the initial investigation of the promiscuity of the heterologously expressed Ste2 receptors in *MAT*α cells towards α-factors, we further wanted to examine the dose-response of the receptors to synthetic α-factors. Therefore, we compared the activation of the mating MAPK signaling pathway, by monitoring Venus expression from the pheromone-induced P_{FUS1} promoter. We reported that the different Ste2 receptors exhibited different dose-responses when stimulated with their cognate α-factors. The different dynamics might have been a result from insufficient expression, improper folding, false incorporation into the membrane, or reduced signal transduction to the native yeast G protein. However, the high sequence homologies of the most crucial Ste2 domains indicated that the listed bottlenecks should not have been the main reasons for the different response dynamics. However, this hypothesis remains to be validated. Only in higher α-factor concentrations, the binding leads to the required conformational change to activate the signal transduction to the mating MAPK signaling pathway [243–245]. We thus conclude that the different Ste2 receptors show different binding affinities to the cognate α-factors.

We further tested the sensitivity of the Ste2 receptors towards non-cognate α-factors. We found that promiscuous Ste2 receptors displayed various response dynamics to the different α-factors. For some of the selected Ste2 receptors, the dose-responses have already been reported previously and match our findings [220]. Apart from the dose-responses of the Ste2 receptors to the different α-factors, we also examined the crosstalk pattern for stimulation with standard synthetic pheromone. We found similar general trends in the crosstalk patterns between the coculture and the dose-response experiment (Figure 134). Interestingly, in some cases, we observed less crosstalk for receptors when stimulated with the standard synthetic pheromone than for the experiment when the pheromone was heterologously expressed in a second strain. We thus assumed that this might indicate that other α-factor variants that are produced from the *mfα1* genes led to different Ste2 receptor crosstalk results since the synthetic α-factors were synthesized according to one mature α-factor variant (

Appendix Table 2).
Overall, we found that the selected Ste2 receptors were functionally expressed, which validated the *in silico* analysis of the third cytoplasmic loop and the seventh transmembrane domain. Interestingly, we found that all selected receptors, with the exception of $Ste2_{Ca}$ and $Ste2_{Ka}$, were promiscuous towards non-cognate α-factors. This finding was unexpected, since stimulation by non-cognate α-factors could lead to a fitness disadvantage, by exhibiting the mating phenotype without successful mating, even though bastardization of yeast strains has previously been reported [511]. One hypothesis could be that species with very high receptor promiscuity, like *E. cymbalariae,*

are domestic in habitats where none of the other selected fungi are found, therefore the evolutionary pressure for high substrate specificity was not required. An alternative hypothesis is that in species with high Ste2 receptor promiscuity, additional parameters apart from the α-factor are required for mating MAPK signaling pathway activation. For example, in *S. pombe*, mating is only initiated when starvation conditions prevail [512].

The investigation and characterization of the different Ste2 receptors was vital for the further use of them in the YCTK. We can conclude that the different receptor properties, like high promiscuity towards α-factors, or for $Ste2_{Ca}$ and $Ste2_{Ka}$, high specificity, allow a versatile utilization and implementation into different multicellular networks and makes the toolkit parts multifarious. Further, the different dose-response dynamics of the Ste2 receptors could be employed for the fine-tuning within multicellular networks. A summary of the crosstalk and dose-response characterization was compiled in Figure 134.

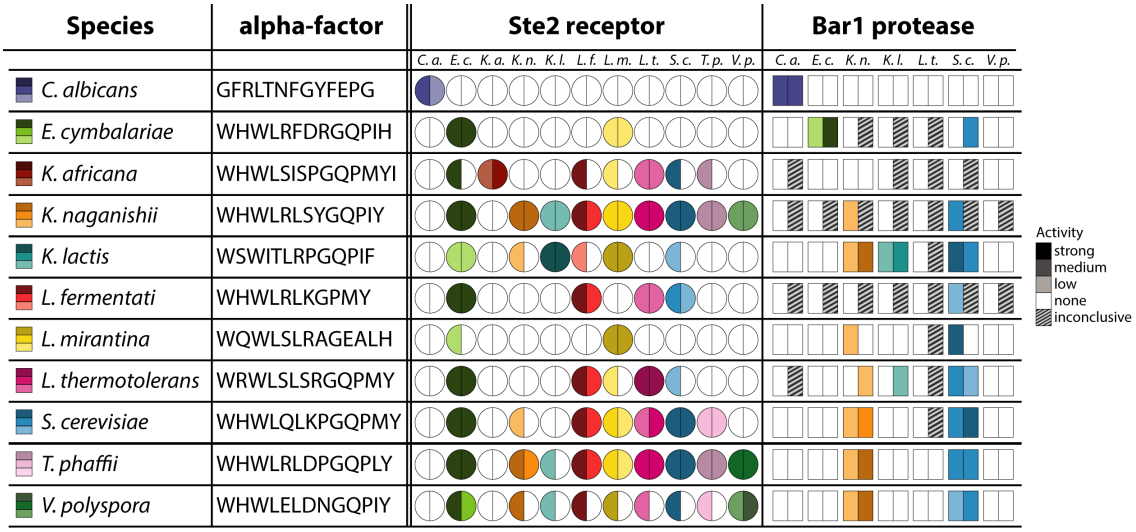

Figure 134: Overview of the promiscuity studies of the Ste2 receptors and Bar1 proteases. The circles represent the Ste2 characterization. The left half displays the results of the Ste2 crosstalk experiments in the *MAT*α background strain cocultivated with an α-factor producing strain (Figure 98) and the right half the results of the *MAT***a** background strain stimulated with synthetic α-factor (Figure 102). Each color represents one species. The color intensity indicates the measured activity of the mating pathway (none, low, medium, strong). The squares represent the Bar1 characterization. The left half of square shows the results of the barrier protease activity of the initial mating pathway reduction experiment preformed in *MAT*α strain background (Figure 105). The right half shows the results of the direct proteomics-based barrier protease activity assay. The color intensity indicates the measured activity of the barrier protease on an α-factor (inconclusive, none, low, medium, strong) (Figure 106).

3.2.8 Barrier part characterization - Bar1

Similar to the characterization of the receiver parts, the characterization and investigation of the promiscuity towards α-factors of the barrier parts, were fundamental for their future use in engineered systems. The examination of the promiscuity of the Bar1 protease was to our knowledge the largest study of its kind and provides additional data for the proposed coevolution of receptors and proteases. We identified α-factor-specific as well as α-factor-promiscuous Bar1 proteases. We could confirm the previously mentioned coevolution hypothesis for some of our barrier proteases but we also found that the hypothesis is not universally applicable.

To complete the toolkit, we included Bar1 barrier proteases that we expressed and characterized to make them accessible for the implementation into engineered multicellular networks. As previously highlighted, we identified seven annotated barrier proteases for the selected species. It is likely that also the other species possess Bar1-like proteases that have not been annotated yet, since it was shown that these proteases improve the mating successes [310]. To verify functional expression of the barrier proteases, we tested their activity on cognate α-factors by indirectly monitoring, if a reduction of the mating signaling pathway activity in the cognate Ste2-expressing strains was observed. The results showed that five out of seven Bar1 barrier proteases were functionally expressed and secreted. No activity of the $Bar1_{Vp}$ and $Bar1_{Lt}$ was found using this coculture experimental setup (chapter 2.2.5.4). It is possible that the annotated proteases were not acting as α-factor proteases or that the expression remained unsuccessful, which could be tested by isolating the protein from the media or by altering the expression conditions.

Similar to the studies of the promiscuity of the Ste2 receptors, we aimed to investigate the promiscuity of the barrier proteases towards different α-factors in coculture. Interestingly, we found that the barrier proteases of *C. albicans*, *E. cymbalariae*, and *K. lactis* exhibited only substrate specificity towards their cognate α-factors. None of the tested Bar1 barrier proteases showed sufficient activity on the α_{Ka}-factor. The barrier proteases of *K. naganishii* and *S. cerevisiae* were comparably promiscuous towards different α-factors. Similar experiments were previously performed to investigate, whether $Bar1_{Sc}$ exhibited promiscuity towards the α_{Ca}-factor and the same results were obtained that $Bar1_{Sc}$ cannot cleave the α_{Ca}-factor [449].

To assess, whether the amino acid sequences of the α-factors indicate barrier protease promiscuity, we compared the activity patterns with the alignment of the α-factors. No evident correlations were identified, and we can thus conclude that the promiscuity of the Bar1s does not correlate with the amino acid sequence of the selected α-factors. In literature, the importance of the C-terminal region of the α-factors for the recognition and subsequent degradation by the barrier proteases was proposed, which could not be validated by our experiments [298].

Further, we correlated the results of the likelihood analysis of the Bar1 proteases with the promiscuity patterns. We can conclude, that $Bar1_{Sc}$ and $Bar1_{Kn}$ that were indicated to be closer related to each other, exhibited a broader substrate promiscuity, while the barrier proteases of *K. lactis* and *E. cymbalariae* that form a separate clade, have a higher substrate specificity. The relationship of the barrier proteases was also in line with the relationships of the species found in the SSU rRNA, as well as the whole-genome phylogenetic tree [450].

It was postulated that the Ste2 receptors and the Bar1 barrier proteases recognize similar or overlapping regions of the α-factors which indicates a coevolution of the two proteins [298]. Our results for *S. cerevisiae*, *K. naganishii*, and *K. lactis* supported this hypothesis, since the Ste2 receptors and barrier proteases recognized similar α-factors. The α_{Lm}-factor showed an exception for *S. cerevisiae* and *K. naganishii*, since we found Bar1 activity but no receptor stimulation. Contradicting the proposed model of coevolution of Ste2 and Bar1 was the protease activity of *E. cymbalariae*. The $Bar1_{Ec}$ protease showed high specificity towards its cognate α-factor, while $Ste2_{Ec}$ was the most promiscuous receptor of our study. We conclude, that the proposed coevolution of Ste2 receptors and Bar1 proteases to recognize the same α-factors could only be partly validated by our results, since it did not apply to all Ste2-Bar1 pairs that we had examined. Interestingly, the α-

factors originating from the same species as the most promiscuous Bar1s were able to stimulate the most Ste2 receptors.

To obtain a more comprehensive understanding of the barrier protease activity, we investigated the protease cleavage sites of the α-factors by the different barrier proteases using LC-MS/MS. The general pattern of protease activities towards cognate and non-cognate α-factors correlated with the results of the Bar1-α-factor-Ste2 crosstalk experiment but also revealed for some examples previously lacking activity. For instance, the initial experiment did not indicate $Bar1_{Sc}$ activity on the α_{Ec}-factor, as well as $Bar1_{Kl}$ did not show visible activity on the α_{Lt}-factor, as it was found in the cleavage experiment. Certainly, some of the results remained inconclusive, which indicates that the method requires further optimization. One limitation was for example that smaller peptide fragments could not be detected for any of the pheromones. The obtained cleavage pattern for $Bar1_{Ca}$ as well as $Bar1_{Sc}$ for their cognate α-factors match previously described findings [298,513]. Interestingly, despite of the proteases, the cleaved fragments of an α-factor were similar, indicating that the different barrier proteases cleaved one α-factor at the same site . Based on the experimental results we can conclude that the selected proteases that showed promiscuity towards non-cognate α-factors, cleaved the α-factor alike, obtaining the same peptide fragments. It would further be possible to investigate the recognition sites of the barrier proteases by di-alanine substitution scanning of the α-factors, as it was performed for the $Bar1_{Ca}$ [298]. In addition, with an improved analytic method as well as by using purified proteases it would be possible to investigate the kinetics of the protease activity. Also, an overall biochemical characterization of all functional barrier proteases, to determine optimal temperature and pH conditions could pursue the hypothesis that all barrier proteases display unusual properties for aspartyl proteases, for example their activity optimum at nearly neural pH conditions [295,298,311,514].

Taken together these characterizations of barrier proteases were to our knowledge the most comprehensive studies of Bar1 promiscuity and activity so far. Our analysis partly validated the proposed coevolution model of Ste2 and Bar1 and applied to a subset of our Bar1 proteases. We can conclude that our results indicated unique cleavage patterns of α-factors by the different Bar1 proteases. Overall, the different properties and especially specificities of barrier protease for α-factors provide versatile parts to be used to alleviate signals and thus constitute an essential design element for multicellular networks. As summary of the Bar1 characterization by cocultivation and LC-MS/MS, as well as the findings for the Ste2 receptor promiscuity was established in Figure 134.

3.2.9 Tuning of sender, receiver, and barrier parts

The results of the tuning experiments of the sender, receiver, and barrier parts showed that by altering the expression of these, the signaling response and therefore subsequently the behavior in the multicellular system can be altered. This is a cornerstone for predictable dynamics in multicellular networks.

Apart from the importance of characterizing the crosstalk between the parts of the toolkit, also the investigation of the tunability of the parts was essential. Increased expression of one part could affect for example a network interaction. To test the tunability, we used the sender, receiver and barrier parts originating from *S. cerevisiae* and expressed them from the $CuSO_4$-inducible P_{CUP1}

promoter. As presumed, a stronger expression of the *mfa1* gene resulted subsequently in increased mating pathway activity in the strain expressing the Ste2 receptor. The maximal expression strength of the P_{CUP1} promoter was reported to be more than two times weaker than the P_{PGK1} promoter that we used during the crosstalk experiments for the *mfa1* gene expression, which we also confirmed with our experiments [71]. We can conclude that even for maximal expression conditions we did not reach saturated stimulation of the Ste2 receptor. In order to be able to express the *mfa1* gene even stronger, an inducible promoter with a larger dynamic range and maximal induction levels should be tested to investigate, whether with increased expression strength saturated stimulation levels of the Ste2 receptor can be reached. Nevertheless, also with the P_{CUP1} promoter, upregulation of the α-factor expression led to an increase of the mating signaling pathway activity in the Ste2-expressing cells. That allows an additional level of control for the engineering of multicellular systems.

For tuned $Ste2_{Sc}$ receptor expression, we additionally examined how the different expression levels responded to different concentrations of α-factor. Depending on the $Ste2_{Sc}$ expression levels, the maximally reached stimulation level differed. We conclude that weaker expression of the receptor resulted in lower mating pathway activity. Based on these results, we postulate that in our case the receptor can be the limiting factor for the mating activity. Different than reported in literature, we did not observe a correlation between the receptor expression levels and the sensitivity towards the α-factor [382]. This incoherence might be explained by the general low dynamic range and maximal induction levels of the P_{CUP1} promoter. We can conclude that tuning of the $Ste2_{Sc}$ receptor expression was achieved and that by increasing the Ste2 receptor expression, an enhanced activity of the mating pathway, without an increase of the basal activity was obtained. However, it might be beneficial to further investigate, if a promoter with a greater tunable range and stronger maximal induction levels, would result to the previously reported change of sensitivity [382].

Also, we tested the tunability of the barrier proteases Bar1. In case of the Bar1 proteases, direct detection of the activity remained challenging. Therefore, we tested the activity in a coculture with a strain that constitutively expressed the Ste2 receptor with addition of different concentrations of synthetic α-factor. Reduced receptor stimulation indicated higher barrier protease activity since the α-factor was cleaved. Derived from the experimental results we can conclude that increased expression of the barrier protease Bar1 led to reduced receptor stimulation. Also, for the barrier protease we could change the response dynamics resulting in altered degradation of the α-factor, which could be used as a design feature in engineered networks. However, we also noted that even under maximal expression conditions, that barrier protease was not able to degrade all α-factor, leading to minimal induction levels of the P_{FUS1} promoter in the receiver strain, indicating Ste2 stimulation.

Taken together we can conclude, that expression of the sender (α-factors), receiver (Ste2 receptors), and barrier parts (Bar1 proteases) was tunable. This constitutes an elementary feature for the establishment of artificial multicellular networks. We determined these attributes for the parts originating from *S. cerevisiae* and it might thus be beneficial to confirm the results for the remaining parts from the other selected species and possibly even over a larger dynamic range.

3.2.10 Utilization of YCTK parts for the construction of multicellular networks

The aim of the characterization of the parts of the YCTK was to subsequently utilize the toolkit for the engineering of multicellular networks that function for instance as self-organized logic population networks or as multicellular response networks.

3.2.10.1 Logic population networks

With the implementation of logic population networks in *S. cerevisiae* we showed that the YCTK can be utilized to construct multicellular networks and we proved that the signal transmission design motif can be expanded and utilized for the design of more complex multicellular systems like AND and OR logic population networks. The self-stimulation network motif remains to be proven.

We wanted to use the YCTK to construct populations that constitute Boolean logic gates. It was previously shown that the α-factors, Ste2 receptor, as well as Bar1 proteases, allow the wiring of cells. Thus, inducer signal propagating that promotes the expression of an α-factor to stimulate receiver cells can be achieved [158]. Differently from previously established logic gates, in our case, the population composition itself constituted the logics, meaning that for example for an AND logic population network, only when both sender populations are part of a coculture, the receiver population should be stimulated. Thus, no external input signal is required but the population composition itself functions as the signal. Using this concept, we constructed logic population networks displaying Boolean logic gate functions, including buffer, inverter, OR, NOR, AND, NAND, XOR, and XNOR population networks. Since our toolkit provides a large number of parts, it would be possible to extend these systems, for instances by establishing sequences of the different population networks.

The results of the buffer population system demonstrated that an α-factor can be used as a wiring molecule for information propagation. We showed that the receiver population reflected the population composition, meaning only in the presence of the sender population, an output signal was transmitted and an output was observed in the receiver cells. When taking the results of the tunability experiment into account, by tuning the expression strength of the α-factor production and the Ste2 receptor expression, we could further modulate the receiver cell's response and set different thresholds. The design motif can be expanded to other logic population networks. To conclude, simple signal transduction in form of an α-factor from a sender population to a receiver population, constituting a buffer network, was achieved.

Employing previously discussed receptor promiscuity, we successfully implemented an OR-like population network. The receiver cells responded to either or both α-factors produced by the two sender cell populations constituted by two buffer motifs. As previously mentioned, also here it could be envisioned to add additional population networks to allow more complex and successive computations. Apart from the implementation into the OR population network, the basic buffer design motif also was used to engineer an AND population network. The results showed that the receiver cells only fully responded in case of both sender populations were part of the coculture. We can conclude that using our population network approach, an AND design motif was established and can thus be further used to engineer even more complex multicellular networks. However, it should be noted that using the current design, we did not obtain a digital response of the receiver cells, most likely due to leaky α-factor production of the sender strains.

The implemented *FUS1* promoter exhibited overall comparatively low leakiness in relation to the maximal expression levels. However, the YCTK also contains alternative promoters that exhibit even further reduced leakiness. Overall, it could be beneficial to adjust the expression of the utilized parts to obtain an optimal system's behavior. In addition, the implementation of recently published approaches of modulating different mating pathway components could be promising. It was shown that by changing the expression of the Ste2 receptor and the associated G proteins, the response of the mating MAPK signaling pathway could be modulated resulting in reduced sensitivity and a more stepwise dose-response [382]. Further, it would be possible to adjust the expression of the output signal by implementing an additional genetic network as a secondary layer to the mating response. One possibility could be to use a pheromone-inducible promoter to express a transcription factor that subsequently regulates the expression of the output signal. This would set an additional threshold for the expression of the output signal. Additionally, expression of the $Bar1_{Kn}$ could reduce the basal expression levels of the α_{Lm}-factor, which was utilized in the current design.

To implement an inverter, we developed a design based on self-stimulation of the receiver cell population, that could be suppressed in case the sender population was part of the coculture, which expressed a barrier protease. From the results we obtained, we conclude that the self-stimulation design motif and its blocking by a barrier protease did not result in the anticipated dynamics.

Hitherto we could not determine, whether the self-stimulation or the signal repression was the limiting factor. The implementation of a self-stimulating positive feedback loop had been previously shown to be functional. However, the functionality of the feedback was depending on the expression strength of the feedback components (α-factor, Ste2 receptor), as well as the cell density [378]. Concluding from our results and the literature findings, an improvement of the system is required but feasible. To identify suitable expression conditions, titrating the expression of the α-factor as well as the Ste2 receptor using inducible promoters would be auspicious. Further, it was discussed in literature that balanced expression strength of the receptor and the α-factor can lead to self- or neighbor-cell stimulation [378]. One reason why we did not obtain our anticipated results could also have been that locally higher α-factor concentrations in close cell proximity resulted in direct stimulation of the receptor and thus the barrier protease could not efficiently suppress the α-factor signal. Therefore, it might be promising to establish conditions enabling populational self-stimulation (neighbor-stimulation) rather than cellular self-stimulation. As mentioned, also the signal repression motif might require further improvement. In our tunability experiments, even for maximal induction, the barrier protease was not able to prevent all α-factors from stimulating the Ste2 receptor, resulting in basal induction levels. In our design, the protease was expressed from the strongest available promoter of the YTK collection. However, we did not obtain the desired response. To ensure full repression of the signal, it could be beneficial to additionally implement an antagonist to the α-factor. Identified α -factor antagonists have been shown to exhibit competing binding affinities to the Ste2 receptor without activating the downstream mating MAPK signaling pathway [491]. However, prior implementation it should be examined, whether the antagonist can also be bound by the Bar1 and would thus reduce the activity of protease on the α-factor. Overall, we need to conclude that the establishment of a population

network-based inverter requires further optimization and identification of the optimal expression conditions. Since the self-stimulation was also utilized in other networks, also for the NOR, NAND, and XNOR population networks we did not obtain functional systems. Even though we utilized stronger promoters for the expression of α-factors and Ste2 receptors in these networks, the increased expression did not result in a functional system. This highlighted once more the necessity of optimizing they system, for example by titrating gene expression, high throughput circuit design, and subsequent testing.

The design concept of the XOR gate contained an additional design motif that has not been further analyzed yet. Here, the barrier protease Bar1 was not suppressing the signal of a self-stimulating feedback loop but rather blocking the α-factor signal from the respective other sender population. Our results indicated that the design motif should generally be functional. However, the multicellular XOR network did not exhibit the desired features, as well as a low fold change of the output signal. For this particular design, we weakly expressed the α-factors to ensure full signal repression by barrier protease, which subsequently led to low stimulation of the $Ste2_{Ec}$ receptor and therefore P_{FUS1}-mediated reporter expression in the receiver population. To obtain improved functionality, exchange of the promoters would be required.

Overall, we showed that the YCTK collection can be used to the build and implement population logic gate-like networks. Also, we can conclude that the necessary optimization of our designs requires multiparameter approaches. It had been shown for the engineering of other multicellular systems that mathematical models can provide helpful guidance for the improvement of these networks [377]. Therefore, using experimentally determined and previously described paraments in a mathematical model could facilitate the optimization of our logic population networks.

3.2.10.2 Multicellular response networks

To obtain a signaling cascade as well as an amplifier, we constructed these inducer-dependent multicellular networks using the parts of the YCTK. For both network architectures, we did not obtain results yet confirming their functionality. The limitation of these networks was the usage of the inducer galactose, which requires cultivation in glucose-free media. Since alternative carbon sources to galactose and glucose could not be utilized due to the genetics of the background strain, further improvement of the networks is required.

The engineering of the multicellular amplifier response network was previously proposed and partly experimentally established [379]. We designed a sensor cell population that can respond with specific α-factor expression to three different input signals. The specific α-factors in turn induce the expression of the same α-factor in amplification receiver cells, resulting in a signal amplification. Our experimental results indicated that the designed multicellular amplifier response network did not exhibit the anticipated output. Even in absence of any external inducers we observed a comparably strong expression of the output signal. This led to the conclusion that the limitation of the network resulted from the leakiness of the inducible promoters of the sender population but possibly also from a leaky expression of the feedback loop. Additionally, the genetic constraints of the strain limited simple testing, since for the different inducer conditions different carbon sources had to be utilized, as previously mentioned. To determine the dynamics, the network should be taken apart and each population and component should be tested individually. We previously discussed multidimensional parameter optimization of self-stimulating

positive feedback loops that also apply to this response network [378]. Besides the examination of the network components, a promoter titration approach to identify optimal expression conditions could be useful.

Next, we implemented a multicellular cascade. The experimental validation that multicellular cascade networks can be established in *S. cerevisiae* had been previously shown, thus was a suitable test system to be built from YCTK collection parts [220]. Each cascade node acts as an inducer-dependent AND gate. Only upon an α-factor signal of the previous node and an external inducer, the signal should be further transmitted to the next node. Our results indicated that the system did not exhibit the anticipated characteristics. To identify, which node of the cascade was the limiting factor, further testing would be required. We could assume that for one or more of the nodes the inducer levels were insufficient to propagate the signal, resulting in the collapse of the multicellular response network. As for the amplifier cascade, the cells were cultured both in glucose and galactose-containing media, which makes overall comparison difficult. While a basal leaky expression was observed, no difference could be detected upon addition of all inducers. Generally, as previously mentioned, in case the Ste2 receptor is not expressed, the basal activity of mating MAPK signaling pathway is increased, resulting in leaky expression of the *mfa1* gene. This leaky expression can lead to unintended signal propagation and should be considered during design improvement.

To conclude, so far, we did not obtain a functional signaling cascade using α-factor-based communication networks. Further optimization is required and several parameters need to be examined to obtain a robust and functional cascade. Nevertheless, our design laid a foundation to successfully establish multicellular signaling networks, that can be further adapted.

Taken together, even though both the amplifier and the cascade did not exhibit the intended features, obtaining a functional system after careful redesign is feasible.

3.2.11 Concluding remarks and outlook

During this study, we compiled and characterized a comprehensive Golden Gate-compatible yeast communication toolkit, that aims to foster and facilitate the engineering of multicellular networks using the synthetic biology workhorse *S. cerevisiae*. We further showed first proof of principle implementations of multicellular system that demonstrated the flexibility of the design motives that the YCTK collection allows (Figure 135).

For the provision of the toolkit, it was indispensable to characterize the introduced responder (promoters), sender (α-factors), receiver (Ste2 receptors), and barrier (Bar1 proteases) parts. With the heterologous expression of 10 non-native α-factors, we validated our *in silico* identification results of the pre-pro-α-factors and showed the recognition of non-native secretion signals. The *in silico* identification revealed processing motives for Kex1, Kex2, and Ste13 processing proteases and thus indicated the evolutionary conservation of α-factor processing in the different yeast species. Also, hybrid pre-pro-α-factors can be generated for the heterologous expression, however, here, we utilized the codon-optimized native pre-pro-α-factor sequence [220]. For some of the selected species, this was the first reported heterologous expression of their α-factors in *S. cerevisiae*. The experimental investigation of the crosstalk of the α-factor, and the Ste2 receptors, provided new insights into receptor promiscuity towards α-factors. Correlating these results with the phylogenetic likelihood analysis of the SSU rRNA and the Ste2 receptors and the comparison to

current models of the interaction of the α-factor with the Ste2 receptor, did not result in a conclusion that would explain the receptor promiscuity [236]. Follow-up experiments, taking the charge and structure of the α-factors into account, could demonstrate a correlation between α-factor recognition of the receptors. Notable is the finding that α-factors of the *Saccharomycetaceae* for which the receptor exhibited high α-factor promiscuity during the crosstalk experiment, tended to stimulate only a low number of non-cognate receptors (Figure 99). It might be interesting to further pursue this phenomenon.

By introducing and characterizing seven barrier parts, consisting of Bar1 proteases, we wanted to extend the range of applications using the YCTK. Even though only five of the proteases exhibited activity, our investigations of barrier protease promiscuity and determination of the cleavage sites of the α-factors was to our knowledge the largest study to date. The proposed coevolution of receptors and barrier protease to interact with the same α-factor sequences could only be partly validated and thus seems not to be universally applicable [298]. This pheonomenon was most obvious for *E. cymbalariae*, whose Ste2 receptor was promiscuous while the Bar1 protease was substrate specific.

The characterization of the responder parts, pheromone-inducible promoters, indicated differences of the promoter dynamics depending on the mating type of the background strain. Further, we found during the temporal characterization of the promoters that in the *MAT*α strain background the promoter strength decreased over time indicating a reduction of the mating pathway activity. Subsequent investigations revealed that the *MAT*α strain only temporarily exhibited the mating phenotype and then resumed growth, suggesting it became insensitive to α-factor stimulation.

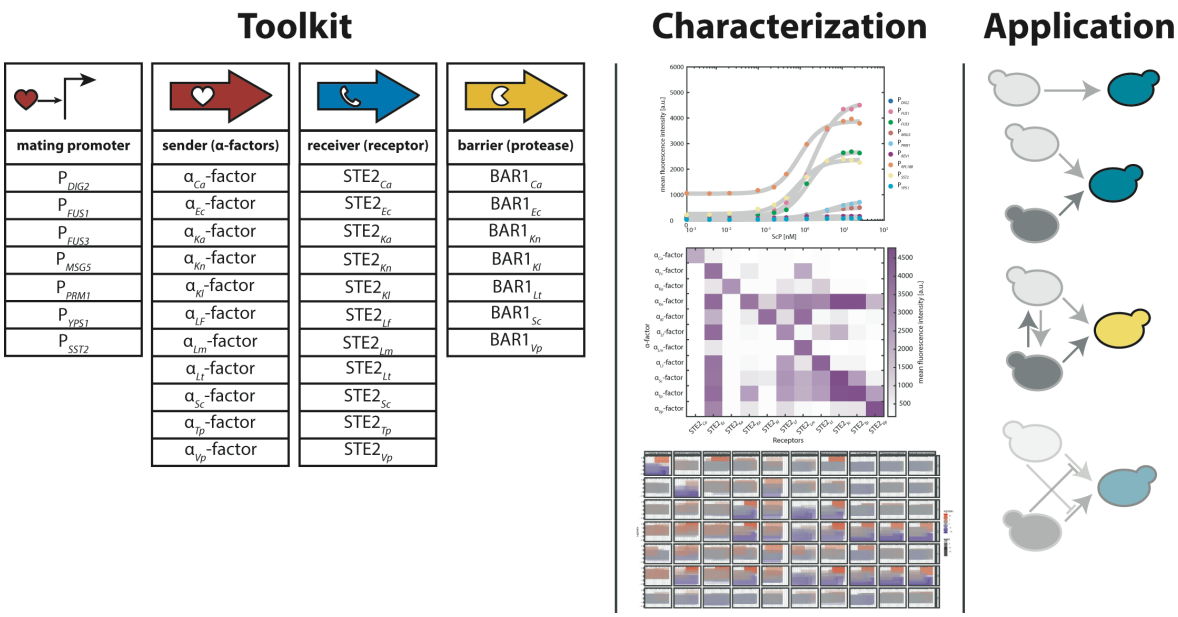

Figure 135: Graphical overview of the yeast communication toolkit and its utilization.

Apart from the characterization, we utilized the YCTK parts to engineer some multicellular networks. The simple signal transduction design motif, that constitutes a buffer-like logic population network, could be extended and adapted for the successful implementation of OR and AND-like

Boolean logic gate population networks. Our engineered systems enabled the receiver population to respond to the population composition by conditional expression of an output signal. For the self-stimulation design motif, that is constituted by α-factor signal repression by a barrier protease, did not result in the desired performance and thus requires further optimization. The improvements of some of the multicellular networks remain especially challenging, since apart from intracellular expression, also parameters like cell density and precise population composition have to be considered.

Overall, we wanted to facilitate the future engineering of multicellular communications networks in *S. cerevisiae* by providing the YCTK. Using the parts of the collection, numerous networks can be envisioned. Several previously established systems in bacterial hosts could be transferred and adapted in *S. cerevisiae* using the toolkit [153,161,186,192]. Another interesting research approach could also be the engineering of spatially organized multicellular systems using YCTK parts. Also, combining multicellular cell-cell communication with metabolic engineering by distributing for example pathways between different populations can be envisioned. Apart from synthetic or applied projects, also basic research question can be addressed utilizing the YCTK collection, for instance, it could be investigated whether two or several mating types are optimal for efficient mating. The YCTK collection includes all required parts and can also be further extended. Simplest, the set of sender and receiver parts could be extended by the implementation of α-factors and Ste2 receptors that were recently described in literature [220]. However, it could also be beneficial to expand the collection by antagonistic α-factors that competitively bind to the Ste2 receptor but do not induce receptor stimulation, thus providing additional design possibilities. Also, more responder parts could be added to the YCTK by selecting or identifying more pheromone-responsive promoters. Alternatively, when the mating MAPK pathway would be decoupled from the native to *S. cerevisiae* transcriptional control by deleting the transcription factor Ste12, a synthetic promoter that binds engineered Ste12 could be implemented, as it was previously shown [220,382]. Also, considering results from systems biology studies of the yeast mating MAPK signaling pathway could result in an improved tunability of the response networks and therefore enhance their functionality [382].

Since the *S. cerevisiae* mating pathway is one of the most intensively studied eukaryotic signaling pathways, the toolkit could be used to integrate other GPC receptors into multicellular networks that may serve as a biosensors or for drug screening setups [337,342]. Previously, different studies addressed the mating MAPK signaling pathway by engineering the Ste5 scaffold protein, thus modulating the signaling dynamics or the pathway for cellular differentiation. To employ these possibilities in multicellular communication networks, the responsible parts could be integrated into the YCTK, extending its application range [361,363,367,515].

To conclude, with the toolkit we are providing standardized and comprehensively characterized key parts of the yeast mating system, to be used together with the YTK collection for the simplified and fast engineering of multicellular communication networks in *S. cerevisiae*.

4 Material & Methods

4.1 Chemicals and enzymes

4.1.1 Chemicals

Table 8: List of chemicals

Chemicals	Company
Agar bacteriology	Applichem
Agarose ultra-pure	Biozym
α-factor	Sigma-Aldrich/BioCat
Amino acid dropout mixes (SD)	Formedium
Amino acid dropout mixes (SC)	Sunrise Science
Ampicillin sodium salt	Applichem
Bacto TM tryptone	BD Biosciences
Bacto TM yeast extract	BD Biosciences
Casein sodium salt	Sigma-Aldrich
Chloramphenicol	Applichem
Disodium phosphate	Sigma-Aldrich
D-glucose	Applichem
Dimethyl sulfoxide (DMSO)	Sigma-Aldrich
dNTPs	Thermo Fisher Scientific
DNA ladder	Thermo Fisher Scientific
Doxycycline	Sigma-Aldrich
EDTA	Roth
Ethanol	Roth
Glucose	Sigma-Aldrich
Glycerol 99.5%	Gerbu Biotechnik
Kanamycin sulphate	Sigma-Aldrich
Lithium acetate dihydrate	Sigma-Aldrich
6x Loading Dye Gel	Thermo Fisher Scientific/New England Biolabs
D-Mannitol	Sigma-Aldrich
Monopotassium phosphate	Sigma-Aldrich
Monosodium phosphate	Sigma-Aldrich
PEG 3350	Sigma-Aldrich
Potassium Chloride	Sigma-Aldrich
Salmon Sperm	Thermo Fisher
Sodium Chloride	Sigma-Aldrich
Sodium phosphate dibasic	Sigma-Aldrich
Tryptone	Roth
Yeast Extract	Applichem
YNB (yeast nitrogen base) (low fluorescence)	Formedium
YPD powder	Roth

4.1.2 Enzymes

Enzyme	Company
Restriction Enzymes and buffer	Thermo Fisher Scientific & New England Biolabs
NEB Golden Gate Assembly Kit	New England Biolabs
PrimeSTAR GXL Polymerase, buffer and dNTPs	Clonetech
T7 DNA ligase	New England Biolabs

4.1.3 Consumables

Consumable	Supplier
Frozen-EZ yeast transformation kit II	Zymo Research
GeneJET PCR Purification Kit	Thermo Fisher Scientific
GeneJET Plasmid Miniprep Kit	Thermo Fisher Scientific
GeneJET Gel Extraction Kit	Thermo Fisher Scientific
Gibson Assembly Master Mix	New England Biolabs
Golden Gate Master Mix	New England Biolabs
Phire Plant Direct PCR kit	Thermo Fisher Scientific

The kits were used according to the manufacturer's protocols.

4.2 Media, buffer and solutions

Luria broth (LB) medium and plates

10 g	Tryptone
5 g	Yeast extract
5 g	NaCl
(15 g	Agar)

ddH_2O was added to a total volume of 1 L and the pH was adjusted to 7.

Super optimal broth (SOB) medium

20 g	Bacto tryptone
5 g	Bacto yeast extract
10 mM	NaCl
2.5 mM	KCl
10 mM	$MgCl_2$
10 mM	$MgSO_4$

ddH_2O was added and the pH was adjusted to pH7 and filled up with ddH_2O to a total volume of 1L.

Super optimal broth with catabolite repression (SOC) medium

20 mM glucose in SOB media.

Yeast peptone dextrose (YPD) medium and plates

50gg	YPD powder
(15 g	Agar)

ddH_2O was added up to a total volume of 1 L.

Low fluorescence synthetic defined (SD) medium and plates

6.9 g	YNB LoFlo
790 mg	Appropriate amino acid dropout mix (SD)
20 g	glucose
(15 g	Agar)

ddH_2O was added up to a total volume of 1 L.

Synthetic complete (SC) medium

5.76 g	appropriate amino acid dropout mix (SC)
13.98 g	YNB
20 g	glucose
100 mL	1 M potassium buffer pH 6.4

ddH_2O was added up to a total volume of 1 L.

Tris-Acetate-EDTA buffer (TAE– 50 x)

242 g	Tris base
57.1g	Glacial acetic acid
100 mL	0.5 M EDTA, pH 8
0.1 mL	10 mM Methionine
1 mL	90% lactic acid

ddH_2O was added up to a total volume of 1 L.

Sodium phosphate buffer pH 6.4

13.3 mL	Na_2HPO_4 (1M)
36.7 mL	NaH_2PO_4 (1M)

High-density-solution (Glycerol-Mannitol-Solution)

200 g	Glycerol
15 g	Mannitol

ddH_2O was added to 200 g glycerol and filled up to a total volume of 1 L. 15 g mannitol were dissolved in the solution and sterile-filtered prior usage.

Quenching solution

40 mL	acetonitrile
40 mL	methanol
20 ML	H_20

Frozen competent cell solution (FCC)

5 % (v/v)	glycerol
10 % (v/v)	DMSO

in ddH_2O

Frozen competent cell transformation mix (per transformation)

PEG 3350 (50% (w/v))	260 µL
Lithium acetate (1 M)	36
Single stranded salmon sperm DNA (2.0 mg/mL)	50
Plasmid DNA / linearized DNA plus ddH_2O	14

Table 9: List of compounds

Compound	Stock concentration	Working concentration
α-factor	1/ 2 mM in SD medium with casein / 80 % 2 µM casein + 20 % DMF 0.1 % TFA	0-26 nM in SD medium with casein
Ampicillin (Amp)	100 mg/mL in ddH_2O	100 µg/mL in ddH_2O
Casein	200 mM in SD medium	200 µM in SD medium
Chloramphenicol (CAM)	34 mg/mL in ethanol	34 µg/mL in ethanol
Doxycycline (DOX)	10 mg/mL in ddH_2O	0.06-20 µg/mL in ddH_2O
Kanamycin (KAN)	50 mg/mL in ddH_2O	50 µg/mL in ddH_2O
Lithium acetate	1 M in ddH_2O	1 M in ddH_2O
PEG 3350	50% w/v in ddH_2O	50% w/v in ddH_2O
Single-stranded salmon sperm DNA	2.0 mg/mL in ddH_2O	

4.3 Molecular cloning methods

4.3.1 Oligonucleotides

The oligonucleotides used in this study were synthesized by Eurofins and IDT.

4.3.2 Polymerase chain reaction (PCR)

PCR was used to amplify DNA fragments for cloning, to verify successful genomic integration or plasmid assembly. PCRs were performed in peqSTAR thermocyclers and subsequently verified by gel electrophoresis. In case of subsequent cloning, DNA fragments were treated with DpnI and then purified using the GeneJet DNA Purification kit.

PCR using GXL polymerase (DNA amplification for cloning)

Reaction Mix:

10 µL	PrimeSTAR GXL Buffer (5x)
4 µL	dNTPs (10 mM)
1 µL	Forward primer (10 µM)
1 µL	Reverse primer (10 µM)
1 µL	DNA template (10 ng/µL)
1-2 µL	PrimeSTAR GXL DNA Polymerase
31-32 µL	ddH_2O

Thermocycler setting:

35 cycles	[	98 °C	30s
		50-60 °C	30s
		68 °C	10-30s/kb
		16 °C	∞

PCR using Dream Taq Polymerase (plasmid assembly verification)

Reaction Mix:

12.5 µL	DreamTaq Green PCR Mastermix (2x)
1 µL	Forward primer (10 µM)
1 µL	Reverse primer (10 µM)
2 µL	DNA template (from 10 µL water, in which 1 colony has been heated at 100°C for 10 min)
8.5 µL	ddH_2O

Thermocycler setting:

		95 °C	5
35 cycles	[	95 °C	30s
		50-60 °C	30s
		72 °C	30s/kb
		16 °C	∞

PCR using the Phire Plant Direct PCR kit (verification genomic integration into *S. cerevisiae*)

Reaction Mix:

12.5 µL	DreamTaq Green PCR Mastermix (2x)
1.25 µL	Forward primer (10 µM)
1.25 µL	Reverse primer (10 µM)
2 µL	DNA template (from 10 µL water, in which 1 colony has been dissolved)
8 µL	ddH_2O

Thermocycler setting:

		98 °C	5
40 cycles	[	98 °C	5s
		50-60 °C	5s
		72 °C	20s
		72 °C	1 min
		16 °C	∞

4.3.3 Gel electrophoresis

PCR-amplified gene fragments or plasmids digested by restriction enzymes were verified using gel electrophoresis. In molecular biology, gel electrophoresis is used to separate DNA by applying an electric field, resulting in DNA fragment separation according to length. PCR products for subsequent cloning were verified by loading 5 µL PCR product or the entire PCR mixture combined with loading dye in an 1 % agarose TAE gel. For colony PCR products, 15 µL of the reaction mixture were loaded onto a gel. For analytical restriction digests, 600 ng were loaded, whereas 3 µL were loaded for plasmids digested for subsequent genomic integration. 135 V were applied to run the gel in a chamber filled with TAE buffer and ran for 15-25 min. The length-separated DNA bands were illuminated with UV light or blue light to verify their lengths.

4.3.4 Cloning

The plasmids of this study were assembled using Gibson Assembly, Circular Polymerase Extension Cloning (CPEC), yeast homologous recombination or Golden Gate Assembly. To confirm if the plasmids were assembled correctly, they were verified by colony PCR or analytical digest and subsequently sequenced.
In case the DNA fragments for cloning were obtained by PCR, they were treated with DpnI to remove template DNA.

PCR DpnI treatment

Reaction mixture:

45 µL	PCR
2 µL	DpnI

Thermocycler setting:

37 °C	30-120 min
56 °C	20 min
16°C	∞

Afterwards, the reaction mixture was purified using the GeneJet PCR Purification kit according to the manufacturer's protocol.

Gibson Assembly/NEB Builder

For the assembly of linear DNA fragments using Gibson assembly, overlapping ends are required and up to 6 parts can be assembled in one stop into a plasmid [516]. Overlapping DNA fragments were at least 15 bp long and more importantly, exhibited a T_m of 60 °C. Prior to the assembly, the DNA fragments were amplified by PCR using the GXL Polymerase, the fragments were verified by gel electrophoresis, treated with DpnI and PCR-purified.
For the Gibson Assembly, the parts were combined in a 1:3 molar ratio of backbone part to insert parts whereupon 100 ng backbone fragment was utilized.

Reaction Mixture:

10 µL	Gibson Assembly Mastermix/NEBuilder Mastermix
100 ng	Backbone DNA fragment
3:1 molar amount	Insert DNA fragments
10 µL – volume DNA	ddH_2O

Thermocycler Setting:

50 °C	15 – 60 min	When 2 parts were assembled 15 min, > 2 parts 60 min
16°C	∞	

Subsequently, the reaction mixture was dialyzed on MF-Millipore Membrane Filter of 0.025 µm pore size. The sample was dialyzed at least 15 min and 5 µL were utilized for the transformation by electroporation into *E. coli*.

Circular Polymerase Extension Cloning (CPEC)

CPEC was used as alternative method to Gibson Assembly, in case Gibson Assembly was unsuccessful [517]. Also, with CPEC, linear fragments with overlapping regions can be assembled. Additionally, the entire newly formed plasmid is amplified. The DNA fragments were amplified by PCR verified by gel electrophoresis and subsequently extracted from the gel using the GeneJET Gel Extraction Kit according to the manufacturer's protocol. Also, here the DNA parts were combined in a 1:3 ratio of backbone: insert DNA fragments and the GXL polymerase was used to join the fragments.

Reaction Mixture:

10 µL	PrimeSTAR GXL Buffer (5x)
4 µL	dNTPs (10 mM)
250 ng	Backbone DNA fragments
3:1 molar ratio	Inserts DNA fragments
2 µL	PrimeSTAR GXL DNA Polymerase
up to 50 µL	ddH_2O

Thermocycler Settings:

		98 °C	30 s
30 cycles	[	98 °C	10 s
		54 °C (0,1 °C/s)	180 s
		68 °C	10 s/kb
		68 °C	10 min
		16 °C	∞

As for Gibson Assembly, the reaction mixture was dialyzed for at least 15 min prior transformation. 5 µL were used for transformation into *E. coli* and an additional 5 µL were loaded on a gel to verify plasmid formation.

Yeast homologous recombination

For yeast homologous recombination, the natural recombination efficiency of *S. cerevisiae* was employed to assemble plasmids [518]. Linear DNA fragments with overlapping ends were transformed in a 1:3 ratio of plasmid backbone to DNA insert fragments. After transformation, *S. cerevisiae* assembled the fragments into a plasmid, which could be purified from the cells and verified after colonies were formed.

Golden Gate Assembly

The Golden Gate Assembly method is a one-pot one-step plasmid-based cloning method that utilizes type II restriction enzymes [519,520]. Pats, that are provided in a library of vectors can be assembled into genetic devices into a plasmid backbone and several devices can be joint together in another assembly step. It is a hierarchical cloning method with alternate usage of two restriction enzymes. For *S. cerevisiae*, a yeast Golden Gate toolkit has been established, providing a basic set of parts and vectors for the construction of functional genetic devices [71].

At first, we assembled custom entry vectors, backbones for our parts and genetic devices, by combining origin or replications for *E. coli* and *S. cerevisiae*, selection markers and genes for visual identification of correctly assembled plasmids. The part-carrying plasmids were combined in a 1:3 ratio of longest: shortest DNA fragments.

Reaction Mixture Entry Vector Assembly:

20 fmol	largest DNA fragment
100 fmol	Insert DNA fragments
0.5 µL	BsaI
1 µL	T4 DNA Ligase Buffer
0.5 µL	T7 DNA Ligase
Remaining volume until 10 µL	ddH_2O

Thermocycler Settings:

50 cycles	[	42 °C	2 min
		16 °C	5 min
		80 °C	10 min
		16 °C	∞

To introduce novel parts into the kit, like promoters, genes, or terminators, the corresponding DNA fragments including the type II restriction enzyme recognition sites were added by PCR. The purified PCR fragments were then introduced into the appropriate backbone in a Golden Gate Assembly reaction using the BsmBI/Esp3I restriction enzyme. The same reaction mixture is also used for the assembly of L2 plasmids.

Reaction Mixture L0/L2 plasmids:

20 fmol	Backbone DNA fragment
100 fmol	Insert DNA fragments
0.5 µL	BsmBI/Esp3I
1 µL	T4 DNA Ligase Buffer
0.5 µL	T7 DNA Ligase
Remaining volume until 10 µL	ddH_2O

Thermocycler Settings:

50 cycles	[	42 °C	2 min
		16 °C	5 min
		60 °C	60 min
		80 °C	10
		16 °C	∞

For the assembly of L1 plasmids from several L0 parts requires the usage of the BsaI enzyme, which can either be supplied as pure enzyme or in the Golden Gate Assembly kit mastermix.

Reaction Mixture L1 plasmids:

20 fmol	Backbone DNA fragment
100 fmol	Insert DNA fragments
0.5 µL	BsaI/Golden Gate Assembly Mix
1 µL	T4 DNA Ligase Buffer
(0.5 µL	T7 DNA Ligase (only when solely BasI is utilized))
Remaining volume until 10 µL	ddH_2O

Thermocycler Settings:

50 cycles	[	37 °C	2 min
		16 °C	5 min
		37 °C	60 min
		80 °C	10 min
		16 °C	∞

After plasmid assembly using Golden Gate, the reaction mixture is dialyzed and subsequently 5 µL is used for the transformation into *E. coli*.

4.3.5 Restriction Enzyme Digest

Either as analytical digest for the verification of correct plasmid assembly or for the genomic integration of constructs into the *S. cerevisiae* genome, restriction enzyme digest was utilized. For an analytical digest, 600 ng were utilized and digested with 1-3 enzymes. Most frequently though, the restriction enzyme digest was used for subsequent genomic integration.

Reaction Mixture:

1 µg	Plasmid
2 µL	Buffer Cutsmart
1 µL	Enzyme 1
Remaining volume until 20 µL	ddH_2O

The reaction mixture was incubated at 37 °C for 3 h and then deactivated for 20 min at 65 °C.

4.3.6 Plasmid purification, concentration determination of DNA and sequencing

For plasmid propagation and subsequent purification, *E. coli* strains harboring the plasmid of interest were cultured in LB media overnight with appropriate antibiotics for plasmid maintenance. The plasmid was purified using the GeneJet Miniprep Kit according to the manufacturer's protocol. During the final elution step, ddH_2O was utilized. For DNA concentration determination, the NanoDrop 2000 spectrophotometer was utilized.
Assembled plasmids were sequenced by Eurofins or Seqlab, to verify whether the assembly was successful.

4.3.7 Preparation of electrocompetent *E. coli* cells and transformation

For plasmid propagation after plasmid assembly, the *E. coli* strain NEB turbo was utilized. To make highly efficient electrocompetent cells, a previously established protocol was used [521]. First, the NEB turbo cells were inoculated into LB for an overnight culture. The next day, the cells were

diluted 1:1000 into fresh 200 mL SOB medium and grown at 30 °C and 200 rpm until an optical density of 0.4-0.6 was reached. After dividing the culture into 50 mL falcons and chilling them for 5 min on ice, the cells were harvested by centrifugation at 4 °C, 2,000 x g for 15 min. The supernatant was removed and the cells were resuspended in 10 mL cold ddH_2O and combined. Then, the cells were underlaid with 10 mL cold glycerol-mannitol solution and were again centrifuged for 15 min at 40 °C and 2,000 x g. For steady slow transition of the cells through the glycerol-mannitol solution resulting in highly competent cells, the breaks of the centrifuge were removed. Last, the supernatant was removed, the cells were resuspended in 200 µL glycerol-mannitol solution and snap-frozen in liquid nitrogen as 50 µL aliquots. They were stored at -80°C.
Prior to transformation, the cells were thawed on ice and an electroporation cuvette as well as water were chilled on ice. In a tube, 5 µL dialyzed plasmid were mixed with 50 µL competent cells and 50 µL chilled water and carefully transferred into the cuvette. To electroporate the cells, a MicroPulser electroporator (BIO-RAD) was utilized and the cells were shocked with the EC1 program. To recover the cells, 1 mL SOC medium preheated to 37 °C was added and the cells were transferred into a tube and further recovered for 30-90 min at 37 °C under shaking conditions. Subsequently, the cells were plated on selective LB plates and incubated at 37 °C overnight.

4.4 Yeast competent cells

For the two projects, two different yeast strains were utilized. While for the metabolic engineering project, the BJ5465 strain background was utilized and the pathways were expressed from 2µ plasmids, for the YCTK-based project, the SEY6210 strain background was used with genomically integrated systems.

4.4.1 Competent BJ5465 cells and transformation

The BJ5465 strain for the acyl-CoA ester project was made competent using the Frozen-EZ yeast transformation kit II according to the manufacturer's protocol. The same kit was also utilized for the transformation of the pathway-harboring plasmids.

4.4.2 Competent SEY6210/SEY6210A cells and genomic integration

To prepare competent SEY6210/SEY6210A cells, the protocol by Gietz *et al.* was adapted [522]. The strain was cultured overnight in YPD media under shaking conditions at 30 °C. For the day culture, the cells were inoculated to an OD of 0.2 into 500 mL 2x YPD. The cells were grown at 30 °C at 200 rpm until and OD of 0.8-1 was reached. The cells were harvested in 50 mL falcons by centrifugation for 5 min at 3,000 x g. After the supernatant was removed, the cells in each falcon were washed with 25 mL sterile water and re-pelleted by centrifugation as before. The cells of each falcon were resuspended in 500 µL FCC solution and divided into 50 µL aliquots. To allow cautious and slow cooling down, the tubes were wrapped in several layers of paper and stored at -80 °C.
To transform the cells, the tubes were thawed at 37 °C for 15 – 30 s. To remove the FCC solution, the cells were centrifuged at 13,000 x g for 2 min. Then, the frozen competent cell transformation mix (see solutions) which contained 1000 ng linearized DNA fragment for genomic integration was used to resuspend the pelleted cells, which were then incubated for 60 min at 42 °C. Afterwards, the cells were centrifuged at 13,000 x g for 30 s, the supernatant was removed and the cells were resuspended in water. Subsequently they were plated on appropriate SD plates and

incubated at 30 °C until colony formation was visible. Successful genomic integration was verified by colony PCR.

4.5 Strains and plasmids

4.5.1 Strains

Table 10: S. cerevisiae nomenclature used in this study.

Exemplary notation	Description
ste2	gene name
Ste2	protein name
ste2Δ	knockout of the *ste2* gene
URA3	homology sequences
P_{FUS1}/*FUS1* promoter	Promoter of the *fus1* gene
FUS1	mRNA levels of *fus1* gene transcript
α-factor$_{Ec}$	α-factor originating from *E. cymbalariae*
Ste2$_{Ec}$	Ste2 originating from *E. cymbalariae*
Bar1$_{Ec}$	Bar1 originating from *E. cymbalariae*

Table 11: List of strains used in the engineered acyl-CoA study.

Strain	Alias	Genotype	Source
sNK44	*S. cerevisiae BJ5465*	*MAT***a** *ura3-52 trp1 leu2-Δ1 his3-Δ200 pep4::HIS3 prb1-Δ1.6R can1 GAL*	ATCC [125,523]
sNK11	*E. coli* NEB turbo	F' proA+B+ laclq ΔlacZM15 / fhuA2 Δ(lac-proAB) glnV galK16 galE15 R(zgb-210::Tn10)TetS endA1 thi-1 Δ(hsdS-mcrB)5	New England Biolabs

Table 12: Bacterial strains for molecular cloning.

Strain	Alias	Genotype	Source
sNK11	*E. coli* NEB turbo	F' proA+B+ laclq ΔlacZM15 / fhuA2 Δ(lac-proAB) glnV galK16 galE15 R(zgb-210::Tn10)TetS endA1 thi-1 Δ(hsdS-mcrB)5	New England Biolabs

Table 13: List of *S. cerevisiae* background strains used in the YCTK project.

Strain	Alias	Genotype	Source
yAA2	SEY6210	*MATα leu2-3,112 ura3-52 his3Δ200 trp1Δ901 lys2-801 suc2Δ9*	[524]
yAA1	SEY6210A	*MAT***a** *leu2-3,112 ura3-52 his3Δ200 trp1Δ901 lys2-801 suc2Δ9*	[524]
yAA408	*MAT*α – P_{FUS1}-*mNeonGreen*	yAA2, *MATα ste3Δ::klTRP1 mfa1Δ::natNT2 mfa2Δ::hphNT1 ste2Δ::[Pfus1-UbiY-mNeonGreen-Tfus1:kanMX]*	A. Anders
yNK157	*MAT*α	yAA408, *ste2Δ*	This study
yAA329	*MAT***a**	yAA1, *LYS2::rttAS2 mfa2Δ::hphNT1 mfa1Δ::klTRP1 bar1Δ::kanMX ste2Δ::natNT*	A. Anders
yNK159	*MAT***a** *far1*Δ	yAA329, *far1Δ::URA3*	This study
yNK160	*MAT*α –*ste2$_{Sc}$*	yNK157, *ura3-52::[P_{PAB1}-ste2$_{Sc}$-T_{ENO1}:LEU2]*	This study
yNK161	*MAT***a** *far1*Δ ste2$_{Sc}$	yNK159, *ura3-52:: [P_{PAB1}-ste2$_{Sc}$-T_{ENO1}:LEU2]*	This study
yNK162	*MAT*α –phero. *ste2$_{Sc}$*	yNK157, *ura3-52::[P_{FUS1}-ste2$_{Sc}$-T_{ENO1}:LEU2]*	This study
yNK163	*MAT*α *far1*Δ	yNK157, *far1Δ::URA3*	This study
yNK164	*MAT*α *far1*Δ ste2$_{Sc}$	yNK163, *ura3-52:: [P_{PAB1}-ste2$_{Sc}$-T_{ENO1}:LEU2]*	This study

yNK165	*MAT***a** *far1*ΔP_{FUS1}-venus	yNK159, *HO*:: *[P_{FUS1}-venus-T_{THD1}-HIS3]*	This study

Table 14: List of *S. cerevisiae* strains used in the YCTK project for promoter characterization.

Strain	Genotype	Source
yNK167	yNK159, *ura3-52*::*[P_{CUP1}-venus-T_{ENO1}-LEU2]*	This study
yNK168	yNK159, *ura3-52*::*[P_{CUP1}-venus-T_{ENO2}-LEU2]*	This study
yNK169	yNK159, *ura3-52*::*[P_{CUP1}-venus-T_{TDH1}-LEU2]*	This study
yNK170	yNK159, *ura3-52*::*[P_{PAB1}-venus-T_{ENO1}-LEU2]*	This study
yNK171	yNK159, *ura3-52*::*[P_{HHF1}-venus-T_{ENO2}-LEU2]*	This study
yNK172	yNK159, *ura3-52*::*[P_{PGK1}-venus-T_{TDH1}-LEU2]*	This study
yNK173	yNK159, *ura3-52*::*[P_{TETO7}-venus-T_{ENO1}-LEU2]*	This study
yNK174	yNK160, *HO*:: *[P_{DIG1}-mRuby2-T_{THD1}-HIS3]*	This study
yNK175	yNK160, *HO*:: *[P_{FUS1}-mRuby2-T_{THD1}-HIS3]*	This study
yNK176	yNK160, *HO*:: *[P_{FUS3}-mRuby2-T_{THD1}-HIS3]*	This study
yNK177	yNK160, *HO*:: *[P_{MSG5}-mRuby2-T_{THD1}-HIS3]*	This study
yNK178	yNK160, *HO*:: *[P_{PRM1}-mRuby2-T_{THD1}-HIS3]*	This study
yNK179	yNK160, *HO*:: *[P_{REV1}-mRuby2-T_{THD1}-HIS3]*	This study
yNK180	yNK160, *HO*:: *[P_{SST2}-mRuby2-T_{THD1}-HIS3]*	This study
yNK181	yNK160, *HO*:: *[[P_{YPS1}-mRuby2-T_{THD1}-HIS3]*	This study
yNK182	yNK160, *HO*:: *[P_{REV1}-mRuby2-T_{THD1}-HIS3]*	This study
yNK183	yNK160, *HO*:: *[P_{RPL18B}-mRuby2-T_{THD1}-HIS3]*	This study
yNK184	yNK160, *HO*:: *[P_{TDH1}-mRuby2-T_{THD1}-HIS3]*	This study
yNK185	yNK160, *HO*:: *[P_{DIG1}-venus-T_{THD1}-HIS3]*	This study
yNK186	yNK160, *HO*:: *[P_{FUS1}-venus-T_{THD1}-HIS3]*	This study
yNK187	yNK160, *HO*:: *[P_{FUS3}-venus-T_{THD1}-HIS3]*	This study
yNK188	yNK160, *HO*:: *[P_{MSG5}-venus-T_{THD1}-HIS3]*	This study
yNK189	yNK160, *HO*:: *[P_{PRM1}-venus-T_{THD1}-HIS3]*	This study
yNK190	yNK160, *HO*:: *[P_{REV1}-venus-T_{THD1}-HIS3]*	This study
yNK191	yNK160, *HO*:: *[P_{SST2}-venus-T_{THD1}-HIS3]*	This study
yNK192	yNK160, *HO*:: *[P_{YPS1}-venus-T_{THD1}-HIS3]*	This study
yNK193	yNK160, *HO*:: *[P_{REV1}-venus-T_{THD1}-HIS3]*	This study
yNK194	yNK160, *HO*:: *[P_{RPL18B}-venus-T_{THD1}-HIS3]*	This study
yNK195	yNK160, *HO*:: *[P_{TDH1}-venus-T_{THD1}-HIS3]*	This study
yNK196	yNK160, *HO*:: *[P_{DIG1}- mTurquoise2-T_{THD1}-HIS3]*	This study
yNK197	yNK160, *HO*:: *[P_{FUS1}- mTurquoise2-T_{THD1}-HIS3]*	This study
yNK167	yNK160, *HO*:: *[P_{FUS3}- mTurquoise2-T_{THD1}-HIS3]*	This study
yNK168	yNK160, *HO*:: *[P_{MSG5}- mTurquoise2-T_{THD1}-HIS3]*	This study
yNK169	yNK160, *HO*:: *[P_{PRM1}- mTurquoise2-T_{THD1}-HIS3]*	This study
yNK170	yNK160, *HO*:: *[P_{REV1}- mTurquoise2-T_{THD1}-HIS3]*	This study
yNK171	yNK160, *HO*:: *[P_{SST2}- mTurquoise2-T_{THD1}-HIS3]*	This study
yNK172	yNK160, *HO*:: *[P_{YPS1}- mTurquoise2-T_{THD1}-HIS3]*	This study
yNK173	yNK160, *HO*:: *[P_{REV1}- mTurquoise2-T_{THD1}-HIS3]*	This study
yNK174	yNK160, *HO*:: *[P_{RPL18B}- mTurquoise2-T_{THD1}-HIS3]*	This study
yNK175	yNK160, *HO*:: *[P_{TDH1}- mTurquoise2-T_{THD1}-HIS3]*	This study
yNK176	yNK162, *HO*:: *[P_{DIG1}-venus-T_{THD1}-HIS3]*	This study
yNK177	yNK162, *HO*:: *[P_{FUS1}-venus-T_{THD1}-HIS3]*	This study
yNK178	yNK162, *HO*:: *[P_{FUS3}-venus-T_{THD1}-HIS3]*	This study
yNK179	yNK162, *HO*:: *[P_{MSG5}-venus-T_{THD1}-HIS3]*	This study

yNK180	yNK162, *HO*:: *[P_{PRM1}-venus-T_{THD1}-HIS3]*	This study
yNK181	yNK162, *HO*:: *[P_{REV1}-venus-T_{THD1}-HIS3]*	This study
yNK182	yNK162, *HO*:: *[P_{SST2}-venus-T_{THD1}-HIS3]*	This study
yNK183	yNK162, *HO*:: *[P_{YPS1}-venus-T_{THD1}-HIS3]*	This study
yNK184	yNK162, *HO*:: *[P_{REV1}-venus-T_{THD1}-HIS3]*	This study
yNK185	yNK162, *HO*:: *[P_{RPL18B}-venus-T_{THD1}-HIS3]*	This study
yNK186	yNK162, *HO*:: *[P_{TDH1}-venus-T_{THD1}-HIS3]*	This study
yNK187	yNK164, *HO*:: *[P_{DIG1}-venus-T_{THD1}-HIS3]*	This study
yNK188	yNK164, *HO*:: *[P_{FUS1}-venus-T_{THD1}-HIS3]*	This study
yNK189	yNK164, *HO*:: *[P_{FUS3}-venus-T_{THD1}-HIS3]*	This study
yNK190	yNK164, *HO*:: *[P_{MSG5}-venus-T_{THD1}-HIS3]*	This study
yNK191	yNK164, *HO*:: *[P_{PRM1}-venus-T_{THD1}-HIS3]*	This study
yNK192	yNK164, *HO*:: *[P_{REV1}-venus-T_{THD1}-HIS3]*	This study
yNK193	yNK164, *HO*:: *[P_{SST2}-venus-T_{THD1}-HIS3]*	This study
yNK194	yNK164, *HO*:: *[P_{YPS1}-venus-T_{THD1}-HIS3]*	This study
yNK195	yNK164, *HO*:: *[P_{REV1}-venus-T_{THD1}-HIS3]*	This study
yNK196	yNK164, *HO*:: *[P_{RPL18B}-venus-T_{THD1}-HIS3]*	This study
yNK197	yNK164, *HO*:: *[P_{TDH1}-venus-T_{THD1}-HIS3]*	This study
yNK181	yNK161, *HO*:: *[P_{DIG1}-venus-T_{THD1}-HIS3]*	This study
yNK182	yNK161, *HO*:: *[P_{FUS1}-venus-T_{THD1}-HIS3]*	This study
yNK183	yNK161, *HO*:: *[P_{FUS3}-venus-T_{THD1}-HIS3]*	This study
yNK184	yNK161, *HO*:: *[P_{MSG5}-venus-T_{THD1}-HIS3]*	This study
yNK185	yNK161, *HO*:: *[P_{PRM1}-venus-T_{THD1}-HIS3]*	This study
yNK186	yNK161, *HO*:: *[P_{REV1}-venus-T_{THD1}-HIS3]*	This study
yNK187	yNK161, *HO*:: *[P_{SST2}-venus-T_{THD1}-HIS3]*	This study
yNK188	yNK161, *HO*:: *[P_{YPS1}-venus-T_{THD1}-HIS3]*	This study
yNK189	yNK161, *HO*:: *[P_{REV1}-venus-T_{THD1}-HIS3]*	This study
yNK190	yNK161, *HO*:: *[P_{RPL18B}-venus-T_{THD1}-HIS3]*	This study
yNK191	yNK161, *HO*:: *[$P_{TD1§}$-venus-T_{THD1}-HIS3]*	This study

Table 15: List of *S. cerevisiae* strains used in the YCTK project for the α-factor characterization.

Strain	Genotype	Source
yNK192	yNK157, *HO*:: *[P_{PGK1}-mfα1$_{Ca}$-T_{THD1}-HIS3]*	This study
yNK193	yNK157, *HO*:: *[P_{PGK1}-mfα1$_{Ec}$-T_{THD1}-HIS3]*	This study
yNK194	yNK157, *HO*:: *[P_{PGK1}-mfα1$_{Ka}$-T_{THD1}-HIS3]*	This study
yNK195	yNK157, *HO*:: *[P_{PGK1}-mfα1$_{Kl}$-T_{THD1}-HIS3]*	This study
yNK196	yNK157, *HO*:: *[P_{PGK1}-mfα1$_{Kn}$-T_{THD1}-HIS3]*	This study
yNK197	yNK157, *HO*:: *[P_{PGK1}-mfα1$_{Lf}$-T_{THD1}-HIS3]*	This study
yNK186	yNK157, *HO*:: *[P_{PGK1}-mfα1$_{Lm}$-T_{THD1}-HIS3]*	This study
yNK187	yNK157, *HO*:: *[P_{PGK1}-mfα1$_{Lt}$-T_{THD1}-HIS3]*	This study
yNK188	yNK157, *HO*:: *[P_{PGK1}-mfα1$_{Sc}$-T_{THD1}-HIS3]*	This study
yNK189	yNK157, *HO*:: *[P_{PGK1}-mfα1$_{Tp}$-T_{THD1}-HIS3]*	This study
yNK190	yNK157, *HO*:: *[P_{PGK1}-mfα1$_{Vp}$-T_{THD1}-HIS3]*	This study

Table 16: List of *S. cerevisiae* strains used in the YCTK project for the Ste2 characterization.

Strain	Genotype	Source
yNK191	yAA408, *ura3-52*:: *[P_{PAB1}-ste2$_{Ca}$-T_{ENO1}-LEU2]*	This study
yNK192	yAA408, *ura3-52*:: *[P_{PAB1}-ste2$_{Ec}$-T_{ENO1}-LEU2]*	This study
yNK193	yAA408, *ura3-52*:: *[P_{PAB1}-ste2$_{Ka}$-T_{ENO1}-LEU2]*	This study
yNK194	yAA408, *ura3-52*:: *[P_{PAB1}-ste2$_{Kl}$-T_{ENO1}-LEU2]*	This study
yNK195	yAA408, *ura3-52*:: *[P_{PAB1}-ste2$_{Kn}$-T_{ENO1}-LEU2]*	This study
yNK196	yAA408, *ura3-52*:: *[P_{PAB1}-ste2$_{Lf}$-T_{ENO1}-LEU2]*	This study
yNK197	yAA408, *ura3-52*:: *[P_{PAB1}-ste2$_{Lm}$-T_{ENO1}-LEU2]*	This study
yNK198	yAA408, *ura3-52*:: *[P_{PAB1}-ste2$_{Lt}$-T_{ENO1}-LEU2]*	This study
yNK199	yAA408, *ura3-52*:: *[P_{PAB1}-ste2$_{Sc}$-T_{ENO1}-LEU2]*	This study
yNK200	yAA408, *ura3-52*:: *[P_{PAB1}-ste2$_{Tp}$-T_{ENO1}-LEU2]*	This study
yNK201	yAA408, *ura3-52*:: *[P_{PAB1}-ste2$_{Vp}$-T_{ENO1}-LEU2]*	This study
yNK202	yNK165, *ura3-52*:: *[P_{PAB1}-ste2$_{Ca}$-T_{ENO1}-LEU2]*	This study
yNK203	yNK165, *ura3-52*:: *[P_{PAB1}-ste2$_{Ec}$-T_{ENO1}-LEU2]*	This study
yNK204	yNK165, *ura3-52*:: *[P_{PAB1}-ste2$_{Ka}$-T_{ENO1}-LEU2]*	This study
yNK205	yNK165, *ura3-52*:: *[P_{PAB1}-ste2$_{Kl}$-T_{ENO1}-LEU2]*	This study
yNK206	yNK165, *ura3-52*:: *[P_{PAB1}-ste2$_{Kn}$-T_{ENO1}-LEU2]*	This study
yNK207	yNK165, *ura3-52*:: *[P_{PAB1}-ste2$_{Lf}$-T_{ENO1}-LEU2]*	This study
yNK208	yNK165, *ura3-52*:: *[P_{PAB1}-ste2$_{Lm}$-T_{ENO1}-LEU2]*	This study
yNK209	yNK165, *ura3-52*:: *[P_{PAB1}-ste2$_{Lt}$-T_{ENO1}-LEU2]*	This study
yNK210	yNK165, *ura3-52*:: *[P_{PAB1}-ste2$_{Sc}$-T_{ENO1}-LEU2]*	This study
yNK211	yNK165, *ura3-52*:: *[P_{PAB1}-ste2$_{Tp}$-T_{ENO1}-LEU2]*	This study
yNK212	yNK165, *ura3-52*:: *[P_{PAB1}-ste2$_{Vp}$-T_{ENO1}-LEU2]*	This study

Table 17: List of *S. cerevisiae* strains used in the YCTK project for the Bar1 characterization.

Strain	Genotype	Source
yNK213	yNK157, *ura3-52*:: *[P_{HHF1}-bar1$_{Ca}$-T_{ENO2}-LEU2]*	This study
yNK214	yNK157, *ura3-52*:: *[P_{HHF1}-bar1$_{Ec}$-T_{ENO2}-LEU2]*	This study
yNK215	yNK157, *ura3-52*:: *[P_{HHF1}-bar1$_{Kl}$-T_{ENO2}-LEU2]*	This study
yNK216	yNK157, *ura3-52*:: *[P_{HHF1}-bar1$_{Kn}$-T_{ENO2}-LEU2]*	This study
yNK217	yNK157, *ura3-52*:: *[P_{HHF1}-bar1$_{Lt}$-T_{ENO2}-LEU2]*	This study
yNK218	yNK157, *ura3-52*:: *[P_{HHF1}-bar1$_{Sc}$-T_{ENO2}-LEU2]*	This study
yNK219	yNK157, *ura3-52*:: *[P_{HHF1}-bar1$_{Vp}$-T_{ENO2}-LEU2]*	This study

Table 18: List of *S. cerevisiae* strains used in the YCTK project for multicellular networks.

Strain	Alias	Genotype	Source
yNK210	yBuffer Sender 1	yNK159, *ura3*-52:: *[P_{TDH3}-mfa1$_{Sc}$-T_{TDH1}-LEU2]*	This study
yNK211	yBuffer Receiver	yNK159, *HO*:: *[P_{HHF1}-sst2$_{Sc}$-T_{ENO1}-P_{FUS1}-mTurquoise2-T_{ADH1}-LEU2]*	This study
yNK212	yInverter Sender 1	yNK159, *ura3*-52:: *[P_{TDH3}- bar1$_{Sc}$-T_{ENO2}-LEU2]*	This study
yNK213	yInverter Receiver	yNK159,*HO*::*[P_{REV1}-mfa1$_{Sc}$-T_{TDH1}-P_{RAD27}-sst2$_{Sc}$-T_{ENO1}-P_{FUS1}-mTurquoise2-T_{ADH1}-LEU2]*	This study
yNK214	yAND Sender 1	yNK159,*HO*::*[P_{REV1}-mfa1$_{Sc}$-T_{TDH1}-P_{RAD27}-sst2$_{Sc}$-T_{ENO1}-P_{FUS1}-mTurquoise2-T_{ADH1}-LEU2]*	This study
yNK215	yAND Sender 2	yNK159, *HO*::*[P_{PGK1}-mfa1$_{Ca}$-T_{TDH1}-P_{PAB1}-sst2$_{Lf}$-T_{ENO1}-P_{FUS1}-mfa1$_{Lm}$-T_{ADH1} -LEU2]*	This study
yNK216	yAND Receiver	yNK159,*HO*::*[P_{PAB1}-sst$_{Lm}$-T_{ENO1}-P_{FUS1}-venus$_{rf}$-T_{ADH1}-LEU2]*	This study

yNK217	yOR Sender 1	yNK159, *ura3*-52::*[P_{PGK1}-mfa1$_{Tp}$ -T_{TDH1}-LEU2]*	This study
yNK218	yOR Sender 2	yNK159, *ura3*-52:: *[P_{PGK1}-mfa1$_{Kn}$ -T_{TDH1}-LEU2]*	This study
yNK219	yOR Receiver	yNK159, *ura3*-52:: *[P_{RPL18B}-ste$_{Sc}$-T_{ENO1}-P_{FUS1}-mTurquoise2-T_{TDH1}-LEU2]*	This study
yNK210	yNOR Sender 1	yNK159, *ura3*-52:: *[P_{TDH3}-bar$_{Sc}$ -T_{ENO2}-LEU2]*	This study
yNK211	yNOR Sender 2	yNK159, *ura3*-52:: *[P_{TDH3}-bar$_{Kl}$-T_{ENO2}-LEU2-URA3]*	This study
yNK212	yNOR Receiver	yNK159, *ura3*-52:: *[P_{RPL18B}- mfa1$_{Kl}$ -T_{TDH1}-P_{POP6}-ste2$_{KL}$-T_{ENO1}- P_{FUS1}-mTurquoise2-T_{ADH1}-LEU2]*	This study
yNK213	yXOR Sender 1	yNK159, *HO*::*[P_{RAD27}- mfa1$_{Ec}$-T_{TDH1}-HIS3]*	This study
yNK214	yXOR Sender 2	yNK159, *HO*:: *[P_{RAD27}- mfa1$_{Sc}$-T_{TDH1}-HIS3]*	This study
yNK215	yXOR Receiver	yNK159, *HO*:: *[P_{RAD27}- mfa1$_{Ec}$ -T_{TDH1}-P_{TDH3}-bar1$_{Sc}$-T_{ENO2}-LEU2]*	This study
yNK216	yXNOR Sender 1	yNK159, *HO*:: *[P_{PSP2}- mfa1$_{Lm}$ -T_{ENO1}-P_{CCW12}-ste2$_{Lm}$-T_{SSA1}- P_{FUS1}-bar1$_{Ca}$-T_{ENO2}- P_{TDH3}-bar1$_{Ec}$-T_{TDH1}-LEU2]*	This study
yNK217	yXNOR Sender 2	yNK159, *HO*:: *[P_{PSP2}- mfa1$_{Ec}$ -T_{ENO1}-P_{CCW12}-ste2$_{Ec}$-T_{SSA1}- P_{FUS1}-bar1$_{Ca}$-T_{ENO2}-P_{TDH3}-bar1$_{Sc}$-T_{TDH1}-LEU2]*	This study
yNK218	yXNOR Receiver	yNK159, *HO*:: *[P_{PSP2}- mfa1$_{Ca}$ -T_{ENO1}-P_{CWC12}-ste2$_{Ca}$-T_{ENO2}-P_{FUS1}-mTurquoise2-T_{ADH1}-LEU2]*	This study
yNK219	yNAND Sender 1	yNK159, *HO*:: *[P_{PGK1}- mfa1$_{Lt}$ -T_{TDH1}-P_{PAB1}-ste2$_{Ca}$-T_{ENO1}-P_{FUS1}-bar1$_{Kl}$-T_{ENO2}-LEU2]*	This study
yNK220	yNAND Sender 2	yNK159, *HO*:: *[P_{PGK1}- mfa1$_{Ca}$-T_{TDH1}-P_{PAB1}-ste2$_{Lt}$-T_{ENO1}-P_{FUS1}-bar1$_{Kl}$-T_{ENO2}-LEU2]*	This study
yNK221	yNAND Reciver	yNK159, *HO*:: *[P_{PSP2}- mfa1$_{Kl}$-T_{ENO2}-P_{PAB1}-ste2$_{Kl}$-T_{ENO1}-P_{FUS1}-mTurquoise$_{I}$-T_{ENO2}-LEU2]*	This study
yNK222	yAmplifier Sender	yNK159, *HO*:: *[P_{CUP1}- mfa1$_{Ca}$ -T_{TDH1}-P_{TETO7}- mfa1$_{Lm}$ -T_{PGK1}-P_{GAL1}- mfa$_{Lf}$ -T_{ENO2}-LEU2]*	This study
yNK223	yAmplifier Receiver 1	yNK159, *HO*:: *[P_{FUS1}- mfa1$_{Ca}$ -T_{TDH1}-P_{RPL18B}- ste2$_{Ca}$ -T_{ENO1}-P_{FUS3}- venus -T_{PGK1}-LEU2]*	This study
yNK224	yAmplifier Receiver 2	yNK159, *HO*:: *[P_{FUS1}- mfa1$_{Lm}$ -T_{TDH1}-P_{PAB1}- ste2$_{Lm}$ -T_{ENO1}-P_{FUS3}- mRuby -T_{ENO2}-LEU2]*	This study
yNK225	yAmplifier Receiver 3	yNK159, *HO*:: *[P_{FUS1}- mfa1$_{Lf}$ -T_{TDH1}-P_{PAB1}- ste2$_{Lf}$ -T_{ENO1}-P_{FUS3}- mTurquoise -T_{ENO2}-LEU2]*	This study
yNK226	yCascade Sender 1	yNK159, *HO*:: *[P_{CUP1}- mfa1$_{Ca}$ -T_{TDH1}-LEU2]*	This study
yNK227	yCascade Sender 2	yNK159, *HO*:: *[P_{FUS1}- mfa1$_{Lm}$ -T_{ENO2}-P_{TETO7}- ste2$_{Ca}$ -T_{TDH1} -LEU2]*	This study
yNK228	yCascade Sender 3	yNK159, *HO*:: *[P_{FUS1}- mfa1$_{Lf}$ -T_{ENO2}-P_{GAL1}- ste2$_{Lm}$ -T_{TDH1} -LEU2]*	This study
yNK229	yCascade Receiver	yNK159, *HO*:: *[P_{FUS1}- venus -T_{ENO2}-P_{PAB}- ste2$_{Lf}$ -T_{TDH1} -LEU2]*	This study

4.5.2 Plasmids

Table 19: List of plasmids used in the engineered acyl-CoA study.

Plasmid	Alias	Description	Source
pNK23	AIB	P_{TEF1}-*aibA*-T_{PGK1} P_{PGK1}-*aibC*-T_{ADH1} P_{ADH1}-*aibB*-T_{HXT7} P_{FBA1}-*liuC*-T_{TDH3}, 2µ, *TRP1*, AmpR-pMB1	This study
pNK30	3HP	P_{TEF1}-*mcr*-T_{PGK1} P_{ADH1}-*acr*-T_{HXT7} P_{FBA1}-*3hpcd*- T_{TDH3} P_{TDH3}-*3hpcs*-T_{ACT1}, 2µ, *LEU2*, AmpR-pMB1	This study
pNK36	PrpE	P_{TDH3}-*prpE*-T_{ACT1}, 2µ, *TRP1*, AmpR-pMB1	This study
pNK37	PrpE-PCC1	P_{TDH3}-*prpE*-T_{ACT1} P_{TEF1}-*accA1*- T_{TDH3} P_{PGK1}-*pccB1*-T_{HXT7}, 2µ, *TRP1*, AmpR-pMB1	This study
pNK42	3HP-CCR	P_{TEF1}-*mcr*-T_{CYC1} P_{ADH1}-*ccr*-T_{HXT7} P_{FBA1}-*3hpcd*-T_{TDH3} P_{TDH3}-*3hpcs*-T_{ACT1}, 2µ, *LEU2*, AmpR-pMB1	This study
pNK44	BUT	P_{GAL1}-*paaH1*-T_{ENO1} P_{GAL10}-*bktB*-T_{SSA1} P_{GAL7}-*ter*-T_{ADH1} P_{TEF2}-*crt*-T_{PGK1}, 2µ, *LEU2*, AmpR-pMB1	This study
pNK54	PrpE-PCC2	P_{TDH3}-*pccE*-T_{ACT1} P_{FBA1}-*prpE*-T_{TDH3} P_{ADH1}-*birA*-T_{HXT7} P_{TEF1} -*accA1*-T_{ADH1} P_{PGK1}-*pccB1*-T_{CYC}, 2µ, *TRP1*, AmpR-pMB1	This study

Table 20: List of level 0 plasmids of the CoA ester toolkit.

Plasmid	Alias	Description	Source
pCTK01	3hpcd L0 P3	*3hpcd*, *camR*-ColE1	This study
pCTK02	3hpcs L0 P3	*3hpcs*, *camR*-ColE1	This study
pCTK03	ACR L0 P3	*acr*, *camR*-ColE1	This study
pCTK04	$birA_{Ec}$ L0 P3	$birA_{Ec}$, *camR*-ColE1	This study
pCTK05	$birA_{Me}$ L0 P3	$birA_{Me}$, *camR*-ColE1	This study
pCTK06	$birA_{Stc}$ L0 P3	$birA_{Stc}$, *camR*-ColE1	This study
pCTK07	ccr_{Ca} L0 P3	ccr_{Ca}, *camR*-ColE1	This study
pCTK08	matB L0 P3	*matB*, *camR*-ColE1	This study
pCTK09	mcr L0 P3	*mcr*, *camR*-ColE1	This study
pCTK10	prpE L0 P3	*prpE*, *camR*-ColE1	This study
pCTK11	accA L0 P3	*accA*, *camR*-ColE1	This study
pCTK12	pccB L0 P3	*pccB*, *camR*-ColE1	This study
pCTK13	pccE L0 P3	*pccE*, *camR*-ColE1	This study
pCTK14	$pccA_{Me}$ L0 P3	$pccA_{Me}$, *camR*-ColE1	This study
pCTK15	$pccB_{Me}$ L0 P3	$pccB_{Me}$, *camR*-ColE1	This study
pCTK16	aibA L0 P3	*aibA*, *camR*-ColE1	This study
pCTK17	aibB L0 P3	*aibB*, *camR*-ColE1	This study
pCTK18	aibC L0 P3	*aibC*, *camR*-ColE1	This study
pCTK19	LiuC L0 P3	*liuC*, *camR*-ColE1	This study
pCTK20	bktB L0 P3	*bktB*, *camR*-ColE1	This study
pCTK21	crt L0 P3	*Crt*, *camR*-ColE1	This study
pCTK22	paaH1 L0 P3	*paaH1*, *camR*-ColE1	This study
pCTK23	Ter L0 P3	*ter*, *camR*-ColE1	This study

Table 21: List of level 0 plasmids of the yeast communication toolkit.

Plasmid	Alias	Description	Source
YCTK001	P_{DIG1} L0 P2	P_{DIG1}, *camR*-ColE1	This study
YCTK002	P_{FUS1} L0 P2	P_{FUS1}, *camR*-ColE1	This study
YCTK003	P_{FUS3} L0 P2	P_{FUS3}, *camR*-ColE1	This study
YCTK004	P_{MSG5} L0 P2	P_{MSG5}, *camR*-ColE1	This study
YCTK005	P_{PRM1} L0 P2	P_{PRM1}, *camR*-ColE1	This study
YCTK006	P_{REV1} L0 P2	P_{REV1}, *camR*-ColE1	This study
YCTK007	P_{SST2} L0 P2	P_{SST2}, *camR*-ColE1	This study
YCTK008	P_{YPS1} L0 P2	P_{YPS1}, *camR*-ColE1	This study
YCTK009	CaP0.001 L0 P3	$mfa1_{Ca}$, *camR*-ColE1	This study
YCTK010	EcP0.002 L0 P3	$mfa1_{Ec}$, *camR*-ColE1	This study
YCTK011	KaP0.003 L0 P3	$mfa1_{Ka}$, *camR*-ColE1	This study
YCTK012	KlP0.004 L0 P3	$mfa1_{Kl}$, *camR*-ColE1	This study
YCTK013	KnP0.005 L0 P3	$mfa1_{Kn}$, *camR*-ColE1	This study
YCTK014	LfP0.006 L0 P3	$mfa1_{Lf}$, *camR*-ColE1	This study
YCTK015	LmP0.007 L0 P3	$mfa1_{Lm}$, *camR*-ColE1	This study
YCTK016	LtP0.008 L0 P3	$mfa1_{Lt}$, *camR*-ColE1	This study
YCTK017	ScP0.009 L0 P3	$mfa1_{Sc}$, *camR*-ColE1	This study
YCTK018	TpP0.010 L0 P3	$mfa1_{Tp}$, *camR*-ColE1	This study
YCTK019	VpP0.011 L0 P3	$mfa1_{Vp}$, *camR*-ColE1	This study
YCTK020	CaR0.001 L0 P3	$ste2_{Ca}$, *camR*-ColE1	This study
YCTK021	EcR0.002 L0 P3	$ste2_{Ec}$, *camR*-ColE1	This study
YCTK022	KaR0.003 L0 P3	$ste2_{Ka}$, *camR*-ColE1	This study
YCTK023	KlR0.004 L0 P3	$ste2_{Kl}$, *camR*-ColE1	This study
YCTK024	KnR0.005 L0 P3	$ste2_{Kn}$, *camR*-ColE1	This study
YCTK025	LfR0.006 L0 P3	$ste2_{Lf}$, *camR*-ColE1	This study
YCTK026	LmR0.007 L0 P3	$ste2_{Lm}$, *camR*-ColE1	This study
YCTK027	LtR0.008 L0 P3	$ste2_{Lt}$, *camR*-ColE1	This study
YCTK028	ScR0.009 L0 P3	$ste2_{Sc}$, *camR*-ColE1	This study
YCTK029	TpR0.010 L0 P3	$ste2_{Tp}$, *camR*-ColE1	This study
YCTK030	VpR0.011 L0 P3	$ste2_{Vp}$, *camR*-ColE1	This study
YCTK031	CaBar10.001 L0 P3	$bar1_{Ca}$, *camR*-ColE1	This study
YCTK032	EcBar10.002 L0 P3	$bar1_{Ec}$, *camR*-ColE1	This study
YCTK034	KlBar10.004 L0 P3	$bar1_{Kl}$, *camR*-ColE1	This study
YCTK035	KnBar10.005 L0 P3	$bar1_{Kn}$, *camR*-ColE1	This study
YCTK038	LtBar10.008 L0 P3	$bar1_{Lt}$, *camR*-ColE1	This study
YCTK039	ScBar10.009 L0 P3	$bar1_{Sc}$, *camR*-ColE1	This study
YCTK041	VpBar10.011 L0 P3	$bar1_{Vp}$, *camR*-ColE1	This study

Table 22: List of level 1 plasmids for promoter characterization.

Plasmid	Alias	Description	Source
pPC001	P_{DIG1}-*mRuby2*	*HO*-P_{DIG1}-*mRuby2*-T_{THD1}-*HIS3-HO*, *ampR*-ColE1	This study
pPC002	P_{FUS1}-*mRuby2*	*HO*-P_{FUS1}-*mRuby2*-T_{THD1}-*HIS3-HO*, *ampR*-ColE1	This study
pPC003	P_{FUS3}-*mRuby2*	*HO*-P_{FUS3}-*mRuby2*-T_{THD1}-*HIS3-HO*, *ampR*-ColE1	This study
pPC004	P_{MSG5}-*mRuby2*	*HO*-P_{MSG5}-*mRuby2*-T_{THD1}-*HIS3-HO*, *ampR*-ColE1	This study
pPC005	P_{PRM1}-*mRuby2*	*HO*-P_{PRM1}-*mRuby2*-T_{THD1}-*HIS3-HO*, *ampR*-ColE1	This study
pPC006	P_{REV1}-*mRuby2*	*HO*-P_{REV1}-*mRuby2*-T_{THD1}-*HIS3-HO*, *ampR*-ColE1	This study
pPC007	P_{SST2}-*mRuby2*	*HO*-P_{SST2}-*mRuby2*-T_{THD1} -*HIS3-HO*, *ampR*-ColE1	This study
pPC008	P_{YPS1}-*mRuby2*	*HO*-P_{YPS1}-*mRuby2*-T_{THD1}-*HIS3-HO*, *ampR*-ColE1	This study
pPC009	P_{REV1}-*mRuby2*	*HO*-P_{REV1}-*mRuby2*-T_{THD1}-*HIS3-HO*, *ampR*-ColE1	This study
pPC010	P_{RPL18B}-*mRuby2*	*HO*-P_{RPL18B}-*mRuby2*-T_{THD1}-*HIS3-HO*, *ampR*-ColE1	This study
pPC011	P_{TDH3}-*mRuby2*	*HO*-P_{TDH3}-*mRuby2*-T_{THD1}-*HIS3-HO*, *ampR*-ColE1	This study
pPC012	P_{DIG1}-*venus*	*HO*-P_{DIG1}-*venus*-T_{THD1}-*HIS3-HO*, *ampR*-ColE1	This study
pPC013	P_{FUS1}-*venus*	*HO*-P_{FUS1}-*venus*-T_{THD1}-*HIS3-HO*, *ampR*-ColE1	This study
pPC014	P_{FUS3}-*venus*	*HO*-P_{FUS3}-*venus*-T_{THD1}-*HIS3-HO*, *ampR*-ColE1	This study
pPC015	P_{MSG5}-*venus*	*HO*-P_{MSG5}-*venus*-T_{THD1}-*HIS3-HO*, *ampR*-ColE1	This study
pPC016	P_{PRM1}-*venus*	*HO*-P_{PRM1}-*venus*-T_{THD1}-*HIS3-HO*, *ampR*-ColE1	This study
pPC017	P_{REV1}-*venus*	*HO*-P_{REV1}-*venus*-T_{THD1}-*HIS3-HO*, *ampR*-ColE1	This study
pPC018	P_{SST2}-*venus*	*HO*-P_{SST2}-*venus*-T_{THD1}-*HIS3-HO*, *ampR*-ColE1	This study
pPC019	P_{YPS1}-*venus*	*HO*-P_{YPS1}-*venus*-T_{THD1}-*HIS3-HO*, *ampR*-ColE1	This study
pPC020	P_{REV1}-*venus*	*HO*-P_{REV1}-*venus* -T_{THD1}-*HIS3-HO*, *ampR*-ColE1	This study
pPC021	P_{RPL18B}-*venus*	*HO*-P_{RPL18B}-*venus* -T_{THD1}-*HIS3-HO*, *ampR*-ColE1	This study
pPC022	P_{TDH3}-*venus*	*HO*-P_{TDH3}-*venus* -T_{THD1}-*HIS3-HO*, *ampR*-ColE1	This study
pPC023	P_{DIG1}-*mTurquoise2*	*HO*-P_{DIG1}-*mTurquoise2*-T_{THD1}-*HIS3-HO*, *ampR*-ColE1	This study
pPC024	P_{FUS1}-*mTurquoise2*	*HO*-P_{FUS1}-*mTurquoise2*-T_{THD1}-*HIS3-HO*, *ampR*-ColE1	This study
pPC025	P_{FUS3}-*mTurquoise2*	*HO*-P_{FUS3}-*mTurquoise2*-T_{THD1}-*HIS3-HO*, *ampR*-ColE1	This study
pPC026	P_{MSG5}-*mTurquoise2*	*HO*-P_{MSG5}-*mTurquoise2*-T_{THD1}-*HIS3-HO*, *ampR*-ColE1	This study
pPC027	P_{PRM1}-*mTurquoise2*	*HO*-P_{PRM1}-*mTurquoise2*-T_{THD1}-*HIS3-HO*, *ampR*-ColE1	This study
pPC028	P_{REV1}-*mTurquoise2*	*HO*-P_{REV1}-*mTurquoise2*-T_{THD1}-*HIS3-HO*, *ampR*-ColE1	This study
pPC029	P_{SST2}-*mTurquoise2*	*HO*-P_{SST2}-*mTurquoise2*-T_{THD1}-*HIS3-HO*, *ampR*-ColE1	This study
pPC030	P_{YPS1}-*mTurquoise2*	*HO*-P_{YPS1}-*mTurquoise2*-T_{THD1}-*HIS3-HO*, *ampR*-ColE1	This study
pPC031	P_{REV1}-*mTurquoise2*	*HO*-P_{REV1}-*mTurquoise2*-T_{THD1}-*HIS3-HO*, *ampR*-ColE1	This study
pPC032	P_{RPL18B}-*mTurquoise2*	*HO*-P_{RPL18B}-*mTurquoise2*-T_{THD1}-*HIS3-HO*, *ampR*-ColE1	This study
pPC033	P_{TDH3}-*mTurquoise2*	*HO*-P_{TDH3}-*mTurquoise2*-T_{THD1}-*HIS3-HO*, *ampR*-ColE1	This study
pPC034		*URA3*-P_{FUS1}-*ste2*$_{Sc}$-T_{ENO1}-*LEU2-URA3*, *ampR*-ColE1	This study
pIPC01		*URA3*-P_{CUP1}-*venus*-T_{ENO1}-*LEU2-URA3*, *ampR*-ColE1	This study
pIPC02		*URA3*-P_{CUP1}-*venus*-T_{ENO2}-*LEU2-URA3*, *ampR*-ColE1	This study
pIPC03		*HO*-P_{CUP1}-*venus*-T_{TDH1}-*HIS3-HO ampR*-ColE1	This study
pIPC04		*URA3*-P_{PAB1}-*venus*-T_{ENO1}-*LEU2-URA3*, *ampR*-ColE1	This study
pIPC05		*URA3*-P_{HHF1}-*venus*-T_{ENO2}-*LEU2-URA3*, *ampR*-ColE1	This study
pIPC06		*HO*-P_{PGK1}-*venus*-T_{TDH1}-*LEU2-HO*, *ampR*-ColE1	This study
pIPC07		*URA3*-P_{TETO7}-*venus*-T_{ENO1}-*HIS3-URA3*, *ampR*-ColE1	This study

Table 23: List of level 1 plasmids for the *mfa1* expression.

Plasmid	Alias	Description	Source
pP001	pCaP1.001	*HO*-P_{PGK1}-*mfa1*$_{Ca}$-T_{THD1}-*HIS3-HO*, *ampR*-ColE1	This study
pP002	pEcP1.002	*HO*-P_{PGK1}-*mfa1*$_{Ec}$-T_{THD1}-*HIS3-HO*, *ampR*-ColE1	This study
pP003	pKaP1.003	*HO*-P_{PGK1}-*mfa1*$_{Ka}$-T_{THD1}-*HIS3-HO*, *ampR*-ColE1	This study
pP004	pKlP1.004	*HO*-P_{PGK1}-*mfa1*$_{Kl}$-T_{THD1}-*HIS3-HO*, *ampR*-ColE1	This study
pP005	pKnP1.005	*HO*-P_{PGK1}-*mfa1*$_{Kn}$-T_{THD1}-*HIS3-HO*, *ampR*-ColE1	This study
pP006	pLfP1.006	*HO*-P_{PGK1}-*mfa1*$_{Lf}$-T_{THD1}-*HIS3-HO*, *ampR*-ColE1	This study
pP007	pLmP1.007	*HO*-P_{PGK1}-*mfa1*$_{Lm}$-T_{THD1}-*HIS3-HO*, *ampR*-ColE1	This study
pP008	pLtP1.008	*HO*-P_{PGK1}-*mfa1*$_{Lt}$-T_{THD1}-*HIS3-HO*, *ampR*-ColE1	This study
pP009	pScP1.009	*HO*-P_{PGK1}-*mfa1*$_{Sc}$-T_{THD1}-*HIS3-HO*, *ampR*-ColE1	This study
pP010	pTpP1.010	*HO*-P_{PGK1}-*mfa1*$_{Tp}$-T_{THD1}-*HIS3-HO*, *ampR*-ColE1	This study
pP011	pVpP1.011	*HO*-P_{PGK1}-*mfa1*$_{Vp}$-T_{THD1}-*HIS3-HO*, *ampR*-ColE1	This study

Table 24: List of level 1 plasmids for the *ste2* expression.

Plasmid	Alias	Description	Source
pR001	pCaR1.001	*URA3*-P_{PAB1}-*ste2*$_{Ca}$-T_{ENO1}-*LEU2-URA3*, *ampR*-ColE1	This study
pR002	pEcR1.002	*URA3*-P_{PAB1}-*ste2*$_{Ec}$-T_{ENO1}-*LEU2-URA3*, *ampR*-ColE1	This study
pR003	pKaR1.003	*URA3*-P_{PAB1}-*ste2*$_{Ka}$-T_{ENO1}-*LEU2-URA3*, *ampR*-ColE1	This study
pR004	pKlR1.004	*URA3*-P_{PAB1}-*ste2*$_{Kl}$-T_{ENO1}-*LEU2-URA3*, *ampR*-ColE1	This study
pR005	pKnR1.005	*URA3*-P_{PAB1}-*ste2*$_{Kn}$-T_{ENO1}-*LEU2-URA3*, *ampR*-ColE1	This study
pR006	pLfR1.006	*URA3*-P_{PAB1}-*ste2*$_{Lf}$-T_{ENO1}-*LEU2-URA3*, *ampR*-ColE1	This study
pR007	pLmR1.007	*URA3*-P_{PAB1}-*ste2*$_{Lm}$-T_{ENO1}-*LEU2-URA3*, *ampR*-ColE1	This study
pR008	pLtR1.008	*URA3*-P_{PAB1}-*ste2*$_{Lt}$-T_{ENO1}-*LEU2-URA3*, *ampR*-ColE1	This study
pR009	pScR1.009	*URA3*-P_{PAB1}-*ste2*$_{Sc}$-T_{ENO1}-*LEU2-URA3*, *ampR*-ColE1	This study
pR010	pTpR1.010	*URA3*-P_{PAB1}-*ste2*$_{Tp}$-T_{ENO1}-*LEU2-URA3*, *ampR*-ColE1	This study
pR011	pVpR1.011	*URA3*-P_{PAB1}-*ste2*$_{Vp}$-T_{ENO1}-*LEU2-URA3*, *ampR*-ColE1	This study

Table 25: List of level 1 plasmids for the *bar1* expression.

Plasmid	Alias	Description	Source
pB001	pCaB1.001	*URA3*-P_{HHF1}-*bar1*$_{Ca}$-T_{ENO2}-*LEU2-URA3*, *ampR*-ColE1	This study
pB002	pEcB1.002	*URA3*-P_{HHF1}-*bar1*$_{Ec}$-T_{ENO2}-*LEU2-URA3*, *ampR*-ColE1	This study
pB004	pKlB1.004	*URA3*-P_{HHF1}-*bar1*$_{Kl}$-T_{ENO2}-*LEU2-URA3*, *ampR*-ColE1	This study
pB005	pKnB1.005	*URA3*-P_{HHF1}-*bar1*$_{Kn}$-T_{ENO2}-*LEU2-URA3*, *ampR*-ColE1	This study
pB008	pLtB1.008	*URA3*-P_{HHF1}-*bar1*$_{Lt}$-T_{ENO2}-*LEU2-URA3*, *ampR*-ColE1	This study
pB009	pScB1.009	*URA3*-P_{HHF1}-*bar1*$_{Sc}$-T_{ENO2}-*LEU2-URA3*, *ampR*-ColE1	This study
pB011	pVpB1.011	*URA3*-P_{HHF1}-*bar1*$_{Vp}$-T_{ENO2}-*LEU2-URA3*, *ampR*-ColE1	This study

Table 26: List of plasmids of the multicellular yeast networks.

Plasmid	Alias	Description	Source
pYG23	pBuffer Sender 1	*URA3*-P_{TDH3}-*mfa1*$_{Sc}$-T_{TDH1}-*LEU2-URA3*, *ampR*-ColE1	This study
pYG26	pBuffer Receiver	*HO*-P_{HHF1}-*sst2*$_{Sc}$-T_{ENO1}-P_{FUS1}-mTurquoise2-T_{ADH1}-*LEU2-HO*, *kanR*-ColE1	This study
pYG29	pInverter Sender 1	*URA3*-P_{TDH3}- *bar1*$_{Sc}$-T_{ENO2}-*LEU2-URA3*, *ampR*-ColE1	This study
pYG30	pInverter Receiver	*HO*-P_{REV1}-*mfa1*$_{Sc}$-T_{TDH1}-P_{RAD27}-*sst2*$_{Sc}$-T_{ENO1}-P_{FUS1}-mTurquoise2-T_{ADH1}-*LEU2-HO*, *kanR*-ColE1	This study

pYG39	pAND Sender 1	*HO*-P_{PGK1}-*mfa1*$_{Lf}$-T_{TDH1}-P_{PAB1}-*sst2*$_{Ca}$-T_{ENO1}-P_{FUS1}-*mfa1*$_{Lm}$-T_{ADH1} -*LEU2-HO*, *kanR*-ColE1	This study
pYG40	pAND Sender 2	*HO*-P_{PGK1}-*mfa1*$_{Ca}$-T_{TDH1}-P_{PAB1}-*sst2*$_{Lf}$-T_{ENO1}-P_{FUS1}-*mfa1*$_{Lm}$-T_{ADH1} -*LEU2-HO*, *kanR*-ColE1	This study
pYG41	pAND Receiver	*HO*-P_{PAB1}-*sst*$_{Lm}$-T_{ENO1}-P_{FUS1}-*venus*$_{f}$-T_{ADH1}-*LEU2-HO*, *kanR*-ColE1	This study
pYG42	pOR Sender 1	*URA3*-P_{PGK1}-*mfa1*$_{Tp}$ -T_{TDH1}-*LEU2-URA3*, *ampR*-ColE1	This study
pYG43	pOR Sender 2	*URA3*-P_{PGK1}-*mfa1*$_{Kn}$ -T_{TDH1}-*LEU2-URA3*, *ampR*-ColE1	This study
pYG45	pOR Receiver	*URA3*-P_{RPL18B}-*ste*$_{Sc}$-T_{ENO1}-P_{FUS1}-*mTurquoise2*-T_{TDH1}-*LEU2-URA3*, *kanR*-ColE1	This study
pYG46	pNOR Sender 1	*URA3*-P_{TDH3}-*bar*$_{Sc}$ -T_{ENO2}-*LEU2-URA3*, *ampR*-ColE1	This study
pYG47	pNOR Sender 2	*URA3*-P_{TDH3}-*bar*$_{Kl}$-T_{ENO2}-*LEU2-URA3*, *ampR*-ColE1	This study
pYG50	pNOR Receiver	*HO*-P_{RPL18B}- *mfa1*$_{Kl}$ -T_{TDH1}-P_{POP6}-*ste2*$_{KL}$-T_{ENO1}- P_{FUS1}-*mTurquoise2*-T_{ADH1}-*LEU2-HO*, *kanR*-ColE1	This study
pYG52	pXOR Sender 1	*HO*-P_{RAD27}- *mfa1*$_{Ec}$-T_{TDH1}-*HIS3-HO*, *ampR*-ColE1	This study
pYG54	pXOR Sender 2	*HO*-P_{RAD27}- *mfa1*$_{Sc}$-T_{TDH1}-*HIS3-HO*, *ampR*-ColE1	This study
pYG55	pXOR Receiver	*HO*-P_{RAD27}- *mfa1*$_{Ec}$ -T_{TDH1}-P_{TDH3}-*bar1*$_{Sc}$-T_{ENO2}-*LEU2-HO*, *kanR*-ColE1	This study
pYG69	pXNOR Sender 1	*HO*-P_{PSP2}- *mfa1*$_{Lm}$ -T_{ENO1}-P_{CCW12}-*ste2*$_{Lm}$-T_{SSA1}- P_{FUS1}-*bar1*$_{Ca}$-T_{ENO2}- P_{TDH3}-*bar1*$_{Ec}$-T_{TDH1}-*LEU2-HO*, *kanR*-ColE1	This study
pYG70	pXNOR Sender 2	*HO*-P_{PSP2}- *mfa1*$_{Ec}$ -T_{ENO1}-P_{CCW12}-*ste2*$_{Ec}$-T_{SSA1}- P_{FUS1}-*bar1*$_{Ca}$-T_{ENO2}- P_{TDH3}-*bar1*$_{Sc}$-T_{TDH1}-*LEU2-HO*, *kanR*-ColE1	This study
pYG71	pXNOR Receiver	*HO*-P_{PSP2}- *mfa1*$_{Ca}$ -T_{ENO1}-P_{CWC12}-*ste2*$_{Ca}$-T_{ENO2}-P_{FUS1}-*mTurquoise2*-T_{ADH1}-*LEU2-HO*, *kanR*-ColE1	This study
pYG78	pNAND Sender 1	*HO*-P_{PGK1}- *mfa1*$_{Lt}$ -T_{TDH1}-P_{PAB1}-*ste2*$_{Ca}$-T_{ENO1}-P_{FUS1}-*bar1*$_{Kl}$-T_{ENO2}-*LEU2-HO*, *kanR*-ColE1	This study
pYG79	pNAND Sender 2	*HO*-P_{PGK1}- *mfa*$_{Ca}$-T_{TDH1}-P_{PAB1}-*ste2*$_{Lt}$-T_{ENO1}-P_{FUS1}-*bar1*$_{Kl}$-T_{ENO2}-*LEU2-HO*, *kanR*-ColE1	This study
pYG80	pNAND Receiver	*HO*-P_{PSP2}- *mfa*$_{Kl}$-T_{ENO2}-P_{PAB1}-*ste2*$_{Kl}$-T_{ENO1}-P_{FUS1}-*mTurquoise*$_{l}$-T_{ENO2}-*LEU2-HO*, *kanR*-ColE1	This study
pYG81	pAmplifier Sender	*HO*-P_{CUP1}- *mfa1*$_{Ca}$ -T_{TDH1}-P_{TETO7}- *mfa1*$_{Lm}$ -T_{PGK1}-P_{GAL1}- *mfa1*$_{Lf}$ -T_{ENO2}-*LEU2-HO*, *kanR*-ColE1	This study
pYG82	pAmplifier Receiver 1	*HO*-P_{FUS1}- *mf1α*$_{Ca}$ -T_{TDH1}-P_{RPL18B}- *ste2*$_{Ca}$ -T_{ENO1}-P_{FUS3}- *venus* -T_{PGK1}-*LEU2-HO*, *kanR*-ColE1	This study
pYG83	pAmplifier Receiver 2	*HO*-P_{FUS1}- *mf1α*$_{Lm}$ -T_{TDH1}-P_{PAB1}- *ste2*$_{Lm}$ -T_{ENO1}-P_{FUS3}- *mRuby* -T_{ENO2}-*LEU2-HO*, *kanR*-ColE1	This study
pYG84	pAmplifier Receiver 3	*HO*-P_{FUS1}- *mfa1*$_{Lf}$ -T_{TDH1}-P_{PAB1}- *ste2*$_{Lf}$ -T_{ENO1}-P_{FUS3}- *mTurquoise* -T_{ENO2}-*LEU2-HO*, *kanR*-ColE1	This study
pYG85	pCascade Sender 1	*HO*-P_{FUS1}- *mfa1*$_{Ca}$ -T_{TDH1}-*LEU2-HO*, *kanR*-ColE1	This study
pYG86	pCascade Sender 2	*HO*-P_{FUS1}- *mfa1*$_{Lm}$ -T_{ENO2}-P_{TETO7}- *ste2*$_{Ca}$ -T_{TDH1} -*LEU2-HO*, *kanR*-ColE1	This study
pYG87	pCascade Sender 3	*HO*-P_{FUS1}- *mfa1*$_{Lf}$ -T_{ENO2}-P_{GAL1}- *ste2*$_{Lm}$ -T_{TDH1} -*LEU2-HO*, *kanR*-ColE1	This study
pYG88	pCascade Reciver	*HO*-P_{FUS1}- *venus* -T_{ENO2}-P_{PAB}- *ste2*$_{Lf}$ -T_{TDH1} -*LEU2-HO*, *kanR*-ColE1	This study

Table 27: List of plasmids for the expression titration of *mfa1*, *ste2*, and *bar1*.

Plasmid	Alias	Description	Source
pT01	P_{CUP1}-*ste2*$_{Sc}$	*URA3*-P_{CUP1}-*ste2*$_{Sc}$ -T_{ENO1}-*LEU2-URA3*, *ampR*-ColE1	This study
pT02	P_{CUP1}-*bar1*$_{Sc}$	*URA3*-P_{CUP1}-*bar1*$_{Sc}$ -T_{ENO2}-*LEU2-URA3*, *ampR*-ColE1	This study
pT03	P_{CUP1}- *mfa1*$_{Sc}$	*HO*-P_{CUP1}- *mfa1*$_{Sc}$ -T_{TDH1}-*HIS3-HO ampR*-ColE1	This study

4.6 Data acquisition and analysis

4.6.1 Cultivation conditions

For the metabolic engineering project, *S. cerevisiae* BJ5465 cells were grown at 30 °C in yeast extract-peptone-dextrose (YPD) medium consisting of 1 % bacto yeast extract, 2 % bacto peptone and 2 % dextrose to prepare competent cells. Yeast strains carrying pathway plasmids were grown at 30 °C on selective plates and at 25°C for liquid cultures, which was required to ensure protease deficiency (see genotype) and that we showed to be beneficial for precursor and PKS expression [123]. A modified synthetic complete medium was used for selective growth in liquid medium. Synthetic complete medium was purchased from Sunrise Scientific lacking tryptophan (SC-TRP) or leucine (SC-LEU). The modified synthetic complete medium contained 13.4 g/L yeast nitrogen base, 5.76 g/L SC-TRP or 5.49 g/L SC-LEU, 20 g/L glucose and 100 mM sodium phosphate buffer pH 6.4 and was used to grow the strains containing 2µ plasmids.
For intracellular acyl-CoA analysis, fresh single colonies were prepared. Each plasmid was transformed into competent cells of *S. cerevisiae* strain BJ5465 and plated onto selective growth agar. The plates were incubated for 3 days at 30°C. Pre-cultures were grown from single colonies in 5 mL selective SC medium for 3 to 4 days at 25°C. Production cultures were then inoculated to a starting OD of 0.05 into 12 mL of selective medium in 100-mL flasks and grown at 25 °C and 200 rpm. Strains carrying *prpE* genes were supplemented with 50 mM sodium propionate to allow propionyl-CoA production. The cells were harvested after 48 h [123].
To determine growth rates, cells were freshly transformed with plasmids. After growing for three days on plates, three/four colonies were picked and cultured in 5 mL media for another three days. Cells were then inoculated at an OD of 0.05 in 24-well plates in 1.5 mL volume with different propionate concentrations, if appropriate, and grown for 70 h at 25 °C [123]. To analyze the growth and to obtain the growth rates, a MATLAB script from Hannes Link was adapted.

For the YCTK project, the yeast cells were always grown at 30 °C. To prepare competent cells, the strains were cultured in 2x YPD (see above), while otherwise SD dropout liquid media or plates were utilized. After genomic integration, the cells were grown on plates for 2-4 days. Liquid overnight cultures were prepared in 24-well plates with 1.5 mL SD dropout or SD complete media and inoculated from single colonies on plates and cultivated for 12-16 hours prior inoculation for experimental procedures.
The day cultures for experiments were inoculated into 24-well plates to an OD OF 0.05 into 2.25 mL SD complete media and grown under shaking conditions at 30 °C for 4 hours. Afterwards, the cultures were either induced with α-factor or mixed with other cultures into 96-well plates to a total volume of 300 µL. For time course experiments, the cultures were incubated up 6 hours, while for all other experiments, the cells were measured 3 hours after transfer onto the 96-well plateS.
To determine the growth and examine cell cycle arrest upon α-factor stimulation, the cells were inoculated into 24-well plates to a starting OD of 0.05. After 4 hours of incubation in a plate reader under shaking conditions at 30°C , α-factor was added, where appropriate, and further incubated for 36 hours. To avoid flocculation, the cells were alternately shaken linearly and orbitally. To plot the growth, a MATLAB script from Hannes Link was adapted.

4.6.2 Metabolite extraction

To determine intracellular concentrations of all acyl-CoA esters from production cultures, the cells were cultivated for 48 h at 25°C at 200 rpm. The protocol for intracellular metabolite extraction was adapted from a previous study [393]. After acyl-CoA ester production, a total OD of 10 was harvested by centrifugation for 3 min at -9 °C at 2,700 x g and supernatant was discarded. The cells were resuspended in 1 mL of pre-chilled quenching solution and transferred into 2 mL screw cap tubes, filled half with 0.5 mm glass beads. Cells were homogenized 10 times for 10 s at 4,800 x g with 2 min on ice between each homogenization pulse (Precellys Evolution, Bertin Instruments). To separate the cell lysate from the beads, the lid of the tubes was removed and a hole was poked into the bottom using a hot needle. The tube containing the metabolite extract was then set into an empty 15-mL falcon, centrifuged for 2 min at 2,700 x g and -9°C, to separate the extract from the beads. After removing the empty homogenizer tube with the remaining beads, the flow-through cell suspension was transferred into prechilled 1.5-mL tubes and centrifuged for at least 20 min at 17,000 g and -9°C to remove any remaining cell debris. The supernatant was transferred into a new tube and the samples were subsequently stored at -80°C for lyophilization or LC-MS/MS analysis [123].

4.6.3 LC-MS/MS analysis and chemical synthesis of acyl-CoA esters

Acyl-CoA esters were measured by fast LC-MS/MS as described previously [525]. An Agilent 1290 Infinity II UHPLC system (Agilent Technologies) was used for liquid chromatography. The column was an Acquity BEH Amide 30 x 2.1 mm with 1.7 µm particle size (Waters GmbH). The temperature of the column oven was 30°C, and the injection volume was 2 µL. LC solvent A was water with 10 mM ammonium formate and 0.1% formic acid (v/v), and LC solvent B was acetonitrile with 0.1% formic acid (v/v). The gradient was 0 min 90% B; 1.3 min 40% B; 1.5 min 40% B; 1.7 min 90% B; 2 min 90% B. The flow rate was 0.4 mL/min^{-1}. An Agilent 6495 triple quadrupole mass spectrometer (Agilent Technologies) was used for mass spectrometry using ion source parameters described in Guder *et al.* [526]. Parameters for multiple reaction monitoring (MRM) were adapted from Zimmermann *et al.* (Table 28) [525]. Absolute concentrations of acyl-CoA esters were estimated by external calibration curves. The corresponding acyl-CoAs were synthesized according to a previous study [527]. Butyryl-CoA and propionyl-CoA were synthesized following the protocol for Symmetric Anhydride Synthesis [527]. For the hexanoyl-CoA, isobyutyryl-CoA, 2-methylbutyryl-CoA and isovaleryl-CoA synthesis, we used Carbonyldiimidazole Synthesis [527]. Methylmalonyl-CoA was synthesized using malonic acid and the malonyl-CoA synthetase MatB [527]. The purity of the products and yields were determined using HPLC-MS and Nanodrop (Nanodrop 2000, Thermo Scientific). The stocks of the compounds were stored at -80°C and diluted into extraction solution to use as standards for LC-MS/MS. All standards were mixed at final concentrations of 2.5 µM, 0.625 µM, 0.156 µM, 0.039 µM, 0.0098 µM and 0.0024 µM. From these calibration curves, the absolute concentration of precursors in cell lysates were determined. Intracellular concentrations were calculated using a specific cell volume of $3.7*10^{-14}$ L/cell and $3*10^{7}$ cells/mL per OD 1 [123,528,529]. The result figures were plotted using MATLAB and revised with Adobe Illustrator, the pathway schemes were generated with ChemDraw and revised using Adobe Illustrator.

Table 28: Multiple reaction monitoring (MRM) parameters

Metabolite	Formula	Q1 (m/z)	Q2 (m/z)
Propionyl-CoA	$C_{24}H_{40}N_7O_{17}P_3S$	822.1	408
Butyryl-CoA	$C_{25}H_{42}N_7O_{17}P_3S$	836.2	408
Isovaleryl-CoA	$C_{26}H_{44}N_7O_{17}P_3S$	850.2	408
Hexanoyl-CoA	$C_{27}H_{46}N_7O_{17}P_3S$	864.2	408
Methylmalonyl-CoA	$C_{25}H_{40}N_7O_{19}P_3S$	866.1	822

4.6.4 Likelihood analysis for the generation of phylogenetic trees

To study the relationship between the different species selected for the YCTK, a likelihood analysis of the SSU rRNAs, the mature α-factors, the pre-pro-α-factors, the Ste2s, and the Bar1s was performed by Stefan Rensing. The SSU rRNA sequences were obtained from SILVA (Table 29), the α-factor, Ste2 and Bar1 sequences from NCBI. The mature α-factor sequences were taken from the *in silico* identification of the *mfa1* genes (chapter 2.2.1.2). Alignments were generated using geneious and then provided Stefan Rensing to perform the likelihood analyses, who provided us the final trees (chapter 2.2.2).

Table 29: Association numbers of the SSU rRNAs in the SILVA database used for the alignment for the likelihood analysis.

Organism	Association number
Candida albicans	AB013586.1.1769
Eremothecium cymbalariae	AY046268.1.1746
Kazachstania africana	AB016510.1.1753
Kazachstania naganishii	AB016512.1.1759
Kluyveromyces lactis	AB054673.1.1766
Lachancea fermentati	FJUO01000029.3972.5759
Lachancea mirantina	FJUN01000016.3.1788
Lachancea thermotolerans	CU928180.1138188.1139986
Saccharomyces cerevisiae	AB278124.1.1714
Tetrapisispora phaffii	AY046245.1.1745
Vanderwaltozyma polyspora	AAZN01000149.13805.15594

4.6.5 Flow cytometry and gating

Most of the data of the YCTK project were obtained by flow cytometry. Flow cytometry allows the detection and measurement of up to 10,000 single cells per second and records physical and chemical properties. To measure the cells, we used the Fortessa Special Order flow cytometer from BD Biosciences. From a 96-well plate or tube, the cells are spired through the sample injection port. Subsequently, the cells pass through the flow cell, in which the cells are mixed with sheath fluid and then further pressed through a nozzle, resulting in the single cell alignment. Afterwards, the cells pass the laser beams and the fluorescence as well as the refracted light are

channeled through filters and mirrors to be detected by sensors. The sensor can only detect a specific spectrum of wavelengths. Generally, the forward scatter, which is in front of the light beam, captures information about the cell size. The side scatter records information about cellular granularity.

The FACS DIVA software was used for data acquisition. The *S. cerevisiae* cells were mostly expressing fluorescence reporter that were detected using different lasers and filters. We measured cells expressing mNeonGreen using the Blue Laser at 488 nm for excitation and detected the emission at 530 nm. For Venus we used the Blue-Green laser (514 nm) and detected the fluorescence at 528 nm, for mTurquoise2 fluorescence detection the Blue-Violet Laser (445 nm) was utilized and the fluorescence was measured at 470 nm, and for mRuby, the Yellow-Green Laser (561 nm) was utilized and the emission was acquired at 610 nm. Since we measured many samples at one time point, the cells were measured from 96-well plates using the high throughput sampler (HTS).

The cells were gated using DIVA and FlowJo (BD Bioscience). Within DIVA, cells were gated while measuring, to exclude events hitting the upper detector limits and events smaller than average yeast cells. Data processing for the promoter characterization, Ste2 sensitivity experiments, and the synthetic multicellular networks were performed using the FlowJo software. FlowJo was further used for raw data visualization.

For the promoter characterization and Ste2 sensitivity (Appendix Figure 4), the first gate that was applied on the recorded single-cell events was to identify single-cell events and thus to out gate multiple detections or aggregates. Next, a gate was added that included all yeast cells and that reduced the debris. The mean fluorescence of the yeast cells was then obtained based on the applied gates and further used to plot figures using MATLAB.

For the multicellular networks, the first two gates were set as above. Afterwards, the gates of the sender and receiver populations was set according to the dedicated constitutively expressed fluorescent protein (Appendix Figure 5). The recorded mean fluorescence intensities of the receiver cell population were exported and utilized to plot the results in MATLAB.

To plot the flow cytometry results, different approaches were taken. If applicable, flow cytometry histograms were exported from FlowJo. For the inducible promoter dose-response characterization and time courses, a MATLAB script was used. For the fitted sigmoidal α-factor dose-response curves and EC50 computation, a MATLAB script from Ritchie Smith was adapted (https://bit.ly/2Zu0kyO). To compute the EC50 and the Hill coefficient, the equation "sigmoid=@(beta,x)beta(1)+(beta(2)-beta(1))./(1+(x/beta(3)).^beta(4))" was used with the curve fitting "[coeffs,r,J]=nlinfit(dose,response,sigmoid,[minResponse maxResponse midResponse 1])". To generate the heatmaps, a heatmap script from Ameya Deoras was customized (https://bit.ly/34g6pgJ).

The plot for the Ste2 crosstalk experiment was generated using a R script by A. Anders. The script plotted the recorded flow cytometry data as histograms. Additionally, a color code indicated the log(par.mean) of the mating pathway activity, which was obtained by calculating the logarithm of the mean fluorescence intensities.

Also, for the Bar1 crosstalk experiment a R script by A. Anders was used. Similar to the previous script, the cytometer data were plotted as histograms. Here, the color code indicated the fold reduction (log(fold.chang)) of the mating pathway activity as a result of α-factor degradation by

Bar1. The fold change was calculated by dividing the log(par.mean) fluorescence intensities obtained in the absence of Bar1 by the mean fluorescence intensities in the presence of Bar1.
A. Anders generated the visualization plot of the Bar1 cleavage experiment. The utilized R script positioned the detected α-factor fragments to the corresponding mature α-factor. The color intensity displays the log of the signal intensity of the LC-MS/MS data. The color code as well as the positing on the y-axis represent the log2ratio of the untreated (no Bar1 protease) to the treated (Bar1 protease).
All figures were further revised using Adobe Illustrator after plotting with FlowJo, MATLAB or R.

4.6.6 α-factor identification and quantification using LC-MS/MS

To quantify α-factor and Bar1 promiscuity towards α-factors using LC-MS/MS, the different α-factor and Bar1 expressing strains were grown over night as previously described. Of each strain three replicates were grown. For the day cultures for the production quantification, the cells were inoculated into 25 mL SD complete media to and OD of 0.05 and grown for 7 hours at 200 rpm at 30 °C. For the Bar1 promiscuity experiment, the Bar1 strains were inoculated into 24 well-plates and grown for 4 hours. Then, synthetic α-factor was added to the cells and further cultivated for 3 hours. Since the α-factors and were applicable α-factor peptide fragments were secreted into and cleaved in the media, the supernatant was separated from the cells by centrifugation for 5 min at 4,000 rpm. 1 mL of the supernatant was taken, snap-frozen in liquid nitrogen and stored at -80 °C until further processing.
For the quantification, synthetic standard peptides were ordered. These standard peptides and the supernatants containing the produced α-factors or α-factor fragments were acidified with trifluoroacetic acid to a final of 1 %. Subsequently, the samples were desalted using C18 microspin columns (Harvard Apparatus) according to the manufacturer's instructions. After the elution of the column the sample was dried, reconstituted and then injected into and analyzed by liquid chromatography-mass spectrometry (LC-MS). The LC-MS/MS analysis of the α-factor peptides and fragments was performed using a Q-Exactive Plus mass spectrometer connected to an electrospray ion source (Thermo Fisher Scientific). The peptide separation was done using a Ultimate 3000 nanoLC-system (Thermo Fisher Scientific), containing an in-house packed C18 resin column (Magic C18 AQ 2.4 µm, Dr. Maisch). First, the samples were loaded onto a C18 precolumn (preconcentration set-up) and then eluted in backflush mode with a gradient from 98 % solvent A (0.15 % formic acid) and 2 % solvent B (99.85 % acetonitrile, 0.15 % formic acid) to 40 % solvent B over 30 min. The flow rate was 300 nL/ min. The data acquisition for the LFQ study was set to obtain one high-resolution MS scan at a resolution of 60000 (*m/z* 200) with scanning range from 375 to 1500 *m/z* followed by MS/MS scans of the 10 most intense ions. For increased efficiency of MS/MS shots, the charged state screening modus was adjusted to exclude unassigned and singly charged ions. The dynamic exclusion duration was 30 sec. The ion accumulation time was 50 ms (both MS and MS/MS). The automatic gain control (AGC) was 3×10^6 for MS survey scans and 1×10^5 for MS/MS scans.
Label-free quantification was performed with the MaxQuant (v1.6.6.0, https://www.nature.com/articles/nbt.1511) and/or Progenesis QI software (Nonlinear Dynamics, version 2.0). Searches were done with Andromeda within Maxquant, or when processed with Progenesis, the output data (MS/MS spectra) were exported in mgf format. MS/MS spectra were then searched

using MASCOT against the α-factor sequences in standard MaxQuant settings with no enzyme, or for Progensis/MASCOT: no enzyme with a mass tolerance set to 10 ppm for precursor ions and 0.02 Da for fragment ions for high energy-collision dissociation (HCD). Results from the database search were imported back to Progenesis and results were evaluated using SafeQuant R-package version 2.2.2. [530]. Due to the limited complexity FDR cut-off was disabled.

5 References

1. Braidwood, R. J. *et al.* Symposium: Did Man Once Live by Beer Alone? *Am. Anthropol.* (1953). doi:10.1525/aa.1953.55.4.02a00050
2. Braidwood, R. J. & Braidwood, L. The earliest village communities of southwestern asia. *Cah. d'Histoire Mond. J. World Hist. Cuad. Hist. Mund.* **1**, (1953).
3. Katz, S. & Voigt, M. Bread and Beer: The Early Use of Cereals in the Human Diet. *Exped. Mag. Univ. Pennsylvania* (1986).
4. McGovern, P. E. *Uncorking the Past: The Quest for Wine, Beer, and Other Alcoholic Beverages*. (2009).
5. Sicard, D. & Legras, J. L. Bread, beer and wine: Yeast domestication in the Saccharomyces sensu stricto complex. *Comptes Rendus - Biologies* (2011). doi:10.1016/j.crvi.2010.12.016
6. McGovern, P. E. *et al.* Fermented beverages of pre- and proto-historic China. *Proc. Natl. Acad. Sci. U. S. A.* (2004). doi:10.1073/pnas.0407921102
7. Pasteur, L. Mémoire sur la fermentation appelée lactique. *Ann. Chim. Phys.* (1858).
8. Pasteur, L. *Nouveaux faits concernant l'histoire de la fermentation alcoolique.* (1858).
9. Barnett, J. A. A history of research on yeasts 5: The fermentation pathway. *Yeast* (2003). doi:10.1002/yea.986
10. Nielsen, J. Yeast Systems Biology: Model Organism and Cell Factory. *Biotechnol. J.* (2019). doi:10.1002/biot.201800421
11. Mortimer, R. K. Evolution and variation of the yeast (Saccharomyces) genome. *Genome Research* (2000). doi:10.1101/gr.10.4.403
12. Fischer, E. & Thierfelder, H. Verhalten der verschiedenen Zucker gegen reine Hefen. *Ber Dtsch Chem Ges* (1894).
13. Fischer, E. Einfluss der Configuration auf die Wirkung der Enzyme. II. *Berichte der Dtsch. Chem. Gesellschaft* (1894). doi:10.1002/cber.189402703169
14. Thiel, A. Lois générales de l'action des diastases, par V ICTOR H ENRI . VIII und 129 Seiten. (Paris, A. H ERMANN , 1903.) . *Zeitschrift für Anorg. Chemie* (1903). doi:10.1002/zaac.19030350145
15. Michaelis, L., Menten, M. L., Goody, R. S. & Johnson, K. A. Die Kinetik der Invertinwirkung/ The kinetics of invertase action. *Biochemistry* (1913). doi:10.1021/bi201284u
16. Barnett, J. A. & Robinow, C. F. A history of research on yeasts 4: Cytology part II, 1950-1990. *Yeast* (2002). doi:10.1002/yea.875
17. Lindegren, C. C. A New Gene Theory and an Explanation of the Phenomenon of Dominance to Mendelian Segregation of the Cytogene. *Proc. Natl. Acad. Sci. U. S. A.* (1946). doi:10.1073/pnas.32.3.68
18. Lindegren, C. C. & Lindegren, G. Selecting, Inbreeding, Recombining, and Hybridizing Commercial Yeasts. *J. Bacteriol.* (1943).
19. Winge, O. *On two types of spore germination, and on genetic segregations in SACCHAROMYCES, demonstrated through single-spore cultures*. (1937).
20. Lindegren, C. C. & Lindegren, G. A New Method for Hybridizing Yeast. *Proc. Natl. Acad. Sci.* (1943). doi:10.1073/pnas.29.10.306
21. Barnett, J. A. A history of research on yeast 10: Foundations of yeast genetics. *Yeast* (2007). doi:10.1002/yea.1513
22. Bardwell, L. A walk-through of the yeast mating pheromone response pathway. *Peptides* **25**, 1465–1476 (2004).
23. Hinnen, A., Hicks, J. B. & Fink, G. R. Transformation of yeast. *Proc. Natl. Acad. Sci. U. S. A.* (1978). doi:10.1073/pnas.75.4.1929
24. Beggs, J. D. Transformation of yeast by a replicating hybrid plasmid. *Nature* (1978). doi:10.1038/275104a0
25. Winzeler, E. A. *et al.* Functional characterization of the S. cerevisiae genome by gene deletion and parallel analysis. *Science (80-.).* (1999). doi:10.1126/science.285.5429.901
26. Liti, G. The natural history of model organisms: The fascinating and secret wild life of the budding yeast S. cerevisiae. *Elife* (2015). doi:10.7554/eLife.05835.001
27. Goffeau, A. *et al.* Life with 6000 genes. *Science (80-.).* (1996). doi:10.1126/science.274.5287.546
28. Duina, A. A., Miller, M. E. & Keeney, J. B. Budding yeast for budding geneticists: A primer on the Saccharomyces cerevisiae model system. *Genetics* (2014). doi:10.1534/genetics.114.163188
29. Hohmann, S. Nobel yeast research. *FEMS Yeast Research* (2016). doi:10.1093/femsyr/fow094

30. Nielsen, J. Production of biopharmaceutical proteins by yeast. *Bioengineered* (2013). doi:10.4161/bioe.22856
31. Hou, J., Tyo, K. E. J., Liu, Z., Petranovic, D. & Nielsen, J. Metabolic engineering of recombinant protein secretion by Saccharomyces cerevisiae. *FEMS Yeast Research* (2012). doi:10.1111/j.1567-1364.2012.00810.x
32. Petranovic, D. & Nielsen, J. Can yeast systems biology contribute to the understanding of human disease? *Trends Biotechnol.* (2008). doi:10.1016/j.tibtech.2008.07.008
33. Petranovic, D., Tyo, K., Vemuri, G. N. & Nielsen, J. Prospects of yeast systems biology for human health: Integrating lipid, protein and energy metabolism. *FEMS Yeast Research* (2010). doi:10.1111/j.1567-1364.2010.00689.x
34. Kim, I. K., Roldão, A., Siewers, V. & Nielsen, J. A systems-level approach for metabolic engineering of yeast cell factories. *FEMS Yeast Research* (2012). doi:10.1111/j.1567-1364.2011.00779.x
35. Liu, Y. & Nielsen, J. Recent trends in metabolic engineering of microbial chemical factories. *Current Opinion in Biotechnology* (2019). doi:10.1016/j.copbio.2019.05.010
36. Lee, S. K., Chou, H., Ham, T. S., Lee, T. S. & Keasling, J. D. Metabolic engineering of microorganisms for biofuels production: from bugs to synthetic biology to fuels. *Current Opinion in Biotechnology* (2008). doi:10.1016/j.copbio.2008.10.014
37. Si, T., Xiao, H. & Zhao, H. Rapid prototyping of microbial cell factories via genome-scale engineering. *Biotechnology Advances* (2015). doi:10.1016/j.biotechadv.2014.11.007
38. Thompson, R. A. & Trinh, C. T. Enhancing fatty acid ethyl ester production in Saccharomyces cerevisiae through metabolic engineering and medium optimization. *Biotechnol. Bioeng.* (2014). doi:10.1002/bit.25292
39. Reyes, L. H., Gomez, J. M. & Kao, K. C. Improving carotenoids production in yeast via adaptive laboratory evolution. *Metab. Eng.* (2014). doi:10.1016/j.ymben.2013.11.002
40. Qin, J. *et al.* Modular pathway rewiring of Saccharomyces cerevisiae enables high-level production of L-ornithine. *Nat. Commun.* (2015). doi:10.1038/ncomms9224
41. Tran, T. N. T. *et al.* Metabolic engineering of Saccharomyces cerevisiae to produce a reduced viscosity oil from lignocellulose. *Biotechnol. Biofuels* (2017). doi:10.1186/s13068-017-0751-y
42. Liu, Z. *et al.* Engineering of a novel cellulose-adherent cellulolytic Saccharomyces cerevisiae for cellulosic biofuel production. *Sci. Rep.* (2016). doi:10.1038/srep24550
43. Chen, R. & Dou, J. Biofuels and bio-based chemicals from lignocellulose: metabolic engineering strategies in strain development. *Biotechnology Letters* (2016). doi:10.1007/s10529-015-1976-0
44. Lee, S. Y. *et al.* A comprehensive metabolic map for production of bio-based chemicals. *Nature Catalysis* (2019). doi:10.1038/s41929-018-0212-4
45. Hong, K. K. & Nielsen, J. Metabolic engineering of Saccharomyces cerevisiae: A key cell factory platform for future biorefineries. *Cellular and Molecular Life Sciences* (2012). doi:10.1007/s00018-012-0945-1
46. Cravens, A., Payne, J. & Smolke, C. D. Synthetic biology strategies for microbial biosynthesis of plant natural products. *Nature Communications* (2019). doi:10.1038/s41467-019-09848-w
47. Siddiqui, M. S., Thodey, K., Trenchard, I. & Smolke, C. D. Advancing secondary metabolite biosynthesis in yeast with synthetic biology tools. *FEMS Yeast Research* (2012). doi:10.1111/j.1567-1364.2011.00774.x
48. Ro, D. K. *et al.* Production of the antimalarial drug precursor artemisinic acid in engineered yeast. *Nature* (2006). doi:10.1038/nature04640
49. Li, Y. *et al.* Complete biosynthesis of noscapine and halogenated alkaloids in yeast. *Proc. Natl. Acad. Sci. U. S. A.* (2018). doi:10.1073/pnas.1721469115
50. Thodey, K., Galanie, S. & Smolke, C. D. A microbial biomanufacturing platform for natural and semisynthetic opioids. *Nat. Chem. Biol.* (2014). doi:10.1038/nchembio.1613
51. Galanie, S., Thodey, K., Trenchard, I. J., Interrante, M. F. & Smolke, C. D. Complete biosynthesis of opioids in yeast. *Science (80-.).* (2015). doi:10.1126/science.aac9373
52. Luo, X. *et al.* Complete biosynthesis of cannabinoids and their unnatural analogues in yeast. *Nature* (2019). doi:10.1038/s41586-019-0978-9
53. Conklin, B. R. *et al.* Engineering GPCR signaling pathways with RASSLs. *Nat. Methods* (2008). doi:10.1038/nmeth.1232
54. Hutchison, C. A. *et al.* Design and synthesis of a minimal bacterial genome. *Science (80-.).* (2016). doi:10.1126/science.aad6253
55. Pretorius, I. S. & Boeke, J. D. Yeast 2.0-connecting the dots in the construction of the world's first functional

synthetic eukaryotic genome. *FEMS Yeast Research* (2018). doi:10.1093/femsyr/foy032
56. Richardson, S. M. *et al.* Design of a synthetic yeast genome. *Science (80-.).* (2017). doi:10.1126/science.aaf4557
57. Jensen, M. K. & Keasling, J. D. Recent applications of synthetic biology tools for yeast metabolic engineering. *FEMS Yeast Research* (2015). doi:10.1111/1567-1364.12185
58. Blount, B. A., Weenink, T. & Ellis, T. Construction of synthetic regulatory networks in yeast. *FEBS Lett.* **586**, 2112–21 (2012).
59. Wöhler, F. Ueber künstliche Bildung des Harnstoffs. *Ann. Phys.* (1828). doi:10.1002/andp.18280880206
60. Yeh, B. J. & Lim, W. A. Synthetic biology: Lessons from the history of synthetic organic chemistry. *Nature Chemical Biology* (2007). doi:10.1038/nchembio0907-521
61. Cameron, D. E., Bashor, C. J. & Collins, J. J. A brief history of synthetic biology. *Nature Reviews Microbiology* (2014). doi:10.1038/nrmicro3239
62. Baldwin, G. *et al. Synthetic Biology - A Primer*. (2015).
63. Endy, D. Foundations for engineering biology. *Nature* (2005). doi:10.1038/nature04342
64. Andrianantoandro, E., Basu, S., Karig, D. K. & Weiss, R. Synthetic biology: New engineering rules for an emerging discipline. *Molecular Systems Biology* (2006). doi:10.1038/msb4100073
65. Purnick, P. E. M. & Weiss, R. The second wave of synthetic biology: From modules to systems. *Nature Reviews Molecular Cell Biology* (2009). doi:10.1038/nrm2698
66. Federici, F., Rudge, T. J., Pollak, B., Haseloff, J. & Gutiérrez, R. A. Synthetic Biology: Opportunities for Chilean Bioindustry and education. *Biol. Res.* (2013). doi:10.4067/S0716-97602013000400010
67. Smolke, C. D. Building outside of the box: IGEM and the BioBricks Foundation. *Nature Biotechnology* (2009). doi:10.1038/nbt1209-1099
68. Casini, A., Storch, M., Baldwin, G. S. & Ellis, T. Bricks and blueprints: Methods and standards for DNA assembly. *Nature Reviews Molecular Cell Biology* (2015). doi:10.1038/nrm4014
69. Lai, H. E., Moore, S., Polizzi, K. & Freemont, P. EcoFlex: A multifunctional moclo kit for E. coli synthetic biology. in *Methods in Molecular Biology* (2018). doi:10.1007/978-1-4939-7795-6_25
70. Leonard, S. P. *et al.* Genetic Engineering of Bee Gut Microbiome Bacteria with a Toolkit for Modular Assembly of Broad-Host-Range Plasmids. *ACS Synth. Biol.* (2018). doi:10.1021/acssynbio.7b00399
71. Lee, M. E., DeLoache, W. C., Cervantes, B. & Dueber, J. E. A Highly Characterized Yeast Toolkit for Modular, Multipart Assembly. *ACS Synth. Biol.* (2015). doi:10.1021/sb500366v
72. Engler, C. *et al.* A Golden Gate modular cloning toolbox for plants. *ACS Synth. Biol.* (2014). doi:10.1021/sb4001504
73. Decoene, T. *et al.* Standardization in synthetic biology: an engineering discipline coming of age. *Critical Reviews in Biotechnology* (2018). doi:10.1080/07388551.2017.1380600
74. Canton, B., Labno, A. & Endy, D. Refinement and standardization of synthetic biological parts and devices. *Nature Biotechnology* (2008). doi:10.1038/nbt1413
75. Chen, Y. Y. *et al.* Synthetic biology: advancing biological frontiers by building synthetic systems. *Genome Biol.* **13**, 240 (2012).
76. Johns, N. I., Blazejewski, T., Gomes, A. L. C. & Wang, H. H. Principles for designing synthetic microbial communities. *Current Opinion in Microbiology* **31**, (2016).
77. Dawes, I. W. Yeast Biotechnology. Edited by D. R. Berry, I. Russell and G. G. Stewart. London: Allen and Unwin. 1987. 512 pages. £60.00. ISBN 0 04 574042 9. *Genet. Res.* (1988). doi:10.1017/s0016672300027737
78. Nielsen, J., Larsson, C., van Maris, A. & Pronk, J. Metabolic engineering of yeast for production of fuels and chemicals. *Current Opinion in Biotechnology* (2013). doi:10.1016/j.copbio.2013.03.023
79. Nielsen, J. & Keasling, J. D. Engineering Cellular Metabolism. *Cell* (2016). doi:10.1016/j.cell.2016.02.004
80. Huang, B. *et al.* Heterologous production of secondary metabolites as pharmaceuticals in Saccharomyces cerevisiae. *Biotechnology Letters* (2008). doi:10.1007/s10529-008-9663-z
81. Stovicek, V., Borodina, I. & Forster, J. CRISPR-Cas system enables fast and simple genome editing of industrial Saccharomyces cerevisiae strains. *Metab. Eng. Commun.* (2015). doi:10.1016/j.meteno.2015.03.001
82. Choi, K. R. *et al.* Systems Metabolic Engineering Strategies: Integrating Systems and Synthetic Biology with Metabolic Engineering. *Trends in Biotechnology* (2019). doi:10.1016/j.tibtech.2019.01.003
83. Bro, C., Regenberg, B., Förster, J. & Nielsen, J. In silico aided metabolic engineering of Saccharomyces cerevisiae for improved bioethanol production. *Metab. Eng.* (2006). doi:10.1016/j.ymben.2005.09.007

84. Nevoigt, E. Progress in metabolic engineering of *Saccharomyces cerevisiae*. *Microbiol. Mol. Biol. Rev.* (2008).
85. Fan, L. H., Zhang, Z. J., Yu, X. Y., Xue, Y. X. & Tan, T. W. Self-surface assembly of cellulosomes with two miniscaffoldins on Saccharomyces cerevisiae for cellulosic ethanol production. *Proc. Natl. Acad. Sci. U. S. A.* (2012). doi:10.1073/pnas.1209856109
86. Ha, S. J. *et al.* Engineered Saccharomyces cerevisiae capable of simultaneous cellobiose and xylose fermentation. *Proc. Natl. Acad. Sci. U. S. A.* (2011). doi:10.1073/pnas.1010456108
87. Kalim Akhtara, M., Turner, N. J. & Jones, P. R. Carboxylic acid reductase is a versatile enzyme for the conversion of fatty acids into fuels and chemical commodities. *Proc. Natl. Acad. Sci. U. S. A.* (2013). doi:10.1073/pnas.1216516110
88. Tang, X., Feng, H. & Chen, W. N. Metabolic engineering for enhanced fatty acids synthesis in Saccharomyces cerevisiae. *Metab. Eng.* (2013). doi:10.1016/j.ymben.2013.01.003
89. Yazawa, H. *et al.* Heterologous production of dihomo-γ-linolenic acid in Saccharomyces cerevisiae. *Appl. Environ. Microbiol.* (2007). doi:10.1128/AEM.01008-07
90. Kimura, K. *et al.* Improvement of stearidonic acid production in oleaginous Saccharomyces cerevisiae. *Biosci. Biotechnol. Biochem.* (2009). doi:10.1271/bbb.90082
91. Shi, S., Valle-Rodríguez, J. O., Khoomrung, S., Siewers, V. & Nielsen, J. Functional expression and characterization of five wax ester synthases in Saccharomyces cerevisiae and their utility for biodiesel production. *Biotechnol. Biofuels* (2012). doi:10.1186/1754-6834-5-7
92. Withers, S. T. & Keasling, J. D. Biosynthesis and engineering of isoprenoid small molecules. *Applied Microbiology and Biotechnology* (2007). doi:10.1007/s00253-006-0593-1
93. Paddon, C. J. *et al.* High-level semi-synthetic production of the potent antimalarial artemisinin. *Nature* (2013). doi:10.1038/nature12051
94. Westfall, P. J. *et al.* Production of amorphadiene in yeast, and its conversion to dihydroartemisinic acid, precursor to the antimalarial agent artemisinin. *Proc. Natl. Acad. Sci. U. S. A.* (2012). doi:10.1073/pnas.1110740109
95. Zhou, K., Qiao, K., Edgar, S. & Stephanopoulos, G. Distributing a metabolic pathway among a microbial consortium enhances production of natural products. *Nat. Biotechnol.* (2015). doi:10.1038/nbt.3095
96. Engels, B., Dahm, P. & Jennewein, S. Metabolic engineering of taxadiene biosynthesis in yeast as a first step towards Taxol (Paclitaxel) production. *Metab. Eng.* (2008). doi:10.1016/j.ymben.2008.03.001
97. Shiba, Y., Paradise, E. M., Kirby, J., Ro, D. K. & Keasling, J. D. Engineering of the pyruvate dehydrogenase bypass in Saccharomyces cerevisiae for high-level production of isoprenoids. *Metab. Eng.* (2007). doi:10.1016/j.ymben.2006.10.005
98. Zhang, F. & Keasling, J. Biosensors and their applications in microbial metabolic engineering. *Trends in Microbiology* (2011). doi:10.1016/j.tim.2011.05.003
99. Nazhand, A. *et al.* Rewiring cellular metabolism for heterologous biosynthesis of Taxol. *Natural Product Research* (2019). doi:10.1080/14786419.2019.1630122
100. Asadollahi, M. A. *et al.* Production of plant sesquiterpenes in Saccharomyces cerevisiae: Effect of ERG9 repression on sesquiterpene biosynthesis. *Biotechnol. Bioeng.* (2008). doi:10.1002/bit.21581
101. Takahashi, S. *et al.* Metabolic engineering of sesquiterpene metabolism in yeast. *Biotechnol. Bioeng.* (2007). doi:10.1002/bit.21216
102. Denby, C. M. *et al.* Industrial brewing yeast engineered for the production of primary flavor determinants in hopped beer. *Nat. Commun.* (2018). doi:10.1038/s41467-018-03293-x
103. Suástegui, M. & Shao, Z. Yeast factories for the production of aromatic compounds: from building blocks to plant secondary metabolites. *Journal of Industrial Microbiology and Biotechnology* (2016). doi:10.1007/s10295-016-1824-9
104. Averesch, N. J. H. & Krömer, J. O. Metabolic engineering of the shikimate pathway for production of aromatics and derived compounds-Present and future strain construction strategies. *Frontiers in Bioengineering and Biotechnology* (2018). doi:10.3389/fbioe.2018.00032
105. Sydor, T., Schaffer, S. & Boles, E. Considerable Increase in Resveratrol Production by Recombinant Industrial Yeast Strains with Use of Rich Medium▽. *Appl. Environ. Microbiol.* (2010). doi:10.1128/AEM.02796-09
106. Hansen, E. H. *et al.* De novo biosynthesis of Vanillin in fission yeast (schizosaccharomyces pombe) and baker's yeast (saccharomyces cerevisiae). *Appl. Environ. Microbiol.* (2009). doi:10.1128/AEM.02681-08

107. Brochado, A. R. *et al.* Improved vanillin production in baker's yeast through in silico design. *Microb. Cell Fact.* (2010). doi:10.1186/1475-2859-9-84
108. Staunton, J. & Wilkinson, B. Combinatorial biosynthesis of polyketides and nonribosomal peptides. *Current Opinion in Chemical Biology* (2001). doi:10.1016/S1367-5931(00)00185-X
109. Kornfuehrer, T. & Eustáquio, A. S. Diversification of polyketide structures via synthase engineering . *Medchemcomm* (2019). doi:10.1039/c9md00141g
110. Smith, S. & Tsai, S. C. The type I fatty acid and polyketide synthases: A tale of two megasynthases. *Natural Product Reports* (2007). doi:10.1039/b603600g
111. Cai, W. & Zhang, W. Engineering modular polyketide synthases for production of biofuels and industrial chemicals. *Current Opinion in Biotechnology* (2018). doi:10.1016/j.copbio.2017.08.017
112. Yuzawa, S., Keasling, J. D. & Katz, L. Bio-based production of fuels and industrial chemicals by repurposing antibiotic-producing type i modular polyketide synthases: Opportunities and challenges. *Journal of Antibiotics* (2017). doi:10.1038/ja.2016.136
113. Zargar, A. *et al.* Leveraging microbial biosynthetic pathways for the generation of 'drop-in' biofuels. *Current Opinion in Biotechnology* (2017). doi:10.1016/j.copbio.2017.03.004
114. Kealey, J. T., Liu, L., Santi, D. V., Betlach, M. C. & Barr, P. J. Production of a polyketide natural product in nonpolyketide-producing prokaryotic and eukaryotic hosts. *Proc. Natl. Acad. Sci. U. S. A.* (1998). doi:10.1073/pnas.95.2.505
115. Wattanachaisaereekul, S., Lantz, A. E., Nielsen, M. L., Andrésson, Ó. S. & Nielsen, J. Optimization of heterologous production of the polyketide 6-MSA in Saccharomyces cerevisiae. *Biotechnol. Bioeng.* (2007). doi:10.1002/bit.21286
116. Choi, J. W. & Da Silva, N. A. Improving polyketide and fatty acid synthesis by engineering of the yeast acetyl-CoA carboxylase. *J. Biotechnol.* (2014). doi:10.1016/j.jbiotec.2014.07.430
117. Rugbjerg, P., Naesby, M., Mortensen, U. H. & Frandsen, R. J. N. Reconstruction of the biosynthetic pathway for the core fungal polyketide scaffold rubrofusarin in Saccharomyces cerevisiae. *Microb. Cell Fact.* (2013). doi:10.1186/1475-2859-12-31
118. Zhou, H., Qiao, K., Gao, Z., Vederas, J. C. & Tang, Y. Insights into radicicol biosynthesis via heterologous synthesis of intermediates and analogs. *J. Biol. Chem.* (2010). doi:10.1074/jbc.M110.183574
119. Zhou, H. *et al.* A fungal ketoreductase domain that displays substrate-dependent stereospecificity. *Nat. Chem. Biol.* (2012). doi:10.1038/nchembio.912
120. Ishiuchi, K. *et al.* Establishing a New Methodology for Genome Mining and Biosynthesis of Polyketides and Peptides through Yeast Molecular Genetics. *ChemBioChem* (2012). doi:10.1002/cbic.201100798
121. Xu, W., Cai, X., Jung, M. E. & Tang, Y. Analysis of intact and dissected fungal polyketide synthase-nonribosomal peptide synthetase in vitro and in saccharomyces cerevisiae. *J. Am. Chem. Soc.* (2010). doi:10.1021/ja107084d
122. Gagne, S. J. *et al.* Identification of olivetolic acid cyclase from Cannabis sativa reveals a unique catalytic route to plant polyketides. *Proc. Natl. Acad. Sci. U. S. A.* (2012). doi:10.1073/pnas.1200330109
123. Krink-Koutsoubelis, N. *et al.* Engineered Production of Short-Chain Acyl-Coenzyme A Esters in Saccharomyces cerevisiae. *ACS Synth. Biol.* (2018). doi:10.1021/acssynbio.7b00466
124. Wattanachaisaereekul, S., Lantz, A. E., Nielsen, M. L. & Nielsen, J. Production of the polyketide 6-MSA in yeast engineered for increased malonyl-CoA supply. *Metab. Eng.* (2008). doi:10.1016/j.ymben.2008.04.005
125. Mutka, S. C., Bondi, S. M., Carney, J. R., Da Silva, N. A. & Kealey, J. T. Metabolic pathway engineering for complex polyketide biosynthesis in Saccharomyces cerevisiae. *FEMS Yeast Res.* (2006). doi:10.1111/j.1567-1356.2005.00001.x
126. Zheng, K., Xie, C. & Hong, R. Bioinspired iterative synthesis of polyketides. *Frontiers in Chemistry* (2015). doi:10.3389/fchem.2015.00032
127. Cardenas, J. & Da Silva, N. A. Engineering cofactor and transport mechanisms in Saccharomyces cerevisiae for enhanced acetyl-CoA and polyketide biosynthesis. *Metab. Eng.* (2016). doi:10.1016/j.ymben.2016.02.009
128. McKay, C. P. What is life - And how do we search for it in other worlds? *PLoS Biology* (2004). doi:10.1371/journal.pbio.0020302
129. Hughes, D. T. & Sperandio, V. Inter-kingdom signalling: Communication between bacteria and their hosts. *Nature Reviews Microbiology* (2008). doi:10.1038/nrmicro1836
130. Torday,J.S. and Rehan, V. K. The Evolution of Cell Communication: The Road not Taken. *Cell Commun. Insights*

(2009). doi:10.4137/cci.s2776

131. Jolly, M. K. *et al.* Operating principles of Notch-Delta-Jagged module of cell-cell communication. *New J. Phys.* (2015). doi:10.1088/1367-2630/17/5/055021
132. Chaiwanon, J., Wang, W., Zhu, J. Y., Oh, E. & Wang, Z. Y. Information Integration and Communication in Plant Growth Regulation. *Cell* (2016). doi:10.1016/j.cell.2016.01.044
133. Teague, B. P. & Weiss, R. Synthetic communities, the sum of parts. *Science (80-.).* (2015). doi:10.1126/science.aad0876
134. Bassler, B. L. Small talk: Cell-to-cell communication in bacteria. *Cell* (2002). doi:10.1016/S0092-8674(02)00749-3
135. Cottier, F. & Mühlschlegel, F. A. Communication in fungi. *International Journal of Microbiology* (2012). doi:10.1155/2012/351832
136. Popat, R., Cornforth, D. M., McNally, L. & Brown, S. P. Collective sensing and collective responses in quorum-sensing bacteria. *Journal of the Royal Society Interface* (2015). doi:10.1098/rsif.2014.0882
137. Williams, P. Quorum sensing, communication and cross-kingdom signalling in the bacterial world. *Microbiology* (2007). doi:10.1099/mic.0.2007/012856-0
138. Merlini, L., Dudin, O. & Martin, S. G. Mate and fuse: How yeast cells do it. *Open Biology* (2013). doi:10.1098/rsob.130008
139. Shong, J., Jimenez Diaz, M. R. & Collins, C. H. Towards synthetic microbial consortia for bioprocessing. *Curr. Opin. Biotechnol.* **23**, 798–802 (2012).
140. Hennig, S., Rödel, G. & Ostermann, K. Artificial cell-cell communication as an emerging tool in synthetic biology applications. (2011). doi:10.1186/s13036-015-0011-2
141. Pereira, C. S., Thompson, J. A. & Xavier, K. B. AI-2-mediated signalling in bacteria. *FEMS Microbiology Reviews* (2013). doi:10.1111/j.1574-6976.2012.00345.x
142. Papenfort, K. & Bassler, B. L. Quorum sensing signal-response systems in Gram-negative bacteria. *Nature Reviews Microbiology* (2016). doi:10.1038/nrmicro.2016.89
143. Monnet, V., Juillard, V. & Gardan, R. Peptide conversations in Gram-positive bacteria. *Critical Reviews in Microbiology* (2016). doi:10.3109/1040841X.2014.948804
144. Marchand, N. & Collins, C. H. Synthetic Quorum Sensing and Cell-Cell Communication in Gram-Positive Bacillus megaterium. *ACS Synth. Biol.* (2016). doi:10.1021/acssynbio.5b00099
145. Dunlap, P. V. Quorum regulation of luminescence in Vibrio fischeri. in *Journal of Molecular Microbiology and Biotechnology* (1999).
146. Weiss, R. & Knight, T. F. Engineered communications for microbial robotics. in *Lecture Notes in Computer Science (including subseries Lecture Notes in Artificial Intelligence and Lecture Notes in Bioinformatics)* (2001). doi:10.1007/3-540-44992-2_1
147. You, L., Cox, R. S., Weiss, R. & Arnold, F. H. Programmed population control by cell-cell communication and regulated killing. *Nature* (2004). doi:10.1038/nature02491
148. Balagaddé, F. K., You, L., Hansen, C. L., Arnold, F. H. & Quake, S. R. Microbiology: Long-term monitoring of bacteria undergoing programmed population control in a microchemostat. *Science (80-.).* (2005). doi:10.1126/science.1109173
149. Khakhar, A., Bolten, N. J., Nemhauser, J. & Klavins, E. Cell-Cell Communication in Yeast Using Auxin Biosynthesis and Auxin Responsive CRISPR Transcription Factors. *ACS Synth. Biol.* **5**, 279–286 (2016).
150. Weber, W., Daoud-El Baba, M. & Fussenegger, M. Synthetic ecosystems based on airborne inter- and intrakingdom communication. *Proc. Natl. Acad. Sci.* **104**, 10435–10440 (2007).
151. Chen, M. T. & Weiss, R. Artificial cell-cell communication in yeast Saccharomyces cerevisiae using signaling elements from Arabidopsis thaliana. *Nat. Biotechnol.* (2005). doi:10.1038/nbt1162
152. Goldberg, S. D., Derr, P., Degrado, W. F. & Goulian, M. Engineered single- and multi-cell chemotaxis pathways in E. coli. *Mol. Syst. Biol.* (2009). doi:10.1038/msb.2009.41
153. Chuang, J. S. Engineering multicellular traits in synthetic microbial populations. *Current Opinion in Chemical Biology* (2012). doi:10.1016/j.cbpa.2012.04.002
154. Bulter, T. *et al.* Design of artificial cell-cell communication using gene and metabolic networks. *Proc. Natl. Acad. Sci. U. S. A.* (2004). doi:10.1073/pnas.0306484101
155. Gerchman, Y. & Weiss, R. Teaching bacteria a new language. *Proceedings of the National Academy of Sciences of*

the United States of America (2004). doi:10.1073/pnas.0400473101

156. Ceroni, F., Algar, R., Stan, G. B. & Ellis, T. Quantifying cellular capacity identifies gene expression designs with reduced burden. *Nat. Methods* (2015). doi:10.1038/nmeth.3339
157. Zhang, H. & Wang, X. Modular co-culture engineering, a new approach for metabolic engineering. *Metabolic Engineering* (2016). doi:10.1016/j.ymben.2016.05.007
158. Regot, S. *et al.* Distributed biological computation with multicellular engineered networks. *Nature* **469**, 207–211 (2011).
159. Tanouchi, Y., Tu, D., Kim, J. & You, L. Noise reduction by diffusional dissipation in a minimal quorum sensing motif. *PLoS Comput. Biol.* (2008). doi:10.1371/journal.pcbi.1000167
160. Tamsir, A., Tabor, J. J. & Voigt, C. A. Robust multicellular computing using genetically encoded NOR gates and chemical 'wiresg'. *Nature* (2011). doi:10.1038/nature09565
161. Silva-Rocha, R. & De Lorenzo, V. Engineering multicellular logic in bacteria with metabolic wires. *ACS Synth. Biol.* (2014). doi:10.1021/sb400064y
162. Koseska, A., Zaikin, A., Kurths, J. & García-Ojalvo, J. Timing cellular decision making under noise via cell-cell communication. *PLoS One* (2009). doi:10.1371/journal.pone.0004872
163. Elowitz, M. B. & Leibier, S. A synthetic oscillatory network of transcriptional regulators. *Nature* (2000). doi:10.1038/35002125
164. McMillen, D., Kopell, N., Hasty, J. & Collins, J. J. Synchronizing genetic relaxation oscillators by intercell signaling. *Proc. Natl. Acad. Sci. U. S. A.* (2002). doi:10.1073/pnas.022642299
165. Danino, T., Mondragón-Palomino, O., Tsimring, L. & Hasty, J. A synchronized quorum of genetic clocks. *Nature* (2010). doi:10.1038/nature08753
166. Anderson, J. C., Voigt, C. A. & Arkin, A. P. Environmental signal integration by a modular and gate. *Mol. Syst. Biol.* (2007). doi:10.1038/msb4100173
167. Ramalingam, K. I., Tomshine, J. R., Maynard, J. A. & Kaznessis, Y. N. Forward engineering of synthetic bio-logical AND gates. *Biochem. Eng. J.* (2009). doi:10.1016/j.bej.2009.06.014
168. Kramer, B. P., Fischer, C. & Fussenegger, M. BioLogic gates enable logical transcription control in mammalian cells. *Biotechnol. Bioeng.* (2004). doi:10.1002/bit.20142
169. Bonnet, J., Yin, P., Ortiz, M. E., Subsoontorn, P. & Endy, D. Amplifying genetic logic gates. *Science (80-.).* (2013). doi:10.1126/science.1232758
170. Siuti, P., Yazbek, J. & Lu, T. K. Synthetic circuits integrating logic and memory in living cells. *Nat. Biotechnol.* (2013). doi:10.1038/nbt.2510
171. Sayut, D. J., Niu, Y. & Sun, L. Construction and enhancement of a minimal genetic AND logic gate. *Appl. Environ. Microbiol.* (2009). doi:10.1128/AEM.01684-08
172. Moon, T. S., Lou, C., Tamsir, A., Stanton, B. C. & Voigt, C. A. Genetic programs constructed from layered logic gates in single cells. *Nature* (2012). doi:10.1038/nature11516
173. Daniel, R., Rubens, J. R., Sarpeshkar, R. & Lu, T. K. Synthetic analog computation in living cells. *Nature* (2013). doi:10.1038/nature12148
174. Friedland, A. E. *et al.* Synthetic gene networks that count. *Science (80-.).* (2009). doi:10.1126/science.1172005
175. Lou, C. *et al.* Synthesizing a novel genetic sequential logic circuit: A push-on push-off switch. *Mol. Syst. Biol.* (2010). doi:10.1038/msb.2010.2
176. Marchisio, M. A. In silico design and in vivo implementation of yeast gene Boolean gates. *J. Biol. Eng.* (2014). doi:10.1186/1754-1611-8-6
177. Maung, N. W. & Smolke, C. D. Higher-order cellular information processing with synthetic RNA devices. *Science (80-.).* (2008). doi:10.1126/science.1160311
178. Auslände, S., Ausländer, D., Müller, M., Wieland, M. & Fussenegger, M. Programmable single-cell mammalian biocomputers. *Nature* (2012). doi:10.1038/nature11149
179. Brenner, K., You, L. & Arnold, F. H. Engineering microbial consortia: a new frontier in synthetic biology. *Trends Biotechnol.* **26**, 483–489 (2008).
180. Macía, J., Posas, F. & Solé, R. V. Distributed computation: The new wave of synthetic biology devices. *Trends in Biotechnology* (2012). doi:10.1016/j.tibtech.2012.03.006
181. Brenner, K., Karig, D. K., Weiss, R. & Arnold, F. H. Engineered bidirectional communication mediates a consensus in a microbial biofilm consortium. *Proc. Natl. Acad. Sci. U. S. A.* (2007). doi:10.1073/pnas.0704256104

182. Macia, J. & Sole, R. How to make a synthetic multicellular computer. *PLoS One* (2014). doi:10.1371/journal.pone.0081248
183. Ji, W. *et al*. A Formalized Design Process for Bacterial Consortia That Perform Logic Computing. *PLoS One* (2013). doi:10.1371/journal.pone.0057482
184. Balagaddé, F. K. *et al.* A synthetic Escherichia coli predator-prey ecosystem. *Mol. Syst. Biol.* **4**, 1–8 (2008).
185. Tolker-Nielsen, T. & Molin, S. Spatial organization of microbial biofilm communities. *Microb. Ecol.* (2000).
186. Basu, S., Gerchman, Y., Collins, C. H., Arnold, F. H. & Weiss, R. A synthetic multicellular system for programmed pattern formation. *Nature* (2005). doi:10.1038/nature03461
187. Karig, D. *et al*. Stochastic Turing patterns in a synthetic bacterial population. *Proc. Natl. Acad. Sci. U. S. A.* (2018). doi:10.1073/pnas.1720770115
188. Borek, B., Hasty, J. & Tsimring, L. Turing Patterning Using Gene Circuits with Gas-Induced Degradation of Quorum Sensing Molecules. *PLoS One* (2016). doi:10.1371/journal.pone.0153679
189. Tabor, J. J. *et al.* A synthetic genetic edge detection program. *Cell* **137**, 1272–81 (2009).
190. Davis, R. M., Muller, R. Y. & Haynes, K. A. Can the natural diversity of quorum-sensing advance synthetic biology? *Frontiers in Bioengineering and Biotechnology* (2015). doi:10.3389/fbioe.2015.00030
191. Scott, S. R. & Hasty, J. Quorum Sensing Communication Modules for Microbial Consortia. *ACS Synth. Biol.* **5**, (2016).
192. Scott, S. R. *et al.* A stabilized microbial ecosystem of self-limiting bacteria using synthetic quorum-regulated lysis. *Nat. Microbiol.* (2017). doi:10.1038/nmicrobiol.2017.83
193. Din, M. O. *et al.* Synchronized cycles of bacterial lysis for in vivo delivery. *Nature* (2016). doi:10.1038/nature18930
194. Hwang, I. Y. *et al.* Engineered probiotic Escherichia coli can eliminate and prevent Pseudomonas aeruginosa gut infection in animal models. *Nat. Commun.* (2017). doi:10.1038/ncomms15028
195. Riangrungroj, P. & Polizzi, K. M. BeQu IK (Biosensor Engineered Quorum Induced Killing): designer bacteria for destroying recalcitrant biofilms . *Microb. Biotechnol.* (2019). doi:10.1111/1751-7915.13465
196. Wang, W. D., Chen, Z. T., Kang, B. G. & Li, R. Construction of an artificial intercellular communication network using the nitric oxide signaling elements in mammalian cells. *Exp. Cell Res.* (2008). doi:10.1016/j.yexcr.2007.11.023
197. Weber, W., Schuetz, M., Dénervaud, N. & Fussenegger, M. A synthetic metabolite-based mammalian inter-cell signaling system. *Mol. Biosyst.* (2009). doi:10.1039/b902070p
198. Bacchus, W. *et al*. Synthetic two-way communication between mammalian cells. *Nat. Biotechnol.* **30**, 991–996 (2012).
199. Carvalho, A. *et al.* Genetically encoded sender-receiver system in 3D mammalian cell culture. *ACS Synth. Biol.* (2014). doi:10.1021/sb400053b
200. Matsuda, M., Koga, M., Nishida, E. & Ebisuya, M. Synthetic signal propagation through direct cell-cell interaction. *Sci. Signal.* (2012). doi:10.1126/scisignal.2002764
201. Weber, W., Daoud-El Baba, M. & Fussenegger, M. Synthetic ecosystems based on airborne inter- and intrakingdom communication. *Proc. Natl. Acad. Sci. U. S. A.* (2007). doi:10.1073/pnas.0701382104
202. Albuquerque, P. & Casadevall, A. Quorum sensing in fungi a review. *Medical Mycology* (2012). doi:10.3109/13693786.2011.652201
203. Dowell, S. J. & Brown, A. J. Yeast assays for G protein-coupled receptors. *Methods Mol. Biol.* (2009). doi:10.1007/978-1-60327-317-6_15
204. Huberman, L. B. & Murray, A. W. Genetically engineered transvestites reveal novel mating genes in budding yeast. *Genetics* (2013). doi:10.1534/genetics.113.155846
205. Arkowitz, R. A. Chemical gradients and chemotropism in yeast. *Cold Spring Harbor perspectives in biology* (2009).
206. Harrison, R. & DeLisi, C. Condition specific transcription factor binding site characterization in Saccharomyces cerevisiae. *Bioinformatics* (2002). doi:10.1093/bioinformatics/18.10.1289
207. Hartwell, L. H. Mutants of Saccharomyces Cerevisiae unresponsive to cell division control by polypeptide mating hormone. *J. Cell Biol.* (1980). doi:10.1083/jcb.85.3.811
208. Michaelis, S. & Barrowman, J. Biogenesis of the Saccharomyces cerevisiae Pheromone a-Factor, from Yeast Mating to Human Disease. *Microbiol. Mol. Biol. Rev.* (2012). doi:10.1128/mmbr.00010-12
209. Banderas, A., Koltai, M., Anders, A. & Sourjik, V. Sensory input attenuation allows predictive sexual response in

yeast. *Nat. Commun.* **7**, 1–9 (2016).

210. Liu, H., Styles, C. A. & Fink, G. R. Elements of the yeast pheromone response pathway required for filamentous growth of diploids. *Science (80-.).* (1993). doi:10.1126/science.8259520
211. Zhou, J., Arora, M. & Stone, D. E. The Yeast Pheromone-Responsive Gα Protein Stimulates Recovery from Chronic Pheromone Treatment by Two Mechanisms That Are Activated at Distinct Levels of Stimulus. *Cell Biochem. Biophys.* (1999). doi:10.1007/BF02738067
212. Kurjan, J. Alpha-factor structural gene mutations in Saccharomyces cerevisiae: effects on alpha-factor production and mating. *Mol. Cell. Biol.* (1985). doi:10.1128/mcb.5.4.787
213. Bender, A. & Sprague, G. F. Yeast peptide pheromones, a-factor and α-factor, activate a common response mechanism in their target cells. *Cell* (1986). doi:10.1016/0092-8674(86)90808-1
214. Kurjan, J. & Herskowitz, I. Structure of a yeast pheromone gene (MFα): A putative α-factor precursor contains four tandem copies of mature α-factor. *Cell* (1982). doi:10.1016/0092-8674(82)90298-7
215. Caplan, S., Green, R., Rocco, J. & Kurjan, J. Glyosylation and structure of the yeast MFα1 α-factor precursor is important for efficient transport through the secretory pathway. *J. Bacteriol.* (1991).
216. Julius, D., Blair, L., Brake, A., Sprague, G. & Thorner, J. Yeast α factor is processed from a larger precursor polypeptide: The essential role of a membrane-bound dipeptidyl aminopeptidase. *Cell* (1983). doi:10.1016/0092-8674(83)90070-3
217. Fuller, R. Enzymes Required For Yeast Prohormone Processing. *Annu. Rev. Physiol.* (1988). doi:10.1146/annurev.physiol.50.1.345
218. Julius, D., Brake, A., Blair, L., Kunisawa, R. & Thorner, J. Isolation of the putative structural gene for the lysine-arginine-cleaving endopeptidase required for processing of yeast prepro-α-factor. *Cell* (1984). doi:10.1016/0092-8674(84)90442-2
219. Dmochowska, A., Dignard, D., Henning, D., Thomas, D. Y. & Bussey, H. Yeast KEX1 gene encodes a putative protease with a carboxypeptidase B-like function involved in killer toxin and α-factor precursor processing. *Cell* (1987). doi:10.1016/0092-8674(87)90030-4
220. Billerbeck, S. *et al.* A scalable peptide-GPCR language for engineering multicellular communication. *Nat. Commun.* (2018). doi:10.1038/s41467-018-07610-2
221. Kuchler, K., Sterne, R. E. & Thorner, J. Saccharomyces cerevisiae STE6 gene product: a novel pathway for protein export in eukaryotic cells. *EMBO J.* (1989). doi:10.1002/j.1460-2075.1989.tb08580.x
222. He, B. *et al.* RAM2, an essential gene of yeast, and RAM1 encode the two polypeptide components of the farnesyltransferase that prenylates a-factor and Ras proteins. *Proc. Natl. Acad. Sci. U. S. A.* (1991). doi:10.1073/pnas.88.24.11373
223. Powers, S. *et al.* RAM, a gene of yeast required for a functional modification of RAS proteins and for production of mating pheromone a-factor. *Cell* (1986). doi:10.1016/0092-8674(86)90598-2
224. Schafer, W. R. *et al.* Enzymatic coupling of cholesterol intermediates to a mating pheromone precursor and to the Ras protein. *Science (80-.).* (1990). doi:10.1126/science.2204115
225. Boyartchuk, V. L., Ashby, M. N. & Rine, J. Modulation of ras and a-factor function by carboxyl-terminal proteolysis. *Science (80-.).* (1997). doi:10.1126/science.275.5307.1796
226. Boyartchuk, V. L. & Rine, J. Roles of prenyl protein proteases in maturation of Saccharomyces cerevisiae a-factor. *Genetics* (1998).
227. Tam, A. *et al.* Dual roles for Ste24p in yeast a-factor maturation: NH2-terminal proteolysis and COOH-terminal CAAX processing. *J. Cell Biol.* (1998). doi:10.1083/jcb.142.3.635
228. Tam, A., Schmidt, W. K. & Michaelis, S. The Multispanning Membrane Protein Ste24p Catalyzes CAAX Proteolysis and NH2-terminal Processing of the Yeast a-Factor Precursor. *J. Biol. Chem.* (2001). doi:10.1074/jbc.M106150200
229. Hrycyna, C. A. & Clarke, S. Farnesyl cysteine C-terminal methyltransferase activity is dependent upon the STE14 gene product in Saccharomyces cerevisiae. *Mol. Cell. Biol.* (1990). doi:10.1128/mcb.10.10.5071
230. Hrycyna, C. A., Sapperstein, S. K., Clarke, S. & Michaelis, S. The Saccharomyces cerevisiae STE14 gene encodes a methyltransferase that mediates C-terminal methylation of a-factor and RAS proteins. *EMBO J.* (1991). doi:10.1002/j.1460-2075.1991.tb07694.x
231. Fujimura-Kamada, K., Nouvet, F. J. & Michaelis, S. A novel membrane-associated metalloprotease, Ste24p, is required for the first step of NH2-terminal processing of the yeast a-factor precursor. *J. Cell Biol.* (1997).

doi:10.1083/jcb.136.2.271

232. Schmidt, W. K., Tam, A. & Michaelis, S. Reconstitution of the Ste24p-dependent N-terminal proteolytic step in yeast a-factor biogenesis. *J. Biol. Chem.* (2000). doi:10.1074/jbc.275.9.6227
233. Berkower, C. & Michaelis, S. Mutational analysis of the yeast a-factor transporter STE6, a member of the ATP binding cassette (ABC) protein superfamily. *EMBO J.* (1991). doi:10.1002/j.1460-2075.1991.tb04947.x
234. Michaelis, S. STE6, the yeast a-factor transporter. *Semin. Cell Dev. Biol.* (1993). doi:10.1006/scel.1993.1003
235. Mackay, V. & Manney, T. R. Mutations affecting sexual conjugation and related processes in Saccharomyces cerevisiae. I. Isolation and phenotypic characterization of nonmating mutants. *Genetics* (1974).
236. Marina Robles, L., Millán-Pacheco, C., Pastor, N. & Del Río, G. STRUCTURE-FUNCTION STUDIES OF THE ALPHA PHEROMONE RECEPTOR FROM YEAST. *TIP* (2017). doi:10.1016/j.recqb.2016.11.002
237. Zuber, J., Danial, S. A., Connelly, S. M., Naider, F. & Dumont, M. E. Identification of destabilizing and stabilizing mutations of Ste2p, a G protein-coupled receptor in saccharomyces cerevisiae. *Biochemistry* (2015). doi:10.1021/bi501314t
238. Boone, C., Davis, N. G. & Sprague, G. F. Mutations that alter the third cytoplasmic loop of the a-factor receptor lead to a constitutive and hypersensitive phenotype. *Proc. Natl. Acad. Sci. U. S. A.* (1993). doi:10.1073/pnas.90.21.9921
239. Gastaldi, S., Zamboni, M., Bolasco, G., Di Segni, G. & Tocchini-Valentini, G. P. Analysis of random PCR-originated mutants of the yeast Ste2 and Ste3 receptors. *Microbiologyopen* (2016). doi:10.1002/mbo3.361
240. Stefan, C. J. & Blumer, K. J. The third cytoplasmic loop of a yeast G-protein-coupled receptor controls pathway activation, ligand discrimination, and receptor internalization. *Mol. Cell. Biol.* (1994). doi:10.1128/mcb.14.5.3339
241. Clark, C. D., Palzkill, T. & Botstein, D. Systematic mutagenesis of the yeast mating pheromone receptor third intracellular loop. *J. Biol. Chem.* (1994).
242. Ćelić, A. *et al*. Sequences in the intracellular loops of the yeast pheromone receptor ste2p required for G protein activation. *Biochemistry* (2003). doi:10.1021/bi0269308
243. Martin, N. P., Ćelić, A. & Dumont, M. E. Mutagenic mapping of helical structures in the transmembrane segments of the yeast α-factor receptor. *J. Mol. Biol.* (2002). doi:10.1006/jmbi.2002.5444
244. Schandel, K. A. & Jenness, D. D. Direct evidence for ligand-induced internalization of the yeast alpha-factor pheromone receptor. *Mol. Cell. Biol.* (1994). doi:10.1128/mcb.14.11.7245
245. Büküşoğlu, G. & Jenness, D. D. Agonist-specific conformational changes in the yeast alpha-factor pheromone receptor. *Mol. Cell. Biol.* (1996). doi:10.1128/mcb.16.9.4818
246. Ballon, D. R. *et al*. DEP-Domain-Mediated Regulation of GPCR Signaling Responses. *Cell* (2006). doi:10.1016/j.cell.2006.07.030
247. Reneke, J. E., Blumer, K. J., Courchesne, W. E. & Thorner, J. The carboxy-terminal segment of the yeast α-factor receptor is a regulatory domain. *Cell* (1988). doi:10.1016/0092-8674(88)90045-1
248. Alvaro, C. G. *et al*. Specific -Arrestins Negatively Regulate Saccharomyces cerevisiae Pheromone Response by Down-Modulating the G-Protein-Coupled Receptor Ste2. *Mol. Cell. Biol.* (2014). doi:10.1128/mcb.00230-14
249. Rotin, D. & Kumar, S. Physiological functions of the HECT family of ubiquitin ligases. *Nature Reviews Molecular Cell Biology* (2009). doi:10.1038/nrm2690
250. Toshima, J. Y., Nakanishi, J. I., Mizuno, K., Toshima, J. & Drubin, D. G. Requirements for recruitment of a G protein-coupled receptor to clathrin-coated pits in budding yeast. *Mol. Biol. Cell* (2009). doi:10.1091/mbc.E09-07-0541
251. Katzmann, D. J., Odorizzi, G. & Emr, S. D. Receptor downregulation and multivesicular-body sorting. *Nature Reviews Molecular Cell Biology* (2002). doi:10.1038/nrm973
252. Prosser, D. C. *et al*. α-Arrestins participate in cargo selection for both clathrin-independentand clathrin-mediated endocytosis. *J. Cell Sci.* (2015). doi:10.1242/jcs.175372
253. Dohlman, H. G. G Proteins and Pheromone Signaling. *Annu. Rev. Physiol.* (2002). doi:10.1146/annurev.physiol.64.081701.133448
254. Guo, M. *et al*. The yeast G protein α subunit Gpa1 transmits a signal through an RNA binding effector protein Scp160. *Mol. Cell* (2003). doi:10.1016/S1097-2765(03)00307-1
255. Metodiev, M. V., Matheos, D., Rose, M. D. & Stone, D. E. Regulation of MAPK function by direct interaction with the mating-specific G?? in yeast. *Science (80-.).* (2002). doi:10.1126/science.1070540

256. Klein, S., Reuveni, H. & Levitzki, A. Signal transduction by a nondissociable heterotrimeric yeast G protein. *Proc. Natl. Acad. Sci. U. S. A.* (2000). doi:10.1073/pnas.97.7.3219
257. Lim, L., Manser, E., Leung, T. & Hall, C. Regulation of phosphorylation pathways by p21 GTPases. The p21 Ras-related Rho subfamily and its role in phosphoryltion signalling pathways. *European Journal of Biochemistry* (1996). doi:10.1111/j.1432-1033.1996.0171r.x
258. Lamson, R. E., Winters, M. J. & Pryciak, P. M. Cdc42 Regulation of Kinase Activity and Signaling by the Yeast p21-Activated Kinase Ste20. *Mol. Cell. Biol.* (2002). doi:10.1128/mcb.22.9.2939-2951.2002
259. Ekkehard, L., Leeuwa, T., Thomas, D. Y. & Dignard, D. Conserved Gβinding (GBB) Sequence Motif in Ste20p/PAK Family Protein Kinase. *Biol. Chem.* (2000). doi:10.1515/BC.2000.055
260. Leeuw, T. *et al.* Interaction of a G-protein β-subunit with a conserved sequence in Ste20/PAK family protein kinases. *Nature* (1998). doi:10.1038/34448
261. Dowell, S. J., Bishop, A. L., Dyos, S. L., Brown, A. J. & Whiteway, M. S. Mapping of a yeast G protein betagamma signaling interaction. *Genetics* (1998).
262. Feng, Y., Song, L. Y., Kincaid, E., Mahanty, S. K. & Elion, E. A. Functional binding between Gβ and the LIM domain of Ste5 is required to activate the MEKK Ste11. *Curr. Biol.* (1998).
263. Inouye, C., Dhillon, N. & Thorner, J. Ste5 RING-H2 domain: Role in Ste4-promoted oligomerization for yeast pheromone signaling. *Science (80-.).* (1997). doi:10.1126/science.278.5335.103
264. Ferrell, J. E. & Cimprich, K. A. Enforced proximity in the function of a famous scaffold. *Molecular Cell* (2003). doi:10.1016/S1097-2765(03)00055-8
265. Pryciak, P. M. & Huntress, F. A. Membrane recruitment of the kinase cascade scaffold protein Ste5 by the Gβγ complex underlies activation of the yeast pheromone response pathway. *Genes Dev.* (1998). doi:10.1101/gad.12.17.2684
266. Butty, A. C., Pryciak, P. M., Huang, L. S., Herskowitz, I. & Peter, M. The role of Far1p in linking the heterotrimeric G protein to polarity establishment proteins during yeast mating. *Science (80-.).* (1998). doi:10.1126/science.282.5393.1511
267. Drees, B. L. *et al.* A protein interaction map for cell polarity development. *J. Cell Biol.* (2001). doi:10.1083/jcb.200104057
268. Johnson, D. I. Cdc42: An essential Rho-type GTPase controlling eukaryotic cell polarity. *Microbiol. Mol. Biol. Rev.* (1999).
269. Madden, K. & Snyder, M. CELL POLARITY AND MORPHOGENESIS IN BUDDING YEAST. *Annu. Rev. Microbiol.* (1998). doi:10.1146/annurev.micro.52.1.687
270. Butty, A. C. *et al.* A positive feedback loop stabilizes the guanine-nucleotide exchange factor Cdc24 at sites of polarization. *EMBO J.* (2002). doi:10.1093/emboj/21.7.1565
271. Chen, G. C., Kim, Y. J. & Chan, C. S. M. The Cdc42 GTPase-associated proteins Gic1 and Gic2 are required for polarized cell growth in Saccharomyces cerevisiae. *Genes Dev.* (1997). doi:10.1101/gad.11.22.2958
272. Evangelista, M. *et al.* Bni1p, a yeast formin linking Cdc42p and the actin cytoskeleton during polarized morphogenesis. *Science (80-.).* (1997). doi:10.1126/science.276.5309.118
273. Elion, E. A. Pheromone response, mating and cell biology. *Current Opinion in Microbiology* (2000). doi:10.1016/S1369-5274(00)00143-0
274. Nern, A. & Arkowitz, R. A. A Cdc24p-Far1p-Gβγ protein complex required for yeast orientation during mating. *J. Cell Biol.* (1999). doi:10.1083/jcb.144.6.1187
275. Nern, A. & Arkowitz, R. A. G proteins mediate changes in cell shape by stabilizing the axis of polarity. *Mol. Cell* (2000). doi:10.1016/S1097-2765(00)80325-1
276. Nern, A. & Arkowitz, R. A. Nucleocytoplasmic shuttling of the Cdc42p exchange factor Cdc24p. *J. Cell Biol.* (2000). doi:10.1083/jcb.148.6.1115
277. Shimada, Y., Gulli, M. P. & Peter, M. Nuclear sequestration of the exchange factor Cdc24 by Far1 regulates cell polarity during yeast mating. *Nat. Cell Biol.* (2000). doi:10.1038/35000073
278. Valtz, N., Peter, M. & Herskowitz, I. FAR1 is required for oriented polarization of yeast cells in response to mating pheromones. *J. Cell Biol.* (1995). doi:10.1083/jcb.131.4.863
279. Burack, W. R. & Shaw, A. S. Signal transduction: Hanging on a scaffold. *Current Opinion in Cell Biology* (2000). doi:10.1016/S0955-0674(99)00078-2
280. Elion, E. A. The Ste5p scaffold. *Journal of Cell Science* (2001).

281. Harris, K. *et al.* Role of scaffolds in MAP kinase pathway specificity revealed by custom design of pathway-dedicated signaling proteins. *Curr. Biol.* (2001). doi:10.1016/S0960-9822(01)00567-X
282. Park, S. H., Zarrinpar, A. & Lim, W. A. Rewiring MAP kinase pathways using alternative scaffold assembly mechanisms. *Science (80-.).* (2003). doi:10.1126/science.1076979
283. Sette, C., Inouye, C. J., Stroschein, S. L., Iaquinta, P. J. & Thorner, J. Mutational analysis suggests that activation of the yeast pheromone response mitogen-activated protein kinase pathway involves conformational changes in the Ste5 scaffold protein. *Mol. Biol. Cell* (2000). doi:10.1091/mbc.11.11.4033
284. Wang, Y. & Elion, E. A. Nuclear export and plasma membrane recruitment of the Ste5 scaffold are coordinated with oligomerization and association with signal transduction components. *Mol. Biol. Cell* (2003). doi:10.1091/mbc.E02-10-0699
285. Cook, J. G., Bardwell, L., Kron, S. J. & Thorner, J. Two novel targets of the MAP kinase Kss1 are negative regulators of invasive growth in the yeast Saccharomyces cerevisiae. *Genes Dev.* (1996). doi:10.1101/gad.10.22.2831
286. Tedford, K., Kim, S., Sa, D., Stevens, K. & Tyers, M. Regulation of the mating pheromone and invasive growth responses in yeast by two MAP kinase substrates. *Curr. Biol.* (1997). doi:10.1016/S0960-9822(06)00118-7
287. White, J. M. & Rose, M. D. Yeast mating: Getting close to membrane merger. *Current Biology* (2001). doi:10.1016/S0960-9822(00)00036-1
288. Bardwell, L. *et al.* Repression of yeast Ste12 transcription factor by direct binding of unphosphorylated Kss1 MAPK and its regulation by the Ste7 MEK. *Genes Dev.* (1998). doi:10.1101/gad.12.18.2887
289. Jeoung, D.-I., Oehlen, L. J. W. M. & Cross, F. R. Cln3-Associated Kinase Activity in Saccharomyces cerevisiae Is Regulated by the Mating Factor Pathway . *Mol. Cell. Biol.* (1998). doi:10.1128/mcb.18.1.433
290. Gartner, A. *et al.* Pheromone-Dependent G 1 Cell Cycle Arrest Requires Far1 Phosphorylation, but May Not Involve Inhibition of Cdc28-Cln2 Kinase, In Vivo . *Mol. Cell. Biol.* (1998). doi:10.1128/mcb.18.7.3681
291. Roberts, C. J. *et al.* Signaling and circuitry of multiple MAPK pathways revealed by a matrix of global gene expression profiles. *Science (80-.).* (2000). doi:10.1126/science.287.5454.873
292. Cherkasova, V., Lyons, D. M. & Elion, E. A. Fus3p and Kss1p control G1 arrest in Saccharomyces cerevisiae through a balance of distinct arrest and proliferative functions that operate in parallel with Far1p. *Genetics* (1999).
293. Thomson, T. M. *et al.* Scaffold number in yeast signaling system sets tradeoff between system output and dynamic range. *Proc. Natl. Acad. Sci. U. S. A.* (2011). doi:10.1073/pnas.1004042108
294. Sprague, G. F. & Herskowitz, I. Control of yeast cell type by the mating type locus. I. Identification and control of expression of the a-specific gene BAR1. *J. Mol. Biol.* (1981). doi:10.1016/0022-2836(81)90280-1
295. Manney, T. R. Expression of the BAR1 gene in Saccharomyces cerevisiae: Induction by the ?? mating pheromone of an activity associated with a secreted protein. *J. Bacteriol.* (1983).
296. Jin, M. *et al.* Yeast dynamically modify their environment to achieve better mating efficiency. *Sci. Signal.* (2011). doi:10.1126/scisignal.2001763
297. Barkai, N., Rose, M. D. & Wingreen, N. S. Protease helps yeast find mating partners [5]. *Nature* (1998). doi:10.1038/24760
298. Jones, S. K., Clarke, S. C., Craik, C. S. & Bennett, R. J. Evolutionary selection on barrier activity: Bar1 is an aspartyl protease with novel substrate specificity. *MBio* **6**, 1–12 (2015).
299. Lee, S. C., Ni, M., Li, W., Shertz, C. & Heitman, J. The Evolution of Sex: a Perspective from the Fungal Kingdom. *Microbiol. Mol. Biol. Rev.* (2010). doi:10.1128/mmbr.00005-10
300. Bardwell, L., Cook, J. G., Inouye, C. J. & Thorner, J. Signal propagation and regulation in the mating pheromone response pathway of the yeast saccharomyces cerevisiae. *Developmental Biology* (1994). doi:10.1006/dbio.1994.1323
301. Dohlman, H. G. & Thorner, J. Regulation of G Protein–Initiated Signal Transduction in Yeast: Paradigms and Principles. *Annu. Rev. Biochem.* (2001). doi:10.1146/annurev.biochem.70.1.703
302. Brown, A. J. *et al.* Functional coupling of mammalian receptors to the yeast mating pathway using novel yeast/mammalian G protein α-subunit chimeras. *Yeast* (2000). doi:10.1002/(SICI)1097-0061(20000115)16:1<11::AID-YEA502>3.0.CO;2-K
303. Fowler, T. J., DeSimone, S. M., Mitton, M. F., Kurjan, J. & Raper, C. A. Multiple sex pheromones and receptors of a mushroom-producing fungus elicit mating in yeast. *Mol. Biol. Cell* (1999). doi:10.1091/mbc.10.8.2559
304. Mayrhofer, S. & Pöggeler, S. Functional characterization of an α-factor-like Sordaria macrospora peptide

pheromone and analysis of its interaction with its cognate receptor in Saccharomyces cerevisiae. *Eukaryot. Cell* (2005). doi:10.1128/EC.4.4.661-672.2005

305. Böhm, J. *et al.* Sexual reproduction and mating-type-mediated strain development in the penicillin-producing fungus Penicillium chrysogenum. *Proc. Natl. Acad. Sci. U. S. A.* (2013). doi:10.1073/pnas.1217943110
306. Chen, B. *et al.* Synthetic biology toolkits and applications in Saccharomyces cerevisiae. *Biotechnol. Adv.* #pagerange# (2018). doi:10.1016/j.biotechadv.2018.07.005
307. Adeniran, A., Sherer, M. & Tyo, K. E. J. Yeast-based biosensors: Design and applications. *FEMS Yeast Research* (2015). doi:10.1111/1567-1364.12203
308. Lim, W. A. Designing customized cell signalling circuits. *Nature Reviews Molecular Cell Biology* (2010). doi:10.1038/nrm2904
309. Baronian, K. H. R. The use of yeast and moulds as sensing elements in biosensors. *Biosensors and Bioelectronics* (2004). doi:10.1016/j.bios.2003.09.010
310. Schaefer, D., Côte, P., Whiteway, M. & Bennett, R. J. Barrier activity in Candida albicans mediates pheromone degradation and promotes mating. *Eukaryot. Cell* (2007). doi:10.1128/EC.00090-07
311. MacKay, V. L. *et al.* The Saccharomyces cerevisiae BAR1 gene encodes an exported protein with homology to pepsin. *Proc. Natl. Acad. Sci. U. S. A.* (1988). doi:10.1073/pnas.85.1.55
312. Hennig, S., Clemens, A., Rödel, G. & Ostermann, K. A yeast pheromone-based inter-species communication system. *Appl. Microbiol. Biotechnol.* (2014). doi:10.1007/s00253-014-6133-5
313. Siu, K. H. & Chen, W. Control of the Yeast Mating Pathway by Reconstitution of Functional α-Factor Using Split Intein-Catalyzed Reactions. *ACS Synth. Biol.* **6**, 1453–1460 (2017).
314. Eriotou-Bargiota, E., Becker, J. M., Xue, C. B. & Naider, F. Antagonistic and Synergistic Peptide Analogues of the Tridecapeptide Mating Pheromone of Saccharomyces cerevisiae. *Biochemistry* (1992). doi:10.1021/bi00117a036
315. Ladds, G., Goddard, A. & Davey, J. Functional analysis of heterologous GPCR signalling pathways in yeast. *Trends in Biotechnology* (2005). doi:10.1016/j.tibtech.2005.05.007
316. Dupré, D. J., Robitaille, M., Rebois, R. V. & Hébert, T. E. The Role of Gβγ Subunits in the Organization, Assembly, and Function of GPCR Signaling Complexes. *Annu. Rev. Pharmacol. Toxicol.* (2009). doi:10.1146/annurev-pharmtox-061008-103038
317. Pierce, K. L., Premont, R. T. & Lefkowitz, R. J. Seven-transmembrane receptors. *Nature Reviews Molecular Cell Biology* (2002). doi:10.1038/nrm908
318. Ostrov, N. *et al.* A modular yeast biosensor for low-cost point-of-care pathogen detection. *Sci. Adv.* (2017). doi:10.1126/sciadv.1603221
319. Hegner, J., Siebert-Bartholmei, C. & Kothe, E. Ligand recognition in multiallelic pheromone receptors from the basidiomycete Schizophyllum commune studied in yeast. *Fungal Genet. Biol.* (1999). doi:10.1006/fgbi.1999.1119
320. Lin, C. H., Choi, A. & Bennett, R. J. Defining pheromone-receptor signaling in Candida albicans and related asexual Candida species. *Mol. Biol. Cell* (2011). doi:10.1091/mbc.E11-09-0749
321. Reiländer, H. & Weiß, H. M. Production of G-protein-coupled receptors in yeast. *Curr. Opin. Biotechnol.* (1998). doi:10.1016/S0958-1669(98)80038-4
322. Krautwurst, D., Yau, K. W. & Reed, R. R. Identification of ligands for olfactory receptors by functional expression of a receptor library. *Cell* (1998). doi:10.1016/S0092-8674(00)81716-X
323. Schlinkmann, K. M. *et al.* Critical features for biosynthesis, stability, and functionality of a G protein-coupled receptor uncovered by all-versus-all mutations. *Proc. Natl. Acad. Sci. U. S. A.* (2012). doi:10.1073/pnas.1202107109
324. Hara, K. *et al.* Chimeric yeast G-protein α subunit harboring a 37-residue C-terminal gustducin-specific sequence is functional in saccharomyces cerevisiae. *Biosci. Biotechnol. Biochem.* (2012). doi:10.1271/bbb.110820
325. Pajot-Augy, E., Crowe, M., Levasseur, G., Salesse, R. & Connerton, I. Engineered Yeasts as Reporter Systems for Odorant Detection. *J. Recept. Signal Transduct.* (2003). doi:10.1081/RRS-120025196
326. King, K., Dohlman, H. G., Thorner, J., Caron, M. G. & Lefkowitz, R. J. Control of yeast mating signal transduction by a mammalian β2-adrenergic receptor and Gs α subunit. *Science (80-.).* (1990). doi:10.1126/science.2171146
327. Price, L. A., Kajkowski, E. M., Hadcock, J. R., Ozenberger, B. A. & Pausch, M. H. Functional coupling of a

mammalian somatostatin receptor to the yeast pheromone response pathway. *Mol. Cell. Biol.* (1995). doi:10.1128/mcb.15.11.6188

328. Price, L. A., Strnad, J., Pausch, M. H. & Hadcock, J. R. Pharmacological characterization of the rat A(2a) adenosine receptor functionally coupled to the yeast pheromone response pathway. *Mol. Pharmacol.* (1996).
329. Kajkowski, E. M., Price, L. A., Pausch, M. H., Young, K. H. & Ozenberger, B. A. Investigation of growth hormone releasing hormone receptor structure and activity using yeast expression technologies. in *Journal of Receptor and Signal Transduction Research* (1997). doi:10.3109/10799899709036610
330. Erickson, J. R. *et al.* Edg-2/Vzg-1 couples to the yeast pheromone response pathway selectively in response to lysophosphatidic acid. *J. Biol. Chem.* (1998). doi:10.1074/jbc.273.3.1506
331. Leplatois, P. *et al.* Neurotensin induces mating in Saccharomyces cerevisiae cells that express human neurotensin receptor type 1 in place of the endogenous pheromone receptor. *Eur. J. Biochem.* (2001). doi:10.1046/j.0014-2956.2001.02407.x
332. Minic, J., Sautel, M., Salesse, R. & Pajot-Augy, E. Yeast System as a Screening Tool for Pharmacological Assessment of G Protein Coupled Receptors. *Curr. Med. Chem.* (2005). doi:10.2174/0929867053507261
333. Pausch, M. H. G-protein-coupled receptors in Saccharomyces cerevisiae: High-throughput screening assays for drug discovery. *Trends Biotechnol.* (1997). doi:10.1016/S0167-7799(97)01119-0
334. Hauser, A. S. *et al.* Pharmacogenomics of GPCR Drug Targets. *Cell* (2018). doi:10.1016/j.cell.2017.11.033
335. Crowe, M. L., Perry, B. N. & Connerton, I. F. G(G(olf) complements a GPA1 null mutation in Saccharomyces cerevisiae and functionally couples to the STE2 pheromone receptor. *J. Recept. Signal Transduct. Res.* (2000). doi:10.3109/10799890009150037
336. Radhika, V. *et al.* Chemical sensing of DNT by engineered olfactory yeast strain. *Nat. Chem. Biol.* (2007). doi:10.1038/nchembio882
337. Fukutani, Y. *et al.* Improving the odorant sensitivity of olfactory receptor-expressing yeast with accessory proteins. *Anal. Biochem.* (2015). doi:10.1016/j.ab.2014.10.012
338. Armbruster, B. N., Li, X., Pausch, M. H., Herlitze, S. & Roth, B. L. Evolving the lock to fit the key to create a family of G protein-coupled receptors potently activated by an inert ligand. *Proc. Natl. Acad. Sci. U. S. A.* (2007). doi:10.1073/pnas.0700293104
339. Dong, S., Rogan, S. C. & Roth, B. L. Directed molecular evolution of DREADDs: A generic approach to creating next-generation RASSLs. *Nat. Protoc.* (2010). doi:10.1038/nprot.2009.239
340. Ault, A. D. & Broach, J. R. Creation of GPCR-based chemical sensors by directed evolution in yeast. *Protein Eng. Des. Sel.* (2006). doi:10.1093/protein/gzi069
341. Adeniran, A., Stainbrook, S., Bostick, J. W. & Tyo, K. E. J. Detection of a Peptide Biomarker by Engineered Yeast Receptors. *ACS Synth. Biol.* **7**, 696–705 (2018).
342. Ehrenworth, A. M., Claiborne, T. & Peralta-Yahya, P. Medium-Throughput Screen of Microbially Produced Serotonin via a G-Protein-Coupled Receptor-Based Sensor. *Biochemistry* (2017). doi:10.1021/acs.biochem.7b00605
343. Mukherjee, K., Bhattacharyya, S. & Peralta-Yahya, P. GPCR-Based Chemical Biosensors for Medium-Chain Fatty Acids. *ACS Synth. Biol.* **4**, 1261–1269 (2015).
344. Di Roberto, R. B., Chang, B., Trusina, A. & Peisajovich, S. G. Evolution of a G protein-coupled receptor response by mutations in regulatory network interactions. *Nat. Commun.* (2016). doi:10.1038/ncomms12344
345. Flower, D. R. Modelling G-protein-coupled receptors for drug design. *Biochimica et Biophysica Acta - Reviews on Biomembranes* (1999). doi:10.1016/S0304-4157(99)00006-4
346. Giaever, G. *et al.* Functional profiling of the Saccharomyces cerevisiae genome. *Nature* (2002). doi:10.1038/nature00935
347. Pryciak, P. M. Designing New Cellular Signaling Pathways. *Chemistry and Biology* (2009). doi:10.1016/j.chembiol.2009.01.011
348. Bashor, C. J., Horwitz, A. A., Peisajovich, S. G. & Lim, W. A. Rewiring Cells: Synthetic Biology as a Tool to Interrogate the Organizational Principles of Living Systems. *Annu. Rev. Biophys.* **39**, 515–537 (2010).
349. Bhattacharyya, R. P., Reményi, A., Yeh, B. J. & Lim, W. A. Domains, Motifs, and Scaffolds: The Role of Modular Interactions in the Evolution and Wiring of Cell Signaling Circuits. *Annu. Rev. Biochem.* (2006). doi:10.1146/annurev.biochem.75.103004.142710
350. Klipp, E. Computational yeast systems biology: A case study for the MAP kinase cascade. *Methods Mol. Biol.*

(2011). doi:10.1007/978-1-61779-173-4_19

351. Klipp, E., Nordlander, B., Krüger, R., Gennemark, P. & Hohmann, S. Integrative model of the response of yeast to osmotic shock. *Nat. Biotechnol.* (2005). doi:10.1038/nbt1114
352. Kiel, C., Yus, E. & Serrano, L. Engineering Signal Transduction Pathways. *Cell* (2010). doi:10.1016/j.cell.2009.12.028
353. Inoue, T. *et al.* Identification of CRE1 as a cytokinin receptor from Arabidopsis. *Nature* (2001). doi:10.1038/35059117
354. Furukawa, K., Randhawa, A., Kaur, H., Mondal, A. K. & Hohmann, S. Fungal fludioxonil sensitivity is diminished by a constitutively active form of the group III histidine kinase. *FEBS Lett.* (2012). doi:10.1016/j.febslet.2012.05.057
355. Salomon, D., Bosis, E., Dar, D., Nachman, I. & Sessa, G. Expression of Pseudomonas syringae type III effectors in yeast under stress conditions reveals that HopX1 attenuates activation of the high osmolarity glycerol MAP kinase pathway. *Microbiol. (United Kingdom)* (2012). doi:10.1099/mic.0.062513-0
356. Furukawa, K. & Hohmann, S. Synthetic biology: Lessons from engineering yeast MAPK signalling pathways. *Mol. Microbiol.* **88**, 5–19 (2013).
357. Strickland, D. *et al.* TULIPs: Tunable, light-controlled interacting protein tags for cell biology. *Nat. Methods* (2012). doi:10.1038/nmeth.1904
358. O'Rourke, S. M. & Herskowitz, I. The Hog1 MAPK prevents cross talk between the HOG and pheromone response MAPK pathways in Saccharomyces cerevisiae. *Genes Dev.* (1998). doi:10.1101/gad.12.18.2874
359. Yang, H. Y., Tatebayashi, K., Yamamoto, K. & Saito, H. Glycosylation defects activate filamentous growth Kss1 MAPK and inhibit osmoregulatory Hog1 MAPK. *EMBO J.* (2009). doi:10.1038/emboj.2009.104
360. Saito, H. Regulation of cross-talk in yeast MAPK signaling pathways. *Current Opinion in Microbiology* (2010). doi:10.1016/j.mib.2010.09.001
361. Bashor, C. J., Helman, N. C., Yan, S. & Lim, W. A. Using engineered scaffold interactions to reshape MAP kinase pathway signaling dynamics. *Science (80-.).* (2008). doi:10.1126/science.1151153
362. Good, M., Tang, G., Singleton, J., Reményi, A. & Lim, W. A. The Ste5 Scaffold Directs Mating Signaling by Catalytically Unlocking the Fus3 MAP Kinase for Activation. *Cell* **136**, 1085–1097 (2009).
363. Zalatan, J. G., Coyle, S. M., Rajan, S., Sidhu, S. S. & Lim, W. A. Conformational control of the Ste5 scaffold protein insulates against MAP kinase misactivation. *Science (80-.).* (2012). doi:10.1126/science.1220683
364. Lai, A., Sato, P. M. & Peisajovich, S. G. Evolution of Synthetic Signaling Scaffolds by Recombination of Modular Protein Domains. *ACS Synth. Biol.* **4**, 714–722 (2015).
365. Babazadeh, R., Furukawa, T., Hohmann, S. & Furukawa, K. Rewiring yeast osmostress signalling through the MAPK network reveals essential and non-essential roles of Hog1 in osmoadaptation. *Sci. Rep.* (2014). doi:10.1038/srep04697
366. Atay, O. & Skotheim, J. M. Spatial and temporal signal processing and decision making by MAPK pathways. **216**, (2017).
367. Galloway, K. E., Franco, E. & Smolke, C. D. Dynamically reshaping signaling networks to program cell fate via genetic controllers. *Science (80-.).* (2013). doi:10.1126/science.1235005
368. Houser, J. R., Ford, E., Nagiec, M. J., Errede, B. & Elston, T. C. Positive roles for negative regulators in the mating response of yeast. *Mol. Syst. Biol.* (2012). doi:10.1038/msb.2012.18
369. Pi, H., Chien, C. T. & Fields, S. Transcriptional activation upon pheromone stimulation mediated by a small domain of Saccharomyces cerevisiae Ste12p. *Mol. Cell. Biol.* (1997). doi:10.1128/mcb.17.11.6410
370. Golemis, E. A. & Brent, R. Fused protein domains inhibit DNA binding by LexA. *Mol. Cell. Biol.* (1992). doi:10.1128/mcb.12.7.3006
371. Redden, H. & Alper, H. S. The development and characterization of synthetic minimal yeast promoters. *Nat. Commun.* (2015). doi:10.1038/ncomms8810
372. Khalil, A. S. *et al.* A synthetic biology framework for programming eukaryotic transcription functions. *Cell* (2012). doi:10.1016/j.cell.2012.05.045
373. Williams, T. C. *et al.* Quorum-sensing linked RNA interference for dynamic metabolic pathway control in Saccharomyces cerevisiae. *Metab. Eng.* **29**, 124–134 (2015).
374. Williams, T. C., Nielsen, L. K. & Vickers, C. E. Engineered quorum sensing using pheromone-mediated cell-to-cell communication in saccharomyces cerevisiae. *ACS Synth. Biol.* **2**, 136–149 (2013).

375. Urrios, A. *et al.* A Synthetic Multicellular Memory Device. *ACS Synth. Biol.* **5**, 862–873 (2016).
376. Urrios, A. *et al.* Plug-and-Play Multicellular Circuits with Time-Dependent Dynamic Responses. *ACS Synth. Biol.* (2018). doi:10.1021/acssynbio.7b00463
377. Hoffman-Sommer, M., Supady, A. & Klipp, E. Cell-to-cell communication circuits: Quantitative analysis of synthetic logic gates. *Front. Physiol.* (2012). doi:10.3389/fphys.2012.00287
378. Youk, H. & Lim, W. A. Secreting and sensing the same molecule allows cells to achieve versatile social behaviors. *Science (80-.).* **343**, (2014).
379. Groß, A., Rödel, G. & Ostermann, K. Application of the yeast pheromone system for controlled cell-cell communication and signal amplification. *Lett. Appl. Microbiol.* **52**, 521–526 (2011).
380. Jahn, M., Mölle, A., Rödel, G. & Ostermann, K. Temporal and spatial properties of a yeast multi-cellular amplification system based on signal molecule diffusion. *Sensors (Switzerland)* (2013). doi:10.3390/s131114511
381. Hoffmann, A. *et al.* Modeling population dynamics in a microbial consortium under control of a synthetic pheromone-mediated communication system. *Eng. Life Sci.* (2019). doi:10.1002/elsc.201800107
382. Shaw, W. M. *et al.* Engineering a Model Cell for Rational Tuning of GPCR Signaling. *Cell* (2019). doi:10.1016/j.cell.2019.02.023
383. Hennig, S., Rödel, G. & Ostermann, K. Artificial cell-cell communication as an emerging tool in synthetic biology applications. *Journal of Biological Engineering* (2015). doi:10.1186/s13036-015-0011-2
384. Koopman, F. *et al.* De novo production of the flavonoid naringenin in engineered Saccharomyces cerevisiae. *Microb. Cell Fact.* (2012). doi:10.1186/1475-2859-11-155
385. Meadows, A. L. *et al.* Rewriting yeast central carbon metabolism for industrial isoprenoid production. *Nature* (2016). doi:10.1038/nature19769
386. Brown, S., Clastre, M., Courdavault, V. & O'Connor, S. E. De novo production of the plant-derived alkaloid strictosidine in yeast. *Proc. Natl. Acad. Sci. U. S. A.* (2015). doi:10.1073/pnas.1423555112
387. Morita, H., Takahashi, Y., Noguchi, H. & Abe, I. Enzymatic formation of unnatural aromatic polyketides by chalcone synthase. *Biochem. Biophys. Res. Commun.* (2000). doi:10.1006/bbrc.2000.3920
388. Srirangan, K. *et al.* Recent advances in engineering propionyl-CoA metabolism for microbial production of value-added chemicals and biofuels. *Critical Reviews in Biotechnology* (2017). doi:10.1080/07388551.2016.1216391
389. Machado, H. B., Dekishima, Y., Luo, H., Lan, E. I. & Liao, J. C. A selection platform for carbon chain elongation using the CoA-dependent pathway to produce linear higher alcohols. *Metab. Eng.* (2012). doi:10.1016/j.ymben.2012.07.002
390. Katz, L. Chapter 6 The DEBS Paradigm for Type I Modular Polyketide Synthases and Beyond. *Methods in Enzymology* (2009). doi:10.1016/S0076-6879(09)04606-0
391. Li, Y., Luxenburger, E. & Müller, R. An alternative isovaleryl CoA biosynthetic pathway involving a previously unknown 3-methylglutaconyl CoA decarboxylase. *Angew. Chemie - Int. Ed.* (2013). doi:10.1002/anie.201207984
392. Steen, E. J. *et al.* Metabolic engineering of Saccharomyces cerevisiae for the production of n-butanol. *Microb. Cell Fact.* (2008). doi:10.1186/1475-2859-7-36
393. Yuzawa, S., Chiba, N., Katz, L. & Keasling, J. D. Construction of a part of a 3-hydroxypropionate cycle for heterologous polyketide biosynthesis in Escherichia coli. *Biochemistry* (2012). doi:10.1021/bi301414q
394. Horswill, A. R. & Escalante-Semerena, J. C. The prpE gene of Salmonella typhimurium LT2 encodes propionyl-CoA synthetase. *Microbiology* (1999). doi:10.1099/13500872-145-6-1381
395. Peter, D. M. *et al.* Screening and Engineering the Synthetic Potential of Carboxylating Reductases from Central Metabolism and Polyketide Biosynthesis. *Angew. Chemie - Int. Ed.* (2015). doi:10.1002/anie.201505282
396. Keren, L. *et al.* Promoters maintain their relative activity levels under different growth conditions. *Mol. Syst. Biol.* (2013). doi:10.1038/msb.2013.59
397. Kaneda, T. Fatty acids of the genus Bacillus: An example of branched chain preference. *Bacteriological Reviews* (1977).
398. Hamilton, R. J. Fatty Acids: Structure, Occurrence, Nomenclature, Biosynthesis and Properties. in *Trans Fatty Acids* (2008). doi:10.1002/9780470697658.ch1
399. WANG, G. -F, KURIKI, T., ROY, K. L. & KANEDA, T. The primary structure of branched-chain α-oxo acid dehydrogenase from Bacillus subtilis and its similarity to other α-oxo acid dehydrogenases. *Eur. J. Biochem.* (1993). doi:10.1111/j.1432-1033.1993.tb17858.x

400. Pulsawat, N., Kitani, S., Kinoshita, H., Lee, C. K. & Nihira, T. Identification of the bkdAB gene cluster, a plausible source of the starter-unit for virginiamycin M production in Streptomyces virginiae. *Arch. Microbiol.* (2007). doi:10.1007/s00203-007-0212-2

401. Denoya, C. D. *et al.* A second branched-chain α-keto acid dehydrogenase gene cluster (bkdFGH) from Streptomyces avermitilis: Its relationship to avermectin biosynthesis and the construction of a bkdF mutant suitable for the production of novel antiparasitic avermectins. *J. Bacteriol.* (1995).

402. Mattevi, A. *et al.* Atomic structure of the cubic core of the pyruvate dehydrogenase multienzyme complex. *Science (80-.).* (1992). doi:10.1126/science.1549782

403. Mattevi, A., Obmolova, G., Sokatch, J. R., Betzel, C. & Hol, W. G. J. The refined crystal structure of Pseudomonas putida lipoamide dehydrogenase complexed with NAD+ at 2.45 Å resolution. *Proteins Struct. Funct. Bioinforma.* (1992). doi:10.1002/prot.340130406

404. Ævarsson, A., Seger, K., Turley, S., Sokatch, J. R. & Hol, W. G. J. Crystal structure of 2-oxoisovalerate and dehydrogenase and the architecture of 2-oxo acid dehydrogenase multienzyme complexes. *Nat. Struct. Biol.* (1999). doi:10.1038/11563

405. Perham, R. N. Domains, Motifs, and Linkers in 2-Oxo Acid Dehydrogenase Multienzyme Complexes: A Paradigm in the Design of a Multifunctional Protein. *Biochemistry* (1991). doi:10.1021/bi00099a001

406. Graybill, E. R., Rouhier, M. F., Kirby, C. E. & Hawes, J. W. Functional comparison of citrate synthase isoforms from S. cerevisiae. *Arch. Biochem. Biophys.* (2007). doi:10.1016/j.abb.2007.04.039

407. Bode, H. B. *et al.* Mutasynthesis-derived myxalamids and origin of the isobutyryl-CoA starter unit of myxalamid B. *ChemBioChem* (2007). doi:10.1002/cbic.200700401

408. Bode, H. B. *et al.* 3-Hydroxy-3-methylglutaryl-coenzyme A (CoA) synthase is involved in biosynthesis of isovaleryl-CoA in the myxobacterium Myxococcus xanthus during fruiting body formation. *J. Bacteriol.* (2006). doi:10.1128/JB.00825-06

409. Bock, T., Müller, R. & Blankenfeldt, W. Crystal structure of AibC, a reductase involved in alternative de novo isovaleryl coenzyme A biosynthesis in Myxococcus xanthus. *Acta Crystallogr. Sect. Struct. Biol. Commun.* (2016). doi:10.1107/S2053230X16011146

410. Liou, G. F., Lau, J., Cane, D. E. & Khosla, C. Quantitative analysis of loading and extender acyltransferases of modular polyketide synthases. *Biochemistry* (2003). doi:10.1021/bi0268100

411. Yuzawa, S. *et al.* Comprehensive in vitro analysis of acyltransferase domain exchanges in modular polyketide synthases and its application for short-chain ketone production. *ACS Synth. Biol.* (2017). doi:10.1021/acssynbio.6b00176

412. Je, W. P., Won, S. J., Sung, R. P., Byoung, C. P. & Yeo, J. Y. Analysis of intracellular short organic acid-coenzyme a esters from actinomycetes using liquid chromatography-electrospray ionization-mass spectrometry. *J. Mass Spectrom.* (2007). doi:10.1002/jms.1240

413. Bond-Watts, B. B., Bellerose, R. J. & Chang, M. C. Y. Enzyme mechanism as a kinetic control element for designing synthetic biofuel pathways. *Nat. Chem. Biol.* (2011). doi:10.1038/nchembio.537

414. Dekishima, Y., Lan, E. I., Shen, C. R., Cho, K. M. & Liao, J. C. Extending carbon chain length of 1-butanol pathway for 1-hexanol synthesis from glucose by engineered Escherichia coli. *J. Am. Chem. Soc.* (2011). doi:10.1021/ja203814d

415. Cheong, S., Clomburg, J. M. & Gonzalez, R. Energy-and carbon-efficient synthesis of functionalized small molecules in bacteria using non-decarboxylative Claisen condensation reactions. *Nat. Biotechnol.* (2016). doi:10.1038/nbt.3505

416. Schadeweg, V. & Boles, E. N-Butanol production in Saccharomyces cerevisiae is limited by the availability of coenzyme A and cytosolic acetyl-CoA. *Biotechnol. Biofuels* (2016). doi:10.1186/s13068-016-0456-7

417. Stout, J. M., Boubakir, Z., Ambrose, S. J., Purves, R. W. & Page, J. E. The hexanoyl-CoA precursor for cannabinoid biosynthesis is formed by an acyl-activating enzyme in Cannabis sativa trichomes. *Plant J.* (2012). doi:10.1111/j.1365-313X.2012.04949.x

418. Tang, Y., Koppisch, A. T. & Khosla, C. The acyltransferase homologue from the initiation module of the R1128 polyketide synthase is an Acyl-ACP thioesterase that edits acetyl primer units. *Biochemistry* (2004). doi:10.1021/bi049157k

419. Ray, L. *et al.* A crotonyl-CoA reductase-carboxylase independent pathway for assembly of unusual alkylmalonyl-CoA polyketide synthase extender units. *Nat. Commun.* (2016). doi:10.1038/ncomms13609

420. Kim, E. J., Son, H. F., Kim, S., Ahn, J. W. & Kim, K. J. Crystal structure and biochemical characterization of beta-keto thiolase B from polyhydroxyalkanoate-producing bacterium Ralstonia eutropha H16. *Biochem. Biophys. Res. Commun.* (2014). doi:10.1016/j.bbrc.2014.01.055

421. Kim, J., Chang, J. H. & Kim, K. J. Crystal structure and biochemical properties of the (S)-3-hydroxybutyryl- CoA dehydrogenase PaaH1 from Ralstonia eutropha. *Biochem. Biophys. Res. Commun.* **448**, 163–168 (2014).

422. Kim, E. J., Kim, Y. J. & Kim, K. J. Structural insights into substrate specificity of crotonase from the n-butanol producing bacterium Clostridium acetobutylicum. *Biochem. Biophys. Res. Commun.* (2014). doi:10.1016/j.bbrc.2014.07.139

423. Brock, M. Generation and phenotypic characterization of Aspergillus nidulans methylisocitrate lyase deletion mutants: Methylisocitrate inhibits growth and conidiation. *Appl. Environ. Microbiol.* (2005). doi:10.1128/AEM.71.9.5465-5475.2005

424. Pronk, J. T., Van der Linden-Beuman, A., Verduyn, C., Scheffers, W. A. & Van Dijken, J. P. Propionate metabolism in Saccharomyces cerevisiae: Implications for the metabolon hypothesis. *Microbiology* (1994). doi:10.1099/00221287-140-4-717

425. Luttik, M. A. H. *et al.* The Saccharomyces cerevisiae ICL2 gene encodes a mitochondrial 2-methylisocitrate lyase involved in propionyl-coenzyme a metabolism. *J. Bacteriol.* (2000). doi:10.1128/JB.182.24.7007-7013.2000

426. Shi, S., Chen, Y., Siewers, V. & Nielsen, J. Improving production of malonyl coenzyme A-derived metabolites by abolishing Snf1-dependent regulation of Acc1. *MBio* (2014). doi:10.1128/mBio.01130-14

427. Sheng, J. & Feng, X. Metabolic engineering of yeast to produce fatty acid-derived biofuels: Bottlenecks and solutions. *Frontiers in Microbiology* (2015). doi:10.3389/fmicb.2015.00554

428. Chen, Y., Daviet, L., Schalk, M., Siewers, V. & Nielsen, J. Establishing a platform cell factory through engineering of yeast acetyl-CoA metabolism. *Metab. Eng.* (2013). doi:10.1016/j.ymben.2012.11.002

429. Kocharin, K., Chen, Y., Siewers, V. & Nielsen, J. Engineering of acetyl-CoA metabolism for the improved production of polyhydroxybutyrate in Saccharomyces cerevisiae. *AMB Express* (2012). doi:10.1186/2191-0855-2-52

430. Berg, I. A., Kockelkorn, D., Buckel, W. & Fuchs, G. A 3-hydroxypropionate/4-hydroxybutyrate autotrophic carbon dioxide assimilation pathway in archaea. *Science (80-.).* (2007). doi:10.1126/science.1149976

431. Hügler, M., Menendez, C., Schägger, H. & Fuchs, G. a Key Enzyme of the 3-Hydroxypropionate Cycle for Autotrophic CO 2 Fixation. *Society* **184**, 2404–2410 (2002).

432. Hügler, M. & Sievert, S. M. Beyond the Calvin Cycle: Autotrophic Carbon Fixation in the Ocean. *Ann. Rev. Mar. Sci.* (2011). doi:10.1146/annurev-marine-120709-142712

433. Liu, C., Wang, Q., Xian, M., Ding, Y. & Zhao, G. Dissection of Malonyl-Coenzyme A Reductase of Chloroflexus aurantiacus Results in Enzyme Activity Improvement. *PLoS One* (2013). doi:10.1371/journal.pone.0075554

434. Alber, B. *et al.* Malonyl-coenzyme A reductase in the modified 3-hydroxypropionate cycle for autotrophic carbon fixation in archaeal Metallosphaera and Sulfolobus spp. *J. Bacteriol.* (2006). doi:10.1128/JB.00987-06

435. Chen, Y., Bao, J., Kim, I. K., Siewers, V. & Nielsen, J. Coupled incremental precursor and co-factor supply improves 3-hydroxypropionic acid production in Saccharomyces cerevisiae. *Metab. Eng.* (2014). doi:10.1016/j.ymben.2014.01.005

436. Huber, G., Spinnler, C., Gambacorta, A. & Stetter, K. O. Metallosphaera sedula gen, and sp. nov. Represents a New Genus of Aerobic, Metal-Mobilizing, Thermoacidophilic Archaebacteria. *Syst. Appl. Microbiol.* (1989). doi:10.1016/S0723-2020(89)80038-4

437. Lee, D. & Kim, K. J. Structural insight into substrate specificity of 3-hydroxypropionyl-coenzyme a dehydratase from metallosphaera sedula. *Sci. Rep.* (2018). doi:10.1038/s41598-018-29070-w

438. Tong, L. Structure and function of biotin-dependent carboxylases. *Cellular and Molecular Life Sciences* (2013). doi:10.1007/s00018-012-1096-0

439. Diacovich, L. *et al.* Kinetic and structural analysis of a new group of Acyl-CoA carboxylases found in Streptomyces coelicolor A3(2). *J. Biol. Chem.* (2002). doi:10.1074/jbc.M203263200

440. Gago, G., Diacovich, L., Arabolaza, A., Tsai, S. C. & Gramajo, H. Fatty acid biosynthesis in actinomycetes. *FEMS Microbiology Reviews* (2011). doi:10.1111/j.1574-6976.2010.00259.x

441. Gago, G., Kurth, D., Diacovich, L., Tsai, S. C. & Gramajo, H. Biochemical and structural characterization of an essential acyl coenzyme A carboxylase from Mycobacterium tuberculosis. *J. Bacteriol.* (2006). doi:10.1128/JB.188.2.477-486.2006

442. Rodríguez, E., Banchio, C., Diacovich, L., Bibb, M. J. & Gramajo, H. Role of an Essential Acyl Coenzyme A Carboxylase in the Primary and Secondary Metabolism of Streptomyces coelicolor A3(2). *Appl. Environ. Microbiol.* (2001). doi:10.1128/AEM.67.9.4166-4176.2001
443. Parthasarathy, R., Bajaj, J. & Boder, E. T. An immobilized biotin ligase: Surface display of Escherichia coli BirA on Saccharomyces cerevisiae. *Biotechnol. Prog.* (2005). doi:10.1021/bp050279t
444. Erb, T. J., Brecht, V., Fuchs, G., Müller, M. & Alber, B. E. Carboxylation mechanism and stereochemistry of crotonyl-CoA carboxylase/reductase, a carboxylating enoyl-thioester reductase. *Proc. Natl. Acad. Sci. U. S. A.* (2009). doi:10.1073/pnas.0903939106
445. Rosenthal, R. G. *et al.* Direct evidence for a covalent ene adduct intermediate in NAD(P)H-dependent enzymes. *Nat. Chem. Biol.* (2014). doi:10.1038/nchembio.1385
446. Rosenthal, R. G., Vögeli, B., Wagner, T., Shima, S. & Erb, T. J. A conserved threonine prevents self-intoxication of enoyl-thioester reductases. *Nat. Chem. Biol.* (2017). doi:10.1038/nchembio.2375
447. Yuzawa, S., Eng, C. H., Katz, L. & Keasling, J. D. Broad substrate specificity of the loading didomain of the lipomycin polyketide synthase. *Biochemistry* (2013). doi:10.1021/bi400520t
448. Urlinger, S. *et al.* Exploring the sequence space for tetracycline-dependent transcriptional activators: Novel mutations yield expanded range and sensitivity. *Proc. Natl. Acad. Sci. U. S. A.* (2000). doi:10.1073/pnas.130192197
449. Janiak, A. M. *et al.* Functional expression of the Candida albicans α-factor receptor in Saccharomyces cerevisiae. *Fungal Genet. Biol.* (2005). doi:10.1016/j.fgb.2005.01.006
450. Shen, X. X. *et al.* Reconstructing the backbone of the saccharomycotina yeast phylogeny using genome-scale data. *G3 Genes, Genomes, Genet.* (2016). doi:10.1534/g3.116.034744
451. Pereira, L. F., Costa, C. R. L., Brasileiro, B. T. R. V. & de Morais, M. A. Lachancea mirantina sp. nov., an ascomycetous yeast isolated from the cachaça fermentation process. *Int. J. Syst. Evol. Microbiol.* (2011). doi:10.1099/ijs.0.020008-0
452. KEGG. Vanderwaltozyma polyspora: Kpol_1063p22. Available at: https://www.genome.jp/dbget-bin/www_bget?vpo:Kpol_1063p22.
453. Chang, F. & Herskowitz, I. Identification of a gene necessary for cell cycle arrest by a negative growth factor of yeast: FAR1 is an inhibitor of a G1 cyclin, CLN2. *Cell* (1990). doi:10.1016/0092-8674(90)90503-7
454. Peter, M. & Herskowitz, I. Direct inhibition of the yeast cyclin-dependent kinase Cdc28-Cln by Far1. *Science (80-.).* (1994). doi:10.1126/science.8066461
455. Kredel, S. *et al.* mRuby, a bright monomeric red fluorescent protein for labeling of subcellular structures. *PLoS One* (2009). doi:10.1371/journal.pone.0004391
456. Chen, Y. Y., Galloway, K. E. & Smolke, C. D. Synthetic biology: Advancing biological frontiers by building synthetic systems. *Genome Biology* (2012). doi:10.1186/gb-2012-13-2-240
457. Hamada, K., Terashima, H., Arisawa, M., Yabuki, N. & Kitada, K. Amino acid residues in the ω-minus region participate in cellular localization of yeast glycosylphosphatidylinositol-attached proteins. *J. Bacteriol.* (1999).
458. Haushalter, R. W. *et al.* Production of anteiso-branched fatty acids in Escherichia coli; next generation biofuels with improved cold-flow properties. *Metab. Eng.* (2014). doi:10.1016/j.ymben.2014.09.002
459. Gilbert, W. V., Zhou, K., Butler, T. K. & Doudna, J. A. Cap-independent translation is required for starvation-induced differentiation in yeast. *Science (80-.).* (2007). doi:10.1126/science.1144467
460. Sharma, P. *et al.* 2A peptides provide distinct solutions to driving stop-carry on translational recoding. *Nucleic Acids Res.* (2012). doi:10.1093/nar/gkr1176
461. Edwards, S. R. & Wandless, T. J. Dicistronic regulation of fluorescent proteins in the budding yeast Saccharomyces cerevisiae. *Yeast* (2010). doi:10.1002/yea.1744
462. Gupta, R. K., Patterson, S. S., Ripp, S., Simpson, M. L. & Sayler, G. S. Expression of the Photorhabdus luminescens lux genes (luxA, B, C, D, and E) in Saccharomyces cerevisiae. *FEMS Yeast Res.* (2003). doi:10.1016/S1567-1356(03)00174-0
463. Souza-Moreira, T. M. *et al.* Screening of 2A peptides for polycistronic gene expression in yeast. *FEMS Yeast Res.* (2018). doi:10.1093/femsyr/foy036
464. Maciejak, A. *et al.* The effects of statins on the mevalonic acid pathway in recombinant yeast strains expressing human HMG-CoA reductase. *BMC Biotechnol.* (2013). doi:10.1186/1472-6750-13-68
465. Shen, C. R. *et al.* Driving forces enable high-titer anaerobic 1-butanol synthesis in Escherichia coli. *Appl. Environ.*

Microbiol. (2011). doi:10.1128/AEM.03034-10

466. Olzhausen, J., Schübbe, S. & Schüller, H. J. Genetic analysis of coenzyme A biosynthesis in the yeast Saccharomyces cerevisiae: Identification of a conditional mutation in the pantothenate kinase gene CAB1. *Current Genetics* (2009). doi:10.1007/s00294-009-0234-1
467. Stirrett, K., Denoya, C. & Westpheling, J. Branched-chain amino acid catabolism provides precursors for the Type II polyketide antibiotic, actinorhodin, via pathways that are nutrient dependent. *J. Ind. Microbiol. Biotechnol.* (2009). doi:10.1007/s10295-008-0480-0
468. Erb, T. J., Fuchs, G. & Alber, B. E. (2S)- Methylsuccinyl-CoA dehydrogenase closes the ethylmalonyl-CoA pathway for acetyl-CoA assimilation. *Mol. Microbiol.* (2009). doi:10.1111/j.1365-2958.2009.06837.x
469. Bernhardsgrütter, I. *et al.* The multicatalytic compartment of propionyl-CoA synthase sequesters a toxic metabolite. *Nat. Chem. Biol.* (2018). doi:10.1038/s41589-018-0153-x
470. Cozens, C. & Pinheiro, V. B. Darwin Assembly: fast, efficient, multi-site bespoke mutagenesis. *Nucleic Acids Res.* (2018). doi:10.1093/nar/gky067
471. Lee, S. K. & Keasling, J. D. A propionate-inducible expression system for enteric bacteria. *Appl. Environ. Microbiol.* (2005). doi:10.1128/AEM.71.11.6856-6862.2005
472. Mattozzi, M. d., Ziesack, M., Voges, M. J., Silver, P. A. & Way, J. C. Expression of the sub-pathways of the Chloroflexus aurantiacus 3-hydroxypropionate carbon fixation bicycle in E. coli: Toward horizontal transfer of autotrophic growth. *Metab. Eng.* (2013). doi:10.1016/j.ymben.2013.01.005
473. O'Kane, P. T., Dudley, Q. M., McMillan, A. K., Jewett, M. C. & Mrksich, M. High-throughput mapping of CoA metabolites by SAMDI-MS to optimize the cell-free biosynthesis of HMG-CoA. *Sci. Adv.* (2019). doi:10.1126/sciadv.aaw9180
474. Lian, J., Si, T., Nair, N. U. & Zhao, H. Design and construction of acetyl-CoA overproducing Saccharomyces cerevisiae strains. in *Food, Pharmaceutical and Bioengineering Division 2014 - Core Programming Area at the 2014 AIChE Annual Meeting* (2014). doi:10.1016/j.ymben.2014.05.010
475. Xu, P., Ranganathan, S., Fowler, Z. L., Maranas, C. D. & Koffas, M. A. G. Genome-scale metabolic network modeling results in minimal interventions that cooperatively force carbon flux towards malonyl-CoA. *Metab. Eng.* (2011). doi:10.1016/j.ymben.2011.06.008
476. David, F., Nielsen, J. & Siewers, V. Flux Control at the Malonyl-CoA Node through Hierarchical Dynamic Pathway Regulation in Saccharomyces cerevisiae. *ACS Synth. Biol.* (2016). doi:10.1021/acssynbio.5b00161
477. Li, S., Si, T., Wang, M. & Zhao, H. Development of a Synthetic Malonyl-CoA Sensor in Saccharomyces cerevisiae for Intracellular Metabolite Monitoring and Genetic Screening. *ACS Synth. Biol.* (2015). doi:10.1021/acssynbio.5b00069
478. Callari, R., Fischer, D., Heider, H. & Weber, N. Biosynthesis of angelyl-CoA in Saccharomyces cerevisiae. *Microb. Cell Fact.* (2018). doi:10.1186/s12934-018-0925-8
479. Schwander, T. The design and realization of synthetic pathways for the fixation of carbon dioxide in vitro. (2018).
480. Cronan, J. E. & Wallace, J. C. The gene encoding the biotin-apoprotein ligase of Saccharomyces cerevisiae. *FEMS Microbiol. Lett.* (1995). doi:10.1016/0378-1097(95)00210-V
481. Stolz, J., Hoja, U., Meier, S., Sauer, N. & Schweizer, E. Identification of the plasma membrane H+-biotin symporter of Saccharomyces cerevisiae by rescue of a fatty acid-auxotrophic mutant. *J. Biol. Chem.* (1999). doi:10.1074/jbc.274.26.18741
482. Maruyama, K. & Kitamura, H. Some effects of propionate on the growth of rhodopseudomonas spheroides S. *Agric. Biol. Chem.* (1975). doi:10.1271/bbb1961.39.1521
483. Erb, T. J. Carboxylases in natural and synthetic microbial pathways. *Applied and Environmental Microbiology* (2011). doi:10.1128/AEM.05702-11
484. Schada von Borzyskowski, L., Rosenthal, R. G. & Erb, T. J. Evolutionary history and biotechnological future of carboxylases. *J. Biotechnol.* (2013). doi:10.1016/j.jbiotec.2013.05.007
485. Erb, T. J. *et al.* Synthesis of C5-dicarboxylic acids from C2-units involving crotonyl-CoA carboxylase/reductase: The ethylmalonyl-CoA pathway. *Proc. Natl. Acad. Sci. U. S. A.* (2007). doi:10.1073/pnas.0702791104
486. Erb, T. J., Brecht, V., Fuchs, G., Müller, M. & Alber, B. E. Carboxylation mechanism and stereochemistry of crotonyl-CoA carboxylase/reductase, a carboxylating enoyl-thioester reductase. *Proc. Natl. Acad. Sci. U. S. A.* (2009). doi:10.1073/pnas.0903939106

487. Klaus, M. & Grininger, M. Engineering strategies for rational polyketide synthase design. *Natural Product Reports* (2018). doi:10.1039/c8np00030a
488. Gajewski, J., Pavlovic, R., Fischer, M., Boles, E. & Grininger, M. Engineering fungal de novo fatty acid synthesis for short chain fatty acid production. *Nat. Commun.* (2017). doi:10.1038/ncomms14650
489. Liu, Z. & Liu, T. Production of acrylic acid and propionic acid by constructing a portion of the 3-hydroxypropionate/4-hydroxybutyrate cycle from Metallosphaera sedula in Escherichia coli. *J. Ind. Microbiol. Biotechnol.* (2016). doi:10.1007/s10295-016-1843-6
490. Raths, S. K., Naider, F. & Becker, J. M. Peptide analogues compete with the binding of alpha-factor to its receptor in Saccharomyces cerevisiae. *J. Biol. Chem*. (1988).
491. Manfredi, J. P. *et al.* Yeast alpha mating factor structure-activity relationship derived from genetically selected peptide agonists and antagonists of Ste2p. *Mol. Cell. Biol.* (1996). doi:10.1128/mcb.16.9.4700
492. Ladds, G., Rasmussen, E. M., Young, T., Nielsen, O. & Davey, J. The sxa2-dependent inactivation of the P-factor mating pheromone in the fission yeast Schizosaccharomyces pombe. *Mol. Microbiol.* (1996). doi:10.1111/j.1365-2958.1996.tb02486.x
493. Ladds, G. & Davey, J. Characterisation of Sxa2, a carboxypeptidase involved in pheromone recovery in fission yeast. in *Biochemical Society Transactions* (1996).
494. Mundt, M., Anders, A., Murray, S. M. & Sourjik, V. A System for Gene Expression Noise Control in Yeast. *ACS Synth. Biol.* (2018). doi:10.1021/acssynbio.8b00279
495. Yamanishi, M. *et al.* A genome-wide activity assessment of terminator regions in saccharomyces cerevisiae provides a 'terminatome' toolbox. *ACS Synth. Biol.* (2013). doi:10.1021/sb300116y
496. Nagai, T. *et al.* A variant of yellow fluorescent protein with fast and efficient maturation for cell-biological applications. *Nat. Biotechnol.* (2002). doi:10.1038/nbt0102-87
497. Matsuyama, T. Recent developments in terminator technology in Saccharomyces cerevisiae. *Journal of Bioscience and Bioengineering* (2019). doi:10.1016/j.jbiosc.2019.06.006
498. Larimer, F. W., Perry, J. R. & Hardigree, A. A. The REV1 gene of Saccharomyces cerevisiae: isolation, sequence, and functional analysis. *J. Bacteriol.* (1989). doi:10.1128/jb.171.1.230-237.1989
499. Zhao, Y., Sohn, J.-H. & Warner, J. R. Autoregulation in the Biosynthesis of Ribosomes. *Mol. Cell. Biol.* (2003). doi:10.1128/mcb.23.2.699-707.2003
500. Grigull, J., Mnaimneh, S., Pootoolal, J., Robinson, M. D. & Hughes, T. R. Genome-Wide Analysis of mRNA Stability Using Transcription Inhibitors and Microarrays Reveals Posttranscriptional Control of Ribosome Biogenesis Factors. *Mol. Cell. Biol.* (2004). doi:10.1128/mcb.24.12.5534-5547.2004
501. Bardwell, L., Cook, J. G., Zhu-Shimoni, J. X., Voora, D. & Thorner, J. Differential regulation of transcription: Repression by unactivated mitogen-activated protein kinase Kss1 requires the Dig1 and Dig2 proteins. *Proc. Natl. Acad. Sci. U. S. A.* (1998). doi:10.1073/pnas.95.26.15400
502. McCullagh, E., Seshan, A., El-Samad, H. & Madhani, H. D. Coordinate control of gene expression noise and interchromosomal interactions in a MAP kinase pathway. *Nat. Cell Biol.* (2010). doi:10.1038/ncb2097
503. Egel-Mitani, M., Flygenring, H. P. & Hansen, M. T. A novel aspartyl protease allowing KEX2-independent MFα propheromone processing in yeast. *Yeast* (1990). doi:10.1002/yea.320060206
504. Vadaie, N. *et al.* Cleavage of the signaling mucin Msb2 by the aspartyl protease Yps1 is required for MAPK activation in yeast. *J. Cell Biol.* (2008). doi:10.1083/jcb.200704079
505. Chasse, S. A. *et al*. Genome-scale analysis reveals Sst2 as the principal regulator of mating pheromone signaling in the yeast Saccharomyces cerevisiae. *Eukaryot. Cell* (2006). doi:10.1128/EC.5.2.330-346.2006
506. Doi, K. *et al*. MSG5, a novel protein phosphatase promotes adaptation to pheromone response in S. cerevisiae. *EMBO J.* (1994). doi:10.1002/j.1460-2075.1994.tb06235.x
507. Blackwell, E. *et al.* Effect of the Pheromone-Responsive G and Phosphatase Proteins of Saccharomyces cerevisiae on the Subcellular Localization of the Fus3 Mitogen-Activated Protein Kinase. *Mol. Cell. Biol.* (2003). doi:10.1128/mcb.23.4.1135-1150.2003
508. Groisman, A. *et al.* A microfluidic chemostat for experiments with bacterial and yeast cells. *Nat. Methods* (2005). doi:10.1038/nmeth784
509. Son, C. D., Sargsyan, H., Naider, F. & Becker, J. M. Identification of ligand binding regions of the Saccharomyces cerevisiae α-factor pheromone receptor by photoaffinity cross-linking. *Biochemistry* (2004). doi:10.1021/bi0496889

510. Naider, F. & Becker, J. M. The α-factor mating pheromone of Saccharomyces cerevisiae: A model for studying the interaction of peptide hormones and G protein-coupled receptors. *Peptides* (2004). doi:10.1016/j.peptides.2003.11.028
511. Greig, D., Louis, E. J., Borts, R. H. & Travisano, M. Hybrid speciation in experimental populations of yeast. *Science (80-.).* (2002). doi:10.1126/science.1076374
512. Nadin-Davis, S. A. & Nasim, A. Schizosaccharomyces pombe ras1 and byr1 are functionally related genes of the ste family that affect starvation-induced transcription of mating-type genes. *Mol. Cell. Biol.* (1990). doi:10.1128/mcb.10.2.549
513. MacKay, V. L. *et al.* Characterization of the bar proteinase, an extracellular enzyme from the yeast Saccharomyces cerevisiae. *Advances in Experimental Medicine and Biology* (1991).
514. Naglik, J. R., Challacombe, S. J. & Hube, B. Candida albicans Secreted Aspartyl Proteinases in Virulence and Pathogenesis. *Microbiol. Mol. Biol. Rev.* (2003). doi:10.1128/mmbr.67.3.400-428.2003
515. Ng, A. H. *et al.* Modular and tunable biological feedback control using a de novo protein switch. *Nature* (2019). doi:10.1038/s41586-019-1425-7
516. Gibson, D. G. *et al.* Enzymatic assembly of DNA molecules up to several hundred kilobases. *Nat. Methods* (2009). doi:10.1038/nmeth.1318
517. Quan, J. & Tian, J. Circular polymerase extension cloning for high-throughput cloning of complex and combinatorial DNA libraries. *Nat. Protoc.* (2011). doi:10.1038/nprot.2010.181
518. Oldenburg, K. R., Vo, K. T., Michaelis, S. & Paddon, C. Recombination-mediated PCR-directed plasmid construction in vivo in yeast. *Nucleic Acids Res.* (1997). doi:10.1093/nar/25.2.451
519. Engler, C., Kandzia, R. & Marillonnet, S. A one pot, one step, precision cloning method with high throughput capability. *PLoS One* (2008). doi:10.1371/journal.pone.0003647
520. Weber, E., Engler, C., Gruetzner, R., Werner, S. & Marillonnet, S. A modular cloning system for standardized assembly of multigene constructs. *PLoS One* (2011). doi:10.1371/journal.pone.0016765
521. Warren, D. J. Preparation of highly efficient electrocompetent Escherichia coli using glycerol/mannitol density step centrifugation. *Anal. Biochem.* (2011). doi:10.1016/j.ab.2011.02.036
522. Gietz, R. D. & Schiestl, R. H. Frozen competent yeast cells that can be transformed with high efficiency using the LiAc/SS carrier DNA/PEG method. *Nat. Protoc.* (2007). doi:10.1038/nprot.2007.17
523. Jones, E. W. Tackling the Protease Problem in Saccharomyces cerevisiae. *Methods Enzymol.* (1991). doi:10.1016/0076-6879(91)94034-A
524. Robinson, J. S., Klionsky, D. J., Banta, L. M. & Emr, S. D. Protein sorting in Saccharomyces cerevisiae: isolation of mutants defective in the delivery and processing of multiple vacuolar hydrolases. *Mol. Cell. Biol.* (1988). doi:10.1128/mcb.8.11.4936
525. Zimmermann, M., Thormann, V., Sauer, U. & Zamboni, N. Nontargeted profiling of coenzyme A thioesters in biological samples by tandem mass spectrometry. *Anal. Chem.* (2013). doi:10.1021/ac401555n
526. Guder, J. C., Schramm, T., Sander, T. & Link, H. Time-Optimized Isotope Ratio LC-MS/MS for High-Throughput Quantification of Primary Metabolites. *Anal. Chem.* (2017). doi:10.1021/acs.analchem.6b03731
527. Peter, D. M., Vögeli, B., Cortina, N. S. & Erb, T. J. A chemo-enzymatic road map to the synthesis of CoA esters. *Molecules* (2016). doi:10.3390/molecules21040517
528. Day, A., Schneider, C. & Schneider, B. L. Yeast cell synchronization. *Methods Mol. Biol.* (2004).
529. Tyson, C. B., Lord, P. G. & Wheals, A. E. Dependency of size of Saccharomyces cerevisiae cells on growth rate. *J. Bacteriol.* (1979).
530. Glatter, T. *et al.* Large-scale quantitative assessment of different in-solution protein digestion protocols reveals superior cleavage efficiency of tandem Lys-C/trypsin proteolysis over trypsin digestion. *J. Proteome Res.* (2012). doi:10.1021/pr300273g

Appendix

Appendix Table 1: Result of the *in silico* identification of α-factors. Green: secretion signaling sequence, red: Kex2 motif, blue: Ste13 motif, yellow: mature α-factor. The table listing the *in silico* identification result for *S. cerevisiae* can be found in Table 3.

Name of organism	Pre-pro-α-factor sequence	α-factor
Ashbya aceri	MKPTLILSLAALAACAPIQPSDLAEAAKVPADAVVGFLELYNVGDMALVP VDNGVHSGILFVNSTLAHLNEPTQPRTRAVSQKWHWLRFGDGQSM	
Ashbya gossypii	MKISLLFSVSALLGAVIAIPVNGSRPEVTIDDVRGNIPEDAVLGFLDLSDVE GLAVRPIQTEERTGLLFVNRQLAEKGTEAASSQGSPKLEKDIARVYKRLME YGHRRIFPAIDL	
Aspergillus fumigatus	MKFLSLVLASFAAAAVQAHITPWCHLPGQGCYML [KRAADA] SDEV [RRSASAVAEAVAEAFP] QSPWCHLPGQGCAKA [KRAAEA] AEEV [KRSA] DVFAEAMAAFEKE	
Babjeviella inositovora	MKLSTVVTTTALVASVISAVPANPTESSVPAATSSAAENTINVPVEAINNAI YLASGEYPLFIEENGKPMVLIVNATLAAQAEEEDADHLN [KRDASPEA] KWGWLTLRFNQPLF [KRQADAEPGA] KWGWLTLRFNQPLF [KRQADAGPEA] KWGWLTLRFNQPLF	α_{Bi}-factor1: KWGWLTLRFNQPLF
Candida albicans	MKFSLTLLTATIATIVAAAPAQYTGQAIDSNQVVEIPESAVEAYFPIDDELT PVFGEIDNKPVILIVNGTTLTSGANNE [KREA] KSKGGFRLTNFGYFEPG [KRDANADA] GFRLTNFGYFEPG [KRDANAEA] GFRLTNFGYFEPGK	α_{Ca}-factor1: KSKGGFRLTNFGYFEPG α_{Ca}-factor2: GFRLTNFGYFEPG
Candida auris	MKFSITAIIAATGSLVAAAPTPSSTDAPSFSEVPSSVESSFGVPTEAIIGQFSF DADEYPLLTVYEDRRYIILLNSTIMEEAYASLNSGNE [KRDAEAEA] KWGWLRFFPGEPFV [KRDAEADAEA] KWGWLRFFPGEPFV [KRDAEADAEA] KWGWLRFFPGEPFV [KRDADAEA] KWGWLRFYPGEPFVKREVEADLEG	α_{Cau}-factor: KWGWLRFFPGEPFV
Candida glabrata	MRFLRFISTVALLITGLATAQPVGEELGETVEVPSEAFIGYLDFGATNDVAI LPISNKTNNGLLFVNTTLYNQATKGEKLSDFT [KRDANPDAEAEA] WHWVKIRKGQGLF [RRSADASPEAEA] WHWVRLRKGQGLF [RRSADASPEAEA] WHWVRLRKGQGLF	α_{Cg}-factor1: WHWVKIRKGQGLF α_{Cg}-factor2: WHWVRLRKGQGLF
Candida intermedia	MKFINTLLLSLAASVVSAAPAATPVDDGSVSVPTEAILGRIDLNPEEFPYIV SDGENTSIVLFNTTILDEAYSGVT [KRDAEP] WGWIKFFPGQPIG [KREADASP] WGWIKFFPGQPIG [KRDAEAEP] WGWIKFFPGQPIG [KRDAEAEP] WGWIKFFPGQPIGKRED	α_{Ci}-factor1: WGWIKFFPGQPIG
Candida orthopsilosis	MKFSITVLTSVAAALVASAPVTPGKIDTPALPIENPLERVVEAFFKGSSIDAE AENKVEDKAVAEAMEDADAKTAAGSQ [KRDAEAKP] HWTTYGYYEPQ [KRDAVAEADAEAKP] HWTTYGYYEPQK	α_{Co}-factor1: HWTTYGYYEPQ
Candida tenuis	MRLSTILTLALTSKFVFSAPVEKVKREDGLDVPDEAIIAVYPIDEYKQPFYAE ADGQNYVVILNTTALGEADLA [KRDADA] FSWNYRLKWQPIS [KRDADADADADA] FSWNYRLKWQPIS [KRDADADADADADA] FSWNYRLKWQPIS	α_{Ct}-factor1:FSWNYRLKWQPIS
Clavispora lusitaniae (Candida lusitaniae)	MKFSLAIIFSLAAAVVSAAPVAPESSSDFQIPEEAIISSQALGDDQLPLLLGE GNATYFVLVNGTTLAEAYGIT [KRDAEA] FDATYLGSSVA [KREANADA] WGWIHFLNTDVIG [KRDAEP] KWKWIHFRNTDVIG [KRDASP] KWKWIKFRNTDVIG [KRDAEADASP] KWKWIKFRNTDVIG [KRDAEADAAP] KWKWIKFRNTDVIG [KRDANAAP] KWRWINFRNTDVIG [KREA] QE	α_{Cl}-factor1:WGWIHFLNTDVIG α_{Cl}-factor2:KWKWIHFRNTDVIG α_{Cl}-factor3: KWKWIKFRNTDVIG α_{Cl}-factor4: KWRWINFRNTDVIG
Eremothecium cymbalariae	MKFYNILSVASIASLVFAAPVSVNDAKEIAATFPQEALLGFLDLTDAENIVI LSLVDEEKSGIALVNKTIWATARSEQAAGIS [KRDADA] WHWLRFDRGQPIH [KRSADAVADA] WHWLRFDRGQPIH [KRSADAVADA] WHWLRFDRGQPIH [KRSADAVADA] WHWLRFDRGQPIHK	α_{Ec}-factor1: WHWLRFDRGQPIH
Eremothecium sinecaudum	MRLNSIVCAFGVAALASAAPVDINLKAATQHDFPKGENFGLPEESILGFID LAKDKDVSVLQVKEGLLFLNSTVLQNSNIEINGSSIE [KRDASP]WKWMKFGRGGSYW[KRDASPDADADAEP]WKWMKFGRGG SYW[KRDASPDADADAEP]WKWVKFGRGGSYW[KRDASPDADADAEP] WKWMKFGRGGSYW[KR]EVSIDANIQT	α_{Es}-factor1: WKWMKFGRGGSYW α_{Es}-factor2: WKWVKFGRGGSYW
Fusarium langsethiae	MKYSILTLAAVASTAFATAIPEPQPDPVAEAEPWCTWKGQPCWKAKMG[KREAKAEAEAEPIPDPVAAPEPNPVAEPNPVAEPNPVAEPMP] WCTWKGQPCWKEKMA [KREAKPEP] WCWWKGQPCWKT [KRNAAPEPMPEP] ANEPRWCWWKGQPCWKSKS [KRDASPEP] WCWWKGQPCWKA[KRDA]SEALTVALHATRGVETRSVAETEHLPRDAA HHA[KRSIVELANVIALSARGSPEEYFKNLYLEEFFPEIPHNATAKRDVKTLQ ED[KR]WCWWKGQPCWKA[KRAAEA]VLHAVDGADGAGAPGGPEEHFD TSNFNPQNFEA[KR]DLMAIKAAARSVVESLEG	α_{Fl}-factor1: WCTWKGQPCWKEKMA α_{Fl}-factor2: WCWWKGQPCWKT α_{Fl}-factor3: ANEPRWCWWKGQPCWKSKS α_{Fl}-factor4: WCWWKGQPCWKA

Hanseniaspora guilliermondii	MKFTTAIASVAAAASFASAAAIDQEQLANGTYIDIPQEAILSFLDLTDSPD VSVYPIKEGSKTGMIFVNSTIVDQAYNETTALT R[KREAVAEADPWA]WIRMXNVARWCYVHQKRC	α_{Hg}-factor1: WIRMXNVARWCYVHQ
Hanseniaspora opuntiae	MKFTTAIASVAAAASFATAAAIDQEQLTNGTYIDIPQESILSFLDLTDSPEV SVYPIKEGSKTGLLFVNSTIVDQAYNETTPLT R[KREAVAEADPWA] WIRMWPGGVMFT [KRDADAEAEAEADPWA] WIRMWPGGVMFT [KRDAEAEADADAEAWA] WIRMWPGGVMFT	α_{Ho}-factor1: WIRMWPGGVMFT
Hanseniaspora osmophila	MKLSTTIAATTAATTALVAGATAAPVSGASNSTSMEVPGEAVKYFLDLSD SPDMALVPINNGNTTGIMFVNTTVIDQAYAETTSLSR [KREASANA] WHWLKFDVGEPLYA [KRDANADADA] SLWHWLKFDVGEPLYA [KRDANADADASA] WHWLKFDVGEPLYA [KRDANADADASA] WHWLKFDVGEPLYA	α_{Hos}-factor1: WHWLKFDVGEPLYA α_{Hos}-factor2: SLWHWLKFDVGEPLYA
Hanseniaspora uvarum (Kloeckera apiculata)	MKFTTAIASVAAAASFASAAAIDQEQLTNGTYIDIPQESILSFLDLTDSPEV SVYPIKEGSKTGLIFVNSTIVDQAYSETTALTR[KREAVAEADPWA] WIRMWPGGVMFT [KRDAEAEAEAEADPWA] WIRMWPGGVMFT [KRDAEAEADAEPWA] WIRMWPGGVMFT	α_{Hu}-factor1: WIRMWPGGVMFT
Kazachstania africana (Kluyveromyces africanus)	MKFTGVLSALSLLSSAVLAETESQSTEAISVPSEAIIGYLDLDGANDVAIIPL VNTTDSGLLFVNTTIYEQASNEDNVSL [KKREADADA] WHWLSIAPGQPMYI [KRDANADADAEA] WHWLSISPGQPMYI [KRDANADADAEA] WHWLSIAPGQPMYI	α_{Ka}-factor1: WHWLSISPGQPMYI α_{Ka}-factor2: WHWLSIAPGQPMYI
Kazachstania naganishii (Saccharomyces naganishii)	MKFSTILSAAALAASAFAAPIEQPEQDLNSTTIPAEAIISYLDLEGDKDIAVV PFSNATDSGLLFVNTTILAQANKEAGTPLQ[KREADADANA] WHWLRLSYGQPIY [KRDANADADADADA] WHWLRLSYGQPIY [KRDANADADADADA] WHWLRLSYGQPIY	α_{Kn}-factor1: WHWLRLSYGQPIY
Kluyveromyces dobzhanskii	MKFSAVLSTTVAIIHAALAAPITSETDLNDTAITIPEEALIGFVDLTGDDISLL PFDNGTHTGVFFLNTTIAKAAFANETSLS[KREASADANADA] WSWISLRPGQPIF[KREANAEAEAEASA]WSWISLRRGQPIF[KREASPEAE AEAEPSA]WSWISLRRGQPIF[KREASPEAEAEPSA] WSWISLRRGQPIF	α_{Kd}-factor1: WSWISLRPGQPIF
Kluyveromyces lactis (Candida sphaerica)	MKFSTILAASTALISVVMAAPVSTETDIDDLPISVPEEALIGFIDLTGDEVSLL PVNNGTHTGILFLNTTIAEAAFADKDDLK[KREADASP] WSWITLRPGQPIF[KREANADANAEASP]WSWITLRPGQPIF [KREANADANADASP]WSWITLRPGQPIF[KREANPEAEADAKPSA]WSWI TLRPGQPIF	α_{Kl}-factor1: WSWITLRPGQPIF
Kluyveromyces marxianus	MRLSAVFVSAIALLSTVIAAPITEKESDDSSIKVPSEAILGFLDLTADDDVGL VKINNGTHSGILFLNTTIASIAYANETILS[KREA]SVEADPWKWLSLRVGQP IY[KREASPEAEAEP]WEWLSLRVGQPLY[KREASPEAEAEAEP] WKWLSFRVGQPIY [KREASPEAEADP] WKWLSFRIGQPIY	α_{Km}-factor1: WKWLSLRVGQPIY α_{Km}-factor2: WEWLSLRVGQPLY
Lachancea dasiensis	MFREFSAYLTLALAMSRAWAAPVNLSSSLSMNEGQSLPAESIVGFLDLTG ADDLALFPVSNATNTGVLIVNTTVLDSATESKKRG[KRNANAEAEP]WQW LRLGRGQPMY[KREANAEAEA]WSWLRLGRGQPMY [KRDANAEPEP]WKWLRLGRGQPMY[KRDASADANANAEP] WRWLRLGRGQPMY[KRDASAAPGAQP]WRWLRLDRGQPMY	α_{Ld}-factor1: WQWLRLGRGQPMY α_{Ld}-factor2: WSWLRLGRGQPMY α_{Ld}-factor3: WKWLRLGRGQPMY α_{Ld}-factor4: WRWLRLGRGQPMY α_{Ld}-factor5: WRWLRLDRGQPMY
Lachancea fermentati	MQRLLILILGLASTLMSVSAAPLTDAASTVDIPQESILGVFEISDYDDIALLP VSNGTHSAVLILNATLIDAAGTSNSDEVE[KRSASP]WHWLRLKGPMY[KR DASPQAEP]WHWLRLKGPMY[KRDANADADP]WHWLRLKGPMY	α_{Lf}-factor1: WHWLRLKGPMY
Lachancea kluyveri	MKLFTTLSASLIFIHSLGSTRAAPVTGDESSVEIPEESLIGFLDLAGDDISVFP VSNETHYGLMLVNSTIVNLARSESANFKG[KREADAEP]WHWLSFSKGEP MY[KREADAEP]WHWLSFSKGEPMY	α_{Lk}-factor1: WHWLSFSKGEPMY
Lachancea lanzarotensis	QQQTTFTSSMFKRLSIYLALALANVSMAAPITTNDSLPAIPQESISGYLDLT GADDLALLPVSNDTHTGILVVNTTILASALASVSQHS[KREAEAEP]WRWL SLARGQPMY[KRDANADAEAEP]WRWLSLARGQPMY [KRDANADAEAEP]WRWLSLARGQPMY[KRDANADAEAEP]WRWLSLA RGQPMY[KRDANADAEAEP]WRW	α_{Lf}-factor1:WRWLSLARGQPMY
Lachancea meyersii	MFKTLSIYVALALAAKGVTAAPISTNESSPALPLESISGYLDLTRADDLALL PVSNDTHTGLLVVNTTILAAAMASESTYT[KREAEAEP]WHWLKLDRGQP MY[KREANAEAEAEP]WHWLRLDRGQPMY[KRDANAEAEAEP]WHWLR LDRGQPMY[KRDANAEAEAEP]WHWLRLDRGQPMY	α_{Lme}-factor1: WHWLKLDRGQPMY α_{Lme}-factor2: WHWLRLDRGQPMY
Lachancea mirantina	MKLTVFWTAFLSFLTTFIVTASAAPVADSANDGSVNIPAESIIGFLDLSDSK DATLVPVSNGTHSGFLFLNSTILSQASTESLK[KRSAQP]WRWLSLRAGEA LH[KREADAEADP]WQWLSLRAGEALH[KREAEAAP]WSWLSLRAGEALH [KRNANAEAEAAP]WRWLSLRAGEALH[KREADAAP]WRWLSLRAGEAL H	α_{Lm}-factor1: WRWLSLRAGEALH α_{Lm}-factor2: WQWLSLRAGEALH α_{Lm}-factor3: WSWLSLRAGEALH
Lachancea nothofagi	MYQTINVCLALTLAVTNVCAAPIKFNDSSPALPLESISGYLDLTGAEDLAL LPVSNATHTGILVVNTTILASALASESNYN[KRDANAEAEAEP]WSWLRLD RGQPMY[KRDANAEAEAEP]WRWLRLDRGQPMY[KREAEAEAEAAAQP] WTWLKLDRGQPMY[KRDANPEAEAEP]WSWLRLDRGQPMY[KRDAEAE AEAEP]WRWLRLDRGQPMY[KRDANAEAEAEP]WRWLRLDRGQPMY	α_{Ln}-factor1: WSWLRLDRGQPMY α_{Ln}-factor2: WRWLRLDRGQPMY α_{Ln}-factor3: WTWLKLDRGQPMY

Lachancea quebecensis	MLKSVSFFLTLALSSITASAAPINITSSDPAIPSESISGFLDLTDAEDLALLPV SNGTHSGVLIVNTTILAQAFGSDDVLT[KRDANAEAEAEP]WRWLSLSRG QPMY[KRDANAEAEAEAEP]WRWLSLSRGQPMY[KRDANAEAEAEP]WR WLRLSRGQPMY[KRDANAEAEAEP]WRWLRLSRGQPMY[KRDANAEAE AEAEP]WRWLSLSRGQPMY[KRDANAEAEAEP]WRWLSLSRGQPMY	α_{Lq}-factor1: WRWLSLSRGQPMY
Lachancea thermotolerans	MLKSFSLFLAFALTSITVSAAPINITDSDPVIPRESICGFLDLTDAEDLALLPV SNGTHSGILVVNTTILAQAFGSDDILT[KRDANAEAEADP]WRWLSLSRG QPMY[KRDANAEADAEP]WRWLSLSRGQPMY[KRDANAEADAEP]WRW LSLSRGQPMY[KRDANAEADAEP]WRWLSLARGQPMY	α_{Lt}-factor1: WRWLSLSRGQPMY α_{Lt}-factor2: WRWLSLARGQPMY
Metschnikowia bicuspidata var. bicuspidata	MKLSIPLIFGAITVASASPASEANLTINGTLIPQEAIISGLTIPEDVYPILNYEN NTATVVFLNGTLLAEAKAYNSETKRDVAYPDREITKRDVEPHTWSWGDA DHELASV[KREAEAEAEADP]WHWVRLKIGQPFF[KRDAEGSADP]WRWV SLTFAKPFF[KRDAEASADP]WHWVALKIGQPFF	α_{Mb}-factor1: WHWVRLKIGQPFF α_{Mb}-factor2: WRWLSLSRGQPMY α_{Mb}-factor3: WHWVALKIGQPFF
Millerozyma farinosa (Pichia farinosa)	MKFSAIVISGLLGAGLVKAAPVDSGAKGKYSRTDLIIPDEAIANRYVVGDD EQPVFAEIDNKPVVYIVNTTKAESIVAKSGITLDDLKESYANATKEEEAKNG [KRDANADAEA]KFHWFTYSNFDPIT[KRDANAAP] KFHWFKYNNFDPIT[KRDANAEASP]KFHWFTYNNFDPIT[KRDANAEAS P]KFHWFKYNNFDPIT[KRDANAAP]KFHWFKYNKYDPIT [KRDANAAP]KFHWFKYNKYDPIT[KRDANAEAAP]KFHWFKYNKYDPIT[KRDANAEAAP]KFHWFKYNKYDPIT[KRDANAEAAP]KFHWFKYNKYDPI TKRET	α_{Mf}-factor1: KFHWFTYSNFDPIT α_{Mf}-factor2: KFHWFKYNNFDPIT α_{Mf}-factor3: KFHWFTYNNFDPIT α_{Mf}-factor4: KFHWFKYNKYDPIT
Naumovozyma castellii (Saccharomyces castellii)	MKLSALLSTVALASTSFAAPIDTTASNENLNSTDIPAEAVIGYLDLGSDSD VAMLPFQNSTSNGLLFVNTTIVQQAAQENDDSVGLA[KREANAEA]GWH WLRLDPGQPLY[KREADADAEA]NWHWLRLDPGQPLY [KREAEADAEA]NWHWLRLDPGQPLY[KREADADAEA]NWHWLRLDPG QPLY[KREADADAEA]NWHWLRLDPGQPLY	α_{Nc}-factor1: GWHWLRLDPGQPLY α_{Nc}-factor2: NWHWLRLDPGQPLY
Naumovozyma dairenensis (Saccharomyces dairenensis)	MKYSHFFNSLALLLSSISLISATQLIDDLTNSDGNIPTEAIIGYLDLGADSDV TLLPFSNNTASGLLFVNATILDQALASSEKSDNNGLSKRACHYAHWGDR CFMNTDPGDLI	no mature pheromone identifited
Penicillium chrysogenum	MKFTSVVVAVIAAGTVQAAALAPSETLPKWCGHIGQGCKRTTDASLDVK RSADALAEAMAGGLPLVLQKWCGHIGQGCYKAKRAADAVDEVKRTSD ALARAFAALEEEDDE	no mature pheromone identifited
Sordaria macrospora	MKFTLPLVIFAAVASATPVAQPIAEAEAQWCRIHGQSCWKV[KRVAEA]FS TAIQGMGGLPTSDESGHLPAQVA[KRQVDELAGIIALTQEDVNAYYDSLN LQDKFAPSTEEEKKDEKVA[KRDAEAEA]QWCRIHGQSCWKKA[KREAEA] QWCRIHGQSCWK[KRDAAPEAAPEANP]QWCRIHGQSCWKA[KRAAEA] VMTAIQSAEAESALLLRDTTFSPVDRVG[KREADP]QWCRIHGQSCW[KRY ASPEA]ACNAPDGSCTKATRDLHAMYNVARAILTAHSDEN	α_{Sm}-factor1: QWCRIHGQSCWKKA α_{Sm}-factor2: QWCRIHGQSCWK α_{Sm}-factor3: QWCRIHGQSCWKA α_{Sm}-factor4: QWCRIHGQSCW
Saccharomyces cerevisiae	MRFPSIFTAVLFAASSALAAPVNTTTEDETAQIPAEAVIGYLDLEGDFDVA VLPFSNSTNNGLLFINTTIASIAAKEEGVSLD[KREAEA]WHWLQLKPGQP MY[KREAEAEA]WHWLQLKPGQPMY[KREADAEA]WHWLQLKPGQPMY [KREADAEA]WHWLQLKPGQPMY	α_{Sc}-factor1: WHWLQLKPGQPMY
Saccharomyces paradoxus	MRFCSVFTAFSFAASSALAAPVNTTTEDEMARIPAEAIIGYLDLEGDFDVA VLPFSNSTNNGLLFINTTIANIAAEEEGVTLN[KREADA]WHWLQLKPGQP MY[KREAEAEADAEA]WHWLQLKPGQPMY[KREAEAEADAEA]WHWLQ LKPGQPMY[KREAEAEADAEA]WHWLQLKPGQPMY	α_{Spa}-factor1: WHWLQLKPGQPMY
Schizosaccharomyces pombe	MKITAVIALLFSLAAASPIPVADPGVVSVSKSYADFLRVYQSWNTFANPDR PNLK[KREFEAAPA]KTYADFLRAYQSWNTFVNPDRPNLK[KREFEAAP]EK SYADFLRAYHSWNTFVNPDRPNLK[KREFEAAP]AKTYADFLRAYQSWNT FVNPDRPNLK[KRTEEDEENEEEDEEYYRFLQFYIMTVPENSTITDVNITAK FES	α_{Sp}-factor1: YADFLRAYQSWNTFVNPDRPNLK α_{Sp}-factor2: YADFLRAYHSWNTFVNPDRPNLK
Saccharomyces kudriavzevii	MRFSSIITAVFAASSALAAPVNTTSESETVQIPAEAIIGYLDLEGDFDVAVLP FANSTNNGLLFINTTIANLATKEESVPLS[KREAEADAEA]WHWLQLKPGQ PMY[KREAEADAEA]WHWLQLKPGQPMY[KREAAADAEA]WHWLQLKP GQPMY[KREAEAEADAEA]WHWLQLKPGQPMY	α_{Sk}-factor1: WHWLQLKPGQPMY
Scheffersomyces stipitis (Pichia stipitis)	MHLRSTAILSAVVFTSVALSAPTSGQNIDIDFPDESIAGAIPLSYDLVPIIGS YQGQNVILIVNSTIAAASEAAASEGKS[KRDANA]WHWTSYGVFEPG[KRD ANANAAP]WHWTSYGVFEPG[KRDANADAAP]WHWTSYGVFEPGK	α_{Ss}-factor1: WHWTSYGVFEPG α_{Ss}-factor2: WHWTSYGVFEPGK
Tetrapisispora blattae (Kluyveromyces blattae)	MKFSTVLSLVSVAASTTLAAPVDTESLYDNSTTVDVPEEAILAFVGFDGTD VALTPFRNETHSGVLFINTTIYESALASEDGTPLV[KREADAEP] HWLRLGRGEPLY[KREAEADAEADA]HWLRLGRGEPLY[KREAEADAEAD A]HWLRLGRGEPLY[KREAEADAEADA]HWLRLGRGEPLY[KREAEADAE ADA]HWLRLGRGEPLY	α_{Tb}-factor1:HWLRLGRGEPLY
Tetrapisispora phaffii	MKLSSVLSTLALTATSAFAAPVSNESVDNASVPAEAIIGYLNFDGANDIAL LPFSNSTTSGVMFINTTIAEQAYEEAGVSLS[KREADA]WHWLRLDPGQPL Y[KRDAEADAEA]WHWLRLDPGQPLY[KRDAEADAEA] WHWLRLDPGQPLY[KRDAEADAEA]WHWLRLDPGQPLY	α_{Tp}-factor1:WHWLRLDPGQPLY

Torulaspora delbrueckii	MKFFNTILSTTLFTYVALAAPVESDPVNIPSEAILGYMDFTEDQDVGVVAY TNSTFSGLIFFNSSIIETKDLT[KRDAEA]GWMRLRLGQPLK[KRDADADAD A]GWMRLSPGKPMK[KREADADAEA]GWMRLRIGQPL	α_{Td}-factor1: GWMRLRLGQPLK α_{Td}-factor2: GWMRLSPGKPMK α_{Td}-factor3: GWMRLRIGQPL
Vanderwaltozyma polyspora	MKFSTVLSTVALAATAVSAAPISRASNETVESVESGLNVPAEAVLGYLDFG EKDDVAMLPFSNGTSNGLLFVNTTIYDAAFADSDDESASLA[KRDAEA]W HWLRLRYGEPIY[KREDSEGVE][KREAAAEP]WHWLRLRYGEPIY[KREDSE SVE][KREAAAEP]WHWLRLRYGEPIY[KREDSESVE][KREANADADA]WH WLRLRYGEPIY	α_{Vp}-factor1: WHWLRLRYGEPIY
Yarrowia lipolytica	MKFSTIALAAVACLVSAAPAAPVGTGSHGPQSIPEEAIVGGLQGTENEIFV FFNDDESGKQGIAIIDAKKAQEAGFMDPQPDSEVAAGNA[KREASPEA] WRWFWLPGYGEPNW[KRDAMP]ADMDKE[KREANPEA]WRWFWLPGY GEPNW[KRDAMP]ADMDKE[KREANPEA]WRWFWLPGYGEPNW[KRDA MP]ADMDKE[KREANPEA]WRWFWLPGYGEPNW	α_{Yl}-factor1: WRWFWLPGYGEPNW
Zygosaccharomyces rouxii	MRLSIALGVTFGAVAGLTAPVEEV[KRDADA]HFIELDPGQPMF[KREAEA] HFIELDPGQPMF[KREAEAEA]HFIELDPGQPMF[KREAEAEA]HFIELDPG QPMF[KREAEADA]HFIELDPGQPMF[KRDADA]HFIELDPGQPMF[KREA EAEA]HFVELDPGQPMF[KREAEADA]HFIELDPGQPMF[KRGEIESAA]	α_{Zr}-factor1: HFIELDPGQPMF α_{Zr}-factor2: HFVELDPGQPMF

Appendix Table 2: List of selected α-factors and synthesized α-factors.

Name of Organism	α-factors	Synthesized α-factors
Candida albicans	α_{Ca}-factor 1: KSKGGFRLTNFGYFEPG α_{Ca}-factor 2: GFRLTNFGYFEPG	α_{Ca}-factor 2: GFRLTNFGYFEPG
Eremothecium cymbalariae	α_{Ec}-factor 1: WHWLRFDRGQPIH	α_{Ec}-factor 1: WHWLRFDRGQPIH
Kazachstania africana	α_{Ka}-factor 1: WHWLSISPGQPMYI α_{Ka}-factor 2: WHWLSIAPGQPMYI	α_{Ka}-factor 1: WHWLSISPGQPMYI
Kazachstania naganishii	α_{Kn}-factor 1: WHWLRLSYGQPIY	α_{Kn}-factor 1: WHWLRLSYGQPIY
Kluyveromyces lactis	α_{Kl}-factor 1: WSWITLRPGQPIF	α_{Kl}-factor 1: WSWITLRPGQPIF
Lachancea fermentati	α_{Lf}-factor 1: WHWLRLKGPMY	α_{Lf}-factor 1: WHWLRLKGPMY
Lachancea mirantina	α_{Lm}-factor 1: WRWLSLRAGEALH α_{Lm}-factor 2: WQWLSLRAGEALH α_{Lm}-factor 3: WSWLSLRAGEALH	α_{Lm}-factor 2: WQWLSLRAGEALH
Lachancea thermotolerans	α_{Lt}-factor 1: WRWLSLSRGQPMY α_{Lt}-factor 2: WRWLSLARGQPMY	α_{Lt}-factor 1: WRWLSLSRGQPMY
Saccharomyces cerevisiae	α_{Sc}-factor 1: WHWLQLKPGQPMY	α_{Sc}-factor 1: WHWLQLKPGQPMY
Tetrapisispora phaffii	α_{Tp}-factor 1: WHWLRLDPGQPLY	α_{Tp}-factor 1: WHWLRLDPGQPLY
Vanderwaltozyma polyspora	α_{Vp}-factor 1:WHWLRLRYGEPIY	α_{Vp}-factor 1: WHWLELDNGQPIY

Appendix Figure 1: Complete amino acid alignment of the selected Ste2 receptors. Annotated in turquoise are the transmembrane and in light red the cytoplasmic loop. In dark blue annotated are the G protein-interacting sites: the third cytoplasmic loop region, and the seventh transmembrane loop.

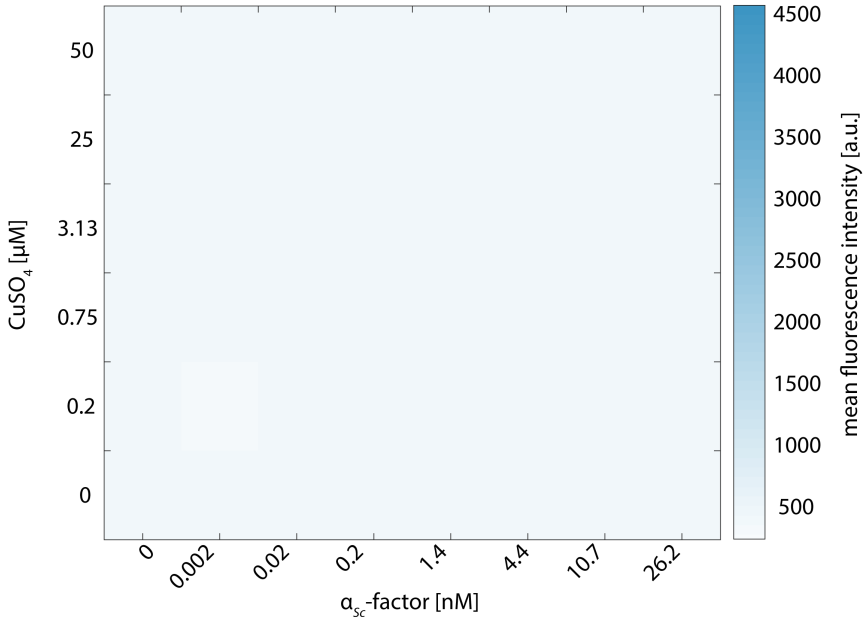

Appendix Figure 2: Results of the *ste2* gene expression titration experiment. The expression of the Ste2 receptor was regulated by amounts of $CuSO_4$ in the media. To investigate the interplay between receptor expression levels and amounts of α-factor, synthetic pheromone was added in different amounts to the Ste2- expressing receptor strains. The rows of the heatmap display different α_{Sc}-factor concentrations and the columns the increasing $CuSO_4$ concentrations. The color code indicates the mating pathway activity as levels of Venus expressed from the P_{FUS1} mating-responsive promoter. Plotted is the mean fluorescence intensity of three biological replicates of 50,000 single-cell events each. The constitutive promoter PAB1 that was previously used for *ste2*$_{Sc}$ gene expression was utilized as a control. Here, heatmap for the *MAT***a** *far1Δ* stain (negative control, no Ste2 receptor was expressed) in increasing $CuSO_4$ and α_{Sc}-factor concentrations. See also Figure 110.

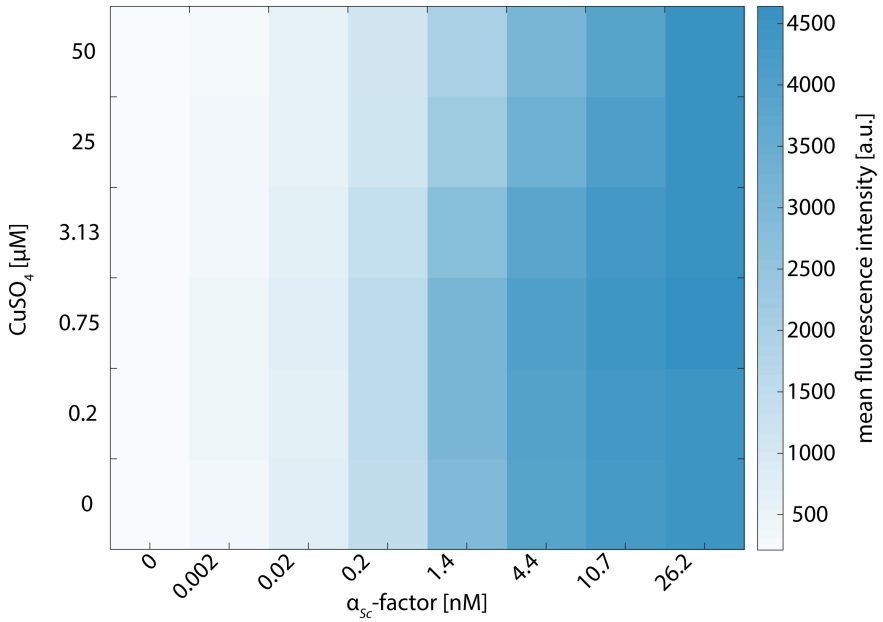

Appendix Figure 3: Results of the *bar1* gene expression titration experiment (negative control). The expression of the Ba11 protease was regulated by amounts of $CuSO_4$ in the media. To investigate the interplay between protease expression levels, amounts of α-factor and resulting mating pathway activation, synthetic pheromone was added in different amounts to the coculture of the Bar1 and Ste2 strain. Higher expression levels of Bar1 should result in reduced

mating pathway activity in the Ste2 receiver strain due to α-factor degradation. The rows of the heatmap display different α_{Sc}-factor concentrations and the columns the increasing $CuSO_4$ concentrations. The color code indicates the mating pathway activity as levels of Venus expressed from the P_{FUS1} mating-responsive promoter in the Ste2 strain. Plotted is the mean fluorescence intensity of three biological replicates of 50,000 single-cell events each. The constitutive promoter HHF1 that was previously used for *bar1*$_{Sc}$ gene expression was utilized as a control. Here, heatmap for the *MAT***a** *far1Δ* stain (negative control, no Bar1 was expressed) in increasing $CuSO_4$ and α_{Sc}-factor concentrations. See also Figure 112.

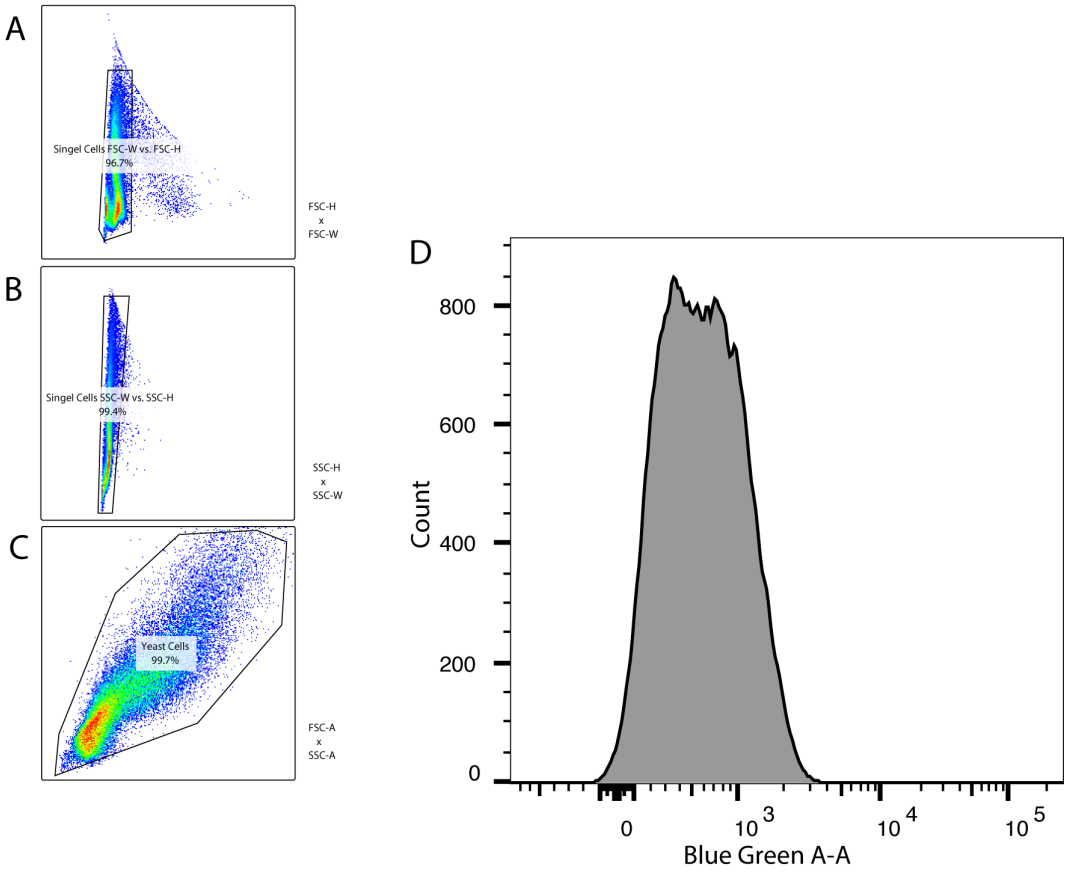

Appendix Figure 4: Visualization of gating on the example of a medium-induced pheromone-responsive promoter. A and B) Gates to select single-cell events in the FSC and SSC channel. Resulting in the removal of multiple detections or aggregates. **C)** Gate to select yeast cells and to remove cell debris. **D)** Final histogram of the recorded yeast cells.

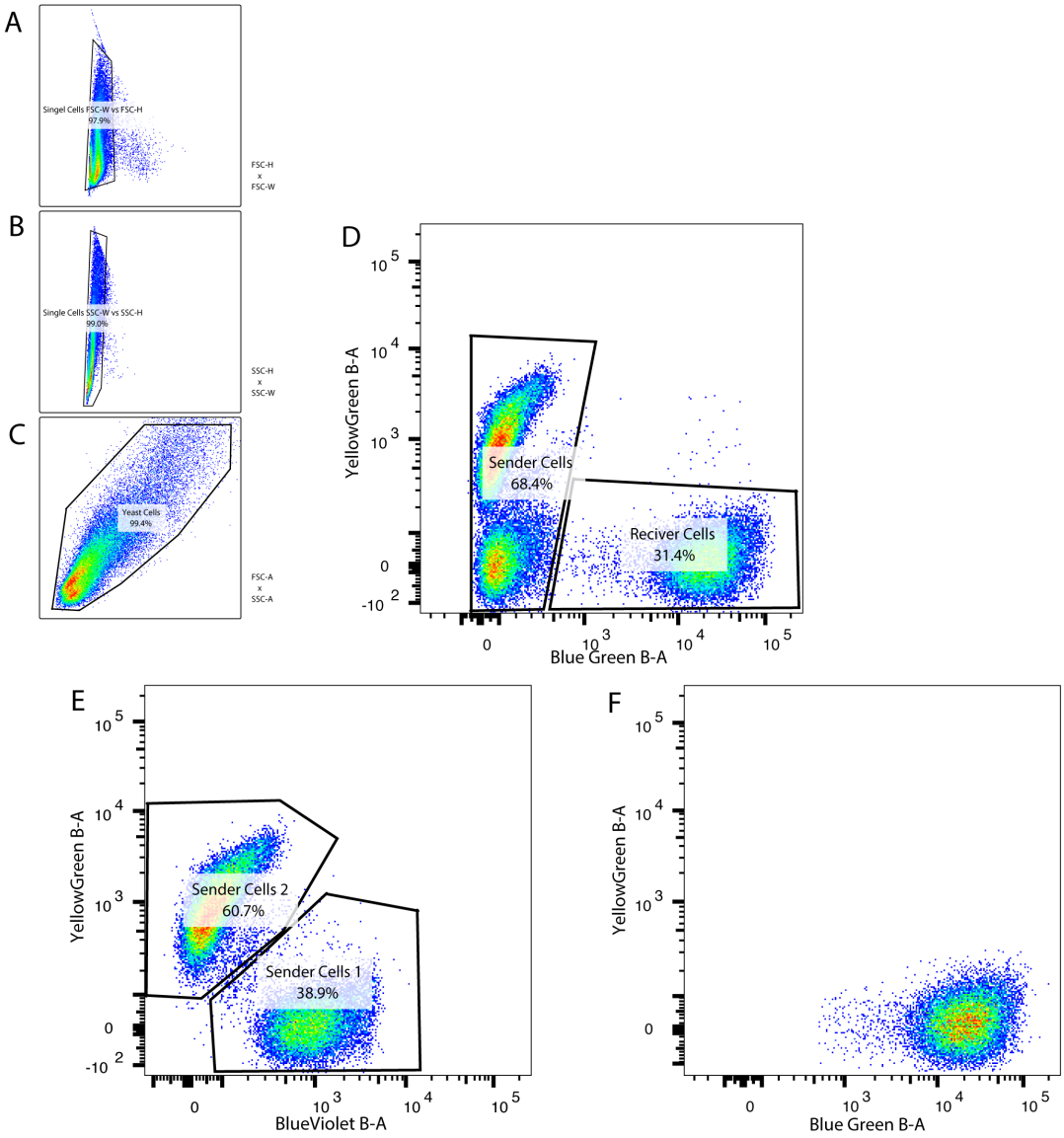

Appendix Figure 5: Visualization of gating on the example of an active AND gate-like population network. A and B) Gates to select single-cell events in the FSC and SSC channel. Resulting in the removal of multiple detections or aggregates. **C)** Gate to select yeast cells and to remove cell debris. **D)** Gating to separate sender and receiver populations based on the dedicated constitutively expressed fluorescent proteins. **E)** Gate to separate the two sender populations. **F)** Separated receiver population for the fluorescence intensity determination.

Acknowledgements

First and foremost, I would like to thank Prof. Victor Sourjik, not only for welcoming me for my doctoral studies in his laboratory but also for trusting and supporting me with a high degree of freedom to follow my own research questions. Thank you!

Over the course of my thesis, Prof. Tobias Erb and Dr. Hannes Link joined my journey as part of my thesis advisory committee. I would like to thank both of them for their great scientific advice, fruitful discussions as well as for their mentoring.

Also, I would like to thank Prof. Michael Bölker, who gave me the opportunity to take over one of his courses to learn how to teach and for joining my defense committee.

I addition, I want to thank Prof. Jay Keasling and Dr. Anna Lechner who allowed me to take the early stage CoA project to Marburg and to continue working with them.

I thank Dr. Alexander Anders for supporting me with the YCTK project as well as for helping me plotting some of the results in the most appealing way.

Dr. Timo Glatter supported me with the proteomics experiments and I would like to thank him for his great efforts to push the limits of the method for the YCTK project further.

I further would like to highlight and thank Prof. Stefan Rensing for great discussions and for his support with the likelihood analysis and phylogenetic studies that were part of the YCTK project.

Also, I thank Silvia González Sierra for keeping the flow cytometer always in excellently shape and supporting me during the long hours using this machine.

Without many that I cannot name all, the laboratory would not run as smoothly as it does - I would like to thank also all of them for their support.

I also would like to thank the students and interns I supervised of the years, the iGEM Team Marburg 2015, Isabelle, Anurag, Lisa, Mary, René and Cooper. I enjoyed the discussions, the teaching and seeing all of you prosper a lot.

I am also thankful to all of the fellow colleagues in the Sourjik Lab who made my doctoral studies special to me. I have to highlight Anne, Max, and Daniel, with whom I experienced a great time beyond the bench, like the founding of GASB and the many events of it.

Also, I want to thank my colleagues who became dear friends, Joana, Anja, Max, Miri, Ron, Daniel, Yu, Alex, and Gabri.

I am deeply grateful to Anne, who supported me over the long and sometimes a bit painful course of my PhD. I am thanking her for discussing science, experiments, and results, that I dreamed about at night, during breakfast and always, spending weekends with me in the laboratory, because I just wanted to do one more experiment, and for literally always being there for me. Thanks for everything that you have done for me.

Vielen Dank, Elke und Knut, für die Unterstützung über die letzten Jahre.

Ich möchte natürlich auch noch meinen Freunden und meiner Familie danken. Gerade meine Familie, besonders Marlies und Bruni, haben mich über die lange Zeit immer sehr unterstützt, auch wenn es schwer zu verstehen war, was ich eigentlich mache, als erster aus der Familie mit einer Doktorarbeit. Ich möchte mich auch bei denen bedanken, die am Anfang meiner Doktorarbeit an meiner Seite waren, doch leider das Ergebnis nicht mehr mit mir feiern können. Besonders bei meiner Oma, die immer an mich glaubte, immer für mich da war und dich ich immer vermissen werde.

Zum Ende der Danksagung will ich meinen wohl größten Dank an meine Mama aussprechen. Ich habe mit ihr tatsächlich in der Elternlotterie das große Los gezogen! Ich bedanke mich für nunmehr 30 Jahre großartige Unterstützung, Rücken freihalten, Ausbügeln und mich motivieren, mir auch mal die Meinung sagen und noch so viele Dinge mehr. Die Doktorarbeit gehört auch dir ein Stück weit! Vielen Dank, einfach für alles!

Curriculum Vitae

Nicolas Krink, né Koutsoubelis
*07.04.1989 in Hagen, Germany
Nicolas.krink@synmikro.mpi-marburg.mpg.de

Education	
Nov. 2014 –2019 Marburg, GER	**Dr. rer. nat. in Biology** *Max Planck Institute for Terrestrial Microbiology Marburg and Center for Synthetic Microbiology (SYNMIKRO)* *Department of Systems and Synthetic Microbiology in the group of Prof. Dr. Victor Sourjik* *International Max-Planck-Research-School Marburg (IMPRS-Mic) fellow* Thesis: From CoA ester supply to a yeast communication toolkit in *Saccharomyces cerevisiae*
Sep. 2012 – Jul. 2014 Paris, FRA	**MSc Interdisciplinary Approaches to Life Sciences** *Center for Research and Interdisciplinarity (CRI), Université Paris V Descartes Cite Sorbonne,* Focus on Systems and Synthetic Biology Thesis: Metabolic Engineering in yeast; completed at the Joint BioEnergy Institute – Prof. Jay Keasling
Oct. 2009 – Aug. 2012 Freiburg, GER	**BSc Biology** *Albert-Ludwigs-University of Freiburg* Focus on Biochemistry, Genetics and Biotechnology Thesis: Quantitative in silico and in vivo characterization of the recombinase addressable data storage

Publications	
2019/2020	**Krink, N.,** Anders, A., Glatter, T. and Sourjik, V. (in preparation) **YCTK – Yeast communication toolkit for multicellular networks in *S. cerevisiae***
Mar. 2018	**Krink-Koutsoubelis, N**., Loechner, A. C., Lechner, A., Link, H., Denby, C. M., Voegeli, B., Erb, T. J., Yuzawa, S., Jakociunas, T., Katz, L., M. K. Jensen, V. Sourjik, J. D. Keasling. (2018) **Engineered production of short chain acyl-coenzyme A esters in S. cerevisiae**. ACS Synth. Biol. 2018, 7, 4, 1105-1115
Jun. 2015	Shih, S. C. C., Goyal, G., Kim, P. W., **Koutsoubelis, N.**, Keasling, J. D., Adams, P. D., Hillson, N. J., and Singh, A. K. (2015) **A Versatile Microfluidic Device for Automating Synthetic Biology**. *ACS Synth. Biol. 4*, 1151–1164.
Dec. 2014	Libis, V. K., Bernheim, A. G., Basier, C., Jaramillo-Riveri, S., Deyell, M., Aghoghogbe, I., Atanaskovic, I., Bencherif, A. C., Benony, M., **Koutsoubelis, N.**, Löchner, A. C., Marinkovic, Z. S., Zahra, S., Zegman, Y., Lindner, A. B., and Wintermute, E. H. (2014) **Silencing of Antibiotic Resistance in E. coli with Engineered Phage Bearing Small Regulatory RNAs**. *ACS Synth. Biol. 3*, 1003–1006.
Dec. 2014	Atanaskovic, I., Bencherif, A. C., Deyell, M., Jaramillo-Riveri, S., Benony, M., Bernheim, A. G., Libis, V. K., **Koutsoubelis, N.**, Zegman, Y., Löchner, A. C., Basier, C., Aghoghogbe, I., Marinkovic, Z. S., Zahra, S., Toulouze, M., Lindner, A. B., and Wintermute, E. H. (2014**) In Situ Characterization of Mycobacterial Growth Inhibition by Lytic Enzymes Expressed in Vectorized E. coli.** *ACS Synth. Biol. 3*, 932–934.